Road and Railway Foundation Response to Moisture Content and Drainage

Xuanxuan Chu

BEng., MSc.

Thesis submitted to the University of Nottingham

for the degree of Doctor of Philosophy

January 2023

ABSTRACT

Attenuation and loss of service capability are closely related to subsurface water in a pavement/track foundation. The strength of the foundation decreases with increasing moisture content. Thus, it is important to investigate foundation soil behaviour. It is beyond the scope of this project to thoroughly cover both pavements and railway tracks, and the analysis of pavement foundations was concentrated on. The findings from the pavement analysis are expected to provide a reference for understanding the foundation response of railway tracks since railways are similar except for the upper structures. This research aims to reveal the significance of drainage and broaden the understanding of foundation behaviour at various moisture contents. The research was performed from various aspects (including simulation analysis and laboratory tests), thus comprehensively demonstrating the effect of moisture content and drainage. Prediction models of resilient modulus were developed for unsaturated soils using data from literature sources. Furthermore, moisture effects and/or drainage benefits were demonstrated on three levels, i.e. simulation analysis, triaxial tests and subgrade box tests. A selected series of studies were analysed and multi-layered elastic simulations were carried out for sensitivity analysis. The sensitivity results provide a reference for parameter selection in the pavement analysis following triaxial tests. Triaxial tests were performed to investigate the stress-strain behaviour and modulus of silty sand at various laboratory-controlled moisture contents and drainage conditions. Subgrade box tests were conducted to study the deformation behaviour under cyclic traffic loading in a more realistic way compared to triaxial tests.

Testing data were collected from previous studies and analysed, and a general trend was revealed among the data. A relationship of resilient modulus with confining pressure, stress states and moisture content was developed, namely the consistency index model and the stress-modified consistency index model. In terms of the model parameters, their relationship with clay content and plasticity index was proposed through regression analysis. These models showed fairly good prediction results of resilient modulus with a wider variety of soil types. Thus, the consistency index as a normalized soil property can extend sensitivity analysis results to different soils. These models were proposed for the first time. The proposed models initially correlated

consistency index with resilient modulus and provided alternative ways for resilient modulus prediction at various moisture contents.

Based on multi-layered elastic theory, a sensitivity analysis was conducted to investigate the variation of pavement response at different moisture contents. The sensitivity analysis involved two aspects, data analysis using predetermined subgrade modulus from model calculations and data analysis using subgrade modulus from literature sources. The variables adopted for the analysis included the thickness and elastic modulus of pavement layers (asphalt concrete, base layer and subbase layer), axle load and subgrade modulus at different moisture contents. Results from the sensitivity analysis included fatigue and rutting life and their sensitivity indices to moisture variation. A design of a polymer drainage layer was also proposed. The critical factors influencing pavement response were identified (e.g. the thickness of asphalt concrete), thus providing a basis for the pavement analysis using unloading modulus from multistage triaxial tests. The comprehensive analysis of the sensitivity of pavement response to moisture content could expand the understanding of moisture effects. This may also help to establish a way to evaluate in-situ pavement structures and pavement design.

Triaxial tests included saturated consolidated undrained and drained triaxial compression tests and unsaturated constant water content triaxial tests. A series of single-stage (monotonic) and multistage loading tests were performed under various confining pressures for saturated and unsaturated tests. Drainage was allowed between loading stages. Results were investigated, including stress-strain behaviour, unloading modulus, cohesion, friction angle, volumetric behaviour (for consolidated drained tests) and matric suction (for unsaturated soils tests). The unloading modulus was adopted as an input into KENPAVE in order to study foundation response in a flexible pavement structure. Effects of drying, wetting and drainage were revealed. The drainage was quantitatively related to pavement response based on pore water pressure reduction. The effects of drainage and moisture content on pavement foundation soils were further comprehensively investigated in a laboratory-controlled manner (i.e. triaxial tests) under different drainage conditions, and the results were compared so as to obtain a sensitivity analysis.

Subgrade box tests were carried out to simulate a more realistic condition. Cyclic

loading was applied at various cyclic stresses, moisture contents and frequencies. The settlement of the subgrade surface was analysed. Moisture distribution with depth before and after loading was checked. It was found that the soil settlement increased with cyclic stress and moisture content. In contrast, with limited repetitions, the settlement did not show a significant increase with frequency. The box tests further revealed the effects of moisture content on foundation soils and were more representative of actual pavement foundations compared with triaxial tests.

ACKNOWLEDGEMENTS

The work presented in the thesis was conducted through facilities at the Nottingham Centre for Geomechanics (NCG) and Nottingham Transportation Engineering Centre (NTEC) of the University of Nottingham. The financial support during the study period provided by the China Scholarship Council (CSC) and the University of Nottingham is thankfully acknowledged.

I would like to thank my supervisors, Dr Andrew Dawson and Dr Nick Thom, for their thoughtful guidance and consistent support throughout my research. They have been really helpful with their great expertise during my study. In particular, Dr Andrew Dawson retired in August 2020 but continued and volunteered to support me. His continuous presence and support have been valuable in the past four years.

I would like to thank Dr Alec Marshall and Dr Lelio Brito for their work in reviewing my thesis. Their comments have helped to greatly improve my thesis. I would like to thank Professor Fuming Wang and Professor Chengchao Guo for their support during my studies. The access to their resources has helped my research to go smoothly.

I would like to thank Dr Juan (Iván) Campos-Guereta Díez for his help and advice on the project and for sharing his FEM code to do calculations. I would also like to thank Dr Ahmed Abed for his guidance on KENPAVE software and coding. I am also grateful to Dr Juan Sebastian Carvajal Munoz for his encouragement and the help to revise the initial outline. I appreciate the help from Dr Ge Cui and Dr Waleed Khan to check and discuss the tests.

I would like to express my gratitude to laboratory technicians, Mr Martyn Barrett, Mr Richard Blakemore, Mr Jon Watson, Mr Andrew Maddison and Mr Lee Hickling for their support with the tests.

I would like to thank Dr Mingming Xu, Dr Junjian Zhang, Dr Jiangyu Wu and Dr Zhengyuan Qin for making the study-life much more enjoyable.

Last but not least, I would like to express my great gratitude to my family, my parents, my siblings and my partner, who supported and encouraged me during my studies. They motivated me to carry on during the more challenging periods of my studies.

DECLARATION

I declare that this thesis has been composed solely by myself and that it has not been submitted, in whole or in part, in any previous application for any other degree or professional qualification. Except where explicitly states otherwise by reference in the text or acknowledgement, the work presented is entirely my own.

TABLE OF CONTENTS

LIST OF FIGURES

LIST OF TABLES

LIST OF NOTATIONS

Roman symbols

a	The minimum of $\log\frac{M_r}{M_{r,opt}}$ (Chapter 2)
a	Cross-section area of the standpipe (mm^2, Chapter 5)
a_s	SWCC parameter
A	Cross-section area of the specimen (mm^2)
A_c	Activity defined as the ratio of plasticity index to the clay-size fraction
A_E	Material constant
A_l	Axle load
$A_i(m)$, $B_i(m)$, $C_i(m)$, $D_i(m)$	Functions independent of coordinates r and z
b	The maximum of $\log\frac{M_r}{M_{r,opt}}$
B	Foundation width (mm)
a_1, a_9, b_1, b_9	Material parameters (Eq. (2.35))
a, b, c, d, g, h, i	Regression coefficients (Eq. (2.42))
b	Destructuring index (Section 2.4.1)
c'	Cohesion intercept of soil particles (kPa)
c_2'	Parameter related to E_{ac}
C_0, C_1, C_2, C_3	Material constants of Eq. (2.33)
C'	Intercept of failure envelope for stress path (kPa)
$C(\psi)$	A correction factor that forces the model through a prescribed suction value of 10^6 kPa at zero moisture content
C_c	Coefficient of curvature
C_u	Coefficient of uniformity
c_v	A normalized indicator independent of specific units
D	Fatigue damage of either bottom-up or top-down cracking
D_f	Foundation depth (mm)
D_r	Damage ratio
d_i	Elementary effects of $(X_1, X_2, \dots, X_k)$
$\overline{d}_i$	The mean elementary effects of $(X_1, X_2, \dots, X_k)$
$\overline{d}_i^*$	Revised $\overline{d}_i$, i.e. absolute value of $\overline{d}_i$
e	Void ratio

$\dot{e}$	The variation of e
e_{max}	Maximum void ratio
e_{min}	Minimum void ratio
E	Elastic modulus (MPa)
E_{ac}	Elastic modulus of asphalt concrete (MPa)
E_{base}	Elastic modulus of base layer (MPa)
E_{drain}	Elastic modulus of polymer drainage layer (MPa)
E_{sub}	Elastic modulus of subbase layer (MPa)
E_{ul}	Unloading modulus (MPa)
ΔE_{ul}	Changes in unloading modulus (MPa)
E_v	Vertical stiffness (MPa)
f	Loading frequency (Hz)
f_1, f_2, f_3, f_4, f_5	Regression coefficients
$\mathrm{FC}_{bottom-up}$	The percentage area affected by cracking that initiates bottom-up (%)
$\mathrm{FC}_{top-down}$	The length of fatigue cracking initiating at the top (mm/m)
F_e	A void ratio function
F_{max}	Maximum loading force of box tests (kN)
F_{min}	Minimum loading force of box tests (kN)
F_{ij}	A second-order tensor that characterises the effect of matric suction
G_s	Specific gravity of soil grains
h	Water head difference at time t
h_1, h_2	Standpipe readings (mm, Chapter 5)
h_{ac}	Thickness of asphalt layer (mm)
h_b	Air-entry head (m)
h_{base}	Thickness of base layer (mm)
h_g	Thickness of the granular layer (mm)
h_{sub}	Thickness of subbase layer (mm)
h_s	Suction head (m)
h_{drain}	Thickness of polymer drainage layer (mm)
h_i	Thickness of the i^{th} layer (mm)
i	Specimen No.
I_c	Consistency index
J_0	Bessel function of order zero.
k	The number of independent variables

$k_0, k_1, k_2, \ldots, k_6$	Regression parameters dependent on material type and physical soil properties
k_1, k_2, k_3	Regression parameters (Eq. (8.11))
k_1, k_2, k_3	Model parameters dependent on stress states (Eqs. (6.9) and (6.10))
$k_{rw}(w_{vol})$	The WRP
$k_w(w_{vol})$	Water permeability (cm/s)
k_{sat}	Saturated coefficient of permeability (cm/s)
k_w	Hydraulic conductivity (cm/s)
m	Model parameter of Eq. (2.24)
m	integration parameter (Eq. (2.51))
m_s	SWCC parameter
M_0	Resilient modulus at the reference stress state (i.e. $p = p_r$, $q_{cyc} = p_r$, and $\psi_m = 0$) (MPa)
M	Constant stress ratio at CS
M'	Slope of stress path failure envelop
M_r	Resilient modulus (MPa)
$M_{r,gra}$	The modulus of granular base/subbase (MPa)
$M_{r,i}$	Measured resilient modulus for specimen i (MPa)
$\widehat{M}_{r,i}$	Predicted resilient modulus for specimen i (MPa)
$\overline{M}_{r,i}$	Mean resilient modulus of all specimens (MPa)
$M_{r,opt}$	Resilient modulus at optimum moisture content (MPa)
$M_{r,rep}$	Representative resilient modulus (MPa)
$M_{r,sat}$	M_r of soil at saturation (MPa)
$M_{r,sg}$	The modulus of subgrade (MPa)
n	The number of specimens (Chapter 5)
n	Model parameter of Eq. (2.24)
n_s	SWCC parameter
N	The number of loading repetitions
N_c, N_q, N_γ	Non-dimensional bearing capacity factors that are all functions of the soil friction angle
N_{bt}	The number of box tests
N_f	The allowable number of loads in flexure to the initiation of fatigue cracking
p'	Effective mean stress (kPa)
p_a	Atmospheric pressure (kPa)
p'_{cs}	Mean effective stress at CS (kPa)

p_{net}	Net mean stress (i.e. $\theta_{net}/3$) (kPa)
p_r	Reference pressure for normalizing p_{net}, simplified as 1 kPa
p_y	Yield stress (kPa)
q, σ_d	Deviator stress (kPa)
q	Flow rate (Chapter 5)
q_{cs}	Deviator stress at CS (kPa)
q_{cyc}	Cyclic stress, i.e. the amplitude of variation in deviator stress during cyclic loading–unloading (kPa)
q_{uc}	Unconfined compression strength
q_u	Ultimate bearing capacity
r	Distance from evaluated point to vertical coordinate axis
R^2	Coefficient of determination
R_m^2	Coefficient of dermination from the proposed modified model (i.e. generalised for all soils)
R_r^2	Coefficient of dermination from the reference (non-generalised) studies
S	Degree of saturation expressed as decimal
s_d	Standard deviation
S_i	Sensitivity index
S_{i,w_1}	Sensitivity index of each response at w_1
S_{opt}	Degree of saturation at w_{opt} expressed as decimal.
$\dot{S}$	The variation in S
t	Time (s)
t_1, t_2	Time corresponding to the head of standpipe h_1 and h_2 (s)
u_a	Pore air pressure (kPa)
u_b	Back pressure (kPa)
u_w	Pore water pressure (kPa)
Δu_w	Variation of pore water pressure
u_m, IMS	Initial matric suction (kPa)
Δu_{w-sat}	Build-up of pore-water pressure under partially saturated conditions (kPa)
w_0, w_1, w_2, w_3, w_4	Moisture contents
Δw	The increment of moisture contents
w_{clay}	Clay content
w_L, LL	Liquid limit
w_P, PL	Plastic limit
w_{opt}, OMC	Optimum moisture content

w_{vol}	Volumetric moisture content
$w_{vol,r}$	Residual volumetric moisture content
$w_{vol,s}$	Saturated volumetric moisture content
a, m, n	SWCC parameters (Chapter 3)
z	Vertical coordinate measured from top surface of layer i (Chapter 2)
$X_1, X_2, \dots, X_k$	Tested factors

Greek Symbols

β	Parameter dependent on material properties
β_{GB}	The test road correction factor
$\beta_0, \beta_1, \beta_2, \beta_3, \beta_4$	Fitting parameters
σ, σ_{ij}	Total normal stress (kPa)
$\sigma',\ \sigma'_{ij}, \delta_{ij}$	Effective normal stress (kPa)
σ_1	Major principal stresses (kPa)
σ'_1	Major principal effective stresses (kPa)
σ'_2	Intermediate principal effective stresses (kPa)
σ_3	Minor principal stresses (kPa)
σ'_3	Minor principal effective stresses
σ_c	Confining pressure (kPa)
σ'_c	Effective confining pressure (kPa)
$\sigma_{c,net}$	Net confining pressure (kPa)
$\Delta\sigma'_c$	Variation of effective confining pressure (kPa)
σ'_v	Effective vertical stress (kPa)
ε_0	Parameter dependent on material properties
ε_1	Major principal strain
ε_3	Minor principal strain
ε_a	Axial strain
ε_c	The maximum compressive strain at the top of the subgrade
ε_{cl}	Linear elastic limit of axial strain
ε_t	The maximum tensile strain at the bottom of asphalt concrete
$\varepsilon_{p,i}$	Plastic strain at the i^{th} layer

ε_r	Resilient strain
ε_{toal}	The total axial strain in one loading process
ε_{vol}	Volumetric strain
ε_q	Triaxial shear strain
u_w	Pore water pressure (kPa)
u_a	Pore air pressure (kPa)
ψ	Total suction (kPa)
π	Osmotic suction (kPa)
χ	Parameter thought to be a function of degree of saturation
τ	Shear stress (kPa)
τ_f	Shear strength of soils (kPa)
τ_{oct}	Octahedral shear stress (kPa)
ϕ'	Internal friction angle of soil particles (˚)
ϕ^b	The angle of shearing resistance associated with matric suction (˚)
$\Phi_i(r,z)$	Burmister's biharmonic functions
ψ_m	Matric suction (kPa)
$\dot{\psi_m}$	The variation of ψ_m
ψ_{m_0}	Initial soil matric suction (kPa)
$\Delta\psi_m$	Relative change in soil matric suction with respect to ψ_{m_0} (kPa)
ψ_{opt}	Matric suction at OMC (kPa)
φ	Effective stress rate factor
γ	Shear strain
γ_{dmax}	Maximum unit weight (kN/m^3)
ν	Specific volume
θ	Bulk stress (kPa)
θ_0	Initial bulk stress (kPa)
θ_{net}	Net bulk stress (kPa)
θ_m	Minimum bulk stress (kPa)
Θ	Normalized volumetric moisture content
κ	A fitting parameter of normalized area of water and normalized volumetric moisture content
ξ	Model parameter
δ_s	Cumulative permanent deformation (mm)
δ_{sg}	The maximum vertical displacement at the top of

	subgrade (mm)
$\delta_{s,i}$	The settlement of test i (mm)
$\bar{\delta}_{s,i}$	The arithmetic mean settlement of $\delta_{s,i}$ (mm)
ρ	Parameter dependent on material properties
ρ_0	The maximum dry density at the optimum moisture content (g/cm^3)
ρ_{opt}	Original dry density (g/cm^3)
λ_p	The slope of SWCC
λ_{p0}	Reference value of the slope of SWCC
η_{ci}	Modified consistency index model parameter
Δ	The variation applied to factor X_i
δ_{ij}	Kronecker delta
χ	Effective stress parameter thought to be a function of degree of saturation

Acronyms/Abbreviations

AASHTO	American Association of State Highway and Transportation Officials
AC	Asphalt concrete
$adj\ R^2$	Adjusted R^2
AVR	Air void ratio
BT	Box tests
CBR	California Bearing Ratio
CD	Consolidated drained
CH	Clay of high plasticity, fat clay
CL	Clay of low plasticity, lean clay
CS	Critical state
CSL	Critical state line
CSR	Cyclic stress ratio
CU	Consolidated undrained
CUSSLT	Consolidated undrained saturated triaxial test
DAVI	Diffused air volume indicator
DDR	Dry density ratio (%)
DE	Elastic modulus of drainage layer

DTH	Thickness of drainage layer
DP	Position of drainage layer
DRA	With drainage
DMRB	Design Manual for Roads and Bridges
ESEM	Environmental SEM
ESR	Effective stress ratio
FHWA	Federal Highway Administration
FDM	Finite difference method
FEM	Finite element method
GMC	Gravimetric moisture content
HAEP	High air entry porous disk
HBM	Hydraulically bound mixture
IDC	Initial drying curve
IMMC	Inner M_r-moisture curve
IWC	Initial wetting curve
LVDT	Linear variable differential transformer
MC, w	Moisture content
MDC-WDP	Main drying curve-wetting drying path
MDD	Maximum dry density
MEPDG	Mechanistic-empirical Pavement Design Guide
MH	Silt of high plasticity, elastic silt
MLE	Multi-layered elastic
ML	Silt
msa	Million standard axle
MSL	Multistage loading
OGDL	Open-graded drainage layer
P60	Flexible pavement with an AC thickness of 60 mm
P180	Flexible pavement with an AC thickness of 180 mm
P300	Flexible pavement with an AC thickness of 300 mm
PI, I_p	Plasticity index
PCC	Portland cement concrete
PD, ε_p	Permanent deformation
PDL	Polymer drainage layer
RC	Relative compaction, defined as the ratio of dry density to maximum dry density

RCM	Percent of recycled clay masonry (%)
RMSE	Root mean square error
RLTT	Repeated load triaxial test
RSS	Residual sum of squares
RT	Repeatability tests
SEM	Scanning electron microscope
SgTop	Subgrade top
SSL	Single stage loading
SWCC	Soil water characteristic curve
TDR	Time domain reflectometer
TH_1, TH_2, …, TH_9	Thickness of asphalt concrete
Unsat	Unsaturated
USCS	Unified Soil Classification System
WRP	Water retention potential

CHAPTER 1 INTRODUCTION

1.1 Background and problem statement

Road and rail network construction plays a significant role in national economic and social development. In the last twenty years or so, especially in countries with rapidly developing economies such as China, the escalating growth in vehicle numbers and weights means that road pavements and railway tracks may have operated beyond their original design capacity. Excess water infiltration into the structure also seriously accelerates structural failure since the foundation's soil is sensitive to water. Damage may originate from excess water due to (e.g.) impeded subgrade drainage, inadequate compaction, moisture-sensitive materials and lengthy drainage pathways, i.e., the strength, modulus and related mechanical properties of the foundation may rapidly degrade in the presence of excess water. Even worse, under repeated traffic loading, pavement or track distress may develop more rapidly, owing to the interaction between excess subsurface water and the challenging stress conditions induced by the loading. Excess resilient deformation may occur, representing the subgrade's recoverable deformation under traffic loading. The accumulation of large plastic strains may then be experienced by the foundations of road and railway tracks. This will endanger the long-term performance and serviceability of pavements under repeated traffic loading.

Through drainage, the build-up of pore water pressure will be dissipated in the foundation and the strength will be enhanced to alleviate the effects of loading and environmentally induced variability. The structural performance of pavements/tracks will be promoted, and the service life shows great extension, up to 2~3 times greater than that of an undrained pavement (Cedergren, 1974). Cedergren (1978) predicted that from 1976 to 1990, $217 billion of the estimated $329 billion in maintenance costs could be avoided if structures with efficient drainage were included in all key pavements. For the annual 200 lane miles of new construction in California, an extension of service life of 10 years amounts to over $5 million for rigid pavements and $8 million for flexible pavements over the service life of pavements constructed during any given year (or 36% of pavement costs) (Forsyth et al., 1987). Inadequate subsurface drainage was found to induce many premature failures (appearing at less than 50% of the expected life) (Christopher & McGuffey, 1997), and thus shorter service life and

higher life-cycle cost (Zaghloul et al., 2004). Zaghloul et al. (2004) found that the life-cycle cost of the pavement structure with poor subsurface drainage systems was over twice as much as that of the same structure with well-drained subsurface systems. Therefore, subsurface drainage must receive more attention as it is a key component in the performance of pavement and track structures.

Apart from the saturated critical condition, foundation soils at shallow depths are commonly subject to partially saturated conditions above the phreatic table. Thus, foundation soils will exhibit different responses from saturated to unsaturated conditions. Current research is focused more on soil testing at various moisture contents, while the soil behaviour due to drainage and the resulting pavement/railway track response is limited. Therefore, it is necessary to better understand the foundation response to various moisture contents and drainage conditions.

1.2 Aims and objectives

This project will focus on pavements. Since both the railway and highway foundations are subjected to similar stress and environmental actions, analysing the principles and methods of foundation mechanical response may benefit both fields (Li & Selig, 1994). The project aims to improve the understanding of the response toward and management of water in the foundation and reveal the significance of drainage to foundations. It may provide the basis for extending pavement/track life and improving service reliability.

The specific objectives of the research are outlined as follows:

1) To identify the main mechanical properties that determine the characteristics of road and railway foundations (e.g., strength, resilient modulus and stress-strain response) by a critical review.
2) To develop prediction models of resilient modulus of foundation soils with consistency index and moisture content through regression.
3) To evaluate the effects of various factors (i.e., optimum/initial moisture content, thickness and modulus of structural layers) on pavement response to moisture content by parametric analysis.
4) To observe the effects of wetting, drying and drainage on the stress-strain behaviour and deformation of foundations by saturated and unsaturated triaxial tests.

5) To study the deformation of foundations at different moisture contents by subgrade box tests to reveal drainage's importance.
6) To draw conclusions on foundation response to moisture content and drainage effectiveness.

1.3 Layout of thesis

In the thesis, ten chapters are presented. Following this Introduction, Chapter 2 presents a review of the literature related to the project. Several aspects are discussed: an overview of road and railway track structures, water-induced structural distresses, water flow in foundations, mechanical properties of foundations, drainage methods and multi-layered elastic analysis. The influencing factors of foundation response include soil conditions, moisture content (MC), matric suction, external stress loading condition and drainage. Referring to the field investigation, drainage simulation and laboratory studies, moisture variation ranges in foundations are determined.

Chapter 3 develops prediction models of the resilient modulus of subgrade soils based on the soil consistency index. The moisture content is normalized by use of the consistency index. Based on regression analysis of previous testing data, prediction models of resilient modulus are developed and validated, namely a consistency index model and a stress-modified consistency index model. These newly proposed prediction models were able to determine resilient modulus at various moisture contents with fair accuracy relying only on simple soil properties. This chapter formed the basis of a paper previously published by the author and others (Chu et al., 2021).

Chapter 4 describes a multi-layered elastic modelling analysis of pavements based on previous relevant research in order to reveal the effect of moisture content on the subgrade. The sensitivity index of fatigue and rutting life is analysed with various factors, including the thickness and modulus of each layer, traffic load and drainage layer. The sensitivity of pavement response to moisture content was comprehensively and quantitatively investigated.

Chapter 5 presents soil selection, specimen preparation and classification, and macro and micro characteristics. Macro characteristics include particle size distribution, hydraulic conductivity, compaction characteristics, Atterberg limits and soil-water characteristic curves. Micro characteristics are particle arrangements evaluated by scanning electron microscope (SEM).

Chapter 6 presents the results of saturated triaxial tests. Consolidated undrained and drained tests (single-stage and multistage loading) are presented. Drainage effects on soil behaviour under saturated conditions are quantitatively investigated. Pavement analysis is conducted using the unloading modulus data from the triaxial tests. Thus, laboratory soil element testing and structural simulation are combined to demonstrate drainage effects under saturation.

Chapter 7 presents the results of unsaturated triaxial tests. It demonstrates the soil behaviour at a constant water content during shearing. The effects of drying, wetting and drainage on unsaturated soil behaviour are studied. This allows the understanding of soil behaviour variations under unsaturated conditions. Combined with the saturated triaxial tests, the soil behaviour is comprehensively revealed.

Chapter 8 presents subgrade box tests. Subgrade settlement under cyclic loading is explored at various stress levels, moisture contents and frequencies. Compared to the triaxial tests, subgrade box tests are more realistic in simulating soil foundations. The chapter also provides a reference for studying permanent soil deformation using subgrade box tests.

Chapter 9 presents a discussion of the findings and recommendations.

Chapter 10 presents the conclusions and future work.

A list of references follows Chapter 10.

CHAPTER 2 LITERATURE REVIEW

2.1 Overview of structures

Road and rail track structures will exhibit different mechanical responses under traffic loading due to their form, due to the materials and soils of which they are constructed and due to their condition (especially moisture condition). Therefore, a better understanding of the structures and their responses can benefit the analysis helping to identify the causes of the distresses and the design of preferred drainage. The components of each structure may differ, while undoubtedly, the subgrade will be the most sensitive of all layers to the change in moisture content. Excess resilient (recoverable) deformation at the pavement surface (causing fatigue cracking of asphalt concrete) can be attributed to inadequate stiffness of either or both aggregate and soil layers (Dawson & Correia, 1996).

The maximization of density is crucial in developing the full-strength potential of the material. At optimum moisture content, the easiest compaction can be performed, and the maximum density will be acquired (Thom, 2008). To achieve the maximum dry density of subgrade soils, construction specifications universally require that, in civil engineering practice, the soils be compacted at (or near) optimum moisture content. Consequently, all placed and many in-situ subgrade soils above the water table should be regarded as materials in a partially saturated state (Drumm et al., 1997; Yang et al., 2005). Due to the environmental conditions (e.g. wetting, drying, freezing and thawing), unsaturated soils will be subjected to seasonal variations in moisture content (Drumm et al., 1997; Khoury & Zaman, 2004; Yang et al., 2008; Khoury et al., 2009). Negative pore water pressure (i.e. matric suction) will vary with the moisture content and affect the resilient modulus of the subgrade as a consequence of the changing effective stress, i.e. the resilient modulus will increase with matric suction rising. Conversely, precipitation, rise in the water table and track flooding can result in the increase of pore water pressures (or reduction in matric suction) and, consequently, reduce the load-bearing capacity and resilient modulus of subgrade soils. With respect to the partially saturated conditions, the soil tests and numerical simulation associated

with unsaturated soil characterization are relatively sophisticated and time-consuming compared with those in the saturated state.

Subgrade in a strong/stiff condition under repeated traffic loads plays a significant role in supporting railway tracks; especially, it becomes vital when carrying vehicles with heavier axle loads (Li & Selig, 1994). Thus, the unsaturated soil behaviour may significantly influence the mechanical properties of compacted pavement subgrades (Sawangsuriya et al., 2008). Hence, the effects of partial saturation should be considered comprehensively under various conditions, e.g. various rainfall intensities, moisture contents, repeated traffic loading, soil types and drainage methods.

2.1.1 Road pavements

Pavements may, fundamentally, be categorized into two types, i.e. flexible and rigid. The manner of operation of rigid and flexible pavements differs essentially in the way in which the load is transmitted to the subgrade (Lebeau & Konrad, 2009). Normally, the pavement contains one or more bound layers placed on one or more unbound aggregate layers, and the latter is also supported by the subgrade. The pavement typically consists of several layers, i.e. surface course, pavement base, subbase and pavement foundation (subgrade), as shown in Figure 2.1.

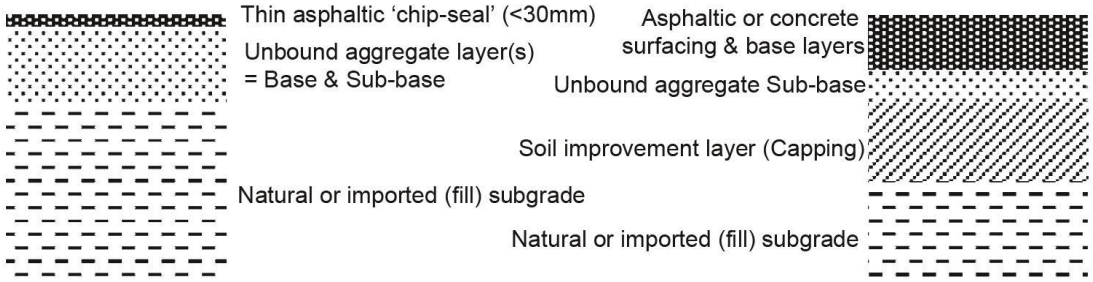

Figure 2.1 Typical pavement structures (*left*=low volume, *right*=higher volume), from Dawson (2008)

With respect to the rigid pavement, a slab of Portland cement concrete with a rigidity much larger than that of the base material is included on the subbase or base layer. Therefore, the slab can make a major contribution to bearing the traffic loading for the rigid pavement. The base (or subbase) layer is mainly needed to facilitate construction and, thereafter, can be used to impede the ejection of a mixture of water and material through joints, cracks, and pavement edges induced by the slab deflection under cyclic traffic loading, i.e. pumping. To achieve this, the base material should be either free-draining or exceedingly resistant to water-induced erosion.

A flexible pavement contains a relatively thin asphalt-wearing course, and vehicle loads are transmitted and distributed by the lower layers. The upper layers only need to be thick enough to distribute the traffic loading sufficiently for the next layer to withstand. Depending on the load distribution properties of the upper layers, lower layers with low-stiffness materials suffer smaller vertical stresses. By providing extra stiffness and dispersing the stresses for the substructure, the base layer increases the load-bearing capacity of roads (Lebeau & Konrad, 2009).

In nearly all cases, the surface layer is bound by bitumen or cement. When there is an embankment, the subgrade consists of imported fill, whereas, regarding a cutting, its subgrade is usually constructed with the in situ natural rock or soil. There are some requirements for the pavement to ensure its serviceability in the long term, e.g. the surface must not deflect much transiently, not deform plastically and provide adequate skidding resistance. The lower unbound layers and subgrades should support the upper layers without much deformation to avoid premature failures (Dawson, 2008).

2.1.2 Railway tracks

Currently, the railway structure is mainly designed in two ways, i.e. slab track and conventional ballasted track. Slab tracks are more suitable for high velocity and high-volume traffic conditions where traffic interruption must be avoided and where traffic is intolerant to track irregularities. However, due to some disadvantages of slab tracks (e.g. sophisticated design and higher initial construction and material costs), conventionally ballasted tracks are still very widely employed (Indraratna et al., 2006; Fatahi & Khabbaz, 2011; Fatahi et al., 2011). The main components of ballasted railway track structures are generally divided into two groups, including superstructure (i.e. the rails, the fastening system and the sleepers/ties) and substructure (i.e. the ballast, the sub-ballast and the subgrade) (Selig & Waters, 1994), as presented in Figure 2.2.

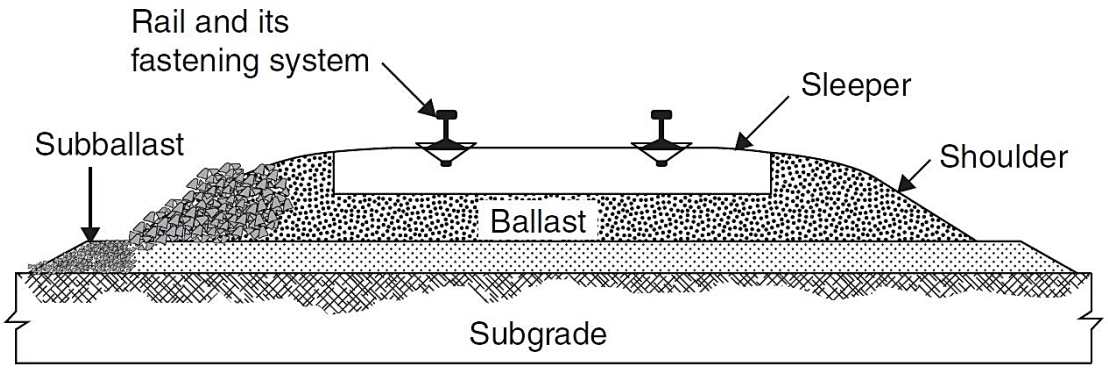

Figure 2.2 Typical railway track structures, from Indraratna (2011)

The rail with adequate strength and stiffness can support the trains and transfer the wheel loading to the underlying sleepers. The fastening system holds the rail in position on the track and is subjected to vertical, lateral and longitudinal forces. Sleepers transmit the loads from the rails to the substructure and maintain the rail gauge without generating excess deflection. As Rushton & Ghataora (2009) noted, the ballast plays a significant role in retaining sleepers and transferring the train load to the substructure. The ballast can permit the rapid drainage of water from the superstructure, while ballast fouling would reduce its permeability. Regarding sub-ballast, it can alleviate the stress on the subgrade, inhibit the migration of fine particles and contribute to draining water laterally. The permeability of the sub-ballast should range from the values for the ballast to that of the subgrade. As an important foundation for the superstructure, stabilized subgrade can contribute significantly to supporting the ballast and sub-ballast and maintaining track performance under repeated wheel loading. However, there are problems with cracking and erosion.

2.2 Water-induced structural distresses

It is well known that the attenuation of structural performance and the loss of service capability are closely related to subsurface water in the pavement/track foundation (Selig & Waters, 1994; Dawson, 2008). Water generally exists in pavement structures in several types, e.g. free water, capillary water, bound moisture, or water vapour. As the only form of water which can be drained with gravity, the free water can impair the strength and stiffness of the foundations, and thus it raises the most concern due to its detrimental effects (Ridgeway, 1982). It will also contribute to the frost-heave action in the subsurface structure of pavements and tracks. Some bound and capillary water can be beneficial to pavement/track material response. However, free water (especially at elevated pressure heads) will always be damaging as it reduces the

effective stress and, consequently, the mechanical performance that relies on inter-particle friction.

Vehicle loading is widely regarded as static, whereas in operation, pavement structures will be almost always subjected to dynamic wheel loading (Yoo & Al-Qadi, 2007). The dynamic component of wheel loads may cause four times as much damage (fatigue distress) in the wheel track as a static load would; the wheel track showing such damage is only about 5% of the road surfaces and excessive permanent deformation by at least 40% (Cebon, 1986). Thus, dynamic loading may induce severe pavement distress compared with that caused by static loading in the presence of water. With respect to track structures, it is also inadequate to adopt static loading alone. The dynamic loading will also cause high-frequency and low-frequency vibrations. The dynamic interaction between the rail and track may exacerbate the degradation of the track structures and differential track settlement will be generated under repeated loading.

Damages may originate from excess water due to (e.g.) impeded subgrade drainage, inadequate compaction, moisture-sensitive materials and lengthy drainage pathways, i.e. the strength, modulus and related mechanical properties of the foundation will decrease due to the existence of excess water. Even worse, under repeated traffic loading, pavement or track distresses will more rapidly develop progressively, owing to the excess subsurface water. The accumulation of large plastic strains may also be encouraged by water infiltration into the foundations of road and railway tracks. The contribution of the subgrade to the total permanent deformation occurring at the pavement surface could be estimated with some theoretical models, e.g. by using a plastic strain formulation (Puppala et al., 1999). Accordingly, it is indispensable to provide drainage in pavement and track structures so as to maintain good overall performance.

2.2.1 Road pavement distress

Regarding road pavements, various distresses have been investigated, e.g. cracking (fatigue, block, edge, reflection, longitudinal and transverse), patching and potholes (patch deterioration and potholes), surface deformation (rutting and shoving), surface defects (bleeding, polished aggregate and ravelling) and miscellaneous distresses (lane-to-shoulder drop-off and water bleeding and pumping) (Miller & Bellinger, 2014). In particular, two major distresses, i.e. fatigue cracking and critical rutting, may develop

due to the settlement and the accumulation of permanent deformation of subgrade soils in the foundation (Brown, 1997) that increases with increased moisture content and pore water pressure.

Excessive moisture content in the pavement structures (i.e. base, subbase and subgrade soils) can generate premature distresses and result in a structural or functional failure of pavement in the absence of counter-measures (Rokade et al., 2012). One or more combined impacts may originate due to water-induced defects, including reduction of subgrade and base/subbase strength, differential expansion (swelling) in expansive subgrade soils, stripping of asphalt in flexible pavements, frost heave and reduction of strength in freeze-thaw areas, migration of fine particles into the base or subbase course impairing the hydraulic conductivity remarkably and durability cracking (D-cracking) (Diefenderfer et al., 2005; Ji & Nantung, 2015). As Miller & Bellinger (2014) noted, the detrimental impacts of free water in pavements generally include several types, e.g. cracking, patching and potholes, surface deformation, surface defects, joint deficiencies and miscellaneous distresses. Consequently, they will contribute to the impairment of pavement serviceability. Build-up of high pore water pressures in a saturated base can be generated under cyclic traffic loading, and can, therefore, cause a significant reduction of shear strength and stiffness in the pavement base and foundation (Tao & Abu-Farsakh, 2008). Based on a field survey, Ji & Nantung (2015) demonstrated the corollary: that the distress in a drained pavement exhibited lower severity and fewer symptoms compared with that of the undrained pavement, i.e. significantly lower rates of slab cracking, no faulting or pumping, and significantly decreased frost penetration.

The two principal non-jointed pavement types (i.e. those surfaced with asphalt concrete and those formed of continuously reinforced concrete) are presented with their distresses, as shown in Table 2.1 and Table 2.2 (Miller & Bellinger, 2014).

Table 2.1 Asphalt concrete pavement distress types, from Miller & Bellinger (2014)

Category	Type
Cracking	Fatigue cracking
	Block cracking
	Edge cracking
	Longitudinal cracking: a. Wheel path longitudinal cracking b. Non-wheel path longitudinal cracking
	Reflection cracking at joints
	Transverse cracking
Patching and Potholes	Patch/patch deterioration
	Potholes
Surface Deformation	Rutting
	Shoving
Surface Defects	Bleeding
	Polished aggregate
	Ravelling
Miscellaneous Distresses	Lane-to-shoulder drop-off
	Water bleeding and pumping

Table 2.2 Reinforced concrete pavement distress types, from (Miller & Bellinger, 2014)

Category	Type
Cracking	Corner breaks
	Durability cracking (D-cracking)
	Longitudinal cracking
	Transverse cracking
Surface Defects	Map cracking and scaling: Polished aggregate
	Pop-outs
Miscellaneous Distresses	Blow-ups
	Transverse construction joint
	Faulting of transverse
	Lane-to-shoulder drop-off
	Lane-to-shoulder separation
	Punchouts
	Spalling of longitudinal joints
	Longitudinal joint seal damage
	Water bleeding and pumping

2.2.2 Railway track distress

Subgrade plays a significant role in maintaining the overall performance of railway tracks under repeated traffic loading. In the past, the role of subgrade as part of the track foundation was not identified comprehensively. Consequently, the subgrade defects

were simply treated by repeatedly adding more ballast under ties or frequent track maintenance (Li & Selig, 1994). Progressive shear failure, excessive plastic deformation, and subgrade attrition with mud pumping are considered as the major concerns for most subgrades of railway tracks under repeated traffic loading. Also, fouling of ballast may happen during tamping and trafficking. Consequently, the effectiveness of drainage will be impaired, inducing further deterioration of the ballast and the hazard of subgrade failure (Rushton & Ghataora, 2009).

Generally, soil attrition derives from the combined effects of several factors, i.e. repeated dynamic loading, free water and fine soil particles existing at the subgrade surface. The soil attrition distress tends to happen if the ballast is placed directly on fine-grained soils or soft rocks. High stress generated at the ballast-subgrade interface may strip the soil or rock at the subgrade surface. Under repeated traffic loading, overstressing can also be created on the subgrade surface and further causes the plastic flow of soil, i.e. the gradual migration of soil particles along the soil path with low resistance. Thus, progressive shear failure derives from the plastic flow. In particular, softening arises in soils with a high clay content as their moisture content grows. The strength reduction is also induced by soil remoulding and the build-up of excess pore water pressure under repeated loading. Regarding excessive vertical plastic deformation, it contains two components, i.e. the vertical component of progressive shear deformation and the vertical deformation attributed to progressive compaction and consolidation of subgrade soils below the rail under repeated traffic loads (Li & Selig, 1994; Miller et al., 2000). Under repeated loading, plastic deformation produced by a single axle load accumulates progressively in the subgrade. As the plastic deformation in the subgrade may develop to a considerable degree under repeated loading, it will influence the track's operation significantly. Besides, the accumulation of plastic deformation is usually non-uniform at various positions, e.g. along and across the track. Consequently, excessive plastic deformation may induce unacceptable variations of track geometry. For the subgrade newly constructed or with cohesive soils that water can infiltrate, excessive plastic deformation can accumulate more rapidly.

In the ballasted railway track, as the track operates over a long term, fresh and clean ballast without adequate maintenance will be fouled by finer materials from surroundings, particle crushing or fine contents of sublayers. With respect to ballast under repeated train loading, breakage and fouling of ballast will induce progressive

variation in the ballast properties. Due to ballast fouling, the ballast's shear strength and drainage capability will decrease (Janardhanam & Desai, 1983). During saturation, the ballast will experience severe particle breakage (Fatahi & Khabbaz, 2011). Due to the breakage, the material will transform into fine particles to migrate into the overlying structure. With the presence of water, mud is developed by mixing fine materials with water. Under cyclic traffic loading, the mud is forced upward into the voids of fresh ballast, i.e. mud pumping. Thus, the clay pumping and ballast breakage will exacerbate the fouling. Furthermore, the fouling may reduce the drainage capacity of the structure and undermine the structural bearing capacity. After the addition of ballast materials to compensate the reduction of track elevation caused by excessive plastic deformation, ballast pockets may arise when there is severe accumulative plastic deformation in the subgrade, as illustrated in Figure 2.3; it also causes soil attrition of the subgrade and the soil particles may migrate into the ballast through mud pumping. The induced ballast pocket will also impede the draining of water out of the ballast; furthermore, the shear resistance and stiffness of the ballast layer will be undermined. Consequently, permanent deformation and mud pumping will be accelerated (Li & Selig, 1994).

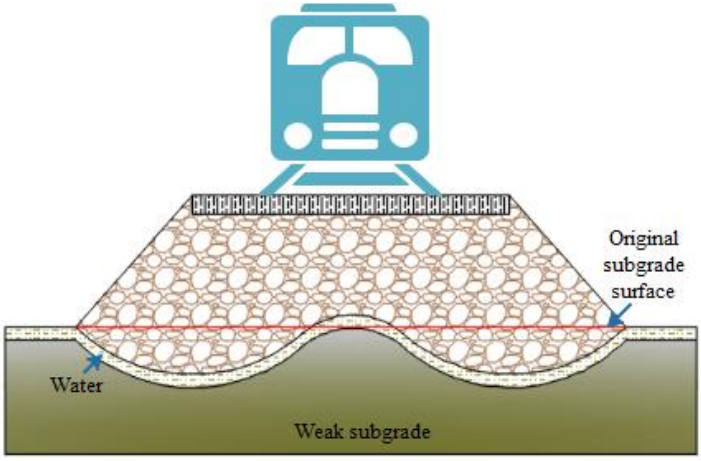

Figure 2.3 Excessive plastic deformation (ballast pocket) in track subgrade

Based on the major causes, subgrade distresses can be classified into three groups, as shown in Table 2.3. The first four types are mainly induced by repeated traffic loading, the two second types by the weight of the train, railway track and subgrade and the last four types by environmental factors (e.g. freezing soil temperature and changing soil moisture content) (Li & Selig, 1994). Generally, the traffic loading-induced problems exist at shallower depths in the subgrade; the weight-induced problems are accompanied by massive migration of the subgrade soils and are relatively deep; the

environmental problems arise at shallower depths or happen at the subgrade surfaces (Li & Selig, 1994).

Table 2.3 Major subgrade problems and their features, from Li & Selig (1994)

Type	Causes	Features	Note
Progressive shear failure	repeated over-stressing	squeezing near subgrade surface	shallower depths in the subgrade
	fine-grained soils	heaves in crib and/or shoulder	
	high moisture content	depression under ties	
Excessive plastic deformation (ballast pocket)	repeated loading soft or loose soils	differential subgrade settlement ballast pockets	shallower depths in the subgrade
Subgrade attrition with mud pumping	repeated loading of subgrade by ballast	muddy ballast	shallower depths in the subgrade
	contact between ballast and subgrade	inadequate sub-ballast	
	clay-rich rocks or soils	-	
	water presence	-	
Liquefaction	repeated loading	large displacement more severe with vibration	shallower depths in the subgrade
	saturated silt and fine sand	can happen in sub-ballast	
Massive shear failure (slope stability)	weight of train, track, and subgrade	high embankment and cut slope	relatively deep depths in the subgrade
	inadequate soil strength	often triggered by the increase in moisture content	
Consolidation settlement	embankment weight	increased static soil stress from a newly constructed embankment	relatively deep depths in the subgrade
	saturated fine-grained soils		
Frost action (heave and softening)	periodic freezing temperature occur in winter/spring period	occur in winter/spring period	shallower depths or at the subgrade surfaces
	free water	rough track surface	
	frost susceptible soils	-	
Swelling/Shrinkage	highly plastic soils	rough track surface	shallower depths or at the subgrade surfaces
	changing moisture content	-	
Slope erosion	running surface and subsurface water	soil washed or blown away	shallower depths or at the subgrade surfaces
	wind	-	
Soil collapse	water inundation of loose soil deposits	ground settlement	shallower depths or at the subgrade surfaces

2.3 Mechanical properties of foundations

The performance of roads and railways depends directly on the mechanical properties of their foundations which should provide reliable bearing capacity for the upper structures and maintain serviceability. As this study aims to investigate and predict the water effects on the subgrade behaviour of pavement/track, the mechanical properties of foundations are introduced. Mechanical properties can be characterised by various parameters, e.g. stiffness, elastic modulus, stiffness modulus, resilient modulus, shear modulus, bulk modulus and Poisson's ratio (Thom, 2008). In the cyclic triaxial test, the resilient modulus M_r is mathematically defined as the ratio of repeated deviator stress q to axial recoverable (i.e. resilient) strain ε_r (Li & Selig, 1994), as follows:

$$M_r = \frac{\Delta\sigma_1{}^2 + \Delta\sigma_1\Delta\sigma_3 - 2\Delta\sigma_3{}^2}{\Delta\sigma_1\varepsilon_1 + \Delta\sigma_3(\varepsilon_1 - 2\varepsilon_3)} \tag{2.1}$$

where σ_1 and σ_3 are the major and minor principal stresses, respectively; ε_1 and ε_3 are the major and minor principal strains, respectively; Δ indicates the change in the value of the stress or strain; for $\Delta\sigma_3 = 0$, $M_r = \frac{\Delta\sigma_1}{\varepsilon_1}$.

To represent the stress-strain behaviour of subgrade soil under normal cyclic traffic loading, M_r of subgrade soil was introduced by AASHTO (1986) as a more rational soil property than the soil support value or modulus of subgrade reaction (Yang et al., 2005) and therefore is widely employed to estimate transient soil deformation under repeated traffic loads.

Failures induced in subgrade soils mainly include two groups, i.e. shear failures where there is distortional movement between particles and settlement failures, where an underlying layer of soil suffers differential compressive deformation and decreases in thickness due to loading (Atkins, 2002), i.e. compaction of unsaturated soil or consolidation of saturated soil. The shear strength of subgrade soil plays a significant role in the design of foundations in practical engineering (e.g. pavement and railway track) (Fredlund & Vanapalli, 2002). It demonstrates the ability of soil to resist shearing under repeated traffic loading. Inadequate shear strength may result in shear deformation.

In the saturated state, the soil has one stress-state variable, i.e. effective normal stress, σ', which can be expressed according to the principle of effective stress (Powrie, 2013) as

$$\sigma' = \sigma - u_w \quad (2.2)$$

where σ is total normal stress and u_w is the pore water pressure, which is generally positive or zero for saturated soil. It allows recognition of the stress components carried by the soil and pore water.

In the partially saturated state, the subgrade soils withstand negative pore water pressure. There exists a difference between the pore water pressure and pore air pressure, i.e. matric suction ($u_a - u_w$). The mechanical response of unsaturated soil now relies on two independent stress-state variables, i.e. net normal stress ($\sigma - u_a$) and matric suction ($u_a - u_w$) (Fredlund & Rahardjo, 1993). Compared with saturated soils, unsaturated soil exhibits matric suction that will affect the mechanical response of the foundations. Matric suction has been considered as an important stress variable in investigating the effects of moisture content on the mechanical behaviour of unsaturated soil in pavement structures. It is widely recognised that matric suction mainly includes two components, i.e. matric and osmotic suction (Krahn & Fredlund, 1972; Edil & Motan, 1984; Fredlund et al., 2012). The relationship can be expressed as

$$\psi = (u_a - u_w) + \pi \quad (2.3)$$

where ψ is the total suction, $(u_a - u_w)$ is matric suction, π is osmotic suction, u_a is pore-air pressure and u_w is pore-water pressure. The total suction indicates the free energy of the soil water, while matric and osmotic suctions are the components of the free energy.

Based on the effective stress concept, the effective stress of unsaturated soil proposed by Bishop (1959) was expressed as

$$\sigma' = \sigma - u_a + \chi(u_a - u_w) \quad (2.4)$$

where χ = parameter thought to be a function of the degree of saturation (χ =0 for dry soils, χ =1 for saturated soils). χ is also found to depend on material state and stress path. However, no unique relationship is found between χ and the degree of saturation (Khalili & Khabbaz, 1998), and, instead, χ is strongly related to the soil structure (Coleman, 1962). As a material parameter, χ is not suitable for the description of stress since the variables used should be independent of material properties (Fredlund & Morgenstern, 1977). Bishop's effective stress exhibited several limitations, e.g. failure to explain the collapse behaviour during wetting of unsaturated soils (Jennings & Burland, 1962) and the dependence of the represented stress space on the material states.

A zero suction state is commonly regarded and accepted as equivalent to a saturated

state despite the shortcomings of this equivalence, i.e. the hysteretic suction levels that correspond to full saturation during drying and wetting are ignored. A continuous relationship as soil moves from positive to negative pore water pressure is not provided. Treating atmospheric air pressure and the suction as zero but allowing a positive or negative pore water pressure for all saturated and unsaturated states is a better alternative as it provides a continuous transition between the saturated and unsaturated states (Sheng et al., 2008).

Considering all the limitations of the effective stress principle, Fredlund & Morgenstern (1977) defined the stress state by two independent non-additive stresses, one described at the macroscopic scale ($\sigma_{ij} - u_a\delta_{ij}$) and the other at the pore scale ($u_a - u_w$). It is fundamentally inadequate to describe the critical state of unsaturated soils only based on the continuum stress state (shear stress, net normal stress and matric suction) and the soil volume (Li, 2003), even though providing an accurate description may be impracticable.

The shear strength of the soil, τ_f, is expressed as a function of the applied σ' rather than σ. Generally, the relationship between the two parameters can be demonstrated by the Mohr-Coulomb failure criterion as follows (Helwany, 2007):

$$\tau_f = c' + \sigma' \tan\phi' \tag{2.5}$$

where c' represents the cohesion intercept derived from linear approximation and ϕ' denotes the angle of internal friction of soil particles. As matric suction develops in the pores with a negative value of u_w, σ' will also increase. Consequently, the soil will present an improved mechanical response. Furthermore, the water pressure and suction in the subgrade soil in the pavement/track structure are affected by the amount of water, e.g. the undrained shear strength relies on the amount of inter-grain water in the soil (Trauner et al., 2005) and it will vary if pore water pressure is dissipated. Instead of using a single term (i.e. σ') as the Bishop model, it is more common to describe the effective stress by considering $(\sigma - u_a)$ and $(u_a - u_w)$ separately as uncombined parameters (Fredlund et al., 1978).

Pavement deformation can generally be grouped into two categories: resilient (recoverable) deformation and plastic (irrecoverable or permanent) deformation. Fatigue cracking of bound layers may derive from resilient deformation, whereas excessive rutting may be attributed to plastic deformations incrementally accumulated over many cycles. The permanent deformation of the soft subsoil in pavement/track is

one of the crucial factors that dominate the design life (Chai & Miura, 2002). Excessive vertical permanent deformations in subgrade soil will undermine the serviceability of the infrastructure. Therefore, it is significant to investigate the permanent response of the underlying foundation to increase the resistance to permanent deformation. Since noticeable rutting still arises under traffic loading in some specific soils (e.g. sands, silty clays and sandy clays) even though they exhibit favourable resilient properties, it is not accurate, nor reliable, to employ resilient modulus to deduce a soil's permanent deformation characteristics (Puppala et al., 1996).

As a penetration test, the California Bearing Ratio (CBR) test is often utilized to assess the load-bearing capacity of the subgrade soil. CBR values are defined as the ratio of the load for measured soil at a given penetration to that for a standard material (i.e. crushed California limestone) required to achieve the same penetration. Typical CBR values vary with the soil grain: fine-grained soils (1.0~5.0), coarse-grained soils (5.0~80.0) and high-quality rock (over 80) (McHenry & Rose, 2012). Since CBR is empirically applicable to a certain set of materials and loading conditions, it may not be suitable to be utilized under various conditions in design (Saad et al., 2005).

The factors influencing the resilient modulus, shear strength and permanent deformation will be discussed and analysed in Section 2.4.

2.3.1 Critical state

During the conventional drained and undrained triaxial compression tests on normally compressed and lightly (or heavily over-consolidated) samples (Wood, 1990), or shear box tests on dense and loose sand samples (Powrie, 2013), the soil samples were observed to develop towards a critical void ratio or specific volume state, at which the soil continues to shear progressively without variations in volume or effective stresses. The development of shear stress (τ), volumetric strain (ε_{vol}) and specific volume (v) with γ during the shear box tests are presented in Figure 2.4 to illustrate the ultimate conditions. With respect to the ultimate state, known as a critical state (CS) during the triaxial test, it can be expressed as

$$\frac{\partial p'}{\partial \varepsilon_q} = \frac{\partial q}{\partial \varepsilon_q} = \frac{\partial v}{\partial \varepsilon_q} = 0 \tag{2.6}$$

where ε_q =triaxial shear strain (γ).

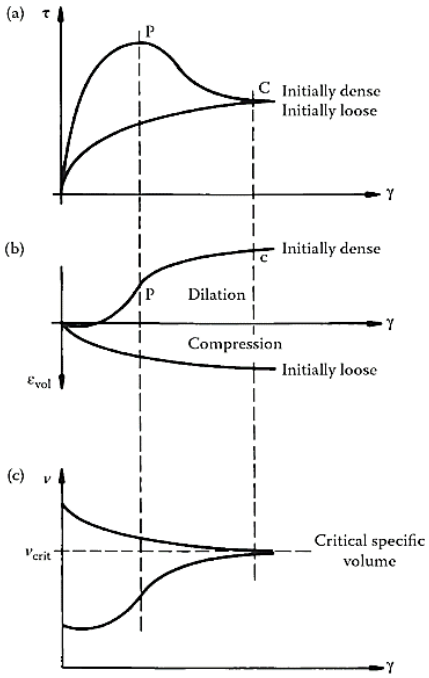

Figure 2.4 Variations of τ, ε_{vol} and ν with γ during idealised shearbox tests, from Powrie (2013)

A three-dimensional plot in the (p', q, ν) space, i.e. CSL, was achieved, as shown in Figure 2.5.

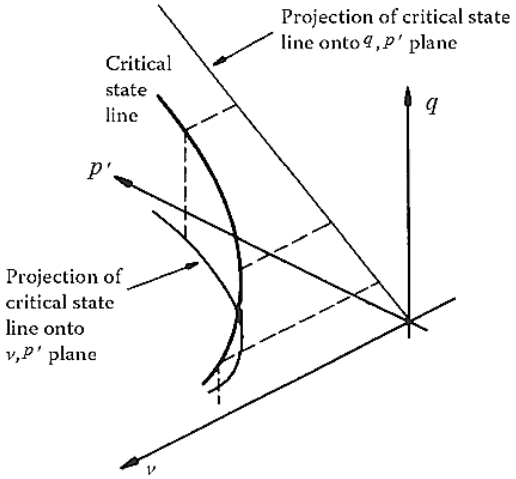

Figure 2.5 CSL in (p', q, υ) space with projections onto (q, p') and (υ, p') planes, from Powrie (2013)

Besides, p', q and ν could be calculated through

$$p' = \frac{1}{3}(\sigma_1' + \sigma_2' + \sigma_3') \tag{2.7}$$

$$q = \frac{1}{\sqrt{2}}\sqrt{(\sigma_1' - \sigma_2')^2 + (\sigma_2' - \sigma_3')^2 + (\sigma_1' - \sigma_3')^2} \tag{2.8}$$

$$\nu = 1 + e \text{ which for saturated soils, } \nu = 1 + wG_s \tag{2.9}$$

where σ_1', σ_2' and σ_3' are major, intermediate and minor principal effective stresses, respectively, e is the void ratio, and G_s is the specific gravity of soil grains. Particularly, in the axial symmetric cases where $\sigma_2' = \sigma_3'$, e.g. oedometer and triaxial tests, the above equations can be rewritten as

$$p' = \frac{1}{3}(\sigma_1' + 2\sigma_3') \tag{2.10}$$

$$q = \sigma_1' - \sigma_3' \tag{2.11}$$

When CS is reached, on the $q - p'$ line, the stress ratio can be expressed as

$$\frac{q_{cs}}{p_{cs}'} = M \tag{2.12}$$

where q_{cs} is the deviator stress at CS, p_{cs}' is the mean effective stress at the CS and M is the constant stress ratio at CS, assuming the soil is frictional only.

2.3.2 Resilient modulus

In view of the substantial contribution of subgrade modulus to the overall performance of roads or railways, it is vital to provide the best prediction of resilient modulus for the roads and railway foundations. Resilient modulus is commonly obtained through repeated load triaxial tests based on AASHTO T307-99 (2012) "Standard Method of Test for Determining the Resilient Modulus of Soils and Aggregate Materials". Various models for resilient modulus have been developed to demonstrate the non-linear stress-strain behaviour of the subgrade soils by incorporating soil physical properties (e.g. moisture content and dry density) (Li & Selig, 1994; ARA, 2004; Liang et al., 2008; Cary & Zapata, 2011) and stress state variables (e.g. deviator stress, confining stress, bulk stress and shear stress) (Monismith et al., 1967; Moossazadeh & Witczak, 1981; Witczak & Uzan, 1988; Garg & Thompson, 1997). Selected models are presented to show the correlation of resilient modulus with stress states and soil properties. The first four equations (Eq. (2.13) ~ (2.16)) are included as a theoretical basis for the model development, and the rest are focused on moisture effects on resilient modulus. This section provides a basis for the consistency index model development in Chapter 3.

a. The $k - \theta$ model associating resilient modulus with bulk stress was presented by Monismith et al. (1967) generally for granular soils as

$$M_r = k_1\left(\theta/p_a\right)^{k_2} \tag{2.13}$$

where k_1 and k_2 are regression parameters dependent on material type and physical soil properties; $\theta = \sigma_1 + \sigma_2 + \sigma_3$, i.e. bulk stress; p_a is the atmospheric pressure.

It is widely used to analyze the stress dependence on material stress, whilst the $k-\theta$ is not specifically accurate to describe the soil behaviour at various locations except for those right below an applied load. When considering the use of the finite element method or the assumption of simplified pavement structure, this model will induce more complications in pavement analysis (Thom, 2008). Constant Poisson's ratio was assumed in this model, whilst Poisson's ratio is not constant and varies with applied stresses (Kolisoja, 1997). It is still insufficient to consider the effects of stresses only by the sum of principal stresses since the same value of θ may represent different stress states. This model did not summarize measured data well when shear stress was significant (Uzan, 1985).

b. The model proposed by Moossazadeh & Witczak (1981), also known as the deviator stress model widely used to represent the resilient modulus of fine-grained subgrade soil, was presented as

$$M_r = k_1 \left(\frac{\sigma_d}{p_a}\right)^{k_2} \tag{2.14}$$

where σ_d is the deviator stress, i.e. $\sigma_1 - \sigma_3$.

Based on the deviator stress, M_r could be easily estimated. A limitation of this model is that moisture conditions were not explicitly incorporated.

c. The Universal model (Witczak & Uzan, 1988) incorporated the effect of both shear stress and bulk stress on M_r as follows

$$M_r = k_1 * p_a\left(\theta/p_a\right)^{k_2}\left(\tau_{oct}/p_a\right)^{k_3} \tag{2.15}$$

where τ_{oct} is the octahedral shear stress, i.e. $\frac{1}{3}\sqrt{(\sigma_1-\sigma_2)^2+(\sigma_2-\sigma_3)^2+(\sigma_1-\sigma_3)^2}$.

Based on the studies, the Universal model outperformed the $k-\theta$ model. The Universal model is recommended for use with cohesive soils if the model development data have various confining stress levels (Santha, 1994).

d. Developed by Fredlund & Rahardjo (1987), M_r of unsaturated soils can be expressed as a function of three stress variables, i.e.

$$M_r = f[(\sigma_3 - u_a), (u_a - u_w), (\sigma_1 - \sigma_3)] \tag{2.16}$$

where u_a is the pore air pressure and $(\sigma_3 - u_a)$ is the net confining pressure.

The model provides a general idea of the relationship between resilient modulus and stress variables (i.e. deviator stress, net confining stress and matric suction). The effects of matric suction were gradually paid more attention to in predicting the resilient modulus.

e. A model was recommended in MEPDG (ARA, 2004) by AASHTO to demonstrate the effect of the degree of saturation on M_r.

$$\log\frac{M_r}{M_{r,opt}} = a + \frac{b-a}{1+e^{\ln(-b/a)+k_4(S-S_{opt})}} \tag{2.17}$$

where $M_{r,opt}$ is the resilient modulus at the optimum moisture content (w_{opt}), a is the minimum of $\log\frac{M_r}{M_{r,opt}}$, b is the maximum of $\log\frac{M_r}{M_{r,opt}}$, k_4 is the regression parameter associated with material properties, S is the degree of saturation expressed as a decimal and S_{opt} is the degree of saturation at w_{opt} expressed as a decimal.

This model considers a degree of saturation so that the water state will be involved. However, matric suction as the direct factor is not considered, and the hysteretic behaviour of M_r with moisture content is not demonstrated (Khoury et al., 2012). The M_r-moisture relationships vary with soil types, particularly with plasticity index (PI), e.g. low PI soils are less susceptible to moisture changes than soils with high PI (Khoury & Zaman, 2004) and the model may be exclusively applicable to some specific soil types.

f. By incorporating the effective stress of unsaturated soils presented by Bishop (1959), the model by AASHTO (1986) is rewritten by Yang et al. (2005) as follows:

$$M_r = k_1(\sigma_d - u_a + \chi\psi_m)^{k_2} \tag{2.18}$$

where σ_d is deviator stress and ψ_m is the matric suction. This model cannot address the effects of drying or a combination of drying and wetting on M_r values of subgrade soils (Khoury et al., 2012).

g. Based on the effective stress, the proposed model by Liang et al. (2008) for partially saturated cohesive soils can be expressed as

$$M_r = k_1 p_a \left(\frac{\theta + \chi\psi_m}{p_a}\right)^{k_2} \left(\frac{\tau_{oct}}{p_a} + 1\right)^{k_3} \tag{2.19}$$

In this model, the matric suction is included, and the suction parameter χ is introduced. It also considers the effects of shear strain. However, the measurement of soil suction may induce complications in the model.

h. As a variation of the Universal Model, a refined model was proposed by Cary & Zapata (2011) as follows:

$$M_r = k_1 p_a \left(\frac{\theta_{net} - 3\Delta u_{w-sat}}{p_a}\right)^{k_2} \left(\frac{\tau_{oct}}{p_a} + 1\right)^{k_3} \left(\frac{\psi_{m_0} - \Delta\psi_m}{p_a} + 1\right)^{k_5} \tag{2.20}$$

where θ_{net} represents net bulk stress, i.e. $\theta - 3u_a$, Δu_{w-sat} is the build-up of pore-water pressure under partially saturated conditions; ψ_{m_0} is the initial soil matric suction

and $\Delta\psi_m$ is the relative change in soil matric suction with respect to ψ_{m_0}; k_5 is a regression constant.

To obtain net bulk stress, pore air pressure needs to be determined. The variation of matric suction included in the model is beneficial, whilst the measurement of matric suction will induce more complexity to the prediction of M_r. During repeated loading, the build-up of pore water pressure could cause changes to the matric suction, which could also impair its accuracy.

i. Based on the MEPDG (ARA, 2004) model, Khoury et al. (2012) proposed two models to assess the M_r-moisture hysteretic behaviour of a subgrade soil along two different environmental paths. A revised model to predict M_r incorporating the effects of moisture content along initial drying curve (IDC) and initial wetting curve (IWC), i.e.

$$\log(\frac{M_r}{M_{r,opt}}) = a_1 + \frac{b_1 - a_1}{1 + e^{\ln\left(\frac{-b_1}{a_1}\right) + k_6 \times (w - w_{opt})}} \tag{2.21a}$$

Through the statistical analysis, model parameters proved to be: a_1 =-0.162, b_1=0.435, and k_6 =0.803, with a coefficient of determination r^2=0.95. The inner M_r-moisture curve (IMMC) was introduced to present the IDC and IWC as a whole, as shown in Figure 2.6.

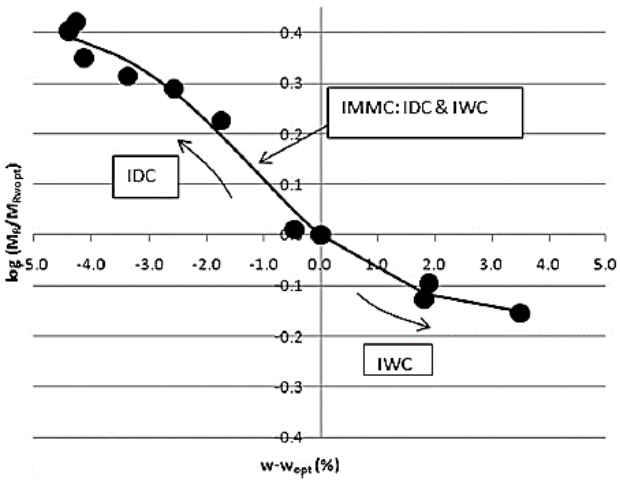

Figure 2.6 M_r-water relationship along the IDC and the IWC (i.e. IMMC) from Khoury et al. (2012)

The following equation was selected to analytically predict the M_r-moisture variation along the main drying curve-wetting drying path (MDC-WDP)

$$\log(\frac{M_r}{M_{r,opt}})_{\text{MDC–WDP}} = a + \frac{b - a}{1 + e^{k_6 \times (w - w_{opt})}} \tag{2.21b}$$

where $\frac{M_r}{M_{r,opt}}$ is resilient modulus ratio, k_6 is a regression parameter and $(w - w_{opt})$ is moisture content variation (%). With the slope of IMMC and the resilient modulus along the IMMC at a specific moisture content $(w - w_{opt})$, the MDC-WDP can be measured, as shown in Figure 2.7.

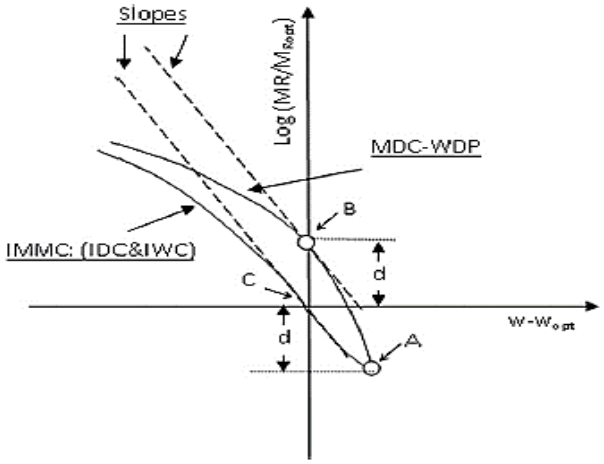

Figure 2.7 Illustration for predicting MWC-WDP, from Khoury et al. (2012)

This model presents the direct effects of moisture content on the M_r. It will be convenient to estimate M_r without requiring more model parameters if the moisture condition is available. However, the matric suction, in its water-related stress state, is not considered. According to the soil water characteristic curve (SWCC), the hysteresis behaviour between matric suction and water content should be incorporated. This may impair the accuracy of the prediction. The model parameters from the regression are based on soil type, so that they may differ from other soil types. Additionally, as mentioned by the authors, the study was limited to predicting the effect of postcompaction moisture content on M_r of one type of soil (i.e. Renfrow). Thus, more studies are needed to extend the scope of application and verify its applicability to other types of soils.

j. To comprehensively predict the resilient modulus, a new equation was proposed incorporating the effect of net stress and matric suction (Ng et al., 2013).

$$M_r = M_0(\frac{p_{net}}{p_a})^{k_1}(1 + \frac{q_{cyc}}{p_a})^{k_2}(1 + \frac{\psi_m}{p})^{k_3} \quad (2.22)$$

where M_0 denotes the resilient modulus at the reference stress state (i.e. q_{cyc} = 0 and ψ_m = 0), p_{net} is the net mean normal stress (i.e. $\theta_{net}/3$) and q_{cyc} is the cyclic stress (i.e. the amplitude of variation in deviator stress during cyclic loading–unloading).

This model allows for a smooth transition between the unsaturated state and saturated state of soils. It is derived from the suction-controlled cyclic triaxial tests,

whilst the direct measurement of matric suction for further application will still be complex.

k. A model for recycled unbound materials was proposed by Azam et al. (2013). This suction-inclusive model incorporated the density ratio to represent the effect of soil density on the resilient modulus. The blend composition was found to significantly affect MDD and OMC of materials. Thus, a new term was added that considered dry density ratio moderated by the effect of RCM content.

$$M_r = k(\frac{\sigma_m}{p_a})^{k_1}\left(\frac{\tau_{oct}}{\tau_{ref}}\right)^{k_2}\left(\frac{\psi_m}{p_a}\right)^{k_3}\left[\frac{DDR\left(1-\frac{k_4 RCM}{100}\right)}{100}\right]^{k_3} \quad (2.23)$$

where σ_m is mean normal stress (i.e. $(\sigma_1+\sigma_2+\sigma_3)/3$), τ_{ref} is reference shear stress (i.e. $\sqrt{2/3}\,\tau_f$), DDR is dry density ratio (%), RCM is the percent of recycled clay masonry (%), and k_4 and k_5 are regression parameters (factors and exponents).

The previous models mainly focus on the behaviour of subgrade soils and/or virgin aggregates, except for recycled products. The proposed model included crushed masonry content, dry density, shear strength, initial matric suction and stress state. Air entry value will not be needed from SWCC to evaluate the effective stress parameter (Azam et al., 2015). The determination of matric suction could make it complex or undermine its accuracy. The applicability to different recycled aggregates and general subgrade soils still needs further studies.

l. Han & Vanapalli (2015) derived a model to predict the variation of the resilient modulus with respect to the soil suction for compacted fine-grained subgrade soils.

$$\frac{M_r - M_{r,sat}}{M_{r,opt} - M_{r,sat}} = \frac{\psi_m}{\psi_{m,opt}}\left\{\frac{\ln\left[2.718+\left(\frac{\psi_{m,opt}}{a}\right)^n\right]}{\ln\left[2.718+\left(\frac{\psi_m}{a}\right)^n\right]}\right\}^{m\xi} \quad (2.24)$$

where $M_{r,sat}$ is M_r of soil at saturation, ψ_{opt} is matric suction at OMC, *m*, *n* and ξ are model parameters, and ξ was found to be equal to 2.0.

It only requires conventional soil properties and alleviates the need for experimental determination of the $M_r - \psi$ relationships, while the stress conditions were not incorporated (Han & Vanapalli, 2015). Compared with models by regression analysis, it is convenient to predict the resilient modulus of subgrade only with soil properties. However, filter paper method measures matric suction based on the previous

calibration, and its accuracy is limited. The measurement of matric suction may limit the application of this model.

m. Considering matric suction, minimum bulk stress and octahedral shear stress, a new prediction model was proposed by Yao et al. (2018).

$$M_r = k_0 p_a (\frac{\psi_m}{p_a} + 1)^{k_1} (\frac{\theta_m}{p_a})^{k_2} (\frac{\tau_{oct}}{p_a} + 1)^{k_3} \quad (2.25)$$

where θ_m is the minimum bulk stress.

This model avoids the issue that the bulk stress exhibited equal values under different combinations of the deviator stress and confining pressure (Yao et al., 2018). The relationships between regression coefficients and physical parameters (plasticity index, liquid limit or plastic limit and percentage passing through the No. 200 (0.075 mm) sieve) were established based on completely weathered granite and then verified within A-4 and A-7 soils. Therefore, its applicability to other types of soil still needs further verification.

n. State and stress variables should be taken as model terms, and basic soil properties should be considered in model parameters. Therefore, matric suction and relative compaction should be incorporated into resilient modulus prediction models. A new model by Zhang et al. (2019) is expressed as

$$M_r = k_0 p_a RC^{k_1} (\frac{\psi_m}{p_a} + 1)^{k_2} (\frac{\theta_m}{p_a})^{k_3} (\frac{\tau_{oct}}{p_a} + 1)^{k_4} \quad (2.26)$$

where *RC* is the relative compaction, defined as the ratio of dry density to maximum dry density, and k_0 is directly proportional to M_r.

Compared with the model by Yao et al. (2018), the new model considered relative compaction of subgrade. However, it also added an extra parameter to the model. It may take more work to achieve these parameters.

2.3.3 Shear strength

Based on the Mohr-Coulomb failure envelope for saturated soils, the failure envelope for unsaturated soil was developed, as illustrated in Figure 2.8 (Fredlund et al., 2012). Mohr circles corresponding to failure conditions of unsaturated soil were plotted in a three-dimensional space, i.e. (τ, $\sigma - u_a$, $u_a - u_w$).

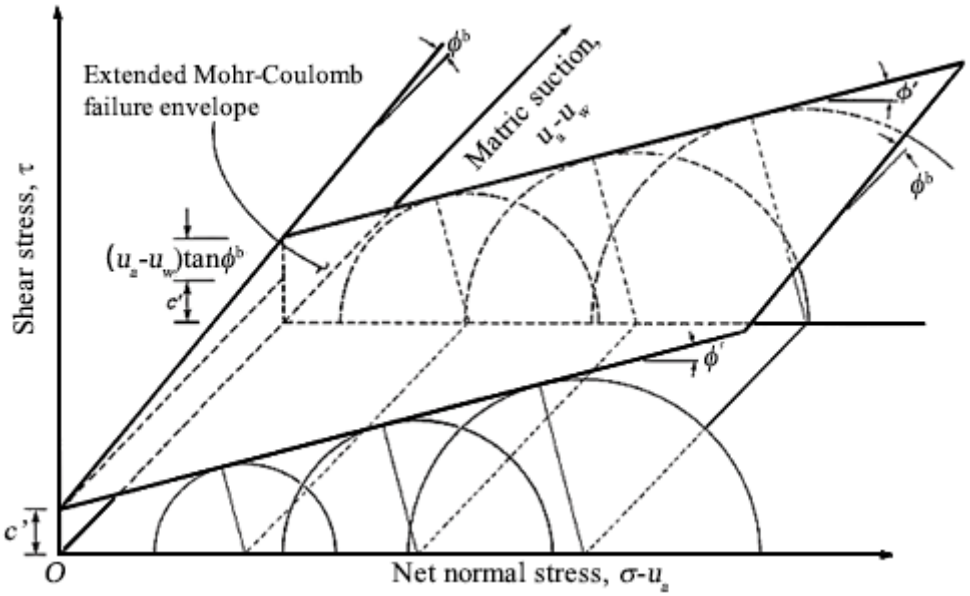

Figure 2.8 Extended Mohr-Coulomb failure envelope for unsaturated soil, from Fredlund et al. (2012)

a. As Helwany (2007) noted, the relationship between τ_f and σ' in the soil was expressed through the Mohr-Coulomb failure criterion as

$$\tau_f = c' + \sigma' \tan\phi' \tag{2.27}$$

This model represents the relationship between shear strength and the applied normal effective stress, and the cohesion and friction between the soil particles are considered. It has provided a strong basis for developing more comprehensive shearing theories.

b. A linear model proposed by Fredlund et al. (1978) for the shear strength of unsaturated soil was presented as

$$\tau_f = c' + (\sigma - u_a)\tan\phi' + (u_a - u_w)\tan\phi^b \tag{2.28}$$

where ϕ^b is the angle of shearing resistance associated with matric suction and $(\sigma - u_a)$ is the net normal stress on the failure plane. The matric suction is considered since it plays a crucial role in unsaturated soil. However, the matric suction will also vary with environmental factors, e.g. moisture content.

c. The model of shear strength for an unsaturated soil at any given value of suction was proposed (Vanapalli et al., 1996) as follows

$$\tau_f = c' + (\sigma - u_a)\tan\phi' + (u_a - u_w)[\Theta^\kappa \tan\phi'] \tag{2.29}$$

where Θ is the normalized volumetric moisture content and κ is a fitting parameter of the normalized area of water and normalized volumetric moisture content. $(u_a -$

$u_w)[\Theta^{\kappa}\tan\phi']$ represents the shear strength contribution of matric suction. Θ can be expressed as

$$\Theta = \frac{w_{vol} - w_{vol,r}}{w_{vol,s} - w_{vol,r}} = \frac{S - S_r}{1 - S_r} \tag{2.30}$$

An alternative approach was also introduced by extending the same philosophical concepts without adopting κ, expressed as

$$\tau_f = c' + (\sigma - u_a)\tan\phi' + (u_a - u_w)[\frac{w_{vol} - w_{vol,r}}{w_{vol,s} - w_{vol,r}}\tan\phi'] \tag{2.31}$$

where w_{vol} is volumetric moisture content, $w_{vol,r}$ is the residual volumetric moisture content and $w_{vol,s}$ is saturated volumetric moisture content. If the SWCC (see Section 2.5.2 for details) is available, the shear strength due to matric suction can be predicted with c' and ϕ' known. Since $w_{vol,r}$ depends on the SWCC, it may be critical to acquire a reliable SWCC to predict the shear strength.

2.3.4 Cumulative permanent deformation

Progressive accumulation of subgrade permanent deformation could cause a premature failure of the pavement due to excess rutting (Lekarp & Dawson, 1998) or reduce the smoothness of railway tracks. Various studies have been performed to predict the cumulative permanent deformation of the subgrade that occurs in a pavement structure or railway trackbed. These may provide a reference for the foundation design in order to prevent excessive settlement under repeated traffic loading. Therefore, two commonly used prediction methods (i.e. layer-wise summation and regression analysis methods) are presented below to lay a theoretical basis for cumulative permanent deformation prediction in this study.

(1) Layer-wise summation method

The procedure of this method includes dividing the subgrade into sublayers, calculating the permanent deformation of each layer, and then summing them up. In a multilayered structure system, the cumulative subgrade deformation can be determined by a summation of the sublayers and expressed as

$$\delta_s = \sum_{i=1}^{n} \varepsilon_{p,i} \times h_i \tag{2.32}$$

where δ_s is the cumulative permanent deformation, $\varepsilon_{p,i}$ is the plastic strain at the i^{th} layer and h_i is the thickness of the i^{th} layer.

In terms of $\varepsilon_{p,i}$, a wide range of prediction models have been proposed (Tseng & Lytton, 1989; Sweere, 1990; Wolff & Visser, 1994; Lekarp & Dawson, 1998; Puppala et al., 1999; El-Basyouny & Witczak, 2005; Korkiala-Tanttu, 2005; Gabr & Cameron, 2013; Azam et al., 2015; Gu et al., 2016; Zhang et al., 2020). In this study, the models incorporating moisture conditions will be presented and discussed in order to show the moisture effects on permanent deformation.

a. A relationship with a cubic polynomial form was proposed for permanent deformation prediction of subgrade soils (Allen & Deen, 1986), expressed as

$$\log \varepsilon_p = C_0 + C_1 \times \log N + C_2 \times (\log N)^2 + C_3 \times (\log N)^3 \quad (2.33)$$

where C_0, C_1, C_2 and C_3 are material constants. For subgrade, $C_0 = -6.5 + 0.38w - 1.1\log(\frac{\sigma_3}{6.89}) + 1.86\log(\frac{\sigma_d}{6.89})$, $C_1 = 10^{-1.1+0.1w}$, $C_2 = 1.8w$ and $C_3 = 0.007 + 0.1w$. w is the moisture content. The stress states and loading repetitions are considered. With the moisture content included in the model parameters, this model can reflect the effects of moisture on the plastic response of subgrade soils. However, due to the hysteretic phenomenon of moisture content, the wetting and drying effects may not be fully revealed. This model was developed based on one particular soil type (with a $\rho_{d,max}$ of 2.093 g/cm^3 at a w_{opt} of 9.7%), and thus it could be dependent on soil types. The data used for the model development was taken from average curves of tests, which would also introduce more errors.

b. Incorporating the material stress state and the number of repeated loading, the assumed explicit relationship between the permanent strain and the resilient strain (Tseng & Lytton, 1989) is expressed for a single-stage repeated load triaxial test (RLTT) as

$$\varepsilon_p(N) = \varepsilon_r \varepsilon_0 e^{-(\frac{\rho}{N})^\beta} \quad (2.34)$$

where ε_r is the resilient strain at N^{th} load cycle, ε_0, ρ and β are parameters dependent on material properties. This model associates the permanent deformation with the resilient strain of subgrade. It only directly considers the number of loading cycles (because other factors are implicitly included in the value of ε_r), which may give the model a simple form. However, the mechanical behaviour of the unbound granular material is highly stress-dependent, and the effects of stress states cannot be demonstrated. Thus, the application of this model will be limited in practice.

c. Based on the model by Tseng & Lytton (1989), El-Basyouny & Witczak (2005) proposed a modified model to increase the prediction accuracy of sublayers and to

facilitate its implementation into the Mechanistic-Empirical Pavement Design Guide (MEPDG). It is demonstrated as

$$\frac{\varepsilon_p(N)}{\varepsilon_r} = \begin{cases} a_1 M_r^{b_1}, & N = 1 \\ a_9 M_r^{b_9}, & N = 10^9 \\ \frac{\varepsilon_0}{\varepsilon_r} e^{-(\frac{\rho}{N})^\beta}, & N \neq 1 \; or \; 10^9 \end{cases} \tag{2.35}$$

where

$$\frac{\varepsilon_0}{\varepsilon_r} = \frac{e^{(\rho)^\beta} \times a_1 M_r^{b_1} + e^{(\frac{\rho}{10^9})^\beta} \times a_9 M_r^{b_9}}{2} \tag{2.36}$$

$$\log \beta = -0.61119 - 0.017368w \tag{2.37}$$

$$\varepsilon_0 = \ln \frac{a_1 M_r^{b_1}}{a_9 M_r^{b_9}} \tag{2.38}$$

a_1, a_9, b_1 and b_9 are material parameters, which can be determined by assuming for $\varepsilon_p = \varepsilon_r$. Compared with Tseng and Lytton's model (1989), the resilient modulus of sublayers is introduced as well as moisture content. The model parameters are also related to the material properties, which enables the model to be more applicable. However, the model parameters still require some repeated load triaxial tests, which will be more time-consuming.

d. Then, the model for predicting permanent deformation proposed in the MEPDG by the AASHTO (2008) is presented as

$$\frac{\varepsilon_p(N)}{\varepsilon_v} = \beta_{GB} \frac{\varepsilon_0}{\varepsilon_r} e^{-(\frac{\rho}{N})^\beta} \tag{2.39}$$

where β_{GB} is the test road correction factor, set as 1.35.

$$\frac{\varepsilon_0}{\varepsilon_r} = \frac{0.15 \times e^{(\rho)^\beta} + 20 \times e^{(\frac{\rho}{10^9})^\beta}}{2} \tag{2.40}$$

$$\rho = 10^9 \times \left[\frac{-4.89285}{1 - (10^9)^\beta}\right]^{\frac{1}{\beta}} \tag{2.41}$$

The MEPDG model introduced the effects of stress states on permanent deformation by relating the laboratory tests to field conditions through vertical strains (Gu et al., 2016). The model parameters are associated with material properties and can be determined by simple tests. It makes the model more efficient in estimating permanent deformation. However, the physical properties (e.g. gradation, angularity and shape) of the soils are not included, which also significantly influences the plastic response of the unbound granular layers (Lekarp et al., 2000a).

e. Through the multistage RLTT, Gabr & Cameron (2013) investigated the plastic behaviour of three types of materials. Based on the experimental results, a prediction model of permanent deformation was developed. It can be described as

$$\varepsilon_p = a\left(\frac{\sigma_m}{p_a}\right)^b \left(\frac{\tau}{\tau_f}\right)^c N^d e^{[(w_{opt}-w)\times(g\times wPI+h)+i\times(\rho_{opt}-\rho_0)]} \quad (2.42)$$

where ρ_{opt} is the maximum dry density at the optimum moisture content, ρ_0 is the initial dry density, wPI is the weighted plasticity index and a, b, c, d, g, h and i are regression coefficients. This model presents the effects of bulk stress, shear stress, loading cycles, moisture content, dry density and plasticity index. The regression coefficients need to be determined with more tests. Considering the wide range of PI values, the model may depend on soil types.

f. Through single-stress-state RLTT, the effects of moisture content and matric suction on the plastic strain of the recycled clay masonry-concrete aggregate mixture was estimated (Azam et al., 2015). A new model with a single set of constants was proposed for the blends, shown as follows

$$\varepsilon_p = aN^b \left(\frac{u_m + 1}{p_a}\right)^c \left(\frac{DDR}{1 + wPI + RCM}\right)^d \quad (2.43)$$

where u_m is the initial matric suction, a, b, c and d are regression coefficients. This model demonstrates the effects of matric suction while it is applicable to specific materials, i.e. recycled clay masonry-concrete aggregate mixture. The effects of shear and confining stress states are not included either.

g. Zhang et al. (2020) argued that the confining pressure and deviatoric stress showed opposite effects on the permanent deformation of soils. Thus, it was unreasonable to combine both into one model. Based on the model by Puppala et al. (2009), a revised model including initial bulk stress and saturation was developed as follows

$$\varepsilon_p = aN^b \left(\frac{\theta_0}{p_a}\right)^c \left(\frac{\tau_{oct}}{p_a}\right)^d S_r^g \quad (2.44)$$

where θ_0 is the initial bulk stress, defined as $(\sigma_1 + \sigma_2 + \sigma_3) - \sigma_d$, a, b, c, d and g are regression coefficients. A more appropriate initial bulk stress term (Zhang et al., 2019) than bulk stress is proposed to differentiate the softening effect from the hardening effect. It is suggested that the mean normal bulk stress contains two stress states with opposite effects, i.e. confining pressure (hardening effects) and deviatoric stress (softening effects). The degree of saturation represents the effect of moisture

conditions. Regarding regression coefficients, many laboratory tests should be conducted to estimate their values, which will also depend on the soil types.

(2) Regression analysis method

Through curve fitting, the relationship of subgrade settlement with time can be developed. Hyperbolic, logarithmic, power and exponential functions have been widely used to establish the prediction model of subgrade settlement. Their basic forms are demonstrated respectively, as follows (Jia et al., 2018)

$$\delta_s = \frac{a}{N+b} - c \tag{2.45}$$

$$\delta_s = a\ln(N+b) - c \tag{2.46}$$

$$\delta_s = aN^b \tag{2.47}$$

$$\delta_s = a + be^{cN} \tag{2.48}$$

where δ_s is the predicted settlement in mm, a, b and c are the fitting parameters.

These models could be applicable to the road and railway tracks with appropriate changes, e.g. incorporating effects of stress states and moisture contents. They are simple to use, while the results could be dependent on the soil types or the monitored sites. It may be more useful to investigate specific sites than complex constitutive models.

Based on the shakedown theory, Dawson & Wellner (1999) and Werkmeister et al. (2001) identified three types of deformation behaviour, including plastic shakedown (Range A), plastic creep (Range B) and incremental collapse (Range C). The permanent deformation behaviour with the number of load cycles dependent on stress levels is illustrated in Figure 2.9. The general characteristics of each type are demonstrated as follows:

Range A: For a limited number of load applications, geotechnical materials exhibit plastic response, and the permanent strain rate shows a rapid decrease; however, after the postcompaction period is completed, the response becomes purely resilient, with no further permanent strain occurring.

Range B: unbound granular materials show a high permanent strain rate in the early loading cycles, which subsequently reduces to a low or constant strain rate. After applying a large number of load repetitions, unbound granular materials may be subjected to progressive increases in plastic strain and progress toward incremental collapse (i.e. Range C).

Range C: unbound granular materials present progressively increasing increments of plastic strains with each load cycle. This behaviour may result in structural failures, and an increasing rate of plastic strain accumulation indicates the start of the failure.

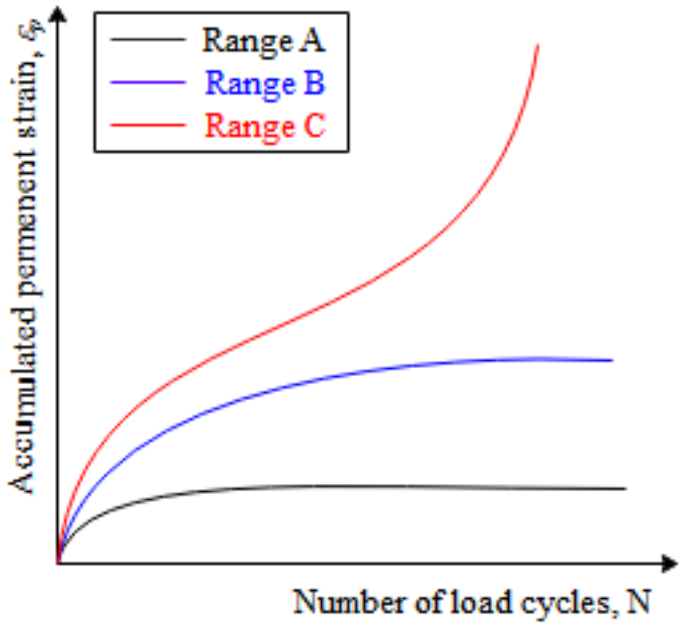

Figure 2.9 Classification of permanent deformation behaviour of unbound granular materials (Arnold et al., 2002)

Thus, from Figure 2.9, it can be seen that these fitting functions show different applicability to the soils within each range. For soils with Range A response, the hyperbolic function (Eq. (2.45)) can better describe the permanent deformation development, the logarithmic model (Eq. (2.46)) for soils with Range B response and the power (Eq. (2.47)) or exponential functions (Eq. (2.48)) for soils with Range C response.

2.4 Factors influencing foundation response

Based on previous studies, the mechanical properties of pavement/railway track foundations (i.e. resilient modulus, shear strength and permanent deformation) depended on various variables. For example, in previous studies, great concerns were raised about the sensitivity of resilient modulus to moisture content, matric suction, external stress, number of load repetitions, stress state, wetting and drying history and soil type (Li & Selig, 1996; Miller et al., 2000; Zaman & Khoury, 2007; Ng et al., 2013; Han & Vanapalli, 2016a; Rasul et al., 2017). The shape of quasi-static stress-strain behaviour is demonstrated by non-linear and hysteretic stress-strain curves that rely on stress level and stress path (Thornton 2000). Shear modulus was generally affected by

matric suction, soil type, void ratio, stress history, total stress and degree of saturation (Fredlund et al., 1978; Miller et al., 2000). In particular, the maximum shear modulus increased as the moisture content decreased (Kim et al., 2003).

Overall, the main impact factors affecting modulus, strength and plastic deformability can be summarized in Table 2.4.

Table 2.4 Main factors affecting modulus, strength and plastic deformability

Factors	Influential variables	Key references
Stress state	Matric suction	Fredlund et al., 2012
	Confining stress	Han and Vanapalli, 2016
	Deviator stress	Yang et al., 2008
Soil condition	Soil structure	Han and Vanapalli, 2016
	Soil dry density	Abu-Farsakh et al., 2007
	Moisture content	Dawson, 2008
Loading condition	Number of load repetitions	Monismith et al. (1972); Li and Selig, 1994; Ni, 2012
	Loading frequency	
	Loading history	

2.4.1 Soil composition

Generally, the impact of water on the structures increases with fines content (e.g. silt or clay). For example, the water in the sub-ballast or on the subgrade layer exhibit more significant effects compared with that in the single-sized-rock ballast (Rushton & Ghataora, 2014). Thevanayagam (1998) noted that the shear strength was significantly influenced by the presence of fines. The relative density increased with fines content. Increased initial confining stress may induce compaction as the finer grains move into the voids between the coarser particles. Consequently, the coarser-grain contacts are enhanced. Therefore, the shear strength may also depend on the initial confining stress history.

The resilient modulus–moisture relationships showed a clear variation by soil types, particularly with plasticity index (Khoury & Zaman, 2004; Khoury et al., 2009), as illustrated in Figure 2.10. The Minco specimens, with a relatively low PI of 8%, exhibited a smaller decrease (or increase) in M_r values after wetting (or drying) than the Port and Kirkland specimens with PI of 14 and 30, respectively.

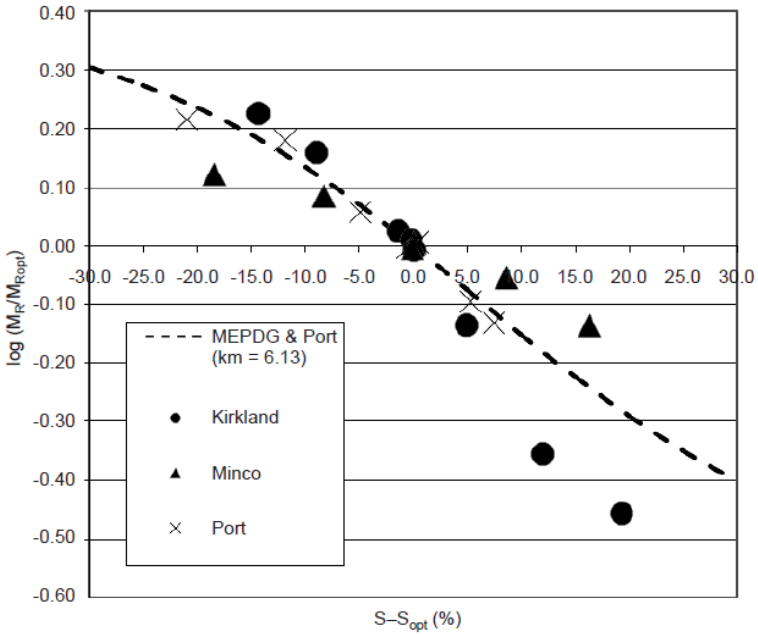

Figure 2.10 The relationship of $\log(M_r/M_{r,opt})$ with $(S - S_{opt})$ (saturation variation), from Khoury et al. (2009)

Han & Vanapalli (2017) conducted cyclic loading tests on three Canadian subgrade soils to investigate the variation of M_r with respect to moisture content and matric suction and found the model parameters were related to soil composition. The sensitivity of the various mechanical properties to suction and moisture changes varies with soil type, e.g. the increase in the representative resilient modulus, $M_{r,rep}$ (through using mean values of deviator stress (σ_d) and confining pressure (σ_c) during the cyclic loading test), of the Indian Head till (when the specimen moisture changed from full saturation to OMC) was more significant compared with the increment in elastic modulus E and unconfined compression strength q_{uc}, while the increase in $M_{r,rep}$ of Toronto silty was far less significant than that of E and q_{uc} (Han & Vanapalli, 2017). M_r of soils with higher plasticity were more sensitive to suction and moisture variations than that of soils with lower plasticity. The basic properties of these two soils are presented in Table 2.5.

Table 2.5 Properties of Indian Head till and Toronto silty clay, from Han & Vanapalli (2017)

Soil	w_L /%	I_p	G_s	w_{opt} /%	γ_{dmax} /kN·m^{-3}	Sand /%	Silt /%	Clay /%
Indian Head till	35.5	19	2.72	15.5	18.46	28	42	30
Toronto silty clay	19.6	6	2.68	13.5	19.15	3	81	16

The effect of soil structure on the idealised isotropic compression behaviour of reconstituted and structured soils is illustrated in Figure 2.11. As the soil was remoulded, the soil structure was disturbed. The remoulding of the soil structure reduces the bearing capacity of soils, whereas the removal of disturbed soils underlying pavement can reduce deflections significantly (Dawson & Correia, 1996). Liu & Carter (2000) defined the 'destructuring index' (i.e. b) to quantify the destructuring rate of the remoulded soils and indicates that the destructuring index was mostly determined by the liquidity index for clay samples of particular mineralogy and with similar geological stress histories but varied depths underneath the surface. Generally, at the same mean effective stress, the void ratio, e, of reconstituted soils was lower than that of structured soils (Liu & Carter, 2002) and the shearing and yielding behaviour were affected, as illustrated in

Figure 2.12. At the initial stage, deviatoric stress increased with b, while the structured soil did not depend on soil structure at the final state due to the complete removal of soil structures. In terms of softening behaviour, the peak strength of structured soil showed a more rapid decrease in the critical state strength than that of remoulded soil.

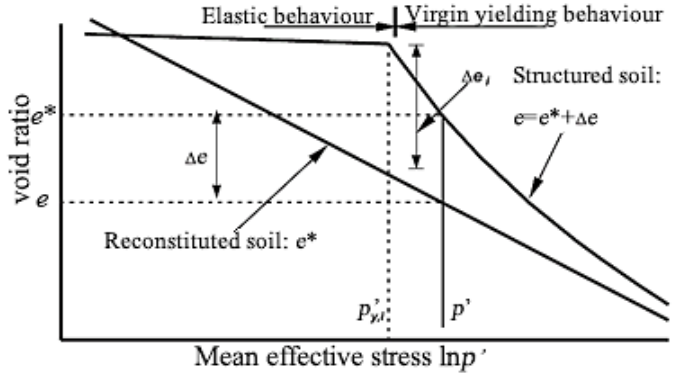

Figure 2.11 Idealization of the isotropic compression behaviour of reconstituted and structured soils, from Liu & Carter (2002)

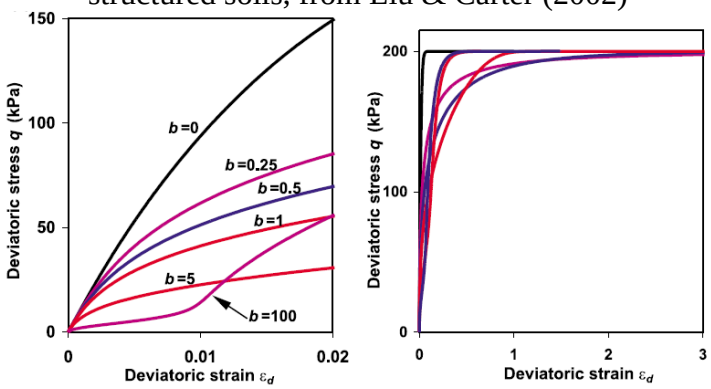

Figure 2.12 Effects of b on stress-strain relationship at two scales, from Liu & Carter (2002)

Based on the review of microstructural effects on compacted soil behaviour by Alonso et al. (2013), the microstructure was found to be critical. Figure 2.13 (Alonso & Pinyol, 2008) illustrates the relationship between yield stress and dry density, $p_y - \rho_d$, according to the analysis of a limited number of soil compaction testing programmes. It shows that for a given ρ_d, the saturated isotropic yield stress p_y increased significantly with soil plasticity and p_y showed a more rapid increase with dry density at higher plasticity. Based on these plots, it may provide a reference for adopting p_y without performing specific tests (e.g. triaxial compression tests).

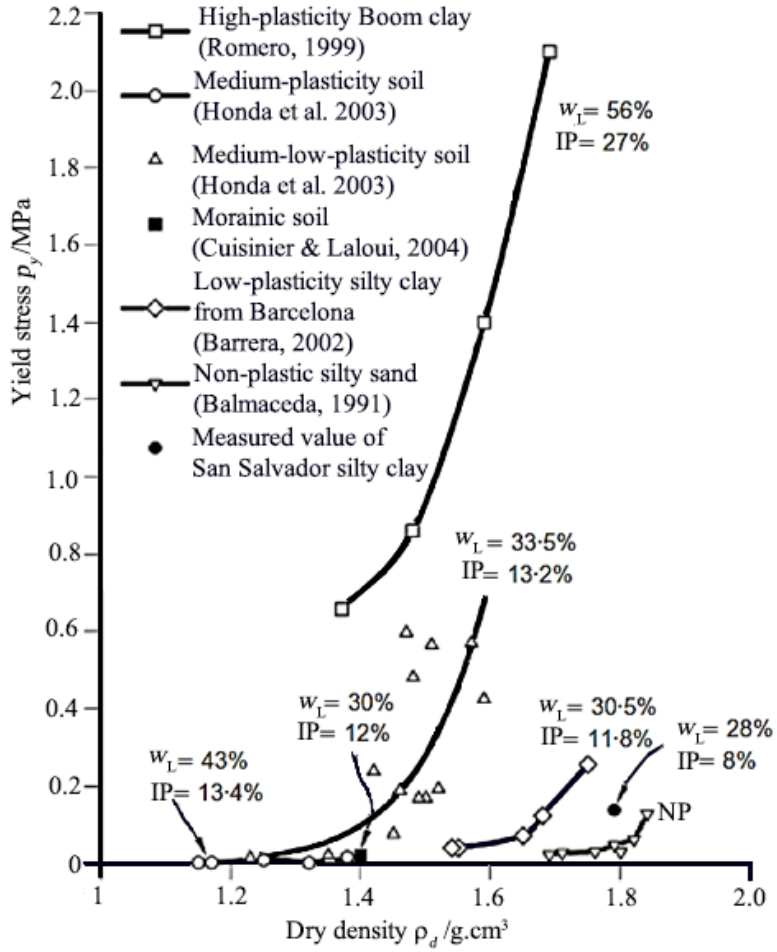

Figure 2.13 Relationship between isotropic p_y at saturated conditions and ρ_d of seven soil types, from Alonso & Pinyol (2008)

Alonso et al. (2013) also revealed the effects of microstructure on the compacted soil behaviour: (a) Geotechnical properties of compacted soils did not depend on the isotropic yield stress and matric suction alone and were distinctly influenced by the microstructure. (b) The sensitivity of the properties to microstructure varied, e.g. the soil permeability may be significantly associated with the microstructure, while less

variation in the drained strength was recognized. (c) The microstructure considerably affected compressibility, collapse and swelling potential. (d) The soil structure may also depend on the stress condition. The applied stress and matric suction paths mainly modify the macro-porosity of compacted soils, whereas matric suction changes may also cause changes to the microstructural void volume in high-plasticity soils. In clayey soils with low-to-medium plasticity, the micro-void ratio tends to retain its original as-compacted value during the following stress–suction paths.

Stark & Eid (1994) found that the magnitude of the drained residual shear strength decreased with increasing liquid limit and also decreased with increasing activity, as illustrated in Figure 2.14. The activity (A_c) is defined as the ratio of the plasticity index to the clay-size fraction. Soil with increasing plasticity will have increasing face-to-face overlaps between soil (clay) particles, thus reducing drained residual shear strength at any particular stress level.

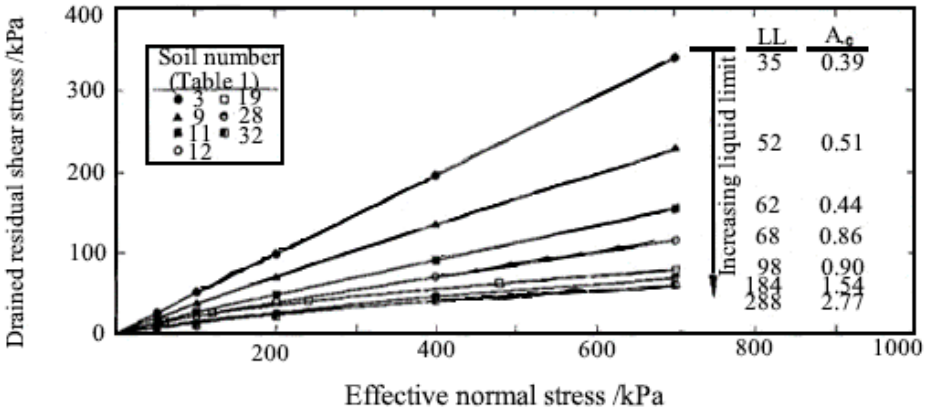

Figure 2.14 Effects of clay mineralogy on drained residual failure envelopes, from Stark & Eid (1994)

2.4.2 Soil density

Soil physical states can be represented by two properties dependent on environmental actions, i.e. moisture content and dry density. The discussion here will mainly focus on the effect of the dry density of the soils, and that of moisture content will be presented in Section 2.4.3 separately. The change in dry density and moisture content can be represented by two basic paths, as shown in Figure 2.15(a) and (b) (Li & Selig, 1994). The effects of dry density on the resilient modulus are presented in Figure 2.16, derived from the work by Seed et al. (1962). It demonstrates that the variation characteristics of resilient modulus with the increase in dry density depend on the moisture content. Basically, the resilient modulus increases as the dry density rises

for most moisture contents, but at a higher moisture content, the resilient modulus decreases as the dry density increases (Li & Selig, 1994).

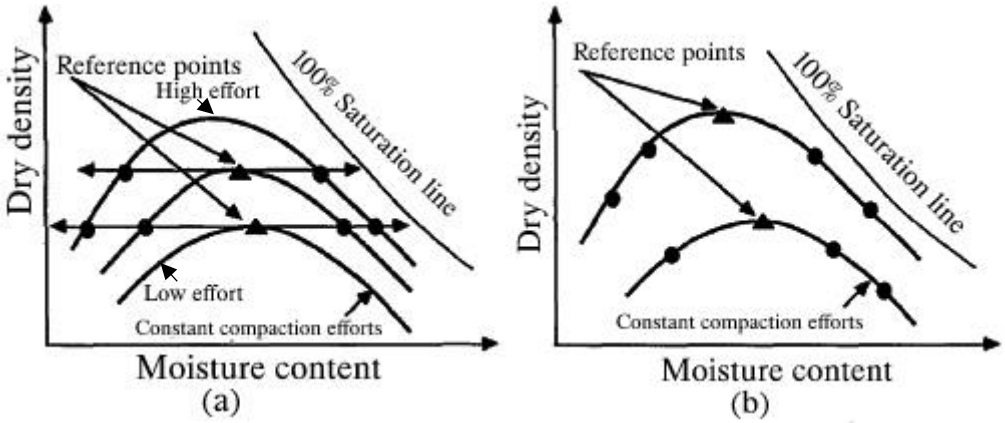

Figure 2.15 Changing paths of dry density and moisture content: (a) at constant dry density; (b) at constant compaction effort, from Li & Selig (1994)

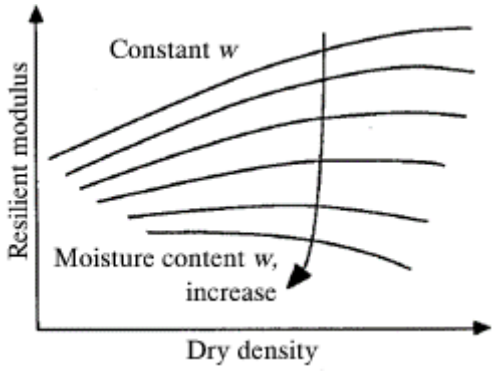

Figure 2.16 Effects of dry density on the resilient modulus, from Li & Selig (1994)

At the corresponding optimum moisture contents, the effects of dry density on the shear resistance at a soil–geo-synthetic interface were measured by Abu-Farsakh et al. (2007). As can be seen from Figure 2.17, the interface shear strength increased as dry density increased. Additionally, the level of the remoulding dry density affected the failure envelopes which was also dependent on soil types. Clay 6 and Clay 25 experienced more significant changes in shear resistance due to dry density variation than Clay 49 (the number corresponds to their plasticity indices). As shown in Figure 2.13 (Alonso & Pinyol, 2008), the relationship between yield stress and dry density, $p_y - \rho_d$, is presented according to the analysis of a limited number of compacted soil types. It shows that the saturated isotropic yield stress p_y rose sharply as ρ_d increased.

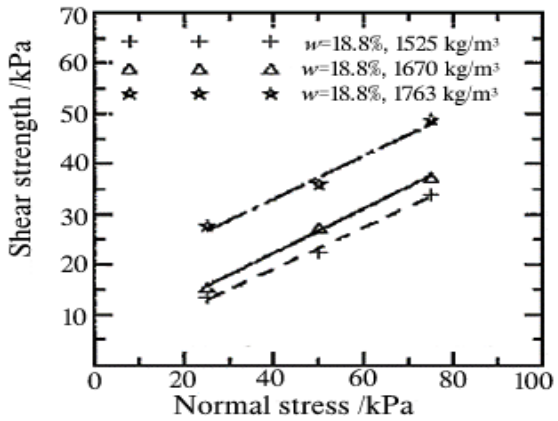

Figure 2.17 Effects of dry densities on the shear strength of the interface between Clay-6 and 4×4 woven geotextiles at optimum moisture content, from Abu-Farsakh et al. (2007)

2.4.3 Moisture content

Due to precipitation, capillary action, evaporation, evapo-transpiration, flooding and water table variation, the moisture content in the subgrade may vary. When saturated, the water will induce positive pore water pressure, which will reduce the load carried by the soil particles due to the reduction in effective stress. Even when unsaturated, increased moisture content reduces matric suction which also reduces effective stress and, hence, mechanical properties. Consequently, the structural bearing capacity will decrease, and the water would further accelerate the deterioration of foundations in pavement and railway track structures under repeated traffic loading and therefore endanger the stability and reliability of transport. Moduli would decrease with higher moisture content, while the permanent deformation and Poisson's ratio increase (Dawson et al., 1996); e.g. with the optimum moisture content rising by 2%, the resilient modulus of cohesive soils reduced significantly, up to 4 times (Ji & Nantung, 2015). Miller et al. (2000) found that the normalized cyclic shear strength was sensitive to the degree of saturation and the cyclic strength may decrease by about 80% with the initial degree of saturation rising from 90 to 100%. It was also obtained that the maximum shear modulus increased by a factor of 3 when moisture content by mass decreased approximately from 10% to 7.5% (Kim et al., 2003). Erlingsson (2010) measured a large increase in the development of permanent deformation in the subgrade by introducing water after the first 500000 load repetitions with a wheel loading of 60 kN and a tyre pressure of 800 kPa. The water level increased to 30 cm beneath the subgrade surface. For example, at the depth range of 35.3-50.5 cm (the uppermost part of the

subgrade), the permanent strain rate increased by approximately 75%. Saevarsdottir & Erlingsson (2013) conducted accelerated pavement tests with a heavy vehicle simulator. For the pavement with fine-graded sandy subgrade, decreased resilient modulus and increased rate of accumulation of permanent deformation occurred as the water table was raised to increase the moisture content, i.e. the water level reached 30 cm beneath the subgrade top. The bottom part of the subbase had the largest increase in resilient strain, by 53%, with the increase in that of the base and the top 30 cm of subgrade by 15% and about 20%, respectively. With respect to all layers, the subgrade exhibited the largest and greatest extent of increase in permanent deformation from 2 mm to 15 mm, while the base showed the smallest increase. However, due to the inconsistency or variable nature of subgrade strength (Sabri, 2015), the values of M_r do not continuously decline over the whole wetting cycle (Rahman & Erlingsson, 2016).

Furthermore, moisture content exhibited a hysteretic behaviour in the relationship with resilient modulus due to the wetting and drying processes (Khoury & Zaman, 2004). M_r showed higher values during the drying cycle than on the wetting cycle at the same moisture content. With regard to non-linearity, increasing moisture content showed few effects (Dawson et al., 1996). Khoury et al. (2009) also found that the resilient modulus-moisture content relationships caused by drying presented higher values than wetting. The changes in resilient modulus with postcompaction are affected by the initial moisture content, e.g. for all the specimens dried to OMC-4%, M_r of specimens prepared at OMC+4% showed higher values than those of specimens prepared at OMC. Ng et al. (2013) stated that at a low cyclic stress, M_r of completely decomposed tuff (PI=14) along a wetting path showed a larger value than that measured along a drying path for the same stress and suction level. With increasing cyclic stress, the difference between the two paths became less prominent.

2.4.4 Matric suction

As Leong & Abuel-Naga (2017) demonstrated, matric suction is associated with capillary effects, while osmotic suction depends on the salt content of the pore water. A strong correlation has been revealed between matric suction and resilient modulus (Khoury & Zaman, 2004). Khoury et al. (2003) demonstrated that the variations in resilient modulus were not induced by osmotic suction. Leong & Abuel-Naga (2017) conducted tests on three series of compacted soils that were prepared using distilled

water and sodium chloride solution and concluded that no effect of osmotic suction or osmotic suction gradient on shear strength of the compacted low plasticity silt specimens was measured. Thus, in most practical situations, the matric suction is far more important than osmotic suction and the effects of matric suction should be prioritized for incorporation in the analysis of the behaviour of unsaturated soil in preference to the effects of total and osmotic suctions.

Matric suction affects the mechanical behaviour of unsaturated soil as a fundamental stress variable and its effects vary with the stress state. The roles of the matric suction in the mechanical response of the soils can be revealed from two aspects, i.e. affecting the effective stress existing in the soil particle through pore water pressure and exerting a force to reinforce the interparticle bonding. With respect to the two mechanisms, the soil response will depend on both suction and the saturation state of the soil (Wheeler & Sivakumar, 1995; Gallipoli et al., 2003).

Resilient and shear moduli increase with matric suction (Gallipoli et al., 2003; Yang et al., 2005; Fredlund, 2006; Khoury et al., 2009; Cary & Zapata, 2011; Han & Vanapalli, 2016b). Using Eq. (2.18) to analyse the experimental data, it was found that resilient modulus correlated better with matric suction than with total suction (Yang et al., 2005), as illustrated in Figure 2.18.

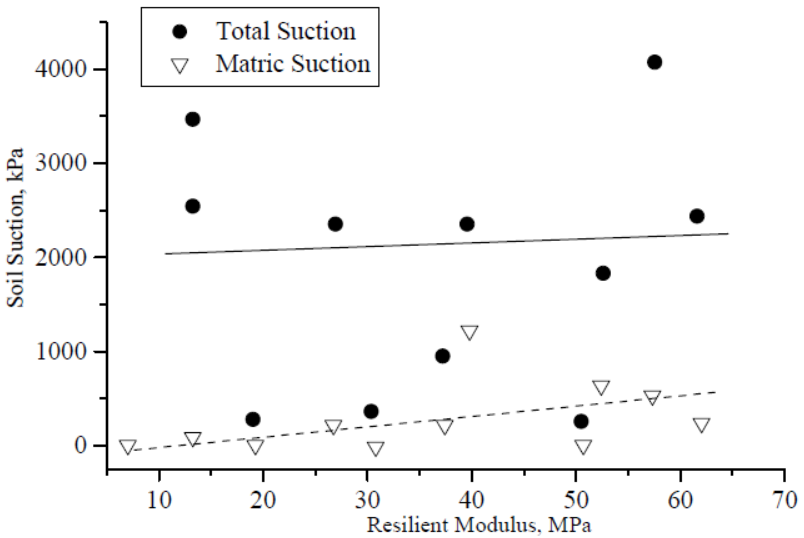

Figure 2.18 Illustration of the relationship between resilient modulus and matric suction for A-7-5 and A-7-6 soils (σ_d=103 kPa, σ_3=21 kPa), from Yang et al. (2005)

Plenty of studies have been performed on the prediction model of resilient modulus of subgrade soils and more model parameters were considered, e.g. confining stress, bulk stress or dry density (Yang et al., 2005; Liang et al., 2008; Cary & Zapata, 2011).

Since the matric suction can reflect the effects of the seasonal variation of moisture content on resilient modulus, the model may be more feasible and reliable by incorporating matric suction than by directly including moisture content in practice. Particularly, at a low moisture content, the resilient modulus is dominated by the significant matric suction for the soil.

Ng et al. (2013) found that resilient modulus increased significantly with matric suction (see Figure 2.19) due to the presence of water tension. It increased by up to one order of magnitude with suction rising from 0 to 250 kPa at a cyclic stress of 30 kPa.

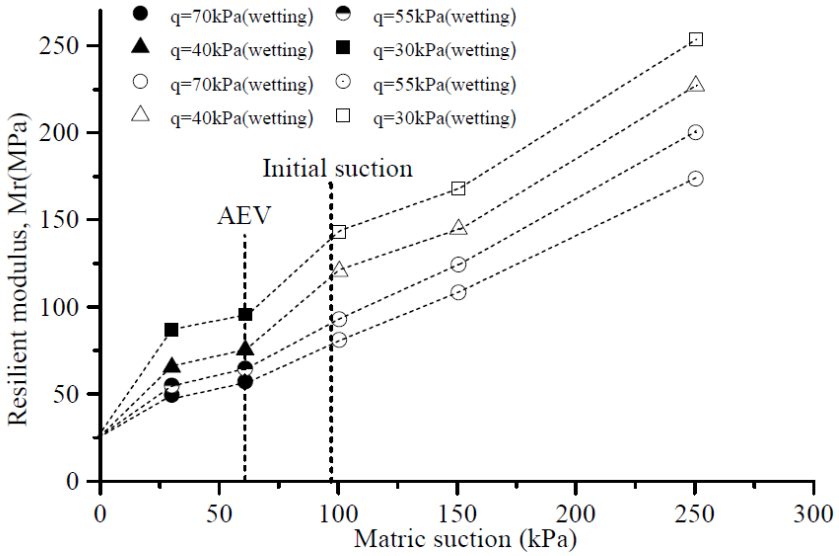

Figure 2.19 Influence of suction on resilient modulus (ψ_m = 0, 30 and 60 kPa in series 1 tests; ψ_m= 100, 150 and 250 kPa in series 2 tests. q is the cyclic stress.), from Ng et al. (2013)

Based on the linear model proposed (Eq. (2.28)) by Fredlund et al. (1978), the effects of matric suction on the shear strength of unsaturated soil are identified. The shear strength shows a nonlinear increase due to increased matric suction (Fredlund et al., 1995), as illustrated in Figure 2.20. A relationship between initial matric suction and permanent strain for all blends of recycled construction and waste material was demonstrated in Figure 2.21(Azam et al., 2015). The permanent strain decreased as matric suction grew. A simple power equation was developed, and the permanent strain was found to correlate better with matric suction than with moisture content.

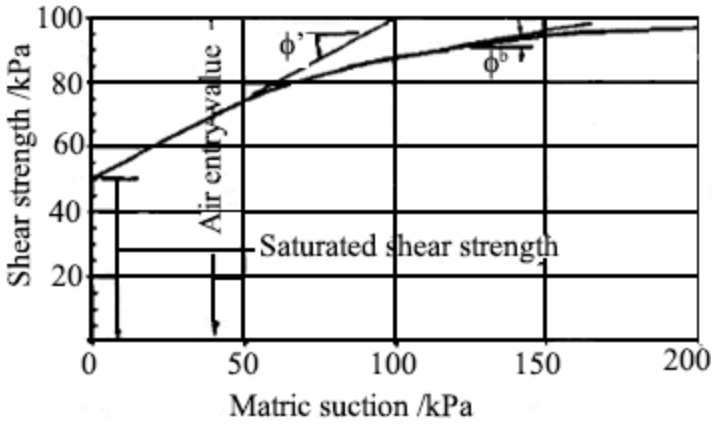

Figure 2.20 A typical relationship between shear strength and increasing matric suction, from Fredlund et al. (1995)

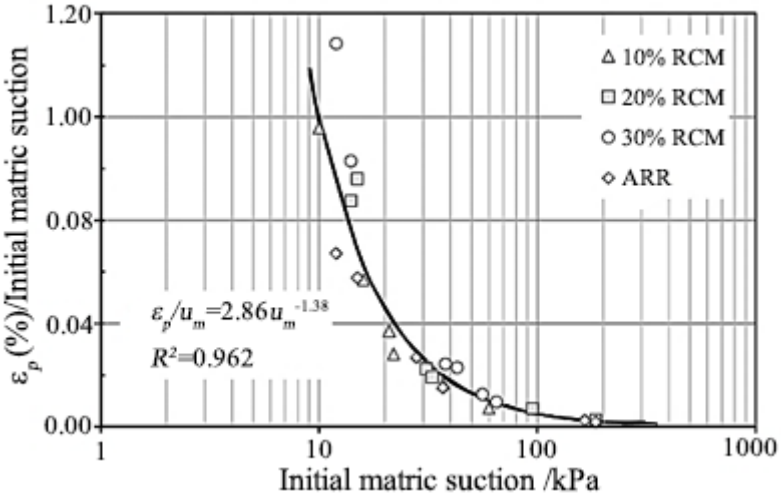

Figure 2.21 Permanent strain/initial matric suction against matric suction for all blends, from Azam et al. (2015)

2.4.5 External stress

More efforts are devoted to exploring the relationship between resilient modulus and stress levels in soils. M_r depends on several external stresses, including external shearing (e.g. deviator stress) and confining stresses (e.g. confining pressure) (Han & Vanapalli, 2016b). The resilient modulus shows an increasing trend as confining stress increases, while the deviator stress has more significant effects on fine-grained subgrade soils (e.g. clay soils) than confining stress (Fredlund et al., 1975; Li & Selig, 1994). Regarding the magnitude of resilient modulus, it depends on the magnitude of deviator stress and confining stress significantly. Yang et al. (2008) found that the resilient modulus increased with increasing deviator stress at the initial matric suction (IMS) of 450 kPa, while decreasing with increasing deviator stress at IMS of 50 and 150 kPa, respectively. Figure 2.22 illustrates the relationships between the resilient

modulus and the deviator stress for the soil classified as A-6 soil in the AASHTO (1986) soil classification system at different IMS. At low IMS, the resilient strain rose significantly as deviator stress increased and accordingly showed a downward trend in M_r. At high IMS, the resilient (recoverable) strain increased slightly as deviator stress grew and showed an increasing M_r. The high IMS (which means the soil experienced a high effective confining stress) increased the resistance of soils to deformation. The recoverable strain showed a smaller increase compared to the increase in the deviator stress.

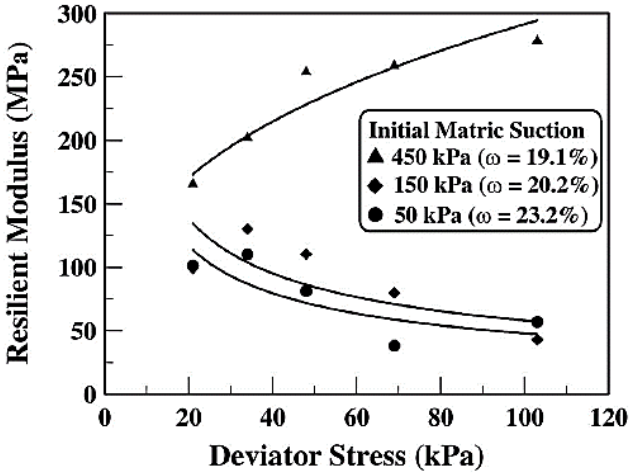

Figure 2.22 Resilient modulus test results for A-6 soils, from Yang et al. (2008)

Maher et al. (2000) investigated the resilient modulus of 8 typical New Jersey subgrade soils. The basic properties of the soils are presented in Table 2.6. Through the resilient modulus test, the A-2-4 and A-4 (fine-grained) soils exhibited similar behaviour. The resilient modulus showed a downward trend as the cyclic deviatoric stress increased, which can be attributed to strain softening. The A-3 soil (fine beach sand) also exhibited a decrease in resilient modulus with increasing deviatoric cyclic stress ratios. However, compared with the A-2-4 and A-4 soils, it showed different characteristics and was less sensitive to moisture variation. When the specimens were on the dry side of optimum, A-6 and A-7 showed slight differences at different levels of deviator stress. The largest difference occurred at the higher applied deviator stresses at the 2% wet of optimum and the soils were more sensitive to strain softening.

Table 2.6 Soil properties and classification, from Maher et al. (2000)

Soil location	AASHTO M 145 Classification	Percent passing 75 μm /%	w_L /%	w_P /%	I_p
Rt. 46	A-2-4	30.1	15	NP	NP
Rt. 80a	A-2-4	33.3	0	NP	NP
Rt. 295	A-3	9.9	0	NP	NP
Rt. 80b	A-4	36.6	20.5	19	1.5
Rt. 206	A-4	43	21	17	4
Cumberland County	A-6	97.5	39.1	20.2	18.9
Cumberland County	A-7	97.7	52.5	25.1	27.4

According to the interface direct shear tests performed on low-plasticity fine-grained soil, the effect of net normal stress on both peak and post-peak shear strength has been identified (Hamid & Miller, 2009). Peak shear stress increased as net normal stress and matric suction increased for soils. Post-peak shear strength of soil showed an increasing trend with net normal stress, while the strength was mostly unaffected by matric suction at a given net normal stress. With shearing beyond peak stress, the air-water menisci were totally damaged, and thus the contribution of suction to the shear strength was negligible. Besides, the amount of compression increased, and dilation decreased as the net normal stress increased.

2.4.6 Loading condition

The subgrade demonstrates differing responses under single static loading than under repeated traffic loading, even with the same magnitudes, e.g. the subgrade will exhibit lower resistance to plastic strain under repeated loadings. Various pavement and track foundation distresses can be attributed to repeated loading (Li & Selig, 1994). Loading conditions, including the number of loading repetitions, loading frequency and loading history, are discussed.

(1) Number of loading repetitions

Based on cyclic load triaxial tests with 100000 load applications, Barksdale (1972) found that the accumulated permanent axial strain of silt and gravel was proportional to the logarithm of the number of loading repetitions and a semi-logarithmic relationship of permanent strain with loading times was proposed. Monismith et al. (1975) studied the permanent deformation of silty clay with RLTT. The results indicate

that the permanent deformation increased and showed an exponential relationship with loading cycles. The model parameters depended on soil types, moisture content and stress levels. Thompson & Nauman (1993) report that the logarithmic permanent deformation showed a linear relationship with the logarithmic loading cycles. It is also found that the effects of loading cycles on cyclic soil behaviour varied with cyclic stress ratio (CSR) (i.e. the ratio of applied cyclic stress to twice the effective confining pressure) at a frequency of 1Hz (Indraratna et al., 2020). With CSR below 0.5, the cyclic axial strain progressively increased to a constant level with loading cycles. With CSR above 0.5, the cyclic axial strain rapidly increased as loading cycles increased. This indicates that soil failure occurred at an early stage.

(2) Loading frequency

It has been extensively believed that the stress-strain relationship and the yield stress of subgrade soils are affected by the loading frequency, as the soil yielding is a time-dependent phenomenon (Thevakumar et al., 2021; Zhao et al., 2021). The threshold stress and cumulative plastic deformation of soils were largely affected by the load frequency (Liu et al., 2006), and the increase in train speed may induce shear failure in a railroad subgrade under repeated loading. The relationship of displacement magnification factors of the subgrade with loading frequencies was studied by Choudhury et al. (2008) with four soil formations (i.e. dense uniform sand, stiff clay, loose sand and soft clay), as shown in Figure 2.23. As the frequency increased to the resonant frequency, the factors of four soils increased to the maximum, and then the values decreased with frequencies. In particular, the soft clay exhibited the largest magnification factor. Liu & Xiao (2010) reported that axial cumulative plastic strain of silt subgrade increased with the load frequency and that the variation was more significant at a higher dynamic stress level or lower relative compaction (RC). The trend is illustrated in Figure 2.24. RC indicates the percentage of dry density to the maximum dry density in the compaction curve. Chen et al. (2013) presented that the dynamic earth pressure in the subgrade increased with the excitation frequency, and the increase was larger at a higher excitation frequency. However, for a reconstituted low plasticity clay (LL=27.5% and PI=10.8), Thevakumar et al. (2021) found that the total axial strain decreased with the loading frequency in comparison of the strain at 0.1 and 0.5 Hz with that at 1Hz, as well as the plastic strain. Generally, the plastic strain showed a larger value at a relatively lower frequency.

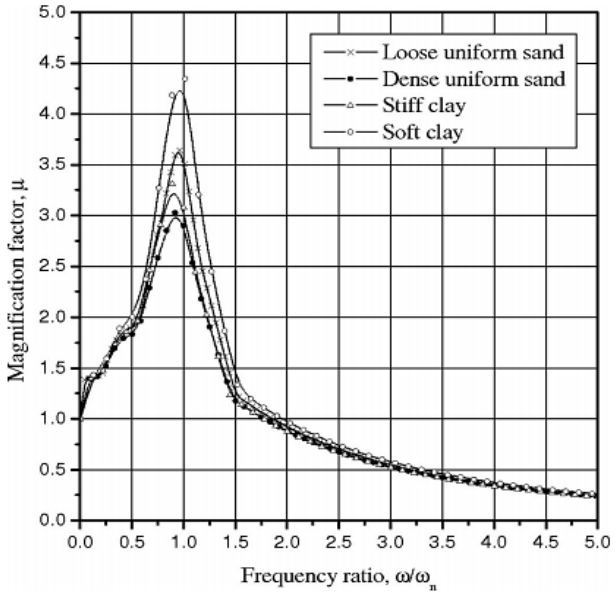

Figure 2.23 The relationship of displacement magnification factor with frequency ratio, from Choudhury et al. (2008)

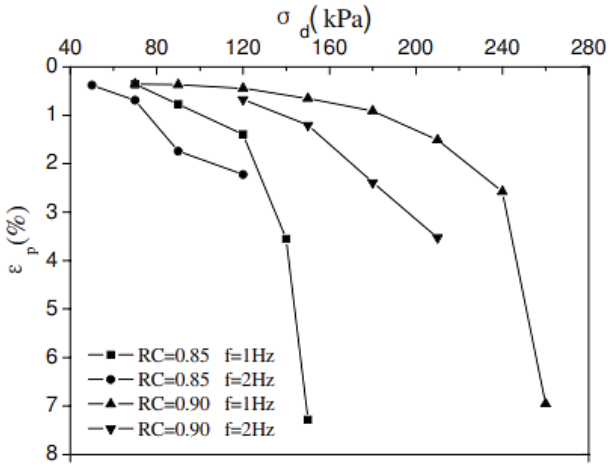

Figure 2.24 The relationship of accumulative permanent strain with dynamic stress, from Liu & Xiao (2010)

(3) Loading history

Based on RLTT on a silty clay (LL = 35, PI = 15), Monismith et al. (1975) studied the influence of stress history on permanent deformation. The repeated load had a frequency of 20 repetitions per minute with a duration of 0.1 s. The experimental results at increasing sequences are illustrated in Figure 2.25. Generally, the permanent strain increased with the level of deviator stress. Without conditioning, the permanent strain showed a larger increase than that with conditioning prior to the test. At a higher stress level, stress history showed a larger effect on the permanent strain. These results are in agreement with the study by Seed et al. (1955).

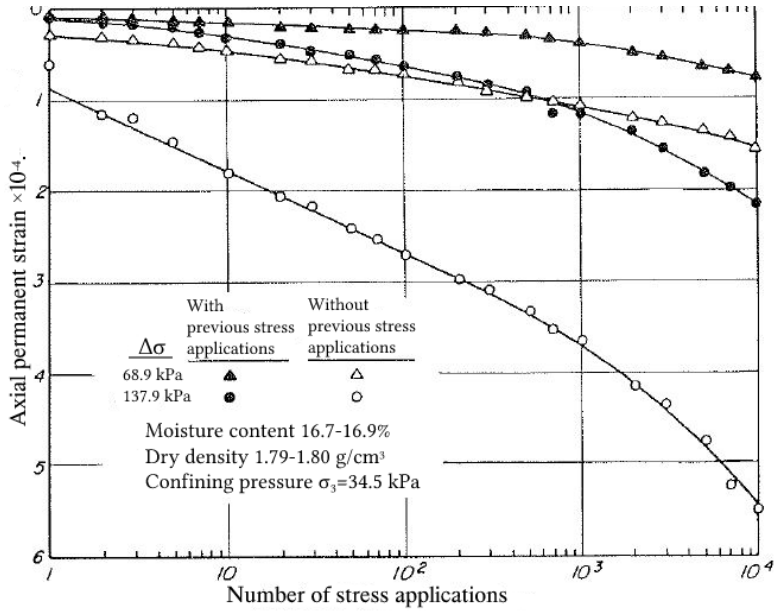

Figure 2.25 The influence of stress history on permanent accumulation, adapted from Monismith et al. (1975)

In practice, the traffic load applied to the subgrade is not continuous and there are intermittent periods between adjacent two vehicles (Nie et al., 2020). Nie et al. (2020) concluded that the intermittent stages of loading imposed significant effects on the accumulation of axial strain, and the axial strain under intermittent loading decreased significantly over the same loading time as that under continuous loading. This can be attributed to the dissipation of pore water pressure during intermittent stages.

Concerning the loading history different from repeated loading, it will also induce variations in soil response (Cui & Delage, 1996). Figure 2.26(a) and (b) shows that the higher suction curves exhibited less volume variation under continuous loading than under step loading and a difference between isotropic yield stress values. During the step loading, the stress increased so suddenly that a dramatic instantaneous (undrained) decrease in the specimen volume arose. The undrained loading induced excess pore water pressure within the specimen, and hence the matric suction would no longer constrain the system. Consequently, the volume reduced remarkably.

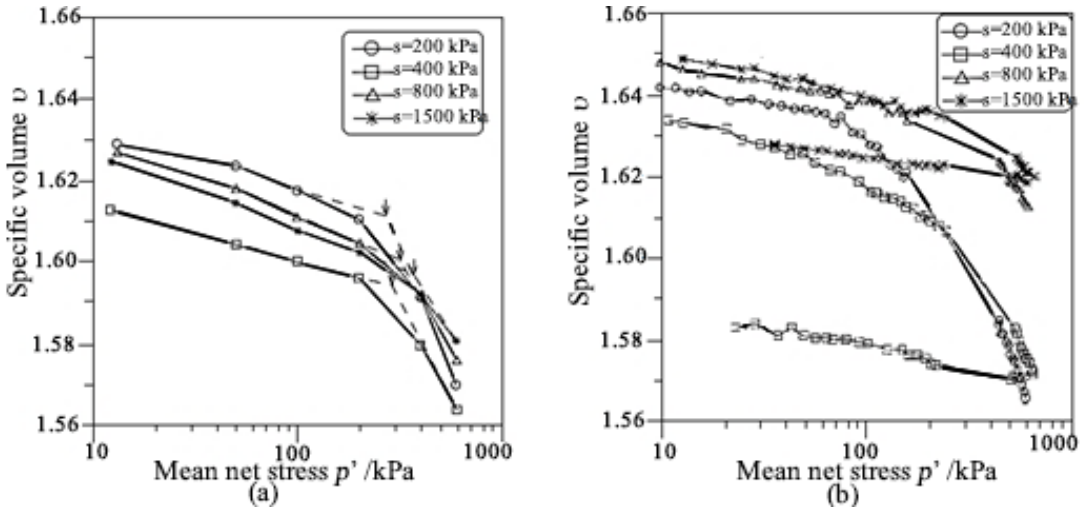

Figure 2.26 Volume changes: (a) under isotropic step loading, (b) under continuous isotropic loading, from Cui & Delage (1996)

2.5 Water flow in foundations

2.5.1 Water source

Water can migrate into the structural pavement section in various ways (Ridgeway, 1980), including surface infiltration, infiltration through the shoulder, cracks and joints, capillary action and water table rise. Surface water infiltration contributes 90~95% of the total moisture in a pavement system. Crack, joint and shoulder infiltrations, possibly supplemented by subgrade capillary action, provide the major routes for water into the subsurface structure (Van Sambeek, 1989; Rokade et al., 2012). Rainfall is the primary source of moisture infiltration in the pavements/railway tracks with a low water table (Al-Qadi et al., 2004). The areas with high water tables may feed the pavement/railway track structure, e.g. when ditches and groundwater may back up. Aquifers, springs and subsurface flow interrupted by the construction may also lead to excessive water in the pavement/track system, while capillary action may draw water in from below or from the margins of the pavement/track (Rokade et al., 2012). Table 2.7 presents the routes of ingress and egress to the pavement structure. In terms of railway tracks, the routes are believed to be similar for concrete slab tracks, as well as for ballasted tracks apart from the route from the pavement surface (cracks and joints). Instead, on the surface of ballasted track, the water will directly infiltrate into the sublayers due to the large void ratio of ballast.

Table 2.7 Routes of ingress and egress, from Apul et al. (2002), Van Sambeek (1989) & Dawson & Hill (1998a)

Direction	Location	Route
Ingress	Pavement surface	Construction joints
		Cracks resulting from shrinkage during/after construction
		Cracks resulting from distress due to loading
		Diffusion through intact materials
	Subgrade	Artesian flow
		Pumping action under traffic loading
		Capillary action of lower pavement layer
		Water vapour rising through subgrade soils
	Road margins	Reverse gradient of permeable layers above formation level
		Lateral or median drain surcharging
		Capillary action of pavement layers
	Other sources	Pavement or ground run-off via unsealed shoulders
		Direct rainfall on pavement during construction
		Frost lenses melting during spring thaw
Egress	Pavement surface	Pumping through existing cracks/joints
		Capillary rise and evaporation through cracks
		Diffusion and evaporation through intact materials
	Subgrade	Infiltration to permeable/low water table subgrade
		Capillary action of subgrade
	Road margins	Gravitational flow in aggregate to lateral or median drain
		Vertical flow in aggregate to open-graded drainage layer below

2.5.2 Hydraulic properties

(1) Permeability

The ability of a soil to allow water to move through the interconnected voids is measured by its permeability, which determines drainage properties of soils. It is expressed as the flow rate through a unit area with a unit hydraulic gradient. In saturated soils, the coefficient of permeability is a function of the void ratio (Lambe & Whitman, 1979). Generally, the coefficient of permeability is assumed to be constant for a given saturated soil when considering some problems, e.g. transient flow. In unsaturated soil, water flow mainly depends on the volumetric moisture content, matric suction and

gravitational potential. As air fills parts of the large pores, water flow may be obstructed in these pores so that water flow will be limited to flow through smaller pores around soil particles. Thus, due to the presence of air in the pores of unsaturated soil, the permeability decreases compared with that of saturated soils. The suction and volumetric moisture content (or degree of saturation) affect the permeability significantly. In unsaturated soil, suction may reduce the void space, but it may draw in air from outside without changing the volume, or it may draw in water expanding the pore space. For example, when the degree of saturation decreases by 20%, the water-relative permeability (WRP) may drop to 36% of the saturated permeability for sand and 18% for clay (Dawson, 2008). The relationship of relative permeability with suction volumetric moisture content is illustrated in Figure 2.27 for coarse- and fine-grained soils.

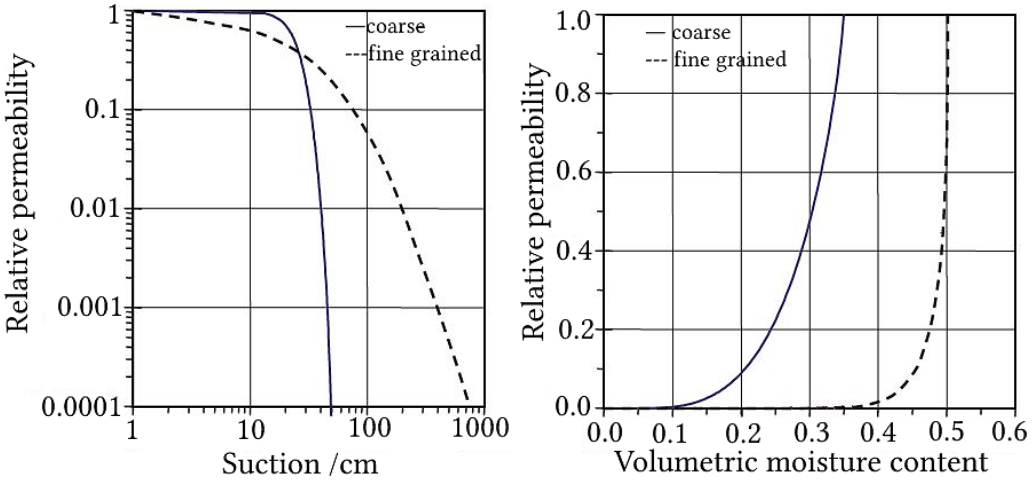

Figure 2.27 The relationship of relative permeability with suction and volumetric moisture content, from Dawson (2008)

Usually, the permeability of unsaturated soil is presented by the WRP which is defined as the ratio of the permeability at a specific volumetric moisture content to the saturated permeability, i.e.

$$k_{rw}(w_{vol}) = \frac{k_w(w_{vol})}{k_{sat}} \tag{2.49}$$

where $k_{rw}(w_{vol})$ is the WRP, $k_w(w_{vol})$ is the water permeability and k_{sat} is the saturated coefficient of permeability. Equations have been proposed by Brooks & Corey (1964) and Van Genuchten (1980), the latter being based on Mualem's model (Mualem, 1976), to measure the WRP.

For a base with a recommended minimum cross slope of 2% in Figure 2.28, it must be fairly coarse to achieve good drainage performance. A correlation between a

minimum degree of saturation and the coefficient of permeability was investigated (McEnroe, 1994). With k_w <1.7×10^{-4} m/s, no drainage occurred due to high air-entry head. With k_w<3.8×10^{-4} m/s, the material remained over 85% saturated. With the k_w reaching 7.4×10^{-4} m/s, a minimum saturated of 50% could be obtained. With k_w>1.7×10^{-3} m/s, the material could achieve a saturation of below 20%. As McEnroe (1994) demonstrated, above 50% of a typical granular material's void space will be undrainable with a permeability below 7.4×10^{-4} m/s. This is due to the suction potential under partially saturated conditions. However, vertical drainage of free water to an underlying water table by gravity and drainage by evaporation will still be achievable.

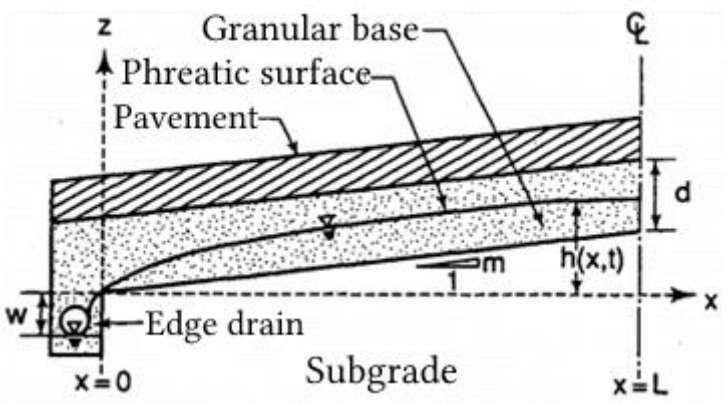

Figure 2.28 Cross section of pavement structure, from McEnroe (1994)

(2) SWCC

Under partially saturated conditions, the matric suction may be generated as a form of negative pore water pressure. It plays an important role in the mechanical behaviour of unsaturated soil because suction contributes to enhancing the stiffness of the soil to bear external loading. During the drying and wetting processes, the matric suction will fluctuate, which may cause plastic volumetric deformations. Generally, increased moisture content will cause volume variation (increase for expansive soils or decrease for collapsible soils) and reduces shear strength and stiffness in soils due to the loss of matric suction. The amount and type of volume variation may vary with soil's physical state, initial soil density, applied stress state and degree of saturation. Soils that vary significantly with moisture content in compression or shrinking/swelling properties are usually regarded as moisture-sensitive soils (Ng & Menzies, 2007). The volumetric behaviour of unsaturated soil does not rely only on the initial and final stress and matric suction but on the stress path from the initial to the final states (Alonso et al., 1990).

SWCC is defined as the relationship between moisture content and matric suction and can be used to help predict the behaviour of unsaturated soil, e.g. the hydraulic conductivity, shear strength and volume change (Pham et al., 2005). Water infiltration or capillary rise (i.e. wetting) will decrease the matric suction in the soil, while water evaporation or gravity drainage (i.e. drying) will increase the matric suction. The hydraulic hysteresis (i.e. the moisture content at a certain suction for a wetting process is lower than that for a drying process) arises in the SWCC of unsaturated soil, as illustrated in

Figure 2.29. The hysteretic behaviour can be mainly attributed to the ink-bottle effect. This effect is demonstrated by considering the ink-bottle capillary tube connected to a water reservoir, as illustrated in Figure 2.30 (Laloui, 2013). If the reservoir is moved downward from the tube top, the capillary tube will keep saturated because the curvature of the meniscus at the tube top can sustain the applied suction. If the water reservoir is moved to the tube bottom and then lifted, the capillary rise will depend on the larger pore. Thus, the capillary tube will not be filled to the same water level, and in terms of the degree of saturation, it will decrease.

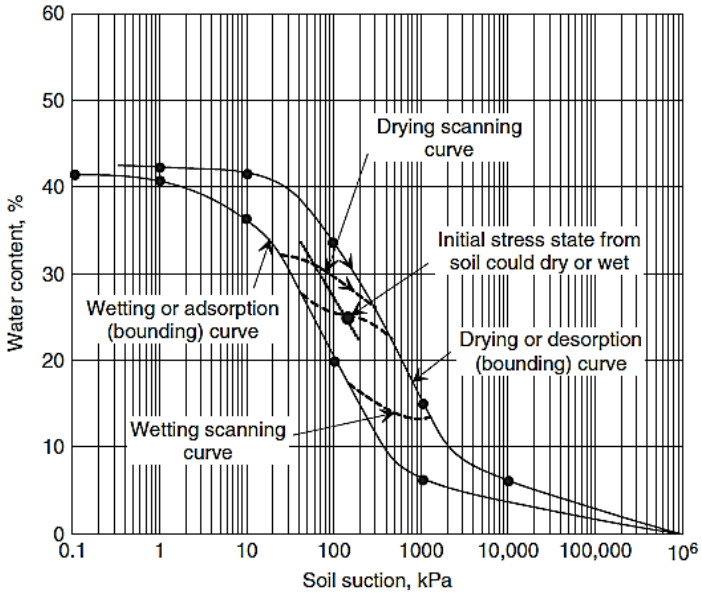

Figure 2.29 Relationship of initial stress state to hysteresis loops of SWCC, from Fredlund et al. (2012)

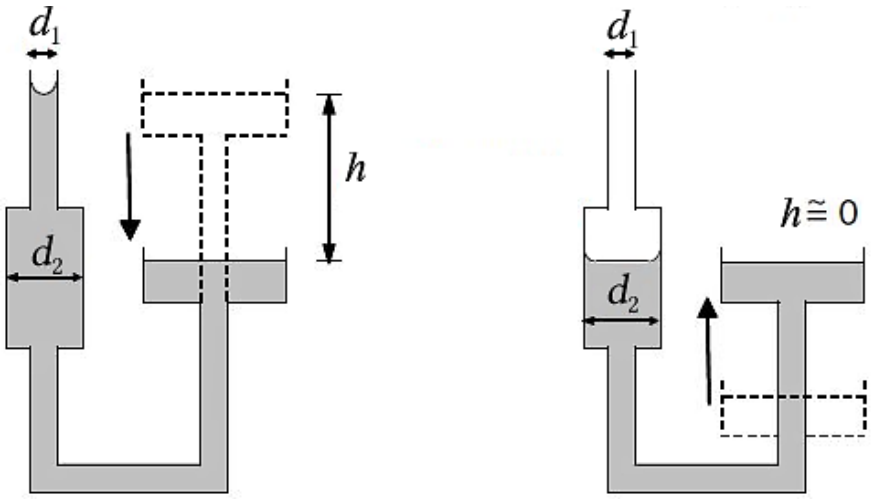

(a) (b)

Figure 2.30 Illustration of the ink-bottle effect. (a) Capillary drainage and (b) Capillary rise, from Laloui (2013)

The effect of hysteresis should be incorporated in utilizing SWCC to predict the matric suction from the moisture content (or vice versa) (Fredlund et al., 2012). As the moisture content of near-surface soils is likely to be affected by a rainstorm and dry periods of weather, it follows that many unsaturated soil in-situ experience changes in matric suction as a function of climate effects - especially as a function of seasonal changes. Thus, due to the seasonally repeated wetting and drying of unsaturated soil, the stiffness and strength of the soils may vary (McCartney & Khosravi, 2012) and will make the strain development unstable or difficult to predict during repeated loading (Birgisson et al., 2007).

SWCC is widely utilized to present the relationship between matric suction and moisture content in the soil. Figure 2.31 (a) shows the hysteresis in the SWCC of silty soil during wetting and drying processes, and (b) demonstrates the different trends of SWCC in various soils (Fredlund & Xing, 1994).

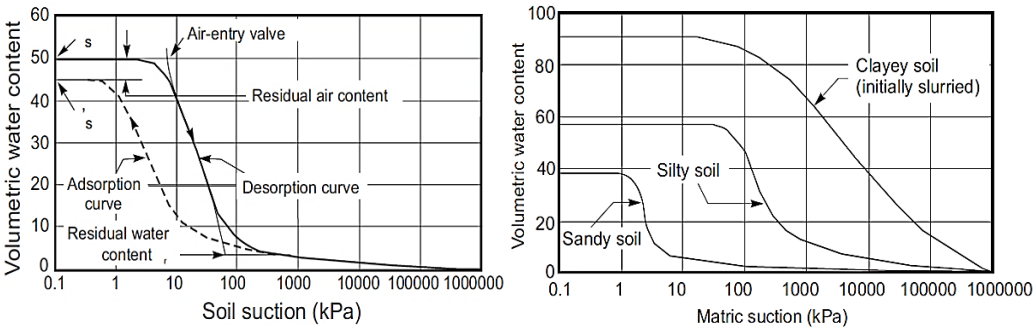

Figure 2.31 (a) Hysteresis in SWCC of silty soil, (b) SWCC for sandy, silty and clayey soils, from Fredlund & Xing (1994)

The SWCC from clayey soils (SC) also shows that the matric suction-moisture content relationship is hysteretic- it differs in wetting and drying conditions, as shown in Figure 2.32.

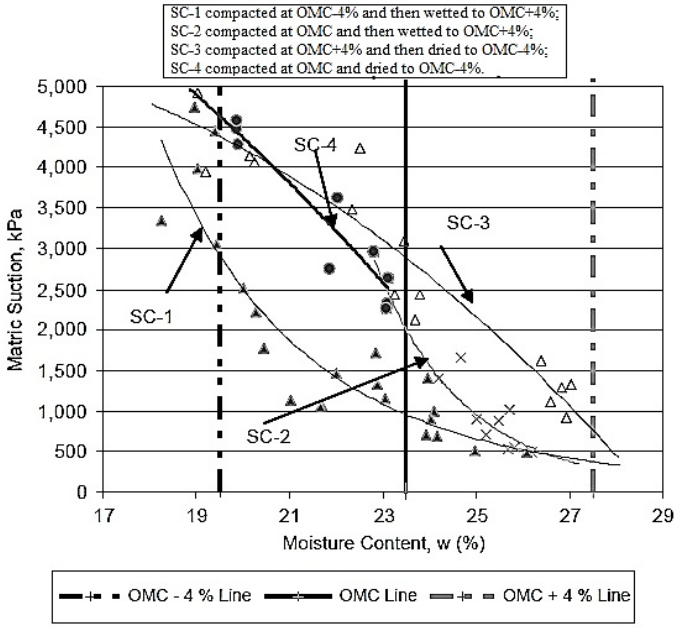

Figure 2.32 SWCC for compacted clay soils, from Khoury & Zaman (2004)

Several elastoplastic models have been developed to investigate the effect of void ratio on the water retention response of unsaturated soil, associating the variation of S with the changes of void ratio and matric suction (e.g. Sun et al. (2007); Mašín (2010)). SWCCs for various void ratios during wetting are presented in Figure 2.33 (Sun et al., 2007). Their results generally demonstrated the relation of suction to the void ratio.

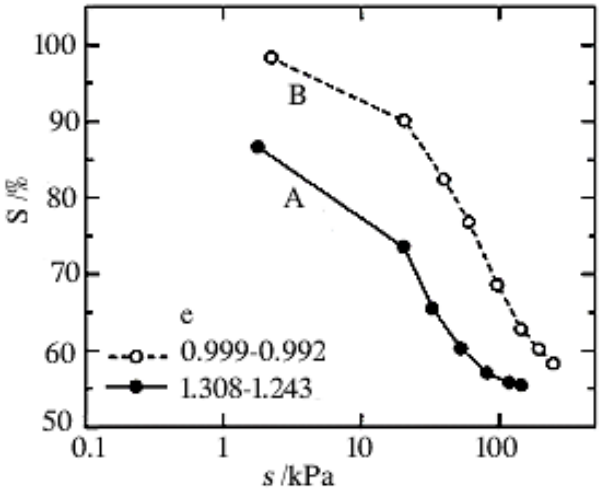

Figure 2.33 SWCC for various void ratios during wetting, from Sun et al. (2007)

The equation proposed by Mašín (2010) is expressed as

$$\dot{S} = \frac{\partial S}{\partial \psi_m}\dot{\psi_m} + \frac{\varphi - S}{e}\dot{e} \tag{2.50}$$

where φ is the effective stress rate factor, and $\dot{S}$, $\dot{\psi_m}$ and $\dot{e}$ indicate the variation in S, ψ_m and e, respectively.

The first term quantifies the dependency of S on suction at a constant void ratio (i.e. SWCC at a constant void ratio), and the second term indicates the dependency of S on void ratio at a constant matric suction. Figure 2.34 (a) and (b) illustrate the effects of the void ratio on the SWCC. λ_p is the slope of SWCC and λ_{p0} is the set reference value.

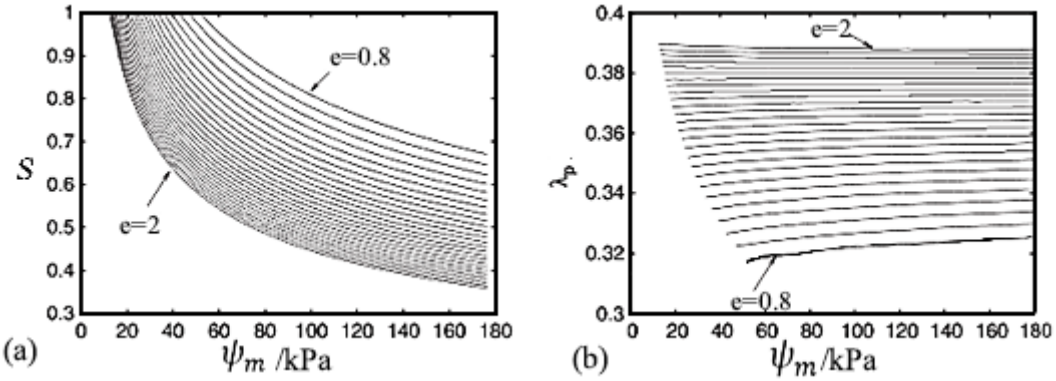

Figure 2.34 (a) Dependency of SWCC on void ratio and (b) dependency of the slope λ_p of the SWCC on ψ_m and e for reference values λ_{p0} = 0.38, s_{e0} = 15 kPa and e_0 = 1.75, from Mašín (2010)

2.5.3 Measurement techniques

(1) Moisture content

Moisture content plays a significant role in evaluating water flow movement in the pavement or railway track. It contributes to revealing the saturation condition. Two groups of methods are developed to measure moisture content, i.e. destructive methods (i.e. gravimetric methods) and non-destructive methods (Dawson, 2008), as shown in Table 2.8. Their features are also summarized and included.

Table 2.8 Summary on the measurement methods of moisture content, adapted from Dawson (2008)

Methods	Features
Gravimetric methods	Simple to conduct, accurate to calibrate other measurement techniques, destructive sampling, inapplicable to in situ real-time measurements
Neutron scattering method	Accurate and precise, inapplicable to automated monitoring due to radioactive source being attended
Time domain reflectometry	ND electromagnetic technology, precise transit time and moisture content measurement with a resolution of 10 picoseconds and 0.1% respectively
Ground penetrating radar	Larger detected soil volume, air/ground launched, non-invasive, resolution and depth of range of the electromagnetic wave dependent of antenna
Capacitance measurement	Non-linear relationship of capacitance and moisture content influenced by soil types
Nuclear magnetic resonance	Fast, NDM with high precision, costly, not suitable for field use and highly dependent on sample calibration
Near infrared reflectance spectroscopy	Accurate, complex calibration and not suitable as routine methods
Seismic methods	Accurate, complex calibration and not suitable as routine methods
Methods based on the thermal properties	Costly and longer measurement time (Veenstra et al., 2005)

(2) Permeability

The saturated permeability can be evaluated in the laboratory or field tests. The laboratory tests include constant head permeability tests, falling head tests and oedometer tests. The field tests consist of pumping tests, injection tests and tracer tests. The direct measurement techniques of permeability in unsaturated soil can be grouped into steady and unsteady methods (Fredlund & Rahardjo, 1993), as shown in Table 2.9. However, generally, the direct measurements are time-consuming, especially for low moisture content conditions. As matric suction increases, the shrinkage of the soil will disrupt the continuity of the water flow. Consequently, the functional coefficient of permeability of the soil mass will not be readily measured by direct methods in the laboratory. The indirect measurements also exhibit limitations, e.g. it is difficult to determine the water volume change accurately, and evaporation will increase the error of measurement.

Table 2.9 Summary of methods for measuring permeability in unsaturated soil, adapted from Dawson (2008)

Methods	Features/Laboratory/field
Steady state methods	Under a constant matric suction, time consuming, difficult to measure low flow rate accurately, laboratory
Thermal methods	Much quicker while not as accurate, laboratory
Instantaneous profile methods	Much quicker while not as accurate, laboratory/field
Multi-step outflow methods	Much quicker while not as accurate, laboratory
Tension infiltrometer methods	Useful for characterizing soil structures, accurate, simple, but difficult to acquire the parameters required and control initial conditions, field
Cone penetrometer methods	Continuous, repeatable, reliable and cost saving, field (Lunne et al., 1997)

(3) Matric suction

Generally, matric suction needs to be measured in practice. Thus, the principal measurement methods of matric suction are presented in Table 2.10.

Table 2.10 Summary of common laboratory and field techniques for measuring matric suction, from Dawson (2008)

Technique/Sensor	Suction component	Measurement range /kPa	Equilibrium time	Laboratory /Field
Tensiometers	Matric	0-100	Several minutes	Laboratory Field
Axis translation techniques	Matric	0-1500	Several hours-days	Laboratory
Electrical/thermal conductivity sensors	Matric	0-1500	Several hours-days	Laboratory Field
Contact filter paper method	Matric	0-10000	2-5 days	Laboratory Field
Non-contact filter paper method	Total	1000-10000	2-14 days	Laboratory Field

2.5.4 Moisture variation

It has been demonstrated that rainfall and drainage play a dominant role in influencing the moisture variation in the pavement subsurface structure (Van Sambeek, 1989; Dawson & Hill, 1998a). By considering these conditions, the range of moisture variation could be determined through previous field investigation, numerical simulation and laboratory studies. Then, the effects of moisture content on soil behaviour can be investigated within a realistic range in compliance with that in

practice. The moisture variation was discussed from three aspects, i.e. field investigation, drainage effect and laboratory tests.

(1) Field investigation

Field investigation has been conducted to reveal seasonal variations of moisture in pavement structures (Heydinger, 2003; Dawson, 2008; Erlingsson et al., 2017). Heydinger (2003) analysed the data from seasonal monitoring program instrumentation at the Ohio Strategy Higher Research Program Test Road (US-23, Delaware County, Ohio). The subgrade soil at the site was classified as A-6 soil (Plastic clay) by AASHTO or CL(Clay) by USCS, with a specific gravity of 2.7. Its optimum volumetric moisture content (w_{vol}) is 31% and 22% by standard and modified Proctor procedures, respectively. The analysis results of data for subgrade soils are presented in Figure 2.35. The measured w_{vol} during TDR probe installation and corresponding gravimetric moisture content (w) are presented in Table 2.11 for AC and PCC pavement sections. The variation of w relative to the OMC (i.e. Δw) was calculated, which ranged from -4% to +7%.

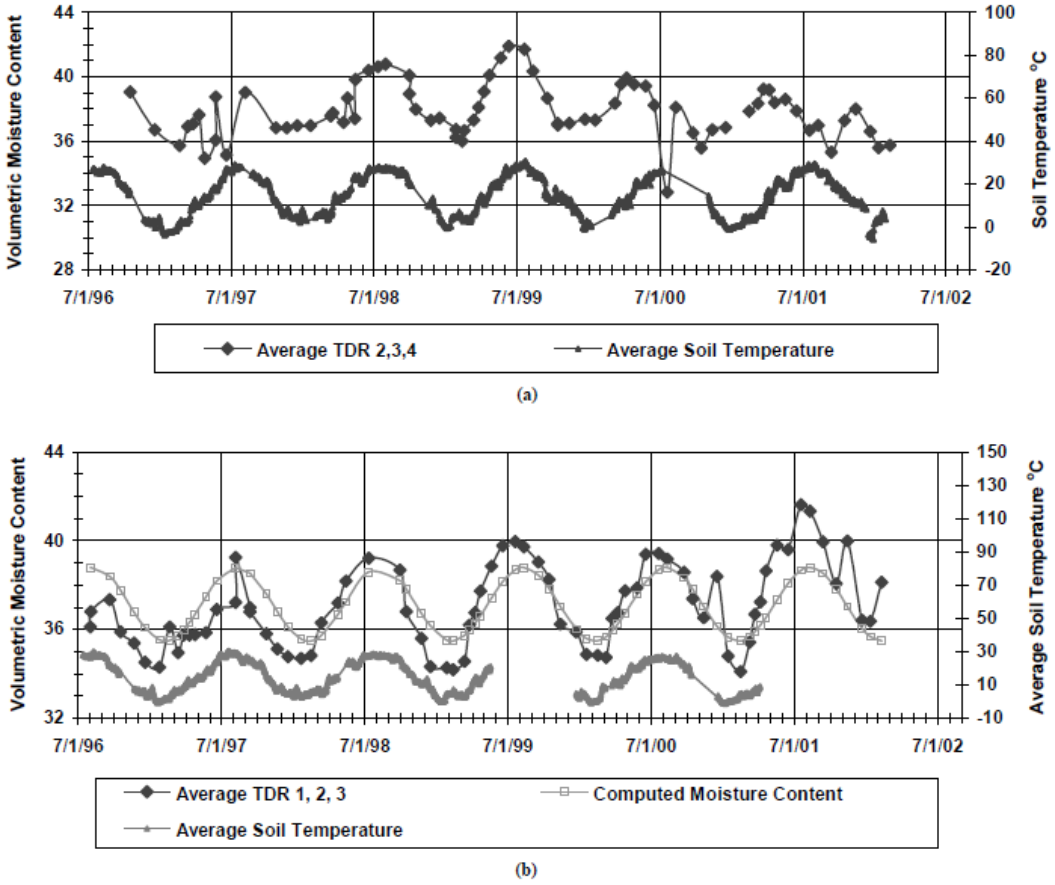

Figure 2.35 Average w_{vol} and soil temperature for (a) PCC and (b) AC, from Heydinger (2003)

Table 2.11 VMC and GMC for AC and PCC sections, adapted from Heydinger (2003)

Road type	Optimum w_{vol} /%	Optimum w /%	w_{vol} range /%	w range /%	Δw /%
AC	31	11.48	35~42	12.96~15.56	+1.48~+4.08
	22	8.15			+4.81~+7.41
PCC	31	11.48	20~24	7.41~8.89	-4.07~-2.59
	22	8.15			-0.74~+0.74

The measurement of in-situ moisture contents in a low-traffic pavement is presented in Figure 2.36 and Figure 2.37 (Dawson, 2008). The flexible pavement consists of 6 cm thick bituminous surfacing, granular base and clayey subgrade. The results show that the pavement edge was the critical zone with a moisture content 2% higher than that near the centreline. From Figure 2.36, the moisture content measured by TDR was nearly equal to 7% during days with no or little rain, while the moisture content of the subgrade could increase from 10% up to 20% and above (Dawson, 2008). For the granular base, the variation due to rainfall was no more than 2%. From Figure 2.37, the variation of the average monthly moisture content was 2% and 5% near the pavement centreline and edge, respectively.

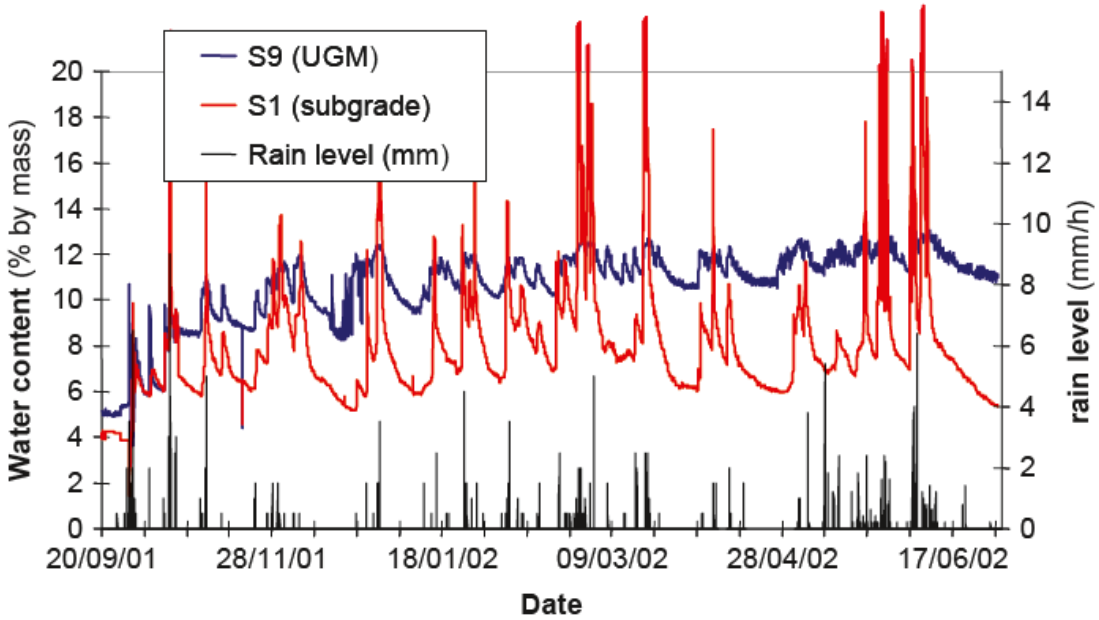

Figure 2.36 Water content variations in the granular base (S9) and in the clayey subgrade (S1) of a low traffic pavement, near the pavement edge, from Dawson (2008)

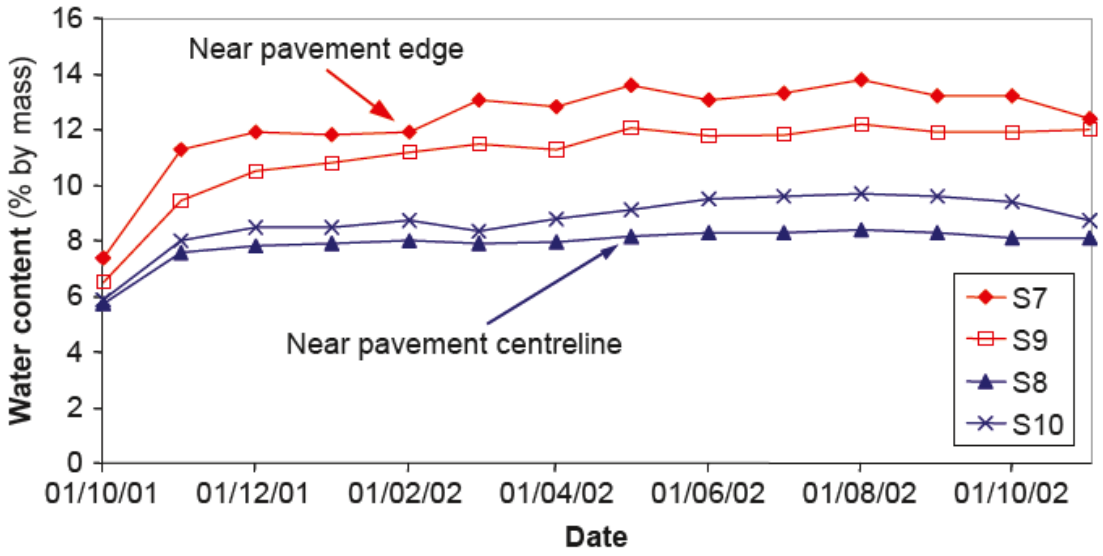

Figure 2.37 Monthly average water contents in the granular base, at the centre and near the edge of the pavement, from Dawson (2008)

The monitored VMC and the daily precipitation at two locations in Sweden over one year are presented in Figure 2.38 (Erlingsson et al., 2017). This data is for a seasonally freezing subgrade – hence the sharp reduction of moisture content when winter comes – and the reason that the higher soil gets a reduction in moisture content earlier than the lower soil and gets a higher moisture content in spring earlier, too. The corresponding GMC was estimated, as shown in Table 2.12. Δ represents the variation of GMC, and it showed a similar magnitude in the subgrade at the two sites.

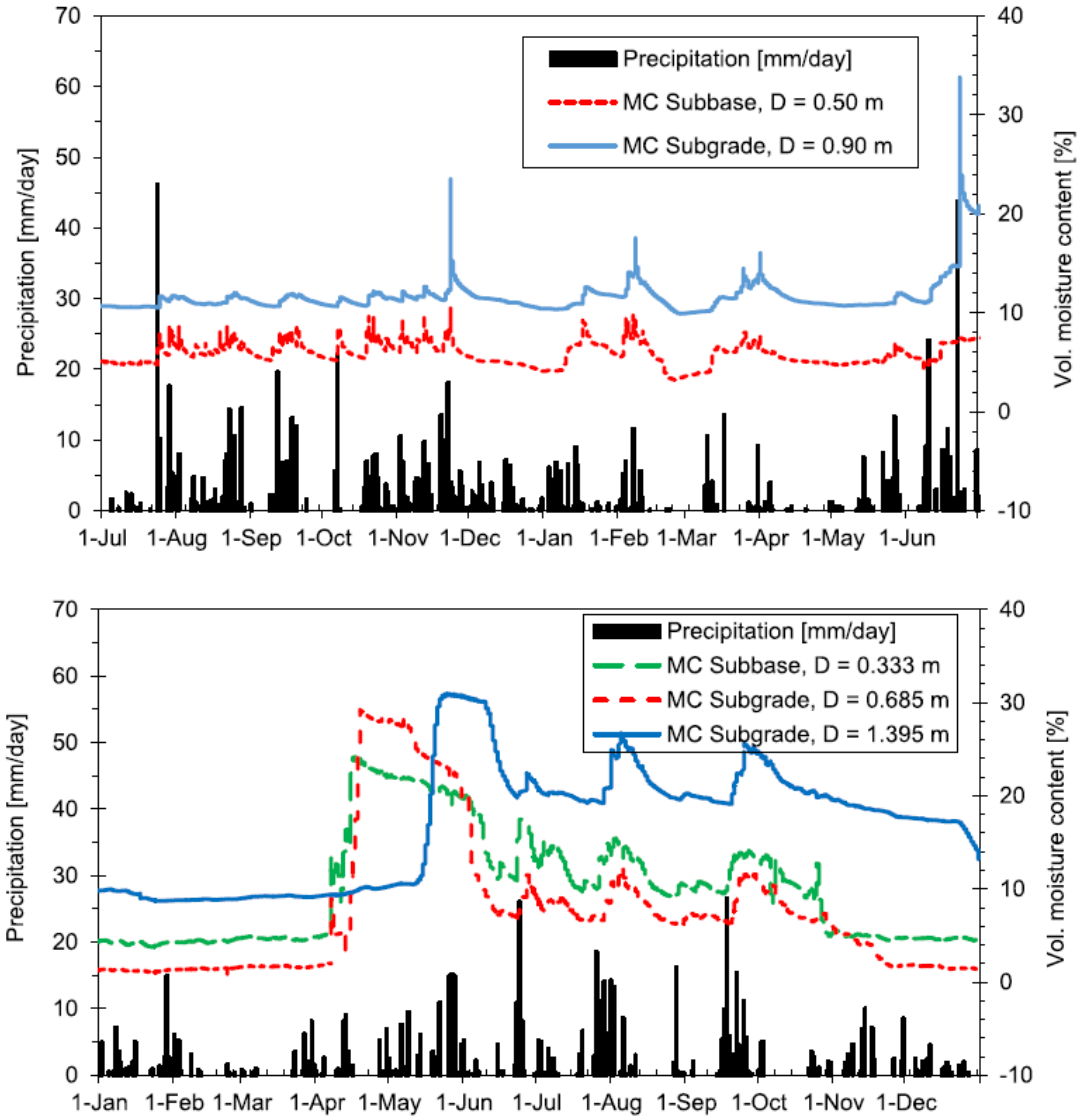

Figure 2.38 Monitored VMC and daily precipitation at two locations in Sweden during one year. (top) Torpsbruk site from 01/07/2010 to 30/06/2011, (down) Svappavaara site from 01/01/2015 to 31/12/2015, from Erlingsson et al. (2017)

Table 2.12 Moisture content variation of subbase and subgrade at two sites, adapted from Erlingsson et al. (2017)

Layers	Moisture content /%	Torpsbruk	Svappavaara
Subbase	w_{vol}	4~10	6~24
	w	1.83~ 4.57	2.74~10.96
	Δw	2.74	8.22
Subgrade	w_{vol}	12~34	2~30
	w	5.48~15.53	0.91~13.7
	Δw	10.05	12.79

(2) Drainage simulation

Based on the analysis by Alonso et al. (2002), it was found that as the depth of the drain increased, the degree of saturation at equilibrium decreased, as shown in Figure 2.39. The drainage effects were improved. When the drain was installed at a depth of 4.5 m, the variation of the degree of saturation in the subbase (i.e. Point D, E and F) were 0.3, 0.32 and 0.45, respectively, which may provide a reference for the possible moisture variation in the subgrade.

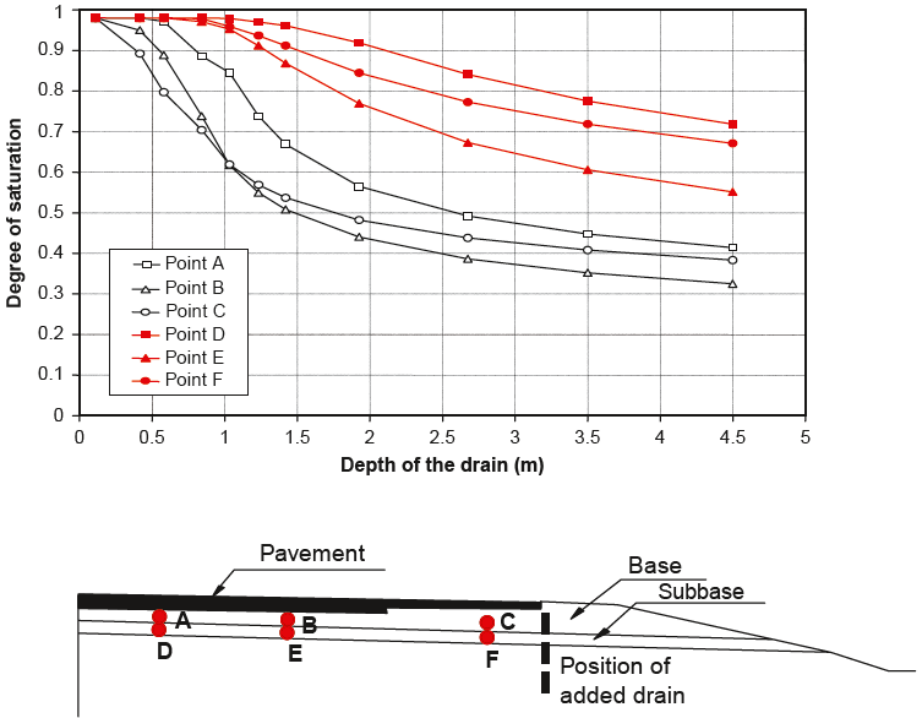

Figure 2.39 Degree of saturation at equilibrium when a drain is installed at the pavement-shoulder contact, from Alonso et al. (2002) and Dawson (2008)

Ghavami et al. (2019) simulated the variation of the degree of saturation in subgrade under different drainage conditions after rainfall, as illustrated in Figure 2.40 and Figure 2.41. According to Hassan & White (1996), a rainfall event was consecutively applied in four steps, shown in Table 2.13. With the drainage layer, the degree of saturation after rainfall decreased by about 20%. From Figure 2.41, the effects of edge drain were demonstrated, and it reduced saturation by 15% in the subgrade.

Table 2.13 Rainfall event details, adapted from Hassan & White (1996)

Flow time /hours	Rainfall intensity /cm·hr^{-1}	Raining/draining conditions
1	0.37	Simultaneous raining and draining
2	0.19	
3	0.15	
4	0.37	
5	0.95	
6	0.87	
7-15	<0.2	Draining only
16	0.9	Simultaneous raining and draining
17	2.47	
18-68	<0.2	Continuous draining only

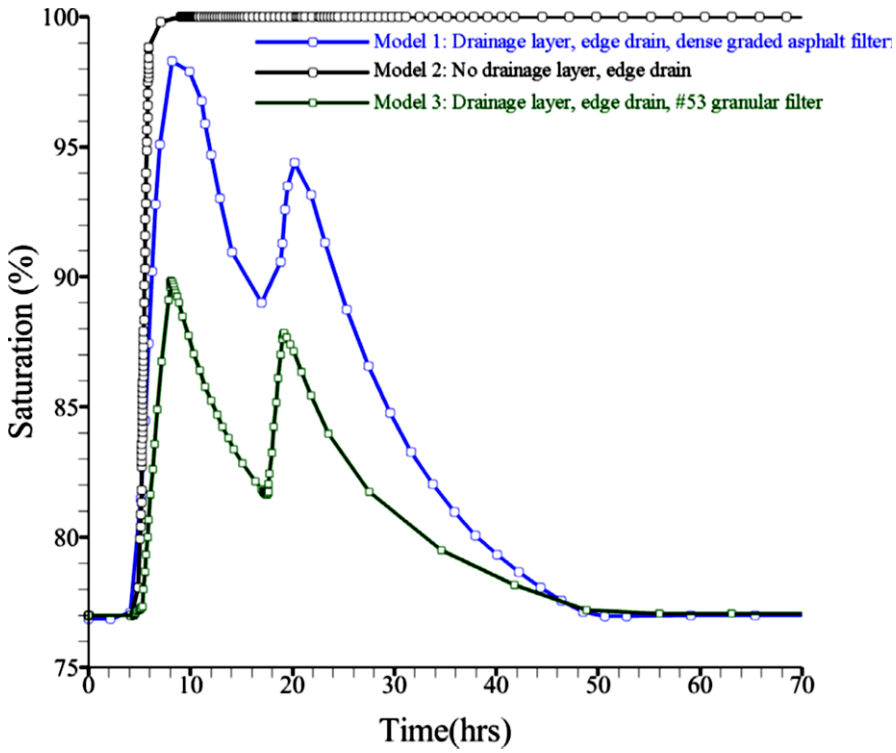

Figure 2.40 Subgrade saturation evolution after rainfall of Models 1, 2 & 3, from Ghavami et al. (2019)

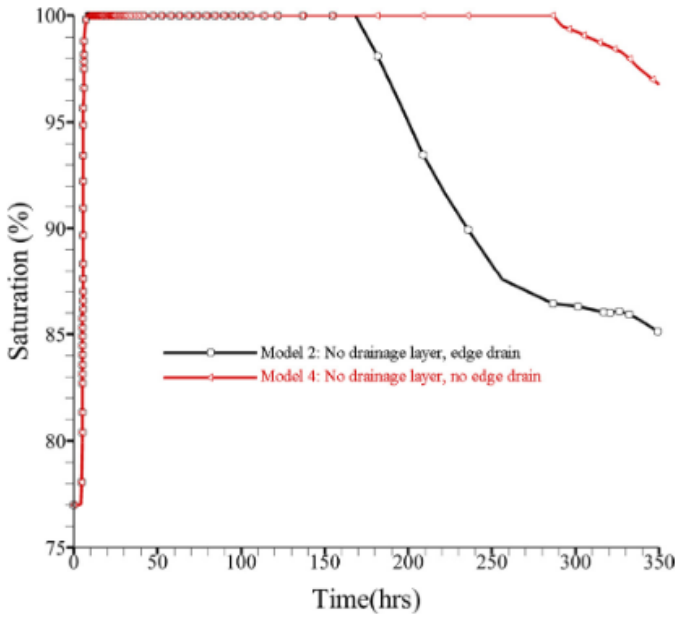

Figure 2.41 Subgrade saturation evolution after rainfall of Models 2 & 4, from Ghavami et al. (2019)

(3) Laboratory studies

Previous studies were reviewed with a focus on the laboratory unsaturated triaxial tests (Brown et al., 1987; Ooi et al., 2004; Yang et al., 2005; Zaman & Khoury, 2007; Khoury et al., 2009; Sawangsuriya et al., 2009; Ozel & Mohajerani, 2011; Han & Vanapalli, 2016b; Khoury, 2018). PI values of all these soils involved varied from 6 to 52. Based on the repeated load triaxial tests, the effects of moisture on the resilient modulus of subgrade were studied generally within a range from OMC-4% to OMC+4%. This range is meant to simulate the possible moisture content variation attributed to the drying and wetting paths in subgrade soils. Detailed analysis of the moisture content and its relationship with resilient modulus was also conducted, as presented in Chapter 3. Considering the severe consequence of subgrade at saturated conditions, saturated triaxial tests should also be conducted. Compared with the drying side of OMC, the wetting side is more critical to influence pavement performance due to the reduction of suction in the subgrade. This may provide a reference for the moisture variation during laboratory testing design.

2.6 Drainage methods

2.6.1 Subsurface drainage

The entry of water into a road pavement was described at the start of Section 2.5.1

(see Table 2.7). Strategies of subsurface drainage were presented by Christopher & McGuffey (1997), including the utilization of permeable base, underdrains, edge drains, filters, outlets and prefabricated geocomposite edge drains. The lateral or median drain may be taken as the most effective drainage route, provided that an underdrain with high conductivity and connecting to the lateral/median drain is included (Dawson & Hill, 1998b).

Regarding subsurface drainage, two general types of subsurface drainage criteria were used by Ridgeway (1982): (a) a time for a certain percentage of drainage and (b) an inflow-outflow criterion. Several combinations of criteria and equations were selected to calculate the required permeability of the drainage layer. Therefore, the effectiveness of the methods could be quantified by measuring and comparing the moisture content or the time to achieve the given moisture content in the corresponding sections.

However, studies on the effects of drainage on foundation performance may still be rare or not comprehensive. They may focus on one of the mechanical properties (e.g. resilient modulus) influenced by drainage rather than consider the properties together. The drainage effects on the subgrade soils and further on the whole structure are not fully explored. Consequently, our knowledge of the sensitivity of foundation response to drainage may still be insufficient for pavement and railway track design.

The following methods for pavement drainage are taken as examples and, following the research by Dawson (2008), the subsurface drainage methods (e.g. permeable base layers as drainage, transverse drainage, longitudinal drainage and underdrains) are demonstrated further. The discussion is mainly focused on the foundation drainage of pavements since that of railways may be similar except for the upper structures.

2.6.1.1 Permeable base layers

Due to high structural stability and permeability requirements, permeable base layers are often constructed by cement (or asphalt)-stabilized open-graded aggregate. For low- to medium-volume highways, it may be more economical to utilize unbound permeable aggregates with the required drainage capacity. Permeability usually shows an opposite trend with structural stability; thus, it should be a concern in the drainage design (Tao & Abu-Farsakh, 2008). White et al. (2004) found that both permeability

and structural stability of the unbound aggregate relied on the gradation, particle shape and angularity significantly.

The typical components of two types of drainage layer (permeable base layer or separate drainage layer) systems are illustrated in Figure 2.42. Two systems include an open-graded drainage layer (OGDL) employed jointly with a longitudinal edge drains/outlet pipe and a daylighted OGDL (Huang, 1993; Diefenderfer et al., 2005). According to the research by Huang (1993), it may be the most effective method to remove the infiltrated water in the pavement structure in the shortest drainage time. Thus, the duration of time at a high water table will decrease in the pavement/track structure. The details of the outlet pipe are shown in Figure 2.43. However, if an efficient collector is not installed for the drainage layer, the drainage layer will serve as a moisture reservoir and further induce hazards. With respect to the railway track foundation, it may have a similar design to that of pavements, as illustrated in Figure 2.44.

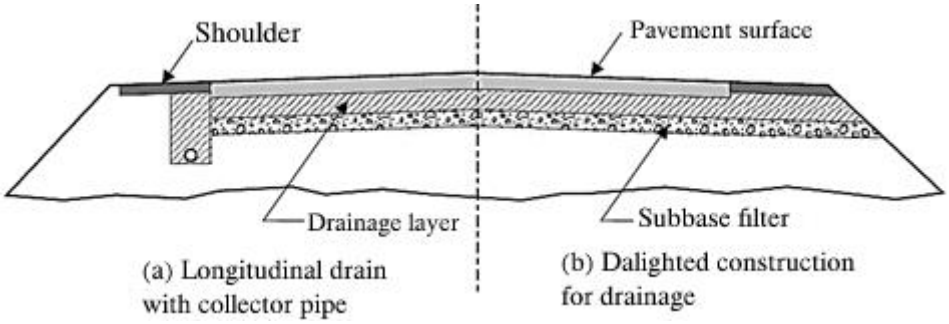

Figure 2.42 Typical components of drainage layer systems with/without collector pipe, from Huang (1993)

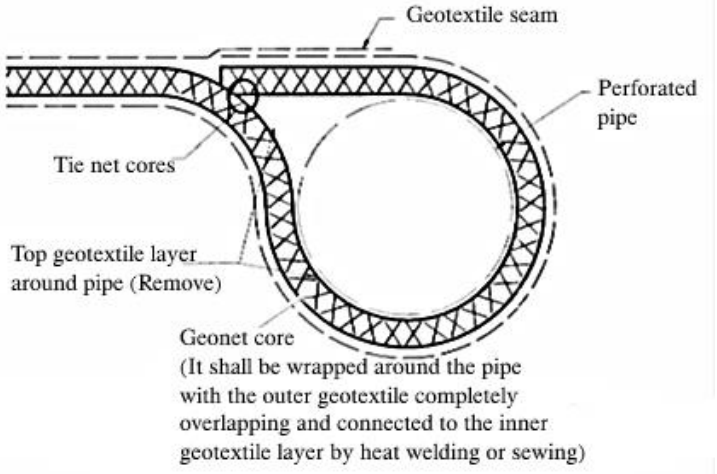

Figure 2.43 Details of the outlet pipe, from Helstrom et al. (2007)

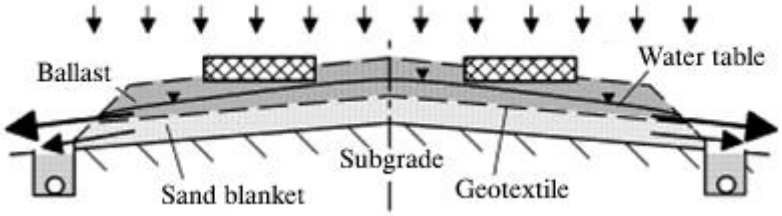

Figure 2.44 Drainage with permeable geotextile below ballast in railway track, from Rushton & Ghataora (2014)

2.6.1.2 Transverse drainage

Transverse drains are set perpendicular to the centreline of the carriageway, as illustrated in Figure 2.45. The transverse drains play a significant role in the transition areas, e.g. joints beneath concrete pavements, since the increasing deterioration of joints may allow water to infiltrate into the subsurface structure. Due to gravity, the water may be collected into the installed perforated collector pipes. Then, the drains will take the water into the side ditches through the pipes. However, distresses may be induced if the water bypasses the pipe.

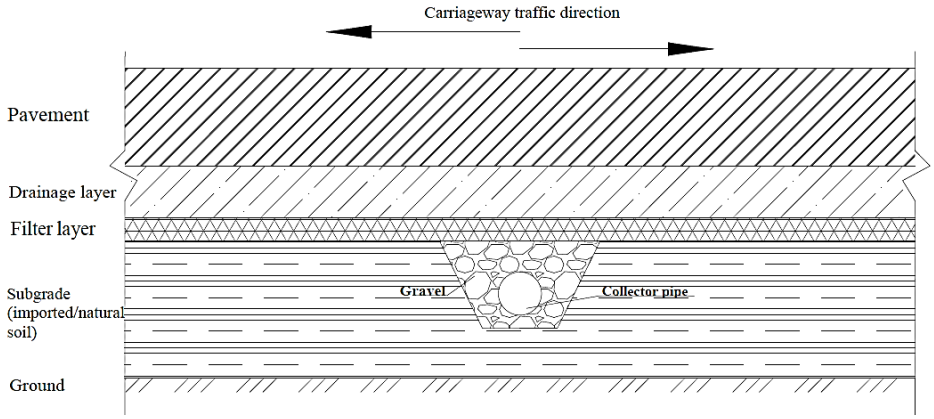

Figure 2.45 Perforated collector pipes as transverse drains in the foundation (Dawson, 2008)

2.6.1.3 Longitudinal drainage

Ditches or trenches are commonly employed as longitudinal drainage methods to prevent/intercept water from infiltrating the foundation of pavement/railway tracks. Currently, a geotextile-wrapped perforated carrier pipe with sufficient discharge capability or porous materials is placed at the bottom of the drains to remove the water. Granular materials with high permeability are used to surround the pipe. Typically, the base of the collector pipe is about 0.5 m from the bottom of the layer to be drained and lies at depths between 1.2 to 2 m below the surface (Dawson, 2008). The geotextile will serve as a filter stopping the migration of fine soil particles, yet without becoming

clogged by particles of soil that would result in a significant reduction in permeability and, hence, function. A typical longitudinal drain is presented in Figure 2.46 (Lebeau & Konrad, 2009). The drain is set at the edge of structures in parallel with the foundation's centreline. When the water level decreases below the drain, the drain will benefit from removing water from the overlying layer or side areas. When the water table rises above the drain, the drain will also remove the water from the subgrade to lower the water table. Lebeau & Konrad (2009) found that drainage time relied on the saturated and effective relative hydraulic conductivity of granular base and subbase materials. Four drainage patterns with different flow paths were revealed as the saturated hydraulic conductivity of subbase materials increased, as illustrated in Figure 2.47. These flow patterns showed different characteristics: a) lateral drainage in a base with relatively high horizontal permeability over a subbase with lower horizontal permeability; b) composite flow where both base and subbase have comparable horizontal permeabilities, but the subbase has a lower vertical permeability; c) vertical flow where the base has a low horizontal permeability compared to that of the subbase; d) funnelled flow where the subgrade has high vertical and horizontal permeabilities compared to the base. It should be noted that in all these, an impermeable subgrade has been assumed.

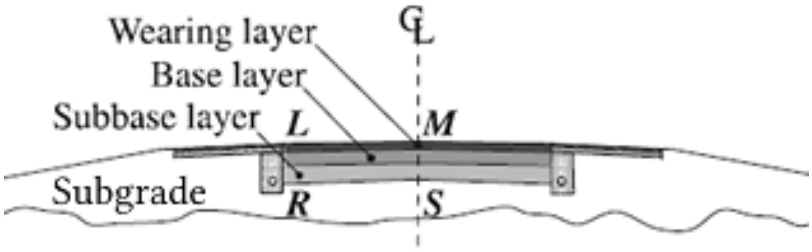

Figure 2.46 Cross section of pavement, including an edge drain, from Lebeau & Konrad (2009)

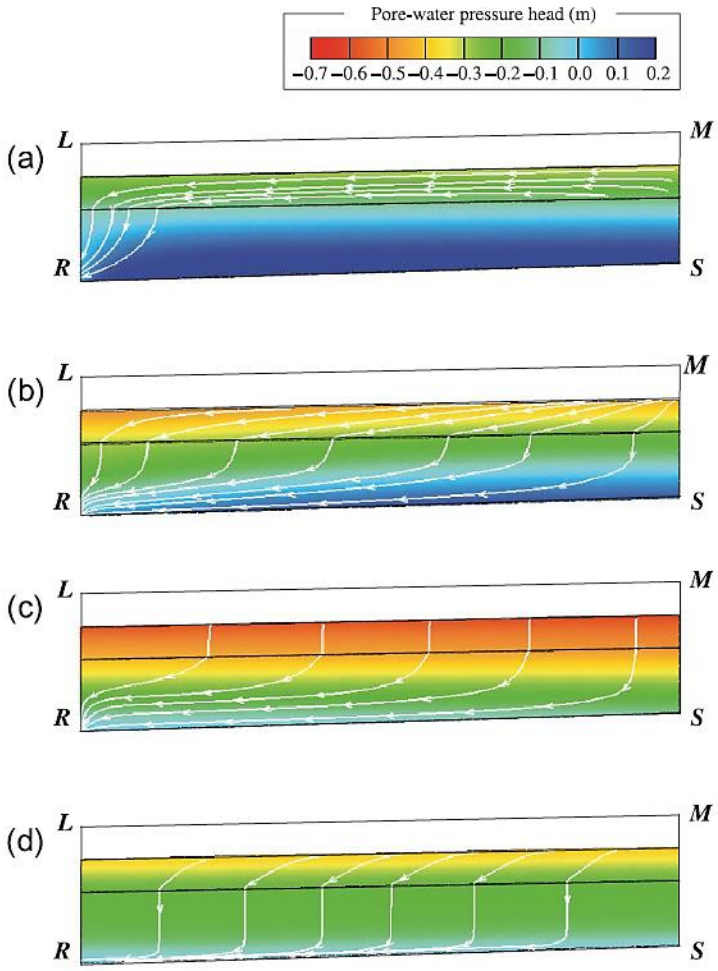

Figure 2.47 Four flow patterns in a pavement. (a) lateral flow, (b) composite flow, (c) vertical flow and (d) funnelled flow, from Lebeau & Konrad (2009)

2.6.1.4 Underdrains

Underdrains can be placed in a trench filled with drainage materials wrapped in geosynthetics (e.g. geotextile). They tend to be constructed centrally right below the position to be drained. A type of underdrain is shown in Figure 2.48.

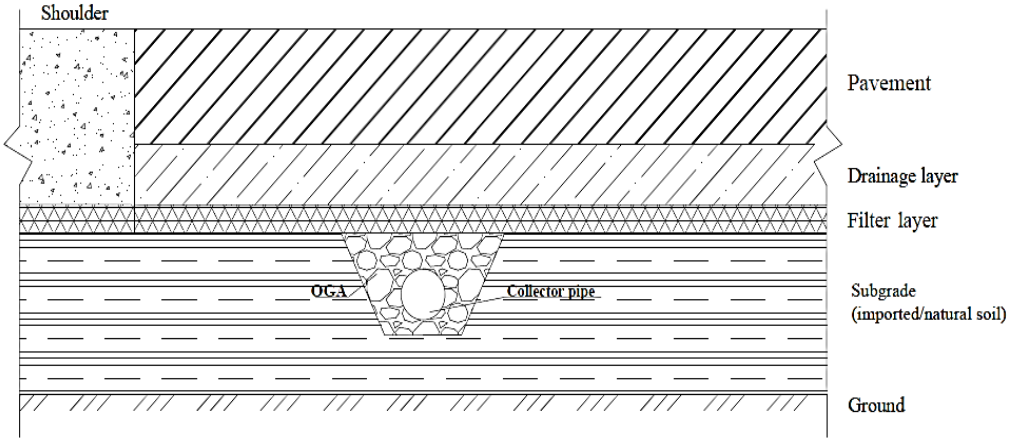

Figure 2.48 Underdrains (Open-graded aggregate) (Dawson, 2008)

2.6.2 Drainage effects on mechanical response

Generally, through drainage, the dissipation of excess pore water pressure in the pavement/track structures will be accelerated. Therefore the loading exerted by the vehicles can be transferred from the pore water to the skeleton of the soil and the foundation will show an improved mechanical response. Drainage strategies prevent water from entering the pavement and remove any existing water into the edge drains. Thus, effective stress will be promoted, and moisture content (or degree of saturation) will decrease to some extent. Then, the negative pore water pressure may increase, i.e. the matric suction, which contributes to the bearing capacity of the underlying soil. As introduced in the Section 2.4.3 and Section 2.4.4, reduced moisture content and increasing matric suction will enhance the structural stability of foundations in pavement/railway track systems. Previous studies (Helstrom et al., 2007; Nazzal et al., 2010; Bahador et al., 2013) investigated the benefits of including a properly constructed drainage layer and showed that pavement structures would not be weakened by including a drainage layer while the strains would be reduced by the drainage.

The study by Ji & Nantung (2015) reported that the moduli of subgrade materials were strongly influenced by adding a drainage layer. For example, a subgrade median modulus of sections with a permeable layer was about double the modulus of the undrained sections. Based on deflection monitoring, the road section with the geocomposite membrane (i.e. a low modulus polyvinyl chloride layer sandwiched between two nonwoven geotextiles) consistently showed less deflection than that without the drainage layer (Al-Qadi et al., 2004). Bahador et al. (2013) found that woven fibreglass and nonwoven polypropylene geotextiles can reduce the total plastic deformation by up to 55 and 35% in paved road sections and by up to 60 and 30% in unpaved road sections, correspondingly, subject to the aggregate base course and asphalt thicknesses. With free-to-drain, the resilient modulus of track foundations showed an increase with the number of cycles and increasing shear stress below the threshold level (Mamou et al., 2017).

However, subsurface drainage features may not benefit all sites and conditions (Diefenderfer et al., 2005). Poor drainage will also induce premature failures to the structures with increasing heavy-duty loads. Thus, suitable drainage strategies should be considered according to the practical conditions to achieve an effective removal of moisture in the underlying structure.

2.6.3 Effectiveness of drainage

The effectiveness of drainage has been investigated within different types of drainage methods. For example, flexible pavement could exhibit a lower deflection by including a subsurface open-graded drainage layer on the subbase with a longitudinal collector pipe since the drainage would maintain the subgrade in a relatively dry state (Diefenderfer et al., 2005). For an asphalt pavement section, the presence of a drainage layer (i.e., a permeable base that was 10 cm thick and 8 m wide with a cross-slope of 2%) reduced the degree of the saturation in the subgrade with a maximum value of 87%, while the subgrade of the section without drainage layer was always saturated (100%) (Ghavami et al., 2016). In terms of underdrains, it is reported that the water table level varied under different conditions, i.e. with and without underdrains. The effects of underdrains on the water surface are illustrated schematically in Figure 2.49. The depth to the water table shows a maximum value at the position right above the underdrain, which has fewer effects with transverse distance from the underdrain (Neale, 2016).

Many researchers investigated drainage methods with permeable geosynthetics in roads or railways, e.g. (Elseifi et al., 2001; Al-Qadi et al., 2004; Fatahi & Khabbaz, 2011; Fatahi et al., 2011; Rushton & Ghataora, 2014). In practice, permeable geotextiles are commonly set between the ballast or sub-ballast and a sand blanket. Geosynthetics with relatively high lateral and transverse permeability can benefit drainage. However, in terms of drainage time, the effectiveness of geocomposites (i.e. those having a highly permeable, lateral core with transversely permeable geotextiles above and below the core) may vary according to the location (Rushton & Ghataora, 2014). The study by Wang et al. (2017) presented that the wicking geotextile could effectively remove water from the road cross section prepared even when the soil was near its optimum moisture content condition. It also implied an effective distance of the geotextile from the soil, which may apply to other permeable or geocomposite drainage layers.

They can also elevate the drainage capability for the capping layer and prevent fine particles from migrating between fine-grained and coarse-grained layers. Woven geotextiles may clog with time and act almost as a plastic sheet retaining water in the subgrade. Thus, geotextiles in the track structure of railroads should be non-woven and needle-punched materials (Fatahi et al., 2011).

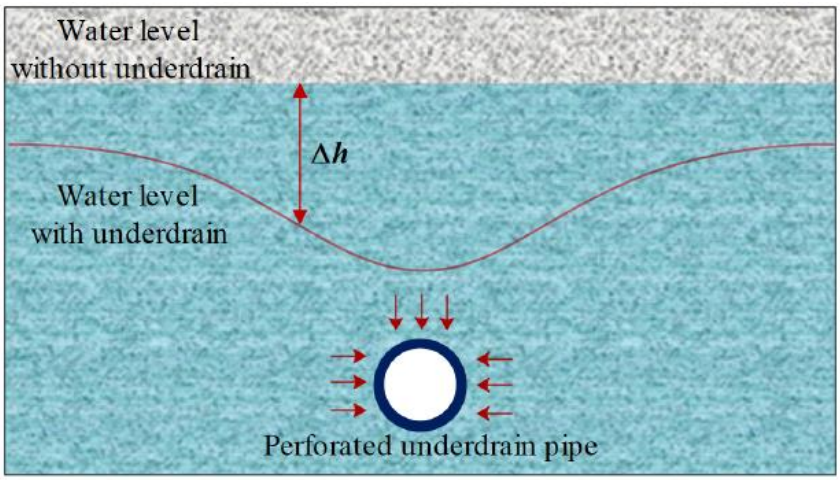

Figure 2.49 Water surface reduction due to underdrains, adapted from Neale (2016)

In terms of the factors affecting drainage, even though pavement/trackbed drainage is beneficial for the rapid removal of excess water, advantages from a subsurface drainage system vary with structural types, rainfall, geometric design and hydraulic properties of materials (Huang, 1993). A rapid water removal could be achieved with the geonet drainage composite placed at the subgrade or below the subgrade. It is also found that the placement of such a drainage layer showed better performance in removing the most damaging waters present during the spring thaw (Christopher et al., 2000). From the study by Raymond et al. (2000), the installation of a drainage system did not stop pumping, i.e. the migration of clay/silt-sized subgrade fines. Under partially drained cyclic loading conditions, the maximum values of volumetric strain showed an upward trend with soil drainage path length. The permeability of the drainage system played a major role in its performance. For a permeable drainage base layer, its drainage effectiveness could be maintained by increasing the hydraulic conductivity and the thickness of the base (White et al., 2004). It was also found that reduced permeabilities (e.g. 10% of the original values) of ballast and subballast due to fouling could induce higher maximum water table and slower fall in the water table, and increased subgrade slopes improved the drainage performance (Rushton & Ghataora, 2009). It is reported that the drainage time of a multilayer pavement relied on both the saturated hydraulic conductivity of the subbase material and the effective relative hydraulic conductivity of the subbase material at the interface of the base and subbase layers (Lebeau & Konrad, 2009; Papanicolaou et al., 2015), as well as the drainage in trackbed depended on the geometry and hydraulic properties of track foundations (Rushton & Ghataora, 2014). An open-graded aggregate layer combined with trenched longitudinal edgedrains and outlet pipes was stated as the most effective

method by Huang (1993), while the efficiency of a drainage system can be improved by incorporating a centre drain in a very wide pavement structure in addition to edgedrains (Mahboub et al., 2003).

Drainage strategies have been increasingly utilized in the design, whilst improper installation and inadequate maintenance of drainage components have often led to poor performance (Christopher & McGuffey, 1997). Without maintenance, pavements with subsurface drainage have been found to perform as poorly as pavements without subsurface drainage. Clogged outlet pipes posed a detrimental effect on the performance of flexible pavements, e.g. increased fatigue cracking, rutting and stripping (ARA, 2004). Following the Federal Highway Administration Federal Highway Administration (1994) definition, the Quality of Drainage is introduced to investigate the effectiveness of the drainage method, also known as the Time to Drain method. Table 2.14 presents drainage quality from 'excellent' to 'very poor' according to the FHWA and AASHTO guide. The time required to reduce the degree of saturation from 100% to 85% or to achieve 50% drainage is recorded to measure the effectiveness of drainage.

Table 2.14 Levels of drainage effectiveness

Effectiveness of drainage	Time to drain	
	FHWA	AASHTO
	85% Saturation	50% Drainage
Excellent	< 2 hours	< 2 hours
Good	2-5 hours	1 day
Fair	5-10 hours	7 days
Poor	>10 hours	1 month
Very poor	>>10 hours	Does Not Drain

2.7 Multi-layered elastic analysis

Given their significant role in transport and their potential economic value and subgrade sensitivity to moisture contents, the structural response of pavements and railway tracks needs to be well understood so that they can be adequately designed – especially as, in practice, deterioration (e.g. surface cracking) has been identified in pavements built to be long-life (Wang et al., 2012). Through experimental analysis, such as laboratory-controlled or field tests, more realistic results can be achieved

relative to computer-based simulation analysis. This experimental approach is straightforward and useful in some circumstances. However, the application of any findings to different conditions (e.g. different environments, loading conditions and material properties) may not be valid. Numerical analysis, as an alternative, employs advanced computer technology (Ghadimi & Nikraz, 2017).

In terms of railway tracks, multi-layered elastic (MLE) theory is a common way to analyse the substructure based on elastic theory and multi-layered system. Thus, many studies have been performed based on the multi-layered elastic theory in terms of the MLE-based programs, e.g. FEART (Fateen, 1972), ILLITRACK (Robnett et al., 1975), GEOTRACK (Chang et al., 1980) and KENTRACK (Rose et al., 2014). Previous studies (Teixeira et al., 2006; Burrow et al., 2007; Rose et al., 2011) based on these programs have proven that it is possible and applicable to utilize MLE methods for the performance-based railway track design. However, it is not realistic to consider all the structures, and thus this study focused on flexible pavements to demonstrate the MLE method.

Several mechanistic computer programs are available for pavement response analysis, e.g. 2-dimensional axisymmetric finite element programs (e.g. ILLI-PAVE and MICH-PAVE), 3-dimensional finite element programs (e.g. ABAQUS and DIANA) and multi-layered elastic (MLE) programs (e.g. CIRCLY, DAMA, KENPAVE, CHEVRON, BISAR, ELSYM5, VESYS, WESLEA, MnLayer and ERAPAVE). Many attempts have been made to investigate the structural response of pavement with finite element or difference methods (FEM or FDM), as shown in Table 2.15. However, the computation time and convergence issues could reduce the value of finite element methods, particularly when many simulations need to be performed. Due to their simplicity, the programs based on multi-layered elasticity are more widely used than finite element-based methods (Ghadimi & Nikraz, 2017). Such software can be used to explore the changing trend of pavement response to moisture content.

Table 2.15 Numerical studies on pavement response

Method	Program	Research objective	Reference
FEM	Viscoelastic continuum damage finite-element program	Fatigue-cracking mechanism in asphalt pavements	Mun et al. (2004)
FEM	Three-dimensional implicit dynamic finite element method	Effects of base and subgrade quality on the fatigue and rutting strains and the vertical surface deflection	Saad et al. (2005)
FEM	ABAQUS	Reinforcement effect of incorporating geosynthetic layer within the base course	Nazzal et al. (2010)
FDM	FLAC	Effects of a geocomposite drainage layer on pavement moisture distribution and plastic deformation	Bahador et al. (2013)
FEM	ABAQUS	The implementation of constitutive models in flexible pavements	Ghadimi & Nikraz (2017)
FEM	ABAQUS	Stress state of test tracks	Lu et al. (2020)

2.7.1 Multi-layered elastic method

The MLE method is commonly adopted as the stress-strain computational tool to achieve a mechanistic-empirical design of pavements and railway tracks. By taking flexible pavement as an example, it is assumed that all layers are numbered sequentially from top to bottom as 1 to n, with the n^{th} layer being an elastic half-space. The basic assumptions to be satisfied are (Huang, 2004):

a) Each layer is homogeneous, isotropic and linearly elastic with an elastic modulus and a Poisson ratio.
b) The material is weightless and infinite to an actual extent.
c) Each layer is of finite thickness, except that the lowest layer is infinite in thickness.
d) Uniform pressure is applied on the surface over a circular area of a limited radius.
e) Continuity conditions are satisfied at the layer interfaces, as indicated by the same vertical stress, shear stress, vertical displacement and radial displacement.

MLE methods exhibit some defects (Chen et al., 1995) in terms of their inability to model the nonlinear resilient behaviour of granular and cohesive soils in a realistic manner, the full (or zero) shear contact that must be assumed between layers and tensile stresses usually generated in a granular material which do not exist in the field. The precision will rely on the material properties assigned to each layer. Yet this approach can still be sufficiently reliable (Suh et al., 2010; Omer & Eghan, 2018) and offer the possibility of a rational solution to the problem (Hossain, 1998).

2.7.2 KENLAYER

The application of KENLAYER to the pavement is taken as an example to demonstrate the use of an MLE to predict pavement structural response. KENLAYER, as a part of KENPAVE by Huang (2004) for typical flexible pavements, can be applied to a multi-layered system under stationary or moving multiple wheel loads (e.g. single, dual, dual-tandem or dual-tridem wheels) with each layer responding differently (e.g. linear elastic, nonlinear elastic or viscoelastic). Based on KENLAYER, flexible pavement structures are analysed as an elastic multilayer system under a circular loaded area. For a linear elastic system, the superposition principle is adopted for multiple wheels. In a nonlinear elastic system, the solutions are superimposed iteratively with a method of successive approximations. It is competent to conduct damage analysis on a seasonal basis by dividing each year into a maximum of 12 periods and assigning a different set of material properties (i.e. modulus of elasticity and Poisson's ratio) in each period. A maximum of 12 load groups (either single or multiple) can be applied to each period. Then, the stress, strain and displacement at each point of the layers can be derived and transformed into pavement performance parameters with empirical models. The strength of KENLAYER lies within its capability of simulating flexible pavement structures either by linear-elastic, nonlinear-elastic and visco-elastic models or by the combinations of these models. Damage analysis can also be conducted for fatigue cracking and permanent deformation, which dominate the pavement design. The main interface of KENLAYER is illustrated in Figure 2.50.

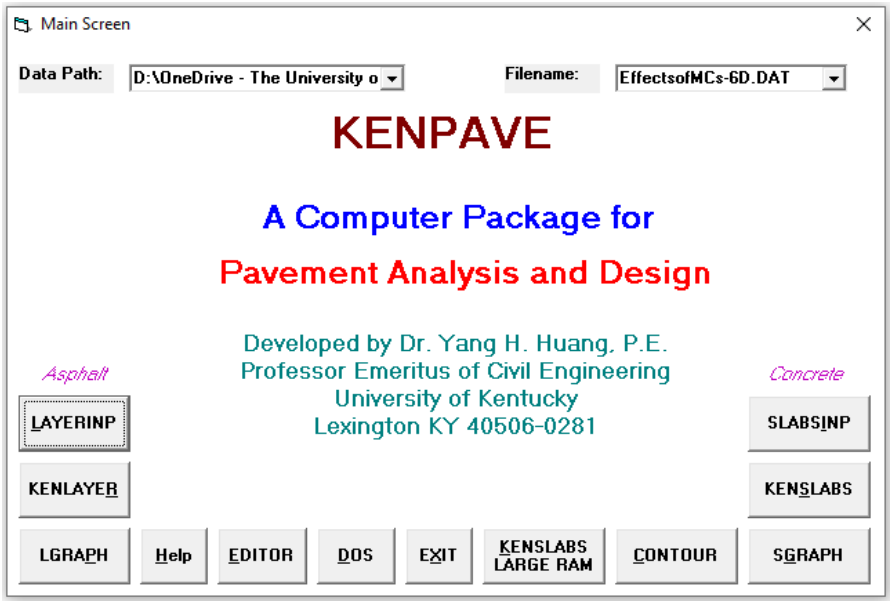

Figure 2.50 Main interface of KENLAYER

The solutions (i.e. stresses, strains, and deflections) of KENLAYER for layer i are presented in terms of Burmister's biharmonic functions (Burmister, 1945; Khazanovich & Wang, 2007), as expressed in Eqs. (2.51) ~ (2.57).

$$\Phi_i(r,z) = \int_0^\infty (A_i(m)e^{mz} - B_i(m)e^{-mz} + C_i(m)ze^{-mz} - D_i(m)ze^{mz})\, J_0(mr)dm \tag{2.51}$$

where $\Phi_i(r,z)$ is Burmister's biharmonic functions, z is the vertical coordinate measured from the top surface of layer i, r is the distance from the evaluated point to vertical coordinate axis, m is the integration parameter, $A_i(m)$, $B_i(m)$, $C_i(m)$, and$D_i(m)$ are functions independent of coordinates r and z, and J_0 is Bessel function of order zero.

$$u_i = -\frac{1+\mu_i}{E_i}\frac{\partial^2\Phi_i}{\partial z \partial r} \tag{2.52}$$

$$w_i = \frac{1+\mu_i}{E_i}\left(2(1-\mu_i)\nabla^2\Phi_i - \frac{\partial^2\Phi_i}{\partial z^2}\right) \tag{2.53}$$

$$\sigma_{zi} = \frac{\partial}{\partial z}\left((2-\mu_i)\nabla^2\Phi_i - \frac{\partial^2\Phi_i}{\partial z^2}\right) \tag{2.54}$$

$$\sigma_{ri} = \frac{\partial}{\partial z}\left(\mu_i\nabla^2\Phi_i - \frac{\partial^2\Phi_i}{\partial r^2}\right) \tag{2.55}$$

$$\sigma_{ti} = \frac{\partial}{\partial z}\left(\mu_i\nabla^2\Phi_i - \frac{1}{r}\frac{\partial\Phi_i}{\partial r}\right) \tag{2.56}$$

$$\tau_{rzi} = \frac{\partial}{\partial r}\left((1-\mu_i)\nabla^2\Phi_i - \frac{\partial^2\Phi_i}{\partial z^2}\right) \tag{2.57}$$

where u_i is radial displacement, w_i is vertical displacement, σ_{zi} is vertical stress, σ_{ri} is radial stress in the horizontal plane, σ_{ti} is tangential stress in the horizontal plane, τ_{rzi} is shear stress, E_i is Young's modulus and μ_i is Poisson's ratio for each layer i. A typical *n*-layer system in cylindrical coordinates is illustrated in Figure 2.51, with the n^{th} layer being of an infinite thickness (Huang 2004).

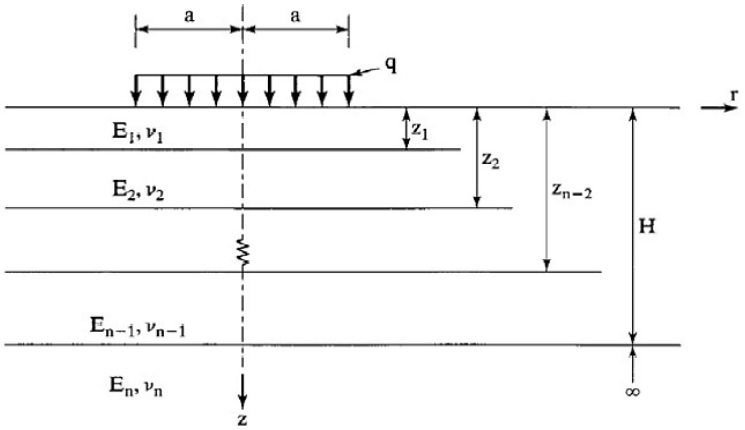

Figure 2.51 An *n*-layer system in cylindrical coordinates, from Huang (2004)

Major disadvantages of KENLAYER include that only modulus values of each layer in the vertical direction can be user-defined and are assumed constant through the thickness even though, in reality, the modulus of granular material are stress-dependent and, thus, will vary with depth and radius in the layer (Huang, 2004; Kumar, 2013). However, such programs can still be fairly reliable (Suh et al., 2010; Omer & Eghan, 2018) and are more widely used than finite-element-based methods due to their simplicity (Thompson et al., 1990). Many studies have been conducted using KENLAYER, e.g. Carvalho et al. (2012); Abed et al. (2019); Bostancioğlu (2021); Mahima & Sini (2021). Considering the research objectives, it is believed that KENLAYER is still applicable with reasonable performance.

2.8 Summary and conclusions

In this chapter, several aspects relevant to the foundation in roads and railway tracks were reviewed, including general structural properties of road pavements and railway tracks, water-induced distress, mechanical properties (i.e. stress-strain behaviour, resilient modulus, shear strength, permanent deformation) of foundations under repeated traffic loading, factors influencing foundation response, water flow, drainage and multi-layered elastic analysis. It is beyond the scope of this project to thoroughly cover both pavements and railway tracks, and the analysis of pavement foundations was concentrated on. It is expected to provide a reference for understanding the foundation response of railway tracks. The main observations are as follows:

- Typically, road pavements consist of a surface course, pavement base, subbase and pavement foundation, and ballasted railway tracks include rails, the fastening system, sleepers (ties), ballast, sub-ballast and subgrade. It is clear that subgrade plays a significant role in supporting pavements/railway tracks with superior performance required under repeated traffic loading. It especially becomes vital when carrying vehicles with heavier axle loads. Thus, the foundation soil has been focused on to broaden the understanding of its behaviour.
- The water-induced distresses in the subsurface structures were identified and summarized. The major distresses were recognized for each structure, i.e. fatigue cracking of overlying bound layers and critical rutting for pavements; progressive shear failure, excessive plastic deformation and subgrade attrition with mud pumping for railway tracks. The contribution of foundations with excess water to the structural distresses was highlighted.

- The key mechanical properties of the foundation were identified as being the resilient modulus, shear strength and permanent deformation resistance. Selective prediction models incorporating the effects of moisture content were reviewed for M_r, τ_f and $\varepsilon_p(N)$ under repeated traffic loading. Therefore, the effects of moisture variation on each property can be quantified. Generally, M_r and τ_f decreased with the excess moisture, while $\varepsilon_p(N)$ showed an opposite trend, and the effects varied with soil types.
- With regard to the factors affecting foundation response, the hysteretic phenomenon of moisture effects and matric suction on resilient modulus was revealed, i.e., the resilient modulus along the drying path was more significant than that along the wetting path. It indicates that the wetting process with lower suctions will be critical to soil response.
- The ingress and egress routes of water into subsurface structures were identified. Surface water infiltration was the main source that contributed the most to excess water. The variation of moisture content in practice generally fluctuated within 11% (drying and wetting). Combined with previous studies, it is believed that the range between OMC to OMC+4% can represent the critical wetting conditions of unsaturated soils.
- An open-graded drainage layer employed jointly with a longitudinal edge drains/outlet pipe, and a daylighted OGDL could be the most effective method to remove excess water. Drainage significantly reduced the water level, dissipated excess pore water pressure and thus enhanced the structural bearing capacity. The effectiveness of drainage depended on structural types, rainfall, geometric design and hydraulic properties of materials. Four flow patterns in granular bases and subbases, resting on an impermeable subgrade, due to drainage were revealed, i.e. lateral flow, composite flow, vertical flow and funnelled flow.
- The multi-layered elastic method has been widely used to analyse pavements and railway tracks due to its simplicity. This method is fairly reliable and offers the possibility of a rational solution to the problem. In particular, KENLAYER as a part of KENPAVE, is able to conduct pavement analysis as an example.

However, based on the literature review, some limitations lie within the previous studies.

- The research on drainage effects is still insufficient. Effects of drainage on shear behaviour have not been fully studied for both saturated and unsaturated soils, and the changing trend of shear strength parameters has not been revealed. In addition, the effects on pavement response have not been further evaluated. Investigations of drainage effects on foundation response under saturated and unsaturated conditions will be significant and comprehensive.
- The sensitivity of structural response (e.g. pavements) to moisture content has not been comprehensively studied. Although the effects of moisture content changes on soil properties have been widely investigated, the effects can vary on different structures. To comprehensively understand the effects on pavement response, it is necessary to conduct a sensitivity analysis of moisture effects on pavement response.
- The prediction models of resilient modulus have been associated with many soil conditions, including degrees of saturation, moisture content, matric suction, confining stress, bulk stress, deviator stress, octahedral shear stress and net mean normal stress as well as with many soil properties (e.g. dry density and PI). These models are flexible by incorporating various variables that affect modulus and are able to achieve reasonably accurate predictions. Despite the progress in the development of prediction models, they were derived from a limited number of soil types and exhibited difficulties in the direct and precise measurement of matric suction during the tests. The model parameters also needed to be determined with more repeated load triaxial tests, which can be time-consuming. Thus, a prediction model having a simpler form which would cover a wide range of soil types is still needed to evaluate the resilient modulus of unsaturated soils under a variety of external conditions.
- The method of predicting the cumulative plastic deformation of foundation soils has been correlated with stress states and soil properties, loading cycles and time. The models incorporating moisture effects may be complicated and limited to one soil type and contain too many model parameters. The moisture effects on cumulative permanent deformation have not been fully reported. Subgrade box tests will reveal the permanent deformation behaviour of subgrade soils in a more realistic way compared to triaxial tests.

CHAPTER 3 PREDICTION OF RESILIENT MODULUS WITH CONSISTENCY INDEX FOR FINE-GRAINED SOILS

3.1 Introduction

Resilient modulus was introduced by the American Association of State Highway and Transportation Officials (AASHTO) and is widely employed to estimate transient soil deformation under repeated traffic loads (AASHTO, 1986). Resilient modulus has been an important indicator used to reflect the resilient behaviour of subgrade soils. Currently, various methods are utilized to obtain the resilient modulus of soils (Thom, 2008), e.g., California bearing ratio (CBR) tests (Brown et al., 1987; Sukumaran et al., 2002), repeated load triaxial tests (Zaman & Khoury, 2007; Khoury et al., 2013; Han & Vanapalli, 2016b), Precision Unbound Material Analyser (Thom et al., 2012; Kwon et al., 2017), K-Mould (Semmelink & De Beer, 1995), Spring box (Edwards et al., 2005), dynamic plate test (Loizos et al., 2003; Asli et al., 2012) and falling weight deflectometer (Ksaibati et al., 2000). Some directly measure a modulus, while others determine the resilient modulus by correlation to another parameter (e.g., CBR value, penetration index and deflection). The users of these tests have found various properties to be significant for predicting resilient modulus, including plasticity index, soil suction, dry unit weight, percent passing 75μm (#200 sieve) and clay content (Puppala, 2008).

The resilient response of pavement foundations has been found to depend on several variables. It is influenced by moisture content, matric suction, external stress, number of load repetitions, stress state, wetting and drying history, soil type and freeze-thaw cycles (Li & Selig, 1996; Miller et al., 2000; Zaman & Khoury, 2007; Ng et al., 2013; Han & Vanapalli, 2016a; Rasul et al., 2017; Ding et al., 2020; Zou et al., 2020). The state conditions affecting resilient behaviour can be summarized as stress state (normal and deviator stress), loading state (frequency, magnitude of load and number of load repetitions), moisture state (moisture content, pore water pressure and matric suction) and particle characteristics (fabric, particle shape, clay content, dry density, compaction degree and packing arrangement due to compaction method). To reach the maximum dry density (MDD) during construction, specifications commonly require

that subgrade soils be compacted at (or near) optimum moisture content (OMC) in practice. Therefore, in-situ subgrade soils should be treated as unsaturated materials. The moisture content of subgrade soils will be subject to seasonal variation, while climate change effects are likely to make the driest and wettest values more extreme. Moisture content directly correlates with resilient behaviour by (e.g.) reducing effective particle friction and increasing compaction. When wetting and/or drying cycles are induced, whether by weather events or seasonal variations, these result in hysteretic moduli changes. Thus, it is very important to incorporate moisture content or its effects into any resilient modulus prediction model.

Based on past test data (Brown et al., 1987; Ooi et al., 2004; Yang et al., 2005; Zaman & Khoury, 2007; Khoury et al., 2009; Sawangsuriya et al., 2009; Ozel & Mohajerani, 2011; Han & Vanapalli, 2016b; Khoury, 2018), relationships of resilient modulus to stress states, soil property index, moisture content, matric suction and degree of saturation have been identified by previous researchers. Various prediction models of resilient modulus have been proposed to demonstrate the non-linear stress-strain behaviour of subgrade soils by incorporating stress state variables (e.g., deviator stress, confining stress, bulk stress, and shear stress), moisture (moisture content, degree of saturation and matric suction) and soil properties (dry density). These models include stress-dependent models (e.g. the $k-\theta$ model (Monismith et al., 1967), the deviator stress model (Moossazadeh & Witczak, 1981), the Uzan model (Uzan, 1985), the Universal model (Kolisoja, 1997), the model used by the Mechanistic-Empirical Pavement Design Guide (MEPDG) (ARA, 2004), suction-based models (Yang et al., 2005; Liang et al., 2008; Ng et al., 2013; Han & Vanapalli, 2015), moisture content-based models (Li & Selig, 1994; Khoury et al., 2013), saturation degree-based models (ARA, 2004), dry density-involved models (Johnson, 1986; Azam et al., 2013; Zhang et al., 2019), plasticity index-related models (Drumm et al., 1990; Cary & Zapata, 2010; Khoury & Maalouf, 2018), genetic algorithm-based models (Nazzal & Tatari, 2013; Ghorbani et al., 2020) and artificial neural network approach (Hanandeh et al., 2020; Zou et al., 2021). The models are well documented and commented upon the references (Lekarp et al., 2000b; Han & Vanapalli, 2016a; Chu, 2020), demonstrating the state of knowledge about the resilient response. Presently, the stress-dependent model suggested by the MEPDG is commonly adopted, even though many other models may show advantages in predicting the resilient modulus of specific soils.

However, these models may be complicated and/or time-consuming, requiring many tests to determine model parameters, or would need to be limited to one soil type. Moisture content has already been shown earlier in the paper to be a key parameter and it has been found that resilient modulus-moisture content relationships are highly dependent on soil types (Ng et al., 2013; Han & Vanapalli, 2016a), and only a few of models are directly focused on moisture content-resilient modulus. Precise measurement of matric suction also requires sophisticated equipment and a cumbersome procedure. In contrast, plasticity information is convenient for a wide variety of soils. Normalizing moisture content relative to plasticity limits (i.e. liquid limit (LL) and plastic limit (PL)) is a common way of characterizing strength (Black, 1962), while strength and stiffness are loosely related (Puppala, 2008; Nagaraj et al., 2012). Thus, it would be significant to explore the effects of moisture state on resilient modulus in order to expand the understanding. The study reported in this Chapter aims to incorporate the moisture state by developing a prediction model of resilient modulus with a consistency index. Based on the testing data collected from previous studies, the relationship between resilient modulus and consistency index was studied and an approach was proposed. Moisture content was normalized through consistency index. The prediction model was also able to incorporate the effects of plasticity index (PI) thereby partly addressing the particle state. It would predict the resilient modulus at varying moisture content in a simple way, since the parameters were well correlated with plasticity index. Based on the modified model, the effects of stress state were incorporated.

Inevitably, there are some limitations to the study reported in this paper. It was derived from fine-grained soils with 50% or more passing the No.200 (0.075 mm) sieve (e.g., silts and clays according to the Unified Soil Classification System, USCS) alone. Even though an attempt has been made to cover a wide range of soils, the 15 soils analysed could not cover every PI value and were not evenly distributed across the range of PIs available. Also, other parameters that affect the resilient modulus were not included, e.g., dry density and hysteretic behaviour due to the wetting and drying process. Nevertheless, it is hoped that the study may provide an alternative method to complex laboratory testing for assessing the resilient modulus of fine-grained soils in the foundation design.

3.2 Materials and methods

3.2.1 Data collection

Based on previously published test results, the resilient modulus data of subgrade soils with various plasticity indices were collected. PI values of the tested soils varied from 6 to 52 in order to cover a wide range of fine-grained soil types; 15 soils were investigated. Among them, four soil chronosequences were recognized, i.e. glacial, marine, tropical and volcanic soils. Their moisture contents ranged from OMC-4% to OMC+4%. This range is meant to represent the possible variability due to the dry and wet extremes of subgrade soils, although this range is still limited for high plasticity soils. The resilient modulus was abstracted from the literature for deviator stress of about 30~40 kPa, which represents the typical stress value to which the subgrade is likely subjected. The basic properties of these soils are presented in Table 3.1. For notation, each soil code consists of two parts, e.g., ‘S06’, ‘S’ represents soil and ‘06’ is the PI value of the soil.

Table 3.1 Basic properties of soils

Soil Name	TSC	Minco	Port	IHT	Renfrow	Pulverized mudstone	Red lake falls	OCSC	Kirkland	Baxter Sandstone	Gault clay	Dried Wahiawa	London clay	Altona S3	Duluth TH23 Slopes
Soil Code	S06	S08	S14	S19	S20	S23	S24	S26	S30	S35	S36	S45	S48	S50	S52
Standard proctor test															
OMC, %	13.5	12.75	14.5	13.9	16.5	17	22	23	19	29.5	n/a	41.6	n/a	33	27.5
MDD, g/cm^3	1.94	1.80	1.76	1.87	1.68	1.83	1.60	1.66	16.4	1.45	n/a	1.25	n/a	1.32	1.44
Atterberg limits															
LL, %	19.6	25	35	35.5	35	50	42	48	50	66	61	87	71	77	85
PL, %	13.6	17	21	16.5	15	27	18	22	20	31	25	42	23	27	33
G_s	2.68	2.69	2.65	2.72	*n/a	2.67	2.69	2.75	2.7	2.75	2.69	3.08	2.73	2.64	2.75
Soil classification															
PI	6	8	14	19	20	23	24	26	30	35	36	45	48	50	52
Soil chronosequence	Glacial	Glacial	Glacial	Glacial	Glacial	Tropical	Glacial	Marine	Glacial	Marine	Marine	Volcanic	Marine	Marine	Glacial
AASHTO	A-4	A-6	A-6	A-6	A-6	A-7-6	A-7-6	A-6	A-7	A-7	A-7-5	A-7	A-7-5	A-7	A-7-6
USCS	CL-ML	CL	CL	CL	CL	CH	CL	CL	CH	CH	CH	MH	CH	CH	CH
Hydrometer analysis															
Percent passing #40 sieve (425μm), %	100	100	100	100	n/a	n/a	100	100	100	n/a	n/a	99	n/a	n/a	100
Percent passing #200 sieve (75μm), %	97	73	83	72	92	n/a	82.4	80	96	n/a	n/a	99	n/a	n/a	96.9
Percent clay <0.002 mm, %	16	22	11	30	n/a	n/a	5.7	32	39	70	39	67	54	77	75.2
Reference	(Han & Vanapalli, 2016b)	(Khoury et al., 2009)	(Khoury et al., 2009)	(Han & Vanapalli, 2016b)	(Khoury, 2018)	(Yang et al., 2005)	(Sawangsuriya et al., 2009)	(Han & Vanapalli, 2016b)	(Khoury et al., 2009)	(Ozel & Mohajerani, 2011)	(Brown et al., 1987)	(Ooi et al., 2004)	(Brown et al., 1987)	(Ozel & Mohajerani, 2011)	(Sawangsuriya et al., 2009)

*n/a represents data not available in the reference.

For fine-grained soils, consistency is a significant characteristic by which to index the firmness of soil and the strength of the soil to withstand irreversible deformation without failure (e.g., cracking or collapsing). As the consistency index increases, the soil states could range from liquid, very soft, soft, firm, stiff and very stiff to hard. Consistency index, I_c, can be derived from Atterberg limits and expressed as

$$I_c = \frac{w_L - w}{w_L - w_P} = \frac{w_L - w}{I_p} \tag{3.1}$$

where w_L is the liquid limit, w_P is the plastic limit, w is the existing moisture content of soils and I_p represents PI. When w reaches the liquid limit, I_c is 0, and when w is equivalent to w_P, I_c is 1. Based on I_c, the moisture content was normalized, and thus the variation of resilient modulus of different soils with moisture contents can be compared.

The variation of resilient modulus with moisture content and consistency index is presented, respectively, as shown in Figure 3.3.1 and Figure 3.2. Moisture states differed from soils, with moisture content lying between 7%~45%, and the moisture content involved in the tests increased with PI. All the soils showed similar trends of resilient modulus with moisture content and consistency index, i.e. as w increased, resilient modulus decreased and the opposite trend at the corresponding consistency index. After normalization by I_c, the soils were tightly distributed, compared with those at varying moisture contents.

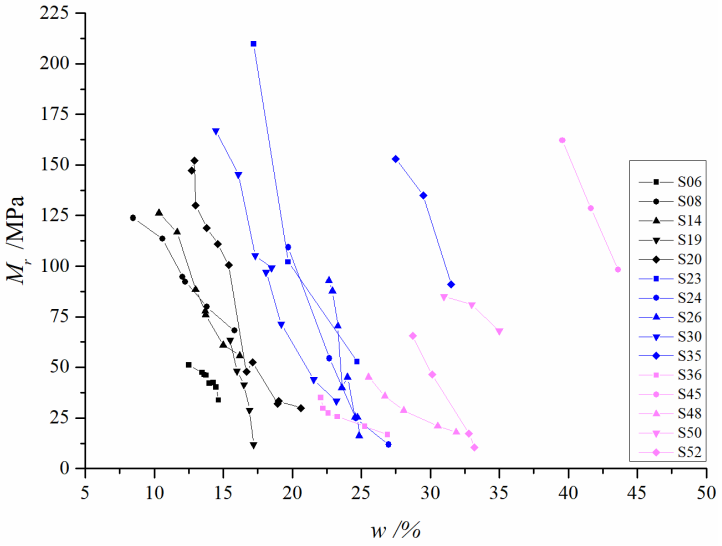

Figure 3.3.1 The variation of resilient modulus with w

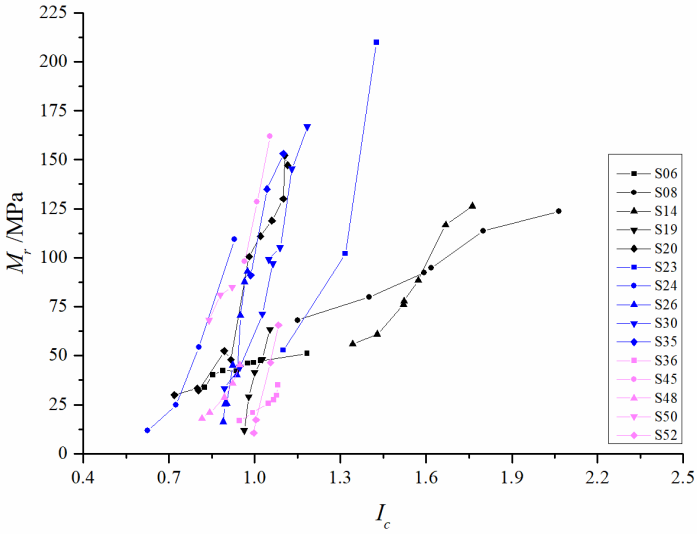

Figure 3.2 The variation of resilient modulus with I_c

3.2.2 Data consistency analysis

The relationship of resilient modulus with consistency index is illustrated for each soil in Figure 3.3~Figure 3.17, and their regression curves are also presented. The consistency index varied from 0.6 to 2.1. According to the coefficient of determination (see Eq. (3.4), discussed below), the resilient modulus showed an excellent linear correlation with the consistency index.

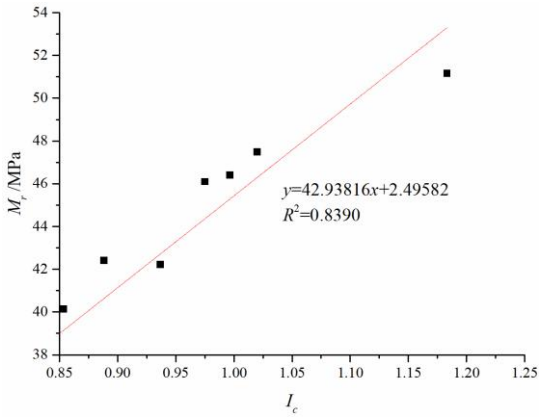

Figure 3.3 Modulus variation of S06

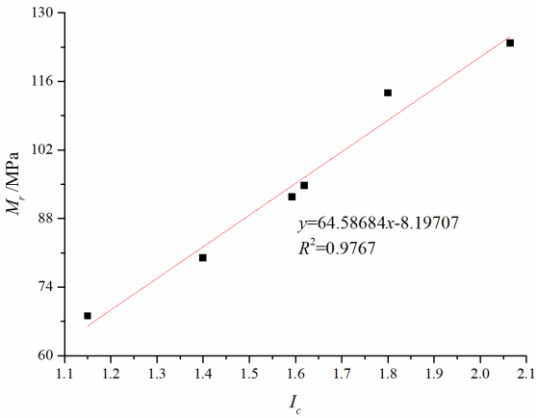

Figure 3.4 Modulus variation of S08

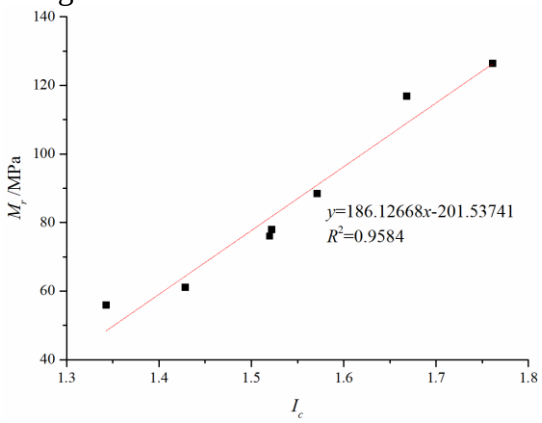

Figure 3.5 Modulus variation of S14

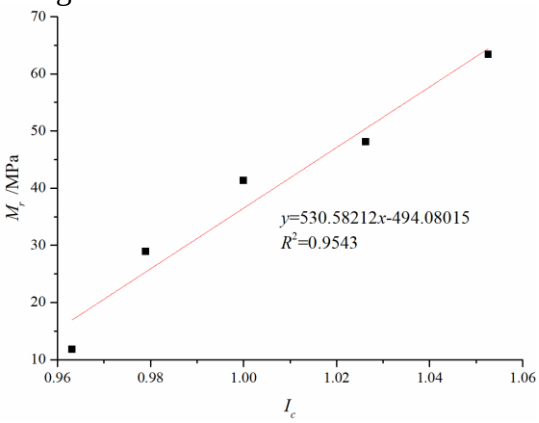

Figure 3.6 Modulus variation of S19

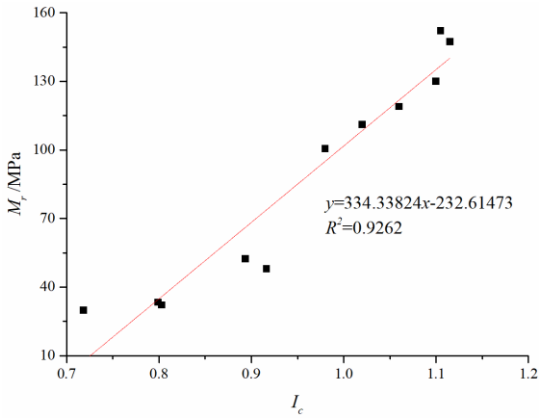

Figure 3.7 Modulus variation of S20

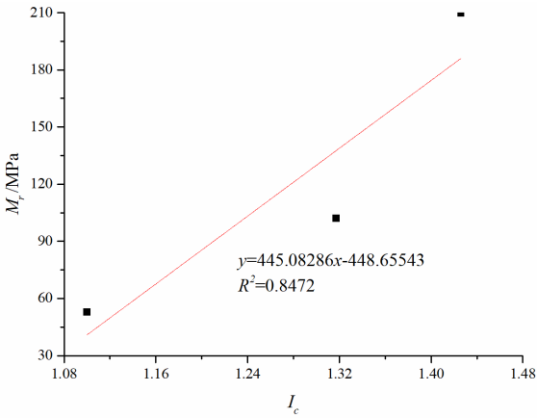

Figure 3.8 Modulus variation of S23

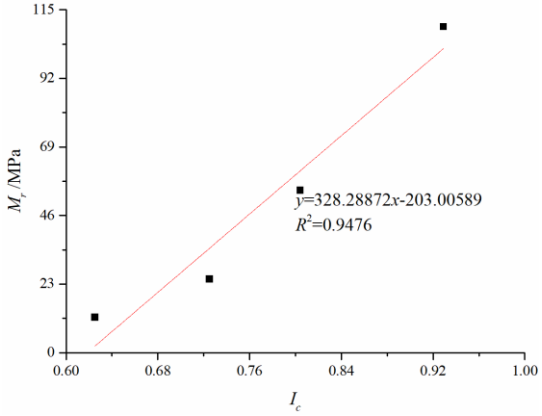

Figure 3.9 Modulus variation of S24

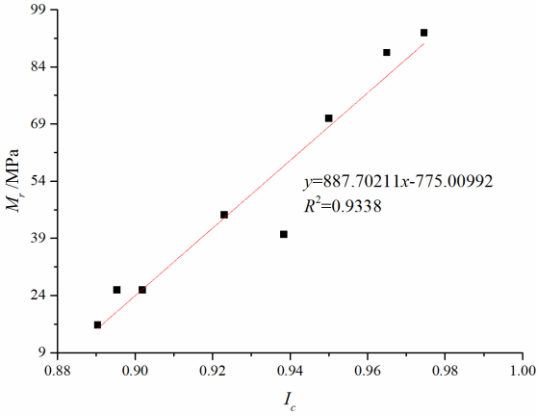

Figure 3.10 Modulus variation of S26

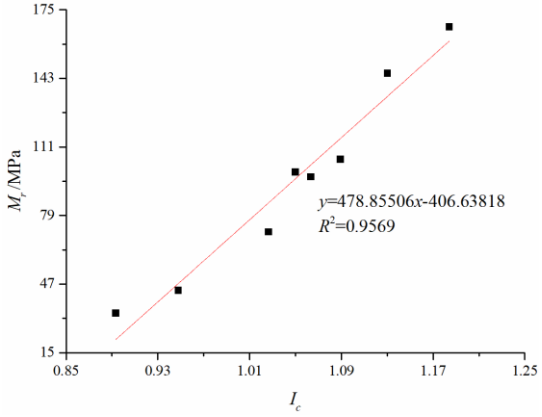

Figure 3.11 Modulus variation of S30

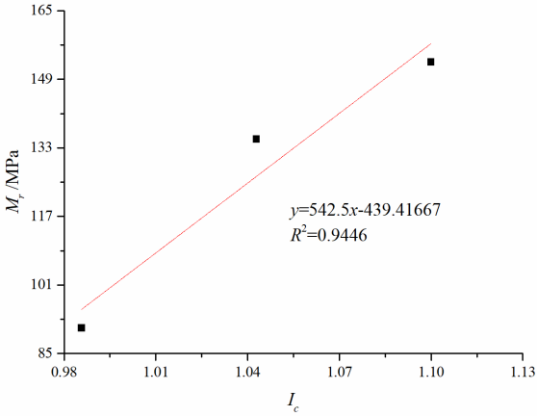

Figure 3.12 Modulus variation of S35

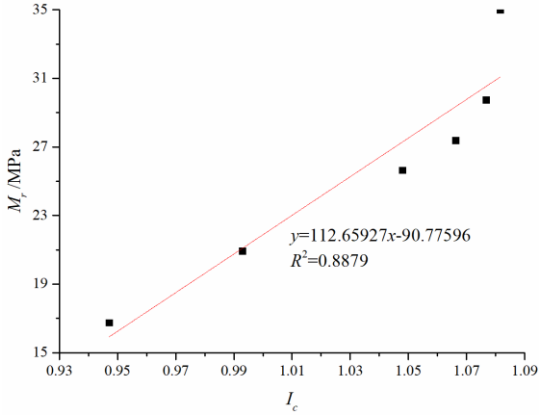

Figure 3.13 Modulus variation of S36

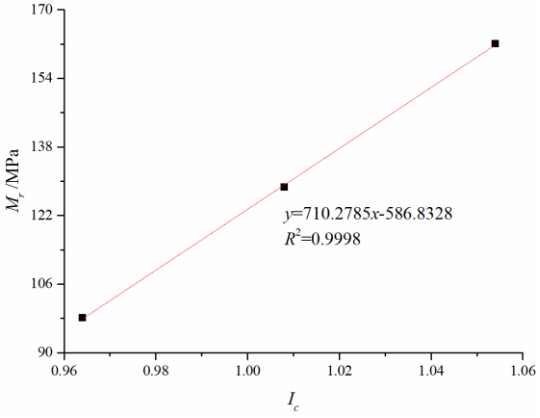

Figure 3.14 Modulus variation of S45

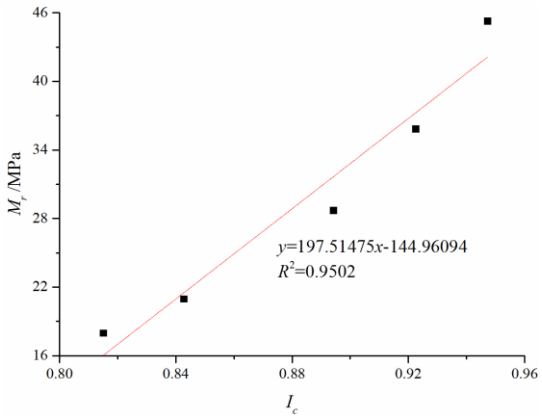

Figure 3.15 Modulus variation of S48

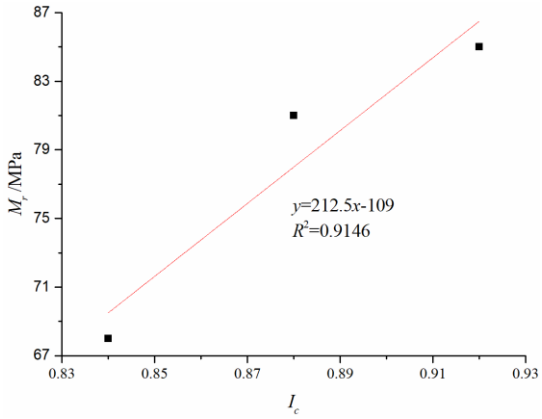

Figure 3.16 Modulus variation of S50

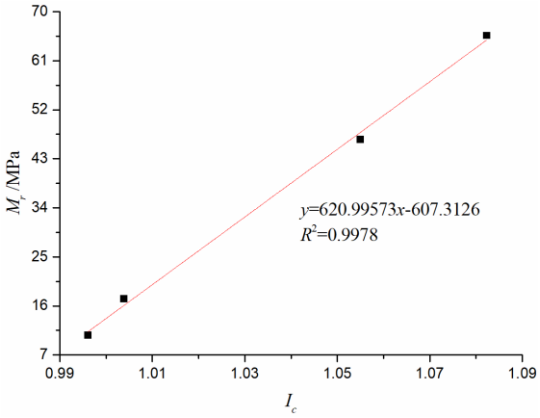

Figure 3.17 Modulus variation of S52

3.2.3 Accuracy estimation

The accuracy of the prediction model for resilient modulus was assessed by four parameters, including the root mean square error (RMSE), residual sum of squares (RSS), the coefficient of determination (R^2) and adjusted R^2 ($adj\ R^2$). They are expressed as

$$RMSE = \sqrt{\sum_{i=1}^{n}\left(\hat{M}_{r,i} - M_{r,i}\right)^2 / n} \tag{3.2}$$

$$RSS = \sum_{i=1}^{n}\left(\hat{M}_{r,i} - M_{r,i}\right)^2 \tag{3.3}$$

$$R^2 = \frac{\sum_{i=1}^{n}\left(\hat{M}_{r,i} - M_{r,i}\right)^2}{\sum_{i=1}^{n}\left(\bar{M}_{r,i} - M_{r,i}\right)^2} \tag{3.4}$$

$$adj\ R^2 = 1 - (1 - R^2)\frac{(n-1)}{(n-k-1)} \tag{3.5}$$

where $M_{r,i}$ is the measured resilient modulus for specimen i, $\hat{M}_{r,i}$ is the predicted resilient modulus for specimen i, $\bar{M}_{r,i}$ is the mean resilient modulus of all specimens,

n is the number of specimens, and k is the number of independent variables. RSS characterises the discrepancy between the data and an estimation model, with a smaller value representing a tighter fit of the model to the data. As more data points were added, R^2 increased. $adj\ R^2$ could reduce the effects of the number of data points on the fitting assessment by compensating for the data points that did not fit the model. $adj\ R^2$ was always less than or equal to R^2. Based on the criteria from Witczak (2002), the goodness of prediction is classified as: excellent ($R^2 \geq 0.9$), good ($0.7 \leq R^2 \leq 0.89$) and fair ($0.4 \leq R^2 \leq 0.69$). For the 15 samples given in and with results illustrated in Figure 3.3~Figure 3.17, only three did not have an excellent classification – and these three were, nevertheless, near the top of the 'good' classification.

3.3 Development of prediction model

3.3.1 Consistency index model

Based on the regression results, a prediction model incorporating a consistency index was derived for the resilient modulus of fine-grained soils. The consistency index model was expressed as

$$M_r = a_1 \times I_c + b_1 \tag{3.6}$$

where a_1 and b_1 are model parameters, and M_r is measured in MPa. It can demonstrate the combined effects of PI and moisture content variation on the resilient modulus of soils. Compared with the current prediction models, it has a simple form and is convenient to apply, but a disadvantage is that it does not consider the stress state and matric suction. For each stress level, model parameters can be determined by regression, and then it can describe resilient modulus at various stress levels. However, such an approach would need more tests and would be time-consuming.

The regression parameters for each soil are summarised in Table 3.2. The measured and predicted resilient modulus values are demonstrated in Figure 3.18. All the data were evenly distributed along the 45^0 line, and the predicted values were in good agreement with the measured values. According to values of the coefficient of determination (i.e. R^2), the relationship of resilient modulus with consistency index was excellently linear for each model. The relationship of the model parameters (a_1 and b_1) with PI is shown in Figure 3.19~Figure 3.24. They show almost no correlation with the plasticity index (the coefficients of determination, R^2, are 0.1130 (a_1) and 0.0978 (b_1)). The parameters for soils S26, S35, S36, S48 and S50 were substantially different from

the other data. Thus, all the soils were divided into two groups, i.e. the glacial group (S06, S08, S14, S19, S20, S23, S24, S30, S45 and S52) and the marine group (S26, S35, S36, S48 and S50). In reality, 'S23' and 'S45' are tropical and volcanic soils, respectively. However, from the analysis, they could be grouped with the trends of glacial soils. Therefore, these two soils were categorised as 'glacial group' for simplicity. Then, it is found that the R^2 values showed a clear increase, i.e. a_1 = 0.7834 and b_1 = 0.7374 for the glacial group, and a_1 = 0.5983 and b_1 = 0.6677 for the marine group. This improvement can be seen by comparing Figure 3.19 to Figure 3.21 or to Figure 3.23 and by comparing Figure 3.20 to Figure 3.22 or Figure 3.24.

Table 3.2 Regression parameters of the prediction model

Soil	PI	$M_r = a_1 \times I_c + b_1$					
		a_1	b_1	R^2	$adj\ R^2$	RMSE	RSS
S06	6	42.938	2.496	0.8390	0.8121	12.905	31.964
S08	8	64.857	-8.197	0.9767	0.9708	45.625	49.715
S14	14	186.127	-201.537	0.9584	0.9501	64.038	178.115
S19	19	530.582	-494.080	0.9543	0.9390	38.167	69.825
S20	20	334.338	-232.615	0.9262	0.9179	147.122	1725.921
S23	23	445.083	-448.655	0.8472	0.6943	104.510	1970.658
S24	24	328.289	-203.006	0.9476	0.9214	73.075	295.144
S26	26	887.702	-775.010	0.9338	0.9228	75.798	407.218
S30	30	478.855	-406.638	0.9569	0.9497	118.935	637.215
S35	35	542.5	-439.417	0.9446	0.8893	43.841	112.66667
S36	36	112.659	-90.776	0.8879	0.8599	13.601	23.348
S45	45	710.279	-586.833	0.9998	0.9996	45.206	0.439
S48	48	197.515	-144.961	0.9502	0.9336	21.679	24.622
S50	50	212.5	-109	0.9146	0.8291	12.021	13.5
S52	52	620.996	-607.313	0.9978	0.9966	44.417	4.428

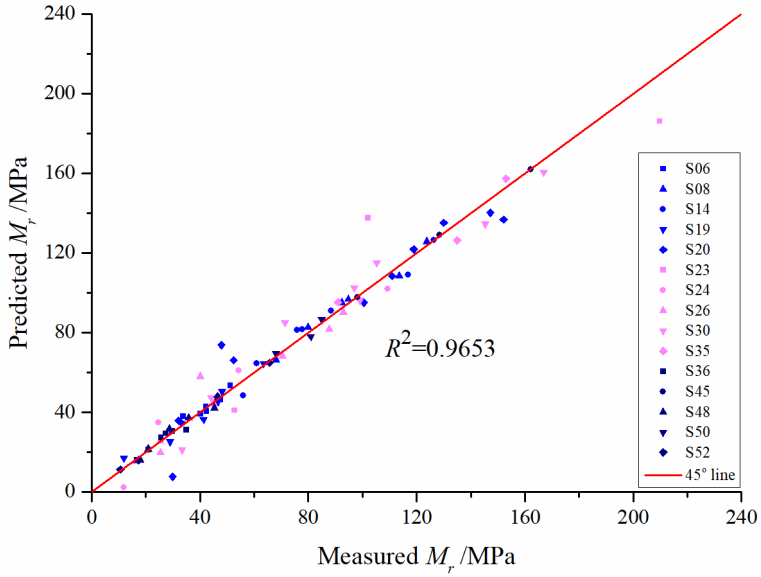

Figure 3.18 Comparison between measured and predicted M_r by consistency index model

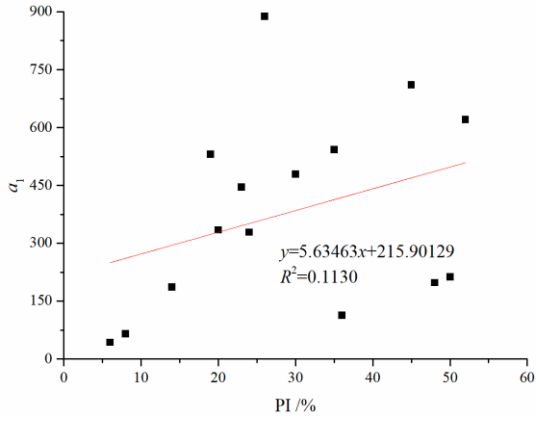

Figure 3.19 Variation of a_1 with PI for all soils

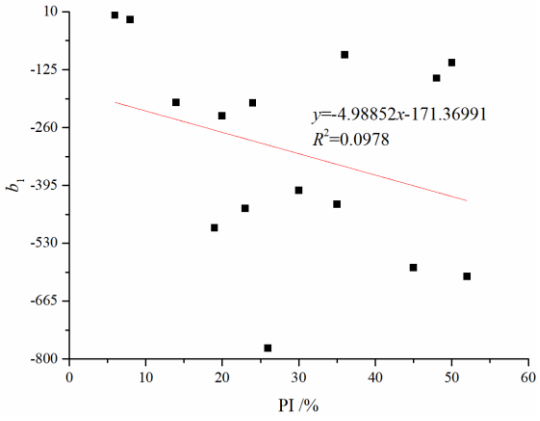

Figure 3.20 Variation of b_1 with PI for all soils

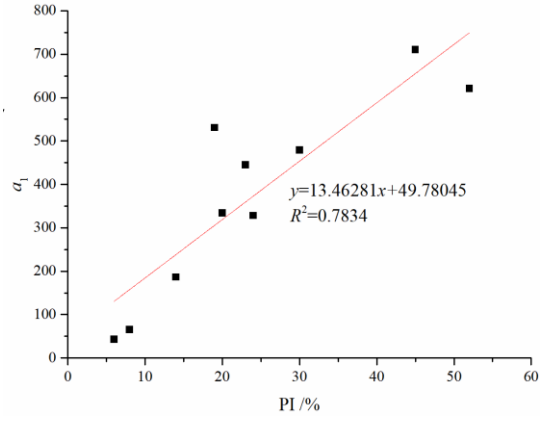

Figure 3.21 Variation of a_1 with PI for glacial group

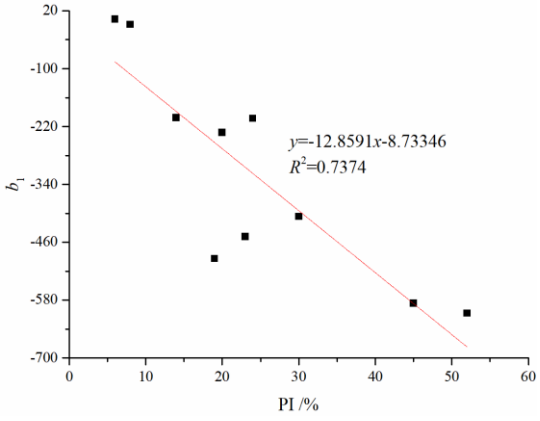

Figure 3.22 Variation of b_1 with PI for glacial group

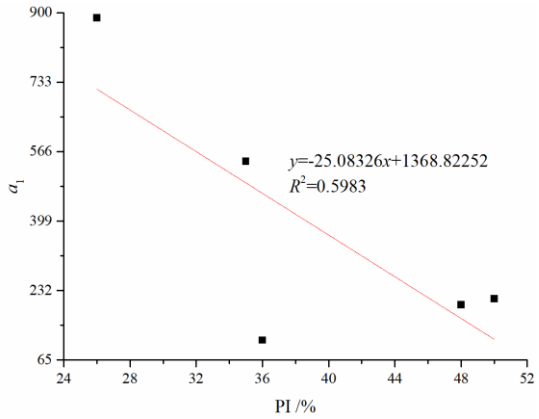

Figure 3.23 Variation of a_1 with PI for marine group

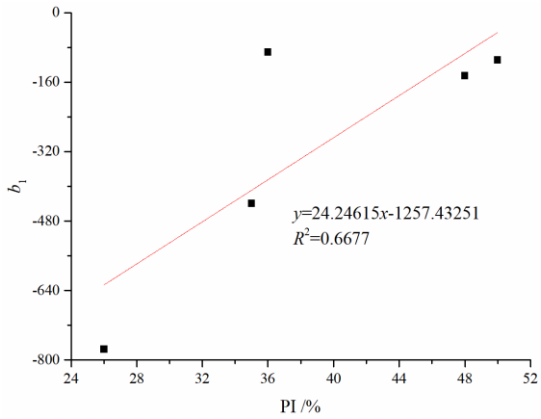

Figure 3.24 Variation of b_1 with PI for marine group

As a result, the model parameters were found to correlate well with PI. Thus, it is practical to obtain these parameters from PI.

For soils in the glacial group, model parameters could be estimated by

$$a_1 = 13.4628 \times I_p + 49.7804, \qquad R^2 = 0.7834 \tag{3.7}$$

$$b_1 = -12.8591 \times I_p - 8.7335, \qquad R^2 = 0.7374 \tag{3.8}$$

For soils in the marine group, model parameters could be evaluated by

$$a_1 = -25.0833 \times I_p + 1368.8225, \qquad R^2 = 0.5983 \tag{3.9}$$

$$b_1 = 24.2462 \times I_p - 1257.4325, \qquad R^2 = 0.6677 \tag{3.10}$$

Thus, by substituting Eqs. (3.7-3.8) and (3.9-3.10) into Eq. (3.1), respectively, Eq. (3.1) can be rewritten as Eq. (3.11) for the glacial group and Eq. (3.12) for the marine group:

$$M_r = 49.7805 \times I_c - 12.8591 \times I_p + 13.4628 \times I_c \times I_p - 8.7335 \tag{3.11}$$

$$M_r = 1368.8225 \times I_c + 24.2462 \times I_p - 25.0833 \times I_c \times I_p - 1257.4325 \tag{3.12}$$

From Eqs. (3.11) and (3.12), it can be seen that the proposed model can describe the effects of plasticity index, moisture content and consistency index on resilient modulus. It might be argued that moisture content is not a fundamental way to describe the condition of a soil and that matric suction is a more rational choice due to its control of effective stress in partially saturated soils. The counterargument that the work described here exploits is that moisture content can be readily determined by simple equipment, which contrasts with the complexities of measuring matric suction. Combined with soil water characteristic curve, it can reflect the effects of matric suction on resilient modulus. For in-situ pavements, it can be utilized to predict the resilient modulus of the subgrade with moisture variation at a deviator stress of 30~40 kPa, as an estimation under the practical condition with simplifications.

3.3.2 Modified consistency index model

Compared with the current prediction models, the consistency index model has a simple form and is convenient to apply. In contrast, the effects of applied stress states on resilient modulus were not considered. In terms of the stress-dependency, a prediction model incorporating bulk stress and octahedral shear stress was recommended by the MEPDG (ARA, 2004), i.e.

$$M_r = k_1 \times p_a \times \left(\frac{\theta}{p_a}\right)^{k_2} \times \left(1 + \frac{\tau_{oct}}{p_a}\right)^{k_3} \quad (3.13)$$

where p_a is the atmospheric pressure (assumed as 100 kPa), θ is bulk stress ($\theta = \sigma_1+\sigma_2+\sigma_3$, where σ_1, σ_2 and σ_3 are the major, intermediate and minor principal stresses, respectively), τ_{oct} is octahedral shear stress ($\tau_{oct} = \sqrt{(\sigma_1-\sigma_2)^2+(\sigma_1-\sigma_3)^2+(\sigma_2-\sigma_3)^2}/3$) and k_1, k_2 and k_3 are model parameters. However, the effects of moisture variations were not demonstrated.

Thus, combining Eqs. (3.6) and (3.13), a modified consistency index model is proposed to describe resilient modulus of unsaturated subgrade soils, expressed as:

$$M_r = k_4 \times (a_1 \times I_c + b_1) \times \left(1 + \frac{q_{cyc}}{p}\right)^{k_5} \times \left(1 + \frac{q_{cyc}}{p_a}\right)^{k_6} \quad (3.14)$$

where q_{cyc} is cyclic deviator stress, p is net mean stress at $q = q_{cyc}$ ($p = \frac{\theta}{3} - u_a$, u_a is the pore air pressure), k_4, k_5 and k_6 are model parameters. The parameter q_{cyc} is introduced to allow the prediction of moduli at cyclic deviator stress levels other than those on which Eq. (3.6) was based (30~40 kPa) and the parameter p is introduced to allow prediction at confining stresses other than those implicit in Eq. (3.6) (25~50 kPa). The first term, k_4, is a coefficient to adjust the modulus to fit Eq. (3.6) when $q_{cyc} \neq$ 30~40 kPa and $p \neq$ 25~50 kPa, otherwise $\left[k_4 \times \left(1 + \frac{q_{cyc}}{p}\right)^{k_5} \times \left(1 + \frac{q_{cyc}}{p_a}\right)^{k_6}\right] \approx 1$. The second term $(a_1 \times I_c + b_1)$ is adopted from Eq. (3.6) to reflect the effects of moisture content and PI. The third term $\left(1 + \frac{q_{cyc}}{p}\right)^{k_5}$ incorporates the effect of the confining stress level. The last term $\left(1 + \frac{q_{cyc}}{p_a}\right)^{k_6}$ quantifies the effects of the cyclic stress level. The ratio q_{cyc}/p is chosen as the means to incorporate the effect of confining stress, rather than p/p_a, because users are only interested in determining M_r when loading is causing a change in q, specifically as the ratio q_{cyc}/p increases. Changes solely in p are of little interest.

3.4 Validation of prediction model

For some of the studied soils, data was available at various confining and deviator stresses. Therefore, these data were utilized to validate the modified consistency index model. It was more comprehensive compared to the model based on the consistency index alone. That was selected and derived from only one deviator stress level for each soil. The available results were fitted to Eq. (3.14) in a similar manner to that used previously when fitting to Eq. (3.6). The predicted and measured resilient moduli are presented in Figure 3.25 and the model parameters are summarised in Table 3.3. R^2, $adj\ R^2$, RMSE and RSS are presented to assess the performance of the prediction model. 323 data points were involved, and all except data for S23 are evenly distributed along the 45^0 line. S23 showed the largest RSS, i.e. the most discrepancy. This may be due to the fact that it was simplified into the glacial group when developing Eq. (3.6), and thus, for Eq. (3.14), this soil may not fit so well. Combined with R^2 and $adj\ R^2$ values, the proposed model performed excellently to determine the resilient modulus.

Table 3.3 Model parameters for modified consistency index model

Soil	$M_r = k_4 \times p_r \times (a_1 \times I_c + b_1) \times \left(1 + \frac{q_{cyc}}{p}\right)^{k_5} \times \left(1 + \frac{q_{cyc}}{p_a}\right)^{k_6}$								
	a_1	b_1	k_4	k_5	k_6	R^2	$adj\ R^2$	RMSE	RSS
S6	13.085	-0.0756	3.921	-0.757	-0.753	0.8688	0.8629	2.6387	15.6296
S8	5.538	-0.699	5.159	1.525	0.572	0.9767	0.9611	2.8768	49.6561
S14	1.495	-1.619	0.417	-4.823	31.729	0.9587	0.9381	5.0222	176.5583
S19	21.385	-19.860	26.514	0.203	-0.649	0.9452	0.9388	4.1225	339.9009
S20	6.368	-4.433	3.6183	0.889	5.445	0.9259	0.9136	12.5472	1731.7639
S23	23.956	-25.286	22.565	0.411	-1.137	0.8635	0.840/8	26.6375	10643.3282
S24	10.467	-6.473	0.880	4.200	-0.7109	0.9476	0.8428	8.5910	295.2187
S26	46.834	-40.922	26.667	-0.366	-0.144	0.9402	0.9389	6.9425	4626.9837
S30	17.962	-15.251	2.690	4.177	1.812	0.9563	0.9389	8.9820	645.4095
S35	39.802	-35.277	36.773	-0.306	-0.773	0.9636	0.9575	5.6756	483.1829
S36	11.161	-8.993	0.405	3.442	2.870	0.8900	0.8166	1.9548	22.9269
S45	37.336	-14.119	7.075	-0.175	-0.688	0.9659	0.9602	3.1143	145.4789
S48	26.835	-19.688	1.275	-1.304	7.739	0.9494	0.8987	2.2342	24.9572
S50	34.441	-20.592	9.089	0.215	-0.783	0.9668	0.9612	1.6712	41.8935
S52	4.033	-3.944	0.920	3.937	4.493	0.9978	0.9933	1.0488	4.3998

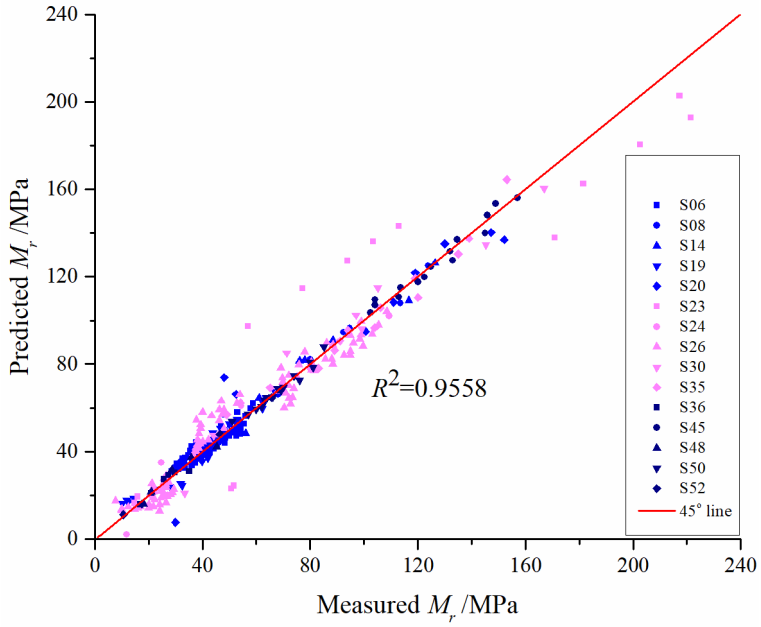

Figure 3.25 Comparison between the measured and predicted resilient modulus

For each model parameter in Eq. (3.14), a possible value based on simple soil properties was sought. Based on an initial trial and error analysis, it was found that the clay content, w_{clay}, also influenced the parameters as well as the plasticity index, I_p. Thus, model parameters were fitted with I_p and w_{clay} by nonlinear regression. Since the clay contents of S20 and S23 were unavailable, they were excluded from the analysis. Various expressions were adopted to fit the data, including polynomials from 1 to 6 orders, exponential, logarithmic and power equations, but all were found not to provide good correlation results. Finally, the following relationship between the model parameters with I_p and w_{clay} was adopted as it showed the best fit:

$$\eta_{ci} = \beta_0 + \beta_1 \times w_{clay} + \frac{\beta_2}{1 + \left(\frac{I_p - \beta_3}{\beta_4}\right)^2} \tag{3.15}$$

where η_{ci} represents the model parameter, w_{clay} is the clay content (%) and β_0, β_1, β_2, β_3 and β_4 are the fitting parameters.

The regression results are presented in Table 3.4. The value of R^2 exhibited a soil-dependent trend. The value of R^2 when considering all the soils ranged from 0.48 to 0.92 but showed significant increases when the soils were categorized into glacial and marine groups. For the glacial group, the value of R^2 lay between 0.7 and 0.98, and especially k_4 and k_6 showed excellent correlation with I_p and w_{clay} with R^2 values of 0.9341 and 0.9835, respectively. For the marine group, the value of R^2 varied from 0.87 to 0.99, and generally exhibited a larger value compared to that of the corresponding

parameter of the glacial group. Despite the limitations of the dataset, this reveals a possible way to obtain the model parameters with reasonable accuracy without doing cyclic modulus tests. With such a wide range of soils, it is not surprising to have such a wide range of values for a parameter.

Table 3.4 Regression results of model parameters

Soil	Parameter	$\eta_{ci} = \beta_0 + \beta_1 \times w_{clay} + \frac{\beta_2}{1 + \left(\frac{I_p - \beta_3}{\beta_4}\right)^2}$					
		β_0	β_1	β_2	β_3	β_4	R^2
All soils	a_1	3.225	0.535	-4.04627e+7	54.149	0.00212	0.6013
	b_1	2.072	-0.292	-43.514	26.840	1.520	0.6402
	k_4	-96.084	0.841	94.859	17.396	28.415	0.7432
	k_5	3.879	-0.042	-8.486	13.289	3.656	0.4866
	k_6	-0.136	0.0277	31.561	14	-5.434e-7	0.9198
Glacial group	a_1	-2.119	0.598	-4139441	53.179	-0.00361	0.8811
	b_1	127.279	-0.483	-129.761	22.312	49.757	0.8875
	k_4	2.1008	0.0269	27.106	19	-1. 313e-5	0.9341
	k_5	5.179	-0.0382	-9.797	13.134	4.618	0.7046
	k_6	-1.133	0.0471	32.344	14	-5.571e-8	0.9835
Marine group	a_1	-16.645	0.706	2.37728e+8	28.287	-0.00095	0.9288
	b_1	15.538	-0.518	-1.13063e+8	29.171	0.00188	0.8715
	k_4	-44.450	0.717	1.31195e+9	29.933	-0.00075	0.9522
	k_5	-1.199	0.013	4.133	36	-7.529e-7	0.9249
	k_6	2.289	-0.105	98494869	43.174	-0.00161	0.9898

The MnROAD soil from Sawangsuriya (2009) was taken as an example to demonstrate the calculation. The calculation procedures are presented as follows:

Step 1) Collection of basic parameters.

I_p=9; w_L=26; w_p=17; w_{clay}(%)=14.5; the soil belongs to the glacial group.

Step 2) Model parameter calculation.

According to Table 3.4 and the basic parameters in Step 1), the model parameters were calculated using Eq. (3.15). Then, the results of the model parameters are shown in Table 3.5. It should be noted that the values of model parameters in Table 3.5 (from model parameter calculation) were different from those in Table 3.8 (from regression analysis).

Table 3.5 Calculation results of model parameters for the MnROAD soil

a_1	b_1	k_4	k_5	k_6
6.524361	-0.8179	29.59685	-0.81354	-0.45005

Step 3) Resilient modulus calculation.

A data point of MnRoad was taken to calculate the resilient modulus (M_r), as shown in Table 3.6.

Table 3.6 Information of the selected data point

w /% by mass	I_c	p /kPa	q /kPa	q/p	Measured M_r /MPa
13.75	1.361	27.67	41	1.482	104.42

Then, the model parameters from **Step 2)** (Table 3.5) were substituted into Eq. (3.14) to predict the resilient modulus of the selected data point.

Therefore, the predicted M_r was 113.84 MPa, which was slightly larger than the measured M_r (104.42 MPa).

3.5 Comparison and analysis

The dependence of the proposed model on the dataset given in Table 3.1 is absolute. Therefore, data of another four soils obtained from previously published testing were selected to provide some independent validation of the proposed modified consistency index model. The basic properties of the four soils used for validation are presented in Table 3.7. The selected datasets are presented in Figure 3.26~Figure 3.28.

Table 3.7 Basic properties of soils for validation

Soil	Red wing	MnROAD	Decomposed tuff	Pickens B-4
Source	(Sawangsuriya et al., 2009)	(Sawangsuriya et al., 2009)	(Ng et al., 2013)	(Rahman, 2017)
Group	Glacial	Glacial	Marine	Volcanic
LL, %	28	26	43	36
PL, %	17	17	29	26
PI	11	9	14	10
AASHTO	A-4	A-4	A-7-6	A-4
OMC, %	13.5	16.0	16.3	18.1
MDD, g/cm^3	1.79	1.77	1.76	1.77

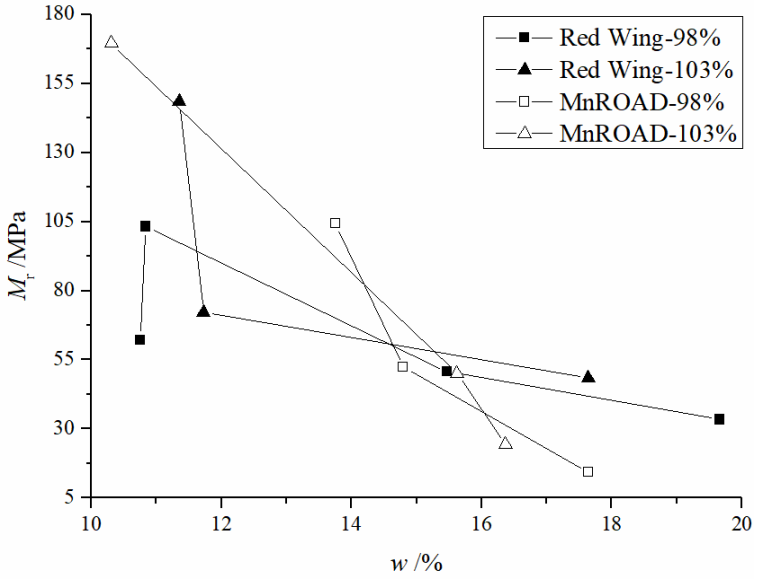

Figure 3.26 M_r of Red Wing and MnROAD (Sawangsuriya et al., 2009)

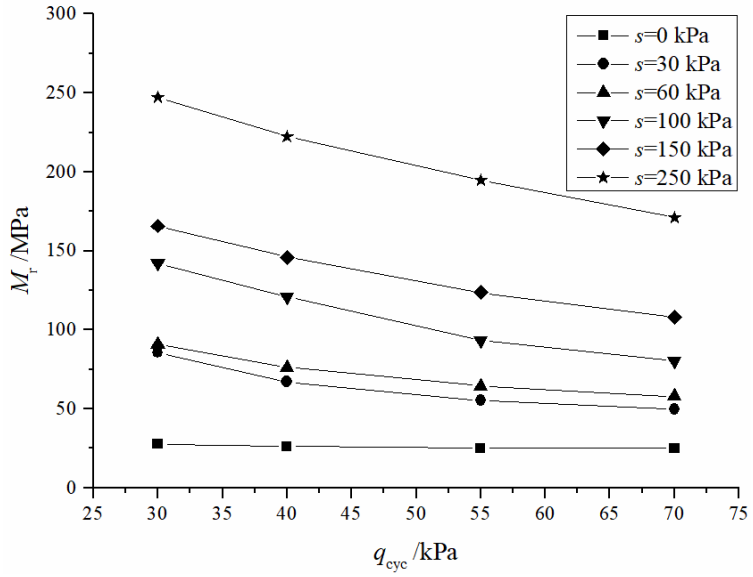

Figure 3.27 M_r of Decomposed tuff (Ng et al., 2013)

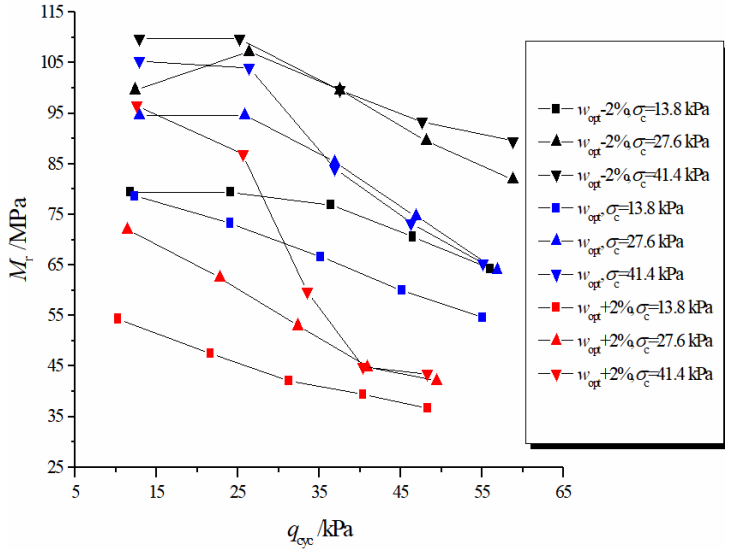

Figure 3.28 M_r of Pickens B-4 (Rahman, 2017)

The prediction results and comparison are presented in Table 3.8 and Figure 3.29. In terms of coefficients of determination, these varied from 0.48 to 0.97. Compared to those in the corresponding reference, the proposed model showed a fairly good prediction of resilient modulus, and particularly for the MnROAD soil, the predictions exhibited the largest R^2 of 0.9659, a better correlation than the reference model discussed earlier in the paper. R_m^2 indicates the coefficient of dermination from the proposed modified model (i.e. generalised for all soils), and R_r^2 indicates the coefficient of dermination from the reference (non-generalised) studies as above. For the Red wing and Pickens B-4 soils, the average of the values given in the references was adopted as R_r^2 for the comparison with R_m^2.

Table 3.8 Prediction results from the modified model and comparison

Soil	Parameters for Eq. (3.14)						Reference
	a_1	b_1	k_4	k_5	k_6	R_m^2	R_r^2
Red wing	3.710	-1.438	1.711	1.724	2.920	0.4845	0.79 (Sawangsuriya et al., 2009)
MnROAD	3.871	-3.515	2.226	2.046	3.77	0.9659	0.76~0.81 (Sawangsuriya et al., 2009)
Decomposed tuff	23.01	-53.61	57.46	-1.08	-0.46	0.6868	0.98 (Ng et al., 2013)
Pickens B-4	16.760	-19.514	11.936	-0.8999	0.221	0.8356	0.89 (Rahman, 2017)

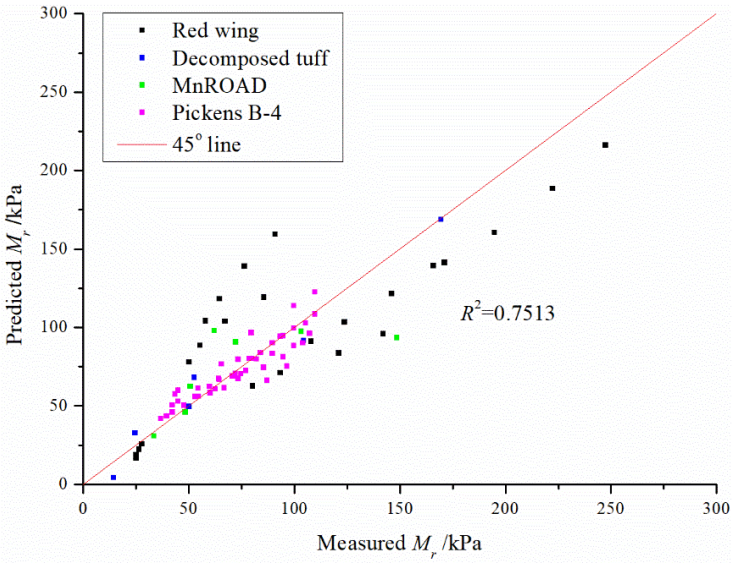

Figure 3.29 Comparison between the measured and predicted resilient modulus for validation

3.6 Summary and conclusions

A prediction model based on the consistency index was proposed for the resilient

modulus of fine-grained soils. A modified model was also proposed, i.e. a consistency index model and a stress-modified consistency index model. The models were able to determine resilient modulus at various moisture contents with fair accuracy relying only on simple soil properties. The study further demonstrated that the parameters of the modified model correlated with the plasticity index and clay content. Further analysis might enable further improvements in predicting the model parameters by relating them to other soil properties (such as degree of compaction). This would further enhance the application of the proposed model.

The consistency index model could reflect the effects of plasticity index and moisture variation on resilient modulus with two regression parameters at approximate in-situ loading conditions. It provides a simple and convenient way for assessing the soil modulus for foundation design.

The stress-modified consistency index model avoided the limitations of the consistency index by incorporating deviator stress and net normal stress. It can be used to predict resilient modulus at various stress conditions as well as at different moisture conditions. The coefficient of determination of the proposed model's parameters varied with soil types. Nevertheless, compared to previous studies, it covered more soil types and gave reasonable, often high, accuracy.

Based on the data analysis, a relationship applicable across all soils with a range of plasticity index values was not achievable. However, a reasonably reliable consistency index model was revealed within a glacial group of soils and another within a marine group of soils. The models were extended to allow for different applied stress conditions.

However, these models did not consider all the possible conditions in unsaturated soils, e.g. wetting and drying paths and dry density. Although the proposed models cover a wide range of soils with various plasticity indices, the study was limited to 15 soils and could not cover all plasticity index values. To further extend the applicability, the proposed models should be verified with extensive laboratory data of soils over a broader range of plasticity indices.

CHAPTER 4 EFFECTS OF MOISTURE CONTENT ON FOUNDATION RESPONSE

4.1 Introduction

The subgrade contributes significantly to supporting upper structures in road pavements and airfields, and the reliability of that support is vital in maintaining excellent performance under repeated traffic loads. A major challenge to this reliability is that subgrade soils are also sensitive to variations in moisture content (MC). When the soil is saturated, positive pore water pressure will be induced under traffic loading, reducing the effective stress as the proportion of the load carried by soil particles reduces. Even when the soil is unsaturated, increased MC reduces matric suction which also reduces effective stress and, hence, mechanical properties. It is found that resilient modulus, M_r, of subgrade generally decreases as moisture increases. However, modulus values show some increasing trends when the soil is above the optimum moisture content since significant plastic deformation occurs due to further post-construction compaction at a higher moisture content (Rahman & Erlingsson, 2016). This could be explained by the refined particle rearrangement (i.e. better particle interlocking) in soil (Yideti et al., 2014) enabled by the drainage of excess water and also because post-construction compaction is enhanced at optimum moisture content.

Various studies have been performed to reveal MC effects on the mechanical response of subgrade soils (Li & Selig, 1995; Miller et al., 2000; Kim et al., 2003; Khoury & Zaman, 2004; Liang et al., 2008; Erlingsson, 2010; Han & Vanapalli, 2017). However, the sensitivity of the pavement response variation to MCs of subgrade under different conditions has still not been comprehensively described, e.g. when increasing the thicknesses and moduli of asphalt concrete (AC) layer and base layer.

In order to maintain an MC associated with an adequate bearing capacity of subgrade, treatment by an ingress-preventing and/or drainage-enhancing procedure is desirable. Non-water reacting double-component polymer materials exhibit excellent properties (Guo et al., 2018), including environmental protection, safe construction, quick response, adjustability, good expansion characteristics of polymer slurry to form a polymer layer and long service life. However, they have not been applied to

foundation drainage. Therefore, a new polymer drainage layer (PDL) is proposed (see Section 4.3), which aims to provide an alternative drainage mechanism and maybe provide a reinforcement effect on the whole structural response.

Since it is unrealistic to cover every aspect of pavement and railway tracks, cases on the pavement were taken as an example to demonstrate the research. In this chapter, pavement simulation analysis based on KENPAVE was performed under various conditions, i.e. various thicknesses and moduli of subbase, base and AC layer, axle load (A_l) and with/without proposed PDL. The effects of moisture content were incorporated by changing the resilient modulus of subgrade, i.e. using the resilient modulus model to calculate the resilient modulus at each moisture content and then inputting the resilient modulus into the model. Based on a one-at-a-time method, the sensitivity index of each response was defined and measured in terms of pavement response variation (i.e. fatigue and rutting life) with moisture content from one condition to another and then used as an indicator of the sensitivity of the response to those different conditions. The mechanical effect of a PDL on the pavement structure will also be investigated. In addition, based on the previous test data (presented in Chapter 4), further data analyses using literature sources were conducted by selecting various elastic moduli and thicknesses of the AC layer and A_l. Fatigue and rutting life, fatigue cracking and permanent deformation were investigated in terms of the pavement response. It may help to broaden understanding of moisture effects on pavement structures and provide a reference, revealing some implications for pavement (or even railway track) drainage design. The quantitative study will also help to better understand the plasticity effects on pavement response.

4.2 Theoretical framework

4.2.1 Research process

Based on the elastic analysis and statistical data, the effects of moisture content on foundation response were studied in two ways, i.e. sensitivity analysis and data analysis using literature sources. The research process is illustrated in Figure 4.1.

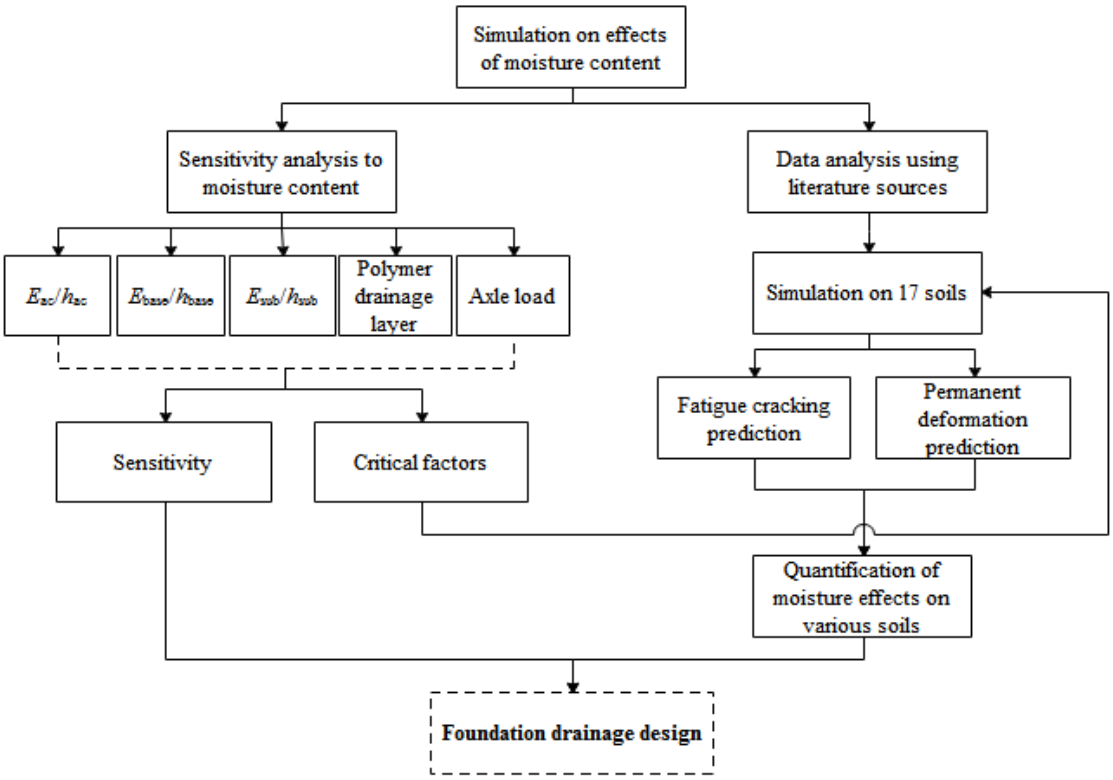

Figure 4.1 Research process for moisture effects

4.2.2 Resilient modulus

The performance of roads and railways depends directly on the mechanical properties of the foundations which should provide reliable bearing capacity for the upper structures and maintain their serviceability. For subgrade soils, it is important to reflect the stress-strain behaviour under normal cyclic traffic loading. Adopted by AASHTO (AASHTO, 1986), the resilient modulus, M_r of subgrade soil is regarded as a more rational soil parameter compared with soil support value or subgrade reaction modulus (Yang et al., 2005) and therefore is commonly applied to the estimation of subgrade deformation under moving traffic. Thus, M_r can be used to investigate and predict the optimum overall performance of road pavement. Mathematically, M_r is described by the relationship of cyclic deviatoric stress q with corresponding axial resilient strain ε_r in the cyclic triaxial test (Li & Selig, 1995), as shown in Eq. (2.21a).

The California bearing ratio (CBR) test is commonly performed to estimate the stiffness of granular materials for road pavements and airfield runways. CBR values show good correlations with some soil properties, e.g. density, moisture content, subgrade modulus, plasticity index and bearing capacity. Based on previous empirical equations, soil resilient modulus can be reasonably evaluated. For the subgrade of

flexible pavements, M_r can be evaluated through CBR tests as follows for $CBR \leq 5$ (Heukelom & Klomp, 1962) and $CBR > 5$ (Powell et al., 1984) through

$$M_{r,sg} = 10 * CBR \; for \; CBR \leq 5 \tag{4.1}$$

$$M_{r,sg} = 17.6 * CBR^{0.64} \; for \; CBR > 5 \tag{4.2}$$

For pavement design, the moduli of subgrade and unbound base layers should be designated at stress levels representative of those they will experience in situ. The latter modulus can be estimated as a function of the subgrade modulus. For granular base and subbase, the moduli can be determined from the subgrade property underneath (Claessen et al., 1977), i.e.:

$$M_{r,gra} = M_{r,sg} * 0.2 * h_g^{0.45} \tag{4.3}$$

where $M_{r,sg}$ and $M_{r,gra}$ (MPa) are the modulus of subgrade and granular base/subbase, respectively, and h_g is the thickness of the granular layer (mm).

Based on the modified model (Eq. (2.21a)) that demonstrates MC effects through the initial drying path and initial wetting path by Khoury et al. (2012), the M_r variation can be determined with increasing moisture contents. Since the study in this Chapter focuses on the sensitivity analysis, the selection of model parameters was simplified, and thus, the statistical analysis results by Khoury et al. (2012) were adopted in this Chapter, i.e. a =-0.162, b =0.435 and k =0.803. From Chu (2020), this model demonstrates the direct effects of MC on M_r. Matric suction has not been explicitly illustrated. By means of the SWCC, the hysteresis behaviour between matric suction and MC should be considered, while the difficulties in direct measurement of suction may reduce the accuracy of modulus prediction. Besides, as noted by Chu (2020), the study showed limitations due to predicting the effect of post-compaction MC on M_r for only one soil type. However, due to the simplicity, this model is introduced to predict M_r of subgrade along the initial wetting path since the wetting process is more critical for design than the drying process. Despite limitations of soil type and the wetting condition, it is expected to serve as an example of investigating M_r variation with moisture content.

4.2.3 Failure models

In terms of the UK design standard, critical stresses and strains consist of: excessive stress/strain (combination of loading magnitude and the number of cycles) inducing fatigue cracking (typically at the bottom of the base) of asphalt concrete, hydraulically bound materials or concrete materials; and excessive subgrade strain causing permanent

deformation of subgrade top (Highway Agency, 2006). The allowable number of load applications is recognized to be related to the maximum tensile strain in the AC layer and compressive strain in the subgrade, which are the most widely adopted criteria for pavement design. In terms of the rutting failure criterion, it does not demonstrate the effect of principal stress axis rotation caused by moving load, which accelerates the permanent deformation of the base and subgrade (Ishikawa et al., 2011; Inam et al., 2012). The failure models will focus on fatigue life and rutting life prediction. Based on the models, the parameter selection would affect the results, but the general trend should be in agreement. This indicates that before sensitivity analysis, the test/field conditions need to be considered and select the suitable model to achieve accurate analysis.

4.2.3.1 Fatigue life prediction

The following assumptions are made: micro-cracking induces modulus loss of the AC layer and initial cracks start at the bottom of the asphalt concrete layer due to tensile stresses caused by flexure; then, cracks develop to the surface under repeated wheel loading; next, repeated tensile strain results in progressive fatigue cracking; finally, pavement failure happens. The allowable number of loads causing the fatigue cracking of asphalt concrete is, thus, associated with tensile strain.

Depending purely on laboratory fatigue tests, fatigue life (Huang, 2004) is predicted as the number of repetitions to failure. In the traditional approach (Ahmed, 2016), it is with the following form (Monismith et al. 1985):

$$\mathrm{N}_f = f_1(1/\varepsilon_t)^{f_2}(1/E_{ac})^{f_3} \tag{4.4}$$

where f_1, f_2 and f_3 are regression coefficients, N_f is the allowable number of loads in flexure to the initiation of fatigue cracking when ε_t is a constant strain at the bottom of the asphalt concrete layer and E_{ac} is the elastic modulus of the asphalt concrete in psi.

Because, in reality, not all cracking is bottom-up, a more realistic prediction of fatigue cracking performance was achieved by the use of the MEPDG models (NCHRP 2004c):

$$\mathrm{FC}_{bottom-up} = \frac{1}{60} \times \frac{6000}{1 + e^{(-2c_2' + c_2' \times \log(D \times 100))}} \tag{4.5}$$

$$\mathrm{FC}_{top-down} = 10.56 \times \frac{1000}{1 + e^{(7.0 - 3.5 \times \log(D \times 100))}} \times 0.189394 \tag{4.6}$$

where $\mathrm{FC}_{bottom-up}$ is the percentage area affected by cracking that initiates bottom-up (%), $\mathrm{FC}_{top-down}$ is the length of fatigue cracking initiating at the top (mm/m), $c_2' =$

$-2.40874 - 39.748 \times (1 + h_{ac}/25.4)^{-2.856}$ and D is the fatigue damage of either bottom-up or top-down cracking. The primary input to these models is D which was calculated in this study based on Miner's law (Huang, 2004). Damage ratio, D_r, is defined as the sum of the ratio between the predicted and allowable number of repetitions for each load group in each period. It can be expressed as

$$\mathrm{D}_r = \sum_{i=1}^{P} \sum_{j=1}^{m} \frac{n_j}{N_j} \tag{4.7}$$

The regression parameters of fatigue life models from various organizations or studies are presented in Table 4.1. These models are simple and convenient ways of predicting N_f for pavement analysis, but they are obtained through continuous loading over a constant range of strains which is inconsistent with the conditions to be expected in situ (where there are, e.g. healing effects due to rest periods from the lack of continuity in moving load, environmental factors and different strains in different loadings) (Ahmed, 2016). Field calibration is required to predict in-situ pavement responses. In this study, considering its simplicity, the parameters from Asphalt Institute were adopted to predict N_f.

Table 4.1 Regression parameters of N_f prediction models

Source		f_1	f_2	f_3
Asphalt Institute		0.0795	3.291	0.854
Shell Research		0.0685	5.671	2.363
Finn model		1.589e-04	3.291	0.854
US Army Corps of Engineers		497.156	5	2.66
Belgian Road Research Centre		4.92e-14	4.76	0
Transport and Road Research Laboratory		1.66e-10	4.32	0
Federal Highway Administration		0.1001	3.565	1.474
ILLINOIS Department of Transportation		5e-06	3	0
Austin Research Engineers		0.4875	3.0312	0.06529
Korean Pavement Design Method	4% *AVR	4e-07	2.79	0
	5% AVR	5e-14	4.62	0
	6% AVR	7e-11	3.82	0
Accelerated Pavement Testing		1.65	2.994	0

Note: *AVR represents air void ratio. The general advantages and disadvantages of these models are presented as follows. **(1) Advantages**: simple form with several parameters involved; convenient to use to achieve reasonable pavement analysis; able to be adjusted to fit in the field condition. **(2) Disadvantages**: limited conditions and factors, e.g. environmental effects, temperature, mixture property, loading frequency and rest periods between loads, were not comprehensively considered; require field shift factor from field calibration for in-situ conditions; limited cracking for regression compared with in-service situations; dependence on the goodness of fit for regression.

4.2.3.2 Rutting life prediction

Permanent deformation is an important factor that should be considered in flexible pavement design. The failure model for rutting life prediction can be expressed as

$$N_r = f_4(1/\varepsilon_c)^{f_5} \tag{4.8}$$

where f_4 and f_5 are regression parameters, N_r is the allowable number of loads resulting in permanent deformation and ε_c is the maximum compressive strain at the top of the subgrade. Various regression parameters of N_r prediction models are presented in Table 4.2. The same caveats apply to N_r as to N_f, when the inconsistencies between idealised loading and in-situ loading are considered. In this study, N_r was predicted with the parameters from Asphalt Institute. In terms of cumulative permanent deformation on subgrade top, it will be evaluated through Eqs. (2.39)~(2.41).

Table 4.2 Regression parameters of N_r prediction models

Source	f_4	f_5
Asphalt Institute	1.365e-09	4.477
Shell Research	6.15e-07	4
US Army Corps of Engineers	1.81e-15	6.527
Belgian Road Research Centre	3.05e-09	4.35
Transport and Road Research Laboratory	1.13e-06	3.75

Note: these models are empirical and derived under specific experimental conditions.

Based on these models, the parameter selection would affect the results, but the general trend should be in agreement. This indicates that before sensitivity analysis, the test/field conditions need to be considered and select the suitable model to achieve accurate analysis.

4.2.4 KENPAVE

KENPAVE by Huang (2004) was adopted to analyse typical pavements as an MLE system under moving multiple wheel loads (e.g. single, dual, dual-tandem or dual-tridem wheels) with elastic responses of each layer. Based on KENLAYER (part of KENPAVE), flexible pavement structures are analysed as an MLE system with n-1 layers, and a n^{th} layer as a semi-infinite elastic half-space, under a circular loaded area. For linear-elastic systems, the superposition principle is adopted for multiple wheels. In a nonlinear elastic system, the solutions are superimposed iteratively with a method of successive approximations. It is common to conduct damage analysis by dividing a year into 12 periods, and material parameters (i.e. modulus of elasticity and Poisson's

ratio) can be applied in each period. A total of 12 load types (either single or multiple) can be applied to each period. Since load types are beyond the scope of this research, only one load type is considered for simplification, i.e. single axle dual wheel load.

Under a rolling wheel load, a stress point in a pavement structure suffers various stresses, including vertical, horizontal, and shear components. Figure 4.2 illustrates the variations of stress at a point with time.

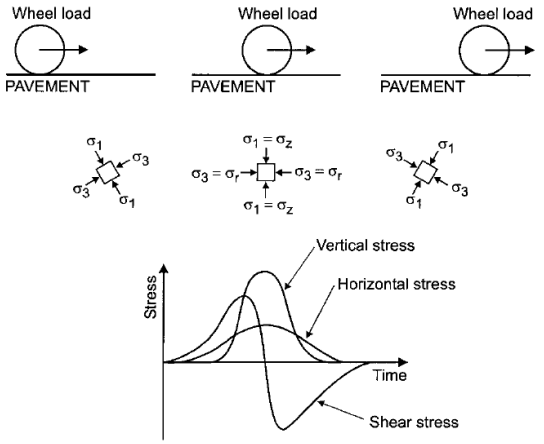

Figure 4.2 Stresses beneath rolling wheel load, from Lekarp et al. (2000b)

4.3 Sensitivity analysis

4.3.1 Sensitivity index

As a simple technique, the Morris One-at-a-Time method is utilized to measure the sensitivity of pavement response to drainage at various conditions. A k-dimensional p-level space is assumed, i.e. k factors (termed $X_1, X_2, \dots, X_k$) are included and each factor can take p values. The elementary effect (i.e. d_i) for the i^{th} input factor is defined as (Morris, 1991)

$$d_i = \frac{f(X_1, \dots, X_{i-1}, X_i + \Delta, X_{i+1}, X_k) - f(X)}{\Delta} \tag{4.9}$$

where Δ is the variation applied to the factor X_i so that $(X_1, \dots, X_{i-1}, X_i + \Delta, X_{i+1}, X_k)$ are the selected inputs. The mean deviation of d_i is expressed as

$$\overline{d}_i = \frac{\sum_{j=1}^{p} d_i(j)}{p} \tag{4.10}$$

where $\overline{d}_i$, the average value at factor X_i, is taken as the measure of this method. A revised method was developed by Campolongo et al. (2007), i.e.

$$\overline{d}_i^* = \frac{\sum_{j=1}^{p} |d_i(j)|}{p} \tag{4.11}$$

In this study, five moisture contents were considered for the subgrade, and particularly w_0 (i.e. w_{opt}) was set as the base condition. Thus, k varied and $p = 4$. In

order to facilitate the comparison of the index among different responses, sensitivity indexes ($S_{i,w_1}, S_{i,w_2}, \ldots, S_{i,w_p}$) from Eq. (4.9) at each moisture content increment of the i^{th} factor were normalized as Eq. (4.12). Then, the sensitivity index S_i at the i^{th} factor is calculated through Eq. (4.13).

$$S_{i,w_1} = \frac{\left|R_{w_1} - R_{w_0}\right|}{\Delta w} \times \frac{w_0}{\left|R_{w_0}\right|} \tag{4.12}$$

$$S_i = \frac{S_{i,w_1} + S_{i,w_2} + S_{i,w_3} + S_{i,w_4}}{4} \tag{4.13}$$

where w_0, w_1, w_2, w_3 and w_4 are moisture contents, Δw is the increment of moisture content, i.e. $w_1 - w_0$, and pavement responses at w_0 are denoted as the reference condition; S_{i,w_1} is the sensitivity index of each response at w_1. w_0 is assumed as 10% in this study. A larger S_i value indicates a higher sensitivity to moisture content increments. In this study, only the moisture content variation of the subgrade was considered. A set of limits were proposed to define the sensitivity levels in Table 4.3 to better understand the effects of each parameter (Nazarian et al., 2003).

Table 4.3 Levels of sensitivity classification (Nazarian et al., 2003)

Sensitivity index	Level of sensitivity	Significance to pavement design
$S_i < 0.25$	Not sensitive	Can be probably estimated with small errors in final results
$0.25 \leq S_i < 0.5$	Moderately sensitive	Must be measured to limit errors in design
$0.5 \leq S_i < 1$	Sensitive	Must be measured with reasonable accuracy for satisfactory design
$S_i \geq 1$	Very sensitive	Must be measured very accurately or the design may not be considered appropriate

4.3.2 Model geometry and property

A four-layer flexible pavement structure is selected to study pavement response to MC variation under different conditions. It includes the AC layer, base, subbase, subgrade and/or proposed PDL. The dimensions and properties of pavement structure are designed in compliance with the Design Manual for Roads and Bridges (DMRB) (Highway Agency, 2006). The general structure is presented in Figure 4.3 as an example (Nunn et al., 1997; Kent County Council, 2000; Highway Agency, 2006). The CBR value of the compacted subgrade is arbitrarily denoted as 20 with infinite thickness, and Poisson's ratio is set as 0.4. The temperature is taken as 20°C (moderate).

The moisture conditions of the subgrade layer considered in this study are assumed as w_{opt} (full modulus), w_{opt}+1%, w_{opt}+2%, w_{opt}+4% and w_{opt}+6%, respectively, to cover a wide range of wetting since it will induce lower subgrade strength and is more critical to structural stability. According to the correlation of M_r with MC shown in Eq. (2.21a), the varying M_r of subgrade soils is estimated for each moisture condition. To achieve M_r, a code with flexible parameter inputs has been developed through MATLAB R2018a to solve the equation, and the results are presented in Figure 4.4.

Based on the density and elastic modulus of the non-water reaction double-component polymer materials obtained in previous experiments (i.e. Table 4.4) (Xu et al., 2012), a composite layer is designed for pavement drainage. The components of the PDL are illustrated in Figure 4.5. The PDL is designed as an ultra-thin polymer layer sandwiched between two permeable geocomposite layers installed at the interface of the subgrade and subbase. This polymer layer was impermeable and was expected to prevent water migration upward or downward. The permeable geocomposite is covered, top and bottom, by permeable geotextiles. The geotextile will limit fine contents in the adjacent layers from migrating into the geocomposite, which would be likely to block water transmission. Thus, this will limit the undermining of the structure due to fines loss. The polymer layer is made of non-water reacting polymer (i.e. double-component polyurethane foam), which exhibits excellent properties (Guo et al., 2018), making it a novel candidate for application in foundation drainage. Furthermore, the polymer layer of the PDL may deliver mechanical benefits to the pavement. In this way, it may provide an alternative approach for pavement drainage design. With high permeability, the geocomposite will accelerate the collection and removal of water from the structural layers.

For the analysis, the impermeable polymer layer is assumed to have been prefabricated in a thin rectangular mould, based on the construction of the ultra-thin anti-seepage wall by the Non-water Reacting Polymer Grouting Technology (Wang et al., 2015). This layer will inhibit the water movement across the layers. During the numerical analysis, the PDL is treated as a polymer layer alone since the stiffness of the polymer layer dominates in the composite structure. Based on the simplified calculation, its mechanical effect on the pavement response will be revealed. Regarding notations, ‘D’ indicates PDL, ‘0’ means no PDL, and E, TH and, P are the elastic modulus, thickness and position of the PDL, respectively. The thickness and elastic

modulus of the polymer layer will be studied. According to the experimental results by Xu et al. (2012), the anti-seepage polymer layer was 5 cm in thickness, which showed good anti-seepage performance. The elastic modulus of the polymer with the density was also revealed, as shown in Table 4.4. Thus, the thickness and modulus of the polymer layer are selected, ranging from 25 mm to 200 mm and from 20 MPa to 229 MPa, respectively. Various positions of the polymer layer will be investigated, i.e. subbase top, 5 cm below subbase top, 5 cm above subbase bottom, subgrade top and 5 cm below subgrade top.

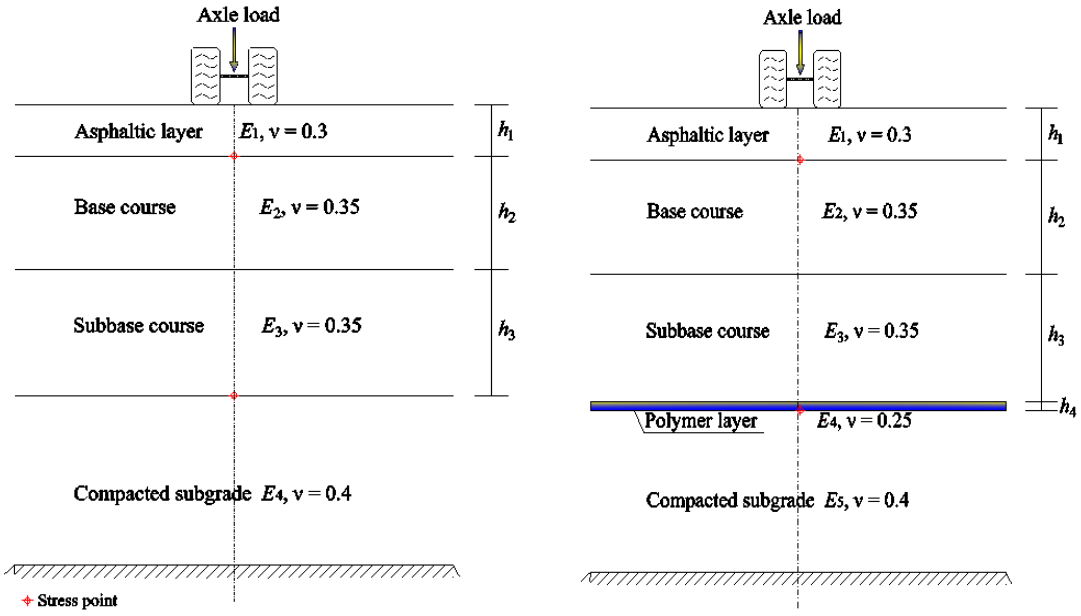

a b

Figure 4.3 Multilayered elastic flexible pavement: (a) without and (b) with polymer layer (e.g. on the top of subgrade)

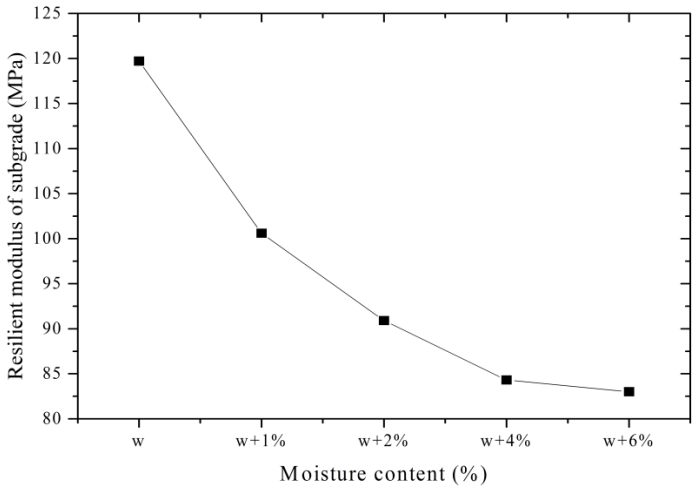

Figure 4.4 Resilient modulus variation of the subgrade with moisture content

Table 4.4 Elastic modulus and density of polymer materials (Xu et al., 2012)

Specimen	1	2	3	4	5	6	7	8	9	10
Density /g·cm^{-3}	0.16	0.27	0.29	0.35	0.36	0.40	0.42	0.47	0.49	0.53
Elastic modulus /MPa	18.2	20.3	40.8	109	136	202	214	218	225	229

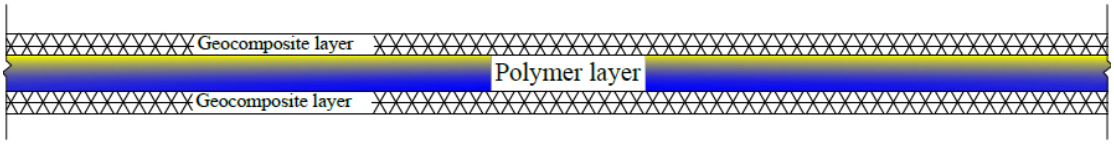

Figure 4.5 Polymer drainage layer

The wheel load was taken to be a single axle with dual wheels, approximated by two circular loaded areas, and the contact pressure depended on the scenarios with different A_l at the same radius. As traffic load was exerted over two circular areas, the maximum stresses, strains or deflections occurred at the centre or the edge of the tyre or directly at stress points located at the midpoint between two dual tyres along the axle. Response at, or immediately below, these stress points were selected and compared for pavement analysis to determine the most critical location. Vertically, stress points at the bottom of the AC layer and the subgrade top were studied.

4.3.3 Parameter selection

Based on HD 26/06 (Highway Agency, 2006), the thickness of each layer is selected. According to the classification of foundation stiffness classes equivalent to the half-space long-term stiffness of the composite foundation under the completed pavement, the assumed subgrade belongs to Foundation Class 2 (stiffness ≥ 100 MPa). Referring to HD 26/06, this foundation should not be adopted for design traffic volume exceeding 80 msa (i.e. million standard axle), unless 150 mm or more of a bound subbase is used, and in this case a subbase with a thickness of no less than 200 mm is adopted. Hydraulically bound mixture (HBM) is denoted as the base material. The value of the stiffness modulus of HBM used is no less than 400 MPa. The thickness of the AC layer in mm (H) over the HBM base is given by (Highway Agency, 2006)

$$H = -16.05 \times (\log(N))^2 + 101 \times \log(N) + 45.8 \quad (4.14)$$

where H is the thickness of the AC layer in mm and N is the design traffic volume in msa with a maximum of 400 msa. The calculated thickness will be rounded up to the next 10 mm with a minimum thickness of 100 mm for < 4 msa, and a thickness of 180

mm for > 80 msa. Derived from the design nomographs for flexible pavement (Figure 4.6), the thickness of the surfacing layer and base is selected. Due to the significant role of AC layers in pavement response, a wide range of values in their thickness and modulus will be chosen.

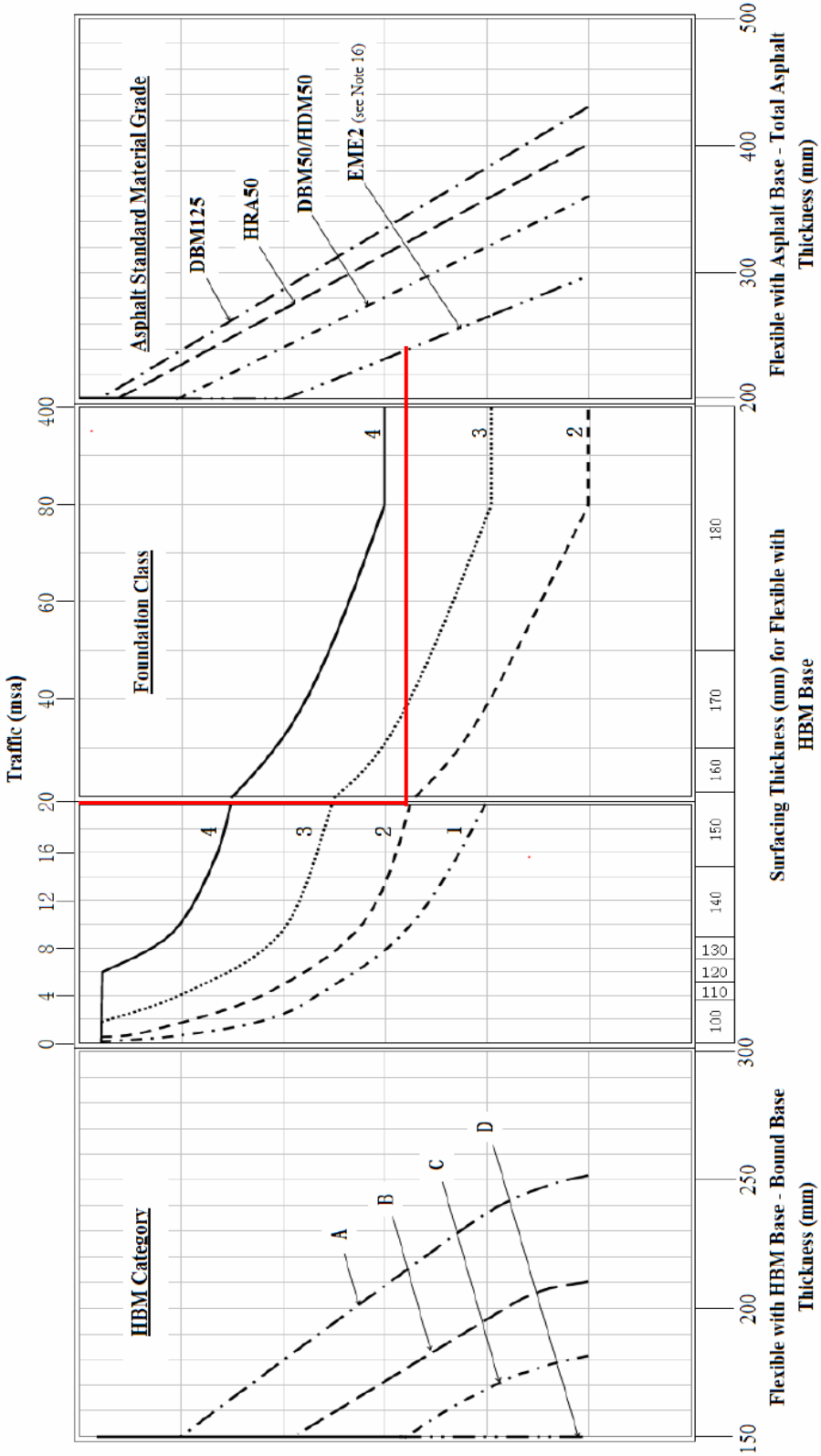

Figure 4.6 Design nomographs for flexible pavement, from HD 26/06 (Highway Agency, 2006) (Example design – red line: traffic, 20 msa; foundation class 2; EME2 asphalt concrete, 235 mm)

As claimed in HD 26/06, for Highways England schemes, the typical figures for long-term elastic stiffness modulus of standard UK asphalt materials for analytical design are required. These are adopted as follows: DBM125: 2500 MPa; HRA50: 3100 MPa; DBM50/HDM50: 4700 MPa; EME2: 8000 MPa (Highway Agency, 2006). Based on these typical figures, interpolation is adopted to cover a wide range of moduli. Considering the factors that affect moisture damage (see Table 4.5), various values of the following parameters will be selected: axle load, thickness and modulus of subbase, base and AC layers, and drainage (with or without proposed PDL).

Table 4.5 Factors affecting moisture damage (Scholz & Rajendran, 2009))

Major Factors	**Descriptions**
Aggregate Properties	Composition (degree of acidity or pH, surface chemistry, type of minerals, source of aggregate) Physical characteristics (angularity, surface roughness, surface area, gradation, porosity, and permeability); Dust and clay coatings; Moisture content; Resistance to degradation
Asphalt Binder Properties	Grade or stiffness; Chemical composition; Crude source and refining process
HMA Mixture Characteristics	Air void level and compaction; Type of HMA (dense-graded, gap-graded, open-graded)
Environmental Factors	Temperature; Freeze-thaw cycles; Moisture vapour; Dampness; Pavement age; Micro-organisms; Presence of ions in the water
Traffic	Percent of trucks; Gross vehicle weight of trucks; Truck tyre pressure
Construction of HMA Pavements	Compaction; Drainage; Weather; Segregation; Contractor experience
Design of HMA Pavements	Air void content; Subsurface drainage; HMA mix selection; Designer experience; Designer site visit

4.3.4 Simulation scenarios

In order to demonstrate the effects of various parameters in a concise way and to exploit the Morris One-at-a-Time approach, all other parameters are fixed at reasonable values while parameters under consideration are varied to reveal their effects (Huang 2004). The spacing of dual wheels is determined by a typical tyre designation 295/80R22.5, i.e. 345 mm. A contact radius of 10.3 cm is assumed in accordance with an 80 kN single axle exerting a contact tyre pressure of 600 kPa.

The matrix for parameter arrangement is presented in Table 4.6 and Table 4.7. Parameters for the polymer layer are tabulated in Table 4.8 in detail.

Table 4.6 Matrix for parameters selection

Variables \ Fixed values		AC v = 0.3		Base v = 0.35		Subbase v = 0.35		Load	PDL
		h_{ac} /mm	E_{ac} /MPa	h_{base} /mm	E_{base} /MPa	h_{sub} /mm	E_{sub} /MPa	A_l /kN	
AC	TH_1 ~ TH_9	-	4700	250	300	200	100	80	n/a
	E_1 ~ E_9	180	-	250	300	200	100	80	
Base	TH_1 150								
	TH_2 200								
	TH_3 250	180	4700	-	300	200	100	80	n/a
	TH_4 300								
	TH_5 350								
	E_1 150								
	E_2 200								
	E_3 250	180	4700	250	-	200	100	80	n/a
	E_4 300								
	E_5 350								
Subbase	TH_1 150								
	TH_2 175								
	TH_3 200	180	4700	250	300	-	100	80	n/a
	TH_4 250								
	TH_5 300								
	E_1 75								
	E_2 100								
	E_3 125	180	4700	250	300	200	-	80	n/a
	E_4 150								
	E_5 200								
AL	AL_1 60								
	AL_2 80								
	AL_3 100	180	4700	250	300	200	100	-	n/a
	AL_4 120								
	AL_5 180								
PDL	Without	180	4700	250	300	200	100	80	Without
	With								With

Table 4.7 Thickness and modulus variables of AC layer

Thickness /mm	25, 50, 75, 100, 150, 180, 225, 270, 300
Elastic modulus /MPa	2000, 2500, 3100, 3500, 4000, 4700, 5700, 6600, 8000

Table 4.8 PDL characteristics (Xu et al., 2012)

Condition	h_{drain} /mm	E_{drain} /MPa	v	Position
D0	0	0	0.25	No PDL
DE1	25	20	0.25	Subgrade top (SgTop)
DE2	25	41	0.25	SgTop
DE3	25	109	0.25	SgTop
DE4	25	202	0.25	SgTop
DE5	25	229	0.25	SgTop
DTH1	25	202	0.25	SgTop
DTH2	50	202	0.25	SgTop
DTH3	100	202	0.25	SgTop
DTH4	150	202	0.25	SgTop
DTH5	200	202	0.25	SgTop
DP1	25	202	0.25	Subbase top (SubTop)
DP2	25	202	0.25	5cm below SubTop (SubTopB5)
DP3	25	202	0.25	5cm above Subbase bottom (SubBottA5)
DP4	25	202	0.25	SgTop
DP5	25	202	0.25	5cm below SgTop (SgTopB5)

4.3.5 Results and discussion

The results under different conditions are illustrated (see Figure 4.7~Figure 4.26) to present the tensile strain at the bottom of asphalt concrete, the compressive strain at the top of the subgrade and the corresponding N_f and N_r. Even though the effects of the thickness and the modulus of AC layer, base and subbase, and A_l on the pavement response are well known in principle, the sensitivity of the pavement response to MC increment at each condition is presented, and they are also presented concerning the effects of the PDL. The mechanical effects of the proposed PDL on the pavement structure are then revealed. The effects of moisture content were incorporated by changing the resilient modulus of subgrade, i.e. using the resilient modulus model to calculate the resilient modulus at each moisture content and then inputting the resilient modulus into the model.

4.3.5.1 Effects of asphalt concrete

Figure 4.7 and Figure 4.8 show that with the increase of AC modulus and thickness (E_{ac} and h_{ac}), N_f and N_r both increased significantly, while showing a decreasing trend with moisture content. Elastic modulus and thickness of AC generated larger effects on N_f than N_r. At a lower modulus and thickness, no clear decreasing trend was

found in N_f with increasing MC. N_r exhibited larger decrease with the same increment of MC, which was consistent with Figure 4.9 and Figure 4.10. At higher moisture contents, the positive effects of increasing AC modulus and thickness on N_r were attenuated. Generally, the sensitivity of N_r was 10-20 times larger than that of N_f. The sensitivity of N_f increased by 1.3 times with the modulus, E_{ac}. The sensitivity of N_f showed a decrease by 91% with h_{ac} increasing from 25 mm to 75 mm, while it increased by about 10 times as the thickness, h_{ac}, varied from 75 mm to 300 mm. Thus, a 6 GPa change in modulus is almost equivalent to a 50 mm change in thickness in terms of the sensitivity of N_f. The sensitivity was significantly influenced by the parameters (i.e. elastic modulus of asphalt concrete). This can provide a perspective for quantitatively analysing the pavement response due to moisture variation. At a thickness of 75 mm, the overall sensitivity of N_f and N_r to moisture variation presented a minimum value. It may indicate that a thinner pavement could maintain a more stable performance at changing moisture conditions. The sensitivity of N_r decreased by 0.9% and 5.2% with AC modulus and thickness, respectively. Thus, in terms of pavement design for rutting control at higher water levels, a thicker or stiffer pavement will not be an effective way to prevent foundation deformation development.

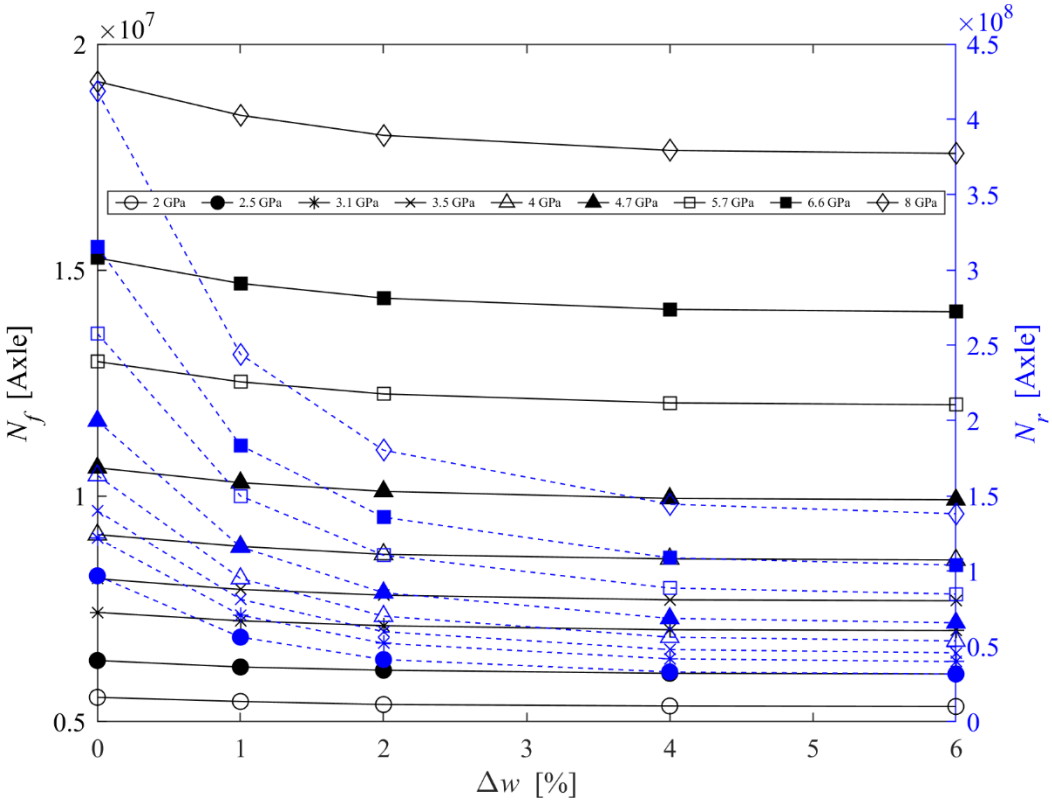

Figure 4.7 N_f and N_r at various E_{ac} (Δw indicates the moisture content of subgrade % above optimum moisture content)

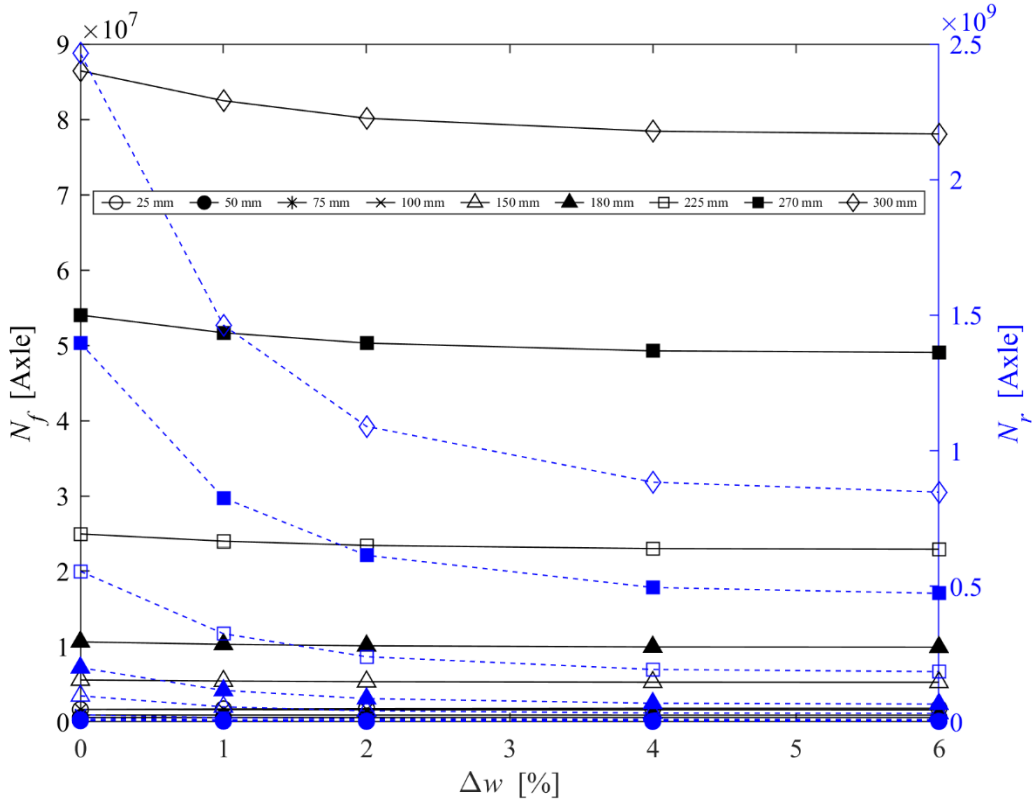

Figure 4.8 N_f and N_r at various h_{ac}

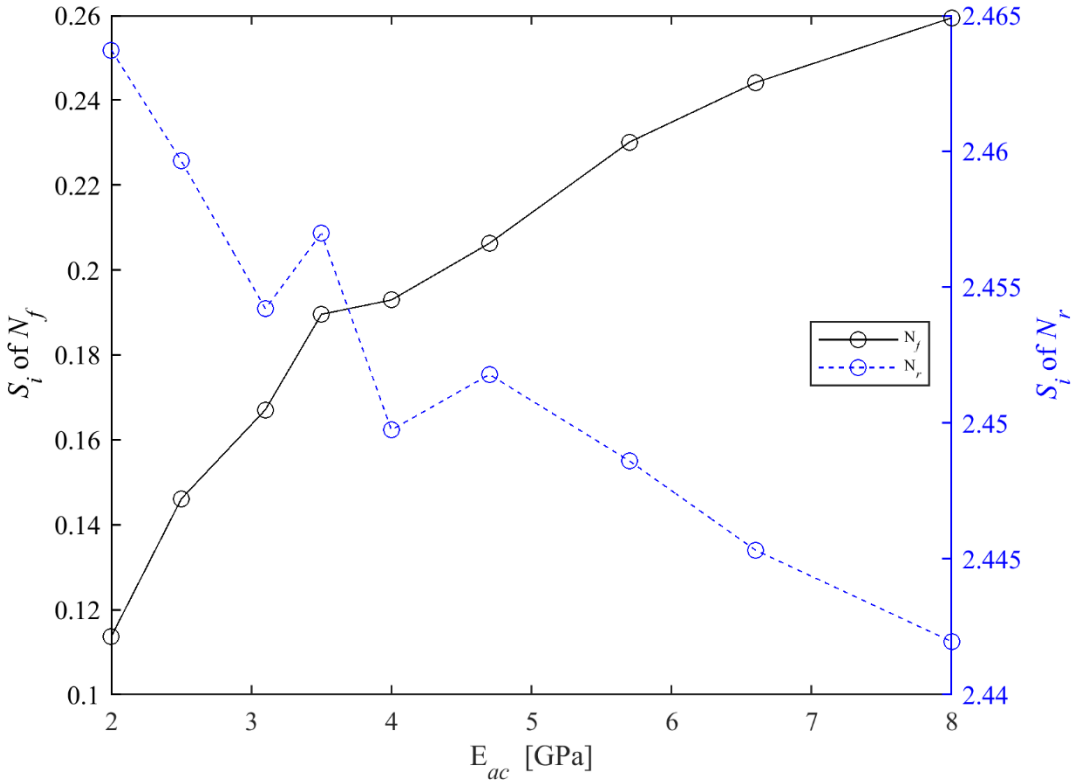

Figure 4.9 S_i of N_f and N_r to MC at various E_{ac}

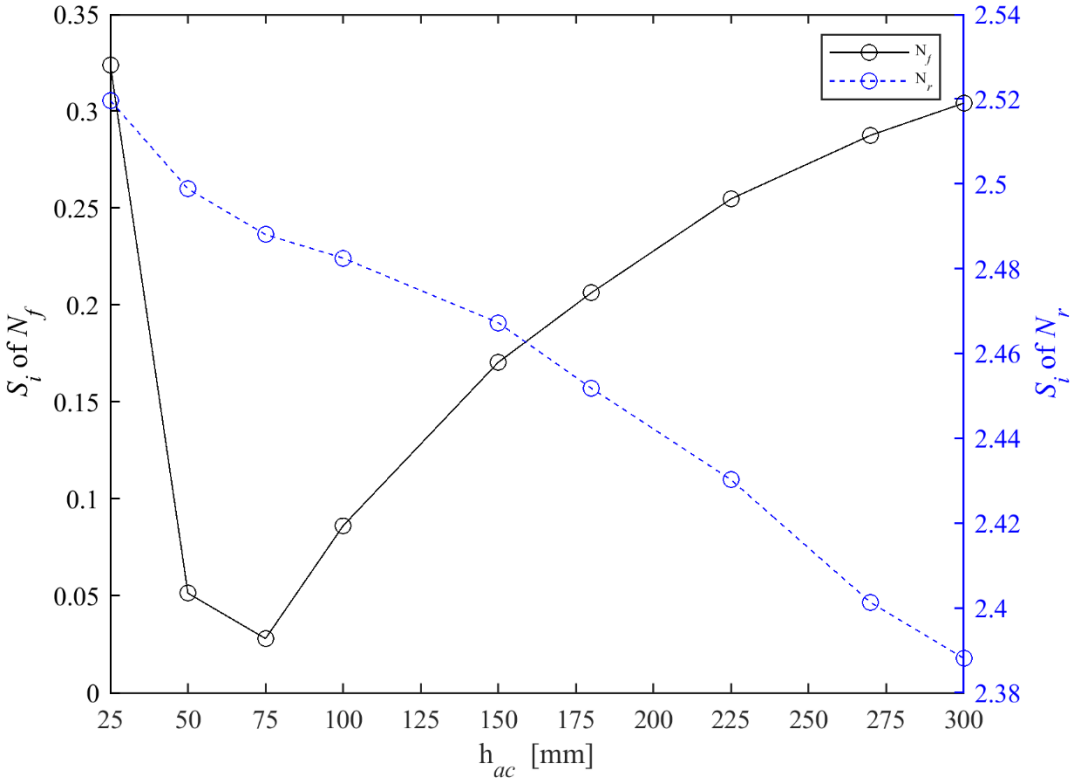

Figure 4.10 S_i of N_f and N_r at various h_{ac}

4.3.5.2 Effects of base layer

N_f and N_r showed similar trends with MC at various base thicknesses and moduli (E_{base} and h_{base}) for the same AC modulus, as shown in Figure 4.11 and Figure 4.12. In terms of the sensitivity in Figure 4.13 and Figure 4.14, N_f and N_r both showed a decreasing trend. The sensitivity of N_f decreased by 11% and 56% along with the base modulus and base thickness (E_{base} and h_{base}), respectively, and the sensitivity of N_r decreased by 4% and 2% accordingly. Although the sensitivity of N_r showed a slight variation with base thickness and modulus (E_{base} and h_{base}), the increase of moduli and thicknesses of base layer can promote the service life of road and reduce the foundation sensitivity to higher water level. It was found that a 200 MPa change in base modulus is equivalent to about a 50 mm change in base thickness in terms of the sensitivity of N_f.

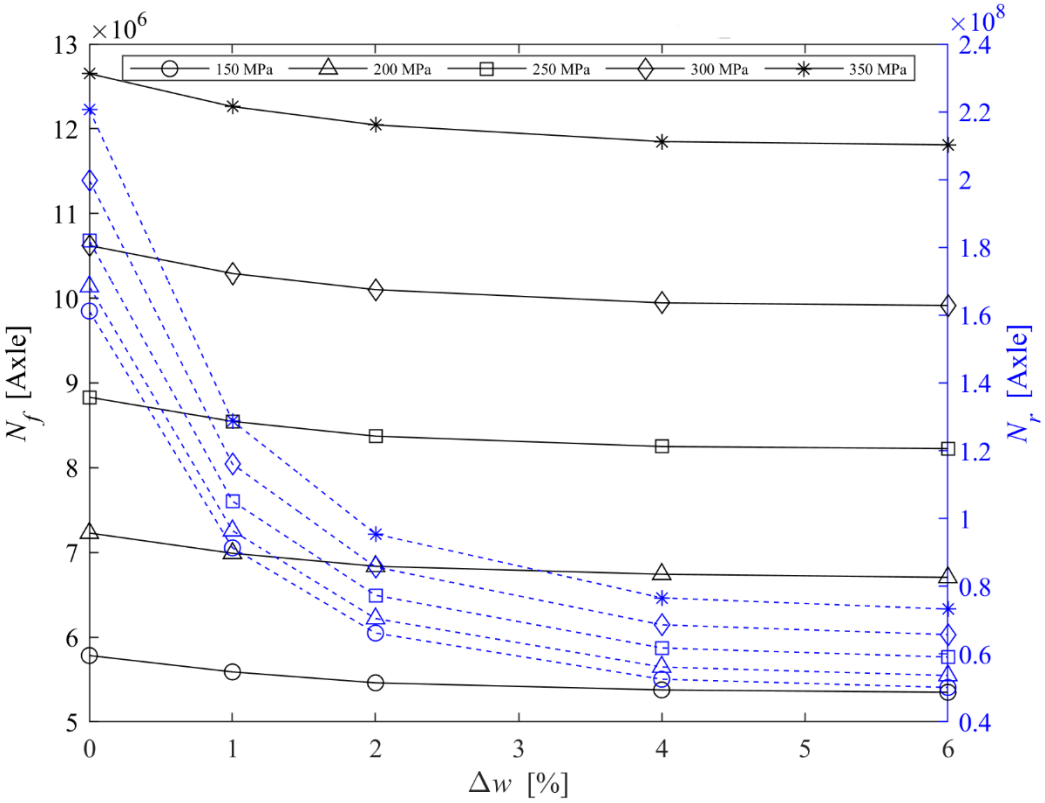

Figure 4.11 N_f and N_r at various E_{base}

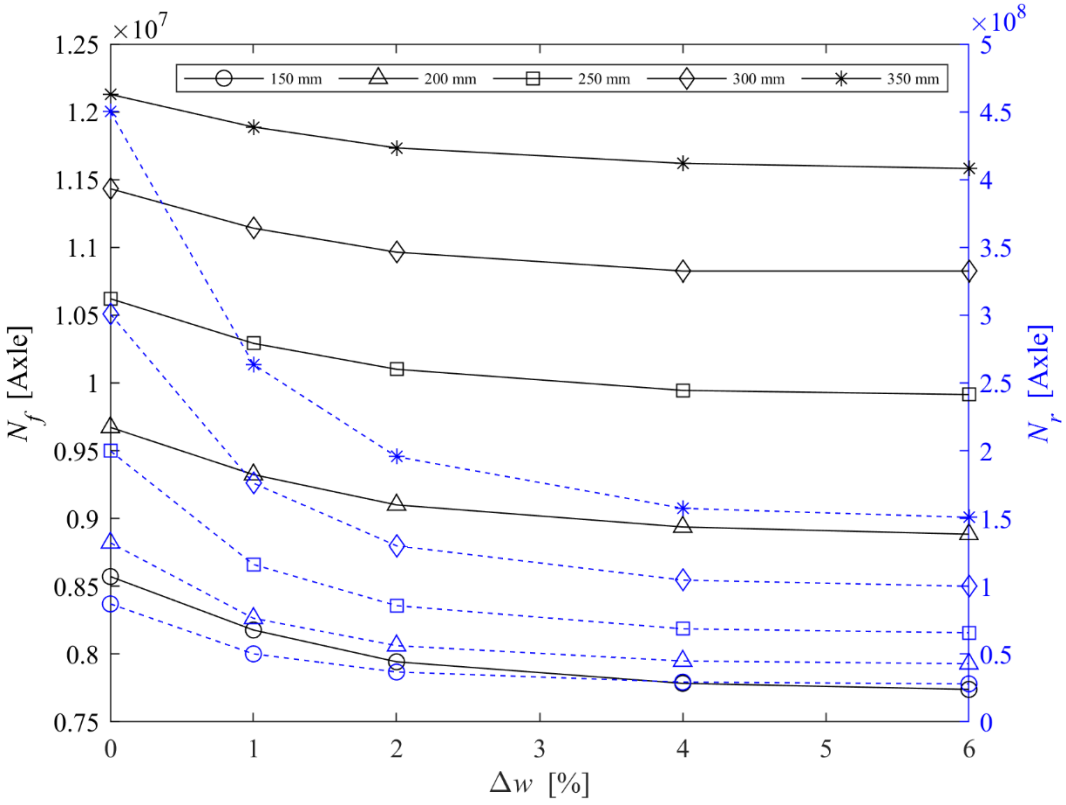

Figure 4.12 N_f and N_r at various h_{base}

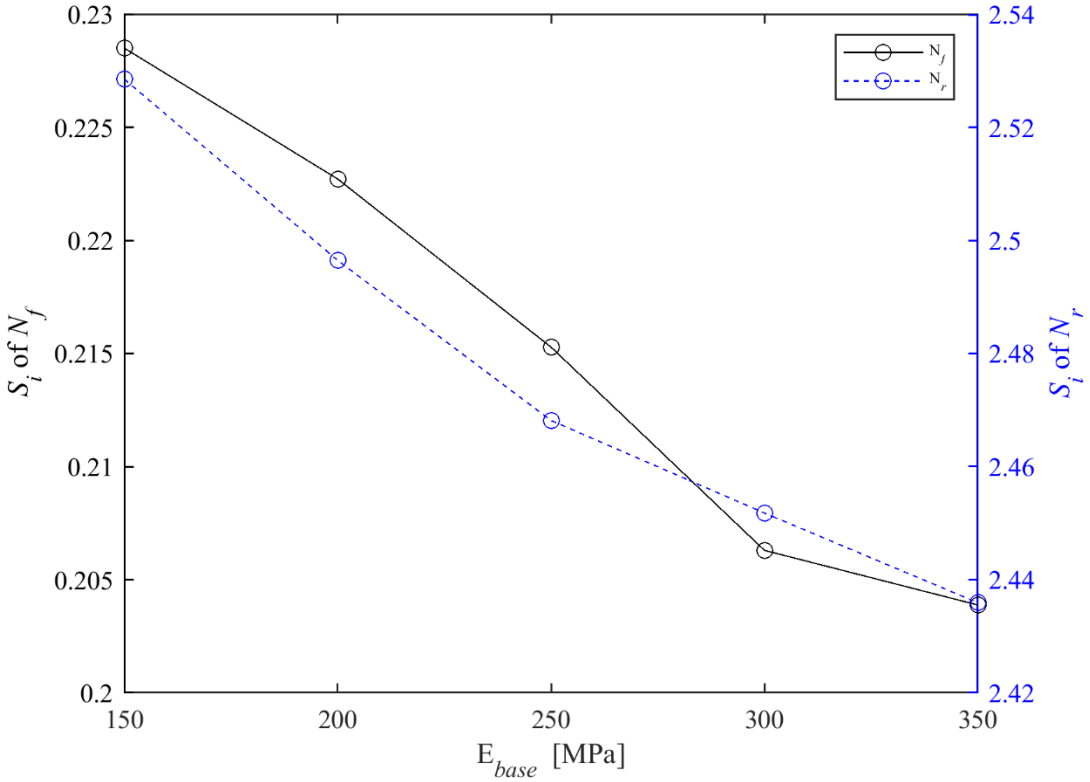

Figure 4.13 S_i of N_f and N_r to MC at various E_{base}

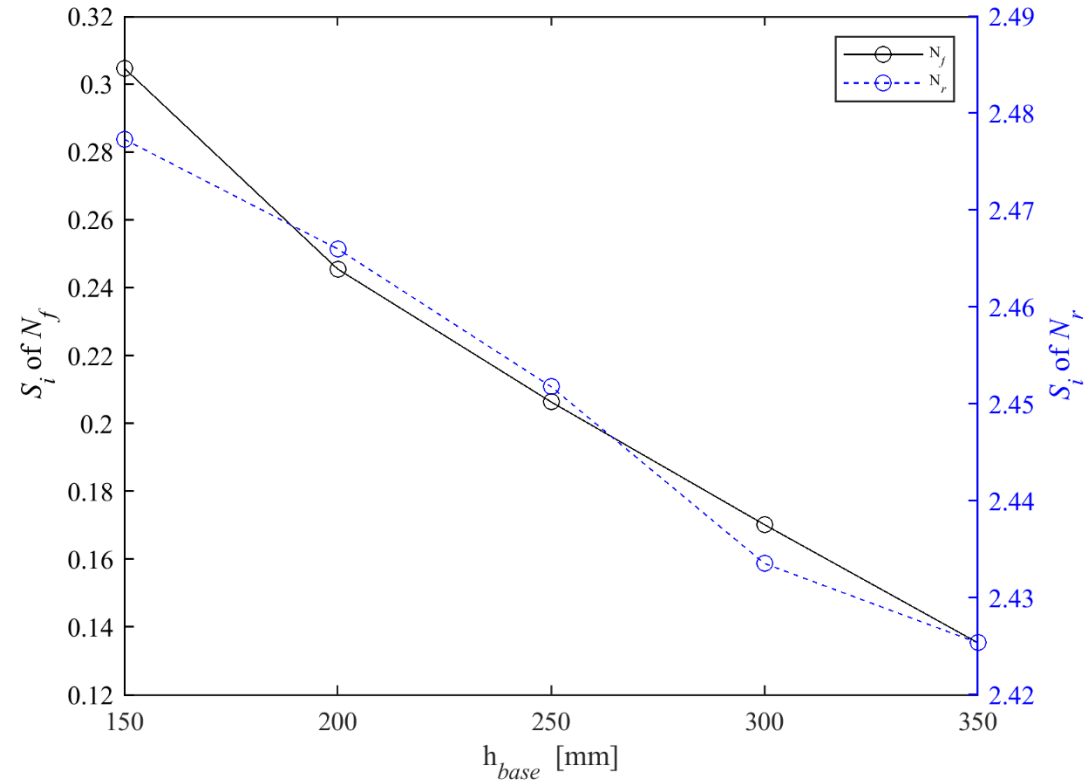

Figure 4.14 S_i of N_f and N_r at various h_{base}

4.3.5.3 Effects of subbase layer

N_r showed a decreasing trend with the increase of subbase modulus (E_{sub}), contrary to that with subbase thickness, h_{sub}, as seen in Figure 4.15 and Figure 4.16. With Δw increasing by 1%, N_f showed different patterns with subbase thickness, i.e. decreasing to a certain point and then increasing. Figure 4.17 and Figure 4.18 illustrate that apart from the change in sensitivity of N_f completely different from that of N_r at various thickness, they did not have a consistent pattern at various modulus. The sensitivity of N_f hardly showed changes with subbase modulus. The sensitivity of N_r started to show a decreasing trend at the modulus (E_{sub}) of 150 MPa. Regardless of the increase of N_f and N_r, a subbase thickness of 200 mm showed a similar effect on their sensitivities to the rising moisture with a h_{sub} of 300 mm. It implies that increasing the thickness of subbase layer at higher water levels may not be an effective way to reduce the sensitivity for pavement design when the subbase reaches a certain thickness.

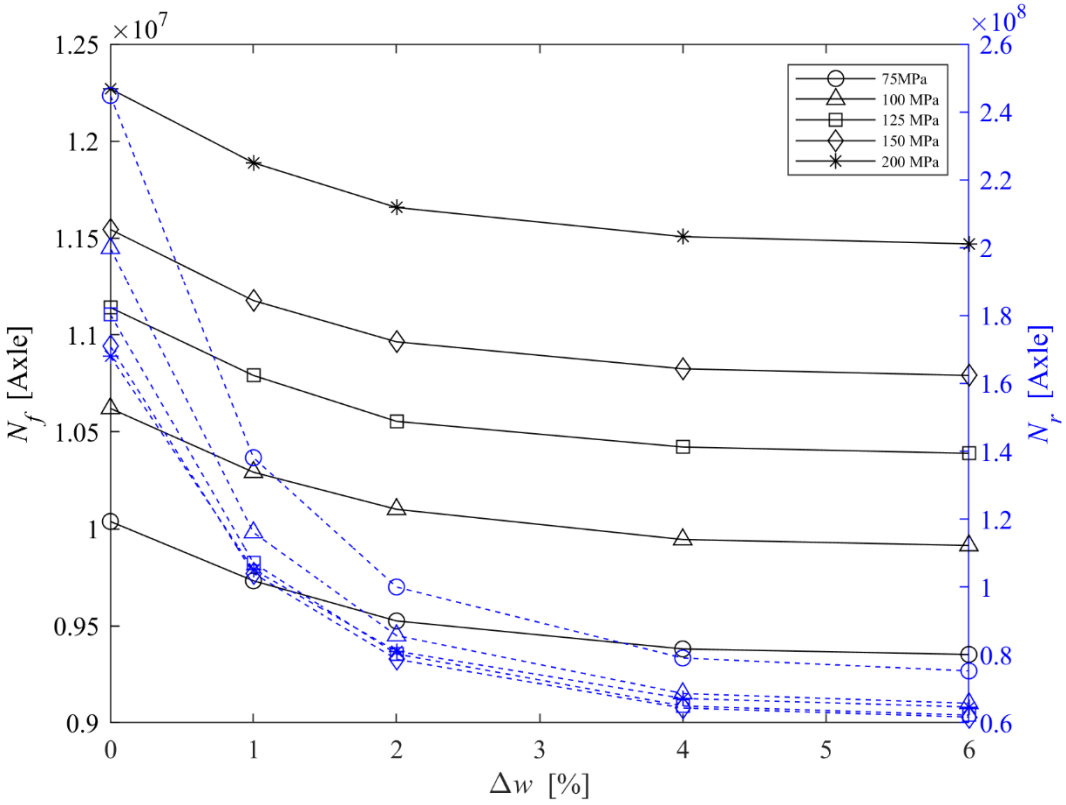

Figure 4.15 N_f and N_r at various E_{sub}

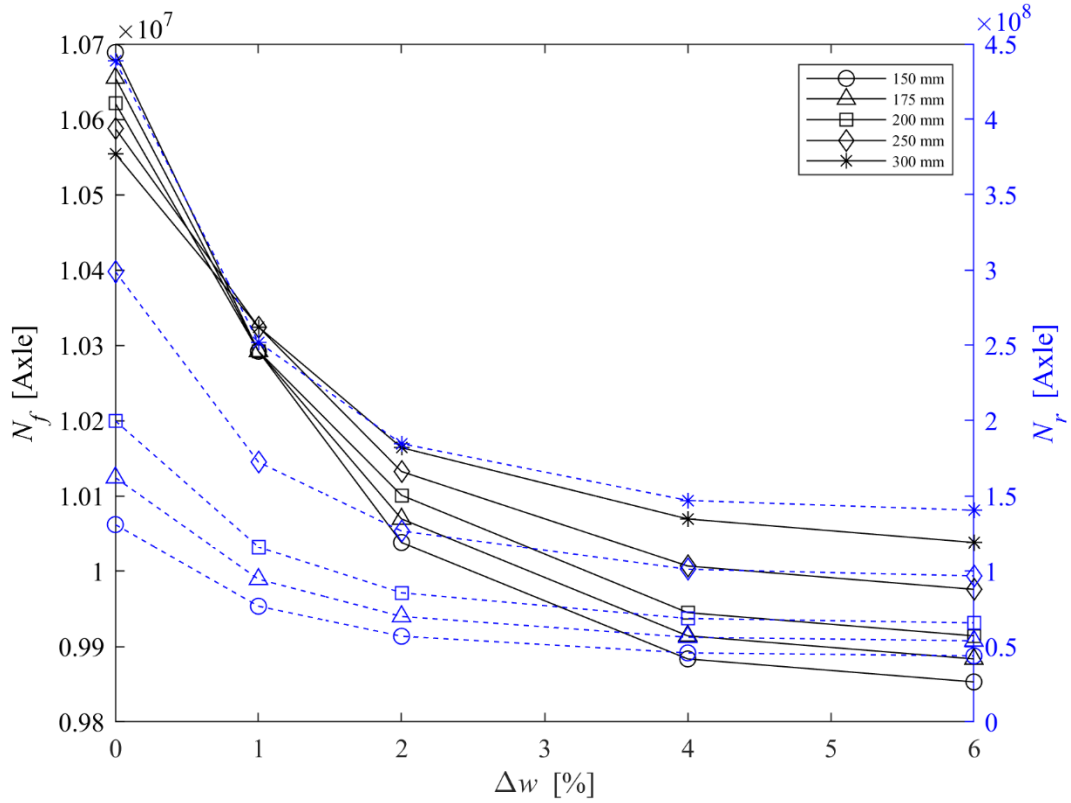

Figure 4.16 N_f and N_r at various h_{sub}

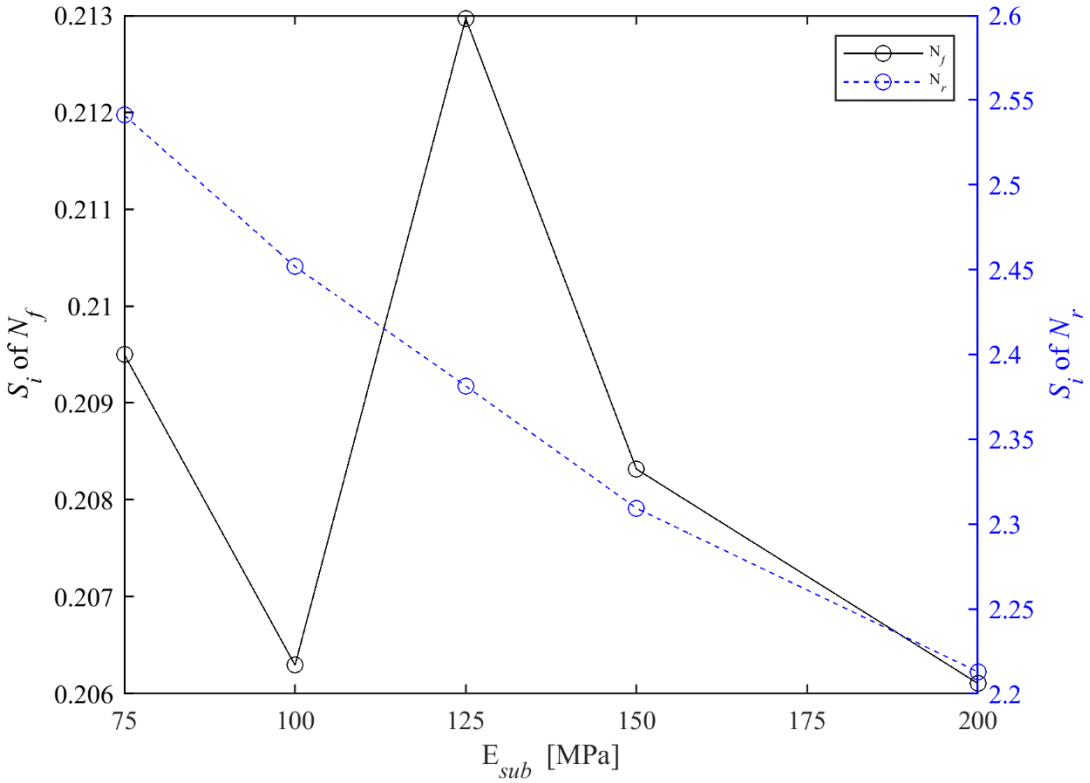

Figure 4.17 S_i of N_f and N_r at various E_{sub}

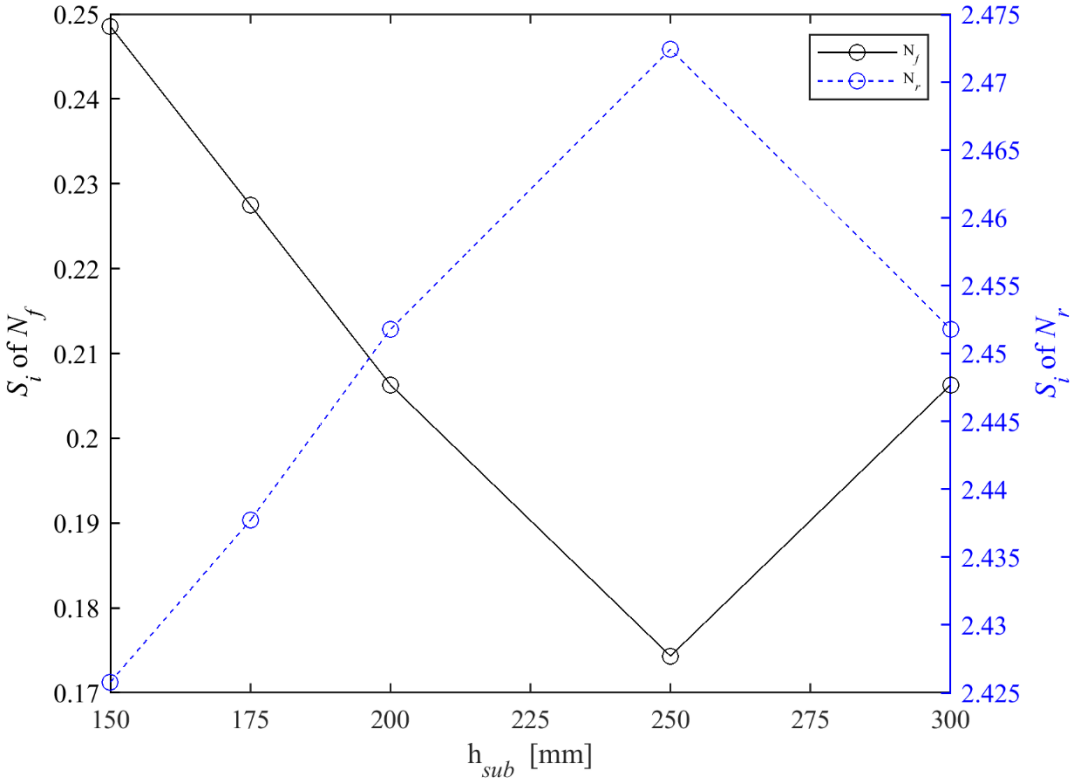

Figure 4.18 S_i of N_f and N_r at various h_{sub}

4.3.5.4 Effects of A_l

N_f and N_r both dropped significantly when the axle load increased from 60 kN to 100 kN, as shown in Figure 4.19. The sensitivity of N_f and N_r in Figure 4.20 showed slight changes and similar trends with axle loading. The sensitivity of N_r was about 12 times the sensitivity of N_f. The axle load imposed larger effects on the sensitivity of rutting life. From the axle load (A_l) of 100 kN, the sensitivity of N_f and N_r was found to become steady. The adverse effects of axle load on fatigue and rutting life attenuated, particularly at higher water levels. At a higher axle load, N_f and N_r showed slight variation with the moisture increase. In terms of the regions subject to similar moisture conditions, the method of limiting the axle load during heavy rainfall or flooding could be more effective for the regions usually experiencing axle loads below 100 kN in order to reduce moisture deterioration.

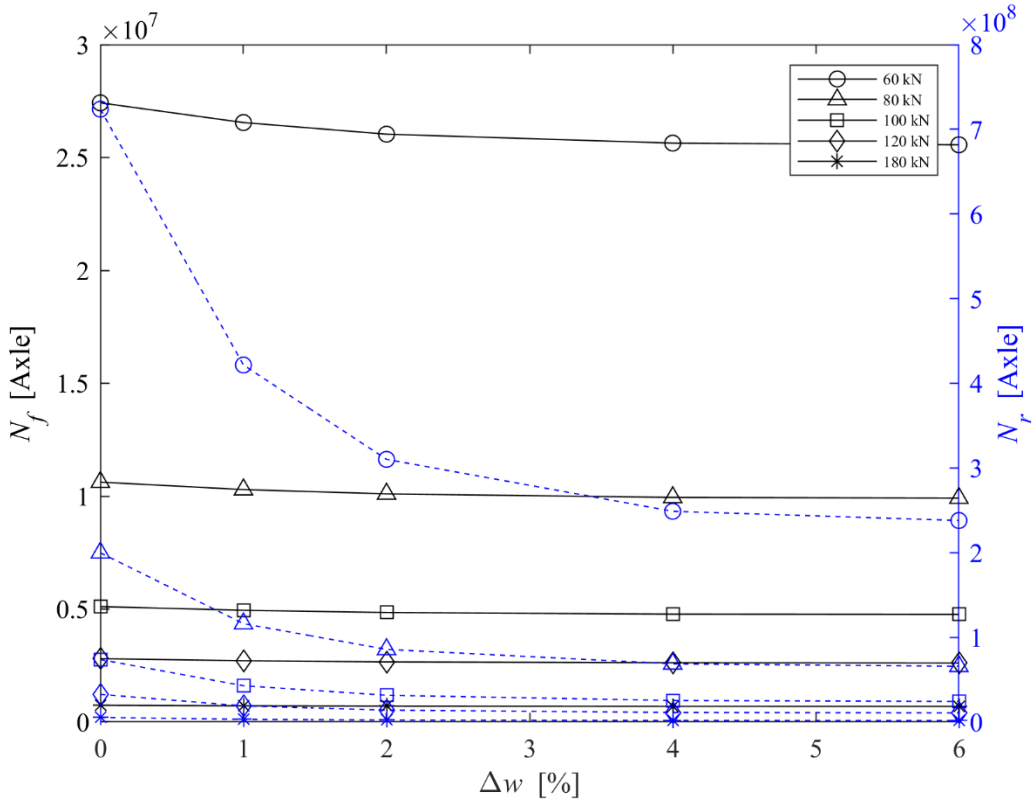

Figure 4.19 N_f and N_r at various A_l

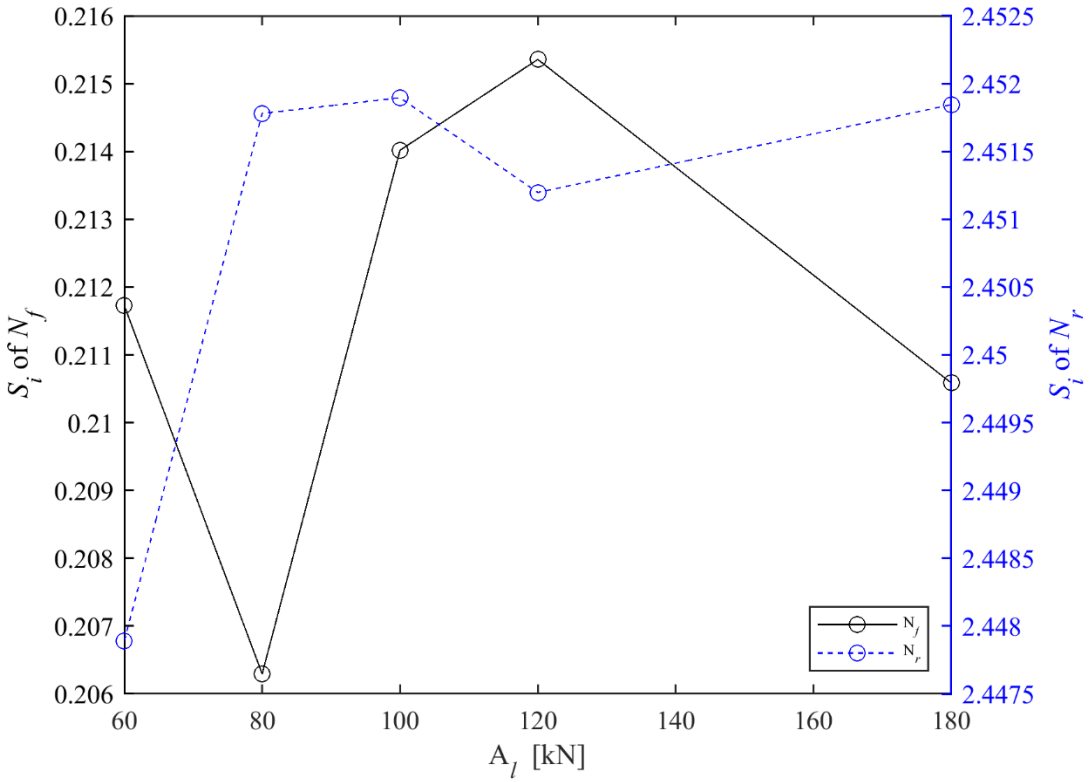

Figure 4.20 S_i of N_f and N_r at various A_l

4.3.5.5 Effects of PDL

The proposed PDL was studied regarding its thickness, modulus and position. The

results are presented in Figure 4.21~Figure 4.26. The insertion of the polymeric drain can certainly be expected to change strains in the highway (or railway) structure, but it may also have a disruptive effect on the relationship between rutting at the surface and the subgrade strain (Tang et al., 2016a; Tang et al., 2016b). For example, Tang et al. (2016b) calibrated the permanent deformation model of Eq. (2.39) and incorporated the effects of geogrids on the subgrade deformation into the model by adjusting the vertical resilient strains. It is found that although the model could demonstrate the geogrid reinforcement on pavement response, an underestimate of the permanent deformation of the subgrade was recognized. However, the disruptive effects of PDL on surface rutting relationship were beyond the scope of the analysis. For simplification, the effects on the relationship were not considered.

Thickness

In Figure 4.21, with the thickness of PDL increasing, N_f and N_r showed clear upward trends, and there was a particularly large effect on N_r. Decreasing trends were noticed in the sensitivity of N_f and N_r at various drain thicknesses, h_{drain}, while the sensitivity of N_r did not vary widely with their thicknesses when over 100 mm, as shown in Figure 4.22. There may be a maximum PDL thickness that should be considered during design in order to reduce the expenditure.

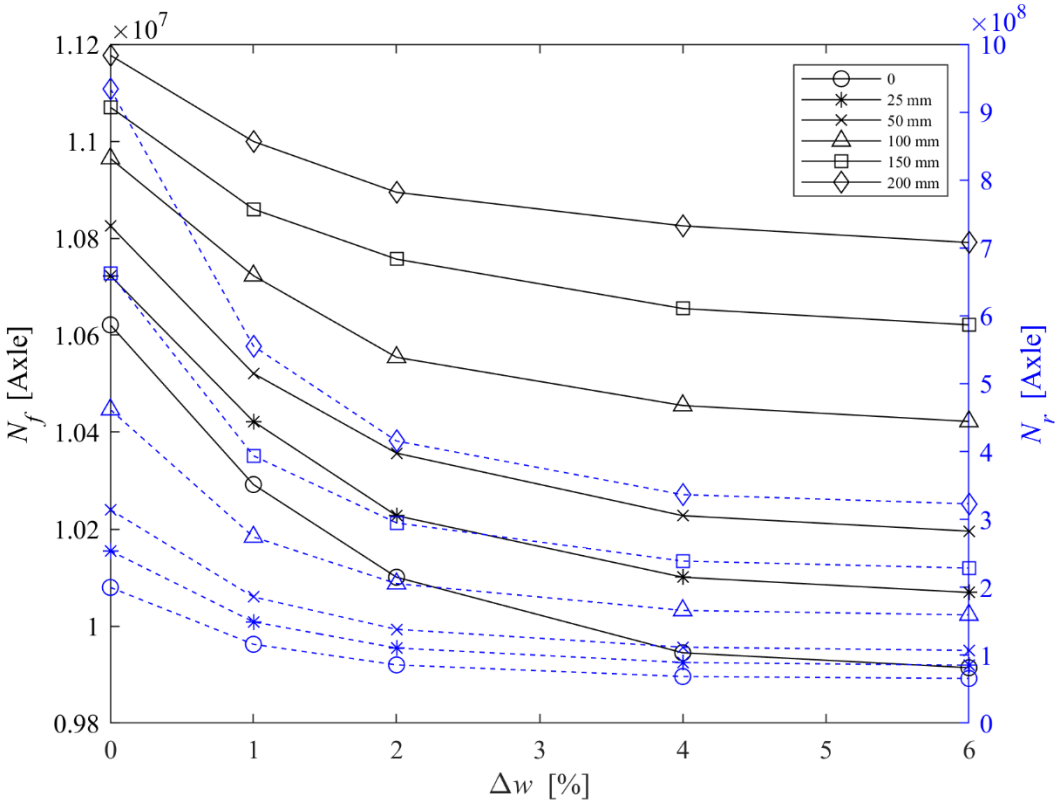

Figure 4.21 N_f and N_r at various h_{drain}

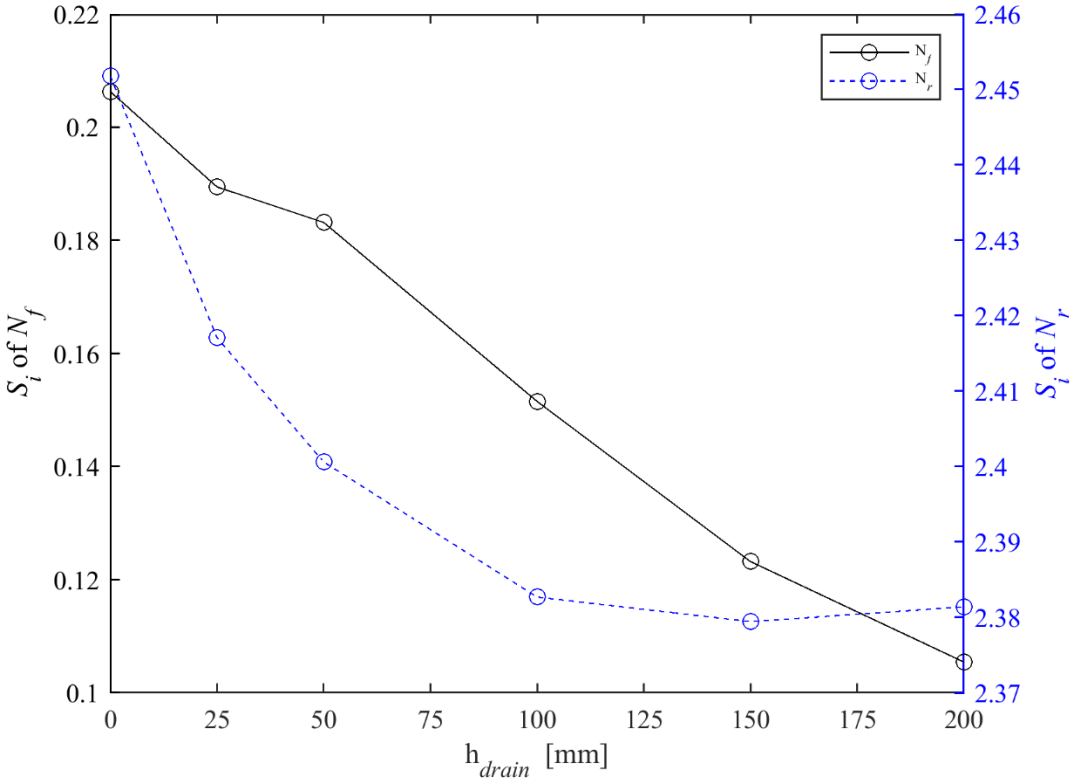

Figure 4.22 S_i of N_f and N_r at various h_{drain}

Elastic modulus

From Figure 4.23, a dramatic difference was observed for N_f and noticeable, though less, for N_r when PDL was incorporated compared with the no-PDL case. At a lower modulus (i.e., from 20 to 109 MPa), N_f and N_r decreased with the PDL modulus, E_{drain}, opposite to that above 109 MPa. As a PDL stiffer than the subgrade was included, the positive effects of PDL on N_f and N_r were indicated. Figure 4.24 demonstrates that the sensitivity of N_f and N_r exhibited opposite trends with increasing PDL modulus, E_{drain}. The sensitivity of N_f did not fluctuate once the modulus, E_{drain}, exceeded 109 MPa, which was close to the subgrade modulus ranging between 83 and 120 MPa. Thus, a PDL modulus at least as great as that of the subgrade is recommended if fatigue and rutting life are not to be compromised.

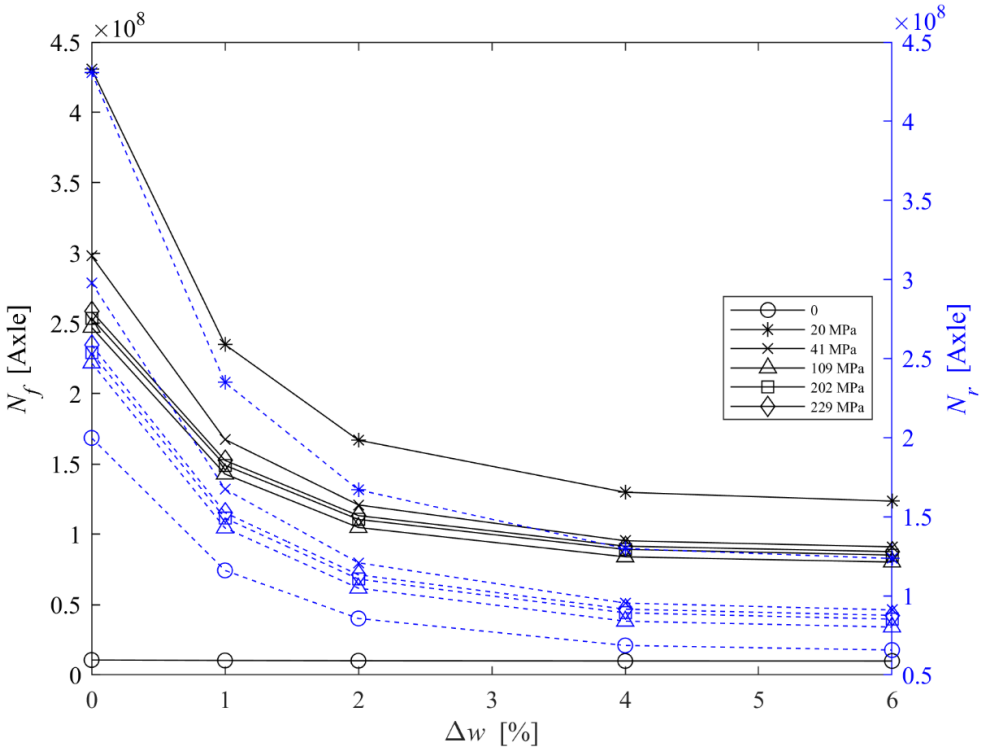

Figure 4.23 N_f and N_r at various E_{drain}

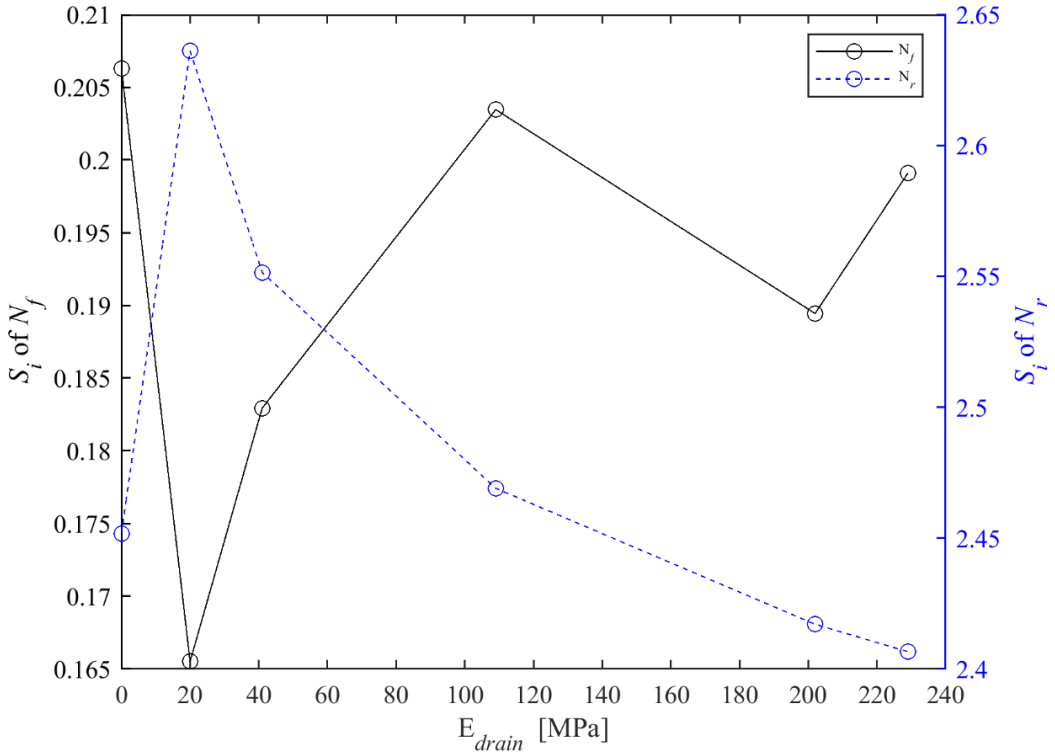

Figure 4.24 S_i of N_f and N_r at various E_{drain}

Position

From Figure 4.25, with the PDL being placed deeper and deeper beneath the top of the subbase, N_f decreased whereas N_r remained largely unchanged. As the drain position, Position$_{drain}$, moved from the subbase top to subgrade top, the sensitivity of

both the N_f and N_r reduced, though the change in the sensitivity was small for N_r (see Figure 4.26). The maximum N_r was found with the PDL placed at the top of subgrade (Figure 4.25), where the sensitivity of N_f had the minimum value. It may indicate that the PDL would exhibit better performance if installed right at the top of subgrade.

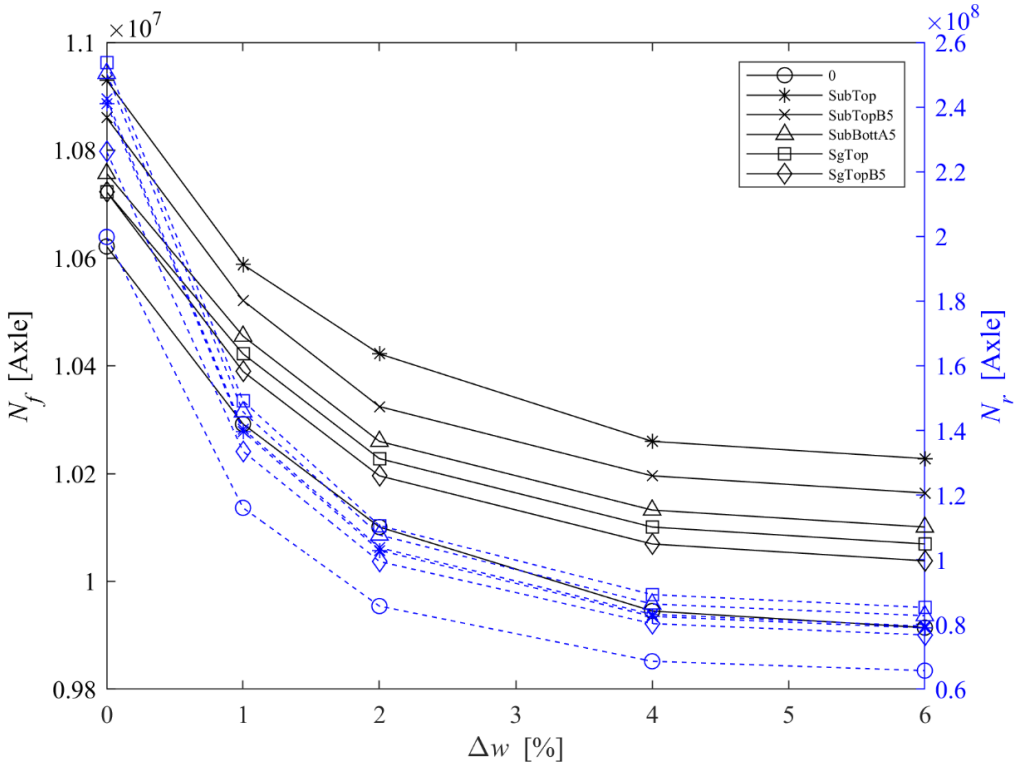

Figure 4.25 N_f and N_r at various Position$_{drain}$

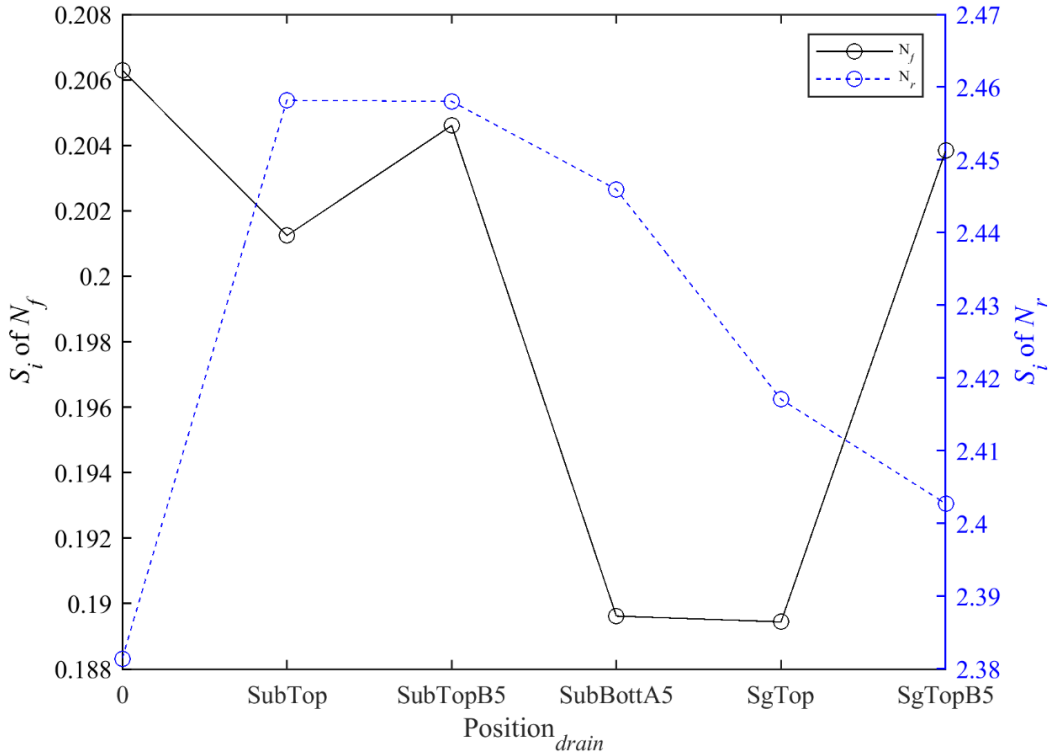

Figure 4.26 S_i of N_f and N_r at various Position$_{drain}$

4.3.5.6 Discussion

Generally, N_f was smaller than N_r, and thus the design life of the whole structure was dominated by fatigue cracking. The sensitivity of N_f to changes in the various factors varied from 0.1 to 0.35 (i.e. relatively insensitive except at various AC thicknesses, h_{ac}, where it was moderately sensitive). Conversely, N_r was very sensitive to such changes (from 2.3 to 2.7). N_r was particularly sensitive to increasing moisture. The effects of moisture content on subgrade modulus were considered in this study. Based on the varying subgrade modulus, pavement analysis was conducted. N_r depends on subgrade strain which is directly linked to E_{sg}; N_f depends on the bending of the asphalt layer, which is much more affected by the layer immediately below, the subbase, than the subgrade. Thus, N_r was more sensitive to moisture content. The implication is that N_r should be accurately determined at different moisture levels - indicating the crucial role of subgrade in pavement design.

Increasing the AC thickness and modulus ($E_{ac}$and h_{ac}) could improve the design life, but at higher MC, the benefits attenuated regarding the N_r. The sensitivity of N_r to moisture increments slightly decreased with the increasing AC modulus, while the sensitivity showed a bit larger variation at various AC thicknesses, h_{ac}. Thus, increasing the thickness of AC may be a more effective means of limiting rutting when moisture content increases to a high level than increasing the AC's elastic modulus.

As expected, the increase in the thickness and modulus of the base layer (E_{base} and h_{base}) was beneficial in reducing the impact of subgrade moisture levels on N_f and N_r, and also in reducing the sensitivity to moisture changes.

Compared with the N_r at various subbase moduli (E_{sub}), N_r showed an upward trend with subbase thickness, h_{sub}. Increasing the thickness could better enhance pavement performance. A thicker granular subbase would also be likely to have greater beneficial filtering so as to prevent the upward migration of fines from the subgrade.

Inevitably, both N_f and N_r decreased with increasing axle loading. The lack of sensitivity to moisture content at higher axle loads (A_l) values may indicate that increasing axle load A_l does not aggravate the effect of excess water in the subgrade. The study reported in this chapter gives a general idea about the effect of axle load, but a more detailed simulation should be conducted as water effects are incorporated.

Regarding sensitivity of N_r to the use of a PDL, it became stable above 100 mm of PDL. With the PDL modulus (E_{drain}) over 109 MPa, N_f and N_r did not change much. When the PDL was placed at the top of the subgrade, the sensitivity was relatively low. Basically, it has the most effect on N_f when it is closest to the asphalt, because asphalt strain is highly influenced by the layer directly beneath; the effect on N_r is less obvious, but the load spread is more efficient when it is just above the subgrade. Considering the mechanical effects of PDL alone, the suggestion for the design of the PDL can thus be deduced as follows: about 100 mm in thickness, not less than 109 MPa in modulus (at least above subgrade modulus) and placed at the top of the subgrade.

4.4 Data analysis using literature sources

Following the analysis based on assumed moisture variation, further sensitivity analysis was conducted using data from the literature sources. The data included the resilient modulus of subgrade soils at corresponding moisture contents.

4.4.1 Model geometry and property

The established model is illustrated, as shown in Figure 4.3(a).

4.4.2 Simulation scenarios

Previous test data of 15 soils (as presented in Section 3.2 of Chapter 3) and two sandy soils (S00A and S00B in Table 4.9) were used in the simulation to quantify the moisture effects on various types of soils, i.e. M_r measured at a deviator stress approximately between 30 and 40 kPa with corresponding moisture contents. 'S' indicates soil, and the number indicates plasticity. Another three variable parameters were selected as an example for simplification, i.e. E_{ac}, h_{ac} and A_l, and the values were the same as those in Table 4.6 and Table 4.7. Based on DMRB (Highway Agency, 2006) and the foundation class (Class 2), the annual traffic volume at an equivalent standard axle load of 80 kN was set as 1 million standard axles, i.e. a low traffic level as defined by the DMRB. A low-traffic design was selected because this leads to thin pavements, which are more affected by foundation stiffness than thick pavements.

Table 4.9 Details of S00A and S00B

Soil name	Binger	Caddo
Soil code	S00A	S00B
Standard proctor test		
OMC, %	12.5	n/a
MDD, kN/m^3	17.8	n/a
Atterberg limits		
LL, %	n/a	n/a
PL, %	0	0
Specific gravity	n/a	n/a
Soil classification		
PI, %	0	0
AASHTO	A-2	A-4
USCS	SC	SC
Hydrometer analysis		
Percent passing #40 sieve (0.425 mm)	n/a	n/a
Percent passing #200 sieve (0.075 mm)	32	n/a
Percent clay <0.002 mm	n/a	n/a
Reference	Khoury & Maalouf (2018)	Khoury & Zaman (2004)

4.4.3 Results and discussion

The response of each property differed depending on the soil. The sensitivity index was compared among all the soils. The distress results for S00A were taken as an example and are illustrated in Figure 4.27~Figure 4.50 (i.e. fatigue and rutting life, fatigue cracking and subgrade deformation). Fatigue and rutting life, fatigue cracking of AC and permanent deformation of subgrade were studied. Variation of the sensitivity index of each soil to moisture content under various conditions was investigated and the difference among all the soils was revealed. Variations of N_f and N_r with moisture content at various E_{ac}, h_{ac} and A_l were consistent with the results presented in Section 4.4.1. The analysis therefore focused on the changes in fatigue cracking and permanent deformation for each soil and their sensitivity indexes.

4.4.3.1 Effects of AC modulus E_{ac}

Generally, with the increase in moisture content, N_f and N_r both significantly decreased in Figure 4.27. Fatigue cracking and permanent deformation increased with increasing moisture contents while decreasing with the AC modulus E_{ac}, as shown in Figure 4.28 and Figure 4.29. A thicker AC layer could improve pavement performance at higher moisture content. From Figure 4.30~Figure 4.34, the sensitivity showed a significant trend with soils, i.e. the soil with higher plasticity generally demonstrated higher sensitivity. For S00A ('S' indicates soil and the number indicates plasticity), there was a slight decrease. S26 exhibited the largest sensitivity, while S08 showed the smallest sensitivity in terms of fatigue cracking and permanent deformation. Regarding N_f, S23 showed the smallest sensitivity. As a cohesionless soil, S00A was expected to show lower sensitivity to moisture variation. For the cohesive soil, the sensitivity did not show monotonic variation with soil plasticity, which may be possibly attributed to the various soil composition. The sensitivity of N_r did not show clear variation with the AC modulus E_{ac}. The sensitivity of fatigue cracking ($FC_{top-down}$ and $FC_{bottom-up}$) and N_r showed larger increases with the AC modulus E_{ac} in the soils with higher plasticity. The benefit of increasing the AC modulus to the pavement may be compromised to some extent for pavements with high-plasticity foundations under varying moisture conditions in terms of moisture sensitivity.

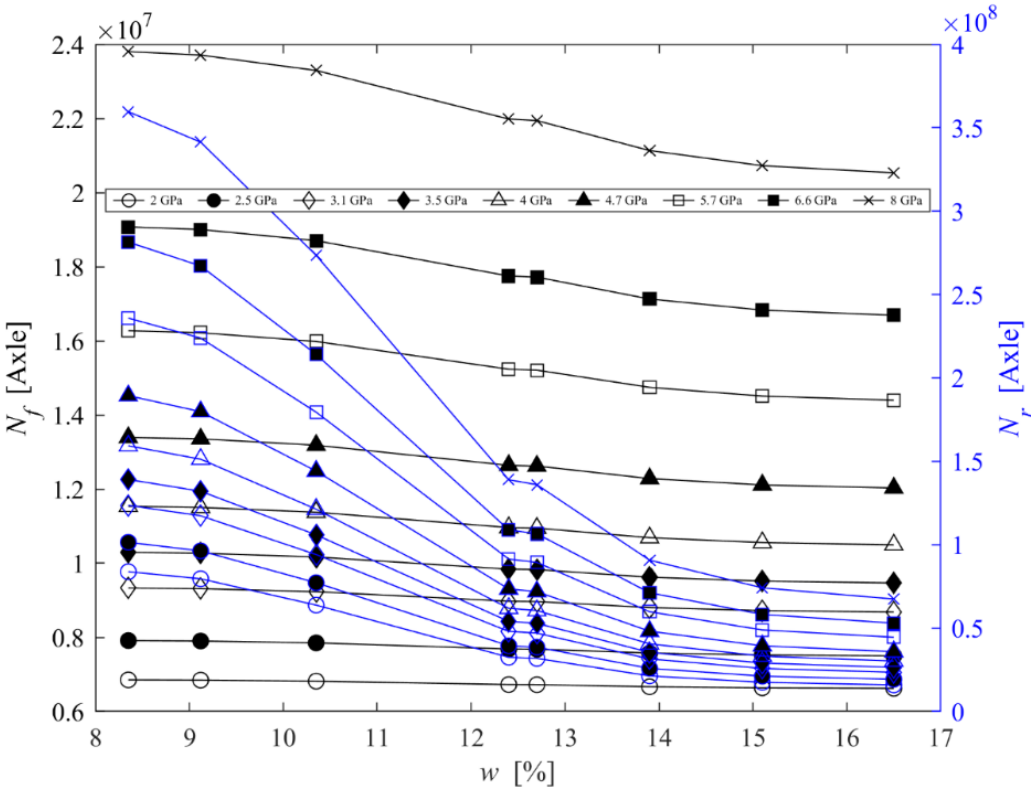

Figure 4.27 N_f and N_r of S00A at various E_{ac}

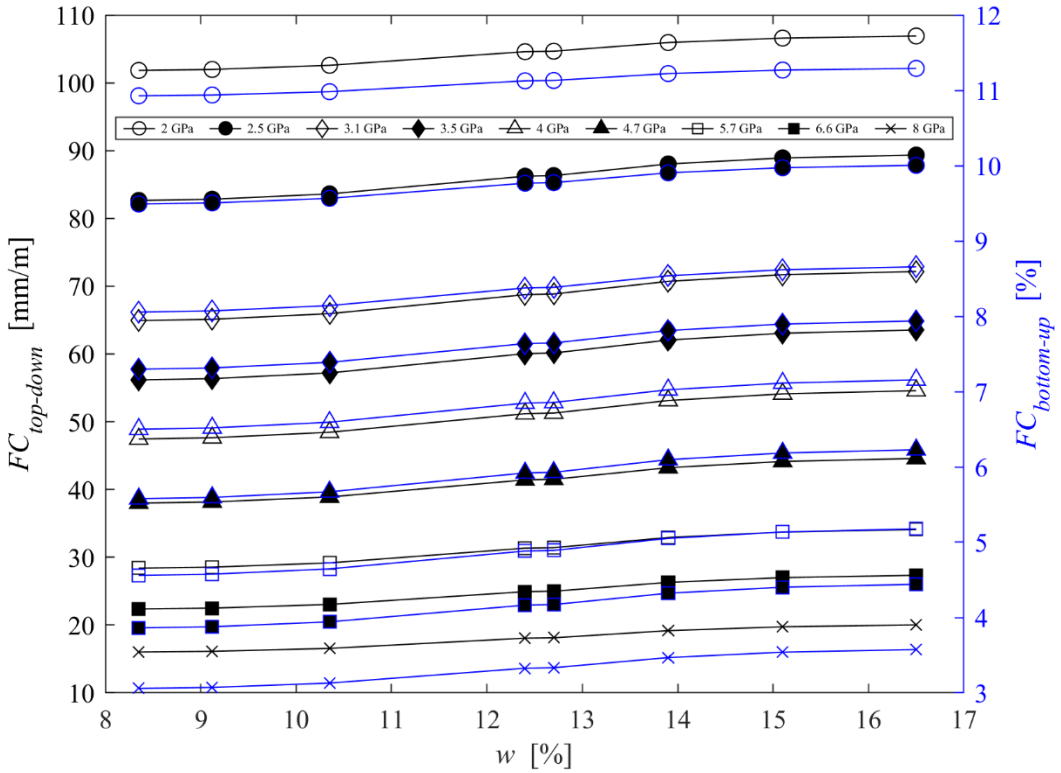

Figure 4.28 $FC_{top-down}$ and $FC_{bottom-up}$ of S00A at various E_{ac}

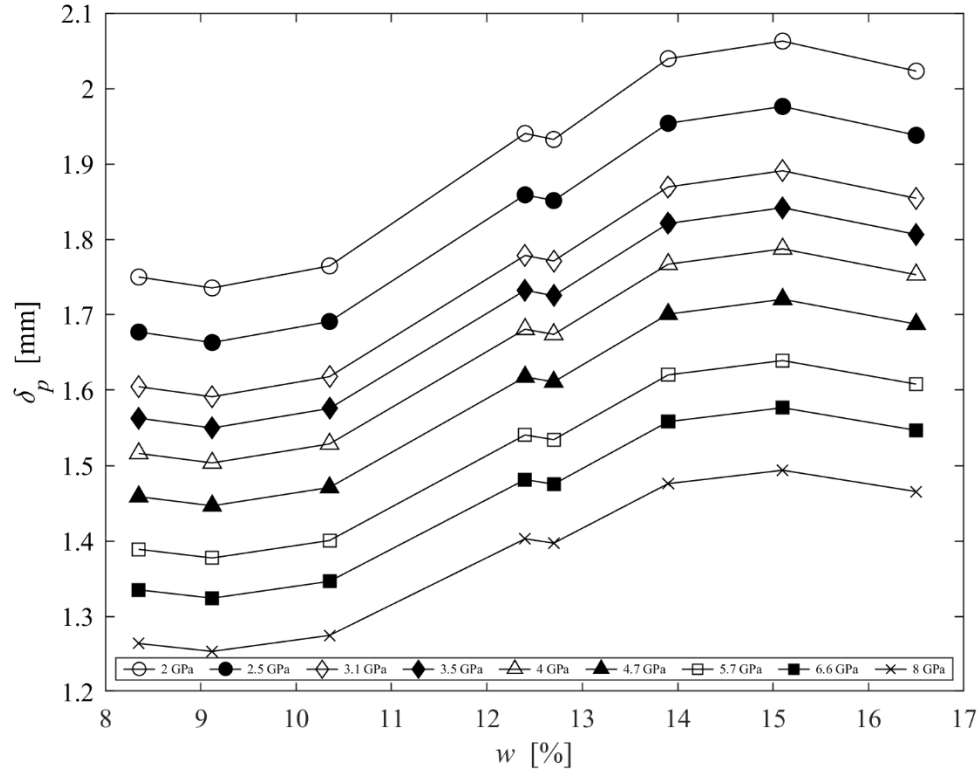

Figure 4.29 δ_p of S00A at various E_{ac}

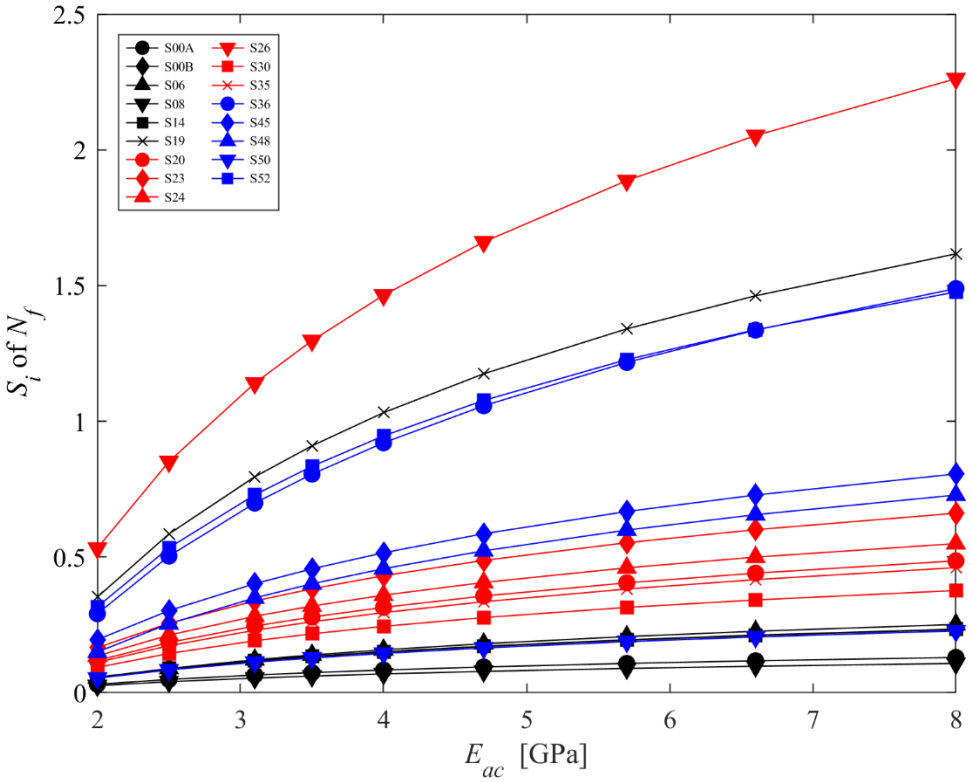

Figure 4.30 S_i of N_f at various E_{ac} for each soil

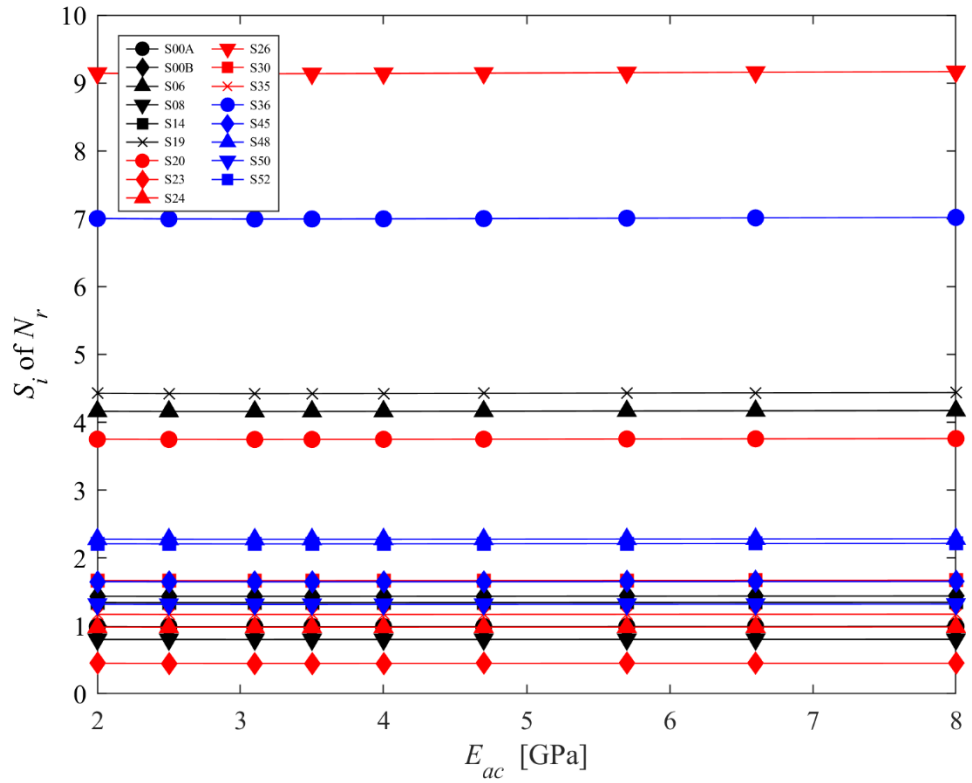

Figure 4.31 S_i of N_r at various E_{ac} for each soil

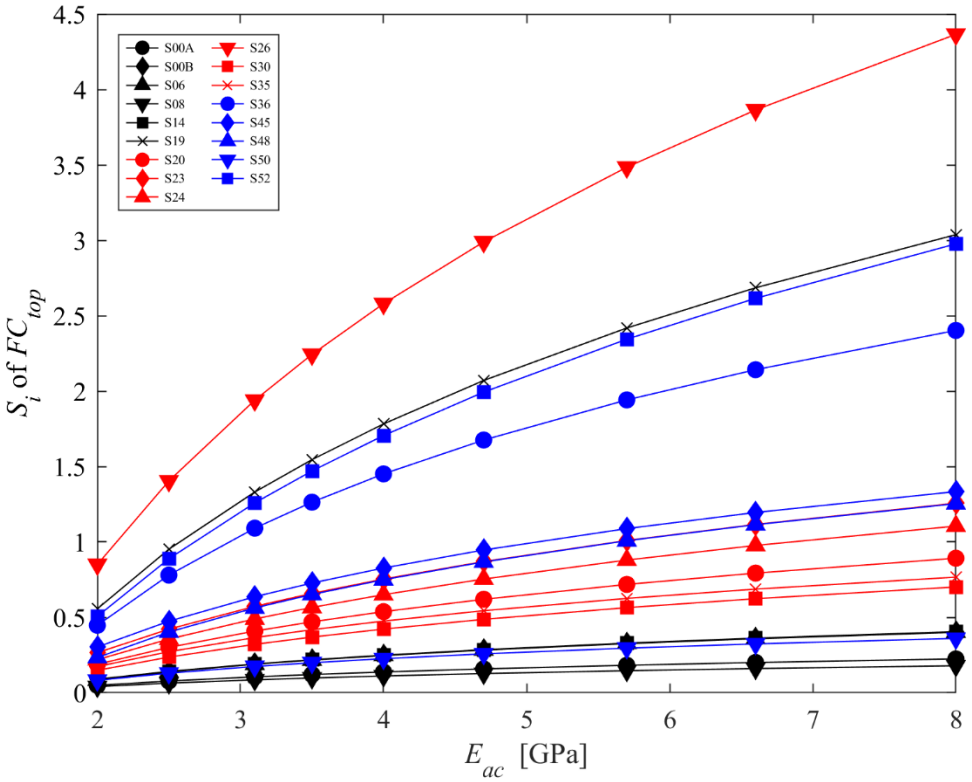

Figure 4.32 S_i of $FC_{top-down}$ at various E_{ac} for each soil

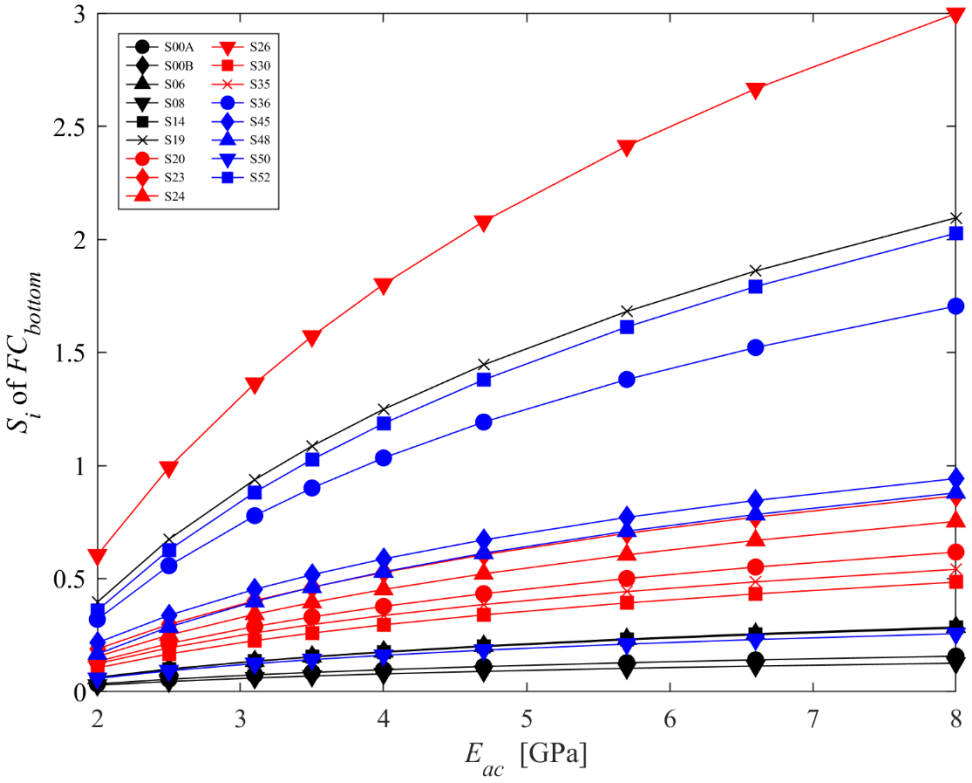

Figure 4.33 S_i of $FC_{bottom-up}$ at various E_{ac} for each soil

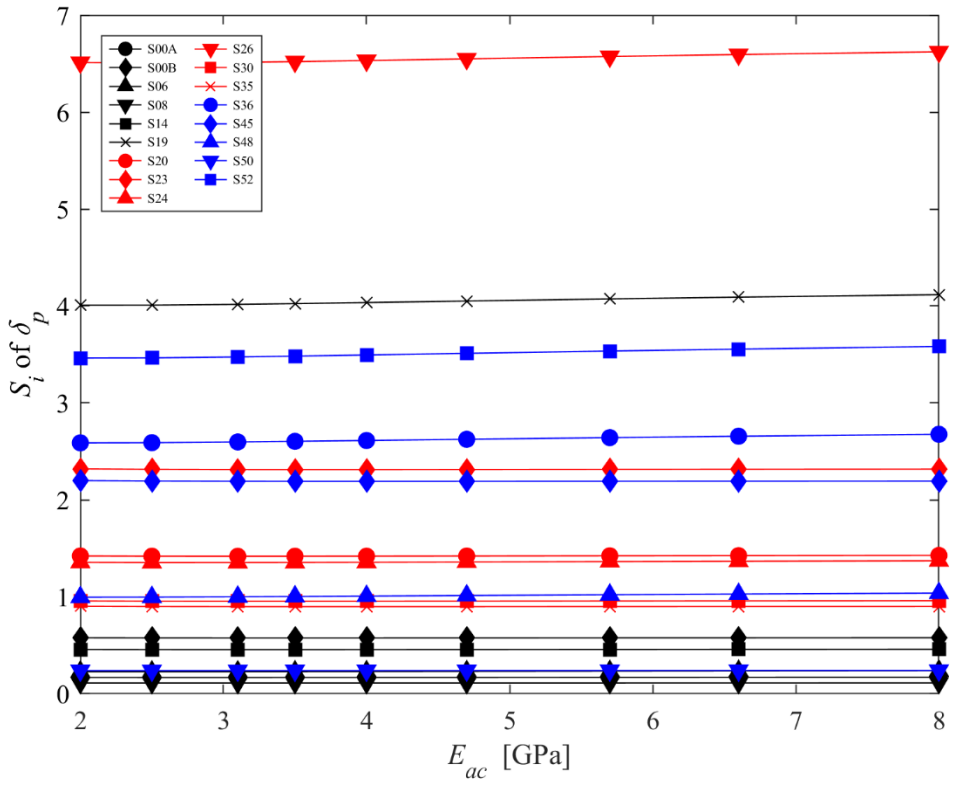

Figure 4.34 S_i of δ_p at various E_{ac} for each soil

4.4.3.2 Effects of AC thickness h_{ac}

From Figure 4.35 and Figure 4.36, N_f, N_r, $FC_{top-down}$ and $FC_{bottom-up}$ showed a decreasing trend with moisture content. Particularly, $FC_{top-down}$ at a h_{ac} of 50 mm exceeded the length of corresponding pavement structures, indicating the pavement experienced complete fatigue failure within the service life. $FC_{top-down}$ at a h_{ac} of 75 mm was close to the length of the pavement structure. Thus, these two h_{ac} values should not be allowed during pavement design, i.e. the thickness of asphalt concrete should be not less than 100 mm based on the currently selected value ranges. For permanent deformation, δ_p, presented in Figure 4.37, it decreased with AC thickness, h_{ac}, while increasing with moisture content. As can be seen from Figure 4.38~Figure 4.42, N_f and N_r, sensitivity of the fatigue distress ($FC_{top-down}$ and $FC_{bottom-up}$) decreased with AC thickness (h_{ac}) from 25 mm to 100 mm, and then showed a strong upward trend, while $FC_{top-down}$ and $FC_{bottom-up}$ showed an opposite trend. Sensitivity of N_r and the deformation δ_p remained stable. This indicates that increasing the thickness of the asphalt concrete layer would attenuate the impact of moisture on the pavement performance. An AC layer with a thickness of 100 mm could be considered for the pavement with higher moisture content in order to reduce its

sensitivity to subgrade moisture content. This is in good agreement with the analysis result in Section 5.3.5. In practice, economic factors should also be considered when attempting to promote pavement performance by increasing the thickness of the AC layer.

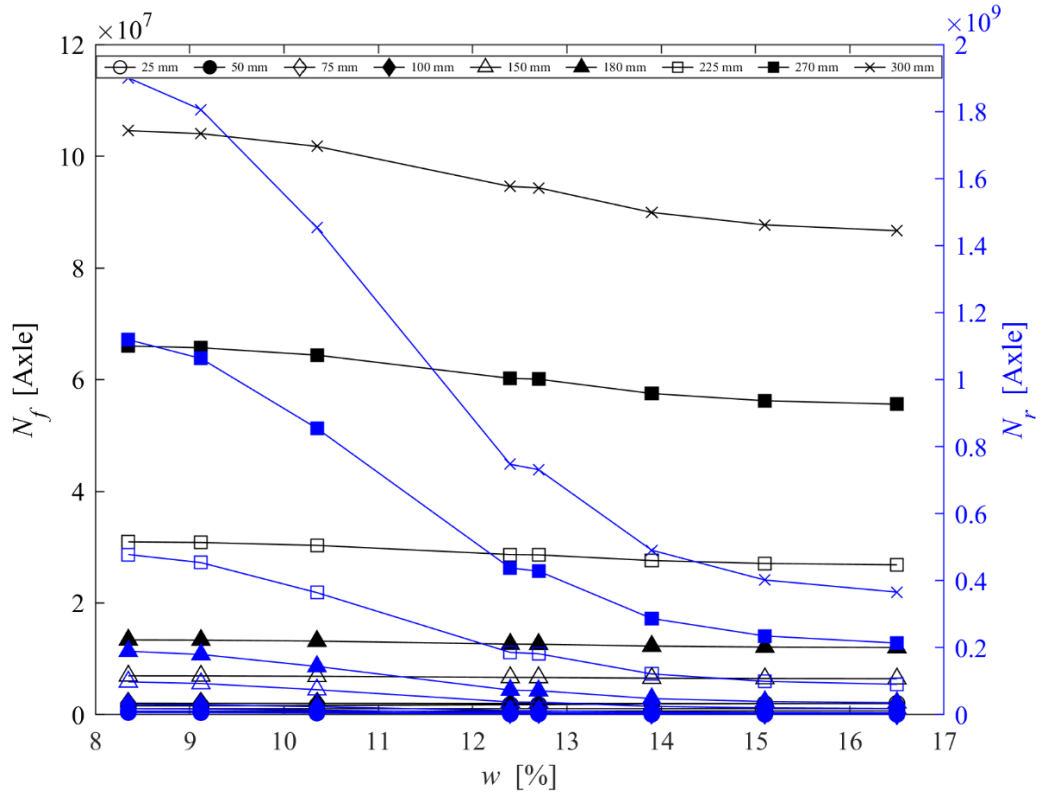

Figure 4.35 N_f and N_r of S00A at various h_{ac}

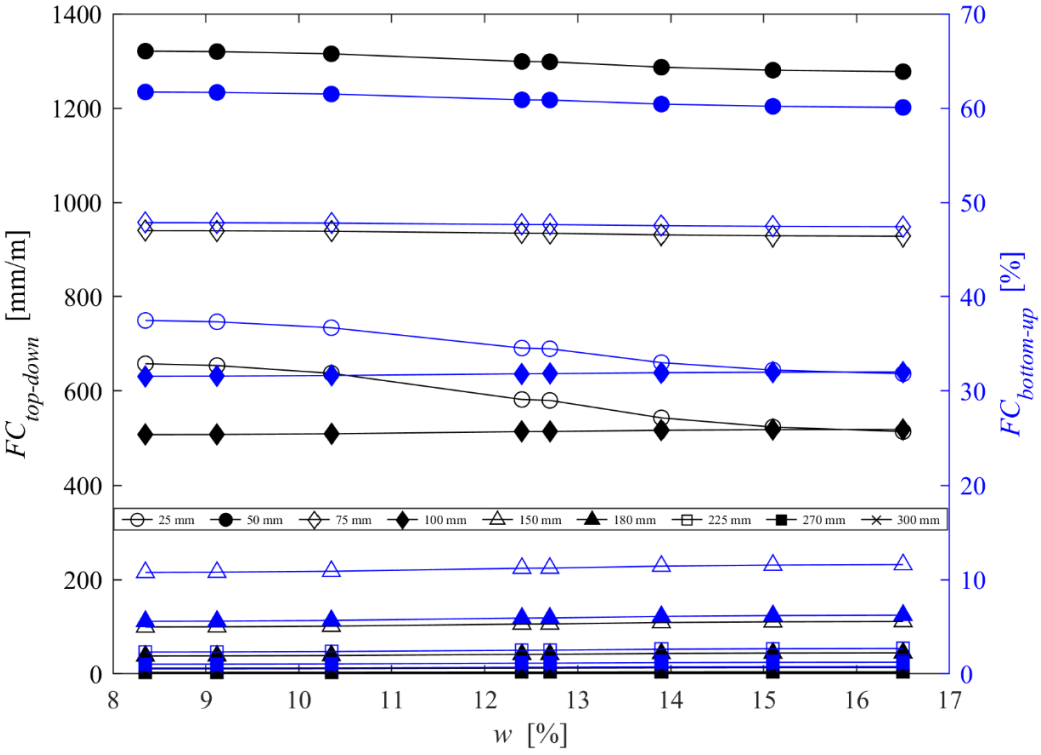

Figure 4.36 $FC_{top-down}$ and $FC_{bottom-up}$ of S00A at various h_{ac}

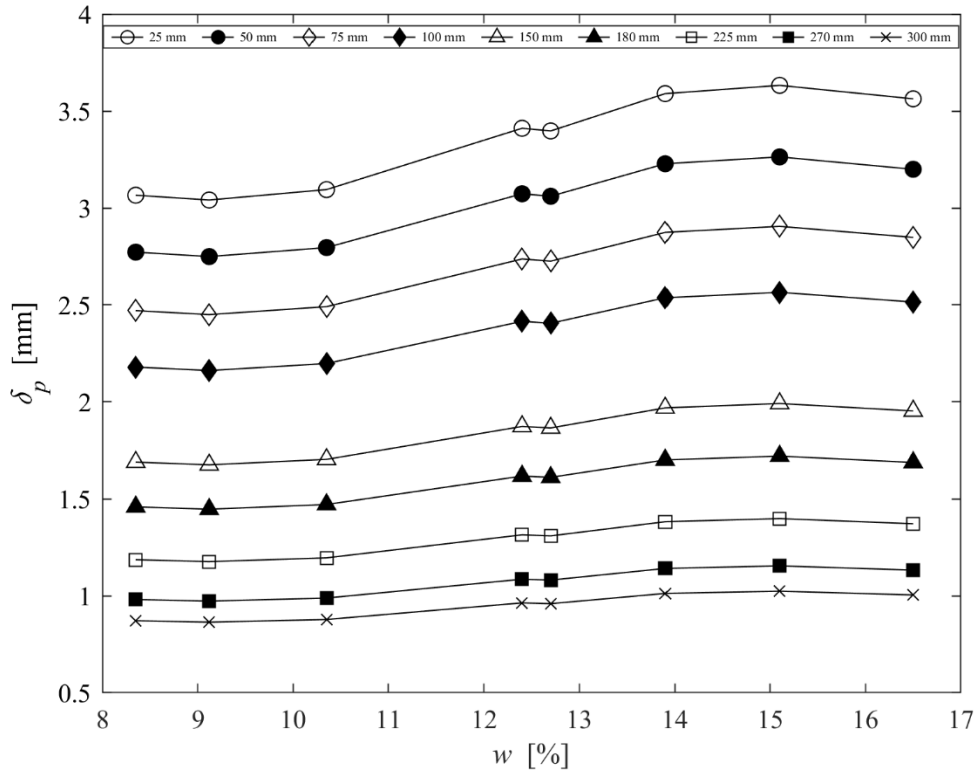

Figure 4.37 δ_p of S00A at various h_{ac}

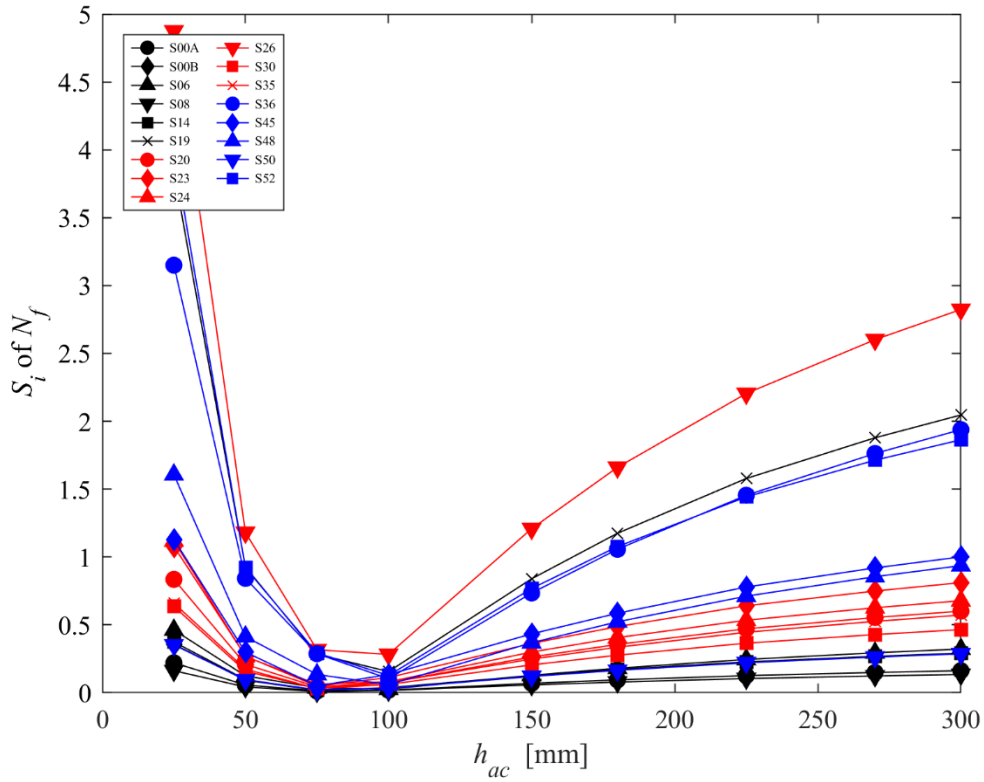

Figure 4.38 S_i of N_f at various h_{ac} for each soil

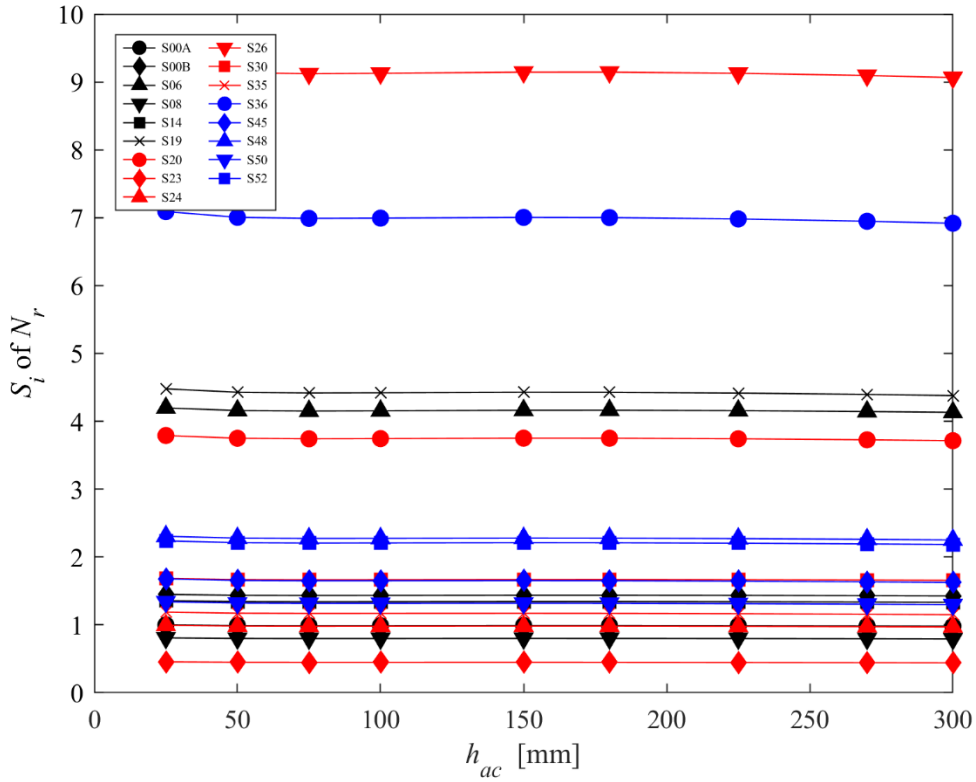

Figure 4.39 S_i of N_r at various E_{ac} for each soil

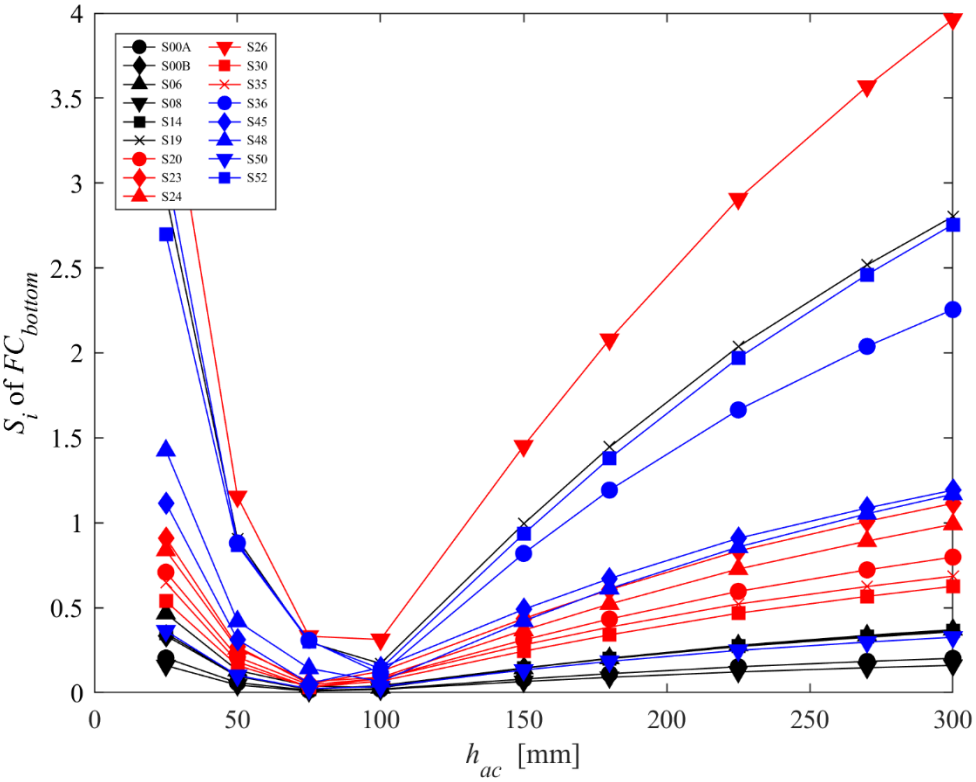

Figure 4.40 S_i of $FC_{top-down}$ at various h_{ac} for each soil

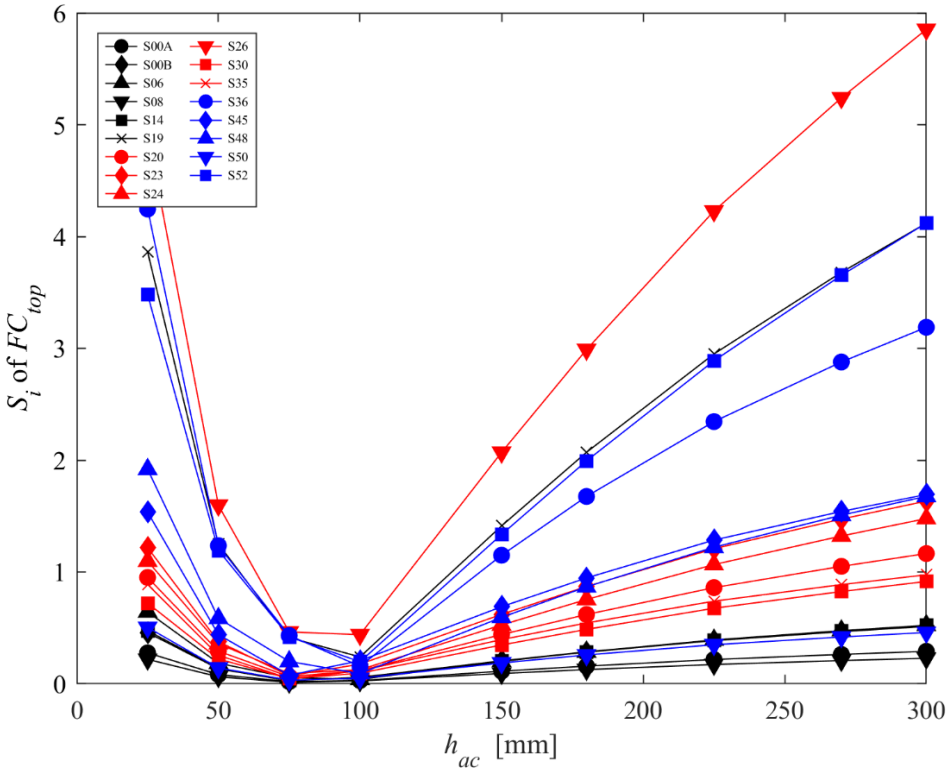

Figure 4.41 S_i of $FC_{bottom-up}$ at various h_{ac} for each soil

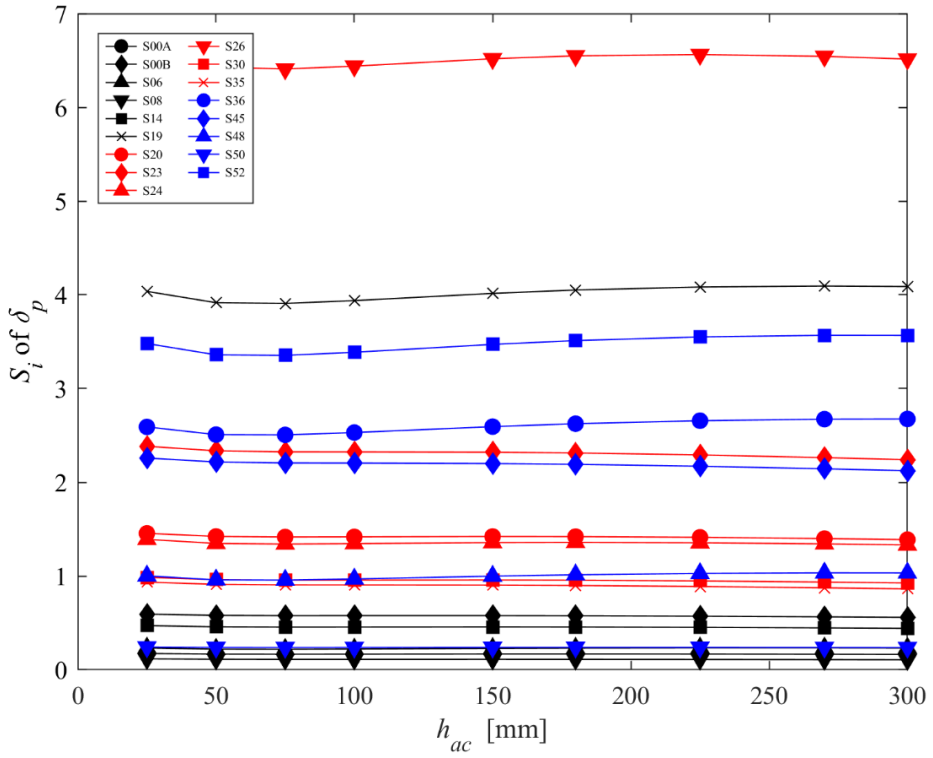

Figure 4.42 S_i of δ_p at various h_{ac} for each soil

4.4.3.3 Effects of A_l

From Figure 4.43~Figure 4.45, N_f, N_r, $FC_{top-down}$, $FC_{bottom-up}$ and δ_p of the subgrade top showed opposite trends with axle load A_l to those with AC modulus E_{ac}.

At an axle load of 180 kN, $FC_{top-down}$ excceded the length of the pavement strucutres, indicating the premature failure when the pavement was subjected to the designed axle load. Thus, this load level should be prevented. The sensitivity did not show significant changes with the axle load A_l in agreement with the results in Section 4.3.5, even though the sensitivity of $FC_{top-down}$ and $FC_{bottom-up}$ exhibited a slight decrease with axle load A_l, as shown in Figure 4.46~Figure 4.50. This is likely attributed to the hydraulic action that was not considered in combination with the axle load. Possibly, the axle load will not change the moisture sensitivity of foundations, e.g., for the areas with similar moisture conditions, the pavement response could show a similar level of variations at various axle loads regardless of their magnitude. In terms of soil types, the sensitivity varied remarkably. Relatively, at the same level of axle loads, although the sensitivity did not monotonically increase with the soil plasticity, a general trend could still be identified, i.e. the soils with higher plasticity showed a larger sensitivity. However, it should be noted that, in practice, the subgrade is subject to the coupling actions of moisture content and traffic loading and, with increasing axle load, it would accelerate the deterioration of the foundation. Thus, the sensitivity would be expected to increase at a higher A_l, which was not reflected from the analysis, and axle load should still be controlled in the region with higher moisture content.

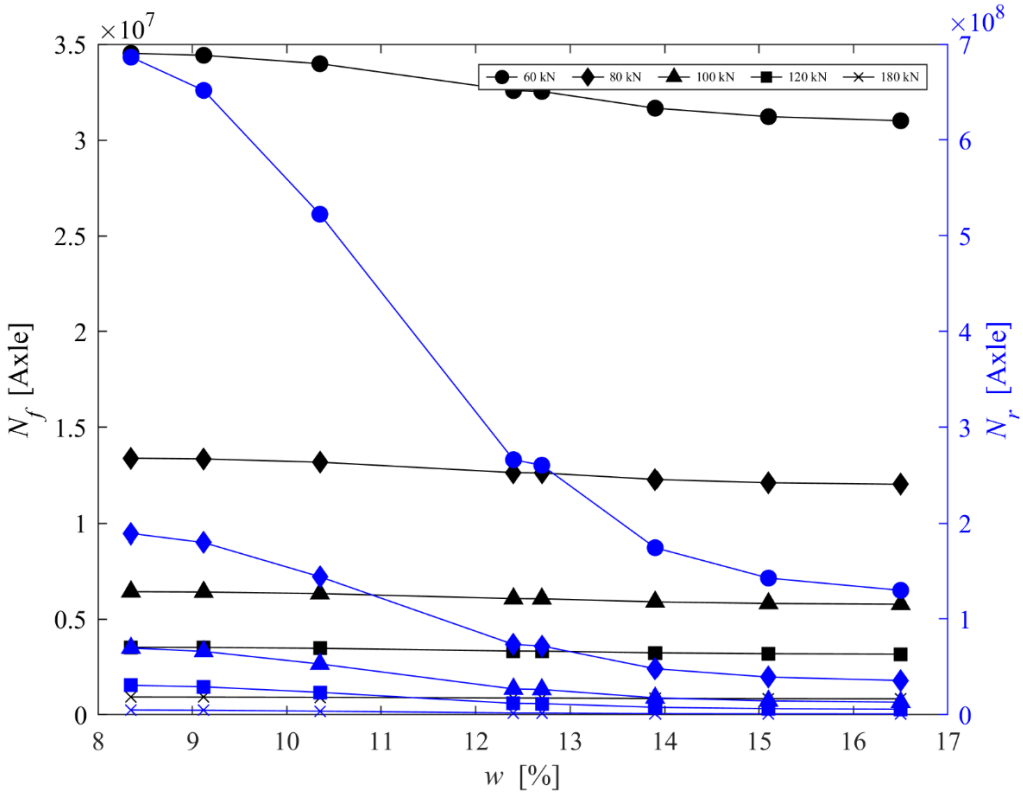

Figure 4.43 N_f and N_r of S00A at various A_l

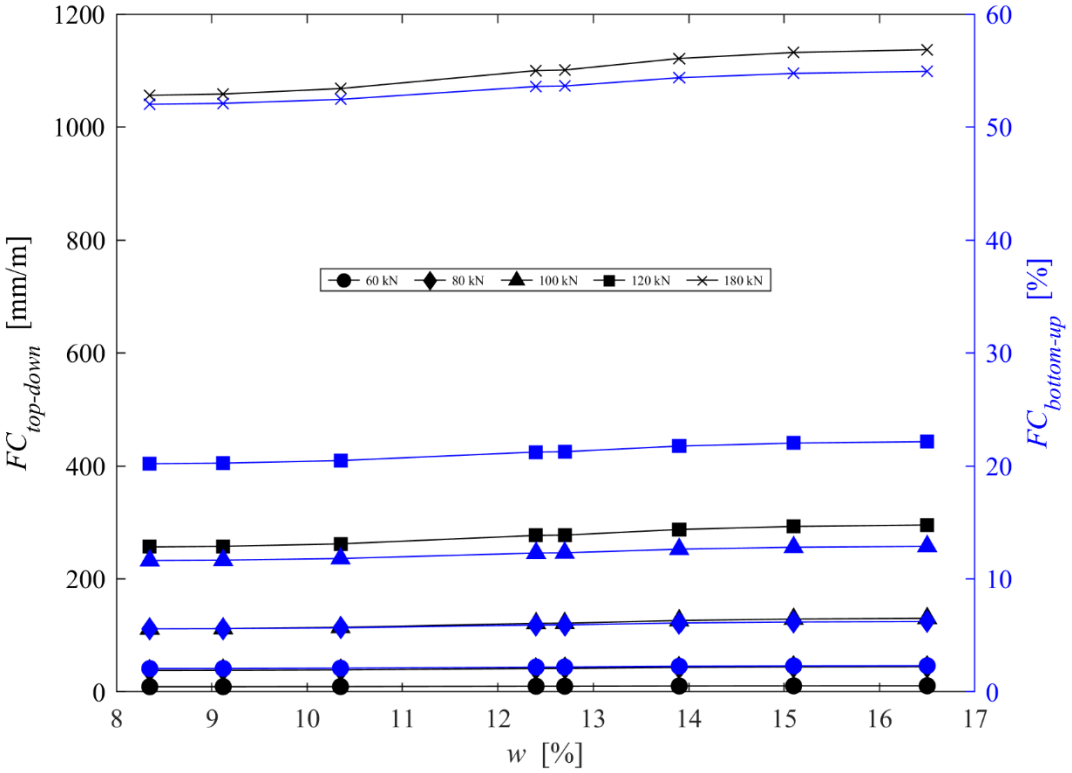

Figure 4.44 $FC_{top-down}$ and $FC_{bottom-up}$ of S00A at various A_l

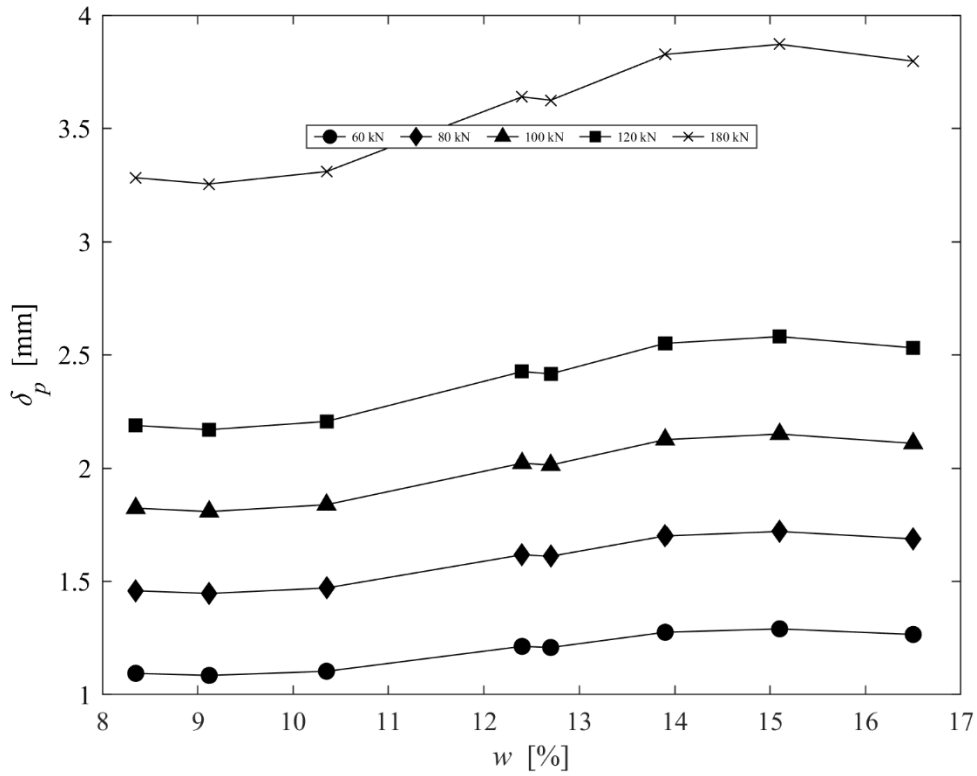

Figure 4.45 δ_p of S00A at various A_l

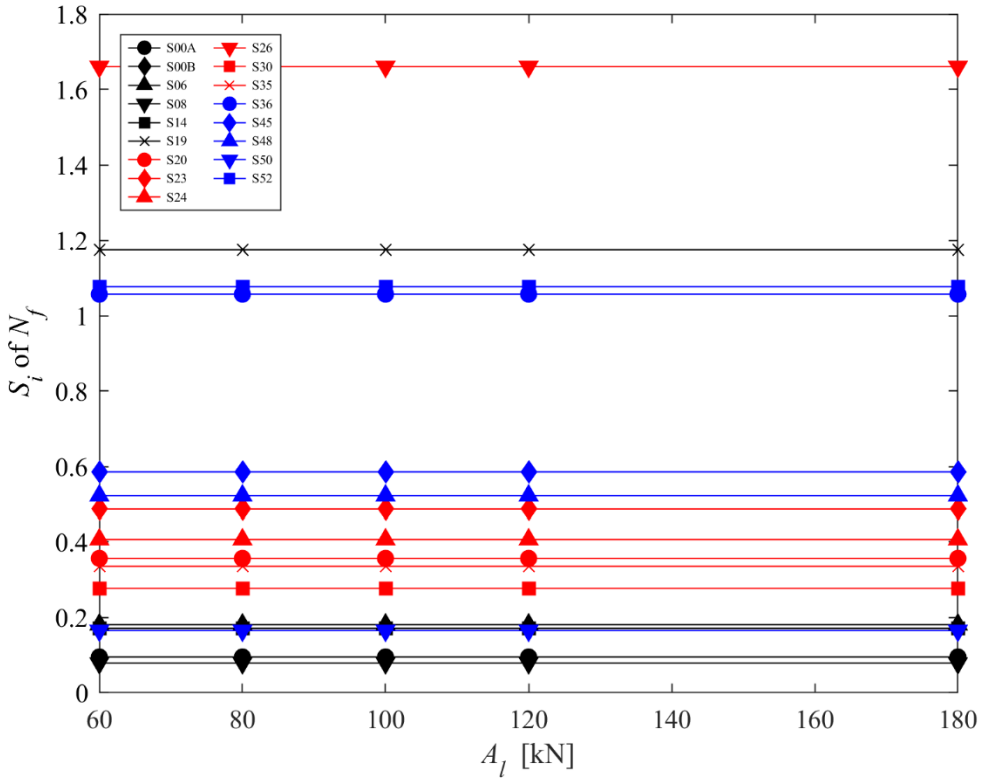

Figure 4.46 S_i of N_f at various A_l for each soil

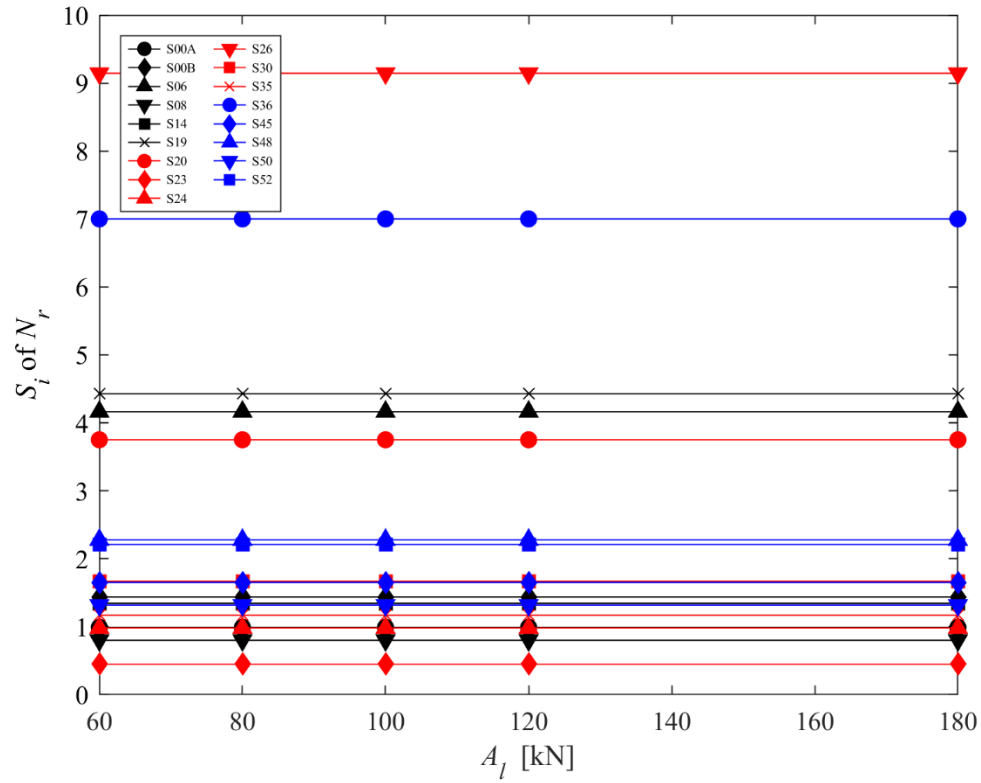

Figure 4.47 S_i of N_r at various A_l for each soil

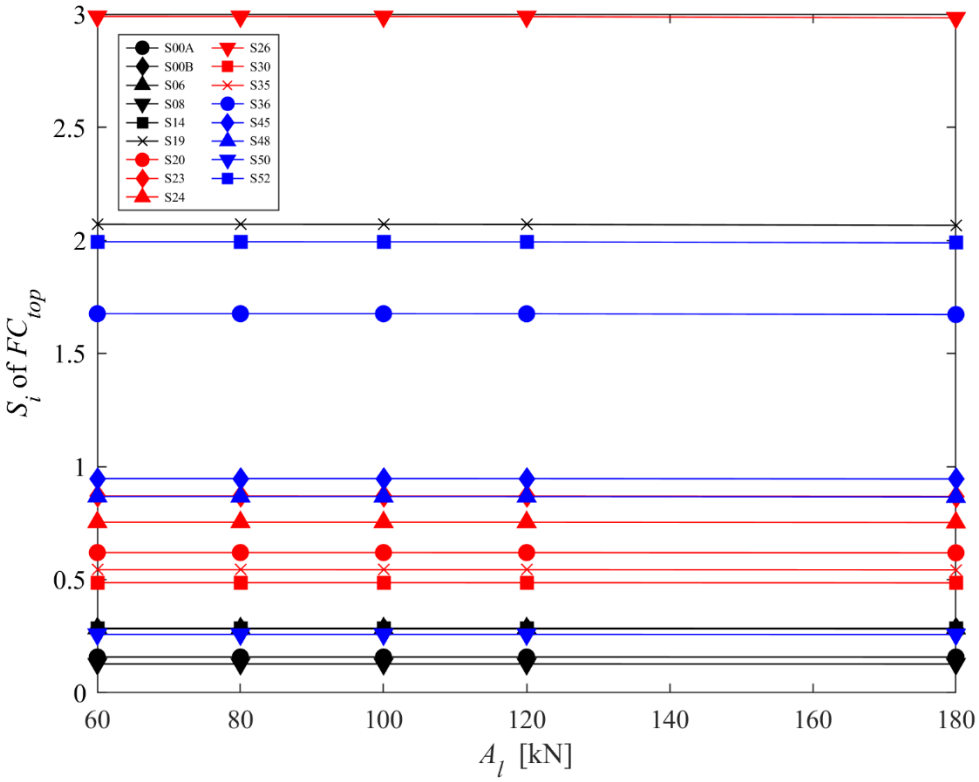

Figure 4.48 S_i of $FC_{top-down}$ at various A_l for each soil

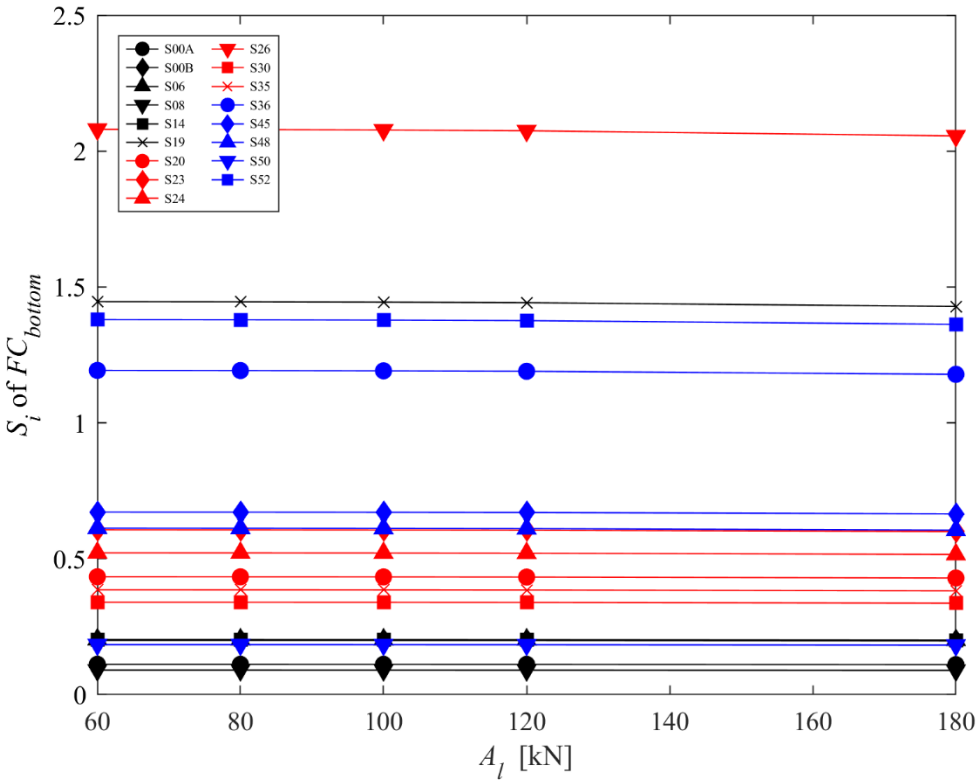

Figure 4.49 S_i of $FC_{bottom-up}$ at various A_l for each soil

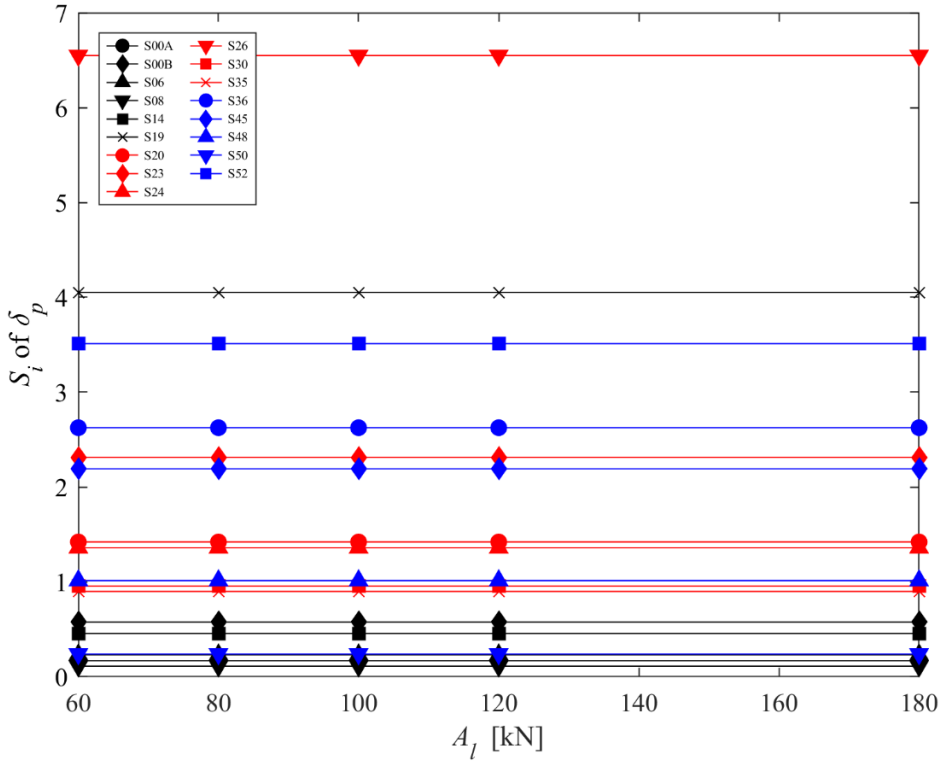

Figure 4.50 S_i of δ_p at various A_l for each soil

4.5 Drainage implications

4.5.1 General implication from the results

Based on the sensitivity analysis, it reveals that the variations of pavement response (i.e. fatigue and rutting life) with the increasing subgrade moisture content showed various trends at different conditions (i.e. E_{ac}, h_{ac}, E_{base}, h_{base}, E_{sub}, h_{sub} and A_l) but emphasized the significance of drainage to the structural performance.

In general, increasing the thickness and modulus of pavement layers (E_{ac}, h_{ac}, E_{base}, h_{base}, E_{sub} and h_{sub}) can promote the service life of the pavement and thus mitigate the deterioration due to excess moisture in subgrade. However, they may not reduce the structural sensitivity to the moisture increase. Since base and subbase layers may serve as permeable drainage layers, it is necessary to consider the possible moisture increase before construction. During the design stage of pavement/railway tracks, analysis of sensitivity to subgrade moisture content could provide a reference for the selection of the dimensions and properties of each layer.

4.5.2 Polymer drainage layer

The designed polymer drainage layer is expected to show good performance in drainage and reinforcement of foundations. In order to achieve its full potential of reinforcement effects, the layer should be designed with a higher modulus than that of

the foundations. Considering the economical and mechanical requirements, the polymer drainage layer is not recommended over 100 mm in thickness. Particularly, the PDL would exhibit better performance if installed right at the top of the subgrade. From the previous studies, the polymer layer can also provide a buffer against impact load and offer thermal insulation, although this needs further laboratory and in-situ analysis to be verified.

4.5.3 Drainage design

The results also indicate a feasible procedure for pavement foundation drainage design. Regardless of the layers above the subgrade, it is also expected to be applicable to railway track foundations. A basic process is proposed for pavement/railway track foundation drainage design by incorporating moisture sensitivity of structural responses, as illustrated in Figure 4.51.

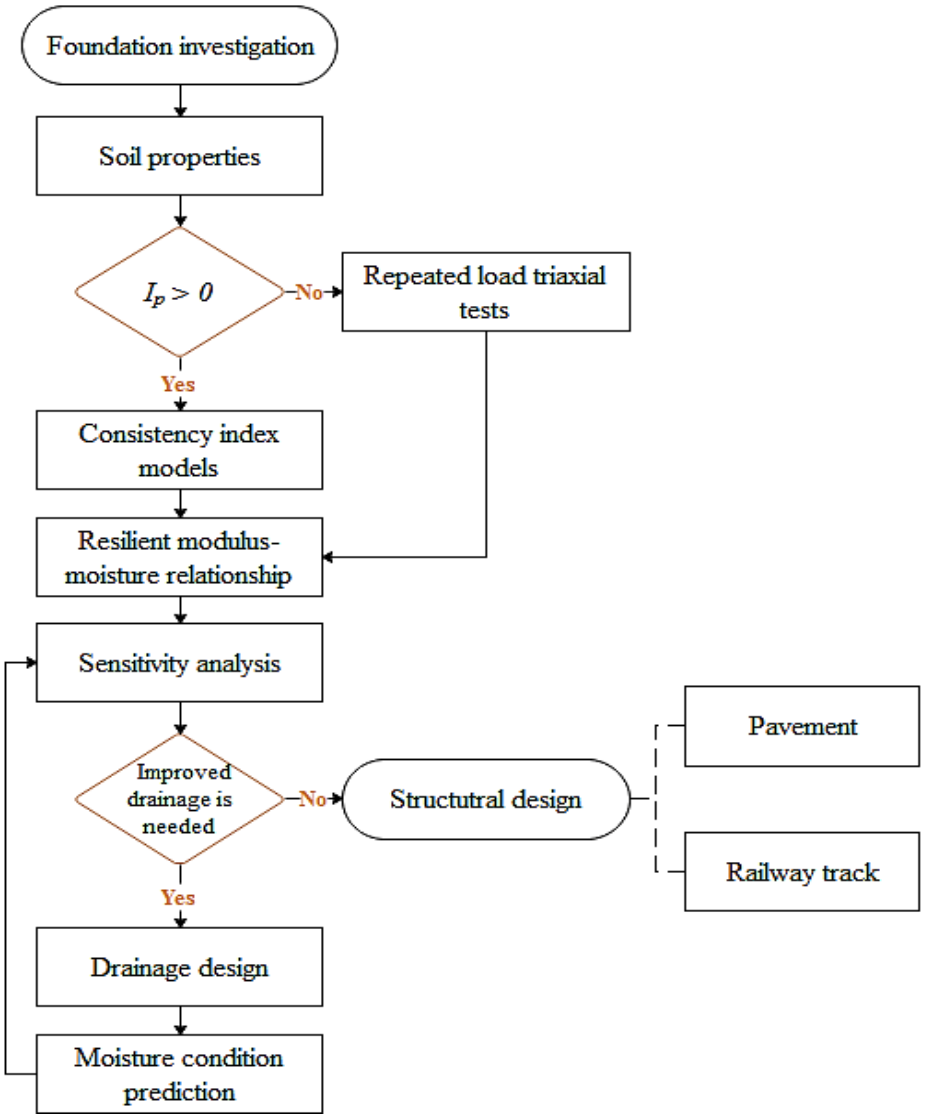

Figure 4.51 Drainage design process

4.6 Summary and conclusions

In this Chapter, based on multi-layered elastic theory, simulations were conducted, including sensitivity analysis and data analysis using literature sources. The effects of asphalt concrete, base layer, subbase, axle load and the proposed polymer drainage layer on the sensitivity of foundation soils to moisture contents were investigated.

Through sensitivity analysis of the selected structure, it was found that N_f was smaller than N_r. Thus, the design life of the whole structure was dominated by fatigue cracking. The sensitivity of N_f and N_r varied to different extents, i.e. from N_f varied between 0.1 and 0.35 (insensitive except at various h_{ac} (i.e. 25, 225, 275 and 300 mm) where it was moderately sensitive) while N_r varied from 2.3 to 2.7 (very sensitive). N_r was very sensitive to the increased moisture. N_r depends on subgrade strain which is directly linked to subgrade modulus; N_f depends on the bending of the asphalt layer, which is much more affected by the layer immediately below, the subbase, than the subgrade. Thus, moisture content showed larger effects on N_r. Therefore, it indicates the crucial role of subgrade conditions in pavement design. The implication is that the N_r should be accurately determined at different moisture levels so as to determine the limiting subgrade condition and/or higher layer thicknesses and stiffnesses so that appropriate drainage can be provided in the design.

Derived from previously published test data, a wide range of soil types were covered, which may represent various types of foundations. Generally, for all types of soils, with the increase of moisture content, fatigue and rutting life decreased, whilst fatigue cracking and permanent deformation increased. For S00A, there was a slight decrease. S26 exhibited the largest sensitivity, while S08 showed the smallest sensitivity in fatigue cracking and permanent deformation. For fatigue life, S23 showed the smallest sensitivity. It indicates that the sensitivity showed a significant trend with soil types, i.e. the soil with relatively higher plasticity generally resulted in higher sensitivity, whilst this trend was not linear with plasticity. This finding of the thesis is not generally known. Thus, the pavement performance was associated with soil types. The sensitivity of the soil to moisture content would largely affect the distress development. The increase of AC elastic modulus and thickness may reduce the permanent deformation and attenuate the effect of moisture on pavement performance while escalating the sensitivity of fatigue and rutting life as well as fatigue cracking to moisture content. Sensitivity did not show significant changes with axle load.

CHAPTER 5 SPECIMEN PREPARATION AND BASIC CHARACTERISTICS

5.1 Introduction

The macroscopic behaviour of soils is basically associated with soil fabric, aggregation and interparticle bonding effects. Without explicitly incorporating the soil microstructural characteristics, the particulate complexities can hardly be clarified (Koliji et al., 2010). In unsaturated soils, air and water phases cause more uncertainty in the particulate analysis. This chapter aims to demonstrate specimen preparation and investigate the basic characteristics of the soil used in this study. The basic characterisation includes particle size distribution, hydraulic conductivity, moisture content-dry density relationship, Atterberg limits and soil water characteristic curve. It serves as a basis for conducting laboratory tests and understanding the macro behaviour of the specimen.

5.2 Soil selection

Specimens are commonly categorised into three groups, i.e. undisturbed specimens, reconstituted specimens and compacted specimens. The advantages and disadvantages of each type of specimen are generally presented in Table 5.1.

Table 5.1 Characteristics of different specimen types, adapted from Bagheri (2018)

Specimen type	Soil type	Advantage	Disadvantage
Undisturbed specimens	Cohesive soil	▪ Represent in-situ soil structures and conditions	▪ Difficulties in sampling process (e.g. trimming block samples) ▪ Disturbance during preparation ▪ Only feasible for cohesive soils
Reconstituted specimens	Cohesive /granular soil	▪ Ease of preparing identical samples ▪ Easy preparation of samples with specific sizes without further treatment	▪ With limited inter-particle bond ▪ Possess a high air entry value.
Compacted specimens	Cohesive /granular soil	▪ Exhibit a lower high air entry value; ▪ More suitable for testing with restricted high suctions, collapse compression in wetting, and unsaturated testing	▪ Different fabrics by compaction on the dry and wet side of optimum ▪ Non-unique water retention even for a given density ▪ Initial conditions highly rely on compaction method/energy and initial water content

Since this study focuses on moisture content and drainage, in order to be practical for the limited study duration, the soil is required to have a reasonable hydraulic conductivity to facilitate drainage and moisture variation within a reasonable time. The soil material should also have high availability for specimen replicates. The typical values of the saturated coefficient of permeability in each type of soil and the corresponding drainage properties are presented in Table 5.2 (Dawson, 2008). Clayey soils take too lengthy a time to conduct the drainage process, drying or wetting. They have also been widely studied before (Yang et al., 2008; Sawangsuriya et al., 2009; Han & Vanapalli, 2016b; Khoury, 2018). Sandy soils cannot allow sufficient time to observe the drainage process due to their high permeability.

Table 5.2 Typical coefficients of permeability of saturated soils (Dawson, 2008)

Soil type	k_w /m·s^{-1}	Degree of permeability	Drainage properties
Clean gravel	>10^{-3}	Very high	Very good
Sandy gravel, clean sand, fine sand	10^{-5}-10^{-3}	High to medium	Good
Sand, dirty sand, silty sand	10^{-7}-10^{-5}	Low	Fair
Silt, silty clay	10^{-9}-10^{-7}	Very low	Poor
Clay	<10^{-9}	Virtually impermeable	Very poor

In terms of hydraulic conductivity, silty sand was found to lie between clayey and sandy soils. The permeability of silty sand with different fine contents (i.e. 5%, 10%, 15%, 20%, 30% and 50%) was investigated. The sand belongs to DB Specialist Sands (Leighton Buzzard sand, Fraction C, 0.3-0.6 mm), purchased from DB Group (Cambridge, UK). The silt was obtained by sieving the "Sheffield soil" already available at the Nottingham Centre for Geomechanics at the University of Nottingham (Tasalloti et al., 2020). A 150-micron mesh was used so that the resulting soil comprised most of the fine sand and smaller fractions - i.e. it was mostly silt with some fine sand. The permeability results show that silty sand with 15% finer soils had a reasonable hydraulic conductivity (as shown in Section 5.5.2 in detail). Thus, compacted specimens formed of this silty sand were used in this study. It should be noted that using such soil may limit the applicability of the results as they will only be based on this silty sand. It is known, for example, that the amount of silt affects the behaviour of silty sands (Lade, 2016).

5.3 Preparation method

Various preparation methods for triaxial testing specimens are available according to specimen and soil types. It is also known that sample preparation methods can have effects on soil behaviour (Lade, 2016). For intact specimens, the preparation method usually consists of sampling with thin-walled tubes, sealing soil inside the tube using wax and tube caps, selecting representative specimens, extruding the soil cylinder and trimming the specimen to fit the triaxial cell. This is mainly applicable to clayey soils.

For reconstituted specimens, a wide range of methods are developed for different soils, including slurry consolidation of clay, air pluviation of sand, depositional techniques for silty sand (i.e. dry funnel deposition, water sedimentation, slurry deposition, mixed dry deposition, air pluviation and moist tamping), under-compaction, compaction method of clay soils (i.e. static, vibratory and kneading), compaction of soils with oversize particles (i.e. compaction of rocks (gravel, cobbles, and boulders) separately and compaction of the soil fraction in the usual manner). The advantages and disadvantages of these specimen preparation methods in triaxial tests were discussed by Lade (2016) and Bagheri (2018). For granular soils, reconstituted specimens are widely used since it is very difficult and unrealistic to obtain non-cohesive soils in their undisturbed and natural state (Frost & Park, 2003). Moist tamping has been widely used in unsaturated soil testing (Ng & Yung, 2008; Maleki & Bayat, 2012; Vo & Russell, 2013; Chen et al., 2018; Pandya & Sachan, 2018). It has the advantage of producing very loose specimens, which generally is considered beneficial (Lade, 2016). For well-graded sand or sand containing significant amounts of fines, moist tamping can eliminate segregation that would clearly occur in air pluviation. Moist tamping using the concept of undercompaction devised by Ladd (1978) would also reduce soil grain segregation and obtain specimens with relatively uniform density. It should be also noted that moist tamping should be cautiously performed to avoid breakage of weak particles.

To easily achieve maximum dry density, construction specifications usually require that the foundation be compacted at or near OMC. In this study, the mechanical behaviour of compacted foundation soil (i.e. silty sand) was investigated. In order to maintain the uniformity of the specimen and obtain specimens with controlled dry density (Frost & Park, 2003), moist tamping was utilized to prepare the specimens layer by layer. The specimen density can be controlled by adjusting the dry weight of soil

specimens that must be fitted into a certain size mould.

5.4 Preparation procedure

For specimens in saturated triaxial tests, preparation procedures are described as follows, thus effectively producing heavily overconsolidated soil. Freshly de-aired water was added into the soil and mixed to achieve the target MC (i.e. optimum moisture content in this study). The mixture was sealed into plastic bags to uniformly distribute the water. Before placing the coarse disk on the base, the base plate should be flushed to remove the air in the channel. A 0.3mm-thick latex membrane was placed around the pedestal and sealed with two O-rings. An internal split mould was directly placed on the pedestal with the membrane inside to prepare the specimen. In order to obtain as homogeneous a specimen as possible, the soil was compacted into five layers, and each layer having the same mass was compacted to the same height. Before dismantling the mould, a vacuum of 3-5 kPa was applied to keep the specimen standing and reduce disturbance. The ratio of the length to diameter was 2:1, and thus cylindrical specimens with a diameter of 38 mm and height of 76 mm were produced. In order to reduce the friction effects of platens and possible buckling of specimens, each specimen end was lubricated with silicone grease. The diameter and height were measured with a vernier calliper. The moisture content was checked after the test using a drying oven.

For specimens in unsaturated triaxial tests, the preparation procedures were generally the same as those in saturated triaxial tests, apart from a high air entry ceramic disk with a value of 500 kPa being used in the base pedestal. Before preparing the specimen, the ceramic disk should be saturated (discussed in Chapter 6). The preparation procedure and tools used are illustrated in Figure 5.1.

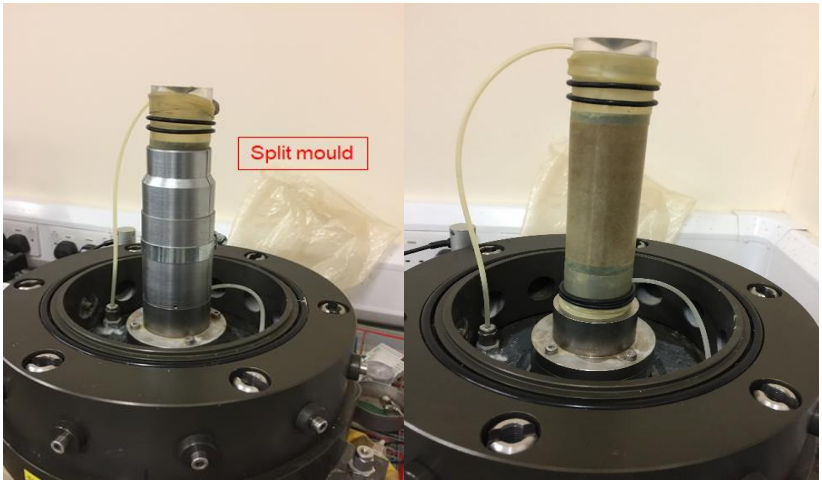

Figure 5.1 Specimen preparation procedures and tools

5.5 Macro characteristics

Basic physical properties of the silty sand were investigated in compliance with BS 1377:1990 by British Standard Institution (1990). Various laboratory tests were conducted, including wet/dry sieving analysis, hydrometer sedimentation, permeability tests, standard Proctor compaction, Atterberg limits and wetting processes to obtain soil water characteristic curve.

5.5.1 Particle size distribution

Wet/dry sieving analysis and hydrometer sedimentation were conducted on the silty sand to obtain the particle size distribution. Through wet sieving, the silt and clay particles were separated from the specimen. Then, dry sieving was performed for the remaining coarser soil. Hydrometer sedimentation was performed for all the collected silt and clay. The results are presented in Figure 5.2. Generally, the soil consists of 85% sand and 15% silt. The results indicate that the sand is non-uniformly graded, i.e. the particle size of sand mainly ranges from 0.3 mm to 0.6 mm with silt at less than 0.15 mm. Fine grains (i.e. silt and clay) could fill the pores between coarser particles. Thus, it will increase the matric potential while reducing the hydraulic permeability. The existence of fine grains will be beneficial to develop relatively high suction in the specimen and thus allow testing on the effects of a wider range of suctions on soil behaviour.

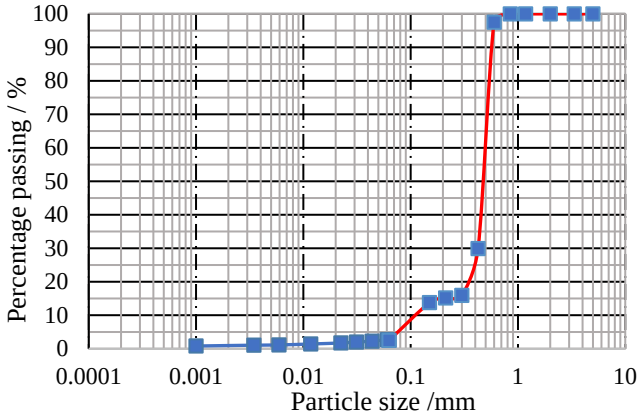

Figure 5.2 Particle size distribution curve of silty sand

5.5.2 Hydraulic conductivity

Saturated permeability is typically estimated in a constant head test for coarse-grained soils and a falling head test for fine-grained soils (Dawson, 2008). Considering the existence of fine grains and low permeability at compacted conditions, falling head

permeability tests were conducted in this study. The mould size was 13 cm in diameter and 10 cm in height. The specimen was produced in the mould following the above preparation procedure and then saturated before testing. The sample was compacted in the cylinder mould (for the permeability tests). Then, a porous disc was placed and fixed on the top of the sample to prevent the top soils from moving. Next, the mould was placed into a container filled with water and immersed. The vacuum was applied to the container, thus removing the air from the sample. When no air bubbles occurred, it was considered as saturation. According to Darcy laws, the flow rate can be calculated through

$$q = k_{sat}\frac{h}{L}A = -a\frac{dh}{dt} \tag{5.1}$$

where q is the flow rate, h is the water head difference at time t, a and A are the cross-section area of the standpipe and the specimen, respectively. Integrating Eq. (5.1) with time from t_1 to t_2 and the corresponding head of the standpipe h_1 and h_2, the saturated permeability can be expressed as

$$k_{sat} = \frac{aL}{A(t_2 - t_1)}\ln\frac{h_1}{h_2} \tag{5.2}$$

Based on initial permeability tests, a reasonable permeability (relatively smaller value) was achieved for the silty sand. Based on the measurement, the coefficient of variation was calculated, i.e. about 23%, which is acceptable. The mean value of measured permeability was 7.13×10^{-6} m/s. This is expected to allow the drainage process to be slow enough for observation while saturation is not too time-consuming.

5.5.3 Standard Proctor compaction

Standard Proctor compaction was conducted to study the relationship of dry density with moisture content. The compaction test result is presented in Figure 5.3. At a w lower than w_{opt}, dry density showed an upward trend, while showing a downward trend at w above w_{opt}. Based on interpolation, the optimum moisture content (OMC) and maximum dry density of silty sand were determined, i.e. 10.5% and 1.85 g/cm^3. The obtained curve is in agreement with typical compaction curves. Based on the above analysis, basic soil properties are presented in Table 5.3.

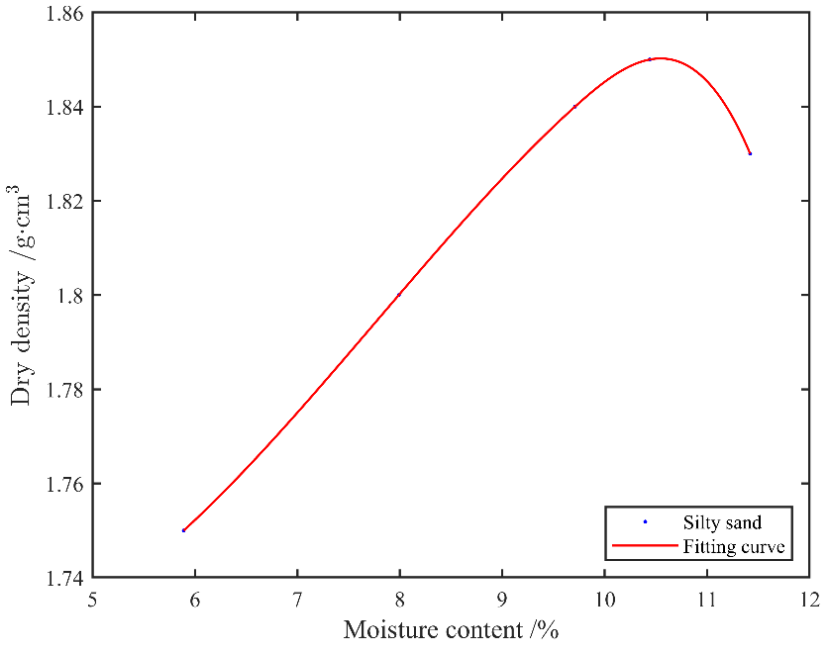

Figure 5.3 The relationship between moisture content and dry density of silty sand

Table 5.3 Summary of basic soil properties

Property	Value
Mean diameter, D_{50}, mm	0.47
Coefficient of uniformity, C_u	4.17
Coefficient of curvature, C_c	3.01
OMC, %	10.5
Maximum dry density (MDD), g/cm^3	1.85
G_s at MDD	2.04
Degree of saturation at MDD, %	70.1
Percent passing #25 sieve (600 μm)	100
Percent passing #240 sieve (0.063 μm)	2.5
Percent clay <0.002 mm	1.05
Fine content, %	15

5.5.4 Atterberg limits

Atterberg limits are commonly used to classify fine-grained soils (O'Kelly et al., 2018). For example, liquid limit (LL) and plasticity index can be used to obtain a plasticity chart to categorise soils (Wesley, 2003), as illustrated in Figure 5.4. Based on the correlation, Atterberg limits have been used to estimate the parameters of shear strength, deformation and critical-state soil mechanics, e.g. determination of

compression index with LL by Skempton & Jones (1944), determination of friction angle with plasticity index by Bjerrum & Simons (1960), Tripathy & Mishra (2011), Sorensen & Okkels (2013) and Farias & Llano-Serna (2016).

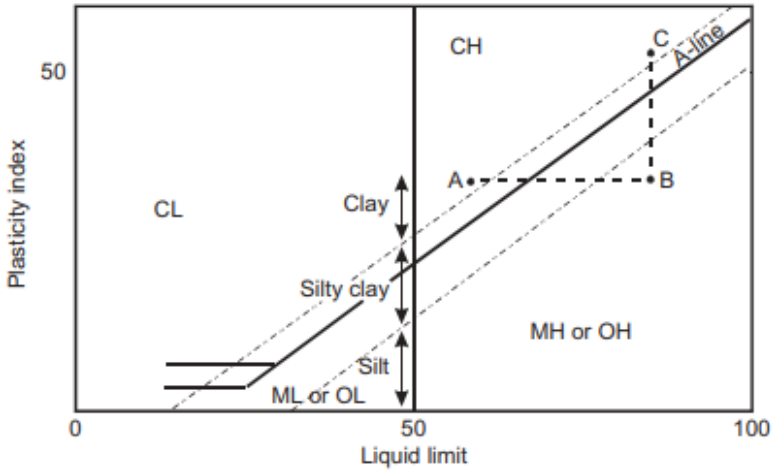

Figure 5.4 Plasticity chart (Wesley 2003)

Atterberg limits were determined for the silty sand, including LL and plastic limit (PL). All the Atterberg limits are summarised in Table 5.4. The plasticity index of the silty sand was determined as 5.4, i.e. low plasticity.

Table 5.4 Summary of Atterberg limits

Soil index	Silty sand	Sand
LL, %	20.5	19.6
PL, %	15.1	n/a
PI	5.4	n/a

5.5.5 Soil water characteristic curve

For unsaturated soils, it is significant to determine the SWCC in order to assess the soil water retention capacity and water flow. SWCC is defined as the relationship between soil suction and gravimetric/volumetric moisture content (or degree of saturation). SWCC is highly influenced by pore characteristics, including pore distribution, pore size and pore connectivity (Mitchell & Soga, 2005). It exhibits a hysteretic phenomenon during wetting and drying paths, i.e. the suction shows a larger value on the drying path than on the wetting path. Thus, it is necessary to measure the suction during both the wetting and drying processes.

Currently, experimental methods are mainly utilized to measure the SWCC, and the principle of measurement is the soil moisture content at various soil water potentials

during the dehumidification process (Pan et al., 2019). A series of discrete data points are acquired from direct measurement of SWCC, which can describe the relationship between soil suction and moisture content. Various mathematical approaches are also proposed to represent the SWCC, e.g. the model by Brooks & Corey (1964), the model by Van Genuchten (1980) and the model by Fredlund & Xing (1994), which are commonly used.

(1) Brooks and Corey model

A two-part power law relationship was proposed by Brooks & Corey (1964), expressed as

$$\Theta = \begin{cases} 1, & \psi \le \psi_m \\ \left(\frac{\psi_m}{\psi}\right)^{\lambda_p}, & \psi > \psi_m \end{cases} \tag{5.3}$$

where Θ is the normalized moisture content, $\Theta = \frac{\theta - \theta_r}{\theta_s - \theta_r}$, θ_s is saturated moisture content, θ_r is residual moisture content, ψ_m is the air entry pressure and λ_p is a pore size distribution index.

In terms of volumetric moisture content, it can also be written as

$$\theta = \begin{cases} \theta_s, & \psi \le \psi_m \\ \theta_r + (\theta_s - \theta_r)\left(\frac{\psi_m}{\psi}\right)^{\lambda_p}, & \psi > \psi_m \end{cases} \tag{5.4}$$

In terms of the suction head h_s and air-entry head h_b, it can be rewritten as

$$\Theta = \begin{cases} 1, & h_s \le h_b \\ \left(\frac{h_b}{h_s}\right)^{\lambda_p}, & h_s > h_b \end{cases} \tag{5.5}$$

(2) van Genuchten model

A three-parameter model by Van Genuchten (1980) is defined as

$$\Theta = \left[\frac{1}{1 + (a_s\psi)^{n_s}}\right]^{m_s} \tag{5.6}$$

where a_s, n_s and m_s are fitting parameters. According to Mualem's relative permeability model (Mualem, 1976), the relationship between n_s and m_s can be expressed as

$$m_s = 1 - \frac{1}{n_s} \tag{5.7}$$

(3) Fredlund and Xing model

Incorporating pore size distribution in a similar way to the van Genuchten model, another model was developed by Fredlund & Xing (1994), presented as

$$\Theta = C(\psi)\theta_s \left[\frac{1}{\ln[e + (\psi/a_s)^{n_s}]}\right]^{m_s} \quad (5.8)$$

where $C(\psi)$ is a correction factor that forces the model through a prescribed suction value of 10^6 kPa at zero moisture content, i.e.

$$C(\psi) = \left[1 - \frac{\ln(1 + \psi/\psi_r)}{\ln(1 + 10^6/\psi_r)}\right] \quad (5.9)$$

Considering the availability and cost of the facility, an unsaturated triaxial cell with a high air entry disk is employed to conduct the tests. Based on the axis translation technique, a target matric suction was applied and the corresponding moisture content in the specimen was determined. The volumetric water content (θ) was the mass of water per mass of dry soil and it was obtained by multiplying gravimetric water content by bulk density.

Basic procedures for SWCC are as follows: after the specimen was installed, seven suction values were selected (50, 25, 15, 10, 5, 3 and 1 kPa in descending order). Based on the axis-translation technique, each target suction was applied and then maintained by setting the pore air pressure and pore water pressure. The back volume changes (volume of back pressure controller) were monitored. The volume change at equilibrium was used to calculate the moisture content variation for each stage. Based on the moisture content and the target matric suction, SWCC was obtained.

At each stage, the suction was changed slowly to allow water equilibrium. The dynamic matric suction was also monitored. When the value was stable, it was considered to reach equilibrium (thus uniform state), which was empirical. During the measurement, the specimen was left to reach equilibrium within sufficient time. Thus, the measurement was believed to represent the samples. The limitations of the axis translation technique include: (1) the suction measurement range was limited by the air entry value of the high-air entry porous disk. (2) It determined the overall matric suction of the specimen, while local moisture distribution and equilibrium were not indicated (or only empirically determined). (3) Accumulation of diffused air bubbles in the water compartment of the high air-entry value ceramic disk can cause a discontinuity between pore-water in the specimen and water in the measurement system.

The SWCC from the test results was fitted using the three models, as shown in Figure 5.5. The model parameters are presented in Table 5.5. It should be noted that outliers were excluded for the FX model considering convergence. It indicates that the model parameters in the study were generally in agreement with the literature. All three

models performed excellently in predicting the SWCC, and the curves demonstrated similar shapes. The Fredlund & Xing model presented the smallest R^2, while the values of R^2 for the other two models showed no significant difference. These models were applicable for describing the SWCC of the silty sand.

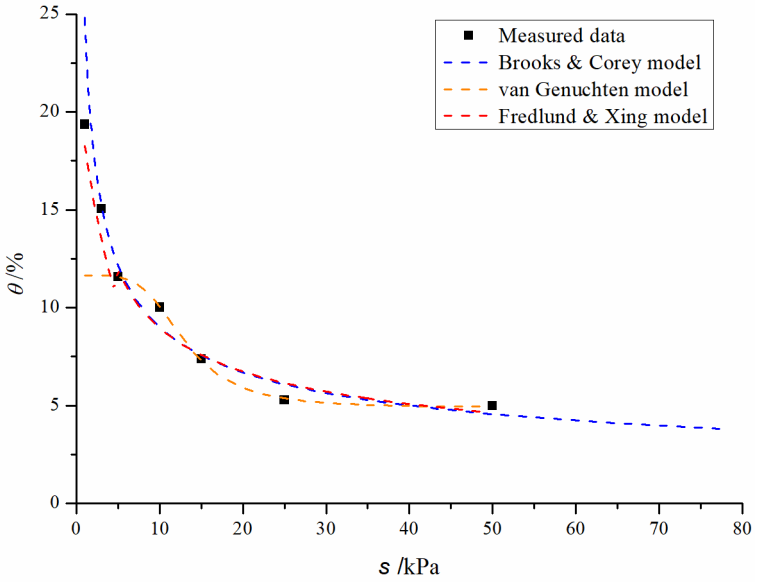

Figure 5.5 SWCC from fitting models

Table 5.5 Model fitting parameters of SWCC

Source	Soil	Model	λ_p	a_s	n_s	m_s	R^2
Thesis	Silty sand	BC model	0.4536	-	-	-	0.9989
		VG model	-	0.0826	4.6258	0.7838	0.9995
		FX model	-	8.07	1.107	3.998	0.9839
Rajesh et al. (2017)	Compacted silty sand	BC model	1.115	-	-	-	0.9757
Baker (2001)	NW12: silty sand	VG model	-	0.0439	3.1398	0.3819	0.965
Song et al. (2012)	Silt	VG model	-	0.052	2.003	0.501	-
	Sand	VG model	-	0.393	8.553	0.883	-
Salour et al. (2014)	Luleå silty sand	FX model	-	34.08	5.59	0.31	> 0.9
Rajesh et al. (2017)	Compacted silty sand	FX model	-	7.88	1.30	0.81	0.9772

Note: BC, VG and FX models indicate Brooks & Corey model, van Genuchten model and Fredlund & Xing model, respectively.

5.6 Micro characteristics by SEM

To develop a knowledge of basic physical properties and mechanical/hydraulic behaviour of intact and reconstituted soils, micro and meso-structural analysis have

been widely conducted. In terms of unsaturated soils, microstructural analysis is commonly focused on compacted soils, which involves the aggregation or matrix of particles at various physical states and their correlations with mechanical/hydraulic behaviour (e.g. strength, compressibility and hydraulic conductivity) (Romero & Simms, 2008). Various techniques have been utilized to analyse particle properties, including (e.g.) time-domain reflectometry, near-infrared spectroscopic measurements, electric impedance tomography, neutron tomography, X-ray computed tomography, dual-energy gamma-ray technique, mercury intrusion porosimetry, scanning electron microscopy (SEM) and nuclear magnetic resonance (NMR). Based on these techniques, the assembly, arrangement and distribution of particles, and the distribution, contacts and connectivity of pores in the soil can be investigated at the particle scale (<100 μm). Considering the advantages of SEM technology, it is employed to study the microscale characteristics of silty sand. It aims to reveal the microstructure of specimens in order to achieve a better understanding of the macroscopic behaviour.

With minimal requirements for specimen preparation, SEM attracts increasing attention to its geotechnical application (Al-Mukhtar et al., 2012; Lin & Cerato, 2014; Mohseni et al., 2017; Wang et al., 2018; Ikeagwuani et al., 2019; Jahandari et al., 2021). It allows observation of specimens in dried states. SEM can be grouped into three categories, conventional SEM, environmental SEM and low vacuum SEM (Van Dam et al., 2002). In particular, environmental SEM for unsaturated soils as an emerging technique has been discussed in detail (Romero & Simms, 2008).

Based on SEM, the basic particle properties of silty sand in this study are analysed. To investigate the particle arrangement of silty sand, three specimens with different degrees of compaction were tested, i.e. 80%, 90% and 100% of the dry density achieved by standard Proctor compaction. Specific amounts of soil and water were mixed together and compacted in the split mould. After compaction, a piece of the sample was taken from each specimen with minimal disturbance. Then, the samples were dried in the oven and used with an electron beam for observation after sputter coating.

The scanning photos from SEM are presented in Figure 5.6~Figure 5.8 to illustrate the bonding between silt and sand. The silt demonstrated a typical cohesive soil structure. It shows that the smaller particles, i.e. silt, were attached to the surface of sand particles or existed as clots among sand particles. The silt amongst sand particles had effects on particle friction and permeability. The sand particles exhibited an

irregular surface. Based on the presence of silt, the sand particles showed closer contact at higher degrees of compaction, i.e. more sand particles in view at the same magnification. This may increase the interlocking of sand particles. Under 100% compaction, the angular shape of sand particles can be identified, and there is a clear indication of breakage of the particles.

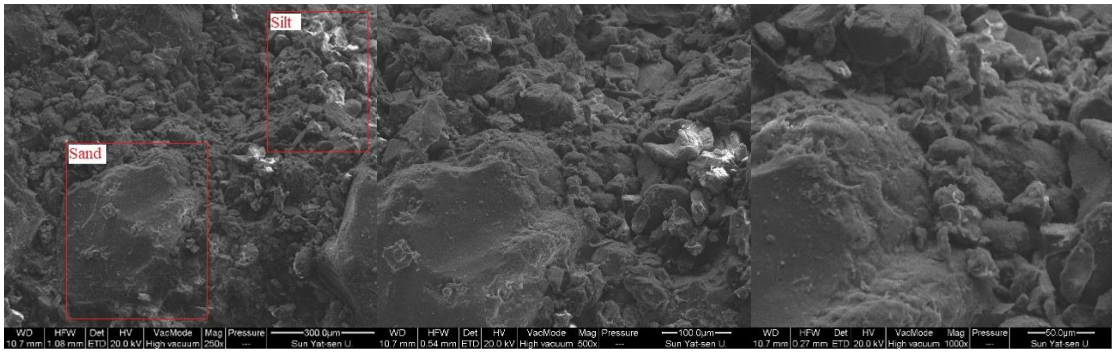

Figure 5.6 SEM photos of soils with 80% compaction at 250x, 500x and 1000x from left to right

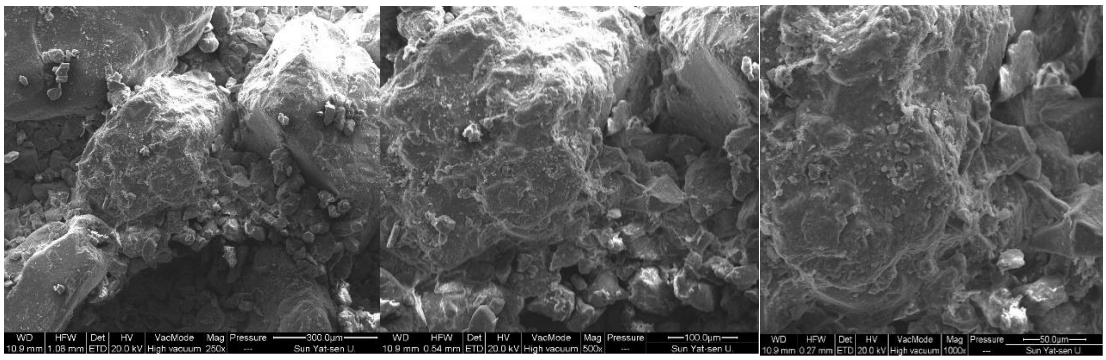

Figure 5.7 SEM photos of soils with 90% compaction at 250x, 500x and 1000x from left to right

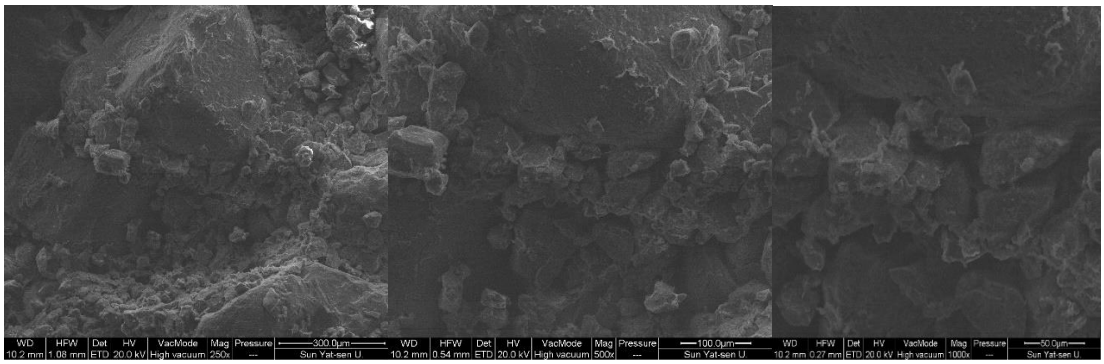

Figure 5.8 SEM photos of soils with 100% compaction at 250x, 500x and 1000x from left to right

Due to the discrepancies in sample preparation and sampling positions, the microstructure may vary apart from the effects of compaction. It could serve as a reference to have a better understanding of the macro behaviour.

5.7 Summary and conclusions

Various specimen preparation methods were presented in terms of specimen types, i.e. undisturbed, reconstituted and compacted specimens. Silty sand is selected to conduct experimental analysis. Based on their advantages and disadvantages, moist tamping was adopted for specimen preparation in this study. A specimen set-up procedure was also developed for adoption in the work described in later chapters.

Macro characteristics were studied, including particle size distribution, hydraulic conductivity, standard Proctor compaction, Atterberg limits and soil water characteristic curve. According to the plasticity index, the soil used showed low plasticity. Fitting models for the SWCC performed excellently in the silty sand, including the Brooks and Corey model, the van Genuchten model and the Fredlund and Xing model. The fitting results verified the applicability of these models to describe the SWCC of the silty sand. The SWCC provides a basis for understanding the correlation between moisture content, suction and soil response.

Based on SEM, the morphology of the specimen was demonstrated. The interparticle arrangement between silt and sand was presented. As the degree of compaction increased, sand particles were found to have closer contact. This further confirmed that specimens were beneficially compacted under 100% compaction.

CHAPTER 6 SATURATED TRIAXIAL TESTS

6.1 Introduction

For both flexible and rigid pavement structures, subgrade plays a significant role in supporting upper layers. Rutting may develop due to settlement and the accumulation of permanent deformation of subgrade soils in the foundation (Brown, 1997) that increases with increased moisture content and pore water pressure. Insufficient stiffness of either or both aggregate and soil layers could induce excess resilient deformation at the pavement surface (Dawson & Correia, 1996). Subsurface water in the pavement foundation is taken as an important factor that reduces the structural performance and service capability of roads and rail tracks (Selig & Waters, 1994; Dawson, 2008). Water generally exists in pavement structures in several forms, e.g. free water, capillary water, bound moisture and/or water vapour. As the only form of water which can be drained by gravity, free water, which can impair the strength and stiffness of the foundations, raises the most concern (Ridgeway, 1982). It can also contribute to frost-heave action in the subsurface structure of pavements. Some bound and capillary water can be beneficial to pavement/track material response, but free water (especially at elevated pressure) will always be damaging as it reduces the effective stress and, consequently, the mechanical performance that relies on inter-particle friction.

Table 2.7 presents various ingress routes of water flow to pavement structures, which will contribute to the water table increase and thus increase the pore water pressure. Through drainage, the build-up of pore water pressure will be dissipated in the foundation and the strength will be enhanced to alleviate the effects of loading and environmental variations. In this way, the structural performance of pavements will be promoted, and the service life will be extended. Inadequate subsurface drainage has been found to induce many premature failures (giving less than 50% of expected life) (Christopher & McGuffey, 1997). Therefore, subsurface drainage should receive serious attention as it is a key component in the performance of pavement structures. Strategies of subsurface drainage were presented by Christopher & McGuffey (1997), including the utilization of permeable base, underdrains, edge drains, filters, outlets and prefabricated geocomposite edge drains. The lateral or median drain may be taken as the most effective route provided an underdrain with high conductivity is included to

bring water to that lateral or median drain (Dawson & Hill, 1998a). Regarding subsurface drainage, two general types of subsurface drainage requirements were used by Ridgeway (Ridgeway, 1982): (a) a time for a certain percentage of drainage and (b) an inflow-outflow criterion. The effectiveness of these methods could be quantified by measuring and comparing the MC or the time to achieve a given MC in the corresponding sections.

The benefits of drainage to enhance foundation performance are widely known. However, studies on the effects of drainage on the foundation soil behaviour and further on pavement performance have not been comprehensive. Through single-stage (i.e. without drainage) and multistage (i.e. with drainage) triaxial tests that were performed, both consolidated drained (CD) and consolidated undrained (CU) shear strength and critical state behaviour are analysed here. In the multistage tests, the pore water pressure was reduced by 100 kPa at a step of -25 kPa in each stage. The increase in the effective stress by the pressure reduction could be linked to the increase in the effective stress by suction variations in the subgrade soils due to environmental influence or drainage during extreme flooding. For example, the 25 kPa increase in the effective stress could be equivalent to the suction increase due to (e.g.) a decrease of about 3% in moisture content from 10% (according to the SWCC in Figure 5.5). The moisture variation will depend on the initial moisture content. In addition, it can also represent extreme cases (e.g. the pavement/railway structures were seriously flooded and inundated), selected in order to clearly illustrate drainage effects. To reduce testing time and acquire more information, during multistage tests, unloading-reloading tests have been performed. Thus, the unloading modulus was obtained as an estimation of the resilient modulus of the subgrade soil. Based on the multi-layered linear elastic theory (Section 2.7) using unloading modulus as an input, relevant pavement responses can be derived. Furthermore, the unloading modulus will be introduced into KENLYAER as an input to perform flexible pavement analysis. Based on the triaxial test results and KENLAYER analysis, the response of a flexible pavement (i.e. horizontal or vertical stress/strain, vertical displacement) at critical positions (i.e. bottom of the asphalt concrete layer and the top of subgrade) are evaluated. In this way, it is hoped to provide reference data for the drainage design of pavements with soft foundations.

6.2 Theoretical framework

6.2.1 Research process

The research process is illustrated in Figure 6.1.

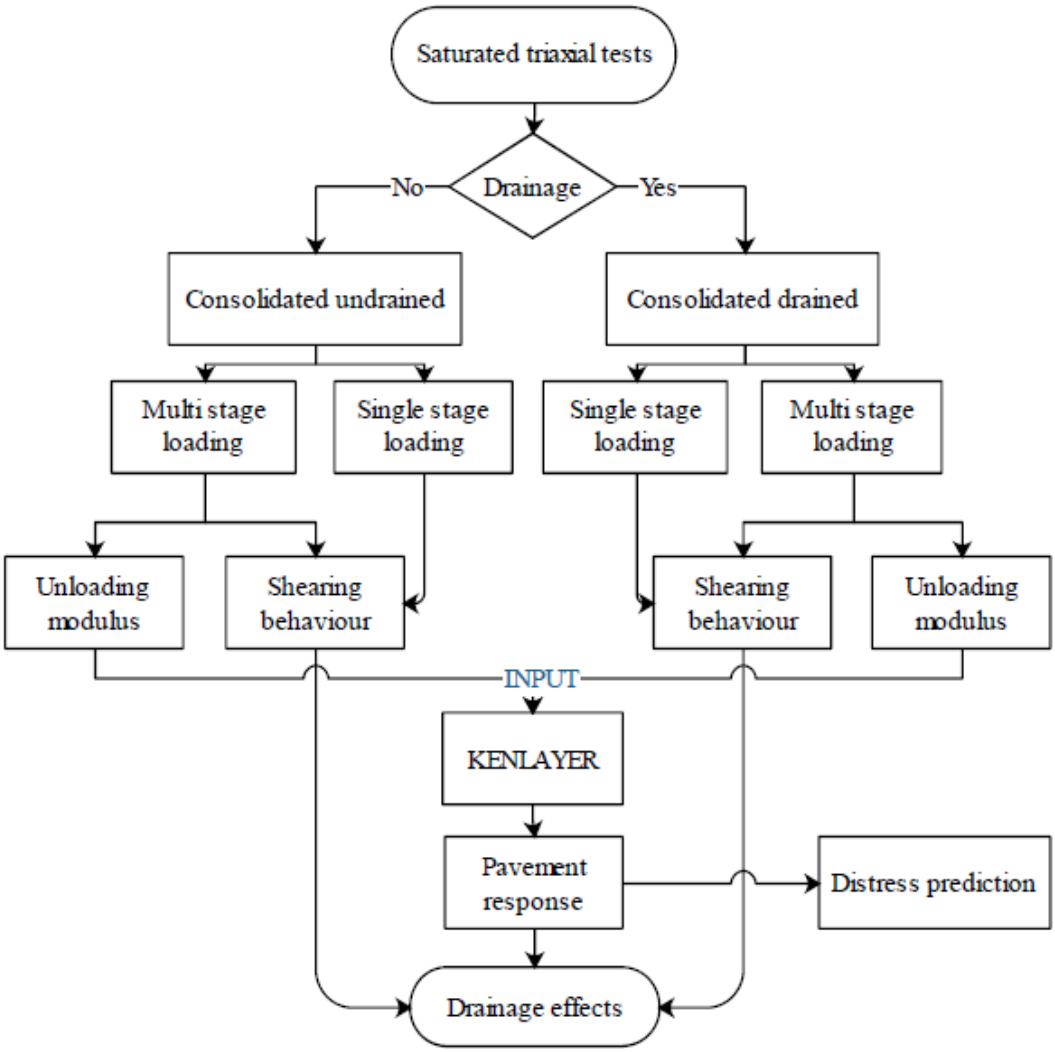

Figure 6.1 Research process of saturated triaxial tests

6.2.2 Effective stress

Due to the different pore water pressure conditions in saturated states, subgrade soil will exhibit consequential differences in stress conditions which will affect the soil's behaviour. Therefore, in order to accurately investigate the mechanical response of the soil, the stress state should be obtained.

In the saturated state, the principle of effective stress is applied. The mechanical state of the soil can be described by a stress-state variable, i.e. effective normal stress σ' which, according to the principle of effective stress (Terzaghi, 1943), can be expressed as

$$\sigma' = \sigma - u_w \tag{6.1}$$

where σ is total normal stress and u_w is the pore water pressure, generally positive or zero for the saturated soil. The relationship is illustrated in Figure 6.2. The effective stress is the part of the total stress that is transmitted to the solid particles and the pore water pressure is the part of the total stress that is transmitted to the water phase. The stress state in a saturated specimen is presented in Figure 6.3.

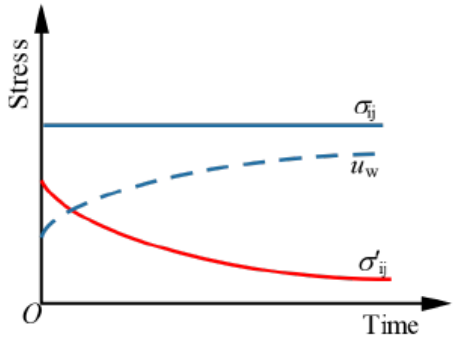

Figure 6.2 General relationship between σ, σ' and u_w (Rees, 2012)

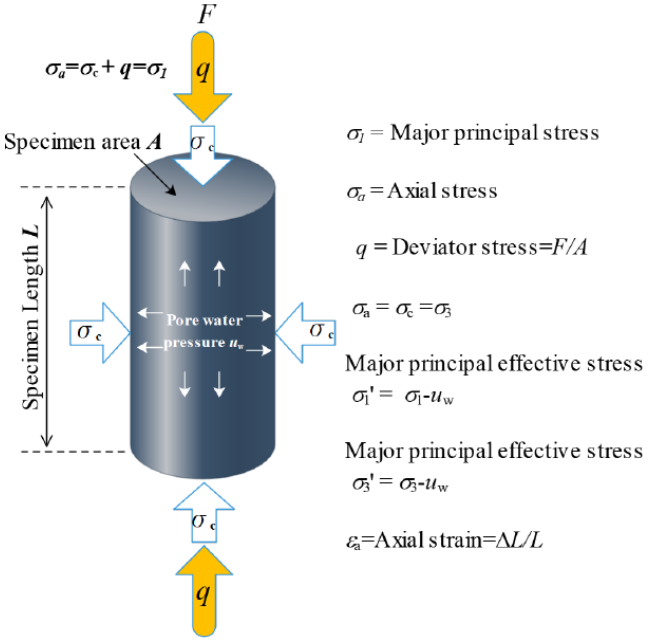

Figure 6.3 Schematic illustration of stress states in triaxial test, adapted from (Rees, 2012)

6.2.3 Critical state

The critical state theory developed by Roscoe et al. (1958) introduces a unified model to investigate the saturated soil behaviour by observing variations (Barnes, 1995) in: the mean effective bulk stress or consolidation stress p'; the shear stress or deviator stress q; the volume change described in terms of specific volume v.

During the conventional drained and undrained triaxial compression tests on normally compressed and lightly (or heavily over-consolidated) samples (Wood, 1990),

or shear box tests on dense and loose sand samples (Powrie, 2013), soil samples have been observed to strain until they reach a critical void ratio or specific volume state, at which condition the soil continues to shear progressively without variations in volume or effective stresses. The development of τ, ε_{vol} and v with γ during shear box tests as well as related equations are presented in Section 2.3.1.

6.2.4 Shear strength

The shear strength of soils indicates the shear resistance presented by the soil to withstand the applied shear stress, as a function of applied normal effective stress, expressed as Eq. (2.5) ($\tau_f = c' + \sigma' tan\,\phi'$), where c' is the cohesion intercept and $\phi'$is the internal friction angle of the soil, i.e. the shear strength parameters. They can be measured using triaxial compression tests. ϕ' can also be derived from the slope of the Mohr-Coulomb failure criterion (i.e. $sin\,\phi' = \frac{\sigma_1' - \sigma_3'}{\sigma_1' + \sigma_3'}$), as shown in Figure 6.4 for soil not exhibiting cohesion (Helwany, 2007). In this situation, the angle θ (see Figure 6.4), σ' and $\tau_f{}'$ can be calculated from

$$\theta = 45^o + \frac{\phi'}{2} \tag{6.2}$$

$$\sigma' = \frac{\sigma_1' + \sigma_3'}{2} - \frac{\sigma_1' - \sigma_3'}{2} sin\,\phi' \tag{6.3}$$

$$\tau = \frac{\sigma_1' - \sigma_3'}{2} cos\,\phi' \tag{6.4}$$

$$\sigma_1' = \sigma_3' \tan^2\left(45^o + \frac{\phi'}{2}\right) + 2c' \tan\left(45^o + \frac{\phi'}{2}\right) \tag{6.5}$$

$$\sigma_3' = \sigma_1' \tan^2\left(45^o - \frac{\phi'}{2}\right) - 2c' \tan\left(45^o - \frac{\phi'}{2}\right) \tag{6.6}$$

A similar interpretation is possible in situations where the soil exhibits cohesive as well as frictional elements of strength.

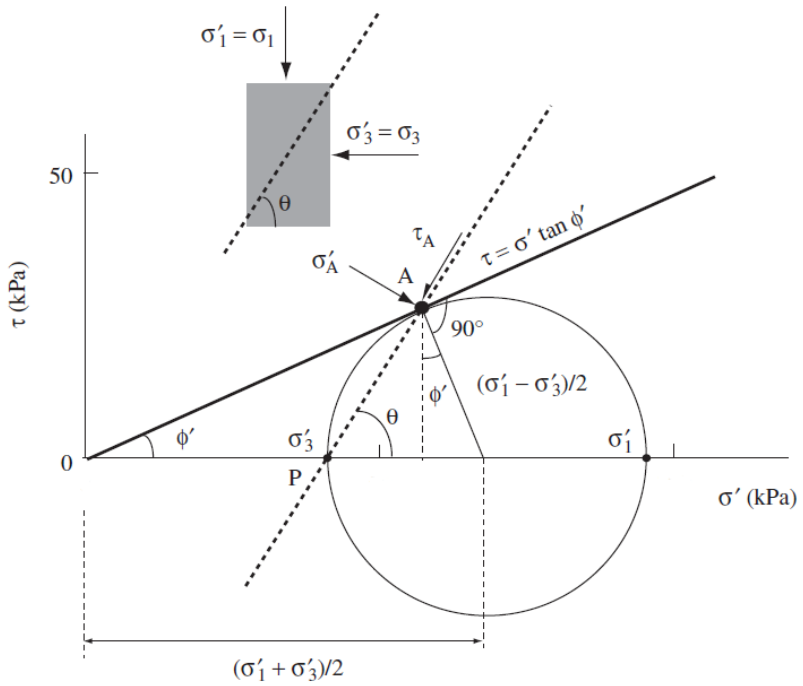

Figure 6.4 Schematic diagram of determination of the Mohr-Coulomb failure criterion for the soil (Helwany, 2007)

6.2.5 Unloading modulus

To reflect the stress-strain behaviour (i.e. resilient response) of subgrade soils under normal cyclic traffic loading, the resilient modulus, M_r, of subgrade soils was introduced by AASHTO (AASHTO, 2002) as a more rational soil property than the soil support value or modulus of subgrade reaction (Yang et al., 2005) which had commonly been used before. Therefore, the resilient modulus, M_r, is widely employed to estimate transient soil deformation under repeated traffic loads. As a significant stiffness parameter to demonstrate the resilient behaviour, M_r is mathematically defined as the ratio of repeated deviator stress q to axial recoverable strain (i.e. resilient strain) ε_r (Li & Selig, 1994) in a more simplified form than as expressed earlier in Eq. (2.1):

$$M_r = \frac{q}{\varepsilon_r} \tag{6.7}$$

Considering the significant contribution of subgrade modulus to the overall performance of roads or railways, it is crucial to provide the best prediction of resilient modulus for road and railway foundations. The unloading deformation will be the truly resilient (i.e. recoverable) deformation, and none of the deformation will be plastic. Therefore, a M_r based on unloading will not include any plastic strain and will therefore allow stress analyses to be performed that apply once all plastic strain is complete. In this study, unloading modulus (i.e. E_{ul}) was adopted as an estimation of M_r to study the drainage effects. E_{ul} has been used in specifications or previous studies as an

indicator of resilient soil response (Deutscnes Institut fur Norrnung, 2001; Zhao et al., 2019). It is a sensible and widely used method. The loading, unloading and reloading paths are illustrated in Figure 6.5, and ε_{toal} indicates the total axial strain in one loading process.

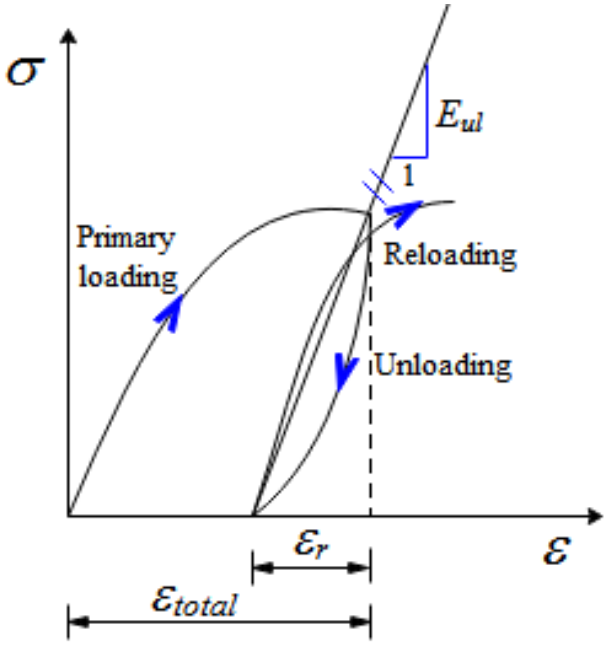

Figure 6.5 Illustration of loading, unloading and reloading paths

6.3 Test apparatus

In accordance with British Standard 1377 (British Standard Institution, 1990), consolidated undrained/drained (CU & CD) triaxial compression tests were conducted with saturated soil specimens. The GDS Saturated Triaxial Testing System was used to perform standard triaxial tests. It is capable of applying the desired stress states to the soil specimen, shearing specimens, and recording the soil response. It can be stress or displacement controlled to perform shearing. The system is illustrated in Figure 6.6 and Figure 6.7. Its primary components are listed in Table 6.2.

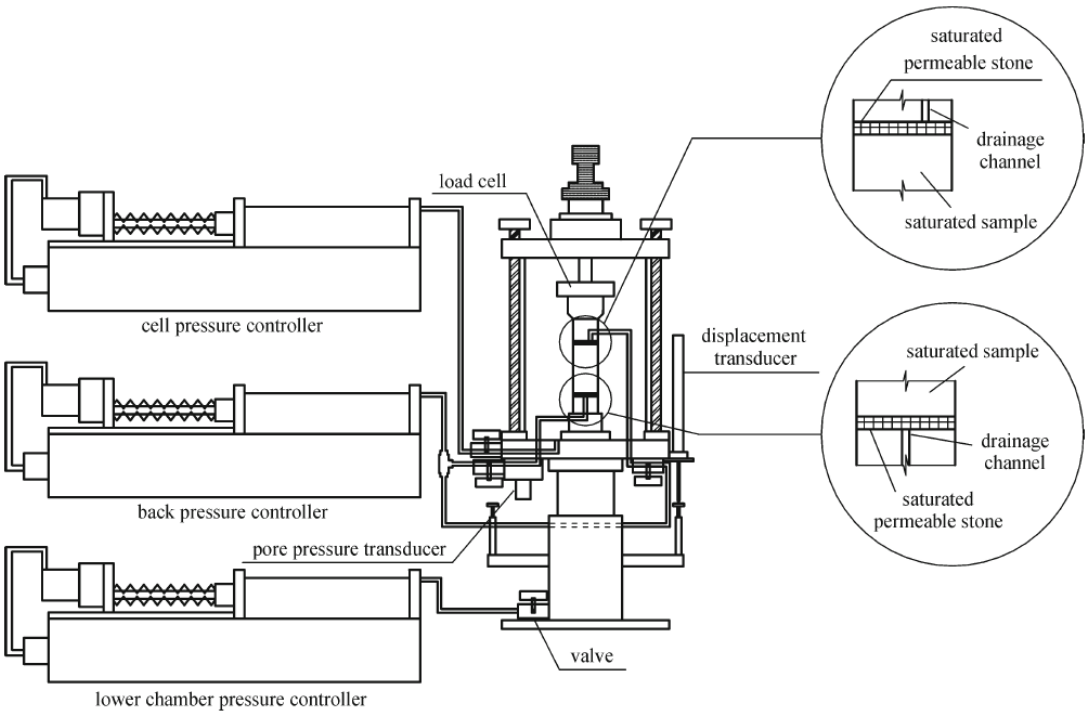

Figure 6.6 Schematic diagram of the saturated triaxial cell (Jiang et al., 2011)

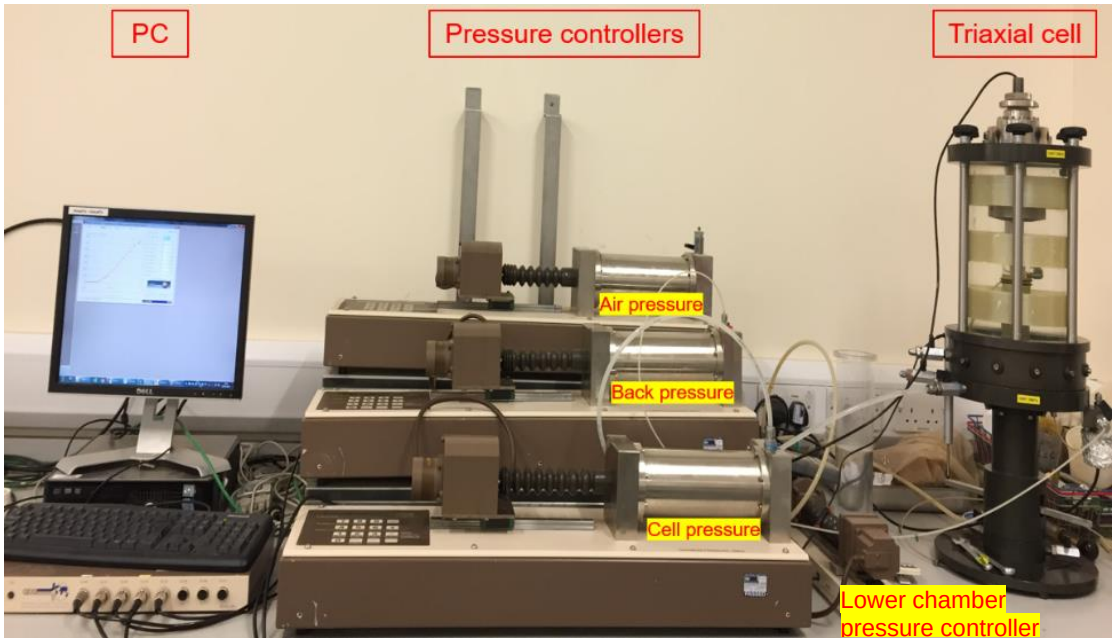

Figure 6.7 Photo of the saturated triaxial testing system

Table 6.1 Primary components of a saturated triaxial system (GDS Instruments)

Component	**Main function**
Triaxial cell	House the specimen and cell fluid.
Pedestal & top-cap	Provide specimen seating and drainage ports.
Rubber membrane, O-rings & porous discs	Seal the specimen from the cell fluid, allowing control over the effective stress and drainage.
Cell pressure / volume controller	Apply confining stress to the specimen by pressurising the cell fluid.
Back pressure / volume controller	Apply back/pore pressure to the specimen and measure volume change.
Air pressure / volume controller	Apply pore air pressure to the specimen and measure volume change.
Internal submersible load cell	Measure the change in axial load F applied to the specimen during shear.
Pore water pressure transducer	Measure the change in pore water pressure u within the specimen.
Axial displacement transducer	Measure the change in height (and hence axial strain) of the specimen.
Data acquisition unit	Convert analogue readings from the load cell, pore water pressure and axial displacement transducers to digital data.
GDSLab control & acquisition software	Control test hardware and record digital readings taken from the data acquisition unit.

6.4 Preparation of triaxial specimens

The basic properties of the test soil are presented in Chapter 5. The soil belonged to silty sand. Freshly de-aired water was mixed into the soil to achieve the target moisture content. The mixture was sealed into plastic bags to uniformly distribute the water. Using a split mould with a rubber membrane inside, the specimen was directly prepared on the pedestal.

In order to reduce the friction effects of platens and possible buckling of specimens, the platen and loading cap's side contacting each specimen end was lubricated by silicone grease but without blocking the pore/back pressure access routes. Considering the control of soil density (Frost & Park, 2003), wet compaction was utilized to prepare the specimens. In order to obtain as homogeneous a specimen as possible, the soil was compacted into five layers, and each layer having the same mass was compacted to the same height. The length to diameter ratio was selected as 2, and thus cylindrical specimens with a diameter of 38 mm and height of 76 mm were produced. At the end

of preparation, a bubble level was placed on the top of the sample to check that it was flat and horizontal. The disturbance to the specimen was kept to a minimum during preparation.

6.5 Test program

The tests aim to investigate the effects of drainage by reducing pore water pressure on the soil shear strength behaviour and the modulus through CD and CU tests. During the shearing stage, pore water pressure was not allowed to build up in CD tests. To achieve the equilibrium of pore water pressure inside the specimen, the displacement rate should be slow enough, i.e. 0.05 mm/min, based on the study of Maleki & Bayat (2012).

Operating at shallow depths, pavement materials are subject to low overlying pressure. Moving traffic load imposes (relatively) large transient and periodic normal and shear stresses and principal stress rotation (Blackmore et al., 2020). Shahu et al. (1999) suggested the use of typical confining pressures of 20, 40 and 100 kPa in railway subgrade testing, while in most pavement structures, it is expected that they can be lower than 35 kPa (Miller et al., 2000). Therefore, the initial effective confining pressures used in this study were selected as 25, 35, 65, 115 and 215 kPa to cover a wide range of stress states from low to high levels.

(1) Drainage control

Soil specimens were saturated using the back-pressure method. The applied back pressure was 500 kPa. Thus, the initial pore water pressure u_{w0} in the specimen was 500 kPa. For single-stage loading, pore water pressure was maintained as constant during shearing in CD tests but varied with shearing in CU tests. In contrast, for multistage loading, pore water pressure was allowed to decrease between stages so as to simulate drainage (see Figure 6.8). For multistage tests, there were five stages of loading-unloading. After reaching peak strength on the loading path, shearing was terminated. The unloading automatically started at the same strain rate as the loading path until the deviator stress was zero. Then, pore water pressure was reduced by (an arbitrary) 25 kPa to the next target pore water pressure by changing the back pressure. Drainage was achieved, and then the back pressure was closed. When the pore water pressure was sensibly constant, it was considered to reach equilibrium. After drainage equilibrium, a reloading path was initiated. In the last loading stage, shearing continued after the peak strength state at the same pore water pressure until reaching a critical

state. These different pore water pressure paths for CD tests, as an example, are illustrated in Figure 6.8. The tests incorporating the reduction of pore water pressure were distinct from the pure CU test. During the tests reported in this thesis, only the first loading-unloading cycle was the pure CU test. Then, manual reduction of pore water pressure was conducted by reducing the back pressure, and then reloading was performed. Thus, although consolidation was possible prior to the loading, the next loading stage itself was undrained.

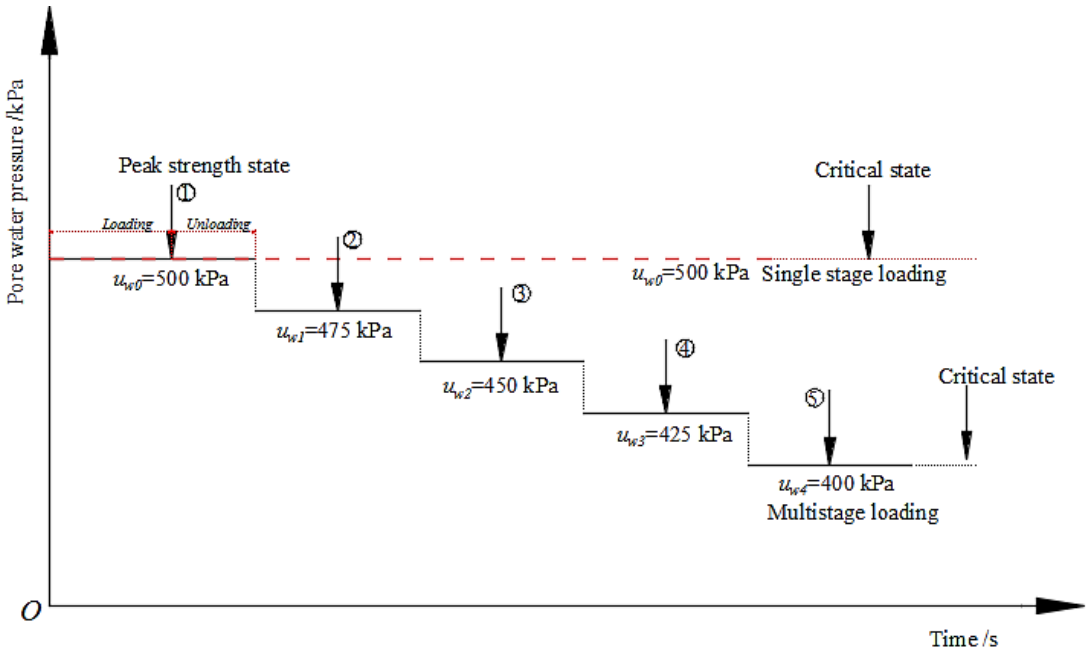

Figure 6.8 Pore water pressure control at single/multistage loading for CD tests

(2) Multistage loading

The tests are divided into two groups, i.e. single-stage loading (SSL) and multistage loading (MSL). SSL means applying the load until the critical state of the soil is reached. MSL (as can be seen from Figure 6.9) means applying the load up to the peak strength of the specimen; afterwards, unloading is conducted until the deviator stress reaches zero; pore water pressure is reduced stepwise to target pore water pressure in order to simulate drainage; after drainage equilibrium, reloading starts; after five stages of reducing pore water pressure, the specimen is sheared until reaching its critical state. Through the MSL procedure, a maximum amount of information can be obtained from a limited number of tests. The effect of variability in the soil can also be avoided from one test to the next (Ho & Fredlund, 1982). By releasing the deviator stress (i.e. unloading), it can prevent creep development in the specimen. It should be noted that the specimen should not be deformed excessively at the early stage beyond its peak strength. From the study by Ho & Fredlund (1982), multistage loading could disturb

the specimen in later stages and thus induce strength and stiffness loss, but it should still give a conservative estimate of the strength and stiffness.

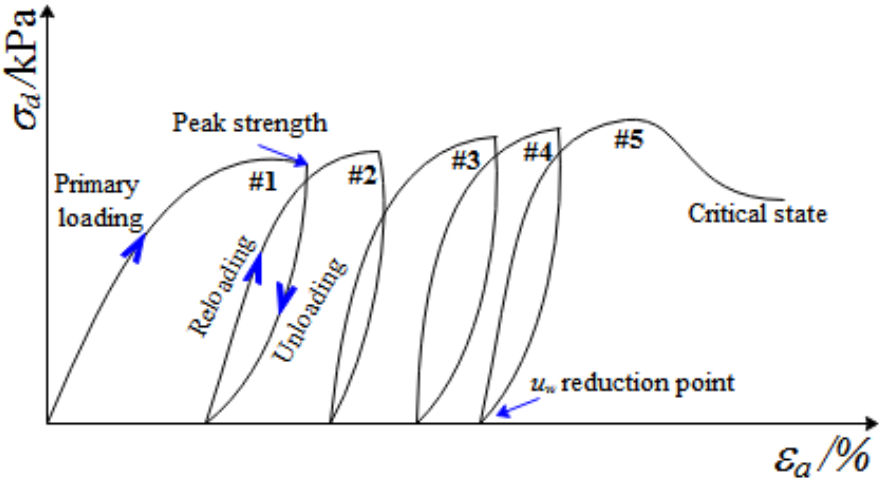

Figure 6.9 Ideal stress-strain curve for a multistage test (Ho & Fredlund, 1982)

(3) Test nomenclature

Regarding the test nomenclature, e.g. 'CD-SSL-25' and 'CD-MSL-25', 'CD' means consolidated drained test, 'SSL' and 'MSL' denote single and multi-stage loading, respectively, and '25' is the initial effective confining stress in kPa. σ_c is confining pressure, σ_c' is effective confining pressure, u_b is back pressure and u_w is pore water pressure.

6.6 Saturated CU SSL triaxial test

6.6.1 Test procedure

For consolidated undrained saturated triaxial tests (CU-SSL), several stages were involved, including flushing, saturation, consolidation and shearing. After placing and sealing the specimen inside the triaxial chamber, the specimen was measured for diameter and height. The specimen was flushed from the bottom with freshly de-aired water for at least four h. During this, a low vacuum (about 5 kPa) was applied to the top for five cycles to effectively remove the air due to back pressure, and each cycle lasted no more than five minutes to avoid undesired increases in the effective consolidation pressure (Lade, 2016). The back-pressure method was adopted to saturate the soil specimen prior to the tests, and when a pore pressure coefficient (i.e. B-value, $B = \frac{\Delta u_w}{\Delta \sigma_c}$) exceeding 0.95 (British Standard Institution, 1990) was measured, the specimen was considered under saturation. This soil was very dense, which belonged to 'very stiff' category. In this case, a B value above 0.95 ensures the soil is saturated.

Following the flushing procedure, the cell pressure and saturation back pressure were simultaneously and gradually increased. At high back pressure and cell pressure, accidental swelling and consolidation of soil specimens may be generated, respectively. Therefore, a difference between cell pressure and back pressure was maintained at 10 kPa to avoid any disturbance to specimens. At the end of the saturation process, the soil specimens were consolidated at an effective confining pressure. Then, the saturated specimens were sheared at a constant loading velocity of 0.05 mm/min for CU triaxial tests, at which the value of strain rate will allow to achieve uniformity of pore water pressures in the specimens. Shear failure tests were conducted under single-stage loading. The initial conditions of the tests are listed in Table 6.2.

Table 6.2 Initial conditions of saturated CU-SSL tests

Tests	σ_c /kPa	u_w /kPa	$\sigma_c^{'}$ /kPa
CU-SSL-25	525	500	25
CU-SSL-35	535	500	35
CU-SSL-65	565	500	65
CU-SSL-115	615	500	115
CU-SSL-215	715	500	215

6.6.2 Test results

(1) Shearing behaviour

The stress-strain behaviour is presented in Figure 6.10 and Figure 6.11. As expected, at higher effective confining pressure, deviator stress showed a larger value. The shear strength parameters, ϕ' and c', were 39° and 54 kPa, respectively. Local suction or particle interlock in the specimen during shearing may also increase the shear strength. The deviator stress and principal effective stress ratio (ESR) (σ_1'/σ_3', shown in Figure 6.11) both increased and then decreased with axial strain. ESR ranged from 4.5 to 5.3. After shear failure, the specimens gradually approached the critical state. Particularly, the specimen at an effective confining pressure of 65 kPa appears to have achieved a critical state with constant deviator stress. When the axial strain reached 30%, the specimens reached the limit of the loading system.

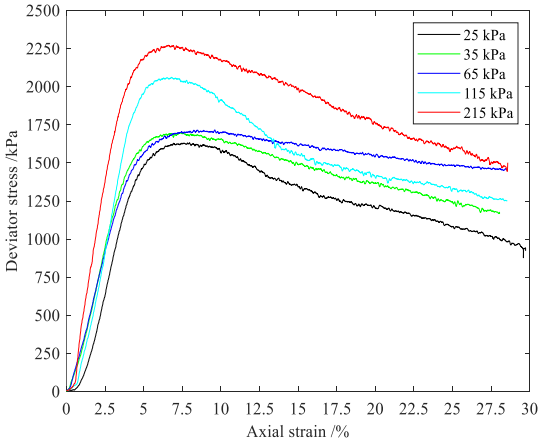

Figure 6.10 $q-\varepsilon_a$ curve of CU-SSL

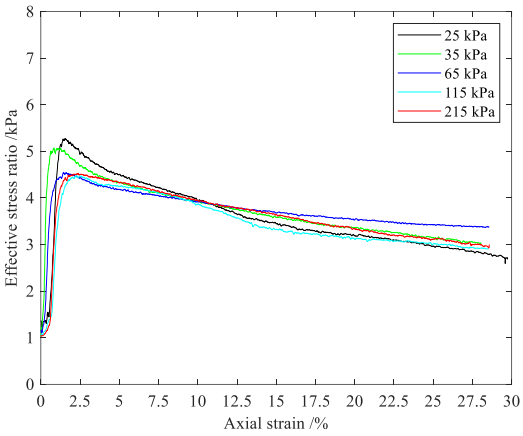

Figure 6.11 ESR$-\varepsilon_a$ curve of CU-SSL

The $q-p'$ curves are presented in Figure 6.12. The stress paths converged to a special path. The compacted soils in this study were also subject to consolidation before shearing to achieve the specific effective normal stress. Thus, the soil behaviour can be interpreted within the framework developed for overconsolidated soils (Özkul & Baykal, 2007). In the undrained tests, the stress paths all lay on an undrained plane (with constant specific volume). These paths initiated underneath the Hvorslev surface (the state boundary surface), ascended almost vertically to the surface and then moved along the surface until the critical state was reached (Barnes, 1995). Generally, the deviator stress of all specimens reached a unique path before failure and then significantly diverged due to the strain softening (Figure 6.12).

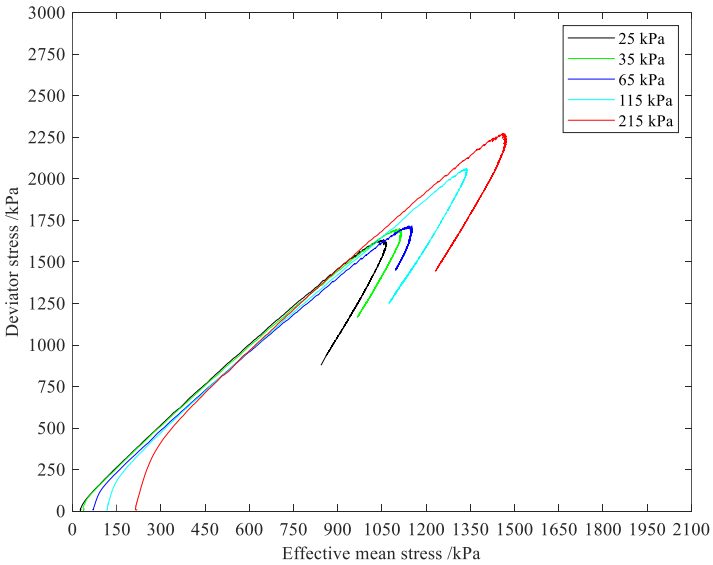

Figure 6.12 $q-p'$ curves for CU-SSL test results

(2) Pore water pressure

Excess pore water pressure slightly increased and then decreased as shearing proceeded, as shown in Figure 6.13. In the initial shearing stage, the pore water pressure

showed a slight build-up. After the shear failure beyond a certain level, excess pore water pressure reached a constant state, apart from that under 35 kPa, which initially reached a stable state and then showed a slight increase. At higher confining pressure, the build-up was larger, while the pore water pressure after failure showed a downward trend. The pore water pressure was positive and then became negative at larger axial strains. The overconsolidated soil would have dilated in a drained test since excess pore water pressure showed a negative change from -20 to -50 kPa. It may be explained by the dilation trend and the potential microstructural changes, such as the opening of local closed pores, which is beyond the scope of this study.

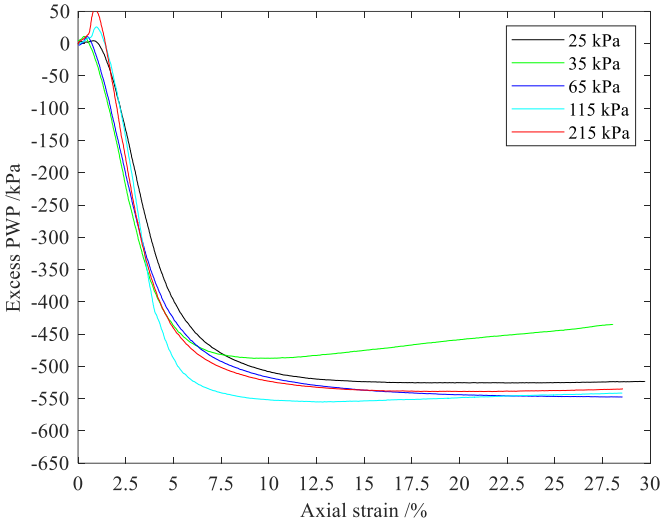

Figure 6.13 Excess pore water pressure variation with ε_a for CU-SSL tests

6.7 Saturated CU MSL triaxial test

6.7.1 Test procedure

Following saturation and consolidation stages (as mentioned in Section 6.6.1), multistage shearing was conducted. Multistage loading followed the procedure listed in Section 6.5. Based on multistage tests, maximum information could be gained from a single specimen. The initial conditions are listed in Table 6.3.

Table 6.3 Initial conditions of saturated CU-MSL tests

Tests	σ_c /kPa	u_w /kPa	σ_c' /kPa
CU-MSL-25	525	500	25
CU-MSL-35	535	500	35
CU-MSL-65	565	500	65
CU-MSL-115	615	500	115
CU-MSL-215	715	500	215

6.7.2 Test results

(1) Shear strength behaviour

The $q - \varepsilon_a$ relationships are presented in Figure 6.14~Figure 6.18. With increased effective stress - as might be achieved by site drainage, the shear strength slightly but gradually increased, and the peak deviator stress values q_f are presented in Figure 6.19. The peaks were also marked with different moisture conditions (potential drainage conditions in actual structures), i.e. D0 (the initial loading cycle without drainage), D1 (the first drainage stage with pore water pressure decreasing by 25 kPa), D2 (the second drainage stage with pore water pressure decreasing by 25 kPa), D3 (the third drainage stage with pore water pressure decreasing by 25 kPa) and D4 (the fourth drainage stage with pore water pressure decreasing by 25 kPa). At higher axial strain, all the specimens reached (or were close to) critical states. The unloading modulus showed an upward trend with the reduction of pore water pressure (drainage), as shown in Figure 6.20.

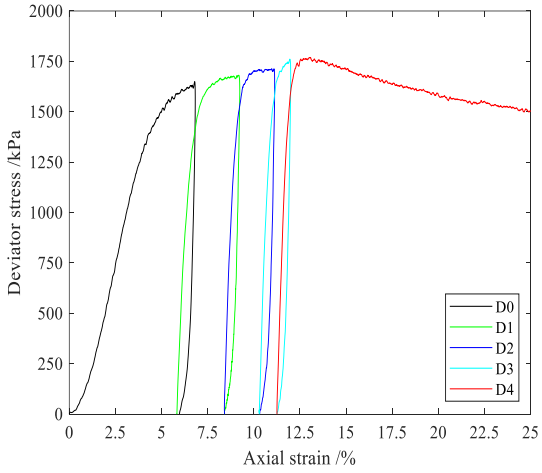

Figure 6.14 $q - \varepsilon_a$ of CU-MSL-25

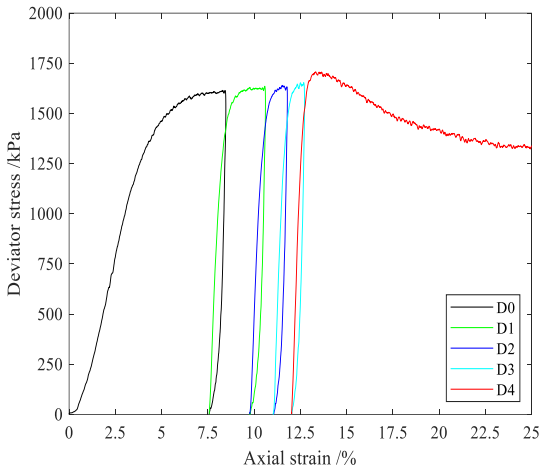

Figure 6.15 $q - \varepsilon_a$ of CU-MSL-35

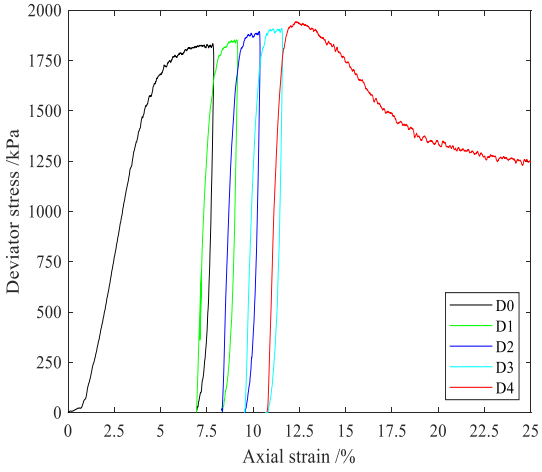

Figure 6.16 $q - \varepsilon_a$ of CU-MSL-65

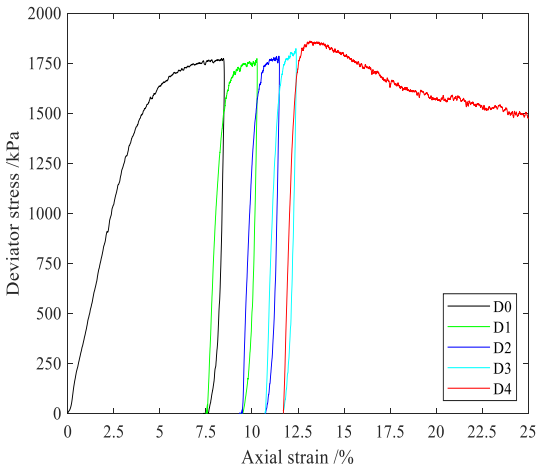

Figure 6.17 $q - \varepsilon_a$ of CU-MSL-115

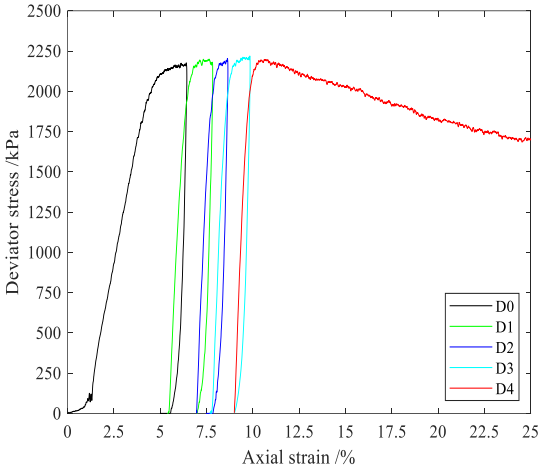

Figure 6.18 $q-\varepsilon_a$ of CU-MSL-215

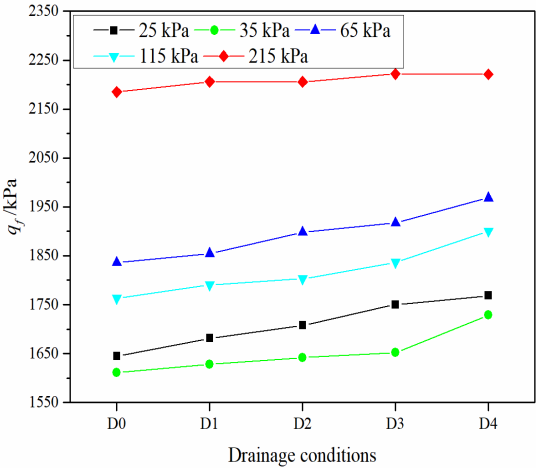

Figure 6.19 q_f changes of CU-MSL with drainage between loading stages

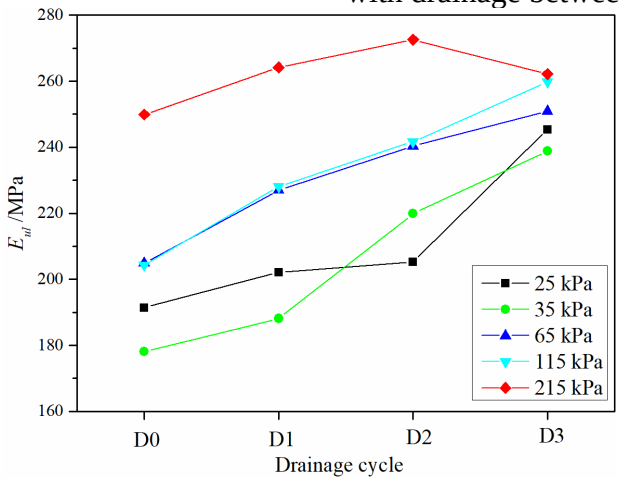

Figure 6.20 Unloading modulus E_{ul} of CU-MSL at each drainage cycle

From Figure 6.21~Figure 6.25, ESR in the first cycle slightly decreased with the effective confining pressure while showing an upward trend with drainage. After the reduction of pore water pressure by 100 kPa in the four stages at a step of -25 kPa, ESR was approximately constant, i.e. the critical state. At the critical state, ESR increased due to the reduction of pore water pressure, compared with that in CU-SSL tests.

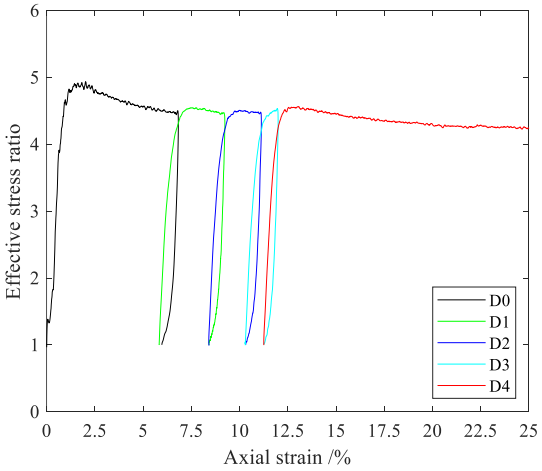

Figure 6.21 ESR$-\varepsilon_a$ of CU-MSL-25

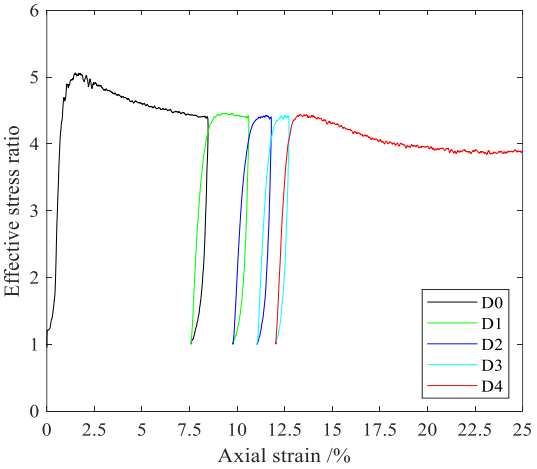

Figure 6.22 ESR$-\varepsilon_a$ of CU-MSL-35

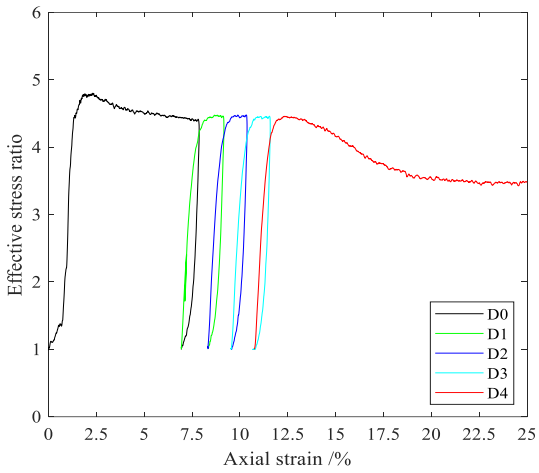

Figure 6.23 ESR$-\varepsilon_a$ of CU-MSL-65

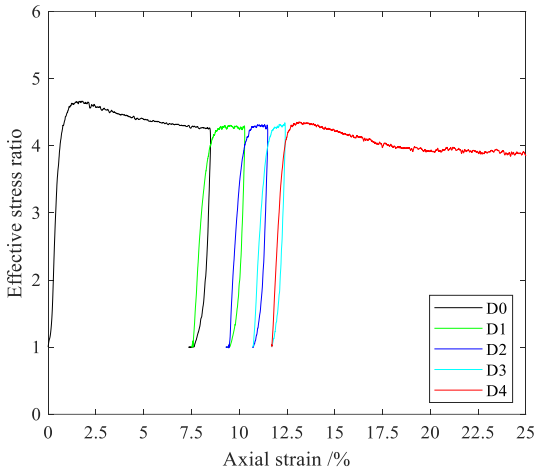

Figure 6.24 ESR$-\varepsilon_a$ of CU-MSL-115

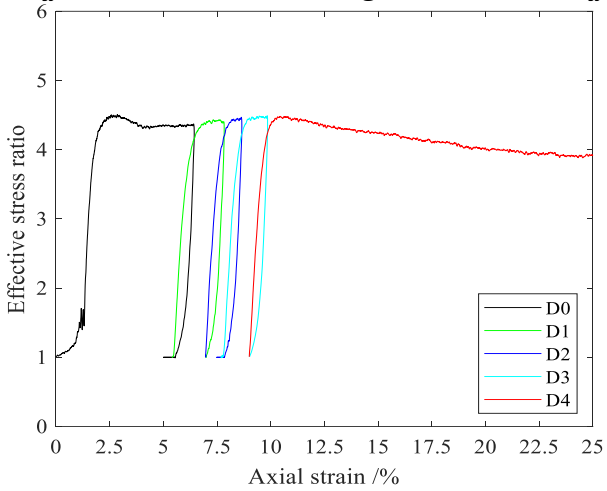

Figure 6.25 ESR$-\varepsilon_a$ of CU-MSL-215

Figure 6.26~Figure 6.30 illustrate the effective stress path of each specimen. It shows that at each σ_c', the deviator stress at failure q_f converged to a unique line. The stress paths all lay on an undrained plane (with constant specific volume). These paths initiated underneath the Hvorslev surface (the state boundary surface), ascended almost vertically to the surface and then moved along the surface until the critical state was reached (Barnes, 1995). To simplify test results and avoid curve overlay, only the first loading-unloading cycle (D0) and the last loading stage (D4) were plotted. With cyclic loading and drainage, the slope of the $q - p'$ loading (or reloading) path showed a clear increase. The initial loading path of each test is very similar to that seen in the single-stage tests (Figure 6.12). The effect of repeated loading - the progressive move rightwards of the reloading stress paths with subsequent load cycles - is evident, but it is noticed that as σ_c' increased, the permanent deformation between cycles reduced so that the primary unloading path was closer to, or even in the same position as, subsequent reloading paths.

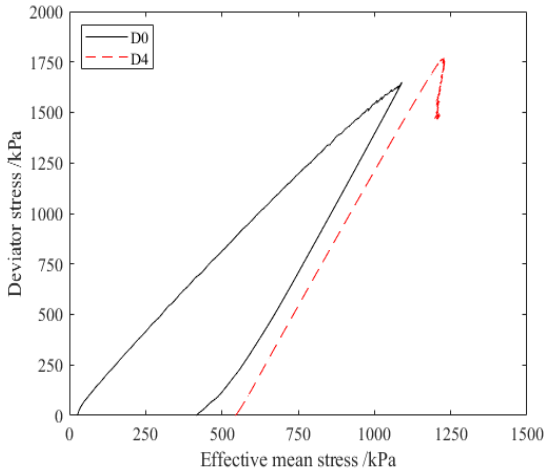

Figure 6.26 $q - p'$ of CU-MSL-25

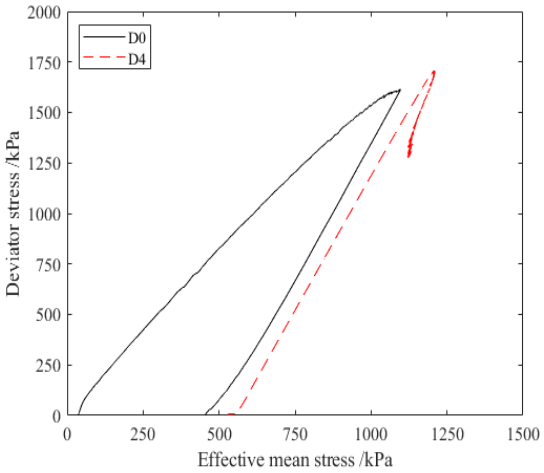

Figure 6.27 $q - p'$ of CU-MSL-35

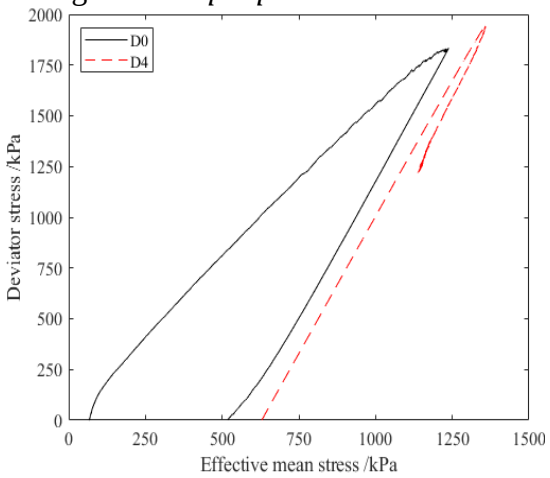

Figure 6.28 $q - p'$ of CU-MSL-65

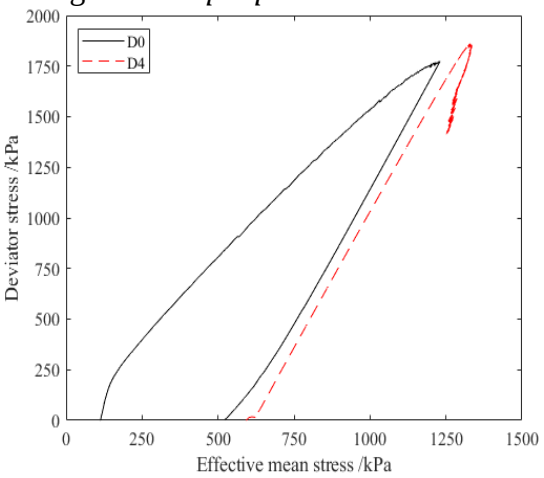

Figure 6.29 $q - p'$ of CU-MSL-115

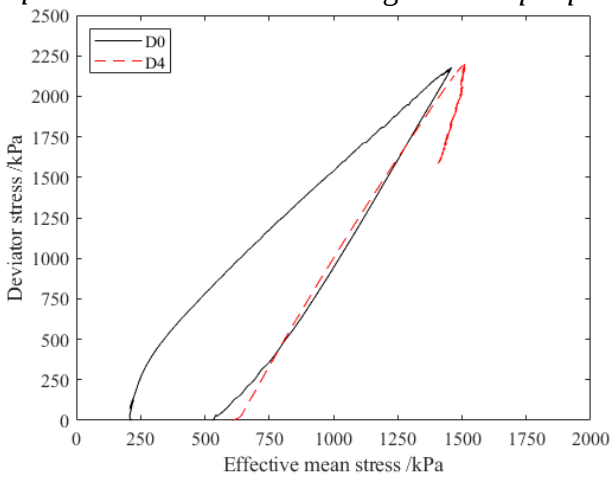

Figure 6.30 $q - p'$ of CU-MSL-215

Figure 6.31~Figure 6.35 illustrate the variation of excess pore water pressure during shearing. The excess was relative to the 500 kPa. During the equilibration stages in CU tests, the u_w rose but not to the original (i.e. zero). In CU tests, u_w reduced due to shear, so u_w was not able to rise back to the original level. During the equilibration, the back-pressure valve was closed. Thus, there was no pressure supply from the platens. The discontinuous points showed the stage from loading to unloading or from

unloading to reloading. Excess pore water pressure decreased with shearing and increased in the unloading stage. It showed the largest increase at the first unloading, and the increase was reduced over the following unloading stages. The similar final u_w indicates that the tendancy to dilate may limit the reduction, i.e. no further reduction occurred at different confining pressure.

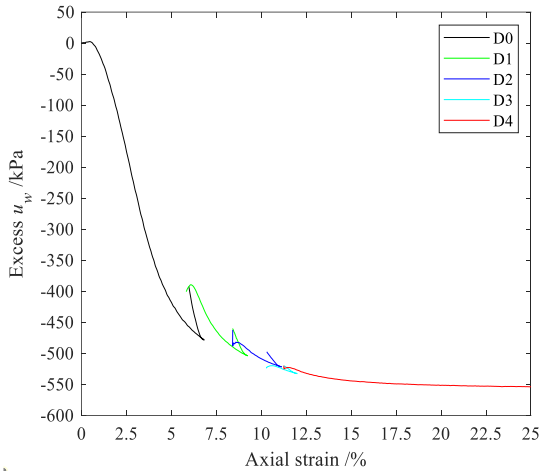

Figure 6.31 Excess u_w of CU-MSL-25

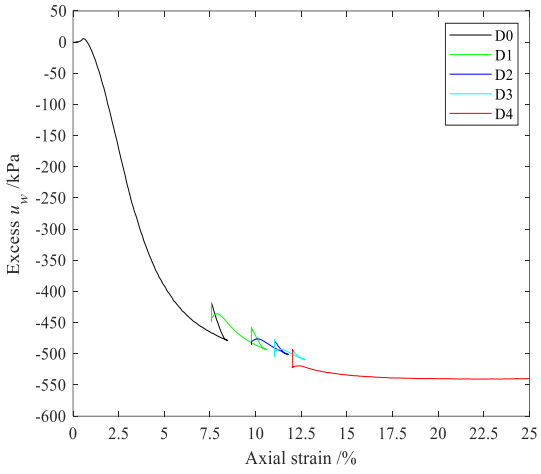

Figure 6.32 Excess u_w of CU-MSL-35

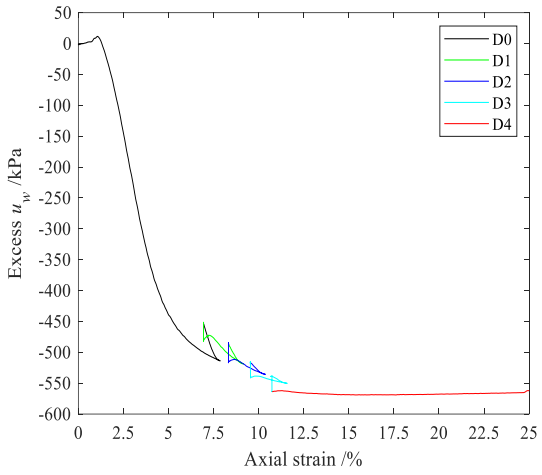

Figure 6.33 Excess u_w of CU-MSL-65

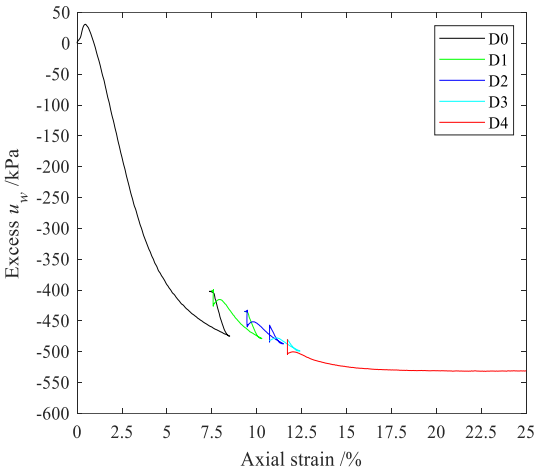

Figure 6.34 Excess u_w of CU-MSL-115

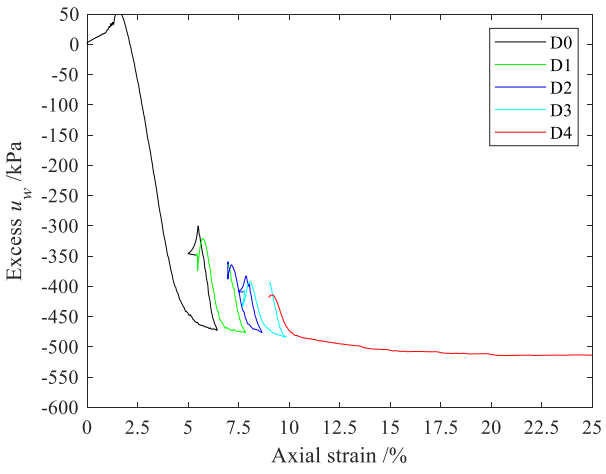

Figure 6.35 Excess u_w of CU-MSL-215

6.8 Saturated CD SSL triaxial test

6.8.1 Test procedure

After saturation and consolidation (as described in Section 6.6.1), shear failure was performed with the drainage line open to maintain a constant pore water pressure, and the critical state was reached. The initial conditions are listed in Table 6.4.

Table 6.4 Initial conditions of saturated CD-SSL tests

Tests	σ_c /kPa	u_w /kPa	$\sigma_c^{'}$ /kPa
CD-SSL-25	525	500	25
CD-SSL-35	535	500	35
CD-SSL-65	565	500	65
CD-SSL-115	615	500	115
CD-SSL-215	715	500	215

6.8.2 Test results

Figure 6.36 illustrates the stress-strain behaviour during CD-SSL tests. At the end of shearing, all the specimens reached the critical state within an axial strain of 25%. Peak and critical state shear strength increased with σ_c'. The specimens at lower σ_c' (i.e. 25 kPa, 35 kPa and 65 kPa) also achieved peak shear strength at a smaller ε_a than those under a higher σ_c' (i.e. 115 kPa and 215 kPa). In terms of ESR shown in Figure 6.37, it also became constant as shear failure developed. At higher σ_c', ESR was smaller at the peak and critical states. From Figure 6.38, the volumetric strain slightly decreased and then increased. This indicates that the specimen experienced contraction at the initial stage and then gradually dilated. The volume change showed a trend to be constant. Generally, volumetric strain decreased as σ_c' increased. This behaviour indicate that the tested soil belongs to the overconsolidated soil. For SSL tests, at higher σ_c', the specimen exhibited smaller volumetric strain, i.e. less dilation. Specimens at higher $\sigma_c^{'}$ were subject to more contraction when reaching the critical state. The dense soils showed much higher shear strength in CD tests than those in CU tests, based on Figure 6.37. These specimens generally followed the typical stress path, as shown in Figure 6.39.

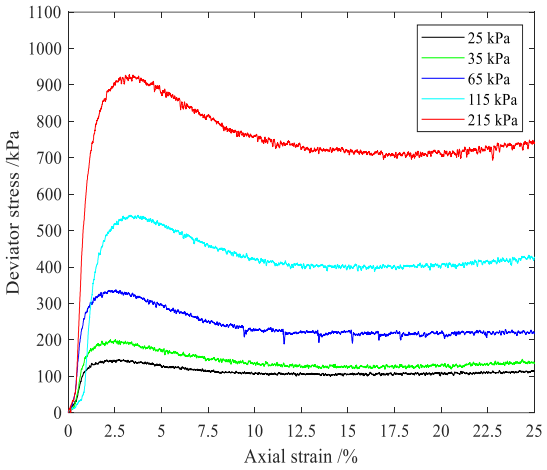

Figure 6.36 $q-\varepsilon_a$ of CD-SSL at different initial σ_c'

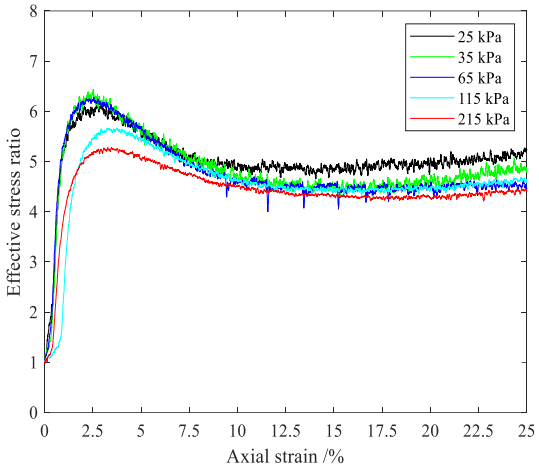

Figure 6.37 ESR$-\varepsilon_a$ of CD-SSL at different initial σ_c'

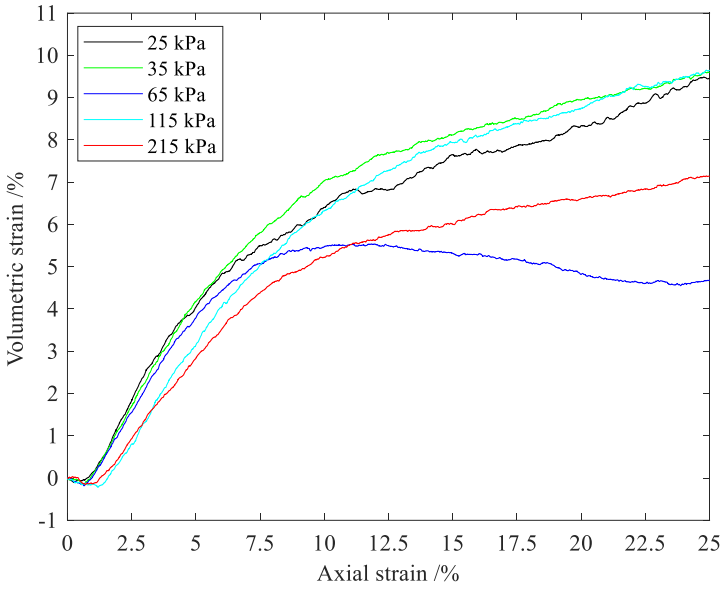

Figure 6.38 $\varepsilon_v-\varepsilon_a$ of CD-SSL at different $\sigma_c^{'}$

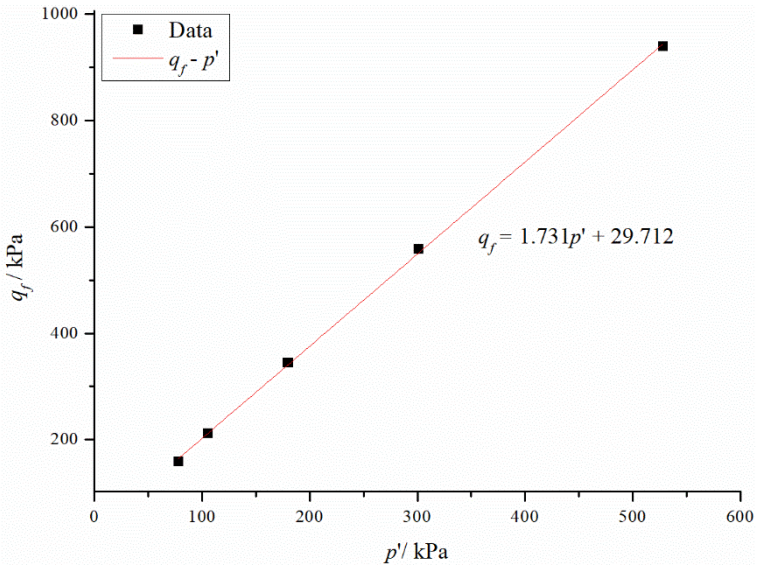

Figure 6.39 Stress path of CD-SSL tests

6.9 Saturated CD MSL triaxial test

6.9.1 Test procedure

The saturation and consolidation stages were, again, as mentioned in Section 6.6.1. Regarding the procedure, only the drainage line for CD-MSL triaxial tests was arranged differently from that for CU-MSL triaxial tests in that it was kept open during shearing at each stage, permitting drainage (in or out) of pore water. After each cycle, the state of the specimen was maintained for 12 hours. When no volume changes were detected in the back pressure controller and pore water pressure reached a constant, it was considered to be at equilibrium. The initial conditions are presented in Table 6.5.

Table 6.5 Initial conditions of saturated CD-MSL tests

Tests	σ_c /kPa	u_w /kPa	$\sigma_c^{'}$ /kPa
CD-MSL-25	525	500	25
CD-MSL-35	535	500	35
CD-MSL-65	565	500	65
CD-MSL-115	615	500	115
CD-MSL-215	715	500	215

6.9.2 Test results

(1) Shear strength behaviour

Following the consolidation stage, the shearing stage starts with compression. For multistage loading tests, the specimens are sheared after drainage equilibrium following the unloading path. Figure 6.40~Figure 6.44 show the variation of deviator stress with axial strain during the shearing stage for multistage loading tests. With the arbitrary drainage between loading stages, the shear strength of all the specimens increased. At the same σ_c', the peak and critical state shear strength in the MSL tests showed significant increases with drainage between loading stages, as shown in Figure 6.45 and Figure 6.46. The unloading modulus in Figure 6.47 increased substantially with σ_c' and showed the largest increases at 25 kPa and 35 kPa. The unloading modulus was employed as an estimation of resilient modulus of the subgrade for analysis of pavement/rail structures. At the same level of drainage, specimens at the σ_c' of 25 kPa showed the largest percentage increase in shear strength and unloading modulus. It may indicate that the drainage could have more effects on the soil at shallower depths in terms of strength.

Based on the Mohr-Coulomb failure criterion, the Mohr circles and the failure envelopes were plotted to obtain the peak strength parameters. With drainage between loading stages, the cohesion intercept showed an increasing trend, while the friction angle (ϕ') exhibited a slight change (Figure 6.48). Even though the silty sand exhibited low plasticity, the interlock between the particles was strengthened with drainage, which was reflected in some apparent cohesion. The cohesion was larger at a larger $\sigma_c^{'}$, while the friction angle showed a slight decrease. The obtained peak ϕ' of silty sand in the thesis was 41°. The Fraction C sand has a critical ϕ' of 31°(Stringer & Madabhushi, 2013). It should be noted that the silty sand in the thesis was different from the pure Fraction C sand and also compacted to reach maximum dry density for testing. The peak ϕ' of mixed soils also increases with fines content due to the increase of both of the critical state ϕ' (Salgado et al., 2000). Typical ϕ' of compacted sand-silt-clay mixtures could reach 40° (Geotechdata.info, 2013). The obtained ϕ' in the thesis could be slightly higher, whilst the value was considered reasonable.

The peak and critical state ESR (i.e. the ratio of maximum principal stress to minimum principal stress) decreased with the increase of σ_c' (Figure 6.49). The figures also show that drainage had few effects on the ESR, except that the specimens at σ_c' of 25 and 35 kPa showed a decrease in the peak ESR. Generally, at large axial strain where constant volume was achieved (see Figure 6.21~Figure 6.25 and Figure 6.49), ESR values were largely independent of σ_c' or drainage. This appears to indicate that the critical shear stress is now only a function of the inter-grain frictional characteristics and that the grain packing is not constrained by the effective confining pressures. Figure 6.50~Figure 6.54 present the effective stress paths at initial σ_c'. The slope of the failure envelope showed a decreasing trend from 1.68 to 1.54 with the increase of initial σ_c'.

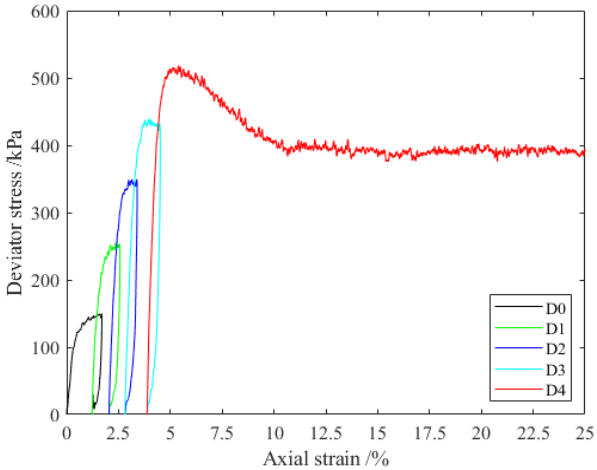

Figure 6.40 $q - \varepsilon_a$ of CD-MSL-25

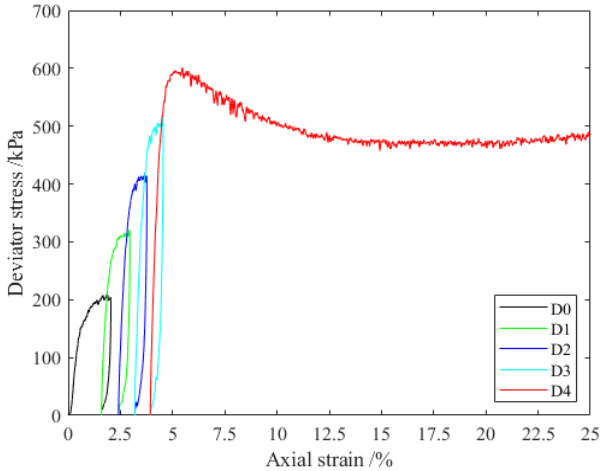

Figure 6.41 $q - \varepsilon_a$ of CD-MSL-35

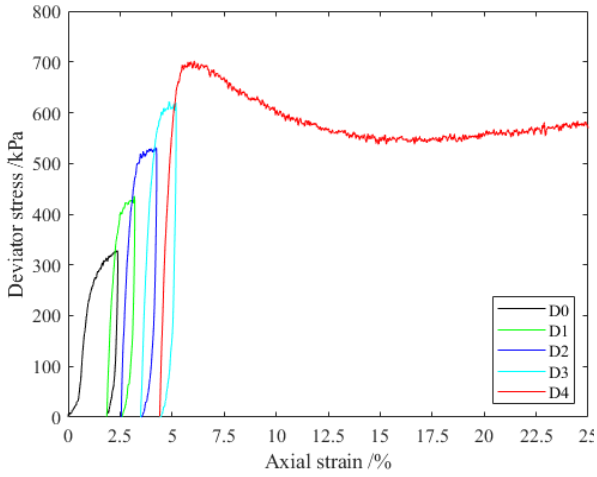

Figure 6.42 $q-\varepsilon_a$ of CD-MSL-65

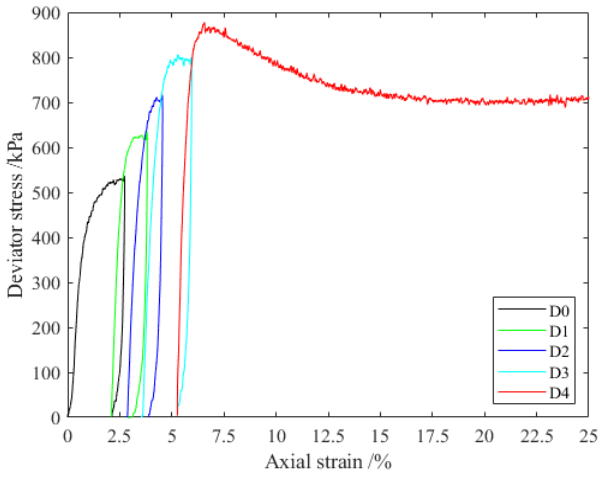

Figure 6.43 $q-\varepsilon_a$ of CD-MSL-115

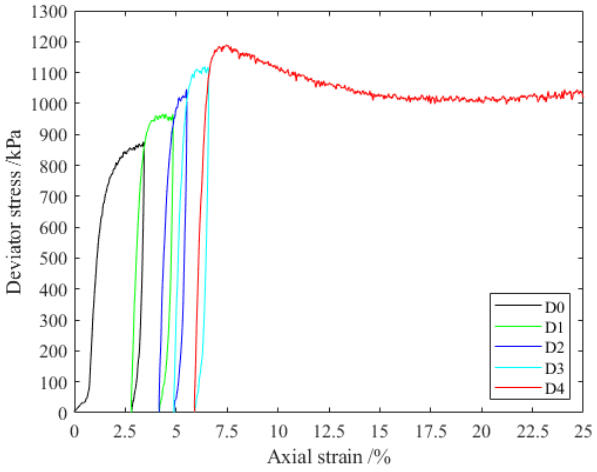

Figure 6.44 $q-\varepsilon_a$ of CD-MSL-215

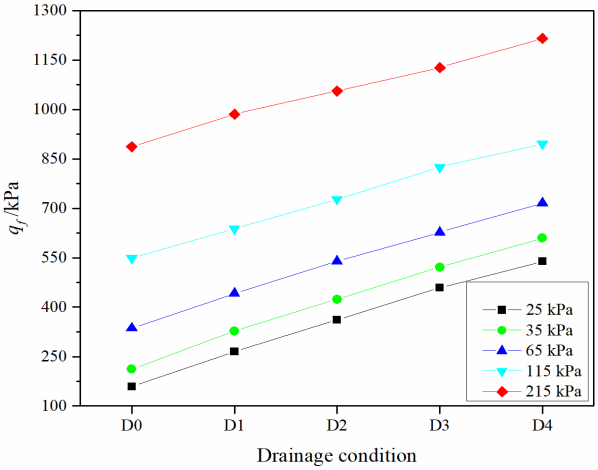

Figure 6.45 q_f variation of CD-MSL with drainage at different initial σ_c'

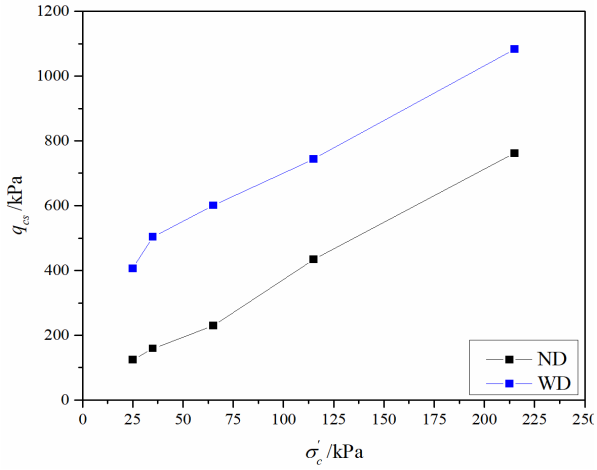

Figure 6.46 q_{cs} variation of CD-MSL at different initial σ_c'

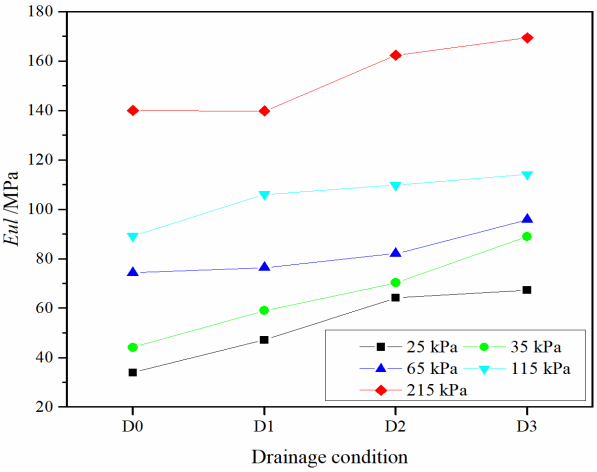

Figure 6.47 E_{ul} of CD-MSL at different initial σ_c'

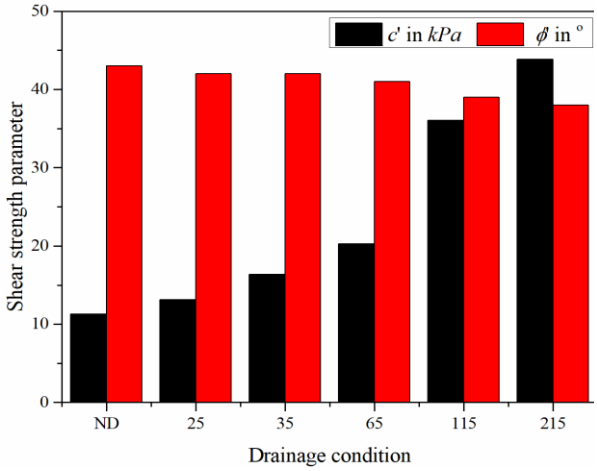

Figure 6.48 c' and ϕ'variation of CD-MSL with drainage

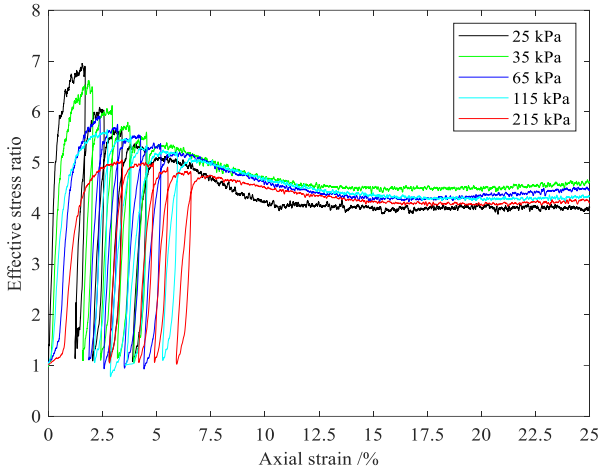

Figure 6.49 ESR$-\varepsilon_a$ of CD-MSL at different initial σ_c'

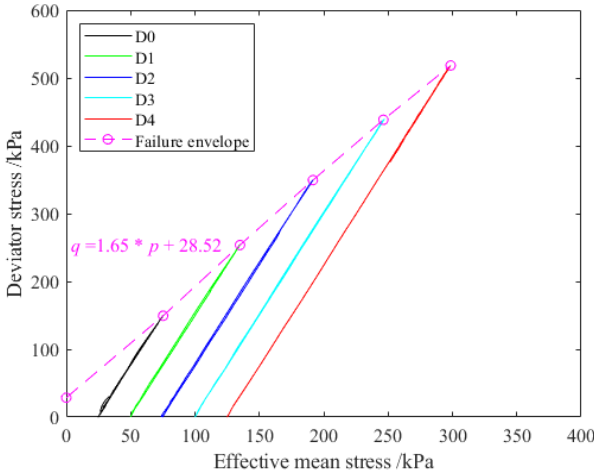

Figure 6.50 $q - p'$ of CD-MSL-25

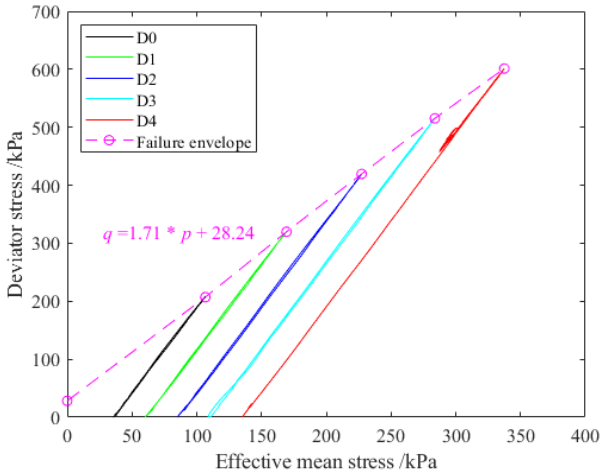

Figure 6.51 $q - p'$ of CD-MSL-35

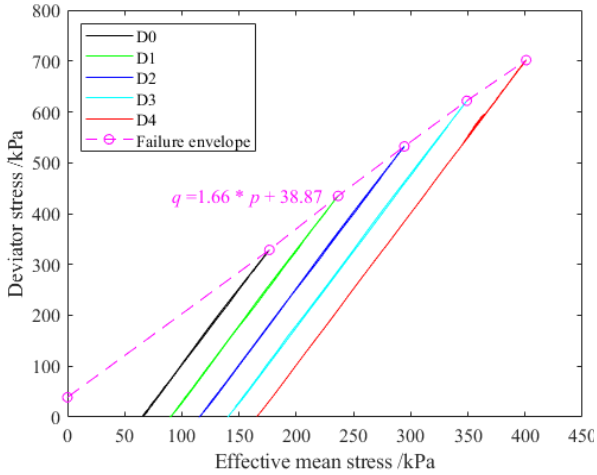

Figure 6.52 $q - p'$ of CD-MSL-65

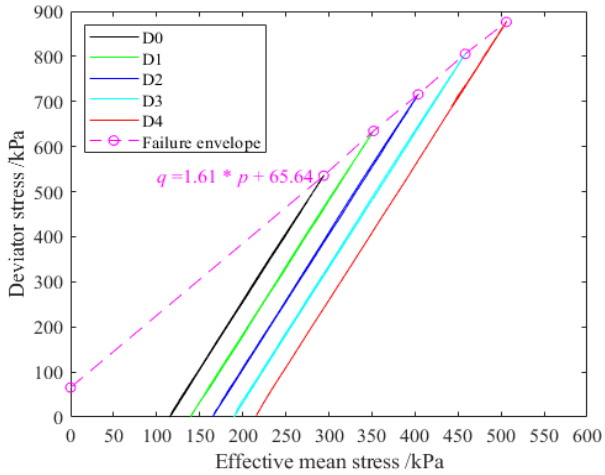

Figure 6.53 $q - p'$ of CD-MSL-115

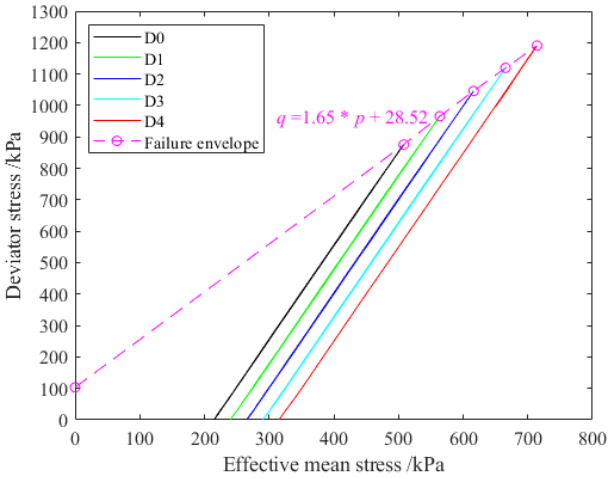

Figure 6.54 $q - p'$ of CD-MSL-215

(2) Volumetric behaviour

The variation of volumetric strain with axial strain during shearing is presented in Figure 6.55~Figure 6.59 for the MSL tests. The specimens exhibited a slight contraction as shearing started. Then, dilation started in all specimens as shearing continued. It is demonstrated that the rate of reduction in volume decreased with strain. ε_v reached a constant in SSL tests, and was most likely developing towards a constant value in the MSL tests (i.e. critical state) as expected. For CD-MSL tests, after drainage, the volume of all the specimens was similar – about 5-6% less than initial – which was a smaller decrease compared to those without arranged drainage for CD-SSL tests (Generally 7-10% except for that of CD-SSL-65 around 4.5%). This may be attributed to the improved strength of soil due to drainage. Through drainage, the enhanced effective stress may be reduced, and the effective stress will have been enhanced, the effect of which can be seen from the increasing cohesion intercept in Figure 6.48.

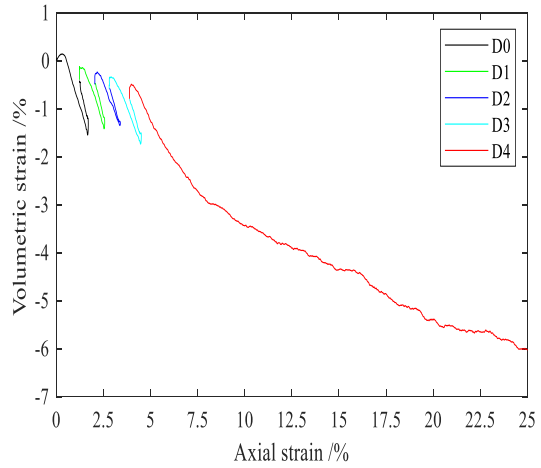

Figure 6.55 $\varepsilon_v - \varepsilon_a$ of CD-MSL-25

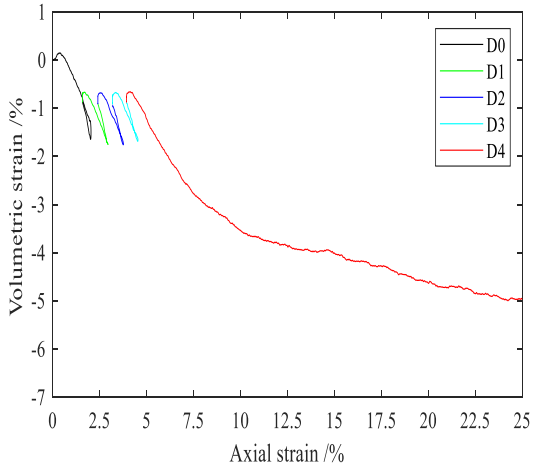

Figure 6.56 $\varepsilon_v - \varepsilon_a$ of CD-MSL-35

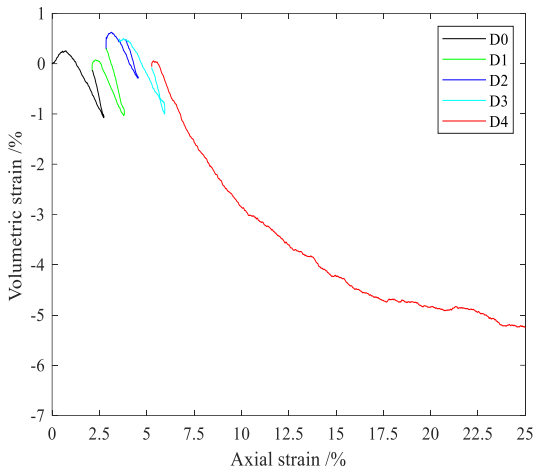

Figure 6.57 $\varepsilon_v - \varepsilon_a$ of CD-MSL-65

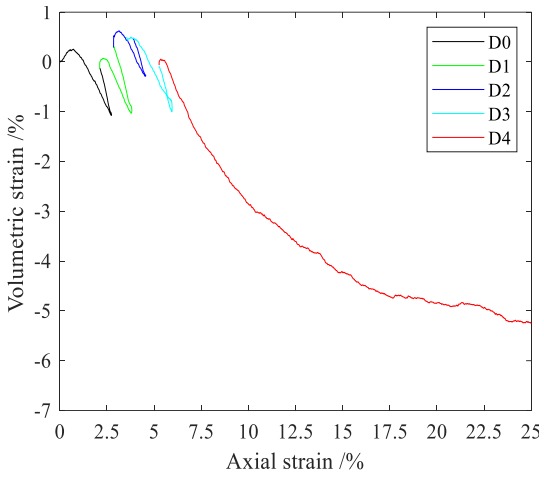

Figure 6.58 $\varepsilon_v - \varepsilon_a$ of CD-MSL-115

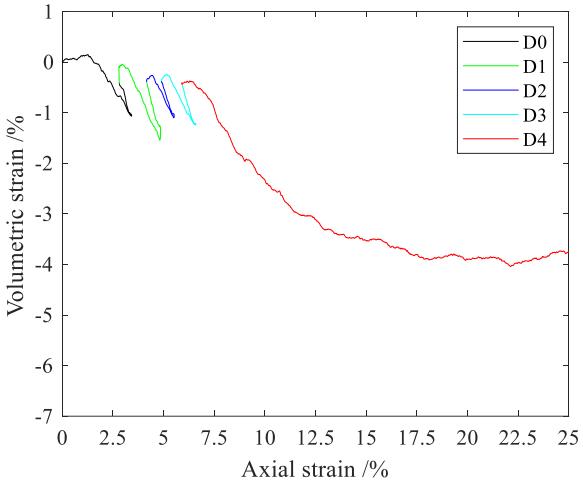

Figure 6.59 $\varepsilon_v - \varepsilon_a$ of CD-MSL-215

6.9.3 Comparison of CU-MSL and CD-MSL tests

The drainage effects on soil response were compared between CU-MSL and CD-MSL tests in relative changes in the shear strength and unloading modulus to the primary loading-unloading path. The relative changes in the peak shear strength (q_f) to the initial peak shear strength are presented in Figure 6.61. Generally, due to the arbitrary drainage between loading stages (reducing pore water pressure), CD-MSL showed a much higher percentage increase in q_f, compared to CU-MSL, i.e. the benefit of relatively small amounts of drainage (25 kPa each step) is evident in increasing soil strength. q_f showed a consistent trend with the defined drainage stages and followed the Mohr-Coulomb failure criterion (Eq. (2.5)). To further validate the test results, in terms of CD-MSL, the relative changes in q_f can be predicted. The prediction process was demonstrated as follows. CD-MSL-25 was taken as an example for analysis. From

D0 to D4, initial σ_c' increased from 25 kPa (σ_c' at D0) to 125 kPa (σ_c' at D4). The increase in q_f in CD-MSL-25 from D0 to D4 was $\left(q_f \text{ at D4} - q_f \text{ at D0}\right)$, i.e., $(\sigma_c' \text{ at D4} - \sigma_c' \text{ at D0})\left(\tan^2\left(45^o + \frac{\phi'}{2}\right) - 1\right)$ according to Eqs. (6.5) and (6.6). Thus, the relative change of q_f to q_f at D0 was $\frac{(\sigma_c' \text{ at D4} - \sigma_c' \text{ at D0})\left(\tan^2\left(45^o + \frac{\phi'}{2}\right) - 1\right)}{q_f \text{ at D0}}$, where ϕ'=41° (Figure 6.48). Finally, the relative change of q_f in CD-MSL-25 from D0 to D4 was calculated as 2.3, which was slightly lower than the measured value (about 2.5) in Figure 6.60. This indicates the consistency between the measurements and theory. It should be noted that, in theory, for purely frictional materials, the relative changes in q_f would always be in proportion to effective confining pressure (σ_c').

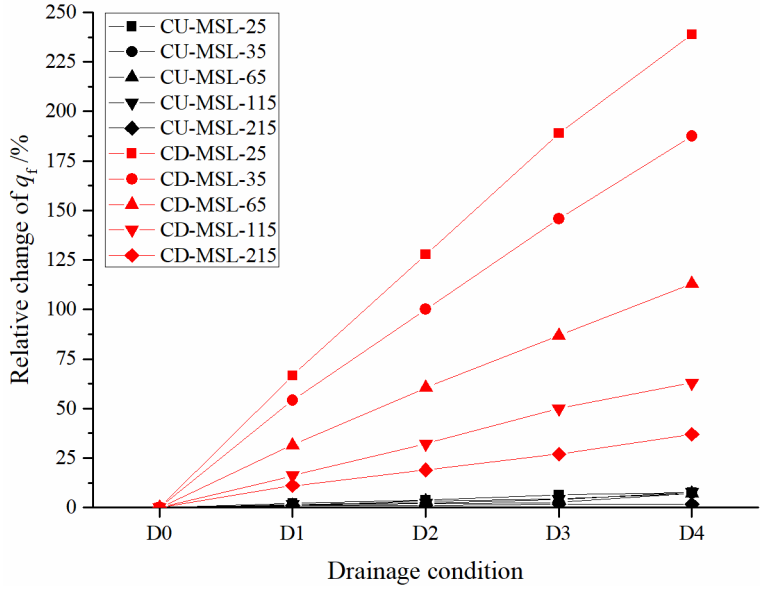

Figure 6.60 Relative change in the peak shear strength

The relative changes in unloading modulus (E_{ul}) to the initial unloading modulus are presented in Figure 6.61. CD-MSL showed a much higher percentage of increases in E_{ul} at a lower σ_c', whilst the percentage of increase at a higher σ_c' showed a similar trend with those of CU-MSL, i.e. drainage is likely to benefit subgrade support modulus at shallow depths (~< 2.5 m) but not so much at greater depths. This indicates that drainage is more effective for the soil under consolidated drained conditions, i.e. the situation where soils can dissipate the pore water pressure freely during in-situ loading. The analysis further clarified drainage effectiveness in a quantitative manner. The loading that is modeled in this Chapter is very brief - i.e. the CU-MSL tests somewhat replicate trains passing over a subgrade that drains a little between one train and the next. On the other hand, the CD-MSL tests would model a railway siding where the

train parks for a while and drainage then takes place under the train. Thus, the results show that shallow-depth drainage under background stress levels, between vehicle loadings, cannot be very effective. At greater subgrade depths (where the live load is a small proportion of the total load), the drainage under the background stress becomes more important, and CU-MSL and CD-MSL moduli showed a similar changing trend.

Lehane & Cosgrove (2000) found that vertical stiffness can be described by effective vertical stress (σ_v') divided by atmospheric pressure (p_a), and one of the expressions they proposed is

$$E_v = A_E F_e \left(\sigma_v'/p_a\right)^{0.5} \text{ for } \varepsilon_a \leq \varepsilon_{cl} \tag{6.8}$$

where E_v is the vertical stiffness, A_E is a material constant, F_e is a void ratio function (i.e. $F_e = \frac{(2.17-e)^2}{1+e}$) and ε_{cl} is the linear elastic limit of axial strain. According to Eq. (6.8), the change in E_{ul} (ΔE_{ul}) could be related to the change in σ_c' (i.e. $\Delta\sigma_c'$) in the form of a power function. Thus, an attempt was made to develop the relationships between ΔE_{ul} and $\Delta\sigma_c'$ (the ΔE_{ul} models, Eqs. (6.9) and (6.10)). E_{ul} data from CD-MSL tests was used to demonstrate the models' accuracy. The fitting results are shown in Table 6.6. Generally, Eq. (6.10) showed a better fitting performance with higher accuracy. This also indicates that $\Delta E_{ul} \sim (\Delta\sigma_c')^k$ is able to predict the changes in unloading modulus (E_{ul}) with excellent performance. However, the specific forms of the ΔE_{ul} models (e.g. Eqs. (6.9) and (6.10) for the tested soil) could be soil-dependent.

$$\Delta E_{ul} = (\Delta\sigma_c')^{k_1} \tag{6.9}$$

$$\Delta E_{ul} = k_2(\Delta\sigma_c')^{k_3} \tag{6.10}$$

where k_1, k_2 and k_3 are model parameters dependent on stress states and materials.

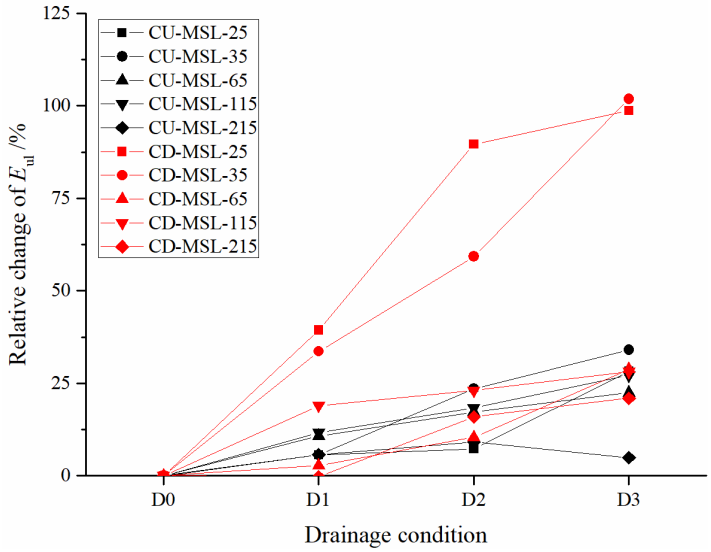

Figure 6.61 Relative change in the unloading modulus

Table 6.6 Fitting results of the ΔE_{ul} models

Test ID	Eq. (6.9)		Eq. (6.10)		
	k_1	R^2	k_2	k_3	R^2
CD-MSL-25	0.8303	0.8744	0.8452	0.8748	0.8744
CD-MSL-35	0.8668	0.9518	0.5962	0.9883	0.9792
CD-MSL-65	0.6427	0.5722	0.0021	2.1218	0.9946
CD-MSL-115	0.7646	0.0659	5.3778	0.3514	0.9745
CD-MSL-215	0.1266	0.1885	0.0044	1.4779	0.9950

6.10 Pavement analysis

Subgrade confining stress varies significantly with depth and pavement structures. Since the confining pressure on the top of the subgrade is generally under 35 kPa as predicted in most pavement structures (Miller et al., 2000), 35 kPa is a typical confining pressure on the top of the subgrade. Therefore, E_{ul} of CD-MSL-35 and -65 (as a representative) was adopted to demonstrate drainage effects on pavement response, as presented in Table 6.7. These stress levels are close to in-situ confining pressure levels. The E_{ul} of CD-MSL-35 and -65 are relatively close to the in-situ subgrade modulus compared to the CU-MSL tests and the tests with higher confinement (e.g. σ_c'= 115 and 215 kPa). Although, in practice, pavement structures deteriorate due to the coupled effects of hydraulic and mechanical factors, and thus, there is less accuracy when incorporating only one factor, it is still valid to broaden understanding of pavement response through an individual study of the important factors. Hence, for simplification, this study was limited to considering the drainage effects on three specific pavement structures as illustrative examples. Through KENPAVE, multi-layered elastic analysis was undertaken. It aims to broaden the understanding of drainage effects on the pavement response. For notation, 'D' is short for 'drainage', 'D0' means the initial cycle without drainage in CD MSL tests, and 'D1' presents the first drainage after unloading in the multistage triaxial tests. E_{sg} is the modulus of subgrade soil.

Table 6.7 Subgrade moduli with drainage

σ_c' /kPa	E_{sg} (E_{ul}) /MPa			
	D0	D1	D2	D3
	σ_c'	σ_c'+25	σ_c'+50	σ_c'+75
35	44.1	58.9	70.2	89.0
65	75.3	76.4	82.1	95.8

6.10.1 Simulation scenarios

The pavement structures were designed with typical dimensions. Based on the Design Manual for Roads and Bridges HD 26/06 (Highway Agency, 2006), flexible pavement structures were selected, as shown in Table 6.8. The selected thicknesses of asphalt concrete were used to represent the thin, medium and thick AC pavements. A single axle dual wheel load was applied, and the contact radius was 10.3 cm based on exerting a contact pressure of 600 kPa under a standard axle load of 80 kN. The spacing of dual wheels was determined by a typical tyre designation 295/80R22.5, i.e. 345 mm. The maximum tensile strain at the bottom of the asphalt concrete layer and the maximum compressive strain at the top of the subgrade layer subgrade were analysed, since they are critical strains (Arshad, 2007). For notations, (e.g. P60), 'P' is short for 'Pavement', and '60' is the thickness of asphalt concrete.

Table 6.8 Pavement model geometry and property

Layer	Property	Pavement with thick base			Pavement with thin base		
		P60	P180	P300	P60	P180	P300
Asphaltic layer $\nu = 0.3$	E_{ac} /GPa	3.5	3.5	3.5	3.5	3.5	3.5
	h_{ac} /mm	60	180	300	60	180	300
Granular layer $\nu = 0.35$	E_g /MPa	200	200	200	200	200	200
	h_g /mm	500	500	500	200	200	200
Subgrade $\nu = 0.40$	E_{sg} /MPa	Varying	Varying	Varying	Varying	Varying	Varying
	h_{sg} /mm	Infinite	Infinite	Infinite	Infinite	Infinite	Infinite

6.10.2 Simulation results

6.10.2.1 Strain

The maximum tensile strain ε_t at the bottom of asphalt concrete and the maximum compressive strain ε_v at the top of the subgrade showed opposite trends with drainage, i.e. ε_t slightly increased while ε_v decreased, as shown in Figure 6.62. The thin AC pavement exhibited the largest changes in ε_t and ε_v with drainage.

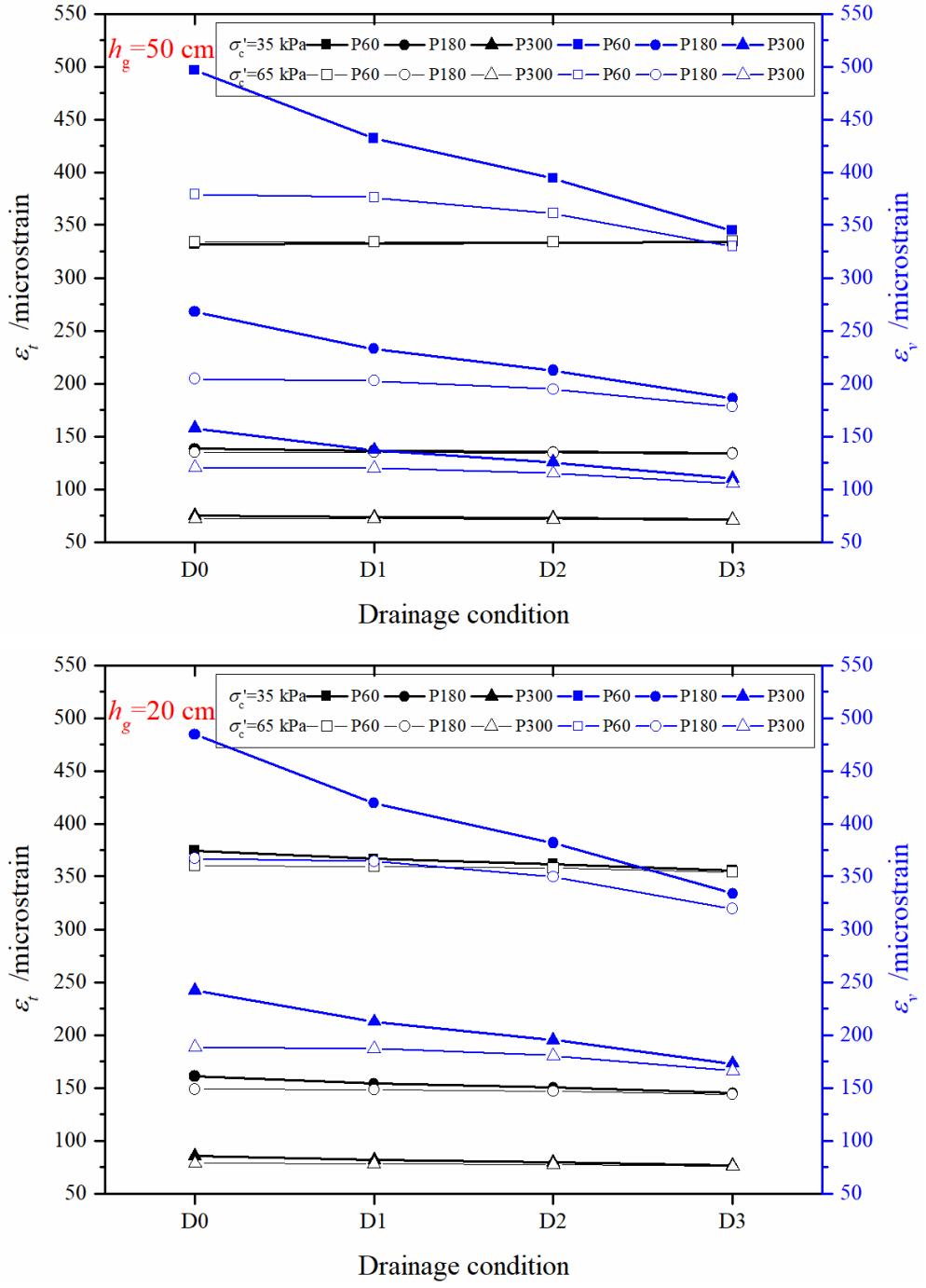

Figure 6.62 ε_t and ε_v variation with drainage

6.10.2.2 Displacement

The maximum vertical displacement δ_{sg} at the top of the subgrade is presented in Figure 6.63. With drainage, the displacement significantly decreased. It indicates the improvement of subgrade soils due to drainage.

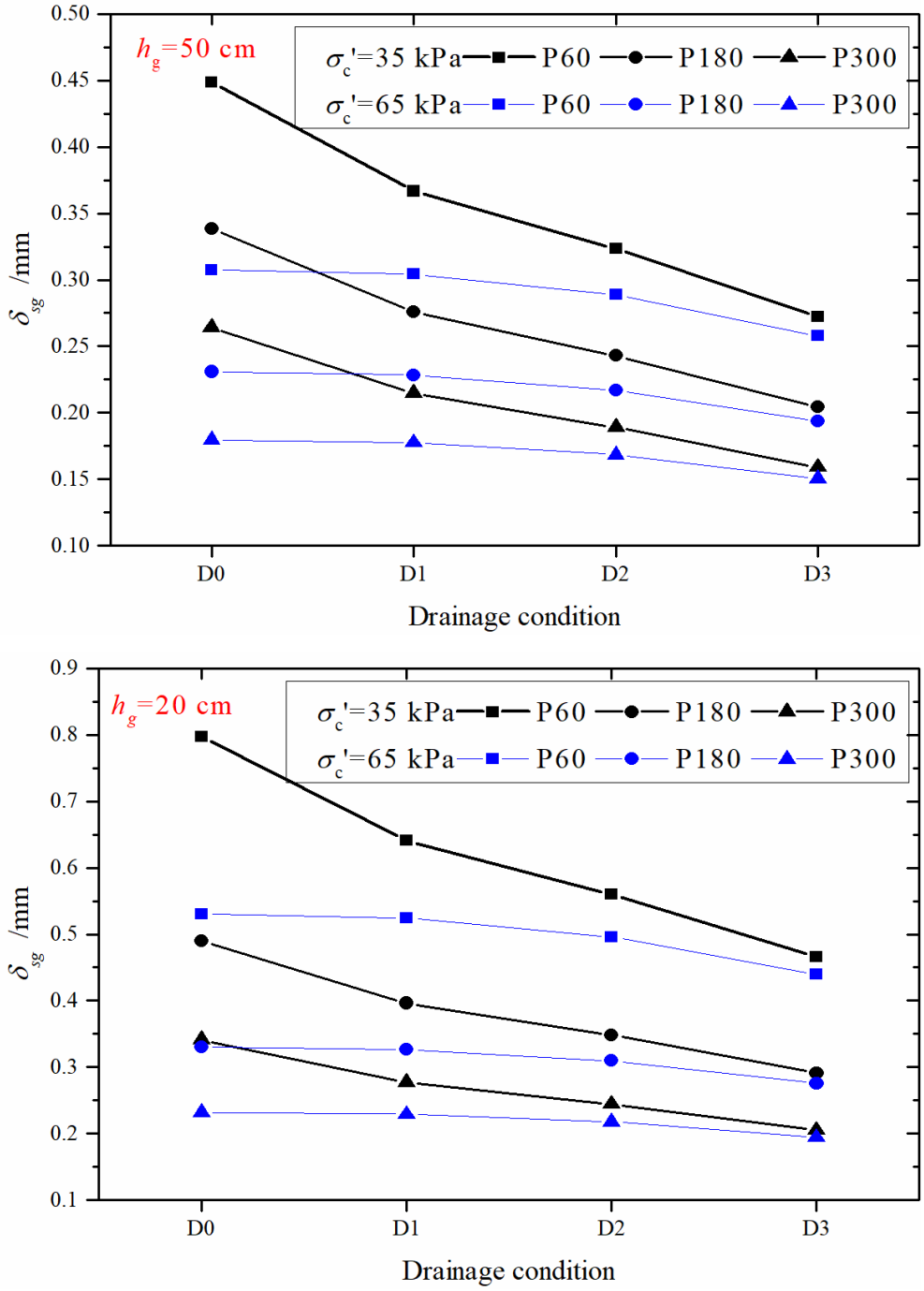

Figure 6.63 δ_{sg} variation with drainage

6.10.2.3 Distress prediction

Fatigue and rutting life (i.e. N_f and N_r) showed different trends with drainage, as shown in Figure 6.64 on a logarithmic scale. As drainage progressed, N_f slightly increased for P60, while slightly decreasing for P180 and P300. For the pavement with a thick base, fatigue life was smaller than rutting life, i.e. fatigue life was the critical life. Their service life was dominated by AC. Although N_r showed an increase with

drainage undertaken, drainage may not aid the fatigue life. For the pavement with a thin base (e.g. for P60), fatigue life was larger than rutting life, i.e. rutting life was the critical life. With efficient drainage installed, the service life of rutting-critical pavements was, therefore, expected to be effectively extended.

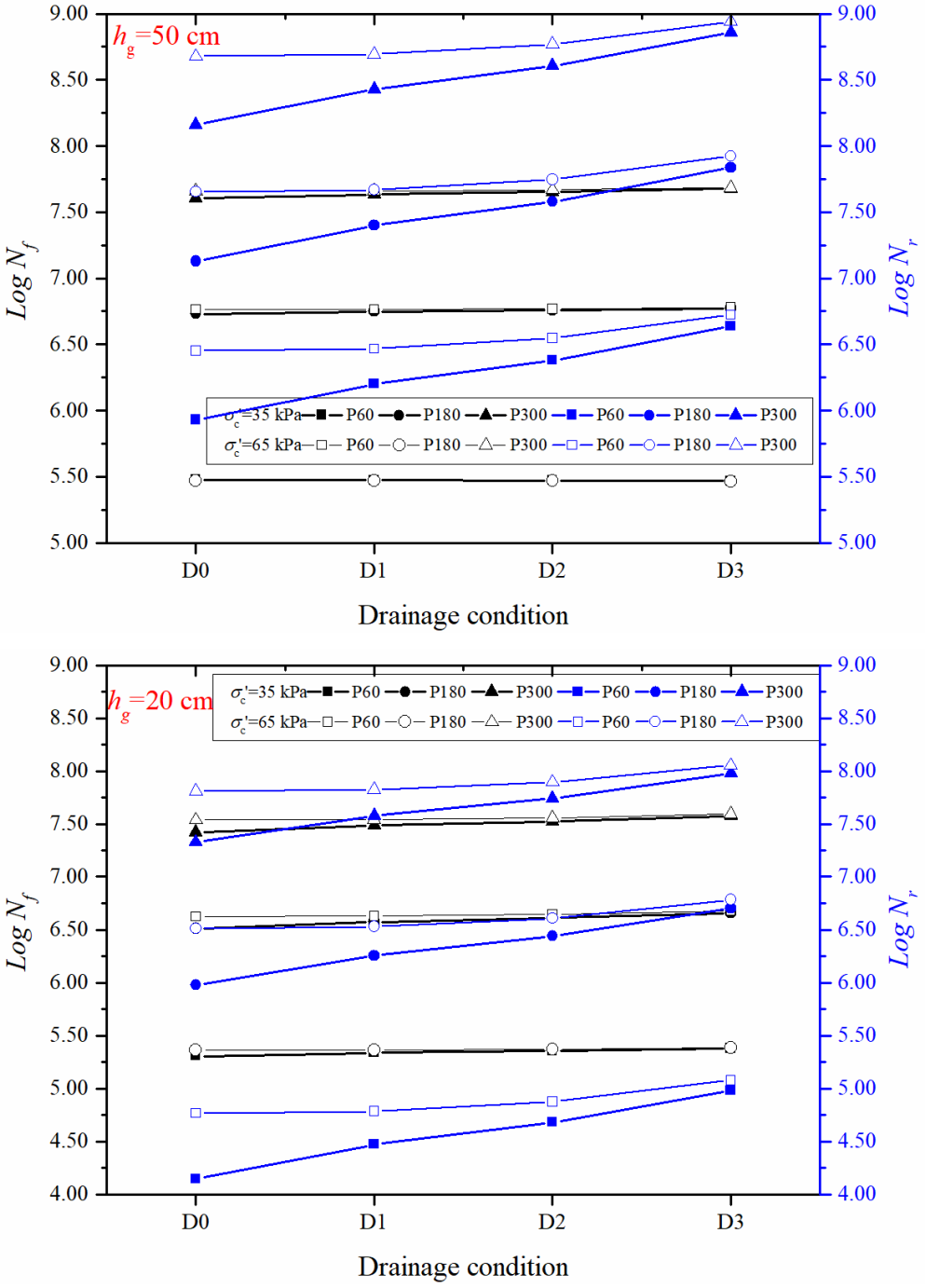

Figure 6.64 N_f and N_r variation with drainage

6.10.2.4 Discussion

The relative change of strain, displacement, and distress to that at D0 are summarized in Table 6.9. '+' indicates an increase in the parameter and '-' means a

decrease. The soil was subject to a decrease of 100 kPa in pore water pressure (i.e. an increase of 100 kPa in effective confining pressure), which could be related to a decrease of about 3% in moisture content from 10% for the unsaturated soil in this study, according to the SWCC in Figure 5.5. For example, under this moisture condition at the σ_c' of 35 kPa , the rutting life increased by about four times and displacement decreased by about 30%, which is significant for the infrastructure operation. The relative change showed a fluctuation and may have an inflection point in terms of AC thickness. It indicates that based on the current pavement design, an optimal AC thickness may exist under which the drainage could achieve the best potential. This would help in avoiding unnecessary expenditure. The distress life at the σ_c' of 35 kPa showed a significantly larger value than at the σ_c' of 65 kPa. This may imply that drainage is more effective in less consolidated foundations. The drainage promoted rutting life more than fatigue life, indicating that drainage effort is best applied to pavements in which rutting failure is critical.

Table 6.9 Relative changes of strain, displacement and distress (in %)

Pavement	σ_c' /kPa	Structure	$D0 \xrightarrow{Drainage\langle D1,D2\rangle} D3$				
			$\frac{\Delta\varepsilon_t}{\varepsilon_t}$	$\frac{\Delta\varepsilon_v}{\varepsilon_v}$	$\frac{\Delta\delta_{sg}}{\delta_{sg}}$	$\frac{\Delta N_f}{N_f}$	$\frac{\Delta N_r}{N_r}$
Pavement with thick base h_g=500 mm	35	P60	+0.79	-30.54	-39.36	-2.56	+411.26
		P180	-3.03	-30.60	-39.61	+10.67	+413.28
		P300	-5.04	-30.14	-39.82	+18.57	+398.28
	65	P60	+0.23	-12.98	-16.17	-0.77	+86.33
		P180	-1.03	-12.93	-16.21	+3.45	+85.87
		P300	-1.71	-12.66	-16.23	+5.84	+83.30
Pavement with thin base h_g=200 mm	35	P60	-5.03	-34.93	-41.59	+18.50	+584.91
		P180	-9.81	-31.09	-40.55	+40.47	+429.64
		P300	-10.35	-28.48	-39.84	+43.29	+348.33
	65	P60	-1.71	-14.82	-17.17	+5.83	+105.05
		P180	-3.42	-13.00	-16.55	+12.13	+86.56
		P300	-3.68	-11.83	-16.17	+13.12	+75.75

6.11 Summary and conclusions

Based on CU and CD triaxial compression tests and multi-layered elastic analysis, soil behaviour and drainage effect were analysed. By incorporating the unloading

modulus of soil as a subgrade, the effects of drainage between loading stages, by reducing pore water pressure (i.e. an increase of 100 kPa in effective confining pressure, corresponding to (e.g.) a decrease of about 3% in moisture content of the unsaturated soil), on the pavement response are simulated. The research achievements are presented as follows:

(1) Generally, in both CU and CD tests, at higher effective confining pressure, the specimens showed higher peak shear strength and an increasing unloading modulus. At the same effective confining pressure, the multistage tests with drainage showed significant increases in peak and critical state shear strength. Due to drainage between loading stages in terms of pore water pressure reduction, the unloading modulus also showed a clear increase. After drainage, the volume of all the specimens showed a smaller decrease in strength than those without drainage.

(2) Compared with SSL tests, MSL tests exhibited strain hardening. The size of the hysteresis loop generally showed a decreasing trend, and the unload-reload loops became stiffer, indicative of strain hardening at high axial strains. In addition, the CU-SSL tests did not show a clearly stable state within the target strain, whilst the CU-MSL tests and CD tests all reached stable critical states. In terms of pore water pressure, CU tests reached equilibrium values that were then maintained at constant values as the shearing proceeded.

(3) The unloading moduli were larger in CU-MSL triaxial tests compared with those in CD-MSL triaxial tests, while peak shear strength was larger in CD-MSL tests. The relative changes in the peak shear strength (q_f) and unloading modulus (E_{ul}) were compared between CU-MSL and CD-MSL. Generally, relative changes were much higher in CD-MSL. This also implies that the drainage (a reduction of 100 kPa in pore water pressure) showed larger effects on the drained shearing behaviour. Combined with decreased excess pore water pressure in CU tests, potential causes of the difference were presented. In CU tests, as shearing proceeded, the pore water pressure of the specimen dropped, thus increasing the effective stress and hence, showing higher strength and stiffness compared to these in CD tests.

(4) The findings obtained at different effective confining pressures may indicate that shallow-depth drainage under background stress levels, between vehicle loadings, cannot be very effective. At greater subgrade depths (where the live load is a small proportion of the total load), the drainage under the background stress becomes

more important, and CU-MSL and CD-MSL moduli showed a similar changing trend.

(5) Through multi-layered elastic analysis, drainage effects on pavement performance were studied. Rutting life showed a clear increase with drainage. With proper drainage installed, the service life of pavements is expected to be effectively extended. The results could also be applicable to sandy soils since the soil used in the test is one type of slightly silty sand. However, the drainage benefited the pavement with a thicker base more with respect to the rutting life. With pore water pressure decreasing by 100 kPa (e.g. equivalent to a decrease in unsaturated moisture content of ~3% according to the SWCC in Figure 5.5), the rutting life increased by about four times. This indicates that drainage effectiveness could be impaired without considering the engineering requirement during design, e.g. drainage improvement for a fatigue-critical pavement may be uneconomic.

However, in this study, the simulation of the flexible pavement is simplified, and limited conditions are considered. The unloading modulus is adopted as an estimation of the resilient modulus of the subgrade. Soil responses in drainage-controlled laboratory tests are idealized, while soils in practice are subject to complicated conditions. The effects of seasonal variation of temperature and moisture content on asphalt layers are not incorporated. Resilient moduli of upper layers are also not constant with time under moving wheel loads. Despite these limitations, the findings are expected to give some reference for future pavement drainage design.

CHAPTER 7 UNSATURATED TRIAXIAL TESTS

7.1 Introduction

Since it is commonly required that the soils be compacted at (or near) optimum moisture content in construction in order to easily reach the maximum dry density, the in-situ subgrade soils should be considered as materials in an unsaturated state above the phreatic line (Drumm et al., 1997; Yang et al., 2005). Subject to environmental effects (e.g. rainfall, evaporation, and freeze-thaw), the subgrade soil could exhibit seasonal moisture variation. The general condition existing in the subgrade is illustrated in Figure 7.1. The moisture conditions of soils are simplified as unsaturated and saturated zones without considering a transition zone.

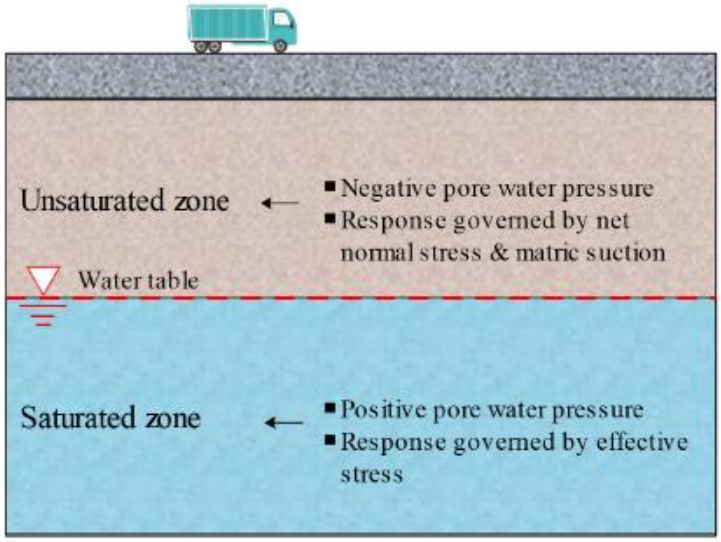

Figure 7.1 Schematic diagram of subgrade soil

Thus, saturated tests often provide the most critical conditions (depending on the normal stress level). However, more information is needed to give a specific understanding of the load-carrying capability of the in-situ subgrade soils in the unsaturated state. This chapter aims to investigate the effects of drying, wetting and drainage on the soil shear strength behaviour and the modulus through constant water content tests. Following Chapter 6, unsaturated triaxial tests were conducted to investigate the response of unsaturated soils, including single-stage and multistage constant water content triaxial tests. The effects of moisture content were revealed in terms of drying, wetting and drainage processes that had been applied during specimen

preparation or between testing stages.

7.2 Theoretical framework

7.2.1 Research process

The research process is illustrated in Figure 7.2 to demonstrate its main characteristics.

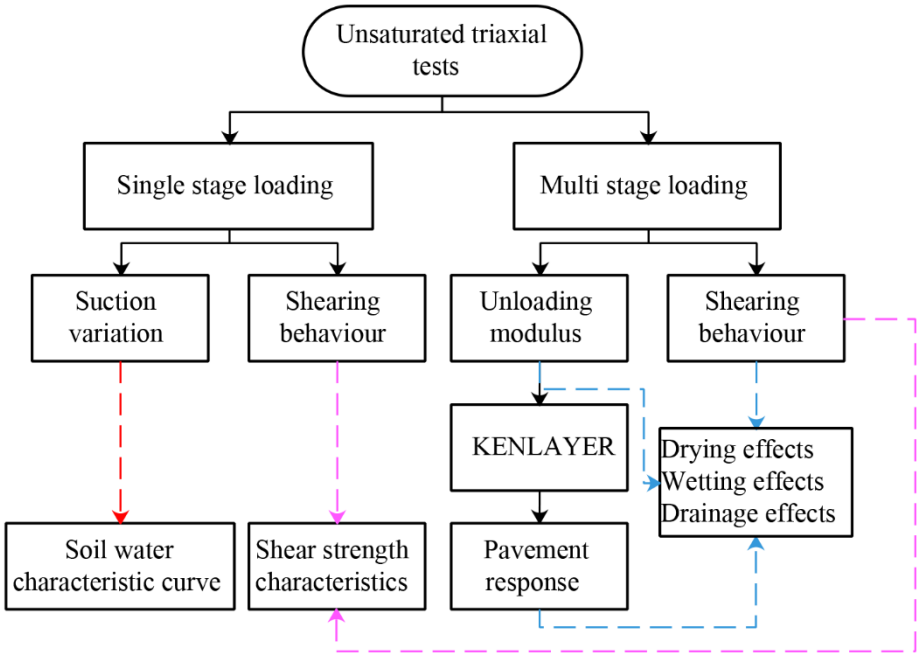

Figure 7.2 Research process for unsaturated triaxial tests

7.2.2 Matric suction

With the development of soil mechanics, matric suction has been considered as an important stress variable in investigating the effects of moisture content on the mechanical behaviour of unsaturated soils in pavement structures. It is widely recognised that soil suction mainly consists of the capillary and adsorptive potentials, i.e. matric and osmotic suction (Krahn & Fredlund, 1972; Edil & Motan, 1984; Fredlund et al., 2012). The total suction indicates the free energy of the soil water, while matric and osmotic suctions are the components of the free energy.

As Leong & Abuel-Naga (2017) demonstrated, matric suction $(u_a - u_w)$ is associated with capillary effects, while osmotic suction depends on the salt content of the pore water. A strong correlation has been revealed between matric suction and resilient modulus (Khoury & Zaman, 2004). Khoury et al. (2013) demonstrated that the variations in resilient modulus were not induced by osmotic suction. Based on analysis of experimental data, it was found that resilient modulus correlated better with matric

suction than with total suction (Yang et al., 2005). Furthermore, based on these studies, the effects of matric suction should be incorporated in the analysis of the behaviour of partially saturated soil in preference to the effects of total and osmotic suctions.

Matric suction affects the mechanical behaviour of unsaturated soils as a fundamental stress variable, and the effects vary with stress states. Matric suction generates capillary inter-particle forces normal to particle contacts, and it plays a more complicated role compared with the pore pressure or mean stress (Sheng et al., 2008). There are two roles of matric suction on the mechanical response of soils, i.e. it affects the effective stress existing between the soil particles (i.e. via negative pore water pressure) and it exerts a force on the particles that may, over time, result in increased intraparticle adhesion. With respect to the two mechanisms, the effects of suction on the response also rely on the saturation state of the soil (Wheeler & Sivakumar, 1995; Gallipoli et al., 2003). When considering suction effects, the distribution of pore fluid imposed by the soil fabric should also be involved to quantify the distribution of pore pressures (Li, 2003).

Referring to resilient modulus, it shows a nonlinear increasing trend at a lower matric suction (Gallipoli et al., 2003; Yang et al., 2005; Yang et al., 2008; Khoury et al., 2009; Cary & Zapata, 2011; Fredlund et al., 2012; Han & Vanapalli, 2016a), whilst the same trend may not be recognized at higher suction levels. It may be induced by the more effective contribution of soil suction on the wetted contact area of soil particles within the low suction region (Vanapalli et al., 1996), while the limited wetted contact area at higher suction levels impairs the effect of suction.

Plenty of studies have been performed on predicting the resilient modulus of subgrade soils and several model parameters have been considered, e.g. confining stress, bulk stress, or dry density (Yang et al., 2005). Since matric suction variations can reflect the effects of the seasonal variation of moisture content under in-situ conditions and directly affect the stress condition in the soil, a resilient modulus model incorporating matric suction could be more reliable than one based on moisture content. Particularly, at a low moisture content, the resilient modulus is dominated by the large matric suction of the soil. Thus, it may benefit the foundation design to have a better understanding and measurement of matric suction.

7.2.3 Axis translation technique

Since the air phase exists in unsaturated soils, it induces negative pore water

pressure due to the influence of the soil pore menisci. For unsaturated soil tests, direct control or measurement of negative pore water pressure (i.e. matric suction) is desirable but is limited when using the traditional saturated triaxial testing system. The limitations are due to two aspects. (1) Porous disks at the specimen ends do not have high air-entry value and thus, air may enter the water compartment in the apparatus when the pressure difference exceeds the value. As a result, the water pressure in the measurement system cannot reflect the pore water pressure in the soil. The measurement system is then filled with air. (2) Cavitation may occur in the water compartment as a gauge pressure of –1 atm is approached. The accumulated bubbles in the water could cause errors in the measurement of pore water pressure.

By translating the reference axis for the measurement of pore air pressure, i.e. by artificially increasing the atmospheric pressure when performing the test, the above-mentioned limitations can be resolved. Consequently, the negative pore water pressure increases by an equal amount to the increase in atmospheric pressure, while the matric suction in the soil specimen remains constant independent of the magnitude of the pore air pressure. In principle, both the pore-air and the pore-water pressures are translated into the positive-pressure range when an axis translation is applied. The method is referred to as the axis translation technique and is commonly used in testing unsaturated soils and is particularly useful at high matric suction over 100 kPa. A saturated ceramic disk with an air-entry value above the matric suction should be installed instead of a porous disk to inhibit air migration into the water compartment. Considering the low coefficients of permeability of the soil specimen and ceramic disk, air could still enter the water pressure measurement system as air bubbles over an extended testing duration. In this case, the system needs to be regularly flushed for a short time to remove the bubbles.

Apart from the advantages of the axis translation technique, various limitations related to this method have been revealed in previous studies (Romero et al., 2003; Romero et al., 2005; Marinho et al., 2008; Bagheri et al., 2019), including (1) the range of matric suction that can be measured or applied is a function of the air-entry value of the ceramic disk, as well as the peak capacity of the air controlling and measurement system; (2) a discontinuity of water flow through the porous filter may be induced by inadequate contact between the pore-water and water compartment in the ceramic disk and, consequently, may greatly extend the equilibrium time or even prevent water

movement under drained conditions (Marinho et al., 2008); (3) accumulation of diffused air bubbles in the water compartment of a high air-entry value ceramic disk can cause a discontinuity between pore-water in the specimen and water in the measurement system (Romero et al., 2003); and (4) difficulties in controlling the evaporation of soil moisture during tests (especially for tests at high temperatures) necessitates a precise installation of auxiliary devices (i.e. vapor traps and a diffused air flushing/volume indicator) (Romero et al., 2003; Romero et al., 2005).

7.2.4 Constant water content triaxial tests

Compared to consolidated drained and undrained tests, constant water content tests may better represent the stress path experienced by the compacted soil under in-situ construction conditions (Thu et al., 2006). Excess pore water pressure varies over time depending on soil characteristics while excess pore air pressure rapidly dissipates. Combined with axis translation, it is widely used to investigate unsaturated soil behaviour. From the previous studies, the challenge in performing constant water content tests is to maintain the uniformity of the pore water pressure in the specimen at the shearing stage (Thu et al., 2006).

After applying the initial stress state, the initial consolidation stage starts by following the same procedure as for consolidated drained tests. When the equilibrium is reached for consolidation, shearing is conducted. During the shearing stage, the pore water pressure valve is kept closed and thus, water cannot migrate out of or into the specimen. An undrained pore water condition is created. Pore water pressure is measured by a transducer connected to the water compartment of a high air entry disk while a constant pore air pressure is maintained.

7.3 Test apparatus

Compared with the triaxial testing system used in consolidated drained and undrained tests, the triaxial testing system for constant water content tests on unsaturated soils shows some differences, i.e. a pore air pressure controller and high air entry ceramic disks are included. The schematic diagram and photos of the system are illustrated in Figure 7.3 and Figure 7.4. The testing system was placed in an air-conditioned room with a constant temperature of about 21˚C and was calibrated prior to testing according to the technical manual. Particularly, the GDS air pressure controllers are 1000cc/2MPa devices with regulation to 1 kPa, i.e. the pressure range is

from zero to 2 MPa and the volumetric capacity (nominal) is 1000cc; pressure and volume resolution of measurement and control are <0.1% full range and 0.5 mm^3, respectively; pressure and volume accuracy of measurement are <0.1% full range and 0.25%, respectively.

For constant water content tests, pore air pressure should be controlled during shearing. The control and measurement of pore air pressure and air volume change can be achieved by the controller. Both pressure control mode and volume change mode are available. Air volume change can be measured when the controller is used in a pressure control mode. A coarse porous disk is placed on the top of specimens to maintain the continuity of the pore air pressure system with the air voids in the specimen.

A high-air entry porous disk (HAEPD) (Figure 7.5) with 500 kPa air-entry value (i.e. the minimum matric suction at which pore air starts to enter a thoroughly saturated ceramic pore) is embedded into the base pedestal in order to maintain the separation of air and water and enable a wide range of matric suctions in the specimen. The water compartment of the disk is connected to the pore water pressure measuring system. Water was flushed through from Port B to Port A in Figure 7.3. The accumulated air bubbles in the water compartment can be flushed out through the water flushing line. Prior to starting the test, the high-air entry ceramic disk was saturated. The three-stage procedure from GDS UNSAT Handbook was followed: (1) flush de-aired water at a back pressure of 30 kPa through the pipes and channels underneath the HAEPD until no further bubbles come out, (2) close the flushing valve and maintain the water pressure underneath the disk until water films appear on the ceramic disk surface, in order to remove air trapped in the disk pores, and (3) pressurize the HAEPD with de-aired water in the triaxial cell by applying a high cell pressure (e.g. 600 kPa) and flow water through the HAEPD for 4-8 hours with the flush valve open to atmosphere. Between tests, the HAEPD was immediately submerged into water to maintain its saturation.

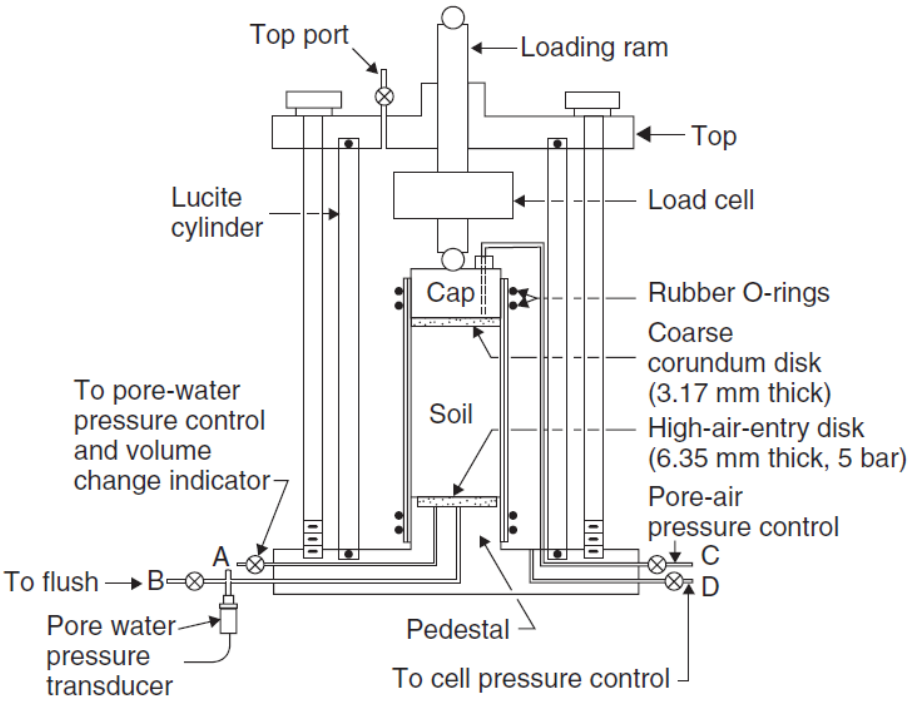

Figure 7.3 Schematic diagram of the unsaturated triaxial cell (Fredlund et al., 2012)

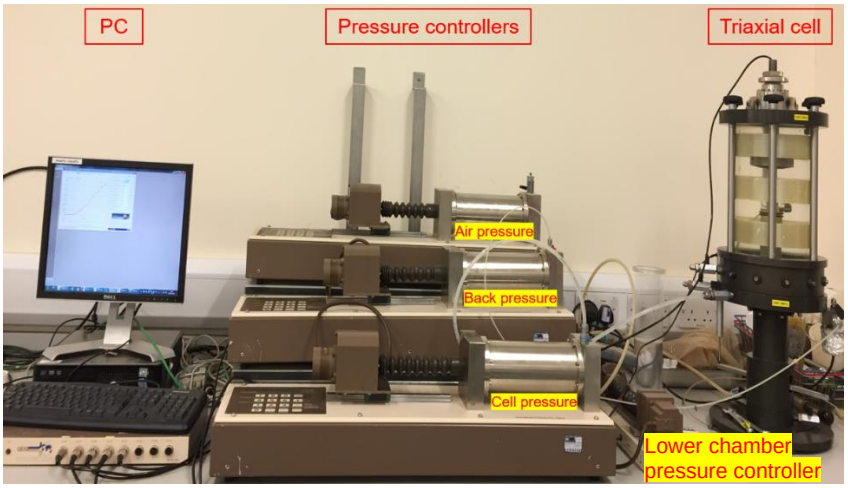

Figure 7.4 Photo of GDS Unsaturated triaxial testing system

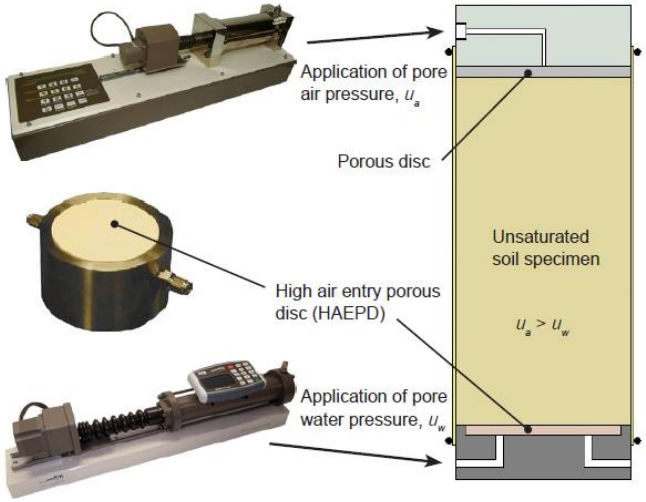

Figure 7.5 Schematic illustration of unsaturated triaxial test set-up (GDS Instruments)

7.4 Preparation of triaxial specimens

The basic properties of the test soil are presented in Chapter 5. The soil is characterised as silty sand. The preparation method of specimens for unsaturated triaxial tests is similar to that of specimens for saturated triaxial tests, except that the specimens were prepared on the high air entry ceramic disk in the pedestal instead of on a porous disk. The physical properties of the unsaturated specimens are presented in Table 7.1.

Table 7.1 Physical properties of unsaturated specimens

e	w /%	S /%	γ_d /g·cm^{-3}	G_s
0.43	10.5	70.1	1.85	2.04

7.5 Test program

During the shearing stage, suction equilibrium should be maintained. To achieve the equilibrium of pore air/water pressure inside the specimen, the strain rate should be slow enough, i.e. 0.01%/min. Single-stage and multistage tests were conducted. For single-stage tests, the specimens experienced shearing until an axial strain of 28% (the equipment's limit). For multistage tests, drying, wetting and drainage processes were performed. A multistage testing protocol was attempted in order to acquire the maximum number of details from a small number of tests and to minimise the impact of soil variability (Ho, 1987). At each stage, the specimen was sheared until the peak strength was reached and then unloaded. The peak state was determined when the deviator stress was detected to start to reduce.

(1) Drying

After the initial loading-unloading stage, the drying process started by applying a higher suction to remove a specific amount of water from the specimens. The moisture content decreased to a specific value to simulate the drying of soils. Prior to the next stage of loading, equilibrium was achieved by maintaining the pore air pressure after completing the drying process and when the matric suction reached a constant value.

(2) Wetting

After three drying stages, a wetting process was performed by increasing the moisture content of the specimen. With the increase of back pressure beyond the pore air pressure, the water in the water compartment of the ceramic disk moved into the specimens. Once again, the equilibrium of suction was realized prior to loading.

(3) Drainage during load-unload cycles

As the drying and wetting processes finished, a free drainage process was simulated by reducing the back pressure to zero during shearing, allowing water to migrate from/to the specimen. This aims to study the effects of free drainage on the mechanical behaviour of soils. The drained water was measured by the back-pressure system, and it can be used to decide the variation of moisture content of the specimen.

(4) Test nomenclature

The same test nomenclature logic is used as in Chapter 6, except that 'Unsat' is introduced to indicate an unsaturated test, and the final number now indicates the initial net confining stress in kPa. For example, 'Unsat-MSL-25' would indicate a multi-stage test on an unsaturated specimen with an initial net confining stress of 25 kPa.

7.6 Unsaturated SSL triaxial test

7.6.1 Test procedure

Different from the traditional saturated testing system, unsaturated testing requires an air pressure-controlled system. An air pressure controller was connected to the sample with a plastic pipe. To determine the volume of the pipe and associated system, the backpressure controller was used to fill the pipe with water prior to testing, and the volume of water required to do so was monitored. The HAEPD should be saturated in the triaxial apparatus before placing specimens. Then, the micropores on the surface of the HAEPD induce a tension film which is able to separate air in the specimen and water in the water compartment of the HAEPD. The HAEPD can best be saturated by first passing water through the disk and then using pressurization to force air into the solution (Fredlund et al., 2012). Regarding saturation procedures suggested by Fredlund et al. (2012), it is either time-consuming to apply 600 kPa air pressure to a triaxial cell with the air pressure controller, or an extra air pump and pressure gauge are needed to increase the pressure up to 600 kPa. Air in the cell water will also dissolve into water, and consequently water with dissolved air may enter ceramic pores, causing later saturation errors once the HAEPD are inside the membrane with the specimen.

Another procedure to saturate the HAEPD is therefore proposed. The HAEPD was first air-dried to remove all the water in the compartment and then mounted on the apparatus. A membrane was used to wrap the pedestal and was sealed with an O-ring. Distilled and de-aired water was added inside the membrane to a height of about 100mm. A loading cap was placed on the top of the membrane and sealed with an O-

ring. The triaxial cell was then assembled and filled up with tap water. The water in the cell was exposed to 600 kPa cell pressure, which caused the water inside the membrane to be under the same pressure. The valve between the water compartment and the measuring system was closed. Water in the membrane flowed through HAEPD for about an hour and the air in the disk dissolved in the water. Then, the valve connected to the water compartment was opened for about 10 min to enable the water in the disk to flow into the compartment and thus, air bubbles accumulated in the compartment which was then flushed to remove the bubbles. The above procedure was repeated five times, after which the HAEPD was considered to be saturated. After each test, the disk was cleaned immediately and covered with distilled de-aired water. Cling film was placed on top and sealed with an O-ring. The valve connected to the backpressure system was opened to flush any air bubbles out of the compartment and then a 30 kPa back pressure was applied until the cling film was filled with water.

After preparing the specimen, the triaxial cell could be assembled. Pore air pressure and confining pressure were simultaneously increased, having a constant difference of 10 kPa. Then, the specimen was consolidated under isotropic conditions. When the target net confining pressure was reached, pore air pressure and confining pressure were maintained while the pore water pressure was measured. The specimen was considered in moisture equilibrium at the end of consolidation as the initial suction prior to shearing was kept constant. The specimen was then sheared by increasing the deviator stress until an axial strain of about 21% was reached.

The shear stage was strain-controlled with drainage pore-air phase and undrained pore-water phase, and the strain rate was selected as 0.01%/min. The critical state was identified for each test at the point when the deviator stress became constant. When the test was completed, the specimen was removed, and the final moisture content was measured. The initial stress conditions are presented in Table 7.2.

Table 7.2 Initial conditions of SSL unsaturated triaxial tests

Tests	σ_c /kPa	u_a /kPa	$\sigma_{c,net}$ /kPa
Unsat-SSL-25	105	80	25
Unsat-SSL-35	115	80	35
Unsat-SSL-65	145	80	65
Unsat-SSL-115	195	80	115
Unsat-SSL-215	295	80	215

7.6.2 Test results

The results of Unsat-SSL tests are presented in Figure 7.6~Figure 7.9. The deviator stress increased with net confining pressure. For the stress-strain behaviour, the deviator stress increased while the strain remained small and reached a constant value, i.e. the critical state, and then decreased with further axial strain after shear failure. Because shearing was designed to be slow enough to maintain the equilibrium of pore water pressure, thus the effective stress ratio followed the same trend with axial strain as did deviator stress. The peak stress ratio decreased with $\sigma_{c,net}$. As the shear failure progressed beyond the peak, the effects of $\sigma_{c,net}$ on shearing behaviour became small. The failure envelope parameters for shear strength and stress path at peak and critical state (Table 7.3) were derived from the best-fit curve. α_{HV} (the angle of the Hvorslev surface) and β_{HV} (the intercept of the Hvorslev surface) are the stress path parameters at the peak state. M (the angle of the critical stage line) is the stress path parameter at the critical state. Thus, the intercept could be slightly different and value of 1.44 kPa could be negligible.

Table 7.3 Failure envelope parameters for shear strength and stress path

Parameters / State	Shear strength		Stress path		
	ϕ' /°	c' /kPa	α_{HV}	β_{HV}	M
Peak state	40	7.21	1.645	15.48	-
Critical state	37	1.44	-	-	1.522

The matric suction (Figure 7.9) generally showed a downward trend with increasing axial strain. It tended to stabilize at the end of shearing, which was in agreement with that at a suction of 162 kPa in the study by Maleki & Bayat (2012). As shearing continued, the specimen exhibited dilation, and pore water pressure increased.

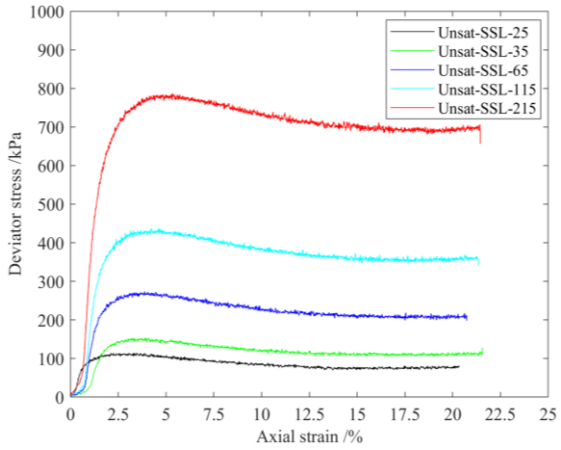

Figure 7.6 $q-\varepsilon_a$ curves of Unsat-SSL

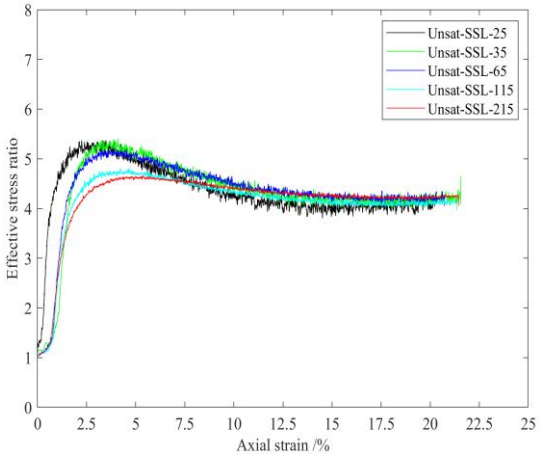

Figure 7.7 ESR$-\varepsilon_a$ curves of Unsat-SSL

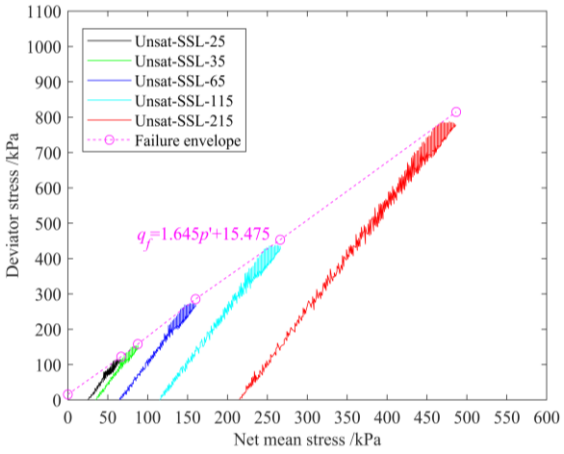

Figure 7.8 $q - p'$ curve of Unsat-SSL

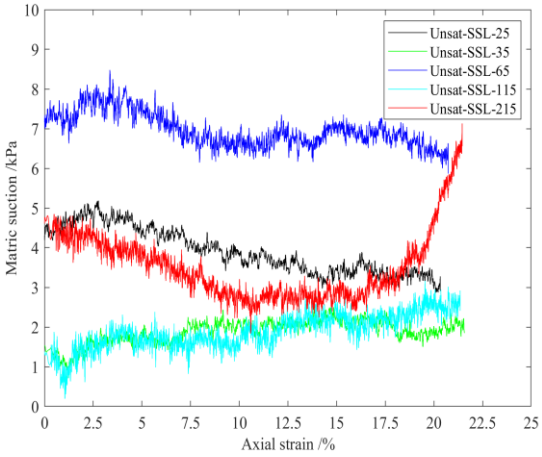

Figure 7.9 Suction with ε_a in Unsat-SSL

7.7 Unsaturated MSL triaxial test

7.7.1 Test procedure

Similar procedures to those in Section 6.6.1 were followed, apart from the multistages. The multistage process contained drying, wetting and drainage procedures, with six loading-unloading cycles. After the initial loading-unloading, moisture contents were changed. The specimen was allowed to reach equilibrium. The matric suction in the specimen (i.e. the difference between pore air pressure and pore water pressure) was monitored. When matric suction became stable and constant, the specimen was considered to reach equilibrium. Then, a reloading-unloading was conducted. Moisture content variations for these six cycles were 0 (initial stage), -1%, -2% and -4% for the drying process, then back to -2% by a wetting stage followed by free drainage during shearing. After the test stopped, the specimen was removed to measure the final moisture content. The moisture content at each stage was calculated based on the water volume change. The testing moisture range was between w_0-4% and w_0. Considering the timeframe of unsaturated testing and the properties of the test soil, a small moisture range was adopted. Initial stress conditions are presented in Table 7.4.

Table 7.4 Initial stress conditions of MSL unsaturated triaxial tests

Tests	σ_c /kPa	u_a /kPa	$\sigma_{c,net}$ /kPa
Unsat-MSL-25	105	80	25
Unsat-MSL-35	115	80	35
Unsat-MSL-65	145	80	65
Unsat-MSL-115	195	80	115
Unsat-MSL-215	295	80	215

7.7.2 Test results

7.7.2.1 Shearing behaviour

The test results are presented in Figure 7.10~Figure 7.20. At the net confining pressures of 25, 35 and 65 kPa, the peak shear strength showed increasing trends with the decrease in moisture content. With wetting, the peak shear strength slightly decreased while increasing with drainage. Regarding the effective stress ratio (ESR), they generally showed an increase as the moisture content decreased. Following the increase in moisture content, the effective stress ratio decreased and then increased as drainage was in progress. At 115 and 215 kPa, the peak shear strength and effective stress ratios presented similar trends with decreasing moisture content while showing a slightly different trend with no stress decrease during wetting compared with those at lower confining pressures. By comparing the responses at w_0-2% (i.e. by comparing stages w_2 and w_4), a general trend can be identified that the shear strength along the drying path was larger than that along the wetting path, i.e. there is a hysteretic effect due to moisture variation. This is in agreement with the previous study (Khoury & Miller, 2011). Their differences decreased with the net stress and became insignificant.

Figure 7.10~Figure 7.14 may also indicate the strain-hardening effect. As the axial strain increased, the size of the hysteresis loop reduced, and the unload-reload loops became stiffer. The shear strength at w_0-2% for $\sigma_{c,net}$= 35 kPa was smaller than that at w_0-2% along the drying path, indicating the moisture effect was not dominant in this process. Thus, the increase in shear strength could also be a consequence of the high strain, distinct from the moisture variation.

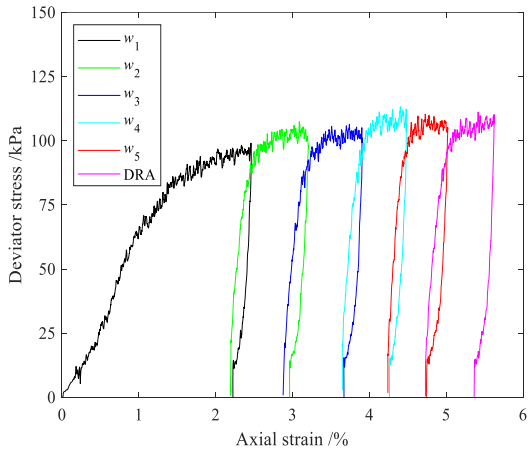

Figure 7.10 $q - \varepsilon_a$ of Unsat-MSL-25 ($w_1 = w_0$; $w_2 = w_0$-1%; w_3=w_0-2%; $w_4 = w_0$-4%; $w_5 = w_0$-2%)

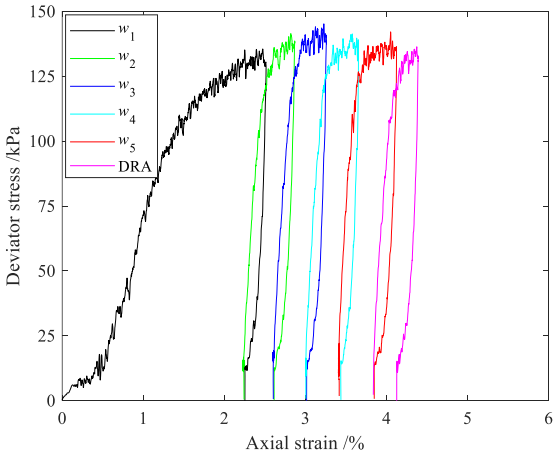

Figure 7.11 $q - \varepsilon_a$ of Unsat-MSL-35 ($w_1 = w_0$; $w_2 = w_0$-1%; w_3=w_0-2%; $w_4 = w_0$-4%; $w_5 = w_0$-2%)

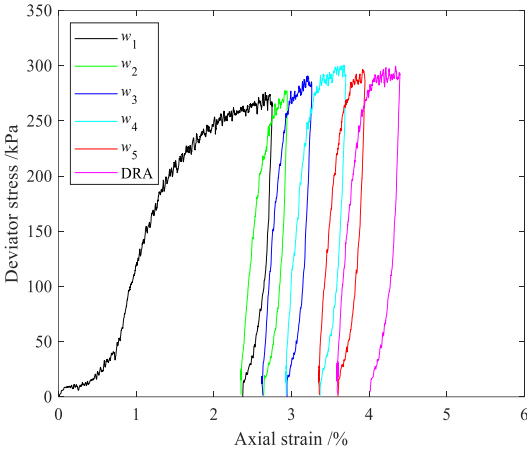

Figure 7.12 $q-\varepsilon_a$ of Unsat-MSL-65 ($w_1 = w_0$; $w_2 = w_0$-1%; w_3=w_0-2%; $w_4 = w_0$-4%; $w_5 = w_0$-2%)

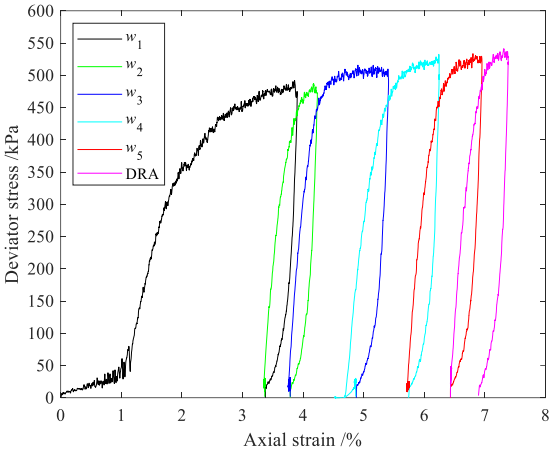

Figure 7.13 $q-\varepsilon_a$ of Unsat-MSL-115 ($w_1 = w_0$; $w_2 = w_0$-1%; w_3=w_0-2%; $w_4 = w_0$-4%; $w_5 = w_0$-2%)

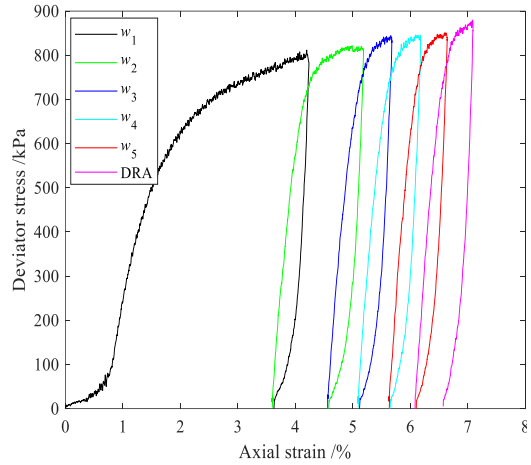

Figure 7.14 $q-\varepsilon_a$ of Unsat-MSL-215 ($w_1 = w_0$; $w_2 = w_0$-1%; w_3=w_0-2%; $w_4 = w_0$-4%; $w_5 = w_0$-2%)

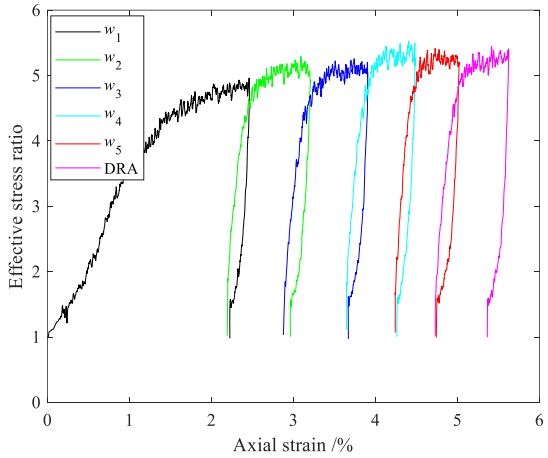

Figure 7.15 ESR$-\varepsilon_a$ of Unsat-MSL-25 ($w_1 = w_0$; $w_2 = w_0$-1%; w_3=w_0-2%; $w_4 = w_0$-4%; $w_5 = w_0$-2%)

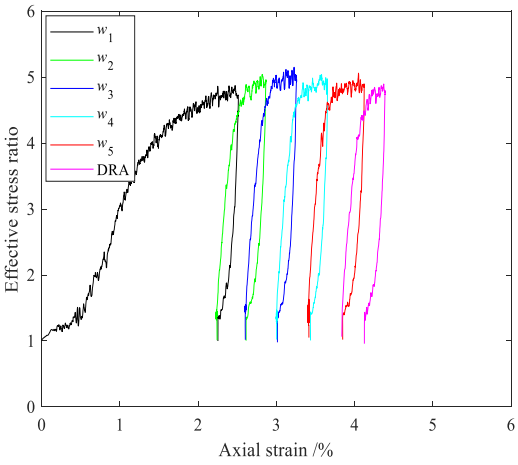

Figure 7.16 ESR$-\varepsilon_a$ of Unsat-MSL-35 ($w_1 = w_0$; $w_2 = w_0$-1%; w_3=w_0-2%; $w_4 = w_0$-4%; $w_5 = w_0$-2%)

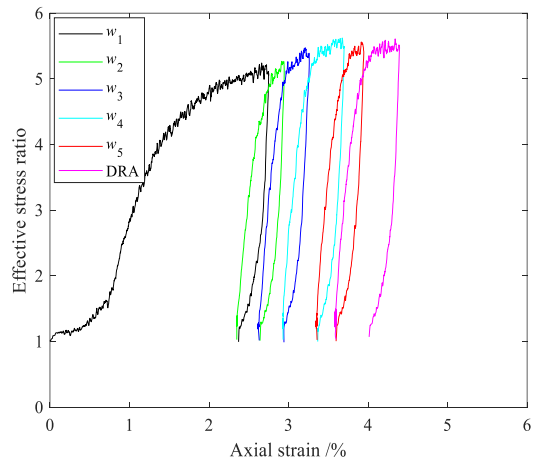

Figure 7.17 ESR$-\varepsilon_a$ of Unsat-MSL-65 ($w_1 = w_0$; $w_2 = w_0$-1%; w_3=w_0-2%; $w_4 = w_0$-4%; $w_5 = w_0$-2%)

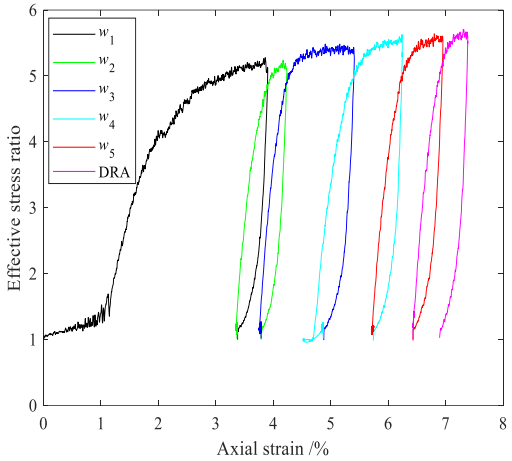

Figure 7.18 ESR$-\varepsilon_a$ of Unsat-MSL-115 ($w_1 = w_0$; $w_2 = w_0$-1%; w_3=w_0-2%; $w_4 = w_0$-4%; $w_5 = w_0$-2%)

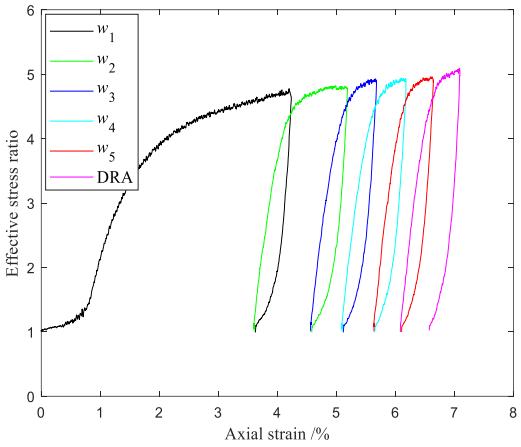

Figure 7.19 ESR$-\varepsilon_a$ of Unsat-MSL-215 ($w_1 = w_0$; $w_2 = w_0$-1%; w_3=w_0-2%; $w_4 = w_0$-4%; $w_5 = w_0$-2%)

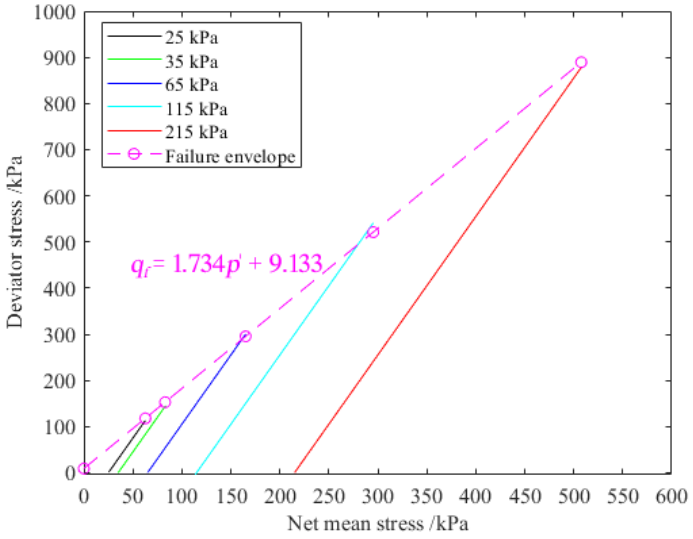

Figure 7.20 $q - p'$ relationship of Unsat-MSL

7.7.2.2 Matric suction

The variation of matric suction is presented in Figure 7.21~Figure 7.25. The labels ('drying', 'wetting' and 'free drainage) indicate different drying, wetting and free drainage stages as mentioned in Section 7.5. 'w_0, w_1, w_2, w_3, w_4' and 'DRA' correspond to each loading-unloading cycle and indicate their moisture conditions. During the drying and wetting processes, matric suction showed clear differences. Within the drying process, matric suction increased as moisture content decreased. Then, the matric suction decreased as the moisture content increased due to wetting. Particularly, the matric suction in the wetting stage (w_4) was lower than that at w_2 (= w_4), due to hysteresis phenomenon. It was also found that matric suction decreased with loading (i.e. shearing) while increasing with unloading. Dilation occurred during shearing. This

may increase the radius of the curvature of air-water interfaces in the specimen. Given the boundary conditions, dilation will mean that the soil pulled in water, increasing the degree of saturation and thus reduced the matric suction according to SWCC in Figure 5.5. In unsaturated conditions, these processes showed fewer effects on the soil response within a small range of moisture variation in silty sand. This also implies that the effectiveness of drainage or moisture-reducing methods varied with the range of moisture content. This may provide a reference for drainage design.

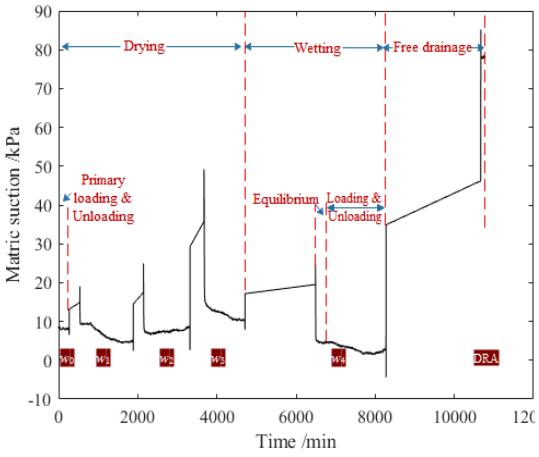

Figure 7.21 Matric suction variation of Unsat-MSL-25

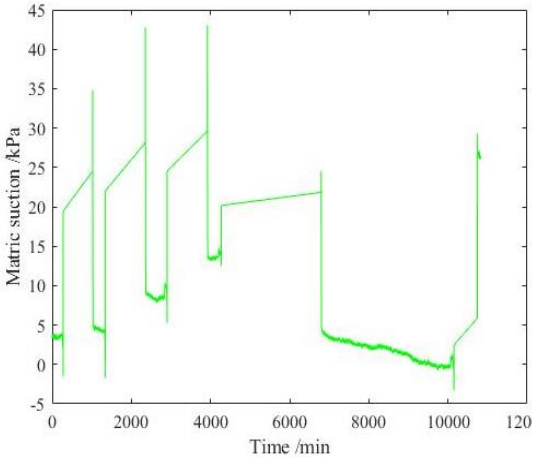

Figure 7.22 Matric suction variation of Unsat-MSL-35

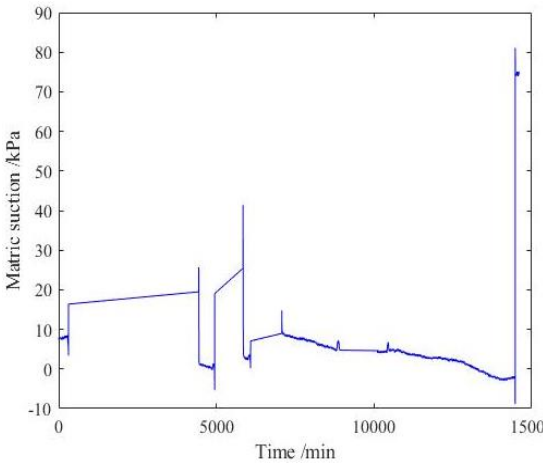

Figure 7.23 Matric suction variation of Unsat-MSL-65

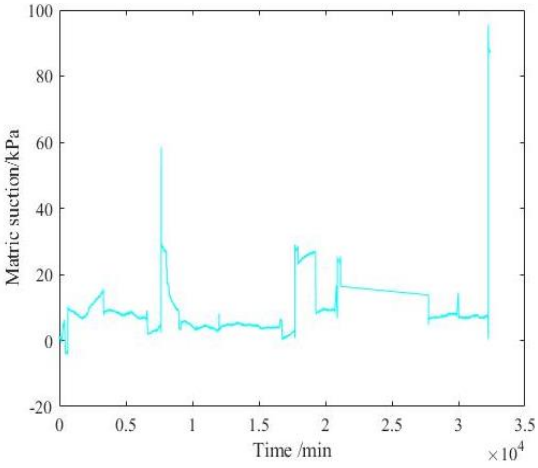

Figure 7.24 Matric suction variation of Unsat-MSL-115

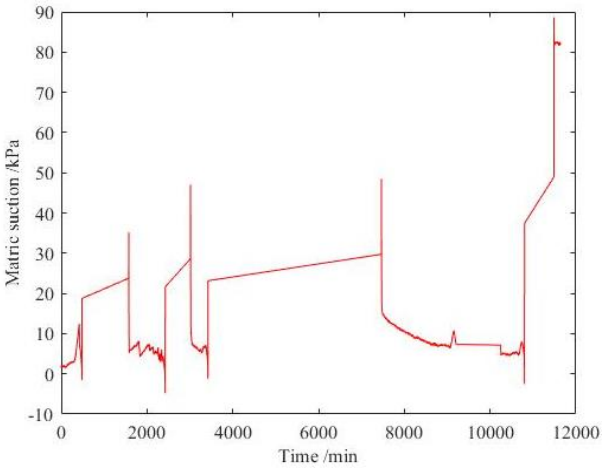

Figure 7.25 Matric suction variation of Unsat-MSL-215

7.7.2.3 Shear strength parameters

Based on the Mohr-Coulomb failure criteria, the failure envelope was determined. Then, the shear strength parameters were measured, as shown in Figure 7.26~Figure 7.27. With the decrease in moisture content, cohesion showed an upward trend. In both wetting and drainage processes, cohesion decreased. The friction angle did not show much difference, indicating no significant consolidation or swelling occurred. In terms of stress path parameters, C' and M were calculated through Eqs. (7.1)~(7.2). They presented a similar trend with cohesion and friction of angle, respectively.

$$C' = \frac{6c' \cos \phi''}{3 - \sin \phi''} \tag{7.1}$$

$$M = \frac{6 \sin \phi''}{3 - \sin \phi''} \tag{7.2}$$

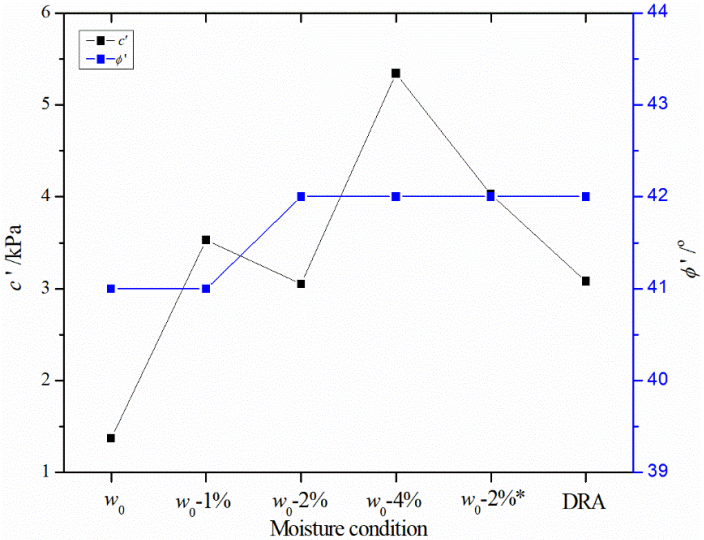

Figure 7.26 Effective friction angle and cohesion at each moisture content

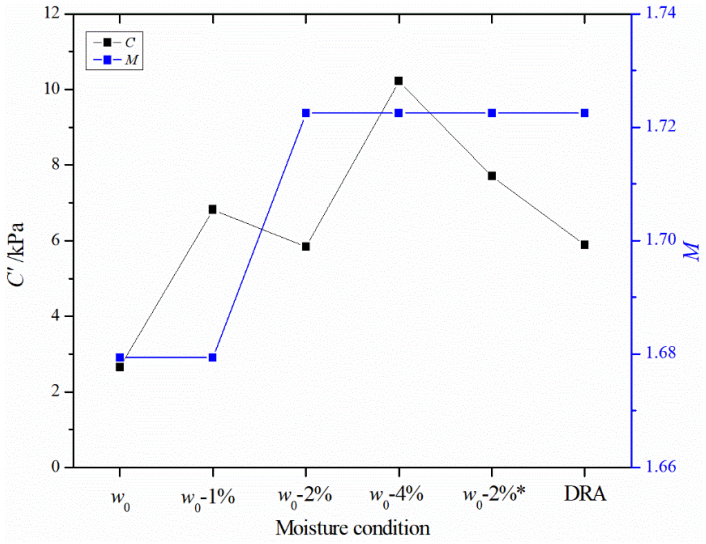

Figure 7.27 Stress path parameters for $q - p'$

7.7.2.4 Shearing strength and unloading modulus

Shear strength q_f from Unsat-SSL and MSL are presented in Figure 7.28 and Figure 7.29. In terms of test uncertainty, the test results from Unsat-SSL tests were compared with those from Unsat-MSL tests at w_0 (i.e. the same initial conditions). The two sets of data showed good agreement, with slight differences, indicating the good repeatability of these tests. q_f from Unsat-MSL tests showed a slight increase as moisture content decreased from w_0 to w_0-4% = w_3. Generally, the moisture variation within the range used did not significantly affect shear strength. To further validate the test results, the relative changes in q_f can be predicted. The prediction process was demonstrated as follows. Unsat-MSL-25 was taken as an example for analysis. From w_1 to w_4, initial σ_c' increased by 5 kPa (i.e. a 5 kPa suction increase according to Figure 5.5). The increase in q_f in Unsat-MSL-25 from w_1 to w_4 was $\left(q_f \text{ at } w_4 - q_f \text{ at } w_1\right)$, i.e., $(\sigma_c' \text{ at } w_4 - \sigma_c' \text{ at } w_1)\left(\tan^2\left(45^o + \frac{\phi'}{2}\right) - 1\right)$. Thus, the relative change of q_f to q_f at w_1 was $\frac{(\sigma_c' \text{ at } w_4 - \sigma_c' \text{ at } w_1)\left(\tan^2\left(45^o + \frac{\phi'}{2}\right) - 1\right)}{q_f \text{ at } w_1}$, where ϕ' =41°. Finally, the relative change of q_f in Unsat-MSL-25 from w_1 to w_4 was calculated as 18.7%, which was slightly lower than the measured value (about 20%) in Figure 7.29. This indicates the consistency between the measurements and theory. It should be noted that, in theory, for purely frictional materials, the relative changes in q_f would always be in proportion to effective confining pressure (σ_c').

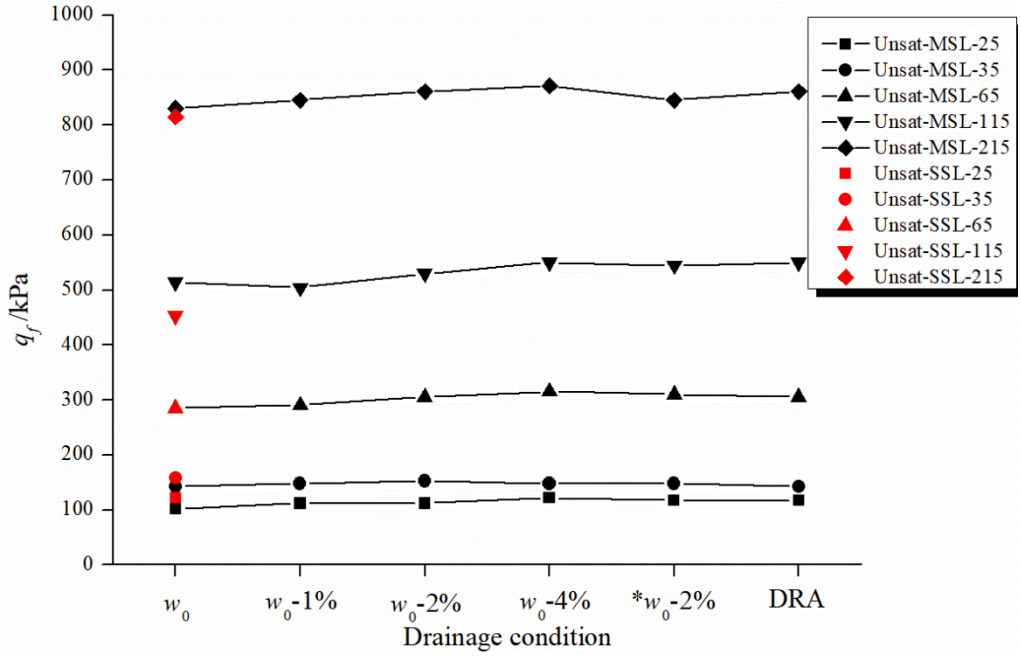

Figure 7.28 Shear strength q_f from Unsat-SSL and MSL tests

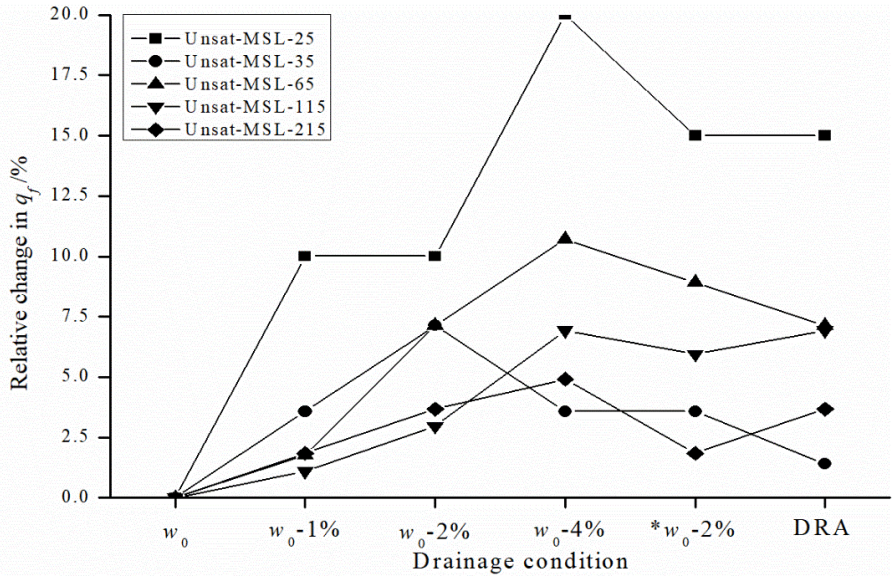

Figure 7.29 Relative changes in shear strength q_f from Unsat-SSL and MSL tests

E_{ul} increased with net confining pressure, as shown in Figure 7.30 and Figure 7.31. As the moisture content decreased from w_0 to w_0-4%, E_{ul} generally increased. Unloading modulus usually decreased a small amount with wetting. After a drying-wetting cycle, E_{ul} showed a decreasing trend. During the drainage process, E_{ul} at 25 and 35 kPa decreased while increasing at 65, 115 and 215 kPa. Although the changing trend of E_{ul} with free drainage (i.e. DRA) was not consistent at all the confining pressures, in unsaturated conditions, the benefit of drainage could still be anticipated in improving the soil performance at higher confining pressures. Compared with those under saturated conditions, E_{ul} under unsaturated conditions showed much larger

values. It indicates the positive effects of suction on soil stiffness.

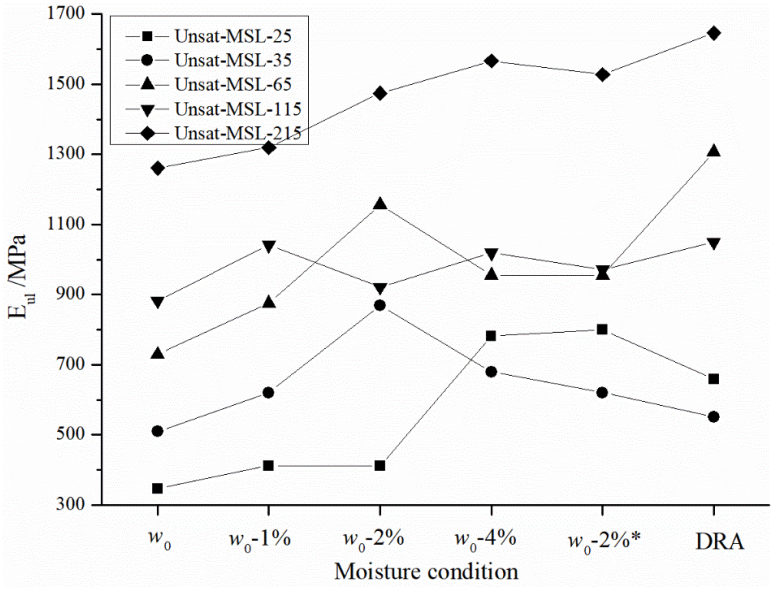

Figure 7.30 Unloading modulus E_{ul} at each moisture condition

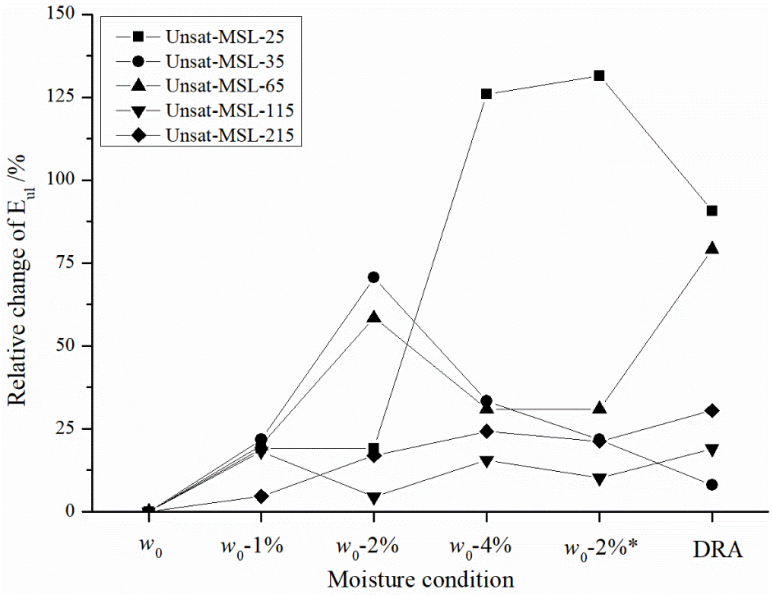

Figure 7.31 Relative changes in unloading modulus E_{ul} at each moisture condition

7.8 Pavement analysis

Since the triaxial stress path is different from that in the subgrade of real roads or railways, the modulus may be unrealistically high. However, E_{ul} values derived at $\sigma_{c,net}$ of 35 and 65 kPa in Unsat-MSL tests were adopted to demonstrate the drying, wetting and drainage effects on pavement response in a similar manner to those in Section 6.10, as presented in Table 7.5. It can also show the variability in results obtained using KENPAVE, and thus general observations can be made. Pavement analysis was conducted with KENPAVE to determine pavement response with an

unsaturated subgrade.

Table 7.5 Unloading modulus at 35 and 65 kPa under different moisture conditions

$\sigma_{c,net}$ /kPa	E_{ul} /MPa					
	w_0	$w_0 - 1\%$	$w_0 - 2\%$	$w_0 - 4\%$	$w_0 - 2\%$*	DRA
35	509.27	620.04	868.82	679.10	620.04	550.04
65	729.54	875.34	1155.73	954.91	954.94	1306.48

Note: * indicates the wetting stage.

7.8.1 Simulation scenarios

The same scenarios were followed as those in Chapter 6, with the variables presented in Table 6.8 (the scenario with a thick base only).

7.8.2 Simulation results

The maximum tensile/compressive strain (ε_t and ε_c), subgrade surface deflection and distress life are presented in Figure 7.32~Figure 7.34.

7.8.2.1 Strain

The tensile strain did not show large differences with the different moisture conditions, while the compressive strain showed a clear trend with the subgrade modulus due to moisture variation, as shown in Figure 7.32. During the drying stages (i.e. from w_0 to w_0-2%), the compressive strain decreased and then increased (from w_0-2% to w_0-4%). This is consistent with the variation of subgrade unloading modulus. The modulus at 35 and 65 kPa both showed an increasing trend from w_0 through to $w_0 - 4\%$, but there was a difference at the drying $w_0 - 2\%$* and at DRA – i.e. the modulus at 35 kPa showed a loss of modulus at later stages whereas the modulus at 65 kPa showed a continuing increase. This may indicate that the drainage effect at 35 kPa was not dominant compared with the previous wetting. Particularly, the curves under $\sigma_{c,net}$ of 35 and 65 kPa overlayed. During drainage, the water from the sample migrated through the HAEPD. Due to the low permeability of the HAEPD, the free drainage during shearing was significantly restricted compared to that which might be expected in situ. The effects of dynamic water movement could reduce the strength of soil and attenuate the benefit of drainage.

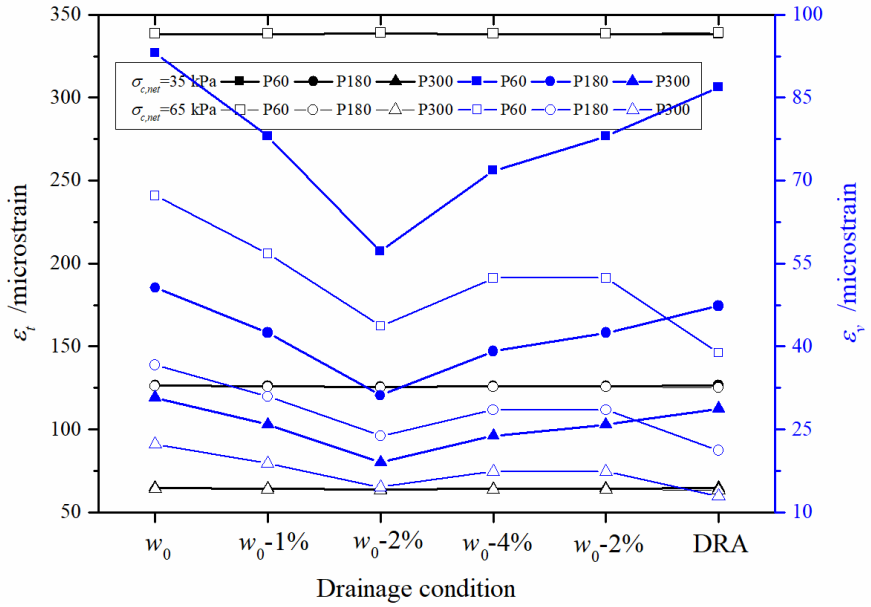

Figure 7.32 Maximum ε_c at the top of subgrade and ε_t at the AC bottom

7.8.2.2 Displacement

From Figure 7.33, the displacement of subgrade top varied between 0.025-0.07 mm. It showed a decreasing trend with decreasing moisture content and then increased with re-wetting. In terms of the whole drainage process, it showed a small downward trend. As the moisture increased by from $w_0 - 4\%$ to $w_0 - 2\%$, the displacement increased and was larger than that at $w_0 - 2\%$ during the drying phase, although the moisture content was the same. This may be caused by the wetting-drying hysteresis effects. Even though the drainage effect in the last cycle showed different trends in terms of different net confining pressure, it still revealed the positive effects due to drainage.

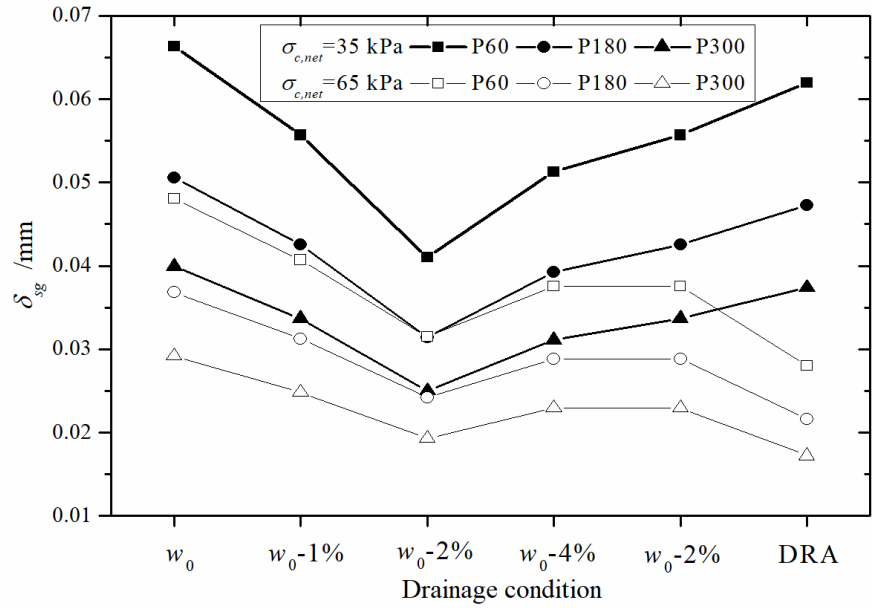

Figure 7.33 Vertical displacement at the top of the subgrade

7.8.2.3 Distress prediction

In terms of distress in Figure 7.34, the fatigue life did not exhibit clear variations, while the rutting life increased and then decreased in terms of $\sigma_{c,net}$ = 35 kPa. Generally, similar trend of distress life was found at $\sigma_{c,net}$ =65 kPa. It indicates the positive drying effects and the disadvantage of wetting. As Mallick et al. (2017) demonstrated, axle loads exceeding 80 kN could increase pavement damage. It may imply that the drainage process should be efficient and traffic loading should be restricted during severe rainfall or flooding due to their wetting effects (Elshaer, 2017; Mallick et al., 2017) in order to extend the pavement service life and reduce the damage.

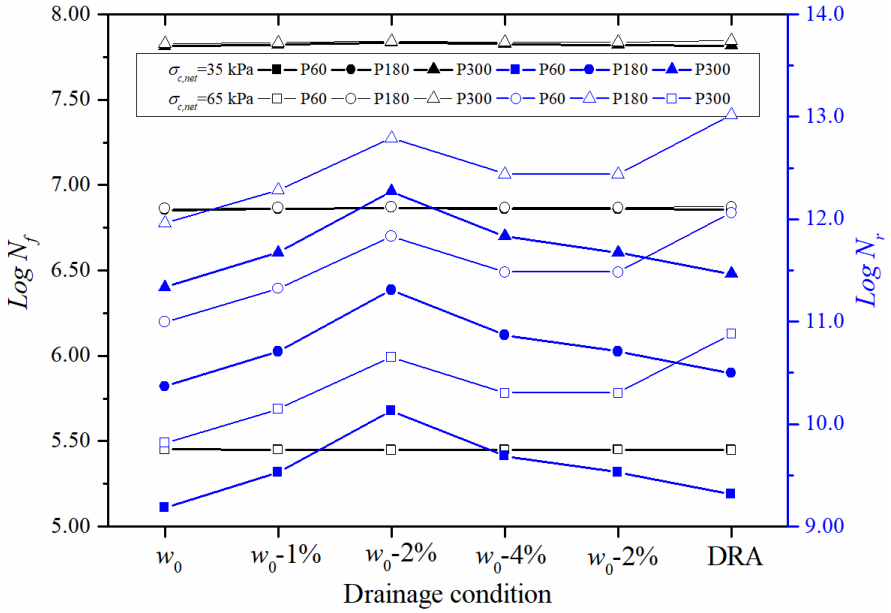

Figure 7.34 Fatigue and rutting life at each drainage condition

7.9 Summary and conclusions

This chapter has presented the results from unsaturated triaxial tests and multi-layered elastic analysis. Single-stage and multi-stage tests were conducted. The stress-strain behaviour, strength parameters and unloading modulus were investigated to reveal the effects of drying, wetting and drainage processes. The results were compared with those of the saturated triaxial tests in Chapter 6.

The peak shear strength generally showed an increasing trend with decreasing moisture content. The shearing behaviour with wetting varied at different net confining pressures. With wetting at lower net confining pressures, the peak shear strength slightly decreased (contrary to those at higher net confining pressures), increasing with drainage. The size of the hysteresis loop reduced, and the unload-reload loops became

stiffer, indicative of strain hardening at high axial strains.

The unloading modulus generally increased with the drying process while decreasing with wetting. After a drying-wetting cycle, the unloading modulus showed a decreasing trend. In the drainage process, the unloading modulus at 25 and 35 kPa decreased while increasing at 65, 115 and 215 kPa. The drying process positively affected pavement response, contrary to the wetting process. The wetting-drying hysteresis was also identified. The unloading modulus showed significantly larger values in unsaturated states than in saturated states.

The maximum tensile strain and fatigue life did not significantly differ with moisture variation. During the drying stages, the compressive strain and subgrade surface displacement generally showed a downward trend. With wetting and drainage, the strain increased. Predicted rutting life showed an opposite trend.

However, there still exist some limitations. The unloading modulus was used as an indicator to quantify subgrade stiffness, which is different from the actual resilient modulus of soils. Unloading modulus was calculated using laboratory triaxial tests, whilst the laboratory-controlled conditions were different from the in-situ conditions, e.g. stress states and moisture distribution. The subgrade modulus used for pavement analysis was significantly higher than those expected in-situ, so it is the general trend that has the most application to in-situ conditions.

CHAPTER 8 SUBGRADE BOX TESTS

8.1 Introduction

Based on the simulation analysis and triaxial tests, it was found that the foundation stiffness decreases due to the existence of more water while the rate of accumulation of permanent deformation increases. Road or railway foundations play a crucial role in maintaining infrastructure performance. However, a more realistic way of investigating subgrade response will improve the understanding of the response to and the management of water in the foundation and thus provide the basis for extending pavement/track life and improving service reliability. In-situ foundations are subject to more complex conditions than those applied in a controlled manner in unit cell laboratory tests. Therefore, in this Chapter, following the controlled laboratory triaxial tests, subgrade box tests were conducted to investigate foundation response to moisture variation under stress states that are more realistic. The aim is that these should serve as a more representative section of the structure in practice and provide theoretical references for better foundation settlement analysis and drainage design. The effects of increasing moisture contents on foundation settlement were studied at various stress levels and frequencies under repeated loading. The settlement under each condition was measured with a linear variable differential transformer (LVDT).

8.2 Theoretical framework

8.2.1 Modes of failure

For road and railway foundations, the constructed foundation depth is generally lower than its width, and thus they should be considered as shallow foundations (Terzaghi, 1943). Due to the imposed load, subgrade soil may be subject to three modes of soil failure: general shear failure, local shear failure and punching shear failure. The type applied in any particular case will depend on soil type, foundation size and depth. The general and local shear failure types are illustrated in Figure 8.1. The basic characteristics of each mode are summarized in Table 8.1.

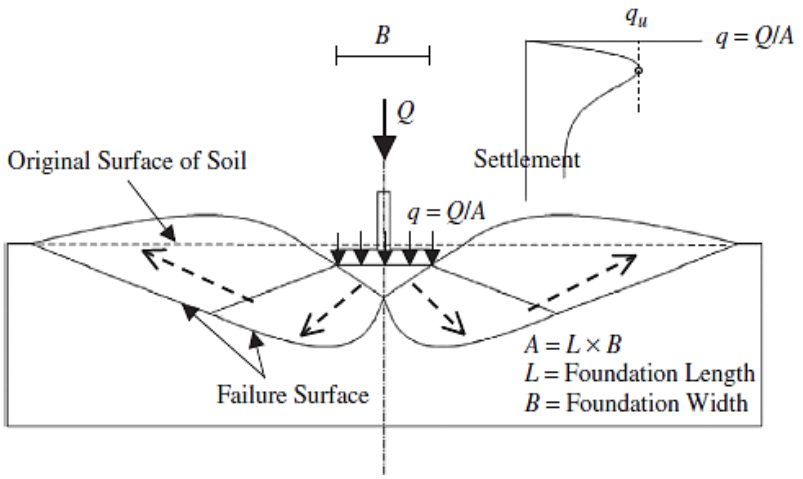

(a)

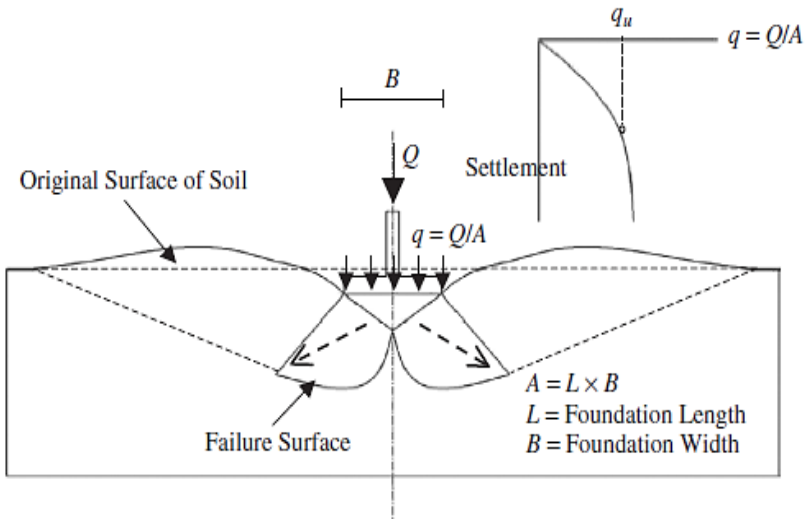

(b)

Figure 8.1 Shear failure modes: (a) general and (b) local (Helwany, 2007)

Table 8.1 Basic characteristics of failure modes (Helwany, 2007)

Modes of failure	Soil type	Failure surface
General shear failure	Dense sands, stiff clays	A distinctive peak in the pressure versus settlement curve
Local shear failure	Medium-dense sands, medium-stiff clays	A progressive failure surface lack of a distinct peak in the curve
Punching shear failure	Loose sands, soft clays	A triangular failure surface lack of distinctive ultimate bearing capacity

8.2.2 Bearing capacity

For subgrade soils, their bearing capacity should be determined so that the pavement/track can be designed so as to prevent excessive settlement. Based on plasticity theory, footing bearing capacity is commonly calculated using the bearing

capacity equation with sufficient accuracy, which accounts for the effects of soil cohesion, surcharge, and soil unit weight in an uncoupled manner by simply superimposing the three terms that reflect these factors (Meyerhof, 1963; Loukidis & Salgado, 2009). The ultimate bearing capacity, q_u (derived from a continuous foundation that generates general shear failure) is expressed as (Terzaghi, 1943)

$$q_u = c'N_c + qN_q + \frac{1}{2}\gamma B N_\gamma \tag{8.1}$$

where c' is the cohesion intercept of soil, q is the overburden pressure at foundation depth ($q = \gamma D_f$), γ is the unit weight of soil, D_f is the foundation depth, B is the foundation width and N_c, N_q and N_γ are non-dimensional bearing capacity factors that are all functions of the soil friction angle, ϕ'.

Adapting Eq. 8.1 gives the bearing capacity under a circular load, as (Meyerhof, 1961)

$$q_u = 1.3c'N_c + qN_q + 0.3\gamma B N_\gamma \tag{8.2}$$

The factors of theoretical bearing capacity are given by (Prandtl, 1920)

$$N_c = (N_q - 1)\cot\phi' \tag{8.3}$$

$$N_q = e^{\pi tan\phi'}\tan^2\left(45^o + \frac{\phi'}{2}\right) \tag{8.4}$$

In terms of N_γ, equations proposed by Meyerhof (1963) (Eq. (8.5)), Hansen (1970) (Eq. (8.6)) and Vesić (1973) (Eq. (8.7)) are widely known, expressed, respectively, as follows.

$$N_\gamma = (N_q - 1)\tan 1.4\phi' \tag{8.5}$$

$$N_\gamma = 1.5(N_q - 1)\tan\phi' \tag{8.6}$$

$$N_\gamma = 2(N_q + 1)\tan\phi' \tag{8.7}$$

When the foundation experiences eccentric and inclined loading, the foundation bearing capacity can significantly decrease due to the loading conditions (Meyerhof, 1963). In this study, the effects of roughness between the soil and the foundation are not considered for simplicity.

8.2.3 Permanent deformation model

In Chapter 2, the permanent deformation models were reviewed and discussed. According to their advantage and disadvantages, the regression analysis method in Section 2.3.4 (i.e. Eqs. (2.47) and (2.48)) was adopted to develop the deformation prediction model due to its simplicity and for convenience. In addition, the models

included in the layer-wise summation method were used as a reference for the main factors influencing subgrade deformation. Water-induced distresses have been widely identified as significant (as demonstrated in Section 2.2 of Chapter 2). The effects of loading cycles on subgrade deformation have also been broadly studied (as demonstrated in Section 2.3.4 of Chapter 2). By considering the objective of the project, i.e. to determine the effects of stress level and moisture content on subgrade deformation development, three main factors were recognized, i.e. the number of load repetitions, moisture content and optimum moisture content.

8.3 Test apparatus

Subgrade box tests were performed with the steel box designed by Fei (2015). It was manufactured to fit the specific MAND loading machine. The basic properties of the subgrade box are presented in Table 8.2.

Table 8.2 Basic properties of subgrade box and soil specimen

Property	Subgrade box	Soil specimen
Length, mm	450	450
Width, mm	200	200
Height, mm	300	230
Thickness, mm	4	-
Material	Case-hardened steel	-

Considering that the natural subgrade, in practice, has low stiffness, a 13 mm-thick rubber sheet (McDowell et al., 2004; Lim et al., 2005) was installed underneath the compacted foundation soil. The rubber sheet had low elastic modulus and, hence, a high degree of deformability and generally showed non-linear stress-strain behaviour (Zakeri et al., 2021). Whether or not to use the rubber sheet to line the sides of the box was determined based on the coefficient of variation using repeatability tests (Section 8.6). The repeatability tests indicate that the box tests were repeated with and without side rubber (Section 8.6), respectively. Then, their test results with and without side rubber were compared to determine the consistency of the results. The condition (with or without sider rubber) facilitating higher test consistency was selected for further testing. From Sol-Sánchez et al. (2015), the effective stiffness modulus of the rubber was discussed. Tested at 5 Hz with plate loading, the static and dynamic bearing modulus of a 20 mm-thick rubber were 7 and 17 MPa, respectively. The testing system is illustrated in Figure 8.2 and Figure 8.3. It includes the PC equipped with software to

apply loading and log data, a loading frame with a hydraulic actuator and an LVDT installed on the top of the frame to measure subgrade settlement and subgrade box. On the top of the subgrade soil, a wooden board was placed to spread the cyclic load and was covered with aluminum foil tape to prevent moisture migration. The side walls were not lubricated but covered with cling film (used in the lab) to protect the steel wall (which may provide some lubrication effects). The dimension of the wooden board is 200×148×57 mm. The subgrade soil underneath the loading platen is 230 mm in thickness. Although the area stressed in the box tests are much smaller than would be stressed in a road or railway foundation by the truck or train loading, nevertheless the area of loading is much larger than the grain size of the subgrade soil under test so should still be representative of subgrade loading.

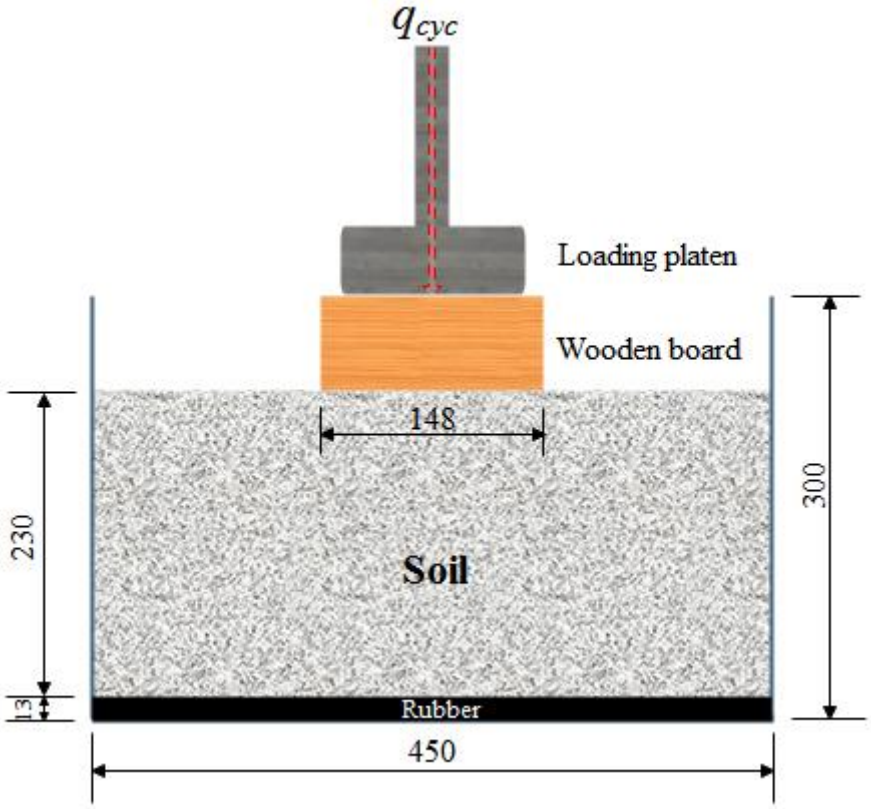

Figure 8.2 Schematic diagram of subgrade box tests

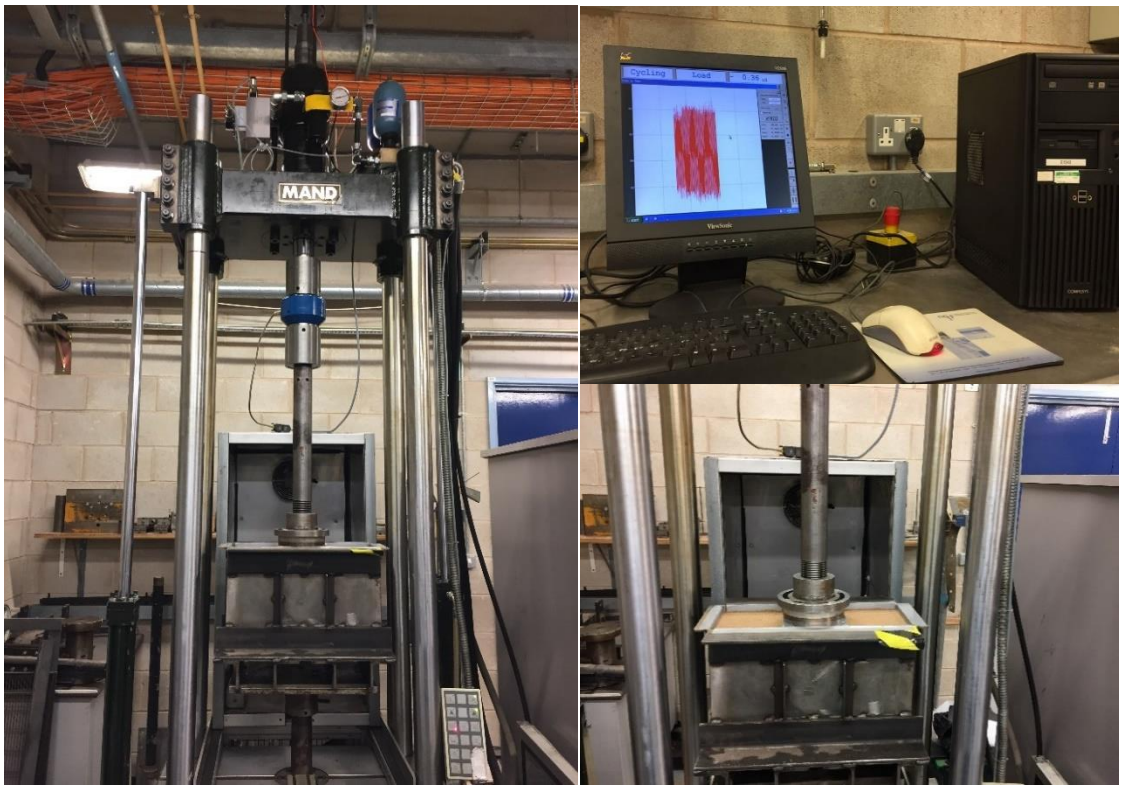

Figure 8.3 Box test apparatus

8.4 Preparation of testing specimens

In practice, density maximization is crucial in developing the soil's full strength, stiffness and potential to resist permanent deformation. When in the condition of optimum moisture content, the easiest compaction can be performed to reach a particular density, or the maximum density will be acquired for a specific compaction effort (Thom, 2008). Thus, to achieve the maximum dry density of subgrade soils, construction specifications universally require that the soils be compacted at (or near) optimum moisture content in practice. The basic properties of the test soil are presented in Chapter 5. The soil is characterised as silty sand.

The subgrade thickness permitted in the box was 230 mm. Initially, moist tamping was performed in order to prepare the subgrade. All soil specimens (the same silty sand used in the triaxial tests) were compacted at optimum moisture content w_{opt}. 36 kg of oven-dried soil was divided into fifths and each fifth was mixed with a specific amount of water to reach w_{opt}. Then the specimen was sealed in a bucket for 24 hours to reach moisture equilibrium. Using a Proctor rammer, it was then manually compacted layer by layer with the same amount of soil each time to reach an equal thickness throughout of 46 mm so as to achieve maximum dry density. Compacting each layer separately

ensures that the specimen obtains a uniform density throughout its depth. The top of the specimen was levelled by hand to secure close contact between the soil and the loading platen. The wooden platen was placed on top of the soil at the centre of the box. A bubble level was also placed on the top of the soil to ensure that the loading platen was completely level, as shown in Figure 8.4.

Figure 8.4 Test specimen after compaction

8.5 Test program

8.5.1 Research process

Based on the subgrade box test, the effects of cyclic stress, loading frequency and moisture content on subgrade settlement were studied. The purpose of the study was to develop an understanding of drainage significance at increasing moisture contents. The research process is illustrated in Figure 8.5. It should be noted that the model development remains to be conducted, which was included to show a full picture of the related study.

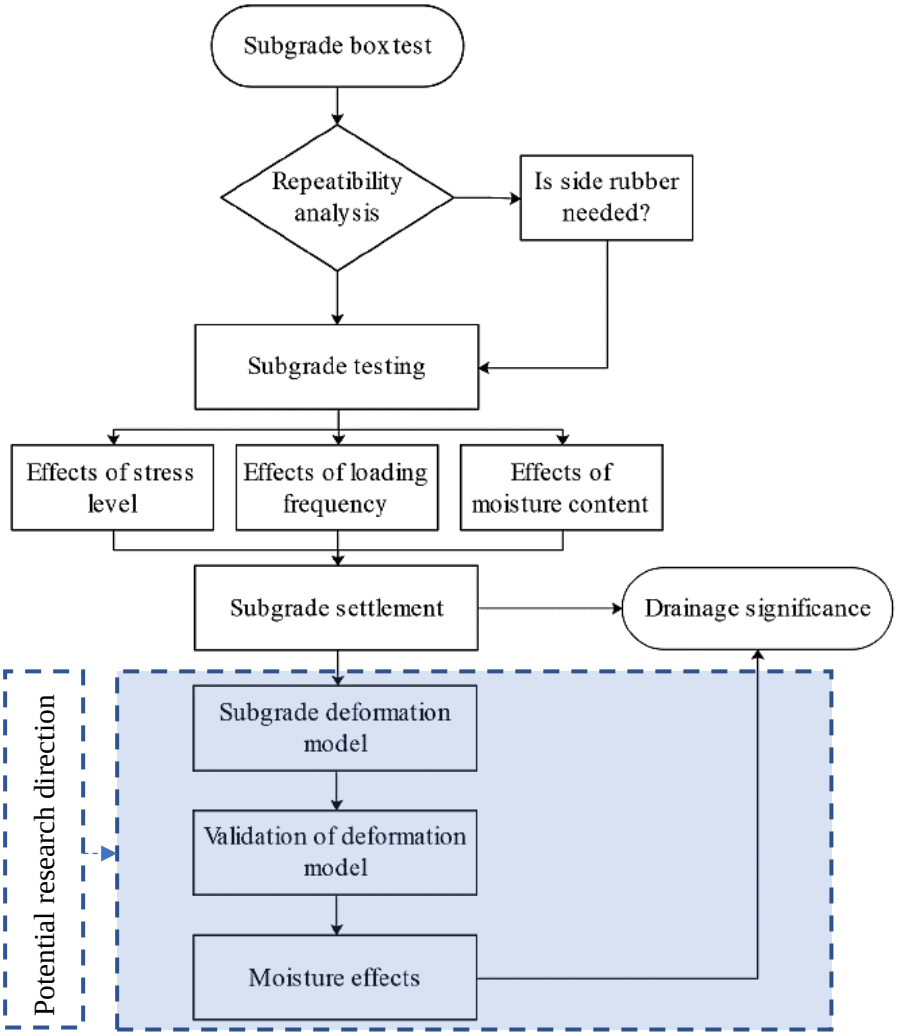

Figure 8.5 Research process for subgrade box tests (Note: potential research direction is not included)

8.5.2 Moisture content

To investigate the effects of moisture content on subgrade settlement, various moisture levels were designed for each test, which ranged from w_{opt} to w_{opt}+4%. The soils were arranged in the same state of compaction and therefore, the moisture content had to start at optimum, but drying the box was not practical. In the subgrade box tests, the wetting process was focused on, i.e. the moisture content was increased up to w_{opt}+4%. The wetting process was performed to simulate the in-situ situation by which subgrade soils constructed at the OMC gradually move towards a saturated state (due to rainfall infiltration, as simulated in the tests described here, and/or absorption of water from the groundwater table below), which is a more critical condition for road/railway structures. Thus, the moisture conditions were different from those in Chapter 7. Before the loading board was positioned into the soil, a specific amount of

water was added to the top of the soil specimen to reach the target moisture content. Then, the specimen was left to absorb the water. Section 8.7.2.1 showed that the actual water distribution was highly non-uniform. However, the tests were intended to simulate what might happen in reality, not achieving a uniform distribution.

The OMC for the soils used is 10.5% by mass, and the saturated moisture content (SMC) is 18.9%. Based on the difference, a series of MCs were adopted for subgrade box tests, including w_1 (w_{opt}), w_2 (w_{opt}+1%), w_3 (w_{opt}+2%), w_4 (w_{opt}+4%) (i.e. 10.5%, 12.5%, 13.5% and 14.5%). By this means, the aim is to cover the range of moisture content that foundation soils experience. Based on visual inspection and the water depth measurement (only under w_{opt} +4% condition), the time for water absorption into the soil was determined, i.e. 12 h for w_{opt}+1%, 24 h for w_{opt}+2% and 3 days for w_{opt}+4%. Excess water would remain on the soil top if testing were to be performed at the saturation moisture content and that might cause hazards if spilled on adjacent electrical apparatus. Thus, considering the laboratory safety guide and the limit of the loading apparatus, the saturation condition was not simulated.

8.5.3 Cyclic loading

Prior to each test, a conditioning stage was performed to maintain close contact between the soil and the wooden board. For conditioning loads, the maximum pressure q_{con} was selected as 10 kPa/0.286 kN and the seating stress was 3.5 kPa/0.1 kN. The number of loading repetitions N was set as 500. A low conditioning load and cycles were applied in case a large settlement was caused prior to the main cyclic loading.

Based on the results presented in Chapter 6, the effective friction angle and cohesion derived from consolidated drained tests were adopted, i.e. 11.2 kPa and 41˚, respectively. Using Eq. (8.1) and Eqs. (8.3)~(8.7), the relevant parameters and the bearing capacity were calculated, as shown in Table 8.3.

Table 8.3 Calculated bearing capacity of subgrade soils

Parameter	Meyerhof (1963)	Hansen (1970)	Vesić (1973)
N_c	93.7	93.7	93.7
N_q	85.37	85.37	85.37
N_γ	139.31	110	150
q_u, kPa	1358.4	1313.5	1374.7
$0.5q_u$, kPa	656.8	687.4	679.2

The applied foundation pressure should not exceed the bearing capacity of the subgrade soil. With regard to an unbound pavement composed of uniform materials, it would be a reasonable design for 10^6 load applications to limit the applied pressure to approximately 50% of q_u (Thom, 2008). For the tests in this study, the number of loading repetitions was limited to 10^5 applications so as to complete the tests in a reasonable timeframe. Three cyclic stress levels were selected 50, 100 and 150 kPa, in order to reveal the deformation's dependency on stress states. All of these were well within the $0.5q_u$ limit. Based on the calculation result in Chapter 5, the maximum compressive stress that the subgrade experienced was about 160 kPa, and from the study of Rahim (2005), a typical in-situ subgrade compressive stress can be 37 kPa. Based on the calculation results by Dai & Van Deusen (1998) and Rose et al. (2011), it is determined that 150 kPa could generally cover the typical maximum in-situ stress to be expected in a rail subgrade due to train load. Another reason for keeping the stresses much less than the calculated $0.5q_u$ limit is that since multi-stage testing is conducted, it is preferred not to cause too much deformation in the earliest stages that might compromise the behaviour in the later stages, and third reason is that the specimen is progressively wetted. Thus, the $0.5q_u$ limit is expected to reduce as the specimen gets wetter. The highest frequency, f, that could be reached reliably by the machine is 5 Hz. For road pavements, it represented a vehicle speed, dependent on the contact tire radius, of about 18 km/h (Huang, 2004). For railway tracks, it represents a train speed lying between 36 and 54 km/h, the speed depending on the combination of rail segment and subgrade. These are slightly lower than those expected in real roads and railway subgrades, but not exceptionally so.

8.6 Repeatability test

Considering the testing scale, stress distribution and water boundary condition, box tests are expected to be more realistic than laboratory-controlled triaxial tests on studying the foundation response. To assess the repeatability of this particular test, it was performed both with and without side rubber lining inside the box to see whether or not the results were consistent. Thus, the applicability, or not, of side rubber was determined. The repeatability was evaluated by the coefficient of variation, c_v. Compared with the standard deviation, s_d, c_v is a normalized indicator independent of specific units. c_v is expressed as:

$$c_v = \frac{s_d}{\bar{\delta}_{s,i}} \tag{8.8}$$

$$s_d = \sqrt{\frac{1}{N_{bt}} \sum_{i=1}^{N_{bt}} (\delta_{s,i} - \bar{\delta}_{s,i})^2} \tag{8.9}$$

$$\bar{\delta}_{s,i} = \frac{\delta_{s,1} + \delta_{s,2} + \cdots + \delta_{s,N}}{N_{bt}} = \frac{1}{N_{bt}} \sum_{i=1}^{N_{bt}} \delta_{s,i} \tag{8.10}$$

where $\delta_{s,i}$ is settlement of test i, $\bar{\delta}_{s,i}$ is arithmetic mean settlement of $\delta_{s,i}$ and N_{bt} is the number of box tests. A lower coefficient of variation indicates higher repeatability.

8.6.1 Repeatability test procedure

The repeatability tests were conducted in the subgrade box. All the specimens had an initial moisture content of 10.5 %. Following the specimen preparation procedure as described in Section 8.4, an as-nearly-as-possible identical dry density was achieved for each test. The bottom rubber was used in all the tests. The cyclic stress was selected as 50 kPa in order to represent one of the stress levels and applied for 10^5 cycles.

Three tests were performed without side rubber and three tests with side rubber. When used, the 3 mm-thick rubber sheets were installed between the soil and side walls, and thus a continuous non-solid surrounding soil environment was provided. In other respects, the same testing procedures and conditions were carefully followed for all the repeatability tests. The test details are presented in Table 8.4. The notation is as follows: 'RT' represents repeatability tests, the first number is the specimen ID and the second number indicates the test sequence.

Table 8.4 Details of repeatability tests

Test ID	Stage	F_{min} /kN	F_{max} /kN	q_{cyc} /kPa	f /Hz	N	w /%
-	Conditioning	0.1	0.286	10	5	500	w_1
RT1-1	Cyclic loading Without side rubber	0.1	1.43	50	5	10^5	w_1
RT1-2		0.1	1.43	50	5	10^5	w_1
RT1-3		0.1	1.43	50	5	10^5	w_1
RT2-1	Cyclic loading With side rubber	0.1	1.43	50	5	10^5	w_1
RT2-2		0.1	1.43	50	5	10^5	w_1
RT2-3		0.1	1.43	50	5	10^5	w_1

8.6.2 Repeatability test results

The results are presented in Figure 8.6 and Figure 8.7. From Figure 8.6, it is evident that the tests without side rubber showed greater consistency. The settlement of

subgrade with cyclic loading showed a similar upward trend for all specimens, but the results with side rubber exhibited a significant difference between the two tests. For RT1 with side rubber, the settlement versus loading cycles was asymptotic to a constant. When the side rubber was used, the water migrated into the gap between the rubber and the box wall possibly due to the increased excess pore water pressure caused by cyclic loading. This could cause interference with the moisture condition of the specimen, especially when extra water was added to the specimen to increase the moisture content. The results and basic calculations are summarised in Table 8.5. The s_d value decreased when no side rubber was installed. c_v in tests with side rubber was three times larger than that in the tests without side rubber. Thus, the tests without side rubber showed higher repeatability and consistency. Thus, the testing results without side rubber were more reproducible. For this reason, side rubber was not used for subsequent box tests.

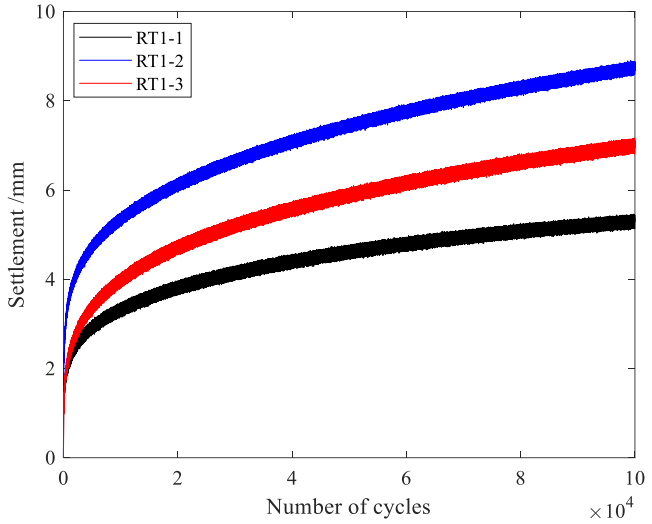

Figure 8.6 Subgrade settlement without side rubber

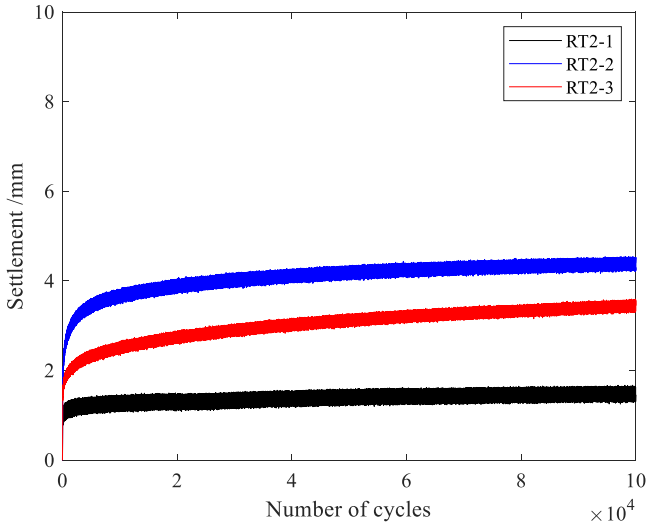

Figure 8.7 Subgrade settlement with side rubber

Table 8.5 Repeatability test results and calculations

Test ID	Side rubber	δ_s /mm	$\bar{\delta}_s$ /mm	s_d /mm	c_v
RT1-1		5.192			
RT1-2	Without	6.731	6.795	1.336	24.07%
RT1-3		8.462			
RT2-1		1.200			
RT2-2	With	4.267	2.907	1.563	53.75%
RT2-3		3.254			

8.7 Subgrade box test

8.7.1 Test procedure

Since the side rubber was not used, the side walls were not lubricated but were covered with cling film (used in the lab) to protect the steel wall (which may provide some lubrication effects). Once the soil had been prepared and installed as described in Section 8.4, the box was lifted into its place inside the MAND frame. Cyclic loading was applied through the MAND's hydraulic actuator. The test started with the conditioning stage for 500 cycles and then the contact was checked through visual inspection and software readings. The box test stage was initially conducted with a moisture content of 10.5%; subsequently, more water was added to bring the specimen to the next moisture content level. Then, the test was conducted at that increased moisture content. When the test finished, post-test moisture content was checked by coring with a sampling tube to see the moisture distribution due to wetting and cyclic loading throughout the thickness. The coring specimen was sliced into ten pieces representing different layers from top to bottom. The calculated moisture content was taken as an average value to estimate the moisture distribution.

The test details are shown in Table 8.6. Each box test includes a conditioning stage and several cyclic loading stages. The cyclic loading was applied at each moisture condition, and the moisture content incrementally increased by surface wetting after each cyclic loading stage (except the last). F_{max} is the notation indicating the upper limit of the loading force corresponding to q_{cyc} and F_{min} is the lower limit (i.e. the seating force) to maintain the contact between the soil specimen and the loading platen. In terms of the test ID, 'BT' represents box test, the first number indicates the specimen ID and the second number indicates the test sequence.

Table 8.6 Box test details

Test ID	Stages	F_{min} /kN	F_{max} /kN	q_{cyc} /kPa	f /Hz	N	w /%
-	Conditioning	0.1	0.286	10	5	500	w_1
BT1-1	Cyclic loading	0.1	1.43	50	5	10^5	w_1
BT1-2		0.1	1.43	50	5	10^5	w_2
BT1-3		0.1	1.43	50	5	10^5	w_3
BT1-4		0.1	1.43	50	5	10^5	w_4
BT2-1	Cyclic loading	0.1	2.86	100	5	10^5	w_1
BT2-2		0.1	2.86	100	5	10^5	w_2
BT2-3		0.1	2.86	100	5	10^5	w_3
BT2-4		0.1	2.86	100	5	10^5	w_4
BT3-1	Cyclic loading	0.1	4.28	150	5	10^5	w_1
BT3-2		0.1	4.28	150	5	10^5	w_2
BT3-3		0.1	4.28	150	5	10^5	w_3
BT3-4		0.1	4.28	150	5	10^5	w_4
BT4-1	Cyclic loading	0.1	1.43	50	1	5000	w_1
BT4-2		0.1	1.43	50	2	5000	w_1
BT4-3		0.1	1.43	50	5	5000	w_1
BT4-4	Cyclic loading	0.1	1.43	50	1	5000	w_2
BT4-5		0.1	1.43	50	2	5000	w_2
BT4-6		0.1	1.43	50	5	5000	w_2
BT4-7	Cyclic loading	0.1	1.43	50	1	5000	w_3
BT4-8		0.1	1.43	50	2	5000	w_3
BT4-9		0.1	1.43	50	5	5000	w_3
BT4-10	Cyclic loading	0.1	1.43	50	1	5000	w_4
BT4-11		0.1	1.43	50	2	5000	w_4
BT4-12		0.1	1.43	50	5	5000	w_4

8.7.2 Test results and discussion

Photos taken after finishing each test are presented in Figure 8.8. After cyclic loading, the top of the subgrade soil showed a similar failure mode. The soil on both sides of the wooden platen was uplifted and always showed a clear pattern similar to that seen in Figure 8.8a. Thus, it was apparent that the failure surface developed to the top and was confined to the near-surface zone, which could be evidence of soil dilation.

The soil underneath the centre went down, which was the source of the recorded settlement.

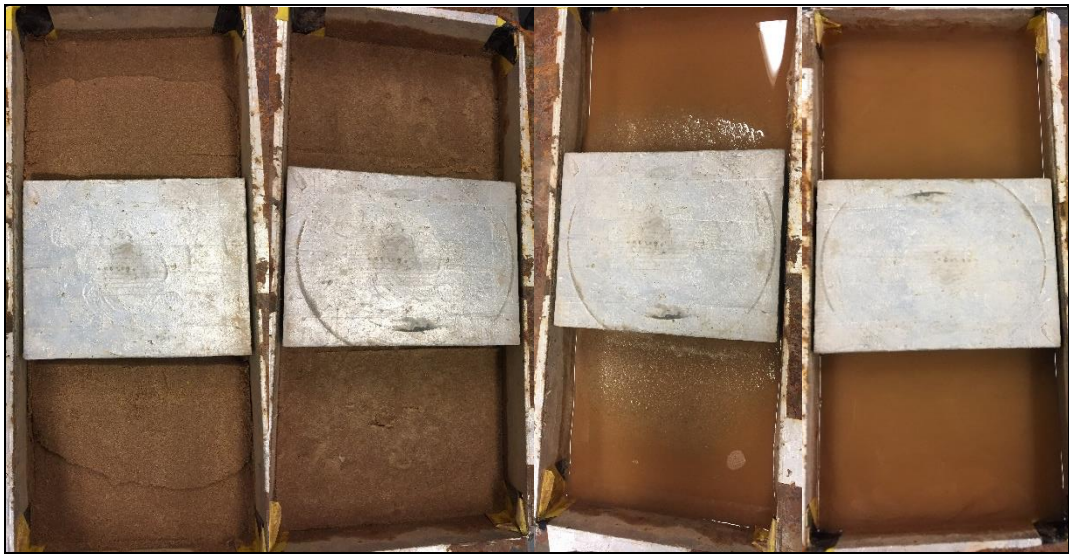

(a) (b) (c) (d)

Figure 8.8 Photos of subgrade box tests with increasing w from left to right

8.7.2.1 Moisture content variation

From Figure 8.8, it can be seen that moisture showed different distribution patterns at different initial moisture contents with cyclic loading. These results were based on sampling at the end of the test. The moisture distribution of undisturbed samples was not monitored. When adding 1% water, it was absorbed and migrated downward directly. Thus, at w_{opt} and $w_{opt} + 1\%$, no extra water was seen on the top. At $w_{opt} + 2\%$, the top of subgrade was flooded before loading, and then the water penetrated the soil due to cyclic loading. Figure 8.8c shows that the soil top appeared as the water level decreased, and fine particles were lifted into the water. As can be seen in Figure 8.8d, at its wettest condition, the top of the subgrade was totally flooded all the time and loosened fine soil particles were found on the top. The observed water level drop during cyclic loading may indicate that it is impractical to keep the surface of a subgrade at a constant water content. The observations may also imply that the water will not soak into the soil when the moisture content is more than a specific value (e.g. 12.5% in this study) without mechanical mixing or the application of external water pressure. At higher nominal moisture contents, the cyclic loading will cause consolidation and the water will be expelled from the soil, which was indicated by the fine particles carried in water on the surface after loading. Under in-situ conditions, a foundation would possibly be flooded when severe rainfall occurred (particularly railway foundations

covered only by highly permeable ballast), which is critical to the performance of the road and railway structures.

General surface moisture states are presented in Figure 8.8, but that figure left the moisture distribution with foundation depth unclear. Therefore, coring was conducted to check the moisture content. The moisture content sampling plan is illustrated in Figure 8.9. From top to bottom, ten points in total were selected to determine the trend of moisture content distribution without and with cycling, respectively. It is intended to represent the moisture condition before and after the test, accordingly. Particularly, in order to reduce the disturbance to the specimen, the moisture profile at the start of the test was estimated from a profile taken at the end of the test (i.e. #1~#10), but remote from the centre where the cyclic load was imposed so as to limit the effect that may have been caused. Since the wetting time (i.e. overnight, ~24 hours) was much larger than the loading time (i.e. 5.5 hours), it is assumed that this would reflect a similar moisture content to what might have been the situation with wetting and no cyclic loading. The moisture profile as a result of wetting and loading was estimated from the centre (i.e. #11~#20) beneath the 'sleeper' position once cyclic loading was complete. Typical results of such moisture content checks are shown in Figure 8.10~Figure 8.13 for tests at $q_{cyc} = 100$ kPa. The depth of the middle of each layer was selected to represent each layer when plotting the curve of mositure content versus depth. It should be noted that the soil surface was covered with water and saturated, while this was not included in Figure 8.12 and Figure 8.13.

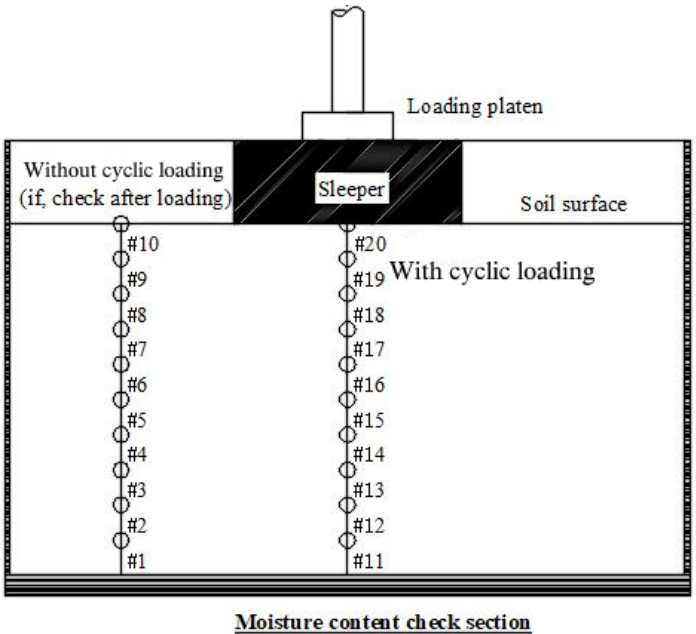

Figure 8.9 Schematic diagram of moisture content check method

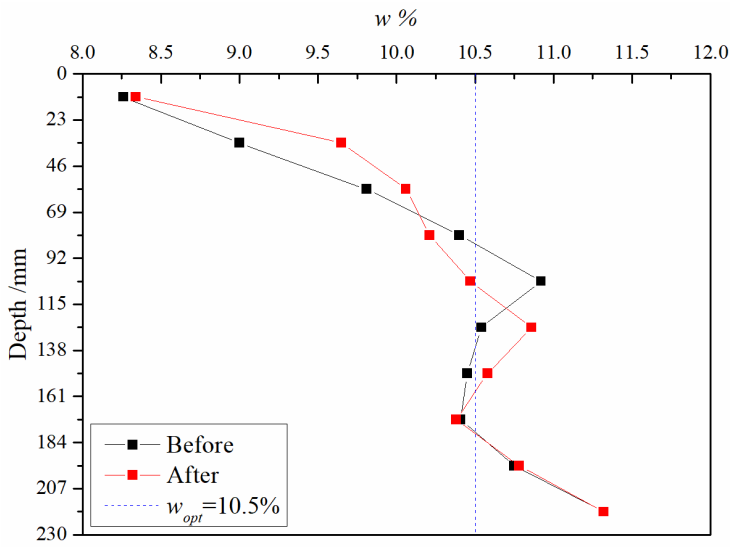

Figure 8.10 Moisture variation at w_{opt}

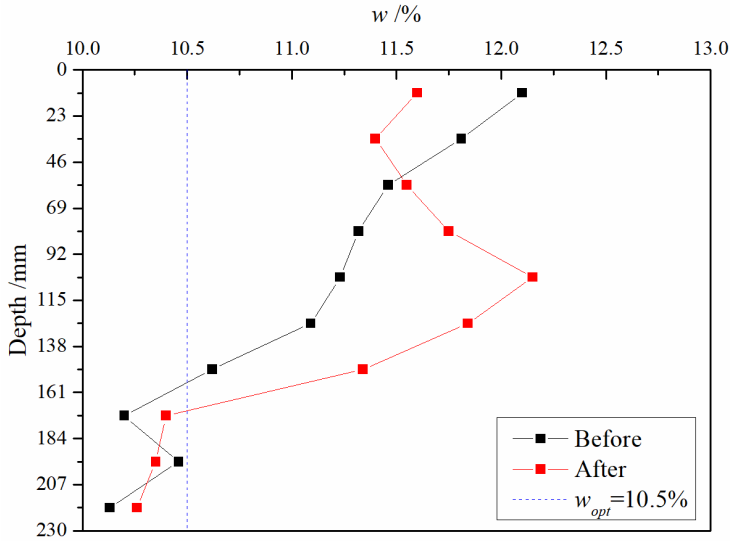

Figure 8.11 Moisture variation at $w_{opt} + 1\%$

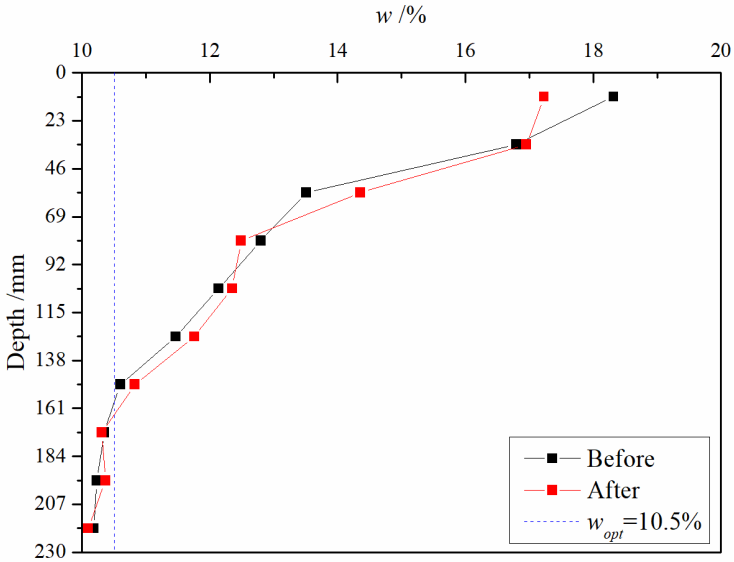

Figure 8.12 Moisture variation at $w_{opt} + 2\%$ (It should be noted that the soil surface was saturated)

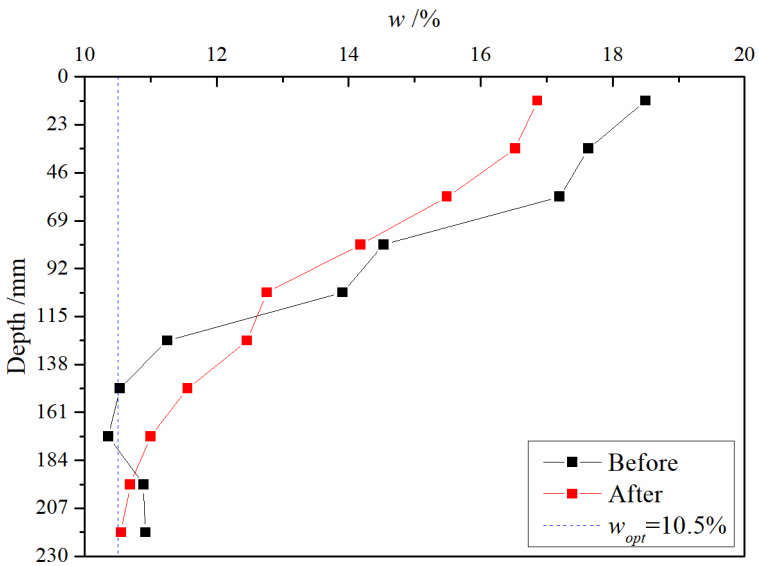

Figure 8.13 Moisture variation at $w_{opt} + 4\%$ (It should be noted that the soil surface was saturated)

The moisture content increased with the depth at w_{opt}, while showing an opposite trend with depth compared with that at $w_{opt} + 1\%$, $w_{opt} + 2\%$ and $w_{opt} + 4\%$. The specimen was highly compacted and thus, it was difficult for water to migrate downward overnight by gravity due to the low permeability. General variation of moisture content ranged within 1% before and after the test, while the moisture content below 172.5 mm from the surface did not show clear variation after cyclic loading. The moisture content in the top 46 mm showed a downward trend, and it might have been an effect of coring. Figure 8.10 shows an opposite trend in moisture content distribution compared to other tests, possibly due to evaporation from the surface when exposed to laboratory warmth. During coring, a coring tube was used to take a cylinder soil through the depth. However, it was noticed that water was squished out as the tube went downward and when the soil was removed from the tube. Thus, moisture loss occurred, which may have led to a lower moisture content measured than expected. Since the soil top was still saturated and covered with water at $w_{opt} + 2\%$ and $w_{opt} + 4\%$, extra (free) water was carefully removed before coring. During coring, the specimen also experienced extrusion, and this may cause water migration. It is also found that the variation of moisture content with depth before the test was different from after the loading. Since the loading time was relatively short, this could be mainly attributed to loading rather than suction and gravity. From all the figures, it can be seen that after a depth of about 161 mm, the moisture content remained constant and the same as the initial value. Due to the high degree of compaction, the soil experienced wetting within

a limited depth, e.g. <~160 mm from the top - the wetting due to water penetration occurred only within a limited depth.

8.7.2.2 Effects of moisture contents

The variation of settlement with moisture content is presented in Figure 8.14~Figure 8.16. It should be noted that the moisture contents in the figures were their nominal values due to the complex moisture distribution of soils. The settlement developed progressively with cyclic loading, apart from the tests at w_{opt} under a q_{cyc} of 50 and 100 kPa which converged to an asymptote. It can be seen that the settlement showed a significant increase as moisture content increased. Settlement showed a substantially larger increase from $w_{opt} + 1\%$ to $w_{opt} + 2\%$ than that from w_{opt} to $w_{opt} + 1\%$. It could be related to the reduced soil suction as the water table level increased on the top of the soil. When the soil top was flooded, the effective stress decreased, and the buoyancy could uplift the particle to show less strength. Since the moisture content showed a larger variation in the upper half of the test box after adding water, the increased settlement would have been mainly induced by the reduced strength of the upper layers. This finding about the sudden settlement is also in agreement with the study by Ionescu (2004).

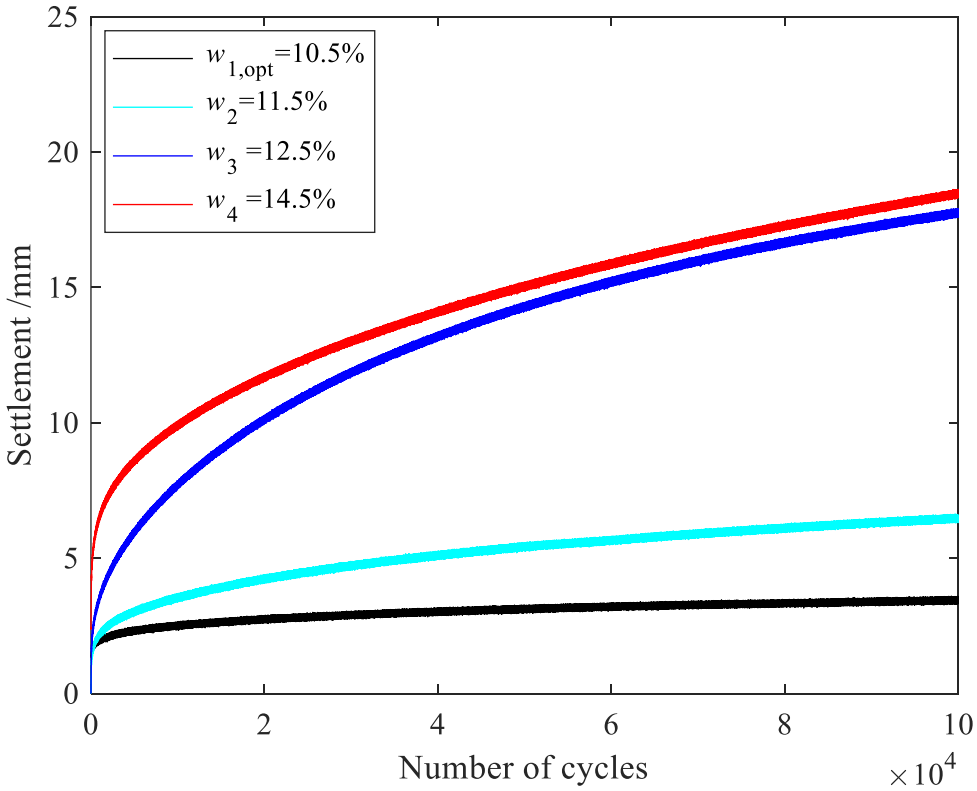

Figure 8.14 Settlement with moisture at 50 kPa

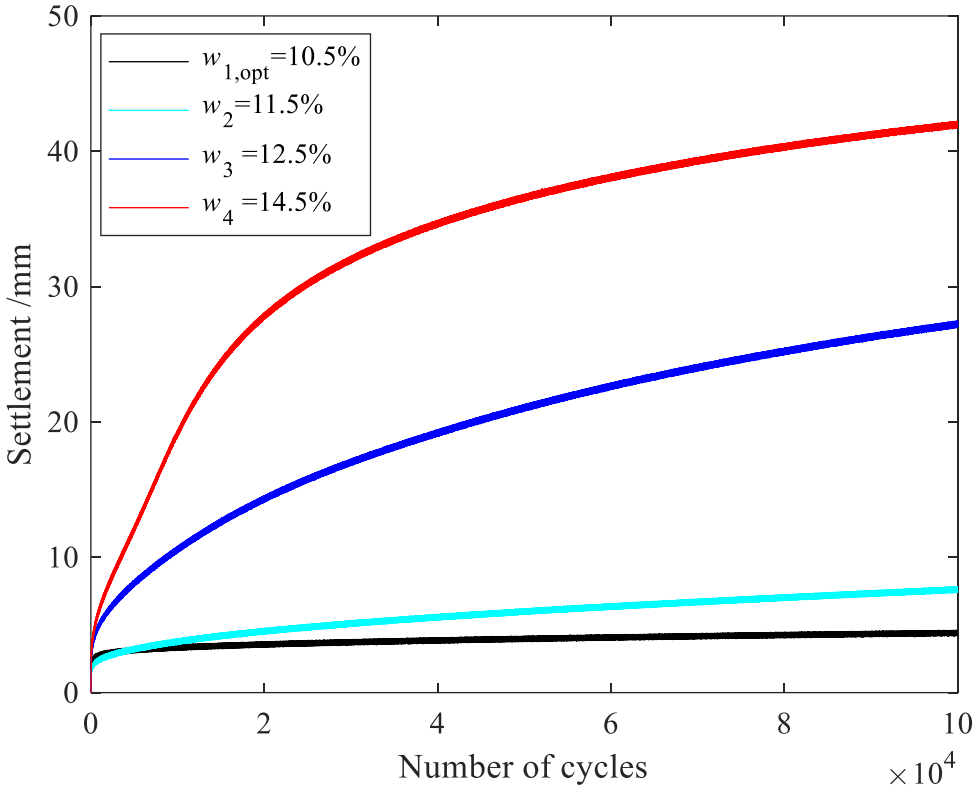

Figure 8.15 Settlement with moisture at 100 kPa

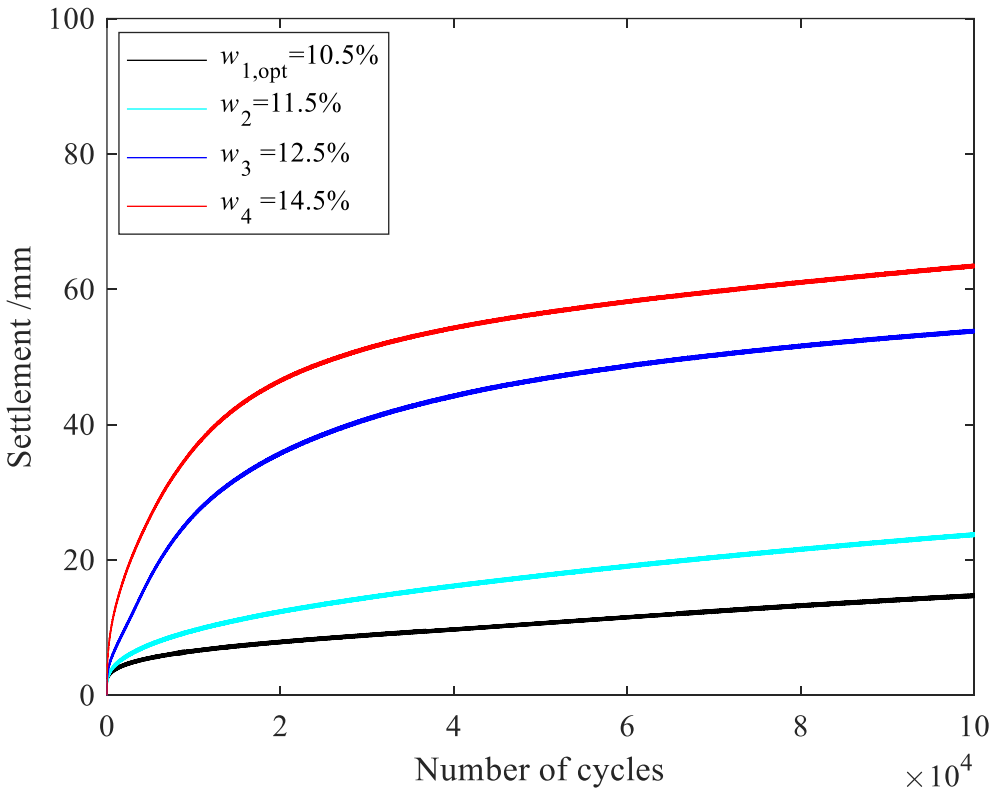

Figure 8.16 Settlement with moisture at 150 kPa

8.7.2.3 Effects of stress levels

The variation of settlement with cyclic stress is presented in Figure 8.17~Figure 8.20. With the increase of cyclic stress, the settlement showed an upward trend at various moisture levels. At w_{opt} and w_{opt}+1%, settlement showed clear but slight increase with q_{cyc}varying from 50 to 100 kPa. At higher moisture contents, it indicates that the increase of the cyclic stress imposed larger effects on subgrade settlement, which also reveals the effect of moisture content consistent with the previously summarized results. Therefore, for regions with frequent flooding, it might be necessary to set weight limits for vehicles on the pavement in order to prevent the development of severe distresses. At w_{opt}, the effect of extra stress was significant (compare 150 kPa result with 100 kPa result in Figure 8.18), but wetting caused all the tests to give a similar or greater settlement when w increased to w_{opt}+ 2%.

Thus, a permitted moisture content-applied dynamic load (i.e. $w-\sigma_d$) envelop might be possible, and a schematic illustration is shown in Figure 8.21. Thus, at the target moisture content (w_t), an allowable loading stress could be estimated. From Figure 8.21, σ_d was considered allowable for Point A ($\sigma_{d,aol}$), threshold for Point B ($\sigma_{d,thr}$) and excessive for Point C ($\sigma_{d,exc}$). In practice, the dynamic stress from vehicles should be maintained so as to be within the envelope. A concept of this envelope is proposed here, and further study is needed to determine and verify its precise position.

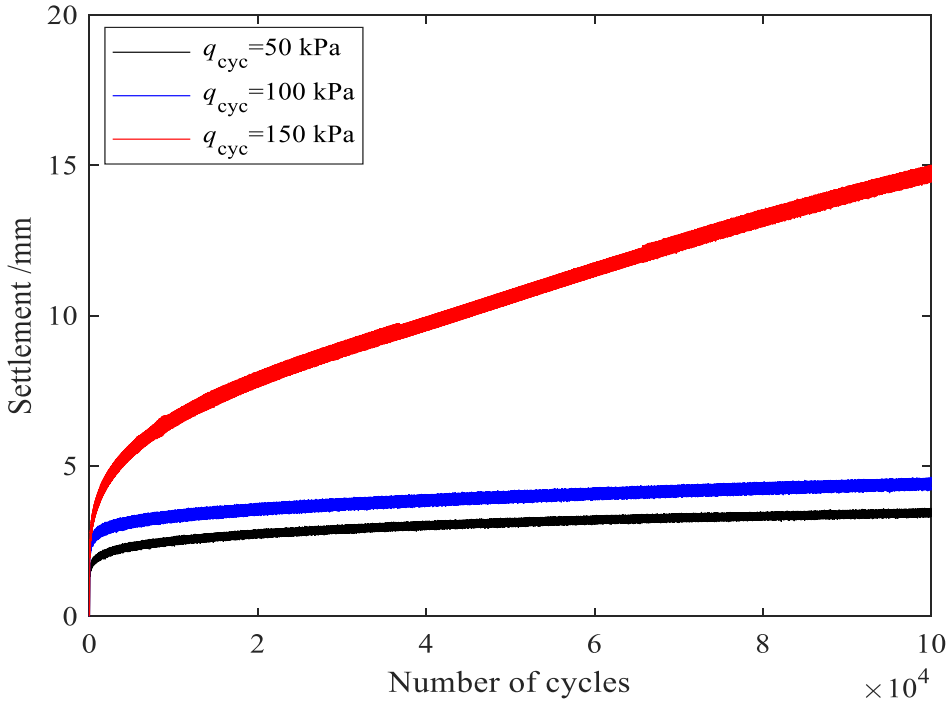

Figure 8.17 Settlement with stress level at w_{opt}

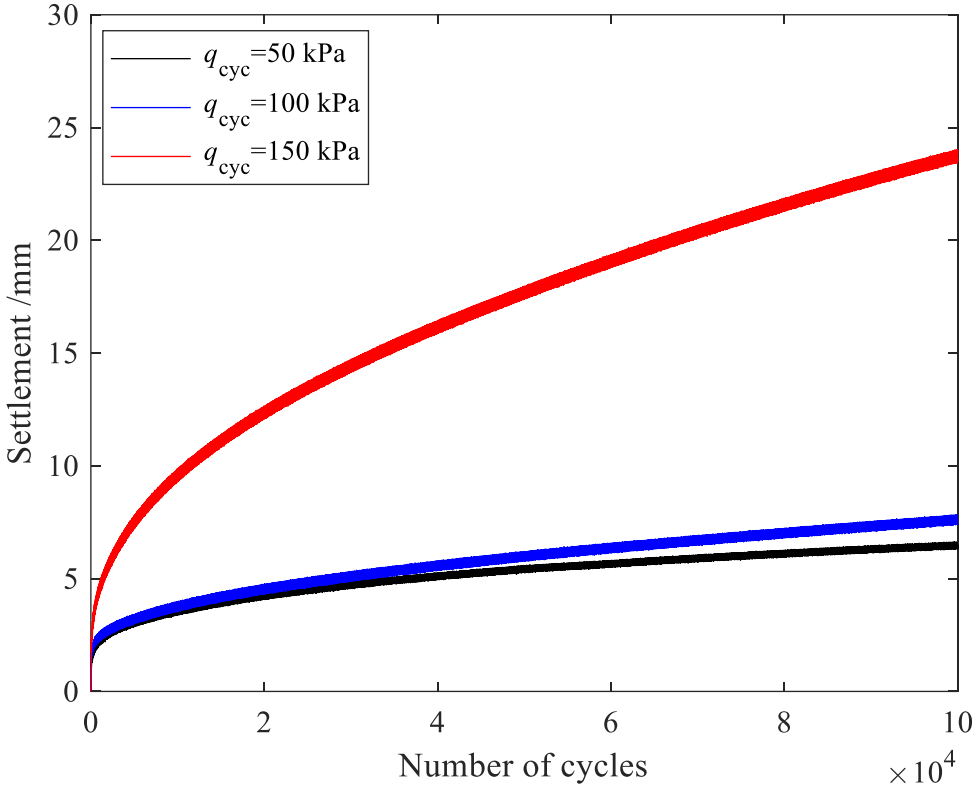

Figure 8.18 Settlement with stress level at w_{opt}+1%

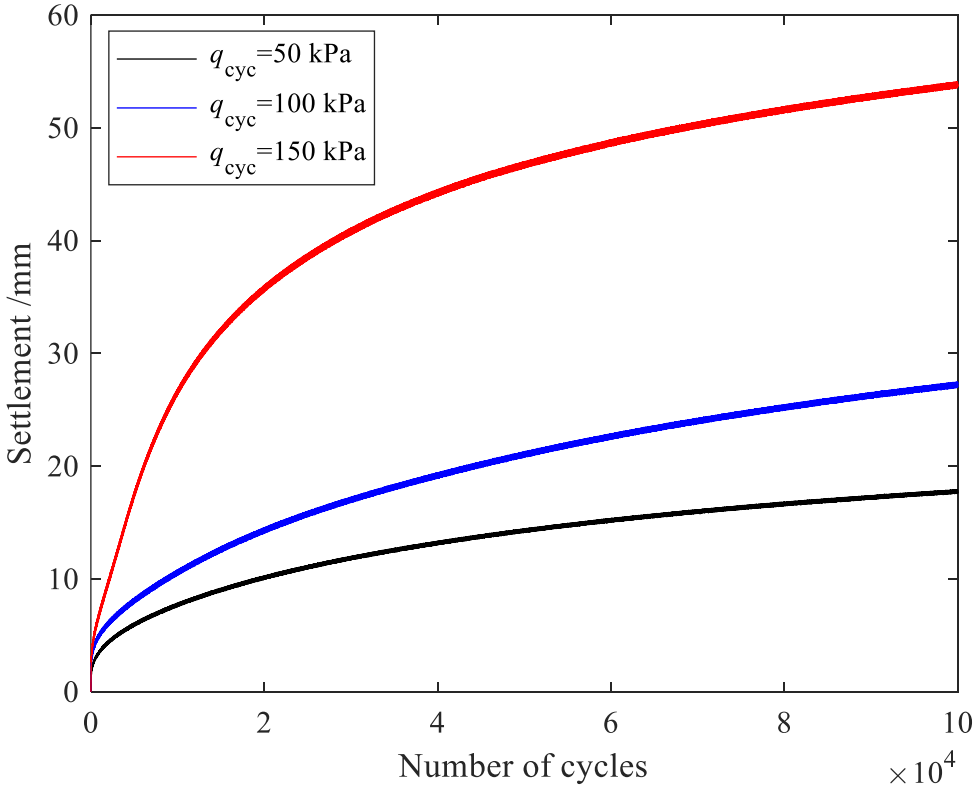

Figure 8.19 Settlement with stress level at w_{opt} + 2%

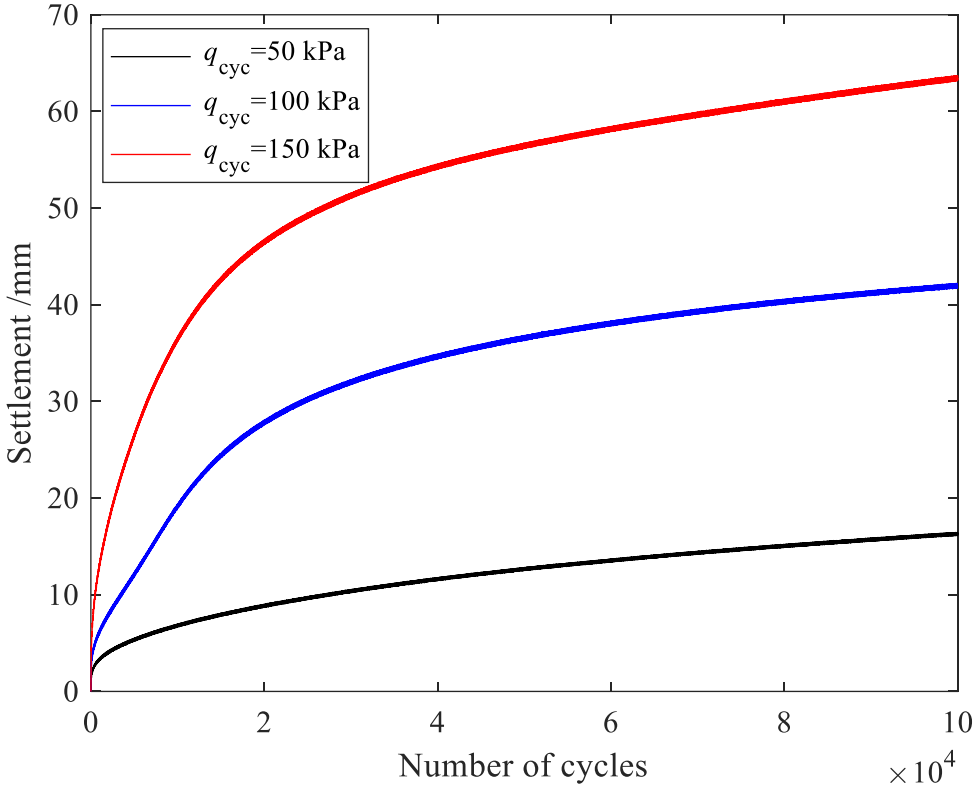

Figure 8.20 Settlement with stress level at w_{opt} + 4%

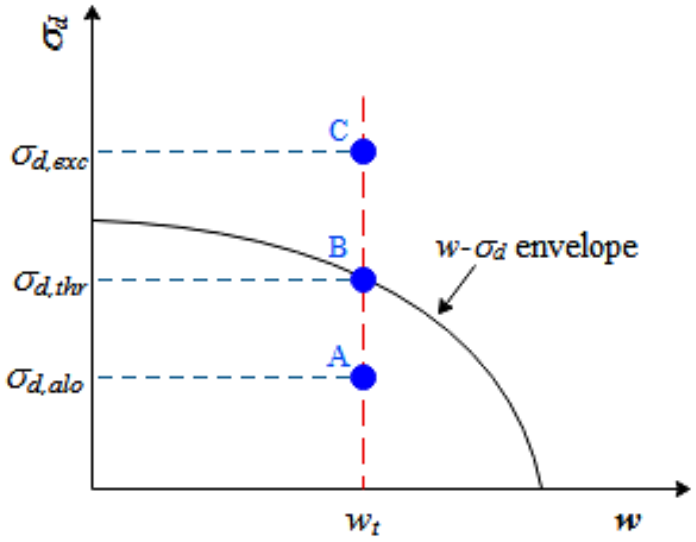

Figure 8.21 Schematic illustration of the wetting-load envelope

8.7.2.4 Effects of loading frequencies

The variation of settlement with increased loading frequency is presented in Figure 8.22~Figure 8.25. Three frequencies were adopted to study its effects on the settlement: 1, 2 and 5 Hz (limited by the capacity of the loading machine). For each stage, the

number of loading repetitions was 5000. The test results obtained at a constant frequency (f) of 5 Hz (i.e. BT1-1~4) were also incorporated in each figure in order to further reveal the frequency effects on the settlement. In terms of the multistage process with f from 1 to 5 Hz, as the frequency increased, the settlement did not show a clear variation in the development trend. Even though there was a step when the new frequency of 5 Hz started in Figure 8.22, the rate of strain development quickly became similar to the previous frequency responses. Thus, it suggests that the loading frequency may not impose significant effects on the strain response under low loading repetitions (e.g. 5000 cycles for each frequency in this study). However, for the whole process, the settlement at the multistage frequencies showed much lower values compared to that at the constant f of 5 Hz. The accumulation rate of settlement was larger at a constant f of 5 Hz, and the effects of loading frequency were enhanced at higher moisture contents. With further cyclic loading, the settlement could progressively develop. It indicates that higher frequency accelerated the development of subgrade settlement; consequently, rutting life is expected to be reduced.

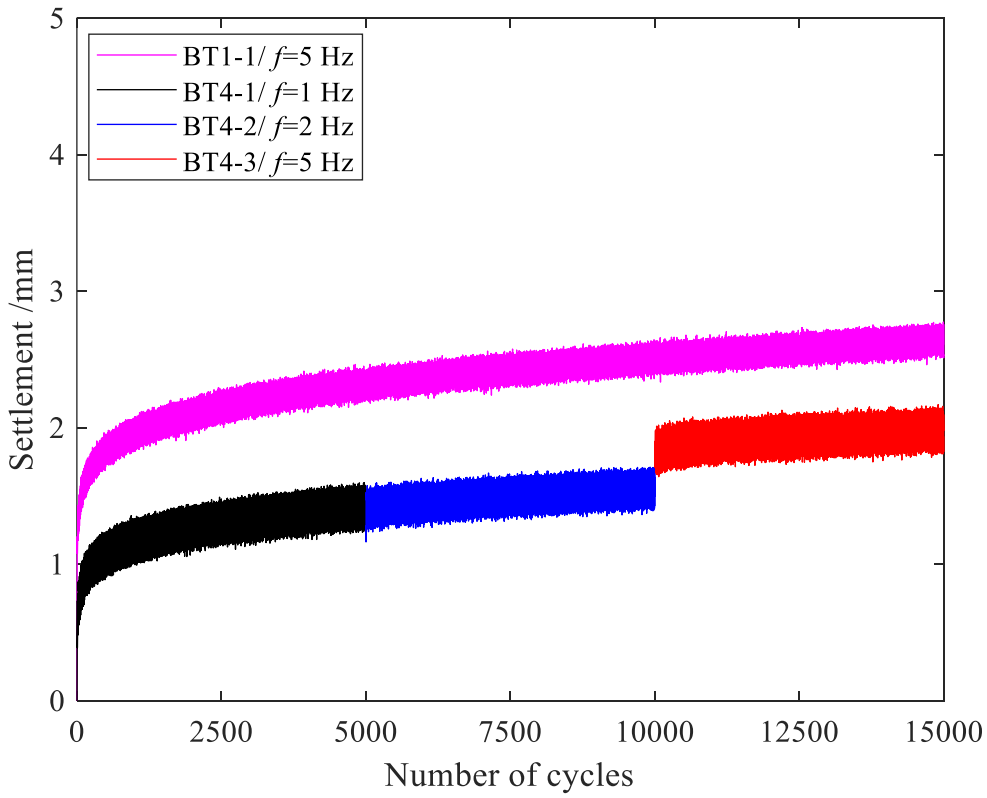

Figure 8.22 Settlement with frequency at w_1

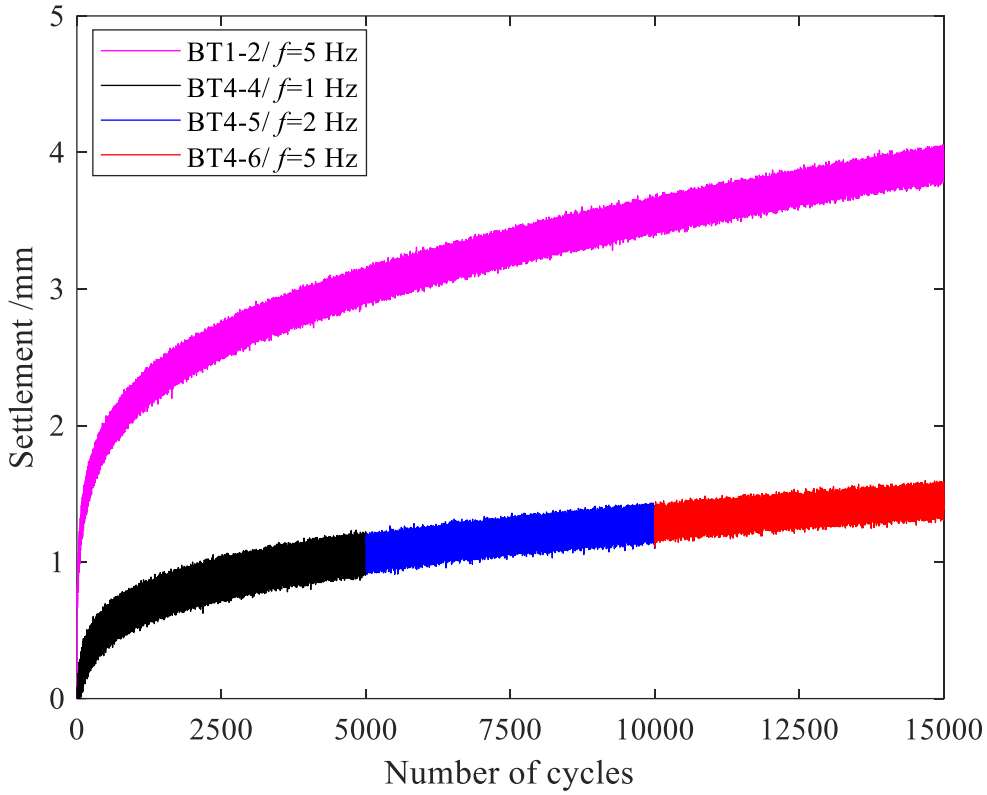

Figure 8.23 Settlement with frequency at w_2

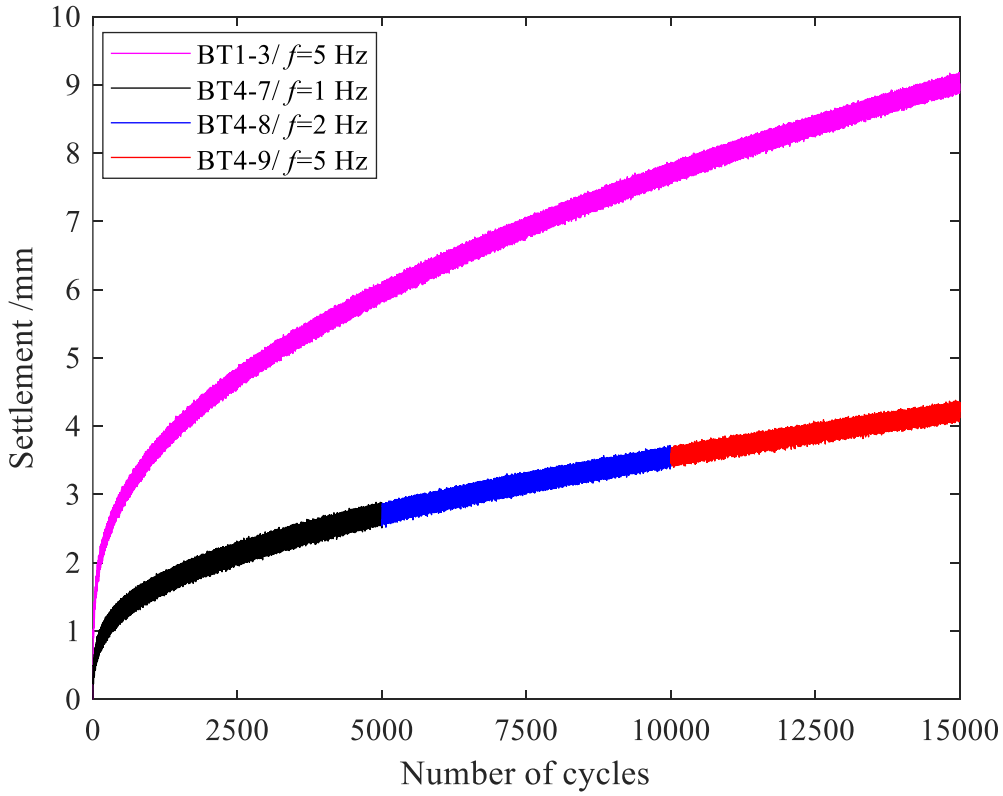

Figure 8.24 Settlement with frequency at w_3

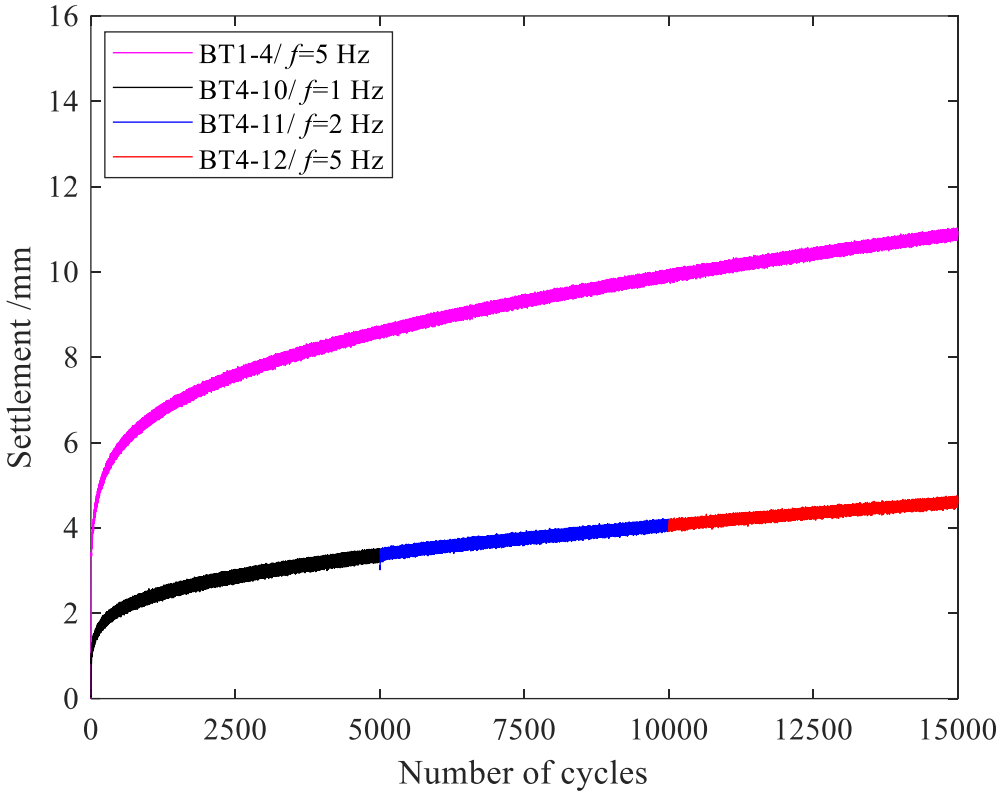

Figure 8.25 Settlement with frequency at w_4

8.7.2.5 Discussion

The test results and related calculations for the subgrade box tests are tabulated in Table 8.7 and Table 8.8. The lower limit of the curve was adopted to quantitatively demonstrate the test results. From Table 8.7 at q_{cyc}=100 kPa, settlement increased by 907.15% when moisture content varied from w_{opt} to w_{opt} + 4%, i.e. when increasing moisture content by 4%. In terms of frequency in Table 8.8, after allowing for the initial development of settlement, subgrade settlement did not show an increase after the same number of repetitions with subsequent increases in frequency. The rate of development was greater at the constant f of 5 Hz compared to that at the end of the multistage sequence for the same f, which can be seen from the difference in the slopes of the curves. If the response is characterized in terms of the settlement rate (δ_s/N), the δ_s/N from the single stage tests was generally 2~7 times higher than that at the end of the multistage sequence. This difference may be attributed to the fact that, at low f, the multistage tests allowed some conditioning that compacts the specimen without building up pore water pressures, or that the threshold deviator stress of subgrade decreased due to the increase of f (Liu & Xiao, 2010). The settlement accumulation at

the constant f of 5 Hz was larger after 15000 cycles, as shown in Table 8.8. It may indicate that an increase in loading frequencies caused a higher deformation rate of the subgrade. This was in agreement with the study by Liu & Xiao (2010) and Chen et al. (2014).

Table 8.7 Summary of test results at increasing moisture content

q_{cyc}	w /%	I_c	f /Hz	N /cycle	δ_s /mm	$\Delta\delta_s$ /mm	$\Delta\delta_s/\delta_s$ /%
50	w_1	1.870	5	10^5	3.254	-	-
	w_2	1.685			6.287	3.033	93.21
	w_3	1.500			17.604	12.87	395.51
	w_4	1.130			18.438	15.18	446.50
100	w_1	1.870	5	10^5	4.142	-	-
	w_2	1.685			7.396	3.254	78.56
	w_3	1.500			26.923	22.781	550.00
	w_4	1.130			41.716	37.574	907.15
150	w_1	1.870	5	10^5	14.201	-	-
	w_2	1.685			23.373	9.172	64.59
	w_3	1.500			53.55	39.349	277.09
	w_4	1.130			63.314	49.113	345.84

Table 8.8 Summary of test results at increasing frequencies

q_{cyc}	w /%	I_c	f /Hz	N /cycle	δ_s /mm	δ_s/N /mm·cycle^{-1}
50	w_1	1.870	1	5000	1.246	-
			2		0.15	-
			5		0.437	8.74e-05
			5	15000	2.524	1.683e-04
50	w_2	1.685	1	5000	1.048	-
			2		0.213	-
			5		0.176	3.52e-05
			5	15000	3.76	2.507e-04
50	w_3	1.500	1	5000	2.537	-
			2		0.85	-
			5		0.704	1.408e-04
			5	15000	8.89	5.927e-04
50	w_4	1.130	1	5000	3.196	-
			2		0.719	-
			5		0.557	1.114e-04
			5	15000	10.76	7.173e-04

8.8 Summary and conclusions

Based on repeatability tests, it was found that the subgrade box test showed better performance without side rubber. Rubber allowed some horizontal movement, which

may have been beneficial when attempting to replicate in-situ response, but possible water migration appeared to offset the advantage.

Comparing the moisture content with and without the effect of cyclic loading, the general variation of moisture content ranged within 1%. In contrast, the moisture content in the bottom half did not show a clear variation.

As moisture content increased from the top, the subgrade settlement significantly increased. At higher moisture content, the soil top was flooded, which has a critical effect on the bearing capacity of the subgrade.

Cyclic stress contributed to subgrade settlement. At higher moisture contents, the increase of cyclic stress imposed larger effects on subgrade settlement.

With a limited number of repetitions, the settlement did not show a significant increase with frequency. Nevertheless, an increase in loading frequencies could cause a higher deformation rate which might then lead to greater settlements with frequency when evaluated at a larger number of cycles. At low f, some conditioning may allow compaction of the specimen without building up pore water pressures. Conversely, the threshold deviator stress of subgrade could decrease due to the increase of f.

CHAPTER 9 DISCUSSION AND RECOMMENDATIONS

9.1 Discussion

Based on simulation analysis and laboratory tests, resilient and plastic foundation responses were investigated. Thus, the effects of moisture content and drainage were revealed, as well as drainage significance. It is beyond the scope of this project to thoroughly cover both pavements and railway tracks, and the analysis of pavement foundations was concentrated on. The findings from pavement analysis are expected to provide references for understanding the foundation response of railway tracks since that of railways may be similar except for the upper structures. According to the previous analysis, the overall discussion is presented as follows. This chapter aims to demonstrate the links between chapters.

9.1.1 Influencing factors of structural response based on sensitivity analysis

Based on the sensitivity analysis (Chapter 4), critical factors can be identified. This will provide a basis for simulating the structural response by mainly considering the critical factors, i.e. pavement analysis based on unloading modulus, as reported in Section 6.10 and Section 7.8. Thus, the drainage effects on pavement response can be further revealed. The analysis process is further presented in Figure 9.1.

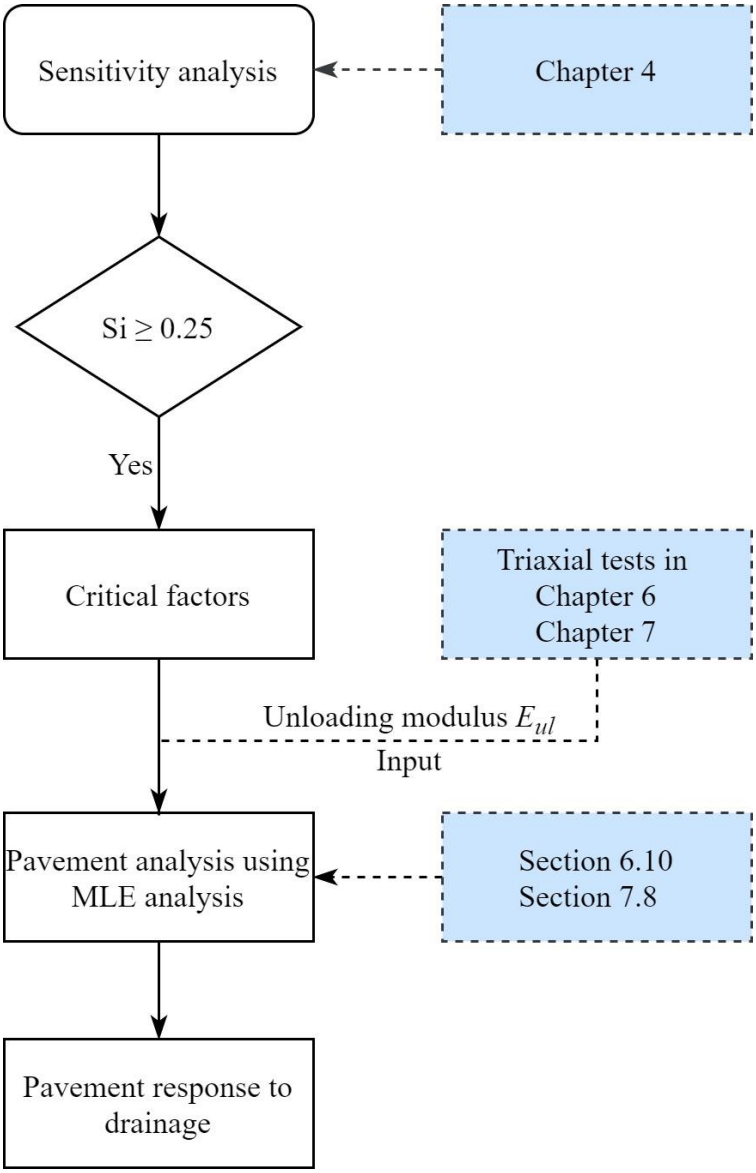

Figure 9.1 Flowchart of sensitivity analysis-based drainage study

9.1.2 Resilient response

Considering the effects of moisture content on the resilient response of unsaturated subgrade (Chu, 2020), it is significant to derive prediction models of resilient modulus incorporating moisture content. The proposed consistency index model and a stress-modified consistency index model were able to predict resilient modulus at various moisture contents with fair accuracy relying only on simple soil properties. The study further demonstrated that the parameters of the modified model correlated with the plasticity index and clay content. Further analysis might enable further improvements in predicting the model parameters by relating them to other soil properties (such as degree of compaction). This would further enhance the application of the proposed

model. Chapter 3 was intended to derive a more general resilient modulus prediction model applicable to soils with a wide variety of plasticity indices. It includes several model parameters and also the normalised moisture content. This will help to expand the findings regardless of soil types in a more general way. For Chapter 4, more assumptions would be necessary if the developed models were used. Considering the objectives, a simpler model would be convenient and feasible.

The unloading deformation is the truly resilient (i.e. recoverable) deformation and none of the deformations will be plastic. Therefore, a M_r based on unloading does not include any plastic strain and therefore allows stress analyses to be performed that apply once all plastic strain is complete. Through triaxial tests, the drainage effects on the unloading modulus were revealed in a laboratory-controlled manner. The unloading modulus showed an upward trend with the drainage between loading periods (i.e. with a decrease of 100 kPa in pore water pressure - an increase of 100 kPa in effective confining pressure, which may be broadly equivalent to a reduction in unsaturated moisture content of ~3% according to the SWCC in Figure 5.5) whilst decreasing with wetting and a drying-wetting cycle. Particularly, comparing Figure 7.28 and Figure 7.30, the unloading modulus showed significantly larger values in unsaturated states than in saturated states, which can be attributed to soil suction.

Since pavement life (as calculated) is a direct function of layer modulus (as shown in Eqs. (4.4) and (4.8)), the observations about unloading modulus and the modulus predicted by consistency index models can be directly related to the calculations reported in Chapter 4. The consistency index is a normalized soil property and has been used, in effect, to normalize results from different soils (as reported in Chapter 4). Thus, sensitivity analysis results and multistage loading results (e.g. unloading modulus) of one type of soil as well as can be extended to a wider variety of soils. The analysis process is further presented in Figure 9.2.

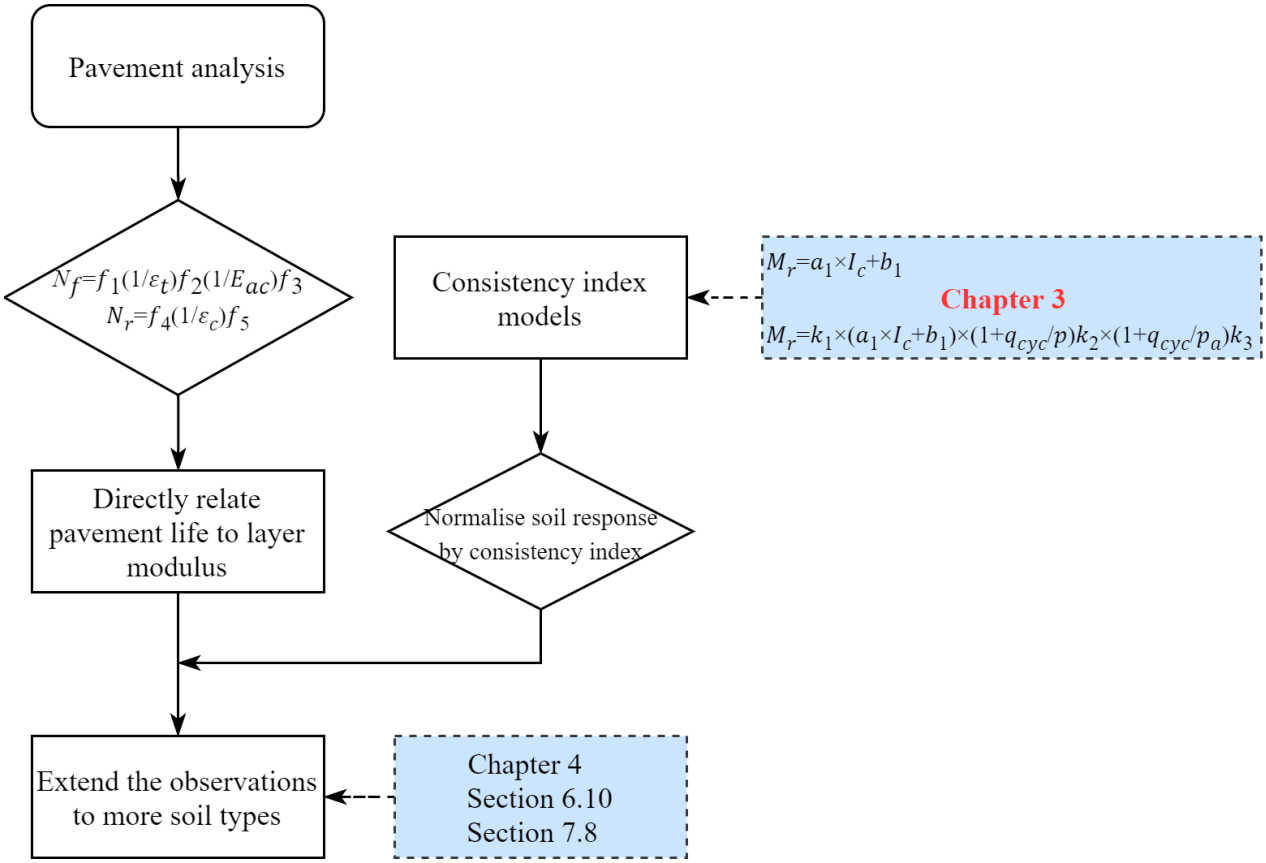

Figure 9.2 Flowchart of resilient response-based analysis

9.1.3 Permanent deformation response

Since permanent deformation was significantly affected by loading cycles and moisture content (as reported in Chapter 8), there was a potential correlation of the deformation with loading cycles and moisture content. The accumulated deformation over the rutting life (N_r, as reported in Chapter 4) could be predicted. Then, the permanent deformation prediction model was related to N_r, i.e. δ_s~(N_r, w, w_{opt}). Loading frequency and stress states could indirectly affect the model parameters and the deformation prediction. The analysis process is further presented in Figure 9.3.

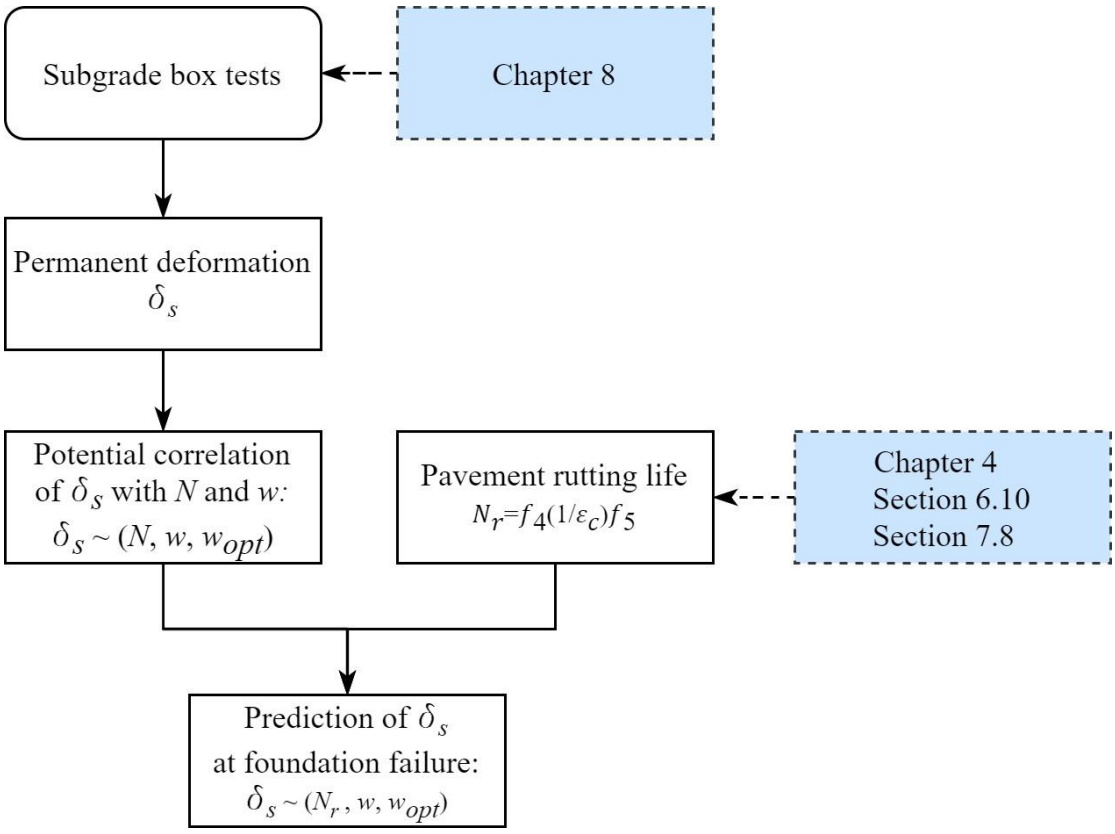

Figure 9.3 Flowchart of permanent deformation-based analysis

9.2 Recommendations

9.2.1 Prediction models

The proposed models provide an alternative way for predicting resilient and plastic responses. They are simple and convenient and lead to fairly good results. They are able to characterize the soil response under the effects of moisture content. Thus, they could be integrated into the drainage design process. With respect to road or railway foundation responses, these models can provide a reliable estimation of the resilient modulus or deformation development with moisture variation. Then, this will provide a basis for drainage design, i.e. based on the prediction results considering possible moisture variation, whether applying drainage or the foundation response after applying drainage could improve can be determined. The design procedure is further demonstrated in Section 9.2.2.3.

By incorporating the effects of plasticity index and moisture variation, the consistency index model could be used to predict resilient modulus with two regression parameters at approximate in-situ loading conditions. The stress-modified consistency index model can be used to predict resilient modulus at various stress conditions as well

as at different moisture conditions. Compared to existing models, the proposed model covered a wider range of soils, which could make it more applicable.

Combined with existing subgrade deformation models, the subgrade deformation could be directly predicted by incorporating the combined effects of cyclic loading and moisture content. It directly includes the water effects, providing a simple way for predicting subgrade deformation due to moisture variation. A prediction process for subgrade resilient modulus and deformation is illustrated in Figure 9.4.

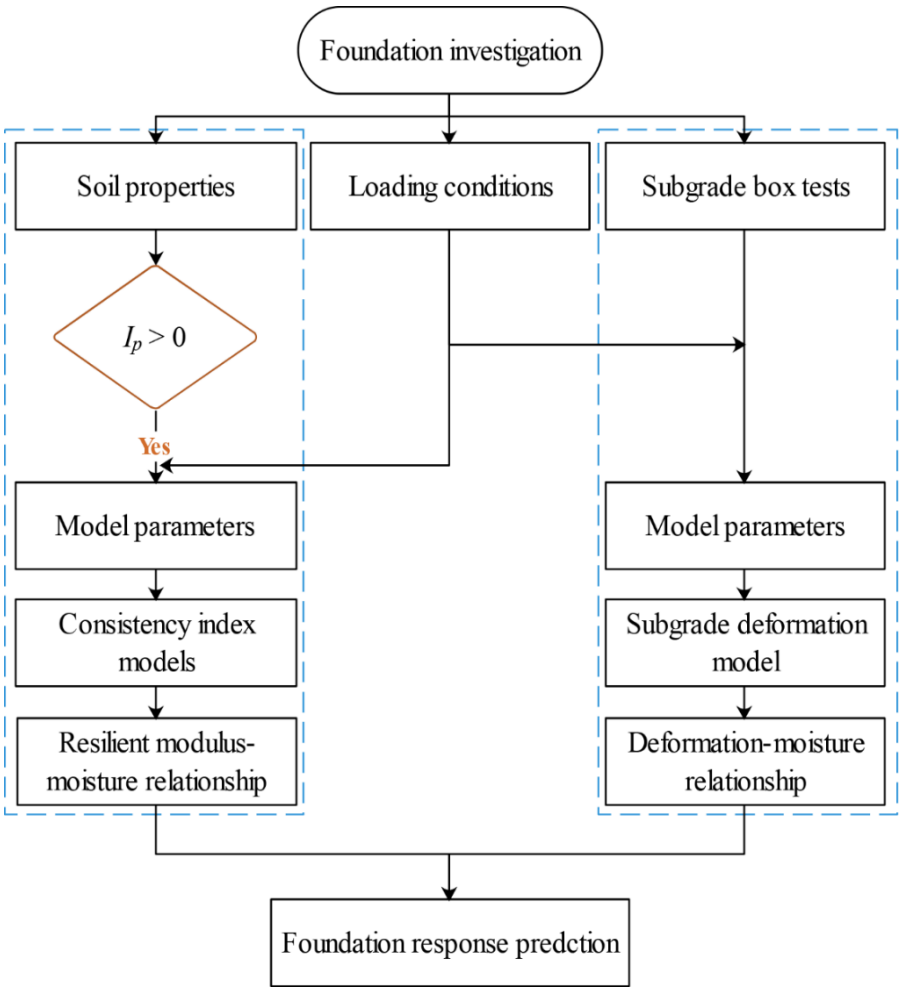

Figure 9.4 Prediction process of consistency index models and the subgrade deformation model

9.2.2 Drainage implications

9.2.2.1 General implication from sensitivity analysis

Based on sensitivity analysis results, a basic determination process of structural properties and dimensions is illustrated in Figure 9.5. Particularly, the structural dimension and properties of flexible pavement structures were included as an example

(i.e. E_{ac}, h_{ac}, E_{base}, h_{base}, E_{sub}, h_{sub} and axle load). It is expected to provide a reference for both roads and railways.

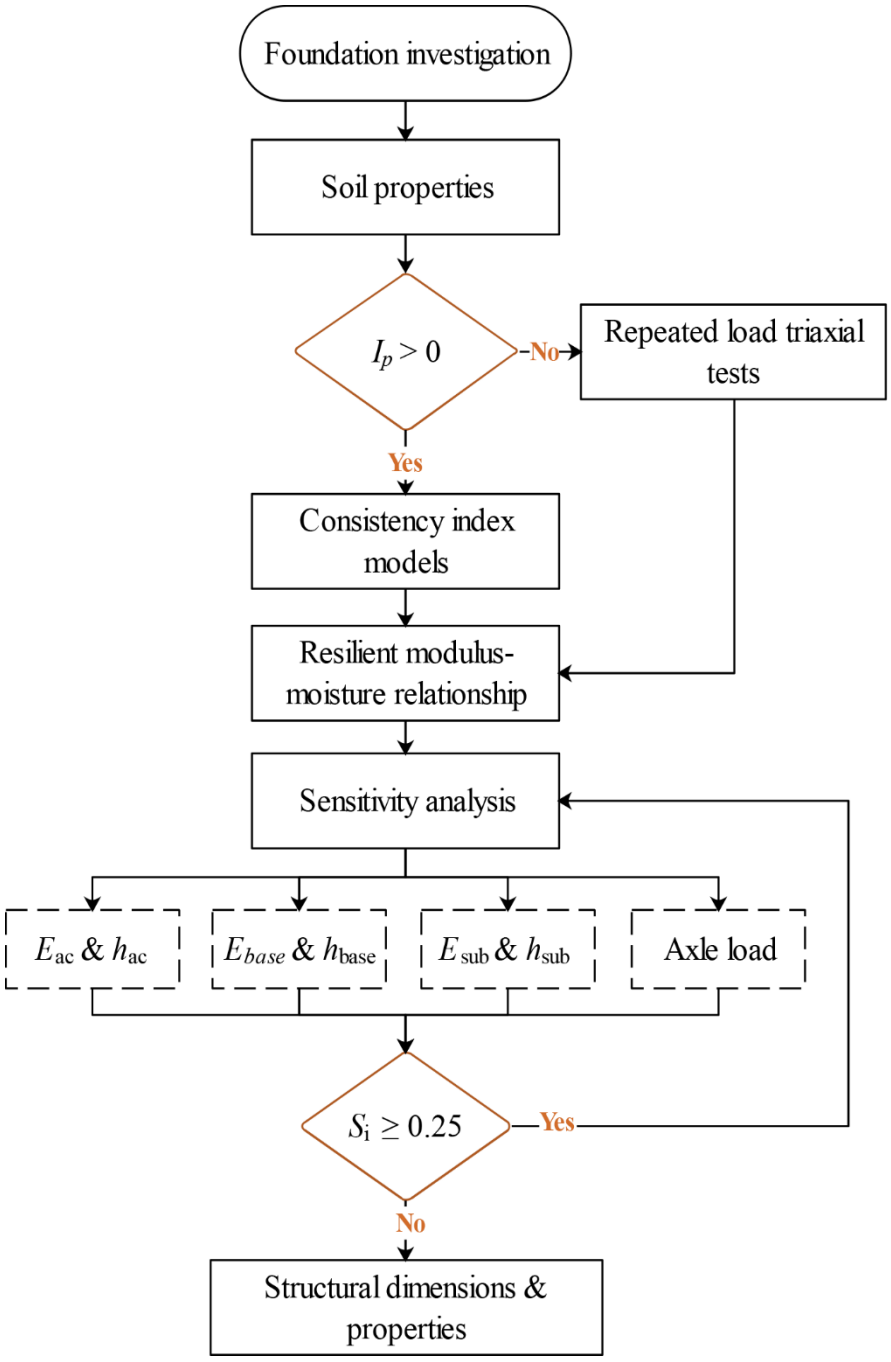

Figure 9.5 Determination of structural properties and dimensions based on sensitivity analysis

9.2.2.2 Polymer drainage layer

The designed polymer drainage layer, PDL, is expected to show good performance in the drainage and reinforcement of foundations. Generally, for the pavement as a whole, the incorporation of PDL can extend the fatigue and rutting life and reduce the sensitivity to moisture content changes, compared to the scenario without PDL. It may

also help reduce the expenditure of upper layers by reducing their thickness due to these benefits. Based on sensitivity analysis (as reported in Section 9.1.1), the optimal properties of PDL could be estimated. The PDL modulus, thickness and position among the structural layers should be considered during drainage design. In order to achieve its full potential of reinforcement effects, the layer should be designed with a higher modulus than the subgrade modulus.

9.2.2.3 Drainage design

A feasible procedure for pavement foundation drainage design was proposed by incorporating the moisture sensitivity of structural responses, as illustrated in Figure 9.6. It is also expected to be applicable to the railway track foundation.

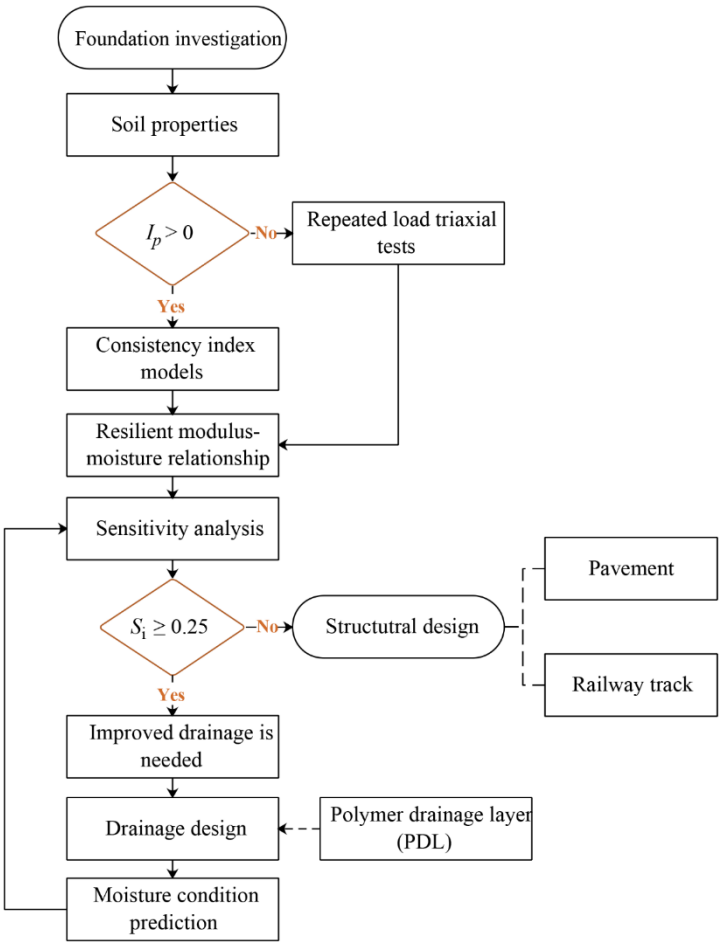

Figure 9.6 Drainage design process

CHAPTER 10 CONCLUSIONS AND FUTURE WORK

10.1 Conclusions

Based on the literature review in Chapter 2, current research on the effects of moisture content and drainage on foundation response is still insufficient. A definitive analysis of foundation sensitivity to moisture content and drainage was scarce. Despite progress in the development of prediction models, existing models were derived from finite soil types. They exhibited difficulties in the direct and precise measurement of matric suction during the tests. The model parameters also needed to be determined with several repeated load triaxial tests, which can be time-consuming. Thus, current models incorporating moisture effects may be complicated and limited to one soil type and contain too many model parameters. Also, the moisture effects on cumulative permanent deformation have not been fully reported. Therefore, data analysis of literature sources was conducted to identify the resilient modulus-moisture content relationship. Sensitivity analysis on assumed values and laboratory-tested soils was performed. Consolidated undrained and drained triaxial tests, unsaturated triaxial tests and box tests were conducted to systematically investigate the influence of moisture content and drainage on soil response. The main achievements are presented as follows:

- A prediction model based on the consistency index was proposed for the resilient modulus of fine-grained soils. A stress-modified model was also proposed, i.e. a consistency index model and a stress-modified consistency index model. The models were able to determine resilient modulus at various moisture contents with fair accuracy relying only on simple soil properties. The study further demonstrated that the parameters of the modified model correlated with the plasticity index and clay content. The consistency index model could reflect the effects of plasticity index and moisture variation on resilient modulus with two regression parameters at approximate in-situ loading conditions. It provides a simple and convenient way for assessing the soil modulus for foundation design. The stress-modified consistency index model avoided the limitations of using the consistency index alone by incorporating deviator stress and net normal stress. It can be used to predict resilient modulus at various stress conditions as well as at different moisture

conditions.

- Regarding a pavement's life, through sensitivity analysis on selected structures, it was found that fatigue life, N_f, was smaller than rutting life, N_r. Thus, the design life of the whole pavement structure was dominated by fatigue cracking. The sensitivity, S_i, of N_f and N_r varied to different extents, i.e. N_f varied between 0.1 and 0.35 (insensitive except at some asphalt thicknesses (i.e. h_{ac} = 25, 225, 275 and 300 mm) where it was moderately sensitive) while N_r varied from 2.3 to 2.7 (very sensitive). N_r was very sensitive to increasing moisture. Therefore, it indicates the crucial role of subgrade moisture conditions in the design of pavements against rutting. The implication is that the N_r should be accurately determined at different moisture levels so as to determine the limiting subgrade condition and/or higher layer thicknesses and stiffnesses so that appropriate drainage can be provided in the design. Derived from previously published test data, a wide range of soil types were covered, which may represent various types of foundations. Generally, for all types of soils, with the increase of moisture content, fatigue and rutting life decreased, whilst fatigue cracking and permanent deformation increased. Based on sensitivity analysis of data from literature sources, it is found that the sensitivity of fatigue cracking and permanent deformation, S_i, to moisture variation was very dependent on the soil types, i.e. the soil with relatively higher plasticity generally demonstrated a higher S_i, whilst this trend was not monotonic with the soil plasticity. Thus, the pavement performance was associated with soil types, and the sensitivity of the soil to moisture content would largely affect the distress development. The increase of AC elastic modulus and thickness may reduce the permanent deformation and attenuate the effect of moisture on pavement performance while escalating the sensitivity of fatigue and rutting life as well as fatigue cracking to moisture content. Axle load, A_l, did not significantly affect the sensitivity, S_i, of fatigue to moisture changes.
- A potential drainage layer based on the non-water reacting double-component polymer was proposed. The incorporation of PDL can extend the fatigue and rutting life and reduce the sensitivity to moisture content changes compared to the scenario without PDL. The optimal design of the polymer layer was recommended, including elastic modulus (not less than subgrade modulus), layer thickness (not more than 100 mm) and installation position (right on the top of the subgrade).

- For the densely compacted soils (i.e. with maximum dry density) in saturated states, generally, at higher effective confining pressure, the soil tested showed higher peak shear strength and an increasing trend in unloading modulus. The multistage tests in CD and CU tests showed significant increases in peak and critical state shear strength with drainage between loading stages compared to those in the corresponding single-stage tests with the same initial effective confining pressure. Due to the drainage between loading stages by reducing pore water pressure, the unloading modulus also showed a clear increase. The shear strength and unloading modulus were larger in consolidated undrained triaxial tests compared with those in consolidated drained triaxial tests. Higher relative changes in CD strength and unloading modulus imply that drainage between loading stages showed larger effects on the drained shearing behaviour and subgrade modulus during the subsequent loading stage. Combined with decreased excess pore water pressure in consolidated undrained tests, potential causes of the difference were presented. After drainage between loading stages, the volume of all the specimens in consolidated drained tests decreased less than those without drainage. The tests also revealed that the effect of drainage between loading stages on foundations at larger depths was limited compared with those at smaller depths (i.e. where there was a smaller effective confining pressure). Through multi-layered elastic analysis, these drainage effects on pavement performance were studied. With drainage between loading stages, vertical displacement at the top of the subgrade and the maximum compressive strain showed a decreasing trend. With drainage between loading stages, maximum tensile strain at the bottom of an overlying asphalt concrete generally in all types of pavements (i.e. thin, medium and thick pavements). Rutting life showed a clear increase with drainage between loading stages. For the pavement with a thick base, fatigue life was smaller than rutting life, i.e. fatigue life was the critical life. Their service life was dominated by AC. Although rutting life showed an increase with drainage undertaken, drainage may not aid the fatigue life. For the pavement with a thin base (e.g. for P60), fatigue life was larger than rutting life, i.e. rutting life was the critical life. With an efficient drainage system installed, the service life of pavements was expected to be effectively extended. Based on the current pavement design, there may exist an optimal AC thickness under which the drainage could achieve the best potential. This would help in avoiding unnecessary

expenditure. The drainage effectiveness should incorporate the engineering requirement design, e.g. drainage improvement for a fatigue-critical pavement may be uneconomic.

- In an unsaturated state, the peak shear strength generally showed an increasing trend with the decrease in moisture content. The shearing behaviour with wetting varied at different net confining pressures. With wetting at lower net confining pressures, the peak shear strength slightly decreased (contrary to those at higher net confining pressures) while increasing with drainage. The unloading modulus generally increased with the drying process while decreasing with wetting. After a drying-wetting cycle, the unloading modulus showed a decreasing trend. In the drainage process, the unloading modulus only improved upon draining when the stress levels were those likely to be experienced in thin or moderately thick pavement construction. The maximum tensile strain and fatigue life did not significantly differ with moisture variation. During the drying stages, the compressive strain and subgrade surface permanent deformation generally showed a downward trend. The tensile strain did not show large differences with the different moisture conditions, while the compressive strain showed a clear trend with the subgrade modulus due to moisture variation. Rutting life showed an opposite trend.
- In a more realistic set-up (i.e. subgrade box tests), comparing the moisture content before and after testing, the general variation of moisture content was within 1%, while the moisture content in the bottom half did not show clear variation with cyclic loading. As moisture content was increased from the top (simulating rainfall effects), the subgrade settlement showed a significant increase. At higher moisture content, the soil top became flooded, which has a critical effect on the subgrade bearing capacity in terms of the increase in subgrade settlement by nine times after flooding. Cyclic stress contributed to subgrade settlement. At higher moisture contents, the results show that the increase of cyclic stress imposed larger effects on permanent subgrade settlement. With a limited number of repetitions, the settlement did not show any clear increase with multistage frequencies, even though a constant higher frequency accelerated the development of subgrade settlement. Consequently, rutting life is expected to be reduced.

10.2 Future work

The work presented in this thesis has extended the understanding of the effects of moisture content and drainage on soil foundation response and provided an alternative way for predicting the resilient and plastic soil response under traffic loading. However, it should be noted that some limitations remain within this study:

- Computations related to pavement response have been made using multi-layered linear elastic pavement analysis mathematical models. Using non-linear finite element models may lead to improved quality of prediction/validation.
- The proposed prediction model of resilient modulus did not consider all the possible conditions in unsaturated soils, e.g., wetting and drying paths and dry density. Although the proposed models cover a wide range of soils with various plasticity indices, the study was limited to 15 soils and could not cover all plasticity index values.
- Soils with varying plasticity indices showed different sensitivity to moisture content and stress levels. The proposed prediction model of permanent deformation was limited to one soil type used in the tests.
- In terms of the case analysis, this study only focused on flexible pavements as an example to demonstrate the drainage and moisture effects on practical structures.

Thus, the following recommendations for future work are made:

- Further laboratory tests or data collection from literature sources on resilient modulus-moisture content relationship with a wider range of soil plasticity indices are needed to further validate the consistency index model and the stress-modified consistency index model, especially those with lower plasticity. It could also be extended to cohesionless soils, perhaps including correction factors.
- Further laboratory tests of soils with a wider range of soil plasticity indices are needed to validate the plastic deformation prediction model and extend the deformation model applicability.
- The analysis of sensitivity to moisture content needs to be extended to other structures, e.g. rigid pavement, ballast and slab railway track.
- Laboratory and in-situ tests are needed to validate the hydraulic and mechanical performance of the proposed polymer drainage layer.
- Further studies should be conducted to determined deformation prediction models

of the subgrade. Thus, this model, plus the consistency models, could be combined to provide a complete model.

REFERENCES

AASHTO (1986). Standard Specifications for Transportation Materials and Methods of Sampling and Testing. American Association of State Highway and Transportation Officials, Washington, DC, USA.

AASHTO (2002). *AASHTO Guide for Design of Pavement Structures,* AASHTO, Washington, D.C.

Abed, A., Thom, N. & Neves, L. (2019). Probabilistic prediction of asphalt pavement performance. *Road Materials and Pavement Design,* 20(sup1)**,** S247-S264.

Abu-Farsakh, M., Coronel, J. & Tao, M. (2007). Effect of soil moisture content and dry density on cohesive soil–geosynthetic interactions using large direct shear tests. *Journal of Materials in Civil Engineering,* 19(7)**,** 540-549.

Ahmed, T. (2016). *Asphalt fatigue failure analysis and modelling: experimental studies and theoretical formulation.* PhD thesis, University of Liverpool.

Al-Mukhtar, M., Khattab, S. & Alcover, J.-F. (2012). Microstructure and geotechnical properties of lime-treated expansive clayey soil. *Engineering Geology,* 139**,** 17-27.

Al-Qadi, I.L., Lahouar, S., Loulizi, A., Elseifi, M.A. & Wilkes, J.A. (2004). Effective approach to improve pavement drainage layers. *Journal of Transportation Engineering,* 130(5)**,** 658-664.

Allen, D.L. & Deen, R.C. (1986). A computerized analysis of rutting behavior of flexible pavement. *Transportation research record,* 1095.

Alonso, E., Canete, A. & Olivella, S. (2002). Moisture transfer and deformation behaviour of pavements: effect of climate, materials and drainage. *Proc. 3rd International Conference on Unsaturated Soils*.)**,** 671-678.

Alonso, E. & Pinyol, N. (2008). Unsaturated soil mechanics in earth and rockfill dam engineering. *In Unsaturated soils: Advances in geo-engineering (eds D. G. Toll, C. E. Augarde, D. Gallipoli and S. J. Wheeler),* June 23 2008, Boca Raton, FL, USA. CRC Press, 1**,** 3-32.

Alonso, E., Pinyol, N. & Gens, A. (2013). Compacted soil behaviour: initial state, structure and constitutive modelling. *Geotechnique,* 63(6)**,** 463-478.

Alonso, E.E., Gens, A. & Josa, A. (1990). A constitutive model for partially saturated soils. *Geotechnique,* 40(3)**,** 405-430.

Apul, D.S., Gardner, K., Eighmy, T., Benoit, J. & Brannaka, L. (2002). A review of water movement in the highway environment: Implications for recycled materials use. *Recycled Materials Resource Center, University of New Hampshire, Durham*.

ARA. (2004). *Guide for mechanistic-empirical design of new and rehabilitated pavement structures*. Report No.: Washington, DC: Transportation Research Board of the National Academies.

Arnold, G., Dawson, A., Hughes, D., Werkmeister, S. & Robinson, D. (2002). Serviceability design of granular pavement materials. *Bearing Capacity of Roads, Railways and Airfields, BCRRA*, 2002, Lisbon, Portugal. CRC Press)**,** 957-966.

Arshad, A. (2007). Flexible pavement design: Transitioning from empirical to mechanistic-based design methods. JURUTERA: July.

Asli, C., Feng, Z., Porcher, G. & Rincent, J.J. (2012). Back-calculation of elastic modulus of soil and subgrade from portable falling weight deflectometer measurements. *Engineering Structures,* 34**,** 1-7.

Atkins, H.N. (2002). *Highway materials, soils and concretes,* 4th Edition, Prentice Hall.

Azam, A., Cameron, D. & Rahman, M. (2013). Model for prediction of resilient modulus incorporating matric suction for recycled unbound granular materials. *Canadian Geotechnical Journal,* 50(11)**,** 1143-1158.

Azam, A.M., Cameron, D.A. & Rahman, M.M. (2015). Permanent Strain of Unsaturated Unbound Granular Materials from Construction and Demolition Waste. *Journal of Materials in Civil Engineering,* 27(3)**,** 04014125.

Bagheri, M. (2018). *Experimental investigation of the time-and rate-dependent behaviour of unsaturated clays.* University of Nottingham.

Bagheri, M., Nezhad, M.M. & Rezania, M. (2019). A CRS oedometer cell for unsaturated and non-isothermal tests. *Geotechnical Testing Journal,* 43(1)**,** 20-37.

Bahador, M., Evans, T. & Gabr, M. (2013). Modeling effect of geocomposite drainage layers on moisture distribution and plastic deformation of road sections. *Journal of Geotechnical and Geoenvironmental Engineering,* 139(9)**,** 1407-1418.

Baker, K.E. (2001). *Investigation of direct and indirect hydraulic property laboratory characterization methods for heterogeneous alluvial deposits: Application to the Sandia-Tech Vadose Zone Infiltration Test Site.* New Mexico Institute of Mining and Technology Socorro.

Barksdale, R.D. (1972). Laboratory evaluation of rutting in base course materials. *Presented at the Third International Conference on the Structural Design of Asphalt Pavements,* September 11-15, Park Lane, London, England. Grosvenor House Publishing, 1**,** 161-174.

Barnes, G. (1995). *Soil mechanics: principles and practice,* Macmillan Press Ltd, Basingstoke, UK.

Birgisson, B., Ovik, J. & Newcomb, D. (2007). Analytical predictions of seasonal variations in flexible pavements: Minnesota road research project site. *Transportation Research Record 1730: Journal of the Transportation Research Board*)**,** 81-90.

Bishop, A.W. (1959). The principle of effective stress. *Teknisk ukeblad,* 39**,** 859-863.

Bjerrum, L. & Simons, N. (1960). Comparison of Shear Strength Characteristics of Normally Con. solidated Clays, NGI-Publ.

Black, W. (1962). A method of estimating the California bearing ratio of cohesive soils from plasticity data. *Geotechnique,* 12(4)**,** 271-282.

Blackmore, L., Clayton, C.R., Powrie, W., Priest, J.A. & Otter, L. (2020). Saturation and its effect on the resilient modulus of a pavement formation material. *Geotechnique,* 70(4)**,** 292-302.

Bostancioğlu, M. (2021). Effect of functional grading on the performance of flexible pavements. *International Journal of Pavement Engineering,* 22(4)**,** 514-523.

British Standard Institution (1990). Methods of Test for Soils for Civil Engineering Purposes. London, UK.

Brooks, R.H. & Corey, A.T. (1964). Hydraulicpropertiesofporousmedia. *Colorado State University, Hydro Paper,* 3**,** 27.

Brown, S.F., Loach, S.C. & O'Reilly, M.P. (1987). Repeated loading of fine grained soils. *In:* TRANSPORT, D. O. (ed.). Transport and Road Research Laboratory and Transport Research Laboratory.

Brown, S.F. (1997). Achievements and challenges in asphalt pavement engineering. *Proc. of 8th Int. Conf. on Asphalt Pavements, Seattle*.

Burmister, D.M. (1945). The general theory of stresses and displacements in layered soil systems. III. *Journal of applied physics*, 16(5)**,** 296-302.

Burrow, M., Bowness, D. & Ghataora, G. (2007). A comparison of railway track foundation design methods. *Proceedings of the Institution of Mechanical Engineers, Part F: Journal of Rail and Rapid Transit*, 221(1)**,** 1-12.

Campolongo, F., Cariboni, J. & Saltelli, A. (2007). An effective screening design for sensitivity analysis of large models. *Environmental modelling & software*, 22(10)**,** 1509-1518.

Carvalho, R., Stubstad, R., Briggs, R., Selezneva, O., Mustafa, E. & Ramachandran, A. (2012). *Simplified techniques for evaluation and interpretation of pavement deflections for network-level analysis*. Report No.: United States. Federal Highway Administration. Office of Infrastructure ….

Cary, C.E. & Zapata, C.E. (2010). Enhanced model for resilient response of soils resulting from seasonal changes as implemented in mechanistic–empirical pavement design guide. *Transportation research record*, 2170(1)**,** 36-44.

Cary, C.E. & Zapata, C.E. (2011). Resilient Modulus for Unsaturated Unbound Materials. *Road Materials and Pavement Design*, 12(3)**,** 615-638.

Cebon, D. (1986). Road damaging effects of dynamic axle loads. *Proceedings, International Symposium on Heavy Vehicle Weights and Dimensions, Kelowna, British Columbia*.

Cedergren, H. (1978). Poor Pavement Drainage Could Cost $15 Billion Yearly. *Engineering News Record*.

Cedergren, H.R. (1974). *Drainage of highway and airfield pavements*, John Wiley and Sons, New York.

Chai, J.-C. & Miura, N. (2002). Traffic-Load-Induced Permanent Deformation of Road on Soft Subsoil. *Journal of Geotechnical and Geoenvironmental Engineering*, 128(11)**,** 907-916.

Chang, C.S., Adegoke, C.W. & Selig, E.T. (1980). GEOTRACK model for railroad track performance. *Journal of Geotechnical and Geoenvironmental Engineering*, 106(11)**,** 1201-1218.

Chen, D., Zaman, M., Laguros, J. & Soltani, A. (1995). Assessment of computer programs for analysis of flexible pavement structure. *Transportation research record*, 1482(137)**,** 123-133.

Chen, J., Alonso, E.E., Gu, C., Cao, Z. & Cai, Y. (2018). Long term cyclic behavior of unsaturated granular soils. *Transportation Geotechnics,* 17**,** 48-55.

Chen, R., Zhao, X., Wang, Z., Jiang, H. & Bian, X. (2013). Experimental study on dynamic load magnification factor for ballastless track-subgrade of high-speed railway. *Journal of Rock Mechanics and Geotechnical Engineering,* 5(4)**,** 306-311.

Chen, R., Chen, J., Zhao, X., Bian, X. & Chen, Y. (2014). Cumulative settlement of track subgrade in high-speed railway under varying water levels. *International Journal of Rail Transportation,* 2(4)**,** 205-220.

Choudhury, D., Bharti, R.K., Chauhan, S. & Indraratna, B. (2008). Response of multilayer foundation system beneath railway track under cyclic loading. *Journal of Geotechnical and Geoenvironmental Engineering,* 134(10)**,** 1558-1563.

Christopher, B.R. & McGuffey, V.C. (1997). *Pavement subsurface drainage systems,* Transportation Research Board.

Christopher, B.R., Hayden, S.A. & Zhao, A. (2000). Roadway base and subgrade geocomposite drainage layers. *Testing and performance of geosynthetics in subsurface drainage.* ASTM International.

Chu, X. (2020). A Review on the Resilient Response of Unsaturated Subgrade Soils. *Advances in Civil Engineering,* Article ID 7367484, 2020**,** 11.

Chu, X., Dawson, A. & Thom, N. (2021). Prediction of resilient modulus with consistency index for fine-grained soils. *Transportation Geotechnics,* 31**,** 100650.

Claessen, A., Edwards, J., Sommer, P. & Uge, P. (1977). Asphalt Pavement Design - The Shell Method. *Proceedings of 4th International Conference on Structural Design of Asphalt Pavements,* August 22-26, Ann Arbor, Michigan. 1**,** 39-74.

Coleman, J. (1962). Stress strain relations for partly saturated soil. *Corespondence to Geotechnique,* 12(4)**,** 348-350.

Cui, Y. & Delage, P. (1996). Yeilding and plastic behaviour of an unsaturated compacted silt. *Geotechnique,* 46(2)**,** 291-311.

Dai, S. & Van Deusen, D. (1998). Field study of in situ subgrade soil response under flexible pavements. *Transportation research record,* 1639(1)**,** 23-35.

Dawson, A. & Correia, A.G. (1996). The effects of subgrade clay condition on the

structural behaviour of road pavements. *In:* CORREIA, G., ed. *Flexible pavements*, 1996, Balkema. CRC Press, 1996**,** 113-119.

Dawson, A., Thom, N. & Paute, J. (1996). Mechanical characteristics of unbound granular materials as a function of condition. *Gomes Correia, Balkema, Rotterdam*)**,** 35-44.

Dawson, A. & Hill, A. (1998a). Prediction and implication of water regimes in granular bases and sub-bases. *International Symposium on Subdrainage in Roadway Pavements and Subgrades*, 11-13 November 1998a, Granada, Spain. Transport Research Laboratory, 1998**,** 121-128.

Dawson, A. & Hill, A. (1998b). Prediction and Implication of Water Regimes in Granular Bases and Sub-Bases. *INTERNATIONAL SYMPOSIUM ON SUBDRAINAGE IN ROADWAY PAVEMENTS AND SUBGRADES, HELD GRANADA, SPAIN, 11-13 NOVEMBER 1998*.

Dawson, A. & Wellner, F. (1999). *Plastic Behavior of Granular Materials*. Report No. Reference PRG99014, United Kingdom: University of Nottingham.

Dawson, A. (2008). *Water in road structures: movement, drainage & effects*, Springer Science & Business Media.

Deutscnes Institut fur Norrnung. (2001). *Determining the deformation and strength characteristics of soil by the plate loading test*. Report No. DIN 18134 : 2001-09: German standard Berlin, Germany.

Diefenderfer, B.K., Galal, K. & Mokarem, D.W. (2005). *Effect of subsurface drainage on the structural capacity of flexible pavement*. Report No.: Virginia Transportation Research Council.

Ding, L., Han, Z., Zou, W. & Wang, X. (2020). Characterizing hydro-mechanical behaviours of compacted subgrade soils considering effects of freeze-thaw cycles. *Transportation Geotechnics*, 24**,** 100392.

Drumm, E., Boateng-Poku, Y. & Johnson Pierce, T. (1990). Estimation of subgrade resilient modulus from standard tests. *Journal of Geotechnical Engineering*, 116(5)**,** 774-789.

Drumm, E.C., Reeves, J.S., Madgett, M.R. & Trolinger, W.D. (1997). Subgrade resilient modulus correction for saturation effects. *Journal of Geotechnical and Geoenvironmental Engineering*, 123(7)**,** 663-670.

Edil, T.B. & Motan, S.E. (1984). Laboratory evaluation of soil suction components.

Geotechnical Testing Journal, 7(4)**,** 173-181.

Edwards, P., Thom, N., Fleming, P.R. & Williams, J. (2005). Testing of unbound materials in the Nottingham asphalt tester springbox. *Transportation research record,* 1913(1)**,** 32-40.

El-Basyouny, M.M. & Witczak, M. (2005). Calibration of alligator fatigue cracking model for 2002 design guide. *Transportation research record,* 1919(1)**,** 76-86.

Elseifi, M.A., Al-Qadi, I.L., Loulizi, A. & Wilkes, J. (2001). Performance of geocomposite membrane as pavement moisture barrier. *Transportation research record,* 1772(1)**,** 168-173.

Elshaer, M.H. (2017). *Assessing the mechanical response of pavements during and after flooding.* PhD thesis, University of New Hampshire.

Erlingsson, S. (2010). Impact of water on the response and performance of a pavement structure in an accelerated test. *Road Materials and Pavement Design,* 11(4)**,** 863-880.

Erlingsson, S., Rahman, S. & Salour, F. (2017). Characteristic of unbound granular materials and subgrades based on multi stage RLT testing. *Transportation Geotechnics,* 13**,** 28-42.

Farias, M. & Llano-Serna, M. (2016). Simple methodology to obtain critical state parameters of remolded clays under normally consolidated conditions using the fall-cone test. *Geotechnical Testing Journal,* 39(5)**,** 855-864.

Fatahi, B. & Khabbaz, H. (2011). Enhancement of ballasted rail track performance using geosynthetics. *GeoHunan International Conference - Advances in pile foundations, geosynthetics, geoinvestigations, and foundation failure analysis and repairs*, June 9-11 2011, Hunan, China. American Society of Civil Engineers, 2011**,** 222-230.

Fatahi, B., Khabbaz, H. & Liem Ho, H. (2011). Effects of geotextiles on drainage performance of ballasted rail tracks. *Australian Geomechanics,* 46(4)**,** 91-102.

Fateen, S.E. (1972). *A finite element analysis of full depth asphalt railway track.* University of Maryland.

Federal Highway Administration (1994). Drainable Pavement Systems - Instructor's Guide, Demonstration Project 87. Publication No. FHWA-SA-94-062. Office of Technology Applications and Office of Engineering, Federal Highway Administration, Washington, DC.

Fei, Q. (2015). *Performance and Maintenance of Fouled Ballast.* PhD Thesis, University of Nottingham.

Forsyth, R.A., Wells, G.K. & Woodstrom, J.H. (1987). Economic impact of pavement subsurface drainage. 1121.

Fredlund, D., Morgenstern, N.R. & Widger, R. (1978). The shear strength of unsaturated soils. *Canadian Geotechnical Journal,* 15(3)**,** 313-321.

Fredlund, D., Vanapalli, S., Xing, A. & Pufahl, D. (1995). Predicting the shear strength function for unsaturated soils using the soil-water characteristic curve. *First International Conference on Unsaturated Soils, Paris, France*.)**,** 6-8.

Fredlund, D. & Vanapalli, S. (2002). Shear Strength of Unsaturated Soils. *Methods of soil analysis: Part,* 4**,** 329-361.

Fredlund, D.G. & Morgenstern, N.R. (1977). Stress state variables for unsaturated soils. *Journal of Geotechnical and Geoenvironmental Engineering,* 103(5)**,** 447-466.

Fredlund, D.G. & Rahardjo, H. (1987). Soil mechanics principles for highway engineering in arid regions. *Transportation research record,* 1137**,** 1-11.

Fredlund, D.G. & Rahardjo, H. (1993). *Soil mechanics for unsaturated soils,* John Wiley & Sons.

Fredlund, D.G. & Xing, A. (1994). Equations for the soil-water characteristic curve. *Canadian Geotechnical Journal,* 31(4)**,** 521-532.

Fredlund, D.G. (2006). Unsaturated soil mechanics in engineering practice. *Journal of Geotechnical and Geoenvironmental Engineering,* 132(3)**,** 286-321.

Fredlund, D.G., Rahardjo, H. & Fredlund, M.D. (2012). *Unsaturated soil mechanics in engineering practice*, John Wiley & Sons.

Fredlund, P., Saltman, S. & Catt, K. (1975). Aldosterone Production by Isolated Adrenal Glomenilosa Cells: Stimulation by Physiological Concentrations of Angiotensin II. *Endocrinology,* 97(6)**,** 1577-1586.

Frost, J. & Park, J. (2003). A critical assessment of the moist tamping technique. *Geotechnical Testing Journal,* 26(1)**,** 57-70.

Gabr, A. & Cameron, D. (2013). Permanent strain modeling of recycled concrete aggregate for unbound pavement construction. *Journal of Materials in Civil Engineering,* 25(10)**,** 1394-1402.

Gallipoli, D., Wheeler, S. & Karstunen, M. (2003). Modelling the variation of degree of saturation in a deformable unsaturated soil. *Géotechnique.,* 53(1)**,** 105-112.

Garg, N. & Thompson, M.R. (1997). Triaxial characterization of Minnesota road research project granular materials. *Transportation research record,* 1577(1)**,** 27-36.

Geotechdata.info. 2013. *Angle of Friction, http://geotechdata.info/parameter/angle-of-friction.html (as of September 14.12.2013)* [Online]. [Accessed November 2022].

Ghadimi, B. & Nikraz, H. (2017). A comparison of implementation of linear and nonlinear constitutive models in numerical analysis of layered flexible pavement. *Road Materials and Pavement Design,* 18(3)**,** 550-572.

Ghavami, M., Hosseini, M.S., Zavattieri, P. & Haddock, J.E. (2016). *Investigating the Need for Drainage Layers in Flexible Pavements*. Report No. FHWA/IN/JTRP-2019/04, West Lafayette, Indiana, United States: Purdue University.

Ghavami, M.S.M., Hosseini, M.S., Zavattieri, P.D. & Haddock, J.E. (2019). Flexible pavement drainage system effectiveness. *Construction and building materials,* 218**,** 99-107.

Ghorbani, B., Arulrajah, A., Narsilio, G., Horpibulsuk, S. & Bo, M.W. (2020). Development of genetic-based models for predicting the resilient modulus of cohesive pavement subgrade soils. *Soils and foundations,* 60(2)**,** 398-412.

Gu, F., Zhang, Y., Droddy, C.V., Luo, R. & Lytton, R.L. (2016). Development of a new mechanistic empirical rutting model for unbound granular material. *Journal of Materials in Civil Engineering,* 28(8)**,** 04016051.

Guo, C., Chu, X. & Wang, F. (2018). The feasibility of non-water reaction polymer grouting technology application in seepage prevention for tailings reservoirs. *Water Science and Technology: Water Supply,* 18(1)**,** 203-213.

Hamid, T.B. & Miller, G.A. (2009). Shear strength of unsaturated soil interfaces. *Canadian Geotechnical Journal,* 46(5)**,** 595-606.

Han, Z. & Vanapalli, S.K. (2015). Model for predicting resilient modulus of unsaturated subgrade soil using soil-water characteristic curve. *Canadian Geotechnical Journal,* 52(10)**,** 1605-1619.

Han, Z. & Vanapalli, S.K. (2016a). State-of-the-Art: Prediction of Resilient Modulus of Unsaturated Subgrade Soils. *International Journal of Geomechanics,* 16(4)**,** 04015104.

Han, Z. & Vanapalli, S.K. (2016b). Relationship between resilient modulus and suction

for compacted subgrade soils. *Engineering Geology,* 211(Supplement C)**,** 85-97.

Han, Z. & Vanapalli, S.K. (2017). Normalizing Variation of Stiffness and Shear Strength of Compacted Fine-Grained Soils with Moisture Content. *Journal of Geotechnical and Geoenvironmental Engineering,* 143(9)**,** 04017058.

Hanandeh, S., Ardah, A. & Abu-Farsakh, M. (2020). Using artificial neural network and genetics algorithm to estimate the resilient modulus for stabilized subgrade and propose new empirical formula. *Transportation Geotechnics,* 24**,** 100358.

Hansen, J.B. (1970). A revised and extended formula for bearing capacity. *Danish Geotechnical Institute,* 28**,** 5-11.

Hassan, H.F. & White, T.D. (1996). *Locating the drainage layer for flexible pavements*. Report No.

Helstrom, C.L., Humphrey, D.N. & Labbe, J.M. (2007). *Performance and effectiveness of a thin pavement section using geogrids and drainage geocomposites in a cold region*. Report No. NETCR60, Maine, United States: University of Maine.

Helwany, S. (2007). *Applied soil mechanics with ABAQUS applications,* John Wiley & Sons.

Heukelom, W. & Klomp, A. (1962). Dynamic testing as a means of controlling pavements during and after construction. *International Conference on the Structural Design of Asphalt Pavements,* Ann Arbor, United States. University of Michigan, 203(1)**,** 495-510.

Heydinger, A.G. (2003). Evaluation of seasonal effects on subgrade soils. *Transportation research record,* 1821(1)**,** 47-55.

Highway Agency (2006). Pavement design and maintenance-foundations, volume 7, HD26/06, design manual for roads and bridges (DMRB). The Stationery Office London.

Ho, D.Y. & Fredlund, D.G. (1982). A multistage triaxial test for unsaturated soils. *Geotechnical Testing Journal,* 5(1/2)**,** 18-25.

Hossain, M. (1998). *Influence of moisture content in granular bases on pavement performance.* Master thesis, Texas Tech University.

Huang, Y.H. (1993). *Pavement analysis and design,* Prentice Hall, Englewood Cliffs, N.J.

Huang, Y.H. (2004). *Pavement analysis and design,* Prentice Hall, Englewood Cliffs,

N.J.

Ikeagwuani, C., Obeta, I. & Agunwamba, J. (2019). Stabilization of black cotton soil subgrade using sawdust ash and lime. *Soils and foundations*, 59(1)**,** 162-175.

Inam, A., Ishikawa, T. & Miura, S. (2012). Effect of principal stress axis rotation on cyclic plastic deformation characteristics of unsaturated base course material. *Soils and foundations*, 52(3)**,** 465-480.

Indraratna, B., Khabbaz, H., Salim, W. & Christie, D. (2006). Geotechnical properties of ballast and the role of geosynthetics in rail track stabilisation. *Ground Improvement*, 10(3)**,** 91-101.

Indraratna, B., Salim, W. & Rujikiatkamjorn, C. (2011). *Advanced rail geotechnology–ballasted track*, CRC press.

Indraratna, B., Singh, M., Nguyen, T.T., Leroueil, S., Abeywickrama, A., Kelly, R. & Neville, T. (2020). Laboratory study on subgrade fluidization under undrained cyclic triaxial loading. *Canadian Geotechnical Journal*, 57(11)**,** 1767-1779.

Ionescu, D. (2004). *Evaluation of the engineering behaviour of railway ballast.* PhD Thesis, University of Wollongong.

Ishikawa, T., Sekine, E. & Miura, S. (2011). Cyclic deformation of granular material subjected to moving-wheel loads. *Canadian Geotechnical Journal*, 48(5)**,** 691-703.

Jahandari, S., Tao, Z., Saberian, M., Shariati, M., Li, J., Abolhasani, M., Kazemi, M., Rahmani, A. & Rashidi, M. (2021). Geotechnical properties of lime-geogrid improved clayey subgrade under various moisture conditions. *Road Materials and Pavement Design*, 2021**,** 1-19.

Janardhanam, R. & Desai, C. (1983). Three-dimensional testing and modeling of ballast. *Journal of Geotechnical Engineering*, 109(6)**,** 783-796.

Jennings, J. & Burland, J. (1962). Limitations to the use of effective stresses in partly saturated soils. *Geotechnique*, 12(2)**,** 125-144.

Ji, R. & Nantung, T. (2015). Quantification of Benefits of Subsurface Drainage on Pavement Performance in Indiana. *Transportation Research Board 94th Annual Meeting*, 2015, Washington DC, United States. Transportation Research Board.

Jia, L., Guo, J. & Yao, K. (2018). In situ monitoring of the long-term settlement of high-fill subgrade. *Advances in Civil Engineering*, 2018, Article ID 1347547**,** 9.

Jiang, M., Hu, H., Peng, J. & Leroueil, S. (2011). Experimental study of two saturated natural soils and their saturated remoulded soils under three consolidated undrained stress paths. *Frontiers of Architecture and Civil Engineering in China,* 5(2)**,** 225-238.

Johnson, T.C. (1986). *Frost action predictive techniques for roads and airfields: A comprehensive survey of research findings,* Cold Regions Research and Engineering Laboratory.

Kent County Council. (2000). *Road Pavement Design Guide*. Report No., Kent Highway Services, Maidstone, UK.

Khalili, N. & Khabbaz, M. (1998). A unique relationship of chi for the determination of the shear strength of unsaturated soils. *Geotechnique,* 48(5)**,** 76–77.

Khazanovich, L. & Wang, Q. (2007). MnLayer: high-performance layered elastic analysis program. *Transportation research record,* 2037(1)**,** 63-75.

Khoury, C.N. & Miller, G.A. (2011). Influence of hydraulic hysteresis on the shear strength of unsaturated soils and interfaces. *Geotechnical Testing Journal,* 35(1)**,** 135-149.

Khoury, N., Musharraf, Z., Nevels, J. & Mann, J. (2003). Effect of soil suction on resilient modulus of subgrade soil using the filter paper technique. *82nd Annual Meeting of the Transportation Research Board*, National Research Council, Washington, DC.

Khoury, N. & Zaman, M. (2004). Correlation between resilient modulus, moisture variation, and soil suction for subgrade soils. *Transportation Research Record: Journal of the Transportation Research Board,* 1874(1)**,** 99-107.

Khoury, N., Brooks, R. & Khoury, C. (2009). Environmental influences on the engineering behavior of unsaturated undisturbed subgrade soils: effect of soil suctions on resilient modulus. *International Journal of Geotechnical Engineering,* 3(2)**,** 303-311.

Khoury, N., Brooks, R., Khoury, C. & Yada, D. (2012). Modeling resilient modulus hysteretic behavior with moisture variation. *International Journal of Geomechanics,* 12(5)**,** 519-527.

Khoury, N., Brooks, R., Boeni, S.Y. & Yada, D. (2013). Variation of resilient modulus, strength, and modulus of elasticity of stabilized soils with postcompaction moisture contents. *Journal of Materials in Civil Engineering,* 25(2)**,** 160-166.

Khoury, N. (2018). Resilient modulus–moisture content relationships for pavement engineering applications. *International Journal of Pavement Engineering,* 19(7)**,** 651-660.

Khoury, N. & Maalouf, M. (2018). Prediction of Resilient Modulus from Post-compaction Moisture Content and Physical Properties Using Support Vector Regression. *Geotechnical and Geological Engineering,* 36(5)**,** 2881-2892.

Kim, D.-S., Seo, W.-S. & Kim, M.-J. (2003). Deformation characteristics of soils with variations of capillary pressure and water content. *Soils and foundations,* 43(4)**,** 71-79.

Koliji, A., Vulliet, L. & Laloui, L. (2010). Structural characterization of unsaturated aggregated soil. *Canadian Geotechnical Journal,* 47(3)**,** 297-311.

Kolisoja, P. (1997). *Resilient deformation characteristics of granular materials*, Tampere University of Technology Finland.

Korkiala-Tanttu, L. (2005). A new material model for permanent deformations in pavements. *Proceedings of the 7th Conference on Bearing Capacity of Roads and Airfields, Trondheim, Norway*.

Krahn, J. & Fredlund, D. (1972). On total, matric and osmotic suction. *Soil Science,* 114(5)**,** 339-348.

Ksaibati, K., Armaghani, J. & Fisher, J. (2000). Effect of moisture on modulus values of base and subgrade materials. *Transportation research record,* 1716(1)**,** 20-29.

Kumar, H. (2013). *Analysis of flexible pavement using Kenlayer*. Master degree, National Institue of Technology Kurukshetra.

Kwon, J., Kim, S.-H., Tutumluer, E. & Wayne, M.H. (2017). Characterisation of unbound aggregate materials considering physical and morphological properties. *International Journal of Pavement Engineering,* 18(4)**,** 303-308.

Ladd, R. (1978). Preparing test specimens using undercompaction. *Geotechnical Testing Journal,* 1(1)**,** 16-23.

Lade, P.V. (2016). *Triaxial testing of soils*, John Wiley & Sons.

Laloui, L. (2013). *Mechanics of unsaturated geomaterials*, John Wiley & Sons.

Lambe, T. & Whitman, R. (1979). Soil mechanics. New York, J. Wiley & Sons.

Lebeau, M. & Konrad, J.-M. (2009). Pavement subsurface drainage: importance of appropriate subbase materials. *Canadian Geotechnical Journal,* 46(8)**,** 987-

1000.

Lehane, B. & Cosgrove, E. (2000). Applying triaxial compression stiffness data to settlement prediction of shallow foundations on cohesionless soil. *Proceedings of the Institution of Civil Engineers-Geotechnical Engineering,* 143(4)**,** 191-200.

Lekarp, F. & Dawson, A. (1998). Modelling permanent deformation behaviour of unbound granular materials. *Construction and building materials,* 12(1)**,** 9-18.

Lekarp, F., Isacsson, U. & Dawson, A. (2000a). State of the art. II: Permanent strain response of unbound aggregates. *Journal of Transportation Engineering,* 126(1)**,** 76-83.

Lekarp, F., Isacsson, U. & Dawson, A. (2000b). State of the art. I: Resilient response of unbound aggregates. *Journal of Transportation Engineering,* 126(1)**,** 66-75.

Leong, E.-C. & Abuel-Naga, H. (2017). Contribution of osmotic suction to shear strength of unsaturated high plasticity silty soil. *Geomechanics for Energy and the Environment,* 15**,** 65-73.

Li, D. & Selig, E.T. (1994). Resilient Modulus for Fine-Grained Subgrade Soils. *Journal of Geotechnical Engineering,* 120(6)**,** 939-957.

Li, D. & Selig, E. (1995). Evaluation of railway subgrade problems. *Transportation research record,* 1489**,** 17.

Li, D. & Selig, E.T. (1996). Cumulative plastic deformation for fine-grained subgrade soils. *Journal of Geotechnical Engineering,* 122(12)**,** 1006-1013.

Li, X. (2003). Effective stress in unsaturated soil: a microstructural analysis. *Geotechnique,* 53(2)**,** 273-277.

Liang, R.Y., Rabab'ah, S. & Khasawneh, M. (2008). Predicting Moisture-Dependent Resilient Modulus of Cohesive Soils Using Soil Suction Concept. *Journal of Transportation Engineering,* 134(1)**,** 34-40.

Lim, W.L., McDowell, G.R. & Collop, A.C. (2005). Quantifying the relative strengths of railway ballasts. *Proceedings of the Institution of Civil Engineers-Geotechnical Engineering,* 158(2)**,** 107-111.

Lin, B. & Cerato, A.B. (2014). Applications of SEM and ESEM in microstructural investigation of shale-weathered expansive soils along swelling-shrinkage cycles. *Engineering Geology,* 177**,** 66-74.

Liu, J., Zeng, Q. & Hou, Y. (2006). Subgrade engineering. *The Architecture and Building Industry Publishing House of China, Beijing*.

Liu, J. & Xiao, J. (2010). Experimental study on the stability of railroad silt subgrade with increasing train speed. *Journal of Geotechnical and Geoenvironmental Engineering,* 136(6)**,** 833-841.

Liu, M. & Carter, J. (2000). Modelling the destructuring of soils during virgin compression. *Geotechnique,* 50(4)**,** 479-483.

Liu, M. & Carter, J. (2002). A structured Cam Clay model. *Canadian Geotechnical Journal,* 39(6)**,** 1313-1332.

Loizos, A., Boukovalas, G. & Karlaftis, A. (2003). Dynamic stiffness modulus for pavement subgrade evaluation. *Journal of Transportation Engineering,* 129(4)**,** 434-443.

Loukidis, D. & Salgado, R. (2009). Bearing capacity of strip and circular footings in sand using finite elements. *Computers and Geotechnics,* 36(5)**,** 871-879.

Lu, Z., Fang, R., Chen, L., She, J. & Xian, S. (2020). Long-term deformation of highway subgrade under coupling effect of traffic load and drying–wetting cycles. *International Journal of Geomechanics,* 20(2)**,** 04019168.

Lunne, T., Powell, J.J. & Robertson, P.K. (1997). *Cone penetration testing in geotechnical practice*, London: Blackie.

Mahboub, K.C., Liu, Y. & Allen, D.L. (2003). Evaluation and analysis of highway pavement drainage.

Maher, A., Bennert, T., Gucunski, N. & Papp Jr, W. (2000). *Resilient modulus properties of New Jersey subgrade soils*. Report No.

Mahima, D. & Sini, T. (2021). Performance evaluation of demolition waste infilled geocell-reinforced subgrade by flexural and rutting analysis. *Road Materials and Pavement Design*)**,** 1-16.

Maleki, M. & Bayat, M. (2012). Experimental evaluation of mechanical behavior of unsaturated silty sand under constant water content condition. *Engineering Geology,* 141**,** 45-56.

Mallick, R.B., Tao, M., Daniel, J.S., Jacobs, J.M. & Veeraragavan, A. (2017). Combined model framework for asphalt pavement condition determination after flooding. *Transportation research record,* 2639(1)**,** 64-72.

Mamou, A., Powrie, W., Priest, J. & Clayton, C. (2017). The effects of drainage on the behaviour of railway track foundation materials during cyclic loading. *Geotechnique,* 67(10)**,** 845-854.

Marinho, F., Take, W. & Tarantino, A. (2008). Measurement of matric suction using tensiometric and axis translation techniques. *Laboratory and field testing of unsaturated soils.* Springer**,** 3-19.

Mašín, D. (2010). Predicting the dependency of a degree of saturation on void ratio and suction using effective stress principle for unsaturated soils. *International Journal for Numerical and Analytical Methods in Geomechanics,* 34(1)**,** 73-90.

McCartney, J.S. & Khosravi, A. (2012). Field-monitoring system for suction and temperature profiles under pavements. *Journal of Performance of Constructed Facilities,* 27(6)**,** 818-825.

McDowell, G.R., Lim, W.L., Collop, A.C., Armitage, R. & Thom, N.H. (2004). Comparison of ballast index tests for railway trackbeds. *Proceedings of the Institution of Civil Engineers-Geotechnical Engineering,* 157(3)**,** 151-161.

McEnroe, B.M. (1994). Drainability of granular bases for highway pavements. *Transportation Research Record 1434.* National Research Council, Washington, D.C.: National Academy Press**,** 23-28.

McHenry, M.T. & Rose, J.G. (2012). *Railroad Subgrade Support and Performance Indicators: A Review of Available Laboratory and In-situ Testing Methods*. Report No. KTC-12-02/FR136-04-6F, Lexington: University of Kentucky.

Meyerhof, G. (1961). Discussion on «Foundations other than piled foundations». *Proceedings of 5th International Conference on Soil Mechanics and Foundation Engineering,* 17-22 July, Paris. Dunod, 3**,** 193-195.

Meyerhof, G.G. (1963). Some recent research on the bearing capacity of foundations. *Canadian Geotechnical Journal,* 1(1)**,** 16-26.

Miller, G., Teh, S., Li, D. & Zaman, M. (2000). Cyclic shear strength of soft railroad subgrade. *Journal of Geotechnical and Geoenvironmental Engineering,* 126(2)**,** 139-147.

Miller, J.S. & Bellinger, W.Y. (2014). *Distress identification manual for the long-term pavement performance program (fifth revised edition)*. Report No.: United States. Federal Highway Administration. Office of Infrastructure Research and Development, FHWA-HRT-13-092.

Mitchell, J.K. & Soga, K. (2005). *Fundamentals of soil behavior*, John Wiley & Sons New York.

Mohseni, E., Saadati, R., Kordbacheh, N., Parpinchi, Z.S. & Tang, W. (2017).

Engineering and microstructural assessment of fibre-reinforced self-compacting concrete containing recycled coarse aggregate. *Journal of Cleaner Production,* 168**,** 605-613.

Monismith, C., Seed, H.B., Mitry, F. & Chan, C. (1967). Prediction of flexible pavement deflections from laboratory repeated-load tests. *NCHRP Report,* 35.

Monismith, C.L., Ogawa, N. & Freeme, C. (1975). Permanent deformation characteristics of subgrade soils due to repeated loading. *Transportation research record,* 537.

Moossazadeh, J. & Witczak, M.W. (1981). Prediction of subgrade moduli for soil that exhibits nonlinear behavior. *Transportation research record,* 810.

Morris, M.D. (1991). Factorial sampling plans for preliminary computational experiments. *Technometrics,* 33(2)**,** 161-174.

Mualem, Y. (1976). A new model for predicting the hydraulic conductivity of unsaturated porous media. *Water resources research,* 12(3)**,** 513-522.

Mun, S., Guddati, M.N. & Kim, Y.R. (2004). Fatigue cracking mechanisms in asphalt pavements with viscoelastic continuum damage finite-element program. *Transportation research record,* 1896(1)**,** 96-106.

Nagaraj, H., Sridharan, A. & Mallikarjuna, H. (2012). Re-examination of undrained strength at Atterberg limits water contents. *Geotechnical and Geological Engineering,* 30(4)**,** 727-736.

Nazarian, S., Abdallah, I., Meshkani, A. & Ke, L. (2003). Use of resilient modulus test results in flexible pavement design. *Resilient Modulus Testing for Pavement Components.* ASTM International.

Nazzal, M.D., Abu-Farsakh, M.Y. & Mohammad, L.N. (2010). Implementation of a critical state two-surface model to evaluate the response of geosynthetic reinforced pavements. *International Journal of Geomechanics,* 10(5)**,** 202-212.

Nazzal, M.D. & Tatari, O. (2013). Evaluating the use of neural networks and genetic algorithms for prediction of subgrade resilient modulus. *International Journal of Pavement Engineering,* 14(4)**,** 364-373.

Neale, C. (2016). *Evaluating use of sub-grade drains with permeable friction course for stormwater drainage: Physical model studies.* Master's thesis, Texas Tech University.

Ng, C.W.W. & Menzies, B. (2007). *Advanced unsaturated soil mechanics and*

engineering, Taylor & Francis, Abington, UK.

Ng, C.W.W. & Yung, S. (2008). Determination of the anisotropic shear stiffness of an unsaturated decomposed soil. *Geotechnique,* 58(1)**,** 23-35.

Ng, C.W.W., Zhou, C., Yuan, Q. & Xu, J. (2013). Resilient modulus of unsaturated subgrade soil: experimental and theoretical investigations. *Canadian Geotechnical Journal,* 50(2)**,** 223-232.

Nie, R., Mei, H., Leng, W., Ruan, B., Li, Y. & Chen, X. (2020). Characterization of permanent deformation of fine-grained subgrade soil under intermittent loading. *Soil Dynamics and Earthquake Engineering,* 139**,** 106395.

Nunn, M., Brown, A., Weston, D. & Nicholls, J. (1997). *Design of long-life flexible pavements for heavy traffic*, TRL Limited.

O'Kelly, B., Vardanega, P.J. & Haigh, S.K. (2018). Use of fall cones to determine Atterberg limits: a review. *Geotechnique,* 68(10)**,** 843-856.

Omer, J. & Eghan, B.A. (2018). Numerical Analysis of Road Pavement Response. *Advancements in Civil Engineering & Technology,* 2(2)**,** 000531.

Ooi, P.S., Archilla, A.R. & Sandefur, K.G. (2004). Resilient modulus models for compacted cohesive soils. *Transportation research record,* 1874(1)**,** 115-124.

Ozel, M. & Mohajerani, A. (2011). Prediction of subgrade resilient modulus for flexible pavement design. *Scientific Research and Essays,* 6(21)**,** 4567-4576.

Özkul, Z.H. & Baykal, G. (2007). Shear behavior of compacted rubber fiber-clay composite in drained and undrained loading. *Journal of Geotechnical and Geoenvironmental Engineering,* 133(7)**,** 767-781.

Pan, T., Hou, S., Liu, Y. & Tan, Q. (2019). Comparison of three models fitting the soil water retention curves in a degraded alpine meadow region. *Scientific reports,* 9(1)**,** 1-12.

Pandya, S. & Sachan, A. (2018). Effect of matric suction and initial static loading on dynamic behaviour of unsaturated cohesive soil. *International Journal of Geotechnical Engineering,* 12(5)**,** 438-448.

Papanicolaou, T., Bressan, F., Wilson, C. & Tsakiris, A. (2015). *Development of a Subgrade Drainage Model for Unpaved Roads*. Report No. TR-654, Iowa, United States: The University of Iowa.

Pham, H.Q., Fredlund, D.G. & Barbour, S.L. (2005). A study of hysteresis models for soil-water characteristic curves. *Canadian Geotechnical Journal,* 42(6)**,** 1548-

1568.

Powell, W., Potter, J., Mayhew, H. & Nunn, M. (1984). *The structural design of bituminous roads*. Report No.

Powrie, W. (2013). *Soil mechanics: concepts and applications*, CRC Press.

Prandtl, L. (1920). Uber die harte plastischer korper. *Mathematisch-Physikalische Klasse,* 1920**,** 74-85.

Puppala, A., Mohammad, L. & Allen, A. (1996). Engineering behavior of lime-treated Louisiana subgrade soil. *Transportation Research Record 1546 : Journal of the Transportation Research Board,* 1546(1)**,** 24-31.

Puppala, A.J., Mohammad, L.N. & Allen, A. (1999). Permanent deformation characterization of subgrade soils from RLT test. *Journal of Materials in Civil Engineering,* 11(4)**,** 274-282.

Puppala, A.J. (2008). *Estimating stiffness of subgrade and unbound materials for pavement design*, Transportation Research Board.

Rahim, A. (2005). Subgrade soil index properties to estimate resilient modulus for pavement design. *International Journal of Pavement Engineering,* 6(3)**,** 163-169.

Rahman, M.M. (2017). Characterization Of Subgrade Resilient Modulus For MEPDG And The Effects On Pavement Rutting.

Rahman, M.S. & Erlingsson, S. (2016). Moisture influence on the resilient deformation behaviour of unbound granular materials. *International Journal of Pavement Engineering,* 17(9)**,** 763-775.

Rajesh, S., Roy, S. & Madhav, S. (2017). Study of measured and fitted SWCC accounting the irregularity in the measured dataset. *International Journal of Geotechnical Engineering,* 11(4)**,** 321-331.

Rasul, J.M., Ghataora, G.S. & Burrow, M.P.N. (2017). The effect of wetting and drying on the performance of stabilized subgrade soils. *Transportation Geotechnics*.

Raymond, G., Bathurst, R. & Hajek, J. (2000). Evaluation and suggested improvements to highway edge drains incorporating geotextiles. *Geotextiles and Geomembranes,* 18(1)**,** 23-45.

Rees, S. 2012. *Part one: Introduction to triaxial testing* [Online]. GDS Instruments. Available: www.gdsinstruments.com [Accessed 2022].

Ridgeway, H.H. (1982). *Pavement subsurface drainage systems*. Report No. NCHRP

SYNTHESIS 96, Washington, DC, 96: Transportation Research Board.

Robnett, Q.L., Thompson, M., Knutson, R.M. & Tayabji, S. (1975). *Development of a structural model and materials evaluation procedures - ballast and foundation materials research program*. Report No. FRA-OR&D-76-255, Illinois, United States: University of Illinois, Urbana-Champaign.

Rokade, S., Agarwal, P. & Shrivastava, R. (2012). Drainage and flexible pavement performance. *International Journal of Engineering Science and Technology,* 4(04)**,** 2002.

Romero, E., Gens, A. & Lloret, A. (2003). Suction effects on a compacted clay under non-isothermal conditions. *Geotechnique,* 53(1)**,** 65-81.

Romero, E., Villar, M. & Lloret, A. (2005). Thermo-hydro-mechanical behaviour of two heavily overconsolidated clays. *Engineering Geology,* 81(3)**,** 255-268.

Romero, E. & Simms, P.H. (2008). Microstructure investigation in unsaturated soils: a review with special attention to contribution of mercury intrusion porosimetry and environmental scanning electron microscopy. *Geotechnical and Geological Engineering,* 26(6)**,** 705-727.

Roscoe, K.H., Schofield, A. & Wroth, C. (1958). On the yielding of soils. *Geotechnique,* 8(1)**,** 22-53.

Rose, J., Trella, M. & Agarwal, N. (2011). Structural Design of Railway Trackbeds: Relative Effects of Various Factors. *ASME/IEEE Joint Rail Conference*, Pueblo CO, United States. American Society of Mechanical Engineers, JRC2011-56016**,** 45-64.

Rose, J.G., Liu, S. & Souleyrette, R.R. (2014). Kentrack 4.0: a railway trackbed structural design program. *Proceedings of the 2014 Joint Rail Conference* April 2-4 2014, Colorado Springs, CO, United States. American Society of Mechanical Engineers, JRC2014-3752**,** V001T001A010.

Rushton, K. & Ghataora, G. (2009). Understanding and modelling drainage of railway ballast. *Proceedings of the Institution of Civil Engineers-Transport*. Thomas Telford Ltd, 162(4)**,** 227-236.

Rushton, K.R. & Ghataora, G. (2014). Design for efficient drainage of railway track foundations. *Proceedings of the Institution of Civil Engineers-Transport,* 167(1)**,** 3-14.

Saad, B., Mitri, H. & Poorooshasb, H. (2005). Three-dimensional dynamic analysis of

flexible conventional pavement foundation. *Journal of Transportation Engineering,* 131(6)**,** 460-469.

Sabri, I.L.M. (2015). Study on the impact of moisture content on subgrade strength. *Proceedings of 5th International Symposium 2015 on Emerging Trends and Challenges in Multidisciplinary Research*, SEUSL. South Eastern University of Sri- Lanka, Oluvil, Sri- Lanka)**,** 71-76.

Saevarsdottir, T. & Erlingsson, S. (2013). Water impact on the behaviour of flexible pavement structures in an accelerated test. *Road Materials and Pavement Design,* 14(2)**,** 256-277.

Salgado, R., Bandini, P. & Karim, A. (2000). Shear strength and stiffness of silty sand. *Journal of Geotechnical and Geoenvironmental Engineering,* 126(5)**,** 451-462.

Salour, F., Erlingsson, S. & Zapata, C.E. (2014). Modelling resilient modulus seasonal variation of silty sand subgrade soils with matric suction control. *Canadian Geotechnical Journal,* 51(12)**,** 1413-1422.

Santha, B. (1994). Resilient modulus of subgrade soils: Comparison of two constitutive equations. *Transportation research record,* 1462.

Sawangsuriya, A., Edil, T.B. & Bosscher, P.J. (2008). Modulus− suction− moisture relationship for compacted soils. *Canadian Geotechnical Journal,* 45(7)**,** 973-983.

Sawangsuriya, A., Edil, T.B. & Benson, C.H.J.T.r.r. (2009). Effect of suction on resilient modulus of compacted fine-grained subgrade soils. 2101(1)**,** 82-87.

Scholz, T.V. & Rajendran, S. (2009). *Investigating premature pavement failure due to moisture*. Report No. FHWA-OR-RD-10-02, Salem, Oregon: Oregon, Deptartment of Transportation, Research Section.

Seed, H.B., Chan, C.K. & Monismith, C.L. (1955). Effects of repeated loading on the strength and deformation of compacted clay. *Proceedings of the 34th Annual Meeting of the Highway Research Board,* January 11-14, Washington, D.C.: Highway Research Board, 34**,** 541-558.

Seed, H.B., Chan, C. & Lee, C.E. (1962). Resilience characteristics of subgrade soils and their relation to fatigue failures in asphalt pavements. *International Conference on the Structural Design of Asphalt Pavements. Supplement,* 20 August, University of Michigan. Ann Arbor, MI United States)**,** 77-113.

Selig, E.T. & Waters, J.M. (1994). *Track geotechnology and substructure management,*

Thomas Telford.

Semmelink, C. & De Beer, M. (1995). Rapid determination of elastic and shear properties of road-building materials with the K-mould. *Proceedings of The Fourth International Symposium On Unbound Aggregates In Roads (Unbar4)*, 17th-19th July, Nottingham, United Kingdom. University of Nottingham)**,** 151-161.

Shahu, J., Kameswara Rao, N. & Yudhbir (1999). Parametric study of resilient response of tracks with a sub-ballast layer. *Canadian Geotechnical Journal,* 36(6)**,** 1137-1150.

Sheng, D., Fredlund, D.G. & Gens, A. (2008). A new modelling approach for unsaturated soils using independent stress variables. *Canadian Geotechnical Journal,* 45(4)**,** 511-534.

Skempton, A.W. & Jones, O. (1944). Notes on the compressibility of clays. *Quarterly Journal of the Geological Society,* 100(1-4)**,** 119-135.

Sol-Sánchez, M., Thom, N., Moreno-Navarro, F., Rubio-Gámez, M. & Airey, G. (2015). A study into the use of crumb rubber in railway ballast. *Construction and building materials,* 75(2015)**,** 19-24.

Song, Y.-S., Hwang, W.-K., Jung, S.-J. & Kim, T.-H. (2012). A comparative study of suction stress between sand and silt under unsaturated conditions. *Engineering Geology,* 124**,** 90-97.

Sorensen, K. & Okkels, N. (2013). Correlation between drained shear strength and plasticity index of undisturbed overconsolidated clays. *Proceedings of the 18th International Conference on Soil Mechanics and Geotechnical Engineering*, Paris. 1**,** 423-428.

Stark, T.D. & Eid, H.T. (1994). Drained residual strength of cohesive soils. *Journal of Geotechnical Engineering,* 120(5)**,** 856-871.

Stringer, M. & Madabhushi, S. (2013). Axial load transfer in liquefiable soils for free-standing piles. *Geotechnique,* 63(5)**,** 400-409.

Suh, Y., Mun, S. & Yeo, I. (2010). Fatigue life prediction of asphalt concrete pavement using a harmony search algorithm. *KSCE Journal of Civil Engineering,* 14(5)**,** 725-730.

Sukumaran, B., Kyatham, V., Shah, A. & Sheth, D. (2002). Suitability of using california bearing ratio test to predict resilient modulus. *Proceedings of Federal*

Aviation Administration Airport Technology Transfer Conference, January 1.)**,** 9.

Sun, D.a., Sheng, D. & Sloan, S.W. (2007). Elastoplastic modelling of hydraulic and stress–strain behaviour of unsaturated soils. *Mechanics of Materials,* 39(3)**,** 212-221.

Sweere, G.T. (1990). *Unbound granular bases for roads.* PhD thesis, Delft University of Technology, Netherlands.

Tang, X., Palomino, A.M. & Stoffels, S.M. (2016a). Permanent deformation behaviour of reinforced flexible pavements built on soft soil subgrade. *Road Materials and Pavement Design,* 17(2)**,** 311-327.

Tang, X., Stoffels, S.M. & Palomino, A.M. (2016b). Mechanistic-empirical approach to characterizing permanent deformation of reinforced soft soil subgrade. *Geotextiles and Geomembranes,* 44(3)**,** 429-441.

Tao, M. & Abu-Farsakh, M.Y. (2008). *Effect of drainage in unbound aggregate bases on flexible pavement performance*. Report No.: Louisiana Transportation Research Center.

Tasalloti, A., Marshall, A.M., Heron, C.M. & Hashemi, M.A. (2020). Geocellular railway drainage systems: Physical and numerical modelling. *Transportation Geotechnics,* 22**,** 100299.

Teixeira, P.F., López-Pita, A., Casas, C., Bachiller, A. & Robuste, F. (2006). Improvements in high-speed ballasted track design: Benefits of bituminous subballast layers. *Transportation research record,* 1943(1)**,** 43-49.

Terzaghi, K. (1943). *Theoretical soil mechanics,* Chapman And Hall, Limited.; London.

Thevakumar, K., Indraratna, B., Ferreira, F.B., Carter, J. & Rujikiatkamjorn, C. (2021). The influence of cyclic loading on the response of soft subgrade soil in relation to heavy haul railways. *Transportation Geotechnics,* 29**,** 100571.

Thevanayagam, S. (1998). Effect of fines and confining stress on undrained shear strength of silty sands. *Journal of Geotechnical and Geoenvironmental Engineering,* 124(6)**,** 479-491.

Thom, N. (2008). *Principles of pavement engineering,* Thomas Telford London.

Thom, N., Cooper, A., Grafton, P., Walker, C., Wen, H. & Sha, R. (2012). A new test for base material characterisation. *Proceedings of the International Symposium on Heavy Duty Asphalt Pavements and Bridge Deck Pavements,* Nanjing, China.

International Society for Asphalt Pavements.

Thompson, M.R., Barenberg, E.J., Carpenter, S.H., Darter, M.I., Dempsey, B.J. & Ioannides, A.M. (1990). *Calibrated Mechanistic Structural Analysis Procedures for Pavement*. Report No.: University of Illinois, Urbana-Champaign.

Thompson, M.R. & Nauman, D. (1993). *Rutting rate analyses of the AASHO road test flexible pavements*.

Thu, T.M., Rahardjo, H. & Leong, E.C. (2006). Shear strength and pore-water pressure characteristics during constant water content triaxial tests. *Journal of Geotechnical and Geoenvironmental Engineering,* 132(3)**,** 411-419.

Trauner, L., Dolinar, B. & Mišič, M. (2005). Relationship between the undrained shear strength, water content, and mineralogical properties of fine-grained soils. *International Journal of Geomechanics,* 5(4)**,** 350-355.

Tripathy, S. & Mishra, A.K. (2011). On the use of Skempton's compression index equation. *Geotechnical and Geological Engineering,* 29(1)**,** 129-135.

Tseng, K.H. & Lytton, R.L. (1989). Prediction of permanent deformation in flexible pavement materials. *Implication of aggregates in the design, construction, and performance of flexible pavements.* ASTM International.

Uzan, J. (1985). Characterization of granular material. *Transportation research record,* 1022(1)**,** 52-59.

Van Dam, T., Sutter, L., Smith, K., Wade, M. & Peterson, K. (2002). *Guidelines for detection, analysis, and treatment of materials-related distress in concrete pavements. Volume 2, Guidelines description and use*. Report No.: United States. Federal Highway Administration.

Van Genuchten, M.T. (1980). A closed-form equation for predicting the hydraulic conductivity of unsaturated soils 1. *Soil Science Society of America Journal,* 44(5)**,** 892-898.

Van Sambeek, R.J. (1989). *Synthesis on subsurface drainage of water infiltrating a pavement structure*. Report No.

Vanapalli, S., Fredlund, D., Pufahl, D. & Clifton, A. (1996). Model for the prediction of shear strength with respect to soil suction. *Canadian Geotechnical Journal,* 33(3)**,** 379-392.

Veenstra, M., White, D.J. & Schaefer, V.R. (2005). *Synthesis of nondestructive testing*

technologies for geomaterial applications. Report No.

Vesić, A.S. (1973). Analysis of ultimate loads of shallow foundations. *Journal of the Soil Mechanics and Foundations Division,* 99(1)**,** 45-73.

Vo, T. & Russell, A.R. (2013). Unsaturated soil interacting with a rotating model wall. *International Journal of Physical Modelling in Geotechnics,* 13(2)**,** 63-78.

Wang, F., Shi, M., Liu, W., Zhong, Y. & Wang, X. (2015). Polymer grouting method for constructing ultra-thin anti-seepage wall. Google Patents.

Wang, F., Han, J., Zhang, X. & Guo, J. (2017). Laboratory tests to evaluate effectiveness of wicking geotextile in soil moisture reduction. *Geotextiles and Geomembranes,* 45(1)**,** 8-13.

Wang, G., Wang, Y., Thompson, R. & Ahn, Y.H. (2012). Long-life pavement design and construction–a case study. *Proceedings of the Ninth Asia Pacific Transportation Development Conference*, June 29-July 1, Chongqing, China. American Society of Civil Engineers.

Wang, M., Li, Z. & Raabe, D. (2018). In-situ SEM observation of phase transformation and twinning mechanisms in an interstitial high-entropy alloy. *Acta Materialia,* 147**,** 236-246.

Werkmeister, S., Dawson, A.R. & Wellner, F. (2001). Permanent deformation behavior of granular materials and the shakedown concept. *Transportation research record,* 1757(1)**,** 75-81.

Wesley, L. (2003). Residual strength of clays and correlations using Atterberg limits. *Geotechnique,* 53(7)**,** 669-672.

Wheeler, S. & Sivakumar, V. (1995). An elasto-plastic critical state framework for unsaturated soil. *Geotechnique,* 45(1)**,** 35-53.

White, D.J., Vennapusa, P. & Jahren, C.T. (2004). *Determination of the optimum base characteristics for pavements*. Report No.

Witczak, M. & Uzan, J. (1988). *The Universal Airport Design System, Report I of IV: Granular Material Characterization*. Report No.

Witczak, M.W. (2002). *Simple performance test for superpave mix design*. Report No. NCHRP 465, Transportation Research Board, Washington, D.C.: The National Academies Press.

Wolff, H. & Visser, A. (1994). Incorporating elasto-plasticity in granular layer pavement design. *Proceedings of the Institution of Civil Engineers-Transport,*

105(4), 259-272.

Wood, D.M. (1990). *Soil behaviour and critical state soil mechanics*, Cambridge university press.

Xu, J., Wang, F., Zhong, Y., Wang, B., Li, X. & Ning, S. (2012). Stress analysis of polymer diaphragm wall for earth-rock dams under static and dynamic loads. *Chinese Journal of Geotechnical Engineering,* 34(9), 1698-1703.

Yang, S.R., Huang, W.H. & Tai, Y.T. (2005). Variation of resilient modulus with soil suction for compacted subgrade soils. *Transportation Research Record: Journal of the Transportation Research Board,* 1913(1), 99-106.

Yang, S.R., Lin, H.D., Kung, J.H.S. & Huang, W.H. (2008). Suction-Controlled Laboratory Test on Resilient Modulus of Unsaturated Compacted Subgrade Soils. *Journal of Geotechnical and Geoenvironmental Engineering,* 134(9), 1375-1384.

Yao, Y., Zheng, J., Zhang, J., Peng, J. & Li, J. (2018). Model for predicting resilient modulus of unsaturated subgrade soils in south China. *KSCE Journal of Civil Engineering,* 22(6), 2089-2098.

Yideti, T.F., Birgisson, B., Jelagin, D. & Guarin, A. (2014). Packing theory-based framework for evaluating resilient modulus of unbound granular materials. *International Journal of Pavement Engineering,* 15(8), 689-697.

Yoo, P. & Al-Qadi, I. (2007). Effect of transient dynamic loading on flexible pavements. *Transportation Research Record 1990: Journal of the Transportation Research Board,* 1990(1), 129-140.

Zaghloul, S., Ayed, A., Ahmed, Z., Henderson, B., Springer, J. & Vitillo, N. (2004). Effect of positive drainage on flexible pavement life-cycle cost. *Transportation research record,* 1868(1), 135-141.

Zakeri, R., Tafreshi, S.M., Dawson, A.R. & Baidya, D.K. (2021). Influence of rubber sheet on dynamic response of machine foundations. *Construction and building materials,* 274, Article 121788, 1-17.

Zaman, M. & Khoury, N. (2007). *Effect of soil suction and moisture on resilient modulus of subgrade soils in Oklahoma*. Report No. ORA 125-6662, Norman, Oklahoma: University of Oklahoma.

Zhang, J., Peng, J., Liu, W. & Lu, W. (2019). Predicting resilient modulus of fine-grained subgrade soils considering relative compaction and matric suction.

Road Materials and Pavement Design)**,** 1-13.

Zhang, J., Peng, J., Zhang, A. & Li, J. (2020). Prediction of permanent deformation for subgrade soils under traffic loading in southern China. *International Journal of Pavement Engineering*)**,** 1-10.

Zhao, H., Indraratna, B. & Ngo, T. (2021). Numerical simulation of the effect of moving loads on saturated subgrade soil. *Computers and Geotechnics,* 131**,** 103930.

Zhao, Y., Yang, H., Huang, L., Chen, R., Chen, X. & Liu, S. (2019). Mechanical behavior of intact completely decomposed granite soils along multi-stage loading–unloading path. *Engineering Geology,* 260**,** 105242.

Zou, W., Ding, L., Han, Z. & Wang, X. (2020). Effects of freeze-thaw cycles on the moisture sensitivity of a compacted clay. *Engineering Geology,* 278**,** 105832.

Zou, W., Han, Z., Ding, L. & Wang, X. (2021). Predicting resilient modulus of compacted subgrade soils under influences of freeze–thaw cycles and moisture using gene expression programming and artificial neural network approaches. *Transportation Geotechnics,* 28**,** 100520.